Design of Photoswitchable Contrast Agents for Magnetic Resonance Imaging

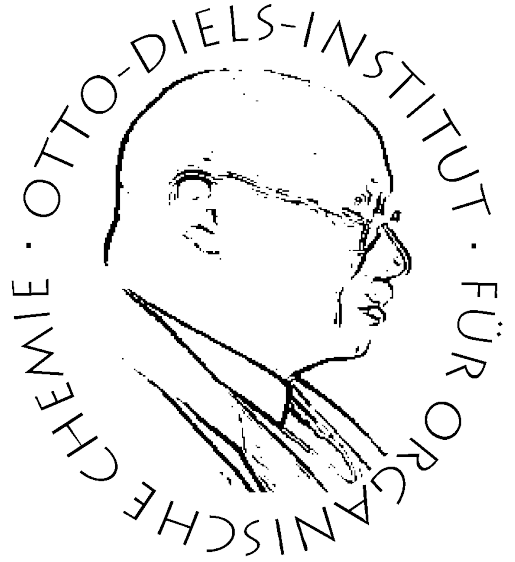

Dissertation

zur Erlangung des Doktorgrades
der Mathematisch-Naturwissenschaftlichen-Fakultät
der Christian-Albrechts-Universität
zu Kiel

vorgelegt von

Marcel Dommaschk

Otto-Diels-Institut für Organische Chemie
Kiel 2016

Referent: Prof. Dr. Rainer Herges
Koreferent:Prof. Dr. Frank D. Sönnichsen

Tag der mündlichen Prüfung: 20.05.2016
Zum Druck genehmigt: 20.05.2016

gez. Prof. Dr. W. J. Duschl, Dekan

Die vorliegende Arbeit wurde unter Anleitung von
Prof. Dr. Rainer Herges
am Otto-Diels-Institut für Organische Chemie
der Christian-Albrechts-Universität
im Zeitraum von Oktober 2011 bis Februar 2016 angefertigt.

Hiermit erkläre ich, Marcel Dommaschk, an Eides statt, dass ich die vorliegende Arbeit selbstständig und nur mit den angegebenen Hilfsmitteln angefertigt habe. Die Dissertation wird ausschließlich an dieser Stelle zur Promotion vorgelegt. Es handelt sich um meinen ersten Promotionsversuch.
Kiel, 25.02.2016

Marcel Dommaschk

Danksagung

Ich bedanke mich bei meinem Betreuer Prof. Dr. Rainer Herges für das außerordentlich vielseitige und fruchtbare Thema meiner Promotion. Er hat mit vielen konstruktiven Vorschlägen meine Arbeit bereichert, aber auch immer genügend Freiraum gelassen eigene Ideen und Projekte zu verfolgen. Dank Prof. Herges konnte ich Kontakte zu uniinternen sowie uniexternen Arbeitsgruppen unterschiedlichster naturwissenschaftlicher Orientierung aufbauen, die zu einer Vielzahl von Kooperationen führten an denen ich mich mit Freude beteiligt habe. Zu nennen ist hier vor allem das Projekt mit Prof. Dr. Wöll (KIT), das zu zwei Publikationen führte, die inhaltlich so weit von meiner eignen Arbeit entfernt sind, dass sie nicht mal in dieser Dissertation erwähnt werden. Natürlich bin ich auch sehr dankbar für die zahlreichen internationalen Tagungen, die ich im Zuge meiner Promotion besuchen konnte. Der nächste Dank gilt dem gesamten Arbeitskreis. Die Stimmung war über all die Jahre stets ganz weit oben, weshalb ich morgens immer gerne aufgestanden bin um zur Uni zu kommen. Zahlreiche Wettbewerbe und Listen, die Kaffeepausen, FAB, THPS2, ... haben den Unialltag in ein regelechtes Event verwandelt. Gegen unseren Sozialraum sieht Las Vegas ziemlich mau aus. Wisst ihr eigentlich, dass ihr sehr geile Kollegen seid? Der Rest des Institutes (die anderen AKs und die Spektroskopie) sind natürlich auch super und sollen hier nicht zu kurz kommen. Vor allem Prof. Frank Sönnichsen danke ich für zahlreiche aufschlussreiche Gespräche und die Übernahme der Zweitkorrektur. Meinen Bachelor Studenten und F3 Praktikanten Morten Peters, Florian Gutzeit, Eike Schaub, Felix Unger, Tobias Plöger und Vanessa Thoms danke ich für die harte Arbeit, die sie bei mir verrichten mussten. Es ist großartig, was ihr hier abgeliefert habt, teilweise. Für das Korrekturlesen dieser Dissertation danke ich außerdem Svea Hinrichsen, Daniel Plaul, Florian Gutzeit, Morten Peters, Lina Harten und Torsten Winkler. Meiner Freundin Svea Hinrichsen danke ich ferner für jeglichen support (nicht nur mit warmen Mahlzeiten) den ich auch außerhalb der Universität täglich genießen darf. Meinen aktuellen und ehemaligen Mitbewohnern Johannes Jensen, Matthias Gens und Christian Schütt danke ich für das lockere WG leben und das auch immer alles reibungslos lief, auch in Zeiten wenn man nurnoch kurz zum Schlafen nach Hause kam und sonst nichts mehr ging. Meiner Familie danke ich ebenfalls für das interessierte Verfolgen meines Fortschrittes aus der Ferne.

Abstract

Magnetically switchable Ni-porphyrins were designed, prepared and investigated in view of their application as switchable contrast agents (CAs) for magnetic resonance imaging (MRI). Molecular bistability and particularly light-induced spin state switching is achieved by covalent attachment of photochromic ligands. The tetradentate porphyrin provides a square planar coordination sphere in which a Ni(II)-ion is diamagnetic and therefore MRI silent. Upon irradiation with green light the attached ligand isomerizes which leads to intramolecular coordination. The fivefold coordinated Ni(II) is paramagentic and hence MRI active. The magnetic switching is called light-driven coordination induced spin state switch (LD-CISSS) and shows no sign of fatigue even after 100,000 cycles at room temperature in solution. We were able to demonstrate that this process can be used to change the NMR relaxation time of solvent protons and thus the MRI contrast even of dilute solutions. The relaxivity in dimethylsulfoxide can be switched by a factor of 6.7 which is by far superior to previous systems based on Gd complexes. The efficiency of the LD-CISSS was improved by increasing the donor strength of the photochromic ligand and by introducing electron-withdrawing groups at the *meso* positions of the porphyrin.

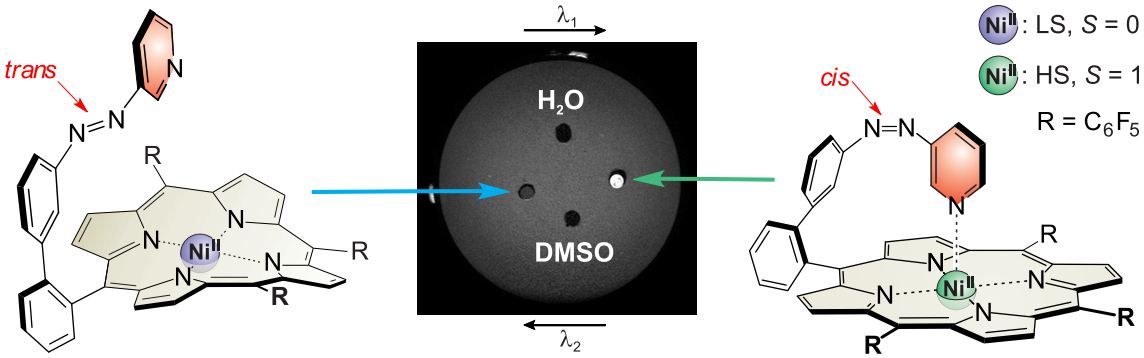

For medical applications (e.g. catheter based interventions) the spin switching must be effected *in vivo*. Towards this end, we were able to provide proof of principle for two important advancements: 1. Ni-porphyrins were functionalized with glycerol dendrimers. The resulting water soluble derivatives have remarkable properties and are the first example of a Ni(II)-based CISSS in water. 2. Ni-chlorins and Ni-isobacteriochlorins were synthesized because these macrocycles can be addressed with light in the near infrared region (NIR) at which blood supported tissue is transparent. These novel Ni-platforms are superior to the Ni-porphyrins in terms of coordination and absorption. The combination of these two approaches with the LD-CISSS molecules is an important step towards magnetic switching under *in vivo* conditions and the development of smart contrast agents for functional imaging.

Kurzdarstellung

Magnetisch schaltbare Ni-Porphyrine wurden designed, synthetisiert und im Hinblick auf ihre Anwendung als schaltbare Kontrastmittel für die Magnetresonanztomographie (MRT) untersucht. Die molekulare Bistabilität durch lichtinduziertes Spin-Switching wurde durch kovalente Verknüpfung mit einem photochromen Liganden erreicht. Porphyrine bieten eine quadratisch planare Koordinationsphäre, in der das Ni(II)-Ion stets diamagnetisch und somit MRT inaktiv ist. Bei Belichtung mit grünem Licht isomerisiert der Ligand wodurch dieser intramolekular koordiniert. Fünfach koordiniertes Ni(II) ist paramagnetisch und daher MRT aktiv. Die magnetische Schaltung wird light-driven coordination induces spin state switch (LD-CISSS) genannt und zeigt auch nach 100.000 Schaltzyklen bei Raumtemperatur in Lösung keine Ermüdungserscheinungen. Wir konnten zeigen, dass NMR Relaxationszeiten sowie MRT Kontraste verdünnter Lösungen geschaltet werden können. Die Relaxivität in DMSO ändert sich dabei um den Faktor 6,7, was weit mehr ist als bei allen bisher präsentierten Gd-Komplexen. Die Effektivität des LD-CISSSs konnte sowohl durch photochrome Liganden mit erhöhter Donorstärke als auch durch elektronenziehende Substituenten am Porphyrin gesteigert werden.

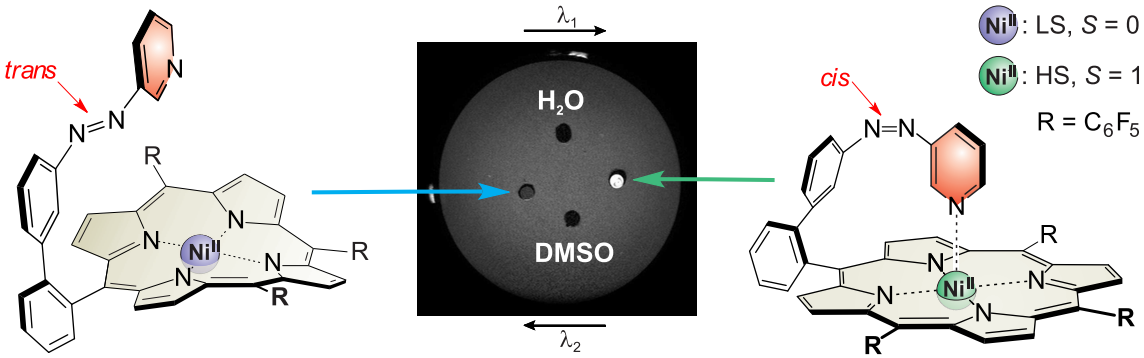

Für medizinische Anwendungen (z.B. katheterunterstützte Interventionen) muss die Spinschaltung *in vivo* funktionieren. Dafür konnten wir mit zwei wichtigen Entwicklungen beitragen: 1. Ni-Porphyrine wurden mit Glycerindendrimeren funktionalisiert. Die dadurch erhaltenen wasserlöslichen Derivate haben einzigartige Eigenschaften und sind das erste Beispiel für einen Ni(II)-basierten CISSS in Wasser. 2. Ni-Chlorine und Ni-Isobakteriochlorine wurden synthetisiert, weil sie mit nahem Infrarotlicht adressiert werden können, welches die höchste Eindringtiefe in durchblutetes Gewebe hat. Diese neuen Ni-Plattformen haben überlegene Koordinations- und Absorbtionseigenschaften. Die Kombination dieser Fortschritte mit den LD-CISSS Molekülen ist der nächste Schritt in Richtung der magnetischen Schaltung *in vivo* und der Entwicklung von intelligenten Kontrastmitteln.

Contents

1 Introduction

1.1 Magnetic Resonance Imaging

Besides the computed tomography (CT), magnetic resonance imaging (MRI) is the most important tool in medical imaging. Both techniques provide tomographic images which can be combined to a three-dimensional picture. This allows non-invasive inspection of the inferior of a human body.[1] The advantages of CT are high resolution, short acquisition times and high contrast of bones. The significant disadvantage of CT is the radiation damage induced by X-rays. Exposure to ionizing radiation can lead to a number of diseases such as cancer. To minimize this risk for patients the exposure time must be as short as possible. MRI has a lower resolution and longer acquisition times during which the patient or the object to be scanned should not move. It is advantageous for the depiction of soft tissue and, most importantly, it avoids ionizing radiation. According to current knowledge MRI is harmless. Hence, MRI scanners and measurement techniques are improved continuously.

The development of MRI started in 1973 with a publication of Lauterbur *et al.*[2] The authors were able to visualize the difference between two tubes, one filled with water and the other one with heavy water, by a two-dimensional image. MRI and nuclear magnetic resonance (NMR) spectroscopy are based on the same physical principles.[3] Atomic nuclei with an intrinsic magnetic moment μ (nuclei with spin quantum number ($I \neq 0$) such as protons ($I = 1/2$) align their magnetic moment in an applied magnetic field. The number of possible orientations ($2I + 1$) is quantized. In an external magnetic field (B_0) these states are no longer degenerated (Zeeman effect). The energy difference ΔE is directly proportional to B_0. Protons ($I = 1/2$) exhibit two nuclear magnetic spin states: parallel ($m_I = 1/2$) and antiparallel ($m_I = -1/2$) with respect to the magnetic field B_0. The parallel orientation is energetically favored (Figure 1.1 left). Boltzmann distribution leads to a small excess of the population of the $m_I = 1/2$ state and thus to a magnetization. The

population difference is small which is the reason for the weak intensity of NMR and MRI compared to other spectroscopic methods.[4] Irradiation with radio frequency disturbs the equilibrium population of the spin states. Upon returning to the original magnetization the system emits radio frequency which is recorded with receiver coils that are as close as possible to the observed object (Figure 1.1 middle). The additional technical challenge of MRI is the transformation of the signals into a three-dimensional image which was investigated by Mansfield who was awarded the Nobel Prize in Physiology or Medicine for his work in 2003 together with Lauterbur.[5] Nowadays clinical MRI scanners have magnetic field strengths of 1-3 T which is lower than conventional NMR spectrometers (200 MHz $\equiv$ 4.7 T).[6] Higher field strengths are rare and can be problematic because eddy currents can be induced in the human brain during the transfer of the patient into the scanner. Hence, the patient has to be brought slowly into the magnetic field. Generally MRI as compared to CT is considered to be better suited to display differences between normal and abnormal tissues. MRI therefore is used to examine ligament and tendon injuries, spinal cord injuries, inflammations and tumors whereas CT is used to display organ injury, broken bones or spinal damage.[7] Motionless body parts like the extremities, the backbone and the head are easier to survey with MRI than active organs like heart or the digestive system. One of the main applications are the identification and localization of tumors as well as inflammations. These are essential information for the surgical removal which cannot be obtained by any other method. Contrast agents can increase the power of a MRI experiment which will be described in section 1.3.

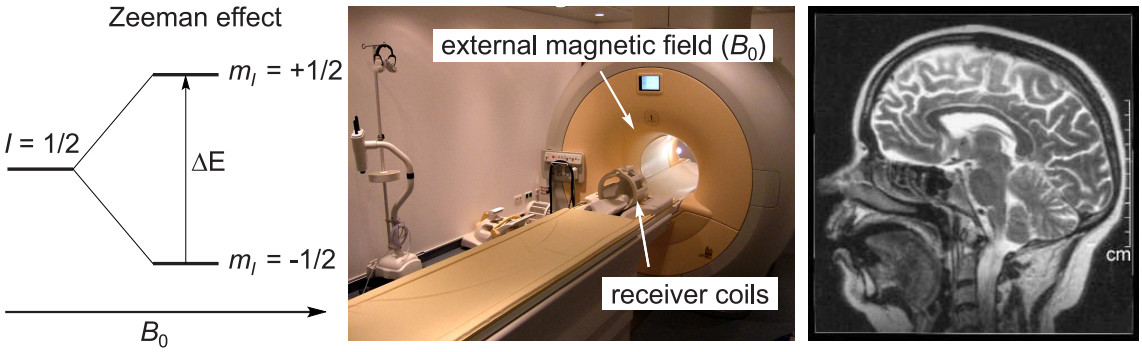

Figure 1.1: Zeeman effect for an $I = 1/2$ nucleus (left), a clinical 3 T MRI scanner with receiver coils for a human head (middle) and a tomographic image of a human head (right, sagittal plane T_2 weighted).

1.2 Relaxation in NMR and MRI

In contrast to NMR spectroscopy, which is focused on the Larmor frequencies to elucidate the molecular structures, MRI uses mainly the relaxation times of the ^{1}H nuclei to obtain three-dimensional structures of objects in *vivo*.[8,9] Almost every molecule in a living organism contains multiple hydrogen atoms. With a natural abundance of 99.99%, the highest gyromagnetic ratio and a biological abundance of 63% ^{1}H nuclei are most qualified for MRI.[10] The relaxation time of a nucleus strongly depends on its environment (Table 1.1).[11] Generally nuclei in molecules with high rotational freedom relax slower than those in immobile molecules. There are two relaxation processes known as longitudinal (T_1) and transversal (T_2) relaxation. To understand these processes the vector model of nuclear magnetic resonance has to be used.

Table 1.1: Relaxation times (T_1 and T_2) of various human tissues at a filed strength of 1.5 T.[11]

Tissue	T_1 / s	T_2 / ms
Cerebrospinal Fluid	0.80−20	110−2000
White Matter	0.76−1.08	61−100
Gray Matter	1.09−2.15	61−109
Meninges	0.50−2.20	50−165
Muscle	0.95−1.82	20−67
Adipose	0.20−0.75	53−94

The excitation in NMR and MRI experiments is achieved by irradiation of the sample with radio frequency whose magnetic field component is orthogonal to the external static field (B_0).[12] The latter is responsible for the population difference between the nuclear magnetic states which gives rise to a macroscopic magnetization (M) in the direction of the magnetic field (B_z) (Figure 1.2). The period of time for which the radio frequency is applied is called pulse. Depending on its strength and duration a pulse transfers a certain fraction of the macroscopic magnetization into the M_{xy} plane where it is precessing around the z-axis. Only the fraction of the macroscopic magnetization within the M_{xy} plane is be measured by the receiver coils because their axes orthogonal to B_0. A 45° pulse transfers half of the magnetization into the M_{xy} plane. A 90° pulse converts M_z completely into M_{xy}. A 180° pulse leads to a population inversion by transferring the magnetization to the -M_z direction, while M_{xy} stays zero.

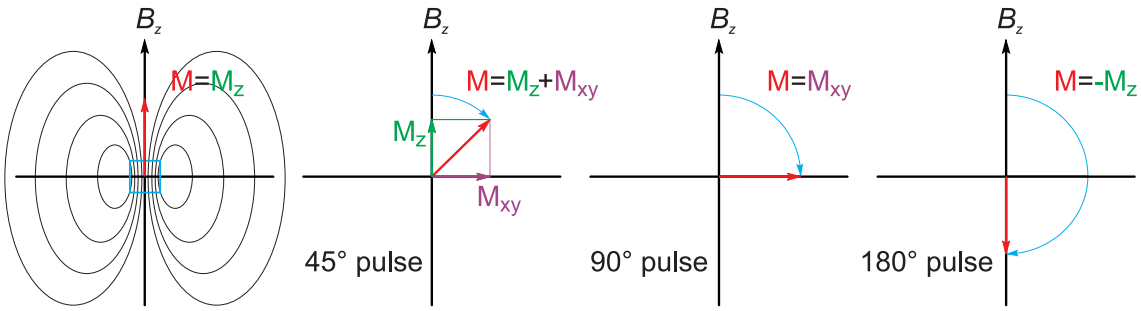

Figure 1.2: Profile of the magnetic field in a NMR and MRI experiment. Orientation of the macroscopic magnetization (M, red) in equilibrium (left) and after a 45°, 90° and 180° pulse. The blue box is the area where the magnetic field is most homogeneous and the measurements are performed.

The system, after some period of time, returns to its original magnetization in direction of B_z. This process is called longitudinal relaxation and the corresponding relaxation time is usually denoted T_1. Hence, T_1^{-1} is the depopulation rate of the excited state by energy transfer to the environment in form of thermal energy.[13,14] Therefore, the longitudinal relaxation is also known as the spin-lattice relaxation. The life time of the excited state is quite long compared to other spectroscopic methods.[4] In exchange the line with of NMR signals is narrow. T_1 can be measured by an inversion recovery experiment (Figure 1.3). A 180° pulse is applied which is followed by a time delay (t). A 90° pulse transfers the remaining magnetization into the M_{xy} plane where it can be measured. A plot of the measured signal intensity over the delay time (t) results in an exponential function whose time constant is the T_1 relaxation time.

The spin-spin or transverse relaxation time T_2 describes the rate of decay of the magnetization within the xy plane.[13,14] It is caused by energy exchange between an excited nucleus with magnetic dipoles (nearby spins). The sequence to measure T_2 starts with a 90° pulse. The measurable magnetization disappears rapidly due to the slightly different Larmor frequencies and the inhomogeneity caused by the experimental setup. This relaxation time is called T_2^*. In homogeneous solutions there are few T_2 processes. Therefore, the majority of the magnetization can be refocused several times by 180° pulses. The results are spin echoes that repeat after the time τ (Figure 1.3). Their intensity decreases with the amount of echoes (n). This decrease is defined as T_2. Since this parameter always includes the spin-lattice relaxation, T_2 is always shorter than T_1 ($T_2 < T_1$) and the corresponding rate is always faster ($T_2^{-1} > T_1^{-1}$).

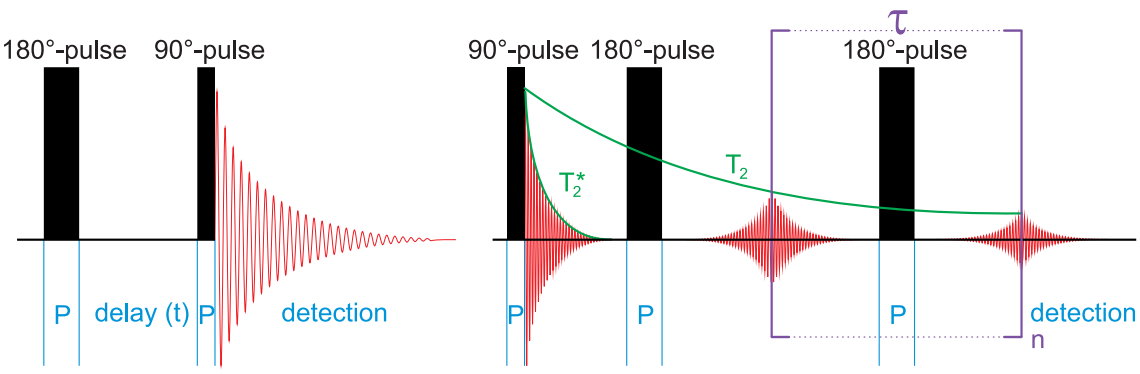

Figure 1.3: Inversion recovery (left) and spin echo experiment (right) of the measurement of T_1 and T_2 relaxation times.

The radiologist chooses a pulse sequence that measures one of the two relaxation times depending on the target and aim of the examination.[15] Both relaxation processes are strongly influenced by paramagnetism.[16,17] The magnetic moment of a single electron is 660 times stronger than the one of the ^{1}H nucleus.[18] Therefore, all paramagnetic compounds have orders of magnitude stronger magnetic moments than the proton. The more unpaired electrons the bigger the impact on a NMR or MRI experiment. The tumbling of a paramagnetic complex creates a fluctuating magnetic field whose interaction with the nuclear magnetic moment of the exited nuclei induces relaxation. This process is most effective when the frequency of the fluctuating field is close to the Larmor frequency of the excited nuclei.[19] The tumbling is described by the rotational correlation time τ_R which is a further important parameter. Depending on the nature of the paramagnetic substance, one of the relaxation times is more affected. Molecules with a single paramagnetic center reduce mainly T_1. On the other hand paramagnetic particles (e.g. iron oxide nanoparticles) reduce mainly T_2. These effects are the basis of MRI contrast agents (CAs).

1.3 MRI Contrast Agents

For special applications or in case the structures in a MR image are not diagnostically conclusive, the radiologist may administer a contrast agent (CA). The application of CAs can furnish information of tremendous importance for a diagnosis or the location of tumors and inflammations. The most frequently applied CAs are Gd(III) complexes. More than 200 million doses have been administered worldwide so far.[20,21] With a seven unpaired electrons ($S = 7/2$) Gd(III) complexes are superior to most of

the other paramagnetic species.[22] They have an enormous impact on MRI contrasts even at low concentrations. The relaxation time of human blood is 1.6-1.8 s (3 T) depending of the hematocrit (volume of erythrocytes in the blood).[23,24] After CA administration the concentration of the Gd(III) complex in the blood vessels is approximately 0.5 mmol l^{-1} which gives rise to a relaxation time of 0.4 s.[25] More details about *in vivo* properties of CAs are discussed in section 4.

Since free Gd(III) is a very toxic ion, it has to be complexed by a strong chelating ligand, mostly cyclic derivatives.[26,27] Most frequently applied are tetraazadodecane (cyclen) derivatives bearing several acetate groups. The parent system is the Gd(III) complex of 1,4,7,10-tetraazacyclododecane-1,4,7,10-tetraacetic acid (Gd-DOTA, **1**)(Figure 1.4). Ligands derived from Gd-DOTA are hepta- or octadentate and therefore exhibit very high association constants to Gd(III) even under *in vivo* conditions.

For the interpretation of MR images it is important to know that a dark spot corresponds to a high intensity. Blood has a long T_1 due to its high mobility (section 1.2). Consequently, the blood vessels appear dark in a T_1 weighted image. Gd(III) CAs are highly hydrophilic and therefore spread mainly in the blood without penetrating lipophilic tissues. As a consequence administration of a CA leads to a brightening of blood supplied areas. A characteristic application is shown in Figure 1.4. CAs usually do not influence the MR image of the human brain because they do not permeate through the blood-brain barrier. Figure 1.4 shows a MR image of the brain of a patient before and after intravenous injection of a contrast agent. The dark matt on the lower left side of the image turns bright after administration of the contrast agent and thus is identified as a brain tumor which established its own blood supply that is independent of the blood-brain barrier.

The examination provided information about the shape and the blood supply of the tumor which were essential for the surgical removal. The efficiency of CAs is quantified by the relaxivity (r_x). There are distinct relaxivities of spin-lattice (r_1) and spin-spin relaxation (r_2). The relationship between the concentration of the agent ($[CA]$) and the relaxation rate (T_x^{-1}) of the solution is linear. The slope is defined as r_x and the intercept is the relaxation rate without CA ($T_{x,0}^{-1}$).

$$T_x^{-1} = T_{x,0}^{-1} + r_x[CA] \qquad x = 1, 2$$

Thus, the relaxivity can be interpreted as the concentration normalized efficiency of a contrast agent to reduce the relaxation time of the NMR active nuclei of the

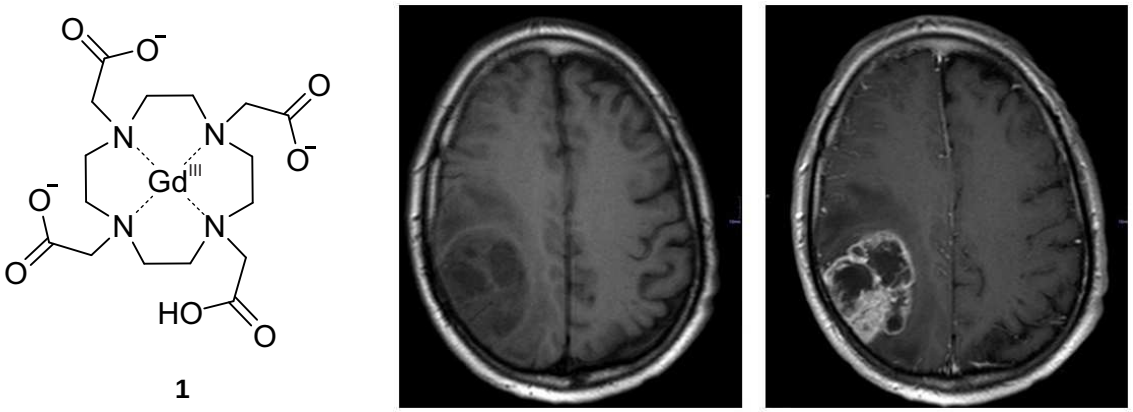

1

Figure 1.4: The MRI CA Gd-DOTA (**1**) (left) and a brain with a tumor before (middle) and after (right) administration of a CA. The image acquisition was performed by the group of Prof. Dr. Jansen and depicted with his permission.

solvent (usually the water protons). The relaxivity depends on further experimental parameters like the magnetic field strength, pH and temperature. The Gd(III) chelates are T_1 CAs which means they are increasing T_1^{-1} and T_2^{-1} more or less equally. On the other hand T_2 CAs like iron nanoparticles are increasing T_2^{-1} by magnitudes more than T_1^{-1}.

1.4 Smart CAs

Several approaches to obtain further information about *in vivo* processes by functionalized Gd(III) complexes have been presented. So-called smart, intelligent or responsive CAs are sensitive to a physiologically relevant parameter.[28] Gd(III) chelates have been developed that are responding to enzymatic activity,[29–35] pH-value,[36–42] carbohydrates,[43,44] thiols[45] and ions like Ca^{2+},[46–51] $Cu^{+/2+}$,[52] K^+,[53] and Zn^{2+}.[54–56] Mn(III)porphyrins that exhibit similar effects have been investigated but they are rarely applied as CAs.[55] The basic principle of all these agents is the same. Besides the magnetic moment and the rotational correlation time (τ_R) (section 1.2) the distance between a paramagnetic center and the observed nuclei (usually the ^{1}H of water molecules) is of tremendous importance for the efficiency of a CA. Therefore, the relaxivity of Gd(III) complexes with a saturated coordination sphere is lower than the one of unsaturated Gd(III) complexes. The relaxation enhancement by direct contact with the paramagnetic metal is known as inner sphere relaxation. If the inner sphere mechanism is possible the contribution to the overall relaxivity

is usually high.[57] In the case of a responsive CA the the inner sphere mechanism becomes available upon contact with the responsive parameter.[28] This gives rise to an enhanced relaxivity which can be monitored by MRI. The first example of a responsive CA was presented by Moats *et al.*[58] They functionalized a Gd(III) chelate with galactose whereby the coordination sphere of the Gd(III) was saturated and the relaxivity of the CA was low. After removing the carbohydrate with the enzyme galactosidase water can directly coordinate to the Gd(III) which increases the relaxivity. Besides this inner sphere relaxation two further mechanisms are operative, namely the outer sphere and the second sphere relaxation.[59] How much each process contributes to the overall relaxivity is experimentally difficult to investigate because it depends on many parameters.[57] An important parameter is the exchange rate (k_{ex}, Figure 1.5) of water molecules coordinated to the metal center.[25] The faster the exchange the higher the contribution of inner sphere mechanism which enhances the potential to design an efficient responsive CA from this system. A CA which is completely MRI silent until activation by a reagent or an external stimulus would be most appreciable.[60] This cannot be realized based on Gd(III) chelates because outer and second sphere relaxivity cannot be switched off. Hence, these molecules will be at least weakly MRI active under any conditions. To realize a CA that can exist in a MRI silent form, the Gd(III) has to be substituted.

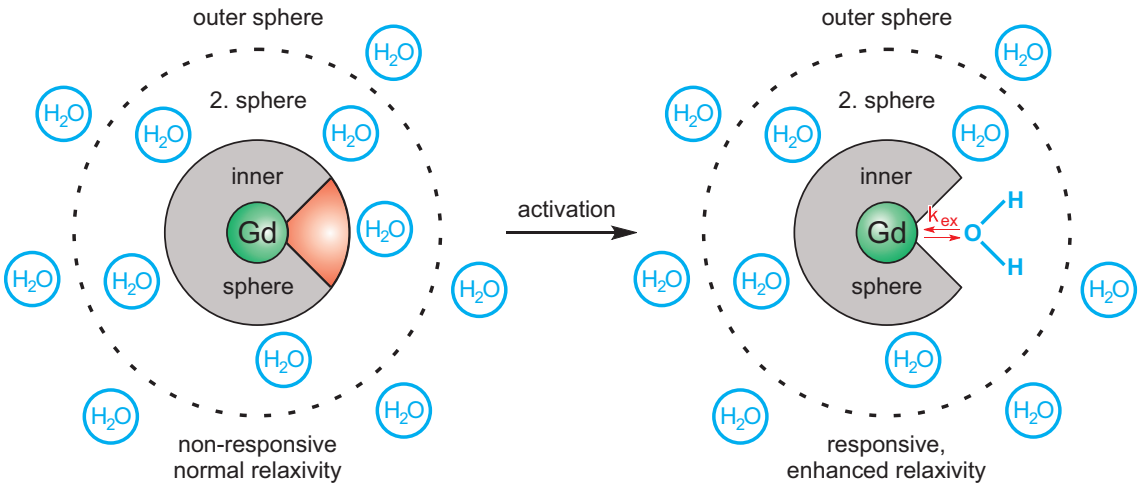

Figure 1.5: The relaxivity enhancement of responsive CAs is due to the increased inner sphere relaxation after the activation.[28,57] The non-responsive form (left) has a saturated coordination sphere. The responsive form (right) is open to coordination by water. The relaxivity is particularly enhanced if the exchange rate (k_{ex}) to the Gd(III) is high.

1.5 Spin State Switching

An activatable CA requires a metal ion that can exist in a diamagnetic and a paramagnetic state. This magnetic bistability is limited to some elements of the 3d transition metals and is mostly a solid state phenomenon known since 1931.[61,62] The driving force of this spin crossover (SCO) is a change of the ligand field strength that can be induced by temperature, pressure and light.[63–67] Typical SCO compounds are octahedral Fe(II)complexes.[68–70] At low temperature they exist in the low spin (LS) state ($^1A_{1g}$) whose zero point energy is lower than the one of the high spin (HS) state ($^5T_{2g}$) (Figure 1.6). With increasing temperature higher energy levels become available. The bond length between Fe(II) and ligand (r(Fe-L)) extends and the entropically favored HS state becomes thermodynamically more stable (Figure 1.6). Besides Fe(II) there are some other 3d metals that exhibit similar or related effects, some even perform spin transition at room temperature.[71–74] In some cases the excited HS state can be populated by irradiation with light which was first observed for $[Fe(ptz)_6](BF_4)_2$ (**2**) (Figure 1.6).[75,76] After excitation with green light ($\lambda = 514\,nm$) the molecule can relax via two inter system crossings (ISC) to the HS state. At temperatures below 50 K the molecule is trapped in this spin state because the forbidden transition to the LS state is not activated. This effect is known as Light-Induced Excited Spin State Trapping (LIESST). Due to the large number of scientists working in the broad field of spin transition complexes numerous publications and reviews are available.[65–79]

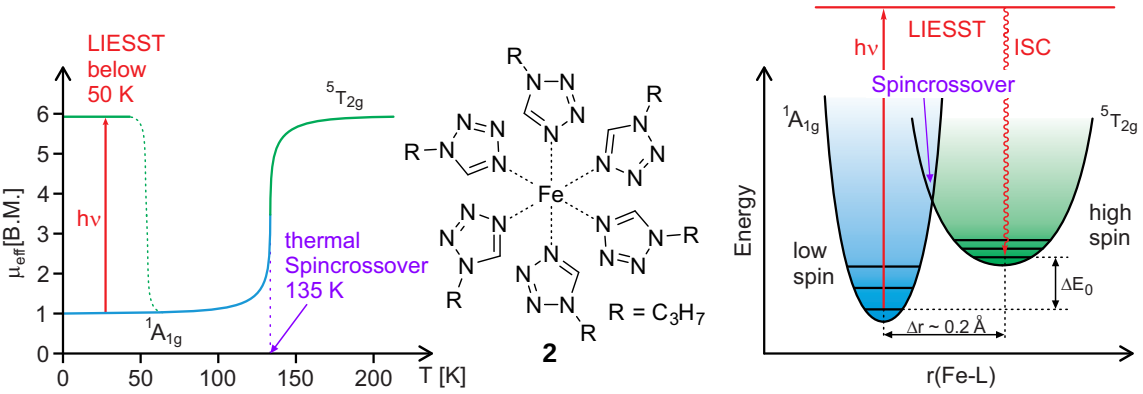

Figure 1.6: $[Fe(ptz)_6](BF_4)_2$ (**2**) (middle) undergoes a thermal SCO at 135 K and a LIESST below 50 K which was observed by the temperature dependence of the Bohr magneton (μ_{eff} in B.M.) (left). The corresponding energy diagram is shown on the right-hand side.

For medical applications the spin state switching has to operate in solution at room temperature or above and in the presence of oxygen. These criteria reduce the number of suitable complexes to zero. Neither temperature nor pressure are appropriate external stimuli under *in vivo* conditions. Due to that, the spin transition complexes which can be addressed with light are most interesting.

1.6 Light-Driven Spin Transitions

The well-known LIESST process only operates at very low temperatures. For spin transitions at higher temperatures the energy barrier between the ground and the excited state must be increased. Since the barrier between two electronic states in a metal complex is intrinsically low, the light-driven spin transition at room temperature requires a different approach. The basic idea is to link a photochromic molecule to the metal center. Photochromism is a phenomenon of organic chemistry.[80] Photochromic compounds have two electronically stable isomers. These are not isoenergetic but the barrier between them is high enough to prevent the immediate isomerization of the metastable form to the thermodynamically stable form. The time scale of the reaction depends on the type of the photochromic molecule. Mainly compounds with long life times of the metastable form at room temperature are of potential interest. This requirement constrains the choice to spiropyranes, diarylethens and azobenzenes (Figure 1.7).[81–83]

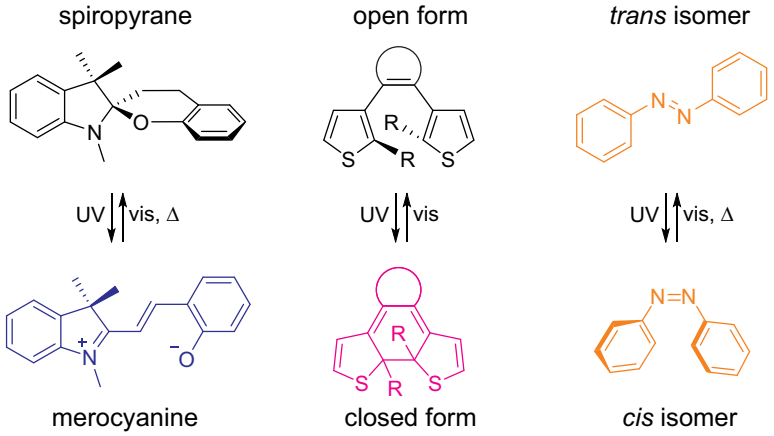

Figure 1.7: Photochromism of spiropyranes (left), diarylethenes (middle) and azobenzenes (right). The parent systems of the three types of photochromic compounds have the color of the drawn structures. The black structures are colorless.

The switch of the configuration entails a massive geometrical movement and change of many molecular properties like UV-vis absorption, dipole moment, conductivity and fluorescence. These molecular switches therefore have been applied for a variety of molecular machines and devices.[84–88]
The combination of a metal complex with a photochromic compound can be beneficial if the metastable isomer gives rise to a different spin state of the metal center than the thermodynamically stable isomer. In that case the isomerization induces the spin transition. So far there are four conceivable approaches to realize this process:

- Switching the ligand field strength
  The isomerization can change the coordination strength of a photochromic ligand. The complex with the less strongly coordinating isomer has a lower SCO temperature than the same complex with the more strongly coordinating isomer. In the interval between both SCO temperatures a Ligand-Driven Light-Induced Spin Change (LD-LISC) is possible.[89,90] The effect was already shown at room temperature[91,92] and even in solution.[93–96] The photochromic ligands are versatile. The metal center is mostly Fe(II) in an octahedral coordination sphere. Therefore, the complexes are stable under inert conditions but are not applicable in presence of oxygen or *in vivo*. Furthermore the switching efficiencies are low and the reversibility of the process is limited to a few cycles.

- Switching the antiferromagnetic coupling
  This concept requires a complex with two metal centers in a single molecule. The photochromic ligand must at least be bidentate and bind to both metals. The configuration of the ligand defines the distance between the paramagnetic metal centers. One isomer must enforce a sufficient distance to prevent magnetic coupling. The other isomer must bring the metal centers close together to induce antiferromagnetic coupling by which the complex becomes diamagnetic. This proposed design has not been realized yet, which is probably due to the difficult tuning of the magnetic coupling in solution.[97]

- Switching the oxidation state
  Magnetic coupling is not limited to metal-metal interaction. Transition metal centers can also couple with so-called non-innocent ligands.[98] Of special interest are Co(II/III) catecholato/semiquinone complexes.[99,100] These ligands can exist in an innocent closed shell catecholato form which is not interacting with the LS Co(III). In the non-innocent semiquinone form one electron is

transfered to the cobalt which is reduced to Co(II) with a HS configuration. The ligand has now a radical character whose spin is coupling with the magnetic moment of the Co(II). The equilibrium between both forms of the complex is called valence tautomerism.[74,101,102] Photochromic coligands can shift the equilibrium. The complex performs a Ligand-Driven Light-Induced Valence Tautomerism (LD-LIVT).[103,104] The LD-LIVT does exclusively operate under inert conditions.

- Switching the coordination number
  Some transition metals exhibit different spin states depending on the coordination number. This requires a metal that is able to form stable complexes of different geometry. Ni(II) is the metal ion that exhibits these properties in an ideal way.[105–115] The switching of the photochromic ligand can induce coordination or decoordination. This effect is known as Coordination-Induced Spin State Switch (LD-CISSS). The spin transition is fully reversible and is operative in solution at room temperature under ambient conditions.[97,116,117] Hence, the LD-CISSS is most qualified to realize a light activatable CA.

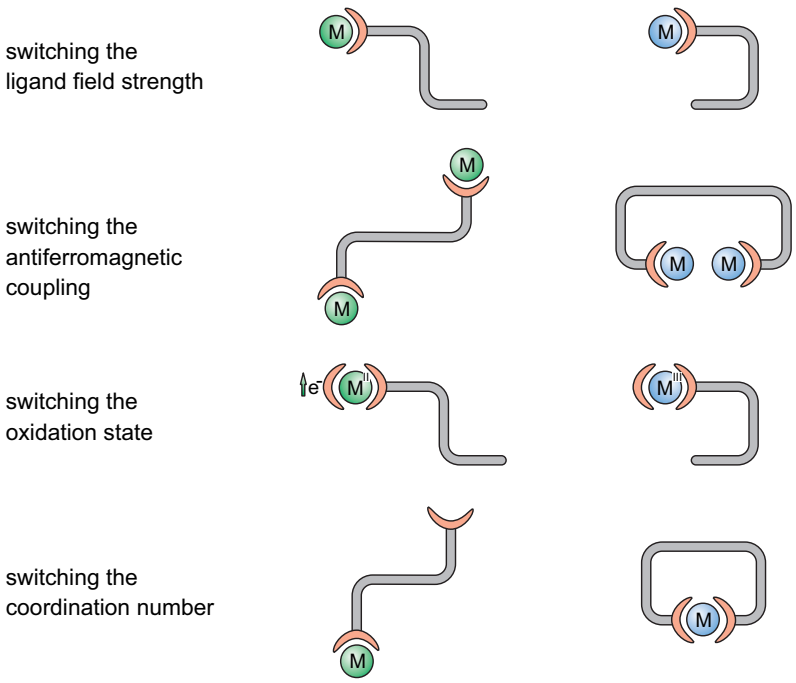

Figure 1.8: Four conceivable approaches to realize a spin transition by the photoisomerization of a ligand.

1.7 Spin Transition of Fe(II) and Ni(II)

Square planar Ni(II) complexes are always LS whereas an octahedral geometry gives always rise to a HS configuration. This spin transition is not a typical SCO phenomenon which is observed exclusively in 3d metal complexes with an electron configuration of d^4-d^7. Ni(II) has an electron configuration of d^8 which disqualifies Ni(II) complexes for a thermal SCO. The origin of the CISSS can be understood by the energy diagram of the molecular orbitals which is quite different compared to classical Fe(II) complexes. A Fe(II) SCO complex has an octahedral geometry (Figure 1.9). The d orbitals are split into the energetically lower t_{2g} (d_{xy}, d_{xz}, d_{yz}) and the e_g ($d_{x^2-y^2}$, d_{z^2}) orbitals. The energy gap between the two sets of orbitals is known as ligand field splitting (Δ). Strong ligands give rise to a high value of Δ and thus to the LS state. In this configuration the electrons are pairing in the t_{2g} orbitals. Weak ligands give rise to small values of Δ. The electrons are distributed according to Hund's rule if Δ is smaller than the spin pairing energy.[118] The SCO can be induced by temperature, pressure and light. Spin change in Ni(II) complexes follows a different scheme due to the lower symmetry of the square planar complex. The d_{z^2} has a relative low energy because there are no ligands in z direction to interact with. The $d_{x^2-y^2}$ has the highest energy and therefore remains unoccupied. The eight d electrons are distributed to the other four orbitals. Hence, the complex has a spin of $S = 0$ and is diamagnetic. Addition of axial ligands increases the energy of the d_{z^2} orbital. The octahedral complex exhibits the familiar e_g/t_{2g} splitting. The d^8 electron configuration gives rise to a spin of $S = 1$.

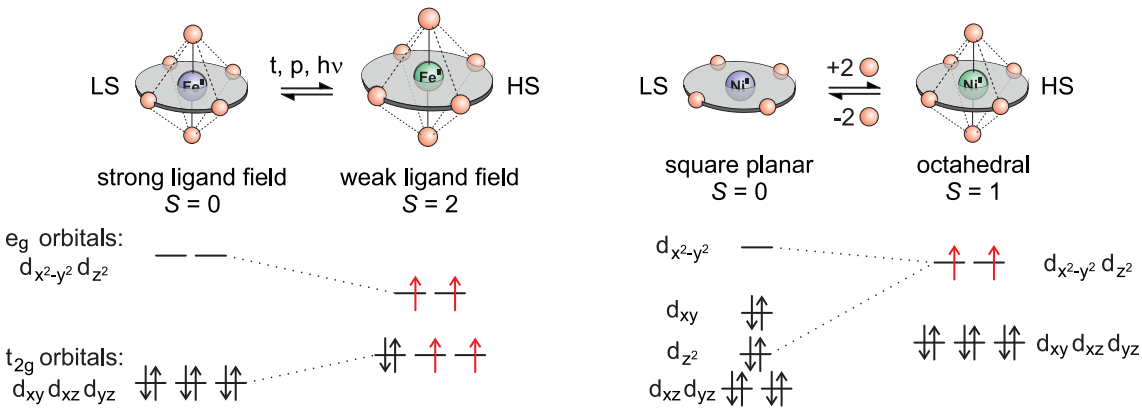

Figure 1.9: Orbital energy diagram of octahedral Fe(II) SCO complexes and Ni(II) CISSS complexes changing from square planar to octahedral geometry.

In contrast to regular SCO complexes the increasing overall ligand field strength leads to the transition from LS to HS. The realization of a CISSS requires a stable square planar Ni(II) complex. This is challenging because Ni(II) can easily adopt octahedral or even tetrahedral geometry.[119–121] Porphyrins have proved their worth for this purpose.[122]

1.8 CISSS of Ni-Porphyrins

Porphyrins are tetradentate rigid macrocycles that provide a perfect square planar coordination sphere for a number of metal ions. The porphyrinato ligand is a dianion. Hence, the complexes with dications like Ni(II) are uncharged. The planar structure of the porphyrin leaves enough space for axial coordination of ligands, which often are nitrogen bases. This type of coordination chemistry is well established.[105–107,109–114] The investigation of the CISSS and the implementation of light control using photoswitchable ligands has been published recently.[97,116,117,122] Porphyrins have four *meso* and eight β positions to introduce functional groups. Natural porphyrins always bear substituents in β positions. Synthetically the *meso* porphyrins are easier accessible by the methods of Adler-Longo and Lindsey.[123–125,138] Especially *meso* aryl porphyrins can be prepared in good yields. For steric reasons the aromatic *meso* substituent is almost perpendicular to the porphyrin plane which decreases aggregation and thus increases solubility. Furthermore, the electronic properties of the porphyrin can be controlled by the nature of the *meso* substituent. This is of special interest for the Ni-porphyrins. Electron-withdrawing *meso* substituents give rise to electron deficiency of the Ni-porphyrin. This increases the affinity of the Ni(II) to accept axial ligands. Consequently, the association constant can be tuned by modification of the *meso* substituents.[113,114] The electron-deficient *meso*-tetrakis(pentafluorophenyl)nickel(II)porphyrin ($NiTPPF_{20}$, **3**) is an established square planar Ni(II) platform for a CISSS whose complex formation with pyridine derivatives is well investigated.[122] It was demonstrated that the *para* substituent of the pyridine is a second parameter for the tuning of the association constant.[108,122] In this case electron-donating substituents increase the coordination. The formation of the octahedral complex proceeds stepwise. A square pyramidal complex is formed initially. The first coordination is quantified by the association constant K_1 and the second by K_2 (Figure 1.10).[115] The five fold coordinated complex is already

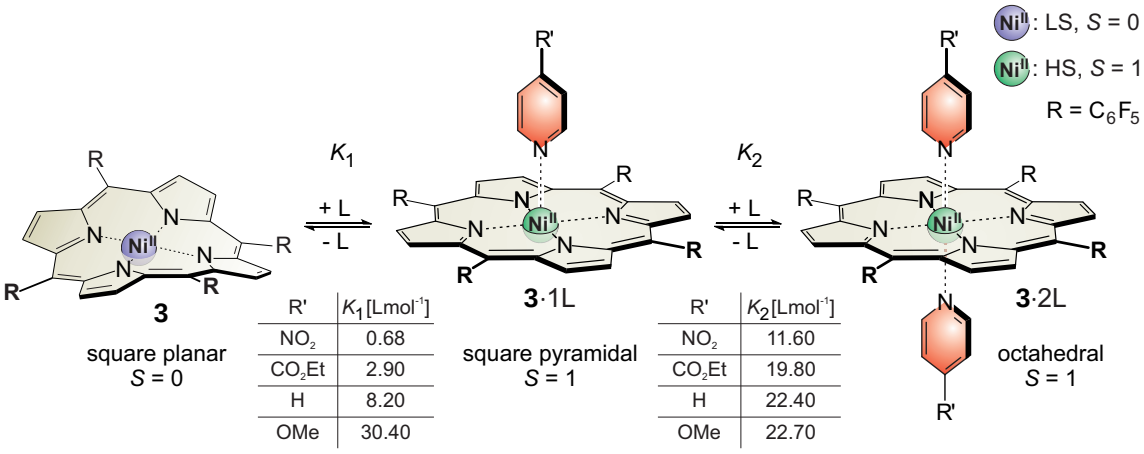

R'	K_1 [Lmol^{-1}]
NO_2	0.68
CO_2Et	2.90
H	8.20
OMe	30.40

R'	K_2 [Lmol^{-1}]
NO_2	11.60
CO_2Et	19.80
H	22.40
OMe	22.70

Figure 1.10: Coordination of *para* substituted pyridine derivatives to NiTPPF$_{20}$, **3**. The association constants for the coordination of the first ligand (K_1) and the second ligand (K_2) are given in the tables.

paramagnetic. Hence, the coordination of the first pyridine is the key step for the spin state switch.

Aliphatic nitrogen bases exhibit even higher association constants than the aromatic bases. For the design of switchable ligands, pyridines are advantageous because their structure is much more rigid. Furthermore, photochromic groups can be introduced much easier than to aliphatic molecules. Therefore, pyridines are utilized to realize a photoswitchable or Light-Driven CISSS (LD-CISSS).

1.9 LD-CISSS

To favor the association of only one isomer of the pyridine containing photochromic compound to a Ni-porphyrin, the geometrical change during the isomerization must be as large as possible. This qualifies azobenzenes. The distance between the two *para* carbon atoms of azobenzene changes from 9 Å in the *trans* configuration to 6 Å in the *cis* configuration.[126–128] The molecule changes from completely planar to a twisted shape. The geometrical change is so drastic that there is no isomerization in solid state which is in contrast to the photochromism of spiropyranes and diarylethenes.[87,88] The introduction of an azo group to pyridine is already established.[129–133] The three regioisomers 2-phenylazopyridine (**4**), 3-phenylazopyridine (**6**) and 4-phenylazopyridine (**5**) are the parent systems with functionalization in *ortho*, *meta* and *para* position (Figure 1.11). 2-Phenylazopyridines (**4**) can be excluded because they are sterically too hindered to coordinate to Ni-porphyrins.

The photochromic group of the 4-phenylazopyridine (**5**) is far away from the Ni-porphyrin. The isomerization has only very little influence on the coordination. The 3-phenylazopyridine (**6**) and its derivatives are most suitable to realize a LD-CISSS. The *trans* isomer is planar and can easily coordinate to the Ni-porphyrin. The *cis* isomer can exist in different conformations, the α form and the β form. The α form can hardly coordinate due to the steric repulsion between the porphyrin and the phenyl group. In contrast to that, the β form can coordinate easily because the phenyl group is turned away from the porphyrin.

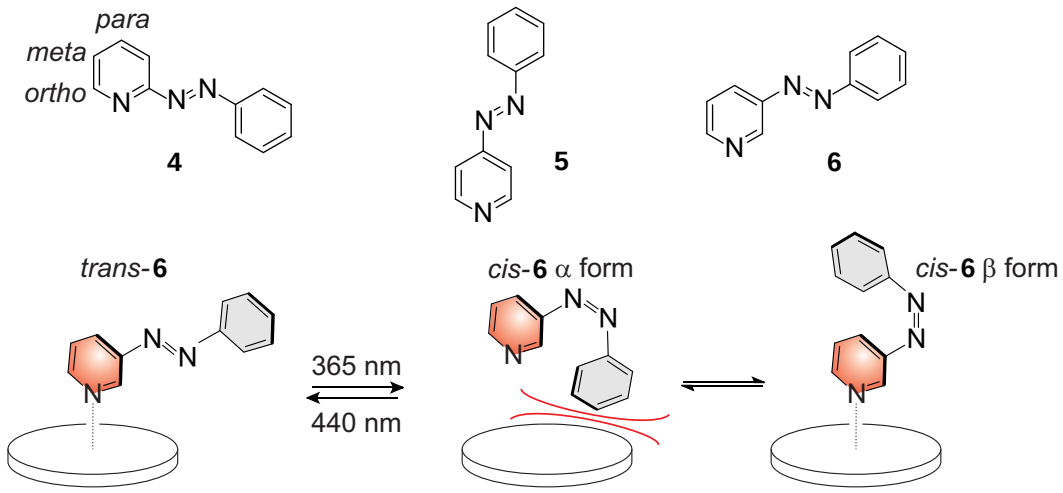

Figure 1.11: The three regioisomers (**4**, **5** and **6**) of phenylazopyridine (top). Photoswitching between *trans*-**6** and *cis*-**6** including the equilibrium between the α and β form (bottom).

To prevent the formation of the *cis* β-form, bulky substituents were introduced to the *para* pyridine position. The repulsion between this substituent and the phenyl group forces the *cis* isomer to preferentially adopt the α-form which can hardly coordinate to the Ni-porphyrin. The association constant of the *cis* isomer can be even further decreased by introduction of *tert*-butyl groups to the *meta* positions of the phenyl substituent (Figure 1.12). Isomerization of those 3-phenylazopyridines from the *trans* to the *cis* configuration leads to decoordination. Molecules of this design are therefore called photodissociable ligands (PDLs). Irradiation with UV light (365 nm) switches the spin state of the nickel from $S = 1$ to $S = 0$. The reverse process is achieved by irradiation with blue light (440 nm) (Figure 1.12). The highest achievable difference in the percentage of paramagnetic Ni(II) is defined as the maximum switching efficiency (SE_{max}).

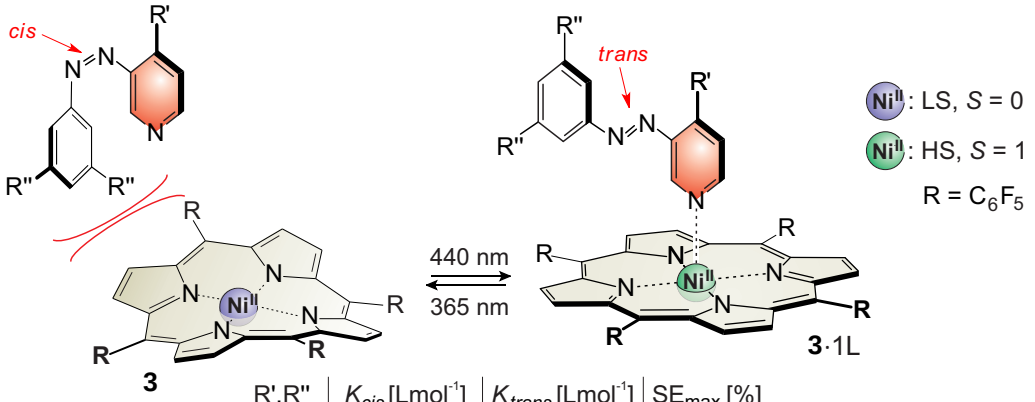

R',R''	K_{cis} [Lmol^{-1}]	K_{trans} [Lmol^{-1}]	SE_{max} [%]
Me, H	2.84	5.83	11
*i*Pr, H	1.96	4.90	15
Me, *t*Bu	1.17	6.27	40

Figure 1.12: LD-CISSS with 3-phenylazopyridine derivatives as PDLs. The association constant of the *cis* isomer (K_{cis}) decreases if the substituents R' and R'' become bulkier. This increases the maximum switching efficiency (SE_{max}).

The LD-CISSS with PDLs is fully reversible and shows no signs of fatigue. A disadvantage of this concept is that the switching efficiency is strongly depending on the ligand concentration. If the concentration is too high, the Ni-porphyrin will always be HS configured due to the circumstances that the photoconversion is not quantitative and the association of the *cis* isomer is not zero. If the concentration is too low, the Ni(II) stays in the LS state because no coordination will occur. An optimal switching efficiency requires a specific ligand concentration which cannot be controlled under *in vivo* conditions. Furthermore the required ligand excess cannot be realized under physiological conditions. This disqualifies the PDLs concept for the application as a photoswitchable MRI CA. For this purpose the spin state of the Ni-porphyrin must become independent of the ligand concentration. To achieve this goal the photochromic ligand was directly attached to the Ni-porphyrin.

1.10 Intramolecular LD-CISSS

The realization of a LD-CISSS with a molecule which has a covalent connection between the Ni-porphyrin and the photochromic ligand requires a very accurate design. There are two possible mechanisms to trigger the association-dissociation processes. The first one is similar to the PDL concept described in the previous chapter. The axial ligand is binding in the *trans* configuration. The *cis* configuration

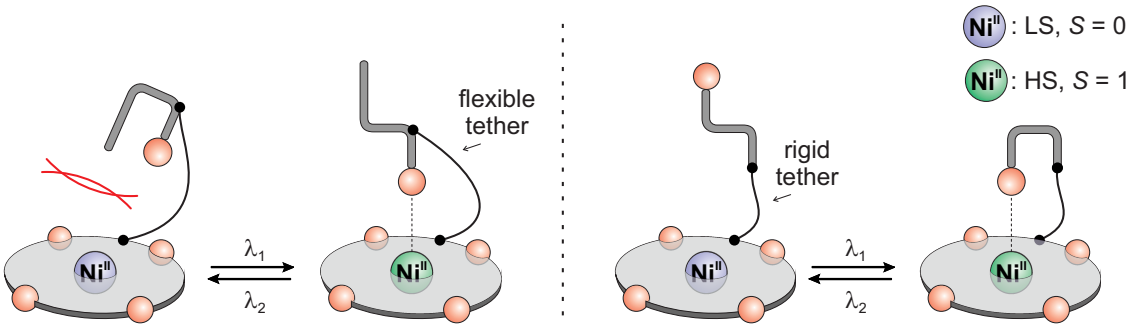

Figure 1.13: The two possible designs to realize an intramolecular LD-CISSS. The PDL-related approach (left) requires a flexible tether to connect the photochromic ligand with the porphyrin. For the structure-oriented record player (RP) approach (right) the tether must be rigid.

causes steric repulsion that induces decoordination of the ligand (Figure 1.13). The tether prevents a complete dissociation of Ni-porphyrin and ligand. To enable the decoordination the tether must be flexible. The second approach requires a rigid tether. The molecule must be designed in a way that only one of the two ligand configurations is able to coordinate. The other isomer must have no conformation which allows the formation of a coordinative bond. Molecules that are able to undergo this kind of an intramolecular LD-CISSS have been coined record players (RPs).
Recently, VENKATARAMANI *et. al* were able to synthesize the first RP (**7**, Figure 1.14).[97] The origin of the spin state switching is the rigid structure of the molecule. In contrast to the PDL concept, the molecule is designed for exclusive coordination in *cis* configuration. The *trans* configuration of RP **7** has no stable conformation in which the distance between the pyridine nitrogen and the Ni(II) is less than 6 Å. Hence, intramolecular coordination is prevented. After isomerization to the *cis* configuration the distance can be reduced to 2.2 Å which is suitable for the coordinative bond of an axial ligand (Figure 1.14). Irradiation with green light ($\lambda_1 = 495 - 530\,\text{nm}$) enriches the paramagnetic *cis* isomer up to 65%. The reverse process is induced by irradiation with blue-violet light ($\lambda_2 = 420 - 435\,\text{nm}$). This isomerization is almost quantitative (less than 5% *cis* isomer left).
The photochromism of RP **7** is fully reversible without showing any signs of fatigue. The spin state of RP (**7**) is not depending on the concentration of a photochromic axial ligand which is a prerequisite of the application as a MRI CA.

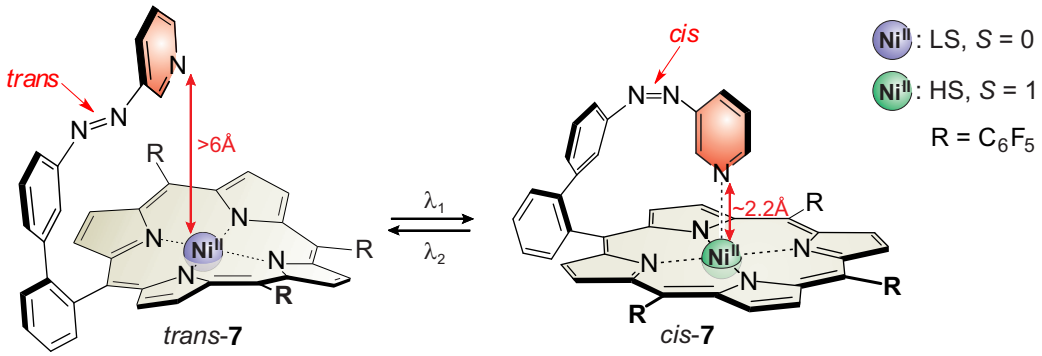

Figure 1.14: The intramolecular LD-CISSS of RP **7**. The square planar coordination of the nickel ion remains unaffected if the ligand is in the trans configuration. The *cis* configuration enables coordination of the covalently linked pyridine. Hence, the Ni-complex has a square pyramidal geometry and is paramagnetic.

2 Scope

This work is devoted to the synthesis and characterization of record players (RPs) and related Ni-porphyrins. The aim is to assess the applicability of molecules performing a Light-Driven Coordination-Induced Spin State Switch (LD-CISSS) as contrast agents (CAs) for magnetic resonance imaging (MRI). All aspects of a future *in vivo* application are supposed to be considered.
Since Ni(II) is a much less paramagnetic metal ion than Gd(III), the magnetic switching efficiency of the RPs must be as high as possible to compete with the Gd(III) CAs. To optimize the magnetic switching it is essential to understand the required experimental conditions, the mechanism and the structure of all relevant species.
The preliminary work with RP **7** could verify that the magnetic susceptibility of a solution can be switched by irradiation with light. The next steps are the investigations regarding the relaxivity and finally the demonstration that MRI contrast can be switched using light. The proof of principle is important to show if further investigations regarding a MRI application are worthwhile.
Another issue is magnetic switching of aqueous solutions. The highly hydrophobic porphyrin has to be functionalized with hydrophilic groups to obtain water soluble derivatives. The Ni-porphyrin is supposed to remain diamagnetic in presence of water which is not trivial because Ni(II) tends to form paramagnetic octahedral aqua complexes. So far, there is no example for a Ni-based CISSS in water.
A further challenge is to address photochromic molecules *in vivo*. The penetration depth of light through tissue is low. The absorption wavelengths of a porphyrin ($\lambda = 400 - 550\,\mathrm{nm}$) are particularly unfavorable. To address a RP *in vivo* other chromophores have to be considered. An absorption within the bio-optical window ($\lambda = 650 - 800\,\mathrm{nm}$) would be most appreciable.
To meet all requirements the RP structure provides several sites for functionalization and modification (Figure 2.1). Hydrophilic groups should be introduced somehow to the porphyrins *meso* positions where they interfere as little as possible with the

photoisomerization. The substituents of the *meso*-aryl units (R) have a tremendous influence on the coordination of axial ligands and therefore have to be chosen carefully.[113] The coordination is also strongly influenced by the pyridine derivative. Variation of the *para* pyridine substituent (R') has a high impact on the association to the Ni(II). Electron donating substituents are known to enhance the coordination just like electron withdrawing *meso*-aryl units (R).[122] The tether between the porphyrin and the ligand can be decorated with substituents. This is a further opportunity to tune the properties of the porphyrin or the photochromic ligand. Finally, the Ni-platform can be modified. Reduction or addition of the double bonds of the porphyrin will preserve the square planar geometry of the Ni-complex but has a drastic influence on the chromophor. The resulting macrocyles exhibit bathochromically shifted absorption bands compared to the corresponding porphyrin.[134] This may be a chance to influence the switching wavelength of the RPs.

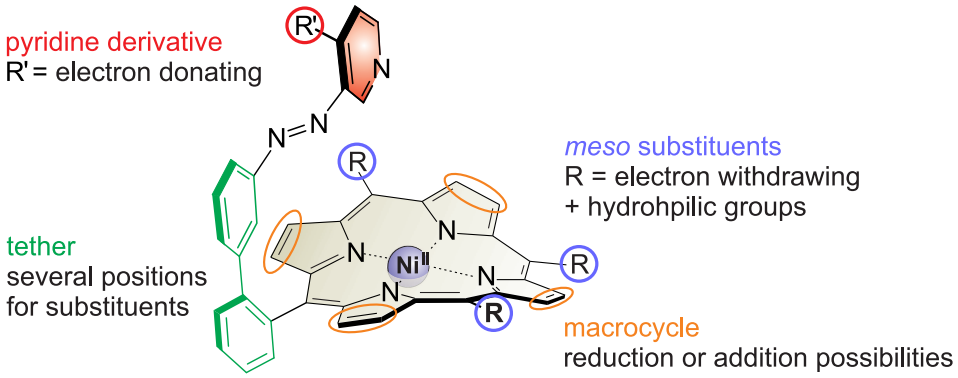

Figure 2.1: The RP can be modified at the pyridine (red), the tether (green), the macrocycle (orange) and the *meso* postions (blue).

3 Investigation of the Intramolecular LD-CISSS

A Ni-complex in the HS state ($S = 1$) has a much lower magnetic moment than a Gd(III) CA ($S = 7/2$). If the RP **7** is supposed to be applied as a CA, the MRI active *cis* form must be as paramagnetic as possible as well as the MRI silent *trans* form must be as diamagnetic as possible. Otherwise the resulting effect will be too small to be observable in a MRI experiment. Both requirements for an optimal magnetic switching efficiency are not given. The *trans* isomer which is supposed to be diamagnetic tends to be paramagnetic at high concentrations due to intermolecular coordination. The *cis* isomer which is supposed to be paramagnetic is in partially diamagnetic due to decoordination of the axial ligand. These both effects decrease the magnetic switching efficiency tremendously and thus, have to be eliminated or drastically reduced to perform photoswitching of MRI contrasts.

3.1 Rational Design of a Room Temperature Molecular Spin Switch. The Light-Driven Coordination-Induced Spin State Switch (LD-CISSS) Approach

Marcel Dommaschk, Christian Schütt, Sugumar Venkataramani, Umasish Jana, Christian Näther, Frank D. Sönnichsen and Rainer Herges

Dalton Trans. **2014**, *43*, 17395-17405.
DOI:10.1039/c4dt03048f

Summary

The rational design and optimization of record player molecules using quantum chemical calculations is presented. The parent system **7** was studied in detail, mainly regarding an optimization of the magnetic switching efficiency. It was demonstrated that the electron-withdrawing *meso* substituents are crucial for the switching of the photochromic ligand. Hence, the coordination must directly be involved in the isomerization process. A wavelength screening reveals that the irradiation wavelength to obtain a photo stationary state (PSS) with the highest possible conversion to the *cis* configuration is 500 nm (up to 75%). The reverse process works best with 430 nm (>95% *trans* isomer). A crystal structure of *trans*-**7** suggests that the paramagnetism at high concentrations is due to the formation of dimers in which two molecules coordinate to each other. Polar solvents like methanol, tetrahydrofuran and dimethylsulfoxide (DMSO) can efficiently suppress this process. Furthermore, these solvents prevent the decoordination of the pyridine of the *cis* isomer. The intramolecular coordination of the pyridine promotes the association of a solvent molecule to the sixth binding site of the nickel. This solvent coordination stabilizes the pyridine-Ni(II) bond which prevents decoordination. Therefore, the equilibrium between the magnetic conformers is shifted towards the paramagnetic form. DMSO turns out to be the solvent in which the LD-CISSS has the highest magnetic switching efficiency.

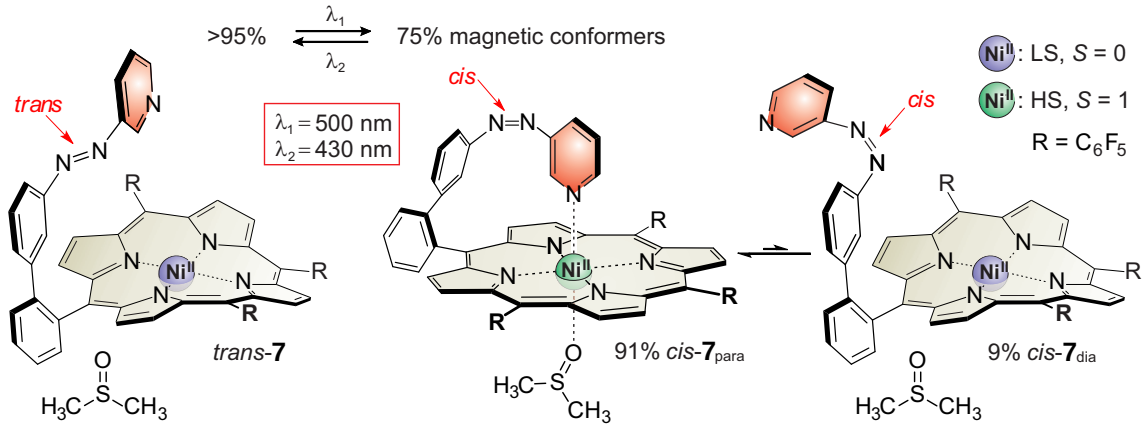

Figure 3.1: DMSO prevents dimer formation of *trans*-**7**, increases the percentage of the paramagnetic form in the conformational equilibrium of the *cis* isomer and improves the photostationary states (*trans*/*cis*) upon irradiation with 500 nm and 430 nm.

Dalton Transactions

PAPER

View Article Online
View Journal | View Issue

Cite this: *Dalton Trans.*, 2014, **43**, 17395

Rational design of a room temperature molecular spin switch. The light-driven coordination induced spin state switch (LD-CISSS) approach†

M. Dommaschk,[a] C. Schütt,[a] S. Venkataramani,[b] U. Jana,[c] C. Näther,[d] F. D. Sönnichsen[a] and R. Herges*[a]

Received 2nd October 2014,
Accepted 10th October 2014

DOI: 10.1039/c4dt03048f

www.rsc.org/dalton

Extensive use of quantum chemical calculations has been made to rationally design a molecule whose spin state can be switched reversibly using light of two different wavelengths at room temperature in solution. Spin change is induced by changing the coordination number of a nickel complex. The coordination number in turn is switched using a photochromic ligand that binds in one configuration and dissociates in the other. We demonstrate that successful design relies on a precise geometry fit and delicate electronic tuning. Our designer complex exhibits an extremely high long-term switching stability (more than 20 000 cycles) and a high switching efficiency. The high-spin state is extraordinarily stable with a half-life of 400 days at room temperature. Switching between the dia- and paramagnetic state is achieved with visible light (500 and 430 nm). The compound can also be used as a molecular logic gate with light and pH as input and the magnetic state as non-destructive read-out.

1. Introduction

Bistability of spin states has long been restricted to solid state systems or very low temperatures. Spin state switching in isolated molecules or in homogenous solution[1] at room temperature, however, is still a challenge.[2–4] A number of interesting applications are waiting to be exploited for these systems, such as switchable contrast agents for MRI,[5,6] light-controlled magnetic levitation, switchable spin labels,[7] or spintronics.[8,9] Unsurprisingly, a number of groups are aiming at this end using different approaches. Starting point of the LD-LISC (light-driven ligand-induced spin change) approach is the spin crossover of Fe^{2+} as a function of the ligand field strength. Photochromic compounds are used as light switchable ligands. The two configurations of the photochromic ligands exhibit different ligand field strengths[10,11] which eventually give rise to different spin states.[12] Redox processes can be used to change the spin state of transition metals.[13] Photo switchable antiferromagnetic coupling was demonstrated in nitroxide substituted diarylethenes.[9,14] A magnetic switch from paramagnetic to ferromagnetic has been achieved by moving two Co-phthalocyanine molecules (S = 1/2) on top of each other (S = 1) with a STM tip.[15] Reversible spin-crossover was also observed by electron injection in single molecules on a surface with an STM tip.[16,17]

Recently we presented the first molecular spin switch that can be operated by visible light at room temperature in homogenous solution with no measurable fatigue over more than 20 000 cycles.[18] Our approach is based on the well-known fact that a number of transition metal ions, such as Fe^{2+}, Fe^{3+}, Mn^{2+}, Mn^{3+}, Co^{2+}, and Ni^{2+} change their spin state upon changing the coordination number. Ni^{2+} was chosen as the transition metal for several reasons: 1. There is a reliable spin state switch between low-spin (S = 0) and high-spin (S = 1) if the coordination is changed from square planar (coordination number CN = 4) to square pyramidal (CN = 5) or square bipyramidal (CN = 6).[19–21] (see Fig. 1) 2. Ni^{2+} high-spin complexes still exhibit reasonably sharp NMR spectra for analysis, and paramagnetic shifts can be used to determine the ratio of high-spin/low-spin Ni ions in solution[22–24] 3. Ni^{2+} complexes are easier to calculate than Fe^{2+} compounds (more reliable convergence of the wavefunction to the lowest electronic state). In the first place we accepted the disadvantage that the high-spin state of Ni^{2+} (S = 1) has a lower magnetic moment than

[a]*Otto-Diels-Institut für Organische Chemie, Christian-Albrechts-Universität, Otto-Hahn-Platz 4, D-24098 Kiel, Germany. E-mail: rherges@oc.uni-kiel.de*
[b]*Indian Institute for Science Education and Research (IISER) Mohali, Knowledge City, Sector 81, SAS Nagar, Manauli PO 140306, India*
[c]*Department of Chemistry, Jadavpur University, Kolkata-700032, India*
[d]*Institut für Anorganische Chemie, Christian-Albrechts-Universität, Max-Eyth-Straße 2, 24098 Kiel, Germany*

†Electronic supplementary information (ESI) available. CCDC 1023485. For ESI and crystallographic data in CIF or other electronic format see DOI: 10.1039/c4dt03048f

View Article Online
Paper Dalton Transactions

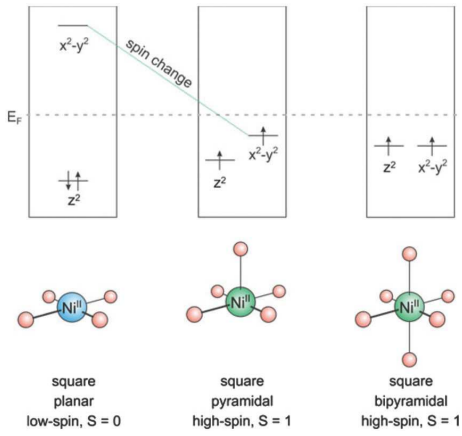

Fig. 1 Schematic illustration of coordination induced spin state switch in Ni-porphyrin.

Fe^{2+} ($S = 2$). We chose Ni-porphyrin as a square planar complex (CN = 4) and an azopyridine tethered to the porphyrin as the photoswitch and light-controlled axial ligand.

We now present a detailed analysis of the prerequisites of the design and optimization of spin switches based on this Light-Driven Coordination Induced Spin State Switch (LD-CISSS) approach. The optimal system is completely diamagnetic (low-spin) in one state and completely paramagnetic (high-spin) in the other state. However, 100% switching efficiency is difficult to achieve in an ensemble of individual molecules. The overall magnetic switching efficiency depends on the (*cis*–*trans*) switching efficiency of the photochromic ligand and on the association constants in both configurations of the ligand. The binding constant should ideally be zero in one state and large in the other. Unfortunately, the situation becomes considerably more complicated under "real" conditions where solvent effects and intermolecular binding interfere. The solvent itself can bind as an axial ligand and convert the nickel complex to the high-spin state, even in the non-binding state of the photochromic ligand. At a first glance, a high binding constant of the photochromic ligand in the binding state should be desirable. However, two problems arise if the association constant is too large. Switching to the non-binding state is thermodynamically less favourable and could be impaired. Moreover, favouring intramolecular binding would also favour intermolecular association. At increasing concentrations an increasing proportion of the complex would form dimers or oligomers and would always be high-spin. Further complications arise from the fact that nickel-porphyrins can add a second axial ligand to form a distorted octahedral complex (Fig. 1). Addition of the first ligand (*e.g.* photochromic ligand) changes spin state from low- to high-spin and activates the addition of a second axial ligand (K_2 usually is larger than K_1). Weakly coordinating solvents that do not bind to the square planar Ni porphyrin could still bind to the square pyramidal complex (binding state of the photochromic ligand) and stabilize the high-spin state which would increase the switching efficiency. Another issue is the life time of the thermodynamically less stable state (usually the *cis* isomer in azobenzenes) which should be large in an ideal system. Many photochromic systems including azobenzenes and spiropyrans undergo thermal back reaction to the more stable state. Coordination could be used to stabilize the binding state of the photochromic ligand if the less stable configuration is binding. A positive feedback from coordination could even improve the switching efficiency of the photochromic ligand. On the other hand the switching of the photochromic ligand often is completely quenched if a chromophore such as a porphyrin is in close proximity or in conjugation. This has to be considered in the design of the tether that connects the porphyrin and the photochromic ligand.

Hence, a number of preconditions have to meet to design molecular spin switches based on the LD-CISSS approach: perfect geometric and electronic design of the switching ligand including the tether, a delicate tuning of the electronic properties of the Ni porphyrin and of the donor strength of the photochromic ligand, the choice of the solvent *etc.* Detailed information about these parameters is of utmost importance for the design of optimized molecular spin switches for various applications such as contrast agents for MRI or switchable spin labels.

We here report on detailed investigations of the above parameters using NMR and UV-vis spectroscopy and single crystal structure analysis. To elucidate the mechanism of the spin switch we performed quantum chemical calculations and compare experimental and theoretical data of two Ni porphyrins (Ni-$TPPF_{20}$ and Ni-TPP).

1.1 General design

The trivial way to change the coordination number of Ni-porphyrin would be to add a ligand to the solution. This would lead to a continuous increase of the higher coordinated complex but not to a switching process, and it would not be reversible. We chose light as the trigger, because it can be applied in different wavelengths for switching back and forth with temporal and spatial control, and unlike chemical triggers light does not leave a trace if it is switched off. So initially we have to design ligands that can be switched between two states: a binding and non-binding form using light of two different wavelengths. To keep the design as simple as possible, we chose 3-phenyl-azopyridine as the photochromic ligand because it combines the switching properties of azobenzene and the coordination of pyridine in a single small molecule. 2-Phenyl-azopyridine and 4-phenyl-azopyridine are not suitable because the first doesn't coordinate to square planar metal complexes (sterical hindrance) and the latter binds in both configurations. Hence, the building blocks to work with are Ni-porphyrin and 3-phenyl-azopyridine. Both units have to be connected with each other by means of a tether in such a way that the lone pair of the pyridine nitrogen is exactly orthogonal to the porphyrin plane in a distance of about 2.2 Å.

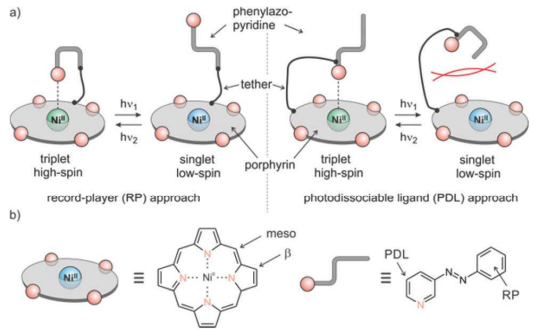

Fig. 2 (a) General design approaches (record player (RP), left), photodissociable ligand (PDL) right. (b) Positions of tether attachment.

There are two points where the tether could be attached to the porphyrin (*meso* or *β*). The other end of the tether can be connected to either the pyridine (PDL design) or the phenyl ring (RP design) of the 3-phenyl-azopyridine unit (Fig. 2). The choice of the position of attachment at the phenyl-azopyridine is of particular importance. A number of azobenzene, azoporphyrin or stilbazole substituted porphyrins are known. However, none of the molecules with *ortho* or *para* connection to the porphyrin exhibits photochromic behavior.[25–29] Conjugation to a chromophore with a low lying S_1 state probably quenches the π–π* excitation of the azo group and thus prevents photochemical isomerisation.[30] Therefore, a direct conjugation path between the azo group and the porphyrin has to be avoided either by an sp^3 atom or a *meta* connection within the tether. Attachment at the *ortho* position of the pyridine ring would prevent coordination by steric hindrance. So we are left with several combinations for attachment and a plethora of conceivable tethers with different lengths and geometries (Fig. 2).

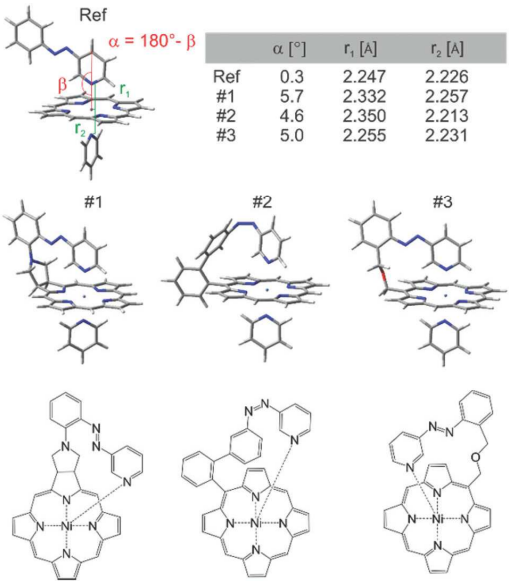

	α [°]	r1 [Å]	r2 [Å]
Ref	0.3	2.247	2.226
#1	5.7	2.332	2.257
#2	4.6	2.350	2.213
#3	5.0	2.255	2.231

Fig. 3 Geometry plots (B3LYP/6-31G*) and structures of Ni-porphyrin with 3-phenyl-azopyridine and pyridine as axial ligands. The reference compound (Ref) without tether is given on top left, and the three highest ranking "record player" structures for LD-CISSS are represented underneath. Note that structure #1 and #3 bind in *trans* configuration and #2 coordinates in its *cis* form. Pyridine has been included in the calculations as a second axial ligand because it is known that Ni-porphyrins prefer a 6-coordinate ligand field. It is assumed that upon changing the coordination number from 4 to 5 and concomitant switching from low-spin to high-spin a solvent molecule would coordinate to complete the square bipyramidal ligand field.

2. Results

2.1 Computational modeling

At this point we used molecular construction kits to build models and performed density functional theory calculations (B3LYP/6-31G*) on more than 36 different structures that looked promising based on geometry and synthesizability. (a selection of structures is presented in ESI†) For obvious reasons the structures were coined "record players" because the porphyrin resembles a disk, the azopyridine works like a tone arm by placing the pyridine nitrogen lone pair (needle) onto the nickel ion.

The structures were ranked according to their theoretically predicted performance. Target parameters are the optimal distance of the pyridine nitrogen and the nickel atom in the binding configuration and a minimal deviation from orthogonal binding to the porphyrin plane. The optimal N–Ni bond length was determined by calculations of phenyl-azopyridine porphyrin complexes without a tether and complete optimisation of all geometry parameters including the N–Ni distance (2.075 Å without and 2.247 Å with pyridine as the sixth ligand, see structure denoted as Ref. in Fig. 3,). Three candidates turned out to comply very well with the geometry constraints above (#1, #2, and #3, Fig. 3).

"Record player" structure #1 is predicted to be high-spin (binding) in its *trans* configuration and low-spin in its *cis* form. A distinct advantage over structures #2 and #3 is the reduced conformational flexibility which should lead to a better switching efficiency. Unfortunately all attempts to synthesize structure #1 failed. The 1,3-dipolar cycloaddition of azomethine ylides to the pyrrole double bonds of porphyrins is known.[31–33] Cross coupling of the pyrrolidine nitrogen with 3-(2-iodo-phenylazo)-pyridine, however, resulted in coupling with the pyridine ring. Several other synthetic attempts failed as well. We therefore discontinued the synthesis in favor of record player #2.

The synthesis of structure #2 with phenyl groups in the porphyrin *meso* positions *via* the mixed aldehyde method was straightforward.[33] Unfortunately, irradiation with light of 365 nm which usually leads to efficient *trans*–*cis* isomerisation in azobenzenes and azopyridines was incomplete (32% *cis*). Photo isomerisation of the *cis* form back to *trans* with 420 nm

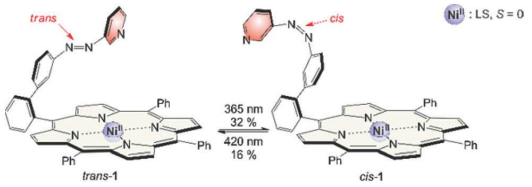

Fig. 4 Record player #2 with phenyl groups in *meso* position (**1**) does not switch efficiently upon irradiation. The photostationary state (PSS) upon irradiation at 365 nm is 32% *cis* and at 420 nm 16% *cis*. Even though the geometry of the *cis* isomer is optimal for coordination, the "tone arm" doesn't bind to the Ni^{2+}.

was incomplete as well (16% *cis* left). Back-isomerisation to the pure *trans* isomer was achieved by heating to 70 °C for several hours. Furthermore the *cis* isomer does not exhibit paramagnetic behavior as expected. Only 5% of the molecules are in the triplet state. Instead of binding to the Ni^{2+}, the azopyridine "tone arm" rotates away from the porphyrin. This hypothesis was corroborated by UHV STM measurements at 5 K.[33] The molecules were deposited on an Au(111) surface and manipulation of the azopyridine unit was achieved by the STM tip. The *trans*–*cis* isomerisation is clearly visible in the STM image. The azopyridine arm points straight away from the porphyrin core and it is bent in *cis* configuration (Fig. 4).

To elucidate the reason for this almost complete failure, we performed further DFT calculations with emphasis on the binding energy of pyridines as axial ligands, and on the singlet–triplet gap of Ni-porphyrins with different substituents in *meso* position. Among 10 different functionals in combination with 5 different basis sets B3LYP/def2TZVP performed best[34] in predicting our experimentally determined association energies including the formation of 1 : 1 and 2 : 1 complexes of porphyrins with pyridines. Simple PBE/DZP seems to be sufficient for geometry optimisation as was confirmed by comparison with our X-ray structures, and by comparing B3LYP/def2TZVP single point association energies at geometries obtained by optimisation with different functionals and basis sets (for computational details see ESI†). In Table 1 and Fig. 5 the corresponding data for Ni-tetraphenyl-porphyrin (Ni-TPP) and Ni-tetrakis(pentafluoro-phenyl)-porphyrin (Ni-$TPPF_{20}$) (the latter as an example for an electron poor porphyrin) are presented. The calculated values are compared with experimental association energies that were obtained by NMR titration at different temperatures.[22] (Table 1, Fig. 5). It is important to note that neither of the Ni-porphyrins binds pyridine as an axial ligand in its singlet spin state.[35] Our calculations reveal a strong repulsion between the Ni ion and the pyridine nitrogen lone pair. Upon including dispersion energy (D3)[36] sandwich type structures were found, however, with no coordination between nickel and the pyridine nitrogen. One can assume that these van der Waals complexes do not exist in homogenous solution due to competition of the pyridine with the solvent. Therefore we conclude that there is no axial coordination in the singlet state at all.

Table 1 Calculated (B3LYP/def2TZVP//PBE/DZP) relative energies (kcal mol^{-1}) of the triplet porphyrins Ni-TPP and Ni-$TPPF_{20}$ as a function of the number of bound pyridines. The energies are relative to the corresponding singlet state. All energies include two pyridine molecules (and thus are based on the same stoichiometry). The number of bound pyridines is given in the headline. So the energies can be directly compared and interpreted as binding energies. The experimental value for ΔH of Ni-TPP (ESI) and Ni-$TPPF_{20}$ are included as well[22]

Porphyrin (triplet state)	0 Py[a]	1 Py[b]	2 Py
Ni-TPP calc.	12.04	−1.96	−4.17
Ni-TPP exp.[c]	—	—	−4.6 (±0.2)
Ni-$TPPF_{20}$ calc.	10.59	−6.96	−11.67
Ni-$TPPF_{20}$ exp.[22]	—	−5.3 (±0.1)	−11.2 (±0.5)

[a] Relative energy includes two uncoordinated pyridine molecules. [b] Relative energy includes one uncoordinated pyridine. [c] Methods for the determination of the association constant see ESI.

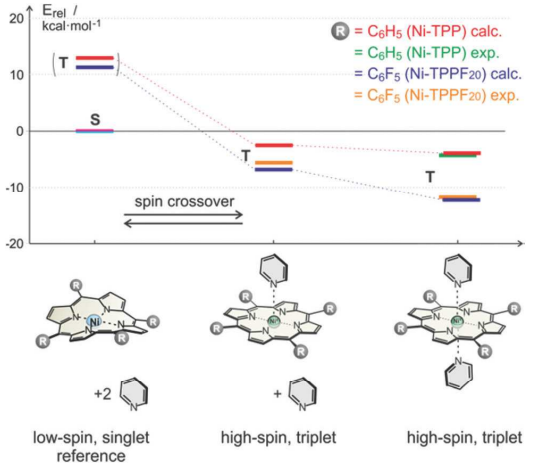

Fig. 5 Calculated (B3LYP/def2TZVP//PBE/DZP) and experimental relative association energies (kcal mol^{-1}) of pyridine to Ni-TPP (calc. red, exp. green) and Ni-$TPPF_{20}$ (calc. blue, exp. yellow) for the respective triplet (high-spin) complexes. The energies are relative to the corresponding porphyrin in its low-spin singlet state (including two unbound pyridine molecules). Note that the experimental[22] and calculated association energies agree quite well. The (very small) experimental binding enthalpy for the 1 : 1 complex of the Ni-tetraphenylporphyrin with pyridine could not be experimentally determined.

Electron withdrawing substituents in *meso* position of Ni-porphyrins increase the binding energy of axial ligands by lowering the d_{z^2} orbital. It has been shown that the association constants of piperidine as axial ligands to Ni-porphyrins with a number of different *para* substituted phenyl groups at *meso* position follow a Hammett relationship. The binding constant (2 : 1 complex) of the *meso*-tetrakis-(4-nitrophenyl) derivative is more than 10 times higher than the association constant of the parent Ni-tetraphenyl-porphyrin.[37] A reverse electronic effect is observed for axial ligands. Electron donor substituents in 4-position of pyridine increase the binding energies to

Ni-porphyrin also following an approximate Hammett (or basicity) relationship.[22,38] Our calculations confirm the increase in binding strength of pyridine as a function of electron withdrawing substituents in *meso*-position of the porphyrin. The calculated association energy of pyridine to Ni-TPPF$_{20}$ (−6.96 kcal mol^{-1}) is 3.6 times higher than to the Ni-TPP (−1.96 kcal mol^{-1}). This effect can be easily rationalized using qualitative MO theory. Triplet (high-spin) Ni-porphyrin has an unpaired electron in the d_{z^2} as well as in the $d_{x^2-y^2}$ orbital. The d_{z^2} orbital is mainly responsible for the binding strength of axial ligands. Electron withdrawing substituents at the porphyrin *meso*-position lower the energy of the d_{z^2} orbital and increase binding. Concomitant with a higher binding energy is a larger singlet–triplet gap in the triplet state. Hence the propensity to undergo spin state change from singlet (low-spin) to triplet (high-spin) should increase with increasing electron withdrawing power of substituents in *meso* position of the porphyrin ring. An analogous effect should also apply for the record player design. This is why we set out to synthesize record player #2 with electron withdrawing pentafluorophenyl substituents (**2**) in the three available *meso* positions. The syntheses and a rough characterisation were presented previously.[18]

2.2 Photochromism

Record player **2** shows an unexpected photochromic behavior. We found that the highest conversion to the *cis* isomer (75%) is achieved by irradiation into the porphyrin Q band at around 495–530 nm. By irradiation into the Soret band of the *cis* isomer at 420–435 nm the molecule can be converted into *trans* configuration almost quantitatively (<3% *cis*) (Fig. 6). The photostationary states (PSS) strongly depend on the solvent (Table 2). Dichloromethane and chloroform decrease switching efficiency which could be due to traces of hydrochloric acid. Coordinating solvents improve *trans*–*cis* isomerisation. It

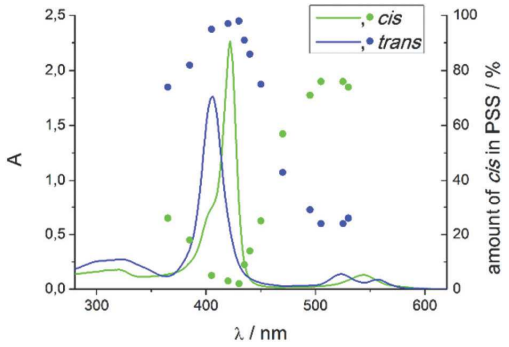

Fig. 6 UV/Vis spectra of *trans* and *cis* record player **2** (blue and green line) and the photo steady states (blue and green points) after irradiation with the corresponding wavelength in dimethylsulfoxide (DMSO). The isomers were separated by HPLC.

Table 2 Photostationary states (PSS) of record player **2** in different solvents. Values are determined by integration of corresponding signals in ^{1}H NMR spectra

Solvent	% *cis* PSS 420 nm	% *cis* PSS 495 nm
Acetone-d$_6$	<5	61
Acetonitrile-d$_3$	<5	65
Benzene-d$_6$	<5	63
Chloroform-d	<5	18
Cyclohexane-d$_{12}$	<5	59
Dichloromethane-d$_2$	<5	45
DMSO-d$_6$	<5	75
Methanol-d$_4$	<5	69
Pentafluoro benzonitrile	<5	67
Tetrachloromethane	<5	57
Tetrahydrofuran-d$_8$	<5	75
Toluene-d$_8$	<5	65

seems that a solvent molecule stabilizes the paramagnetic *cis* isomer by formation of the six fold coordinated complex.

This stabilisation also affects the thermal half-life of the *cis* form. In coordinating solvents the *cis* isomer is highly stable. The half-life in DMSO is about 400 days (20 °C), which, to our knowledge, is the highest value ever observed for an azo compound. In non-coordinating solvents it is much shorter (dichloromethane: 63 d (20 °C), chloroform: 29 d (20 °C)), but still longer than for usual azo compounds.[39,40] The photo physics of the isomerisation is very unusual and not yet understood. Particularly the energy transfer from the porphyrin to the azopyridine unit is unclear. Mechanistic investigations on metal free and Zn containing record player molecules are under way. The fact that the *meso* phenyl substituted nickel record player (**1**) has poor switching properties (Fig. 7) leads to the conclusion that the isomerisation is strongly coupled to the spin state switch.

This pertains to both directions. Irradiation into the Q band (495–530 nm) will only enrich the *cis* isomer if coordination takes place, and irradiation into the Soret band (405–435 nm) will only convert the molecule to its *trans* configuration if a decoordination occurs. Upon irradiation with a shorter wavelength (365 nm) the photochromic behaviors of **1** and **2** become quite similar and independent of the spin state switch. In this region the ππ* band of the azopyridine is located. So the spin state switch seems only to be crucial for

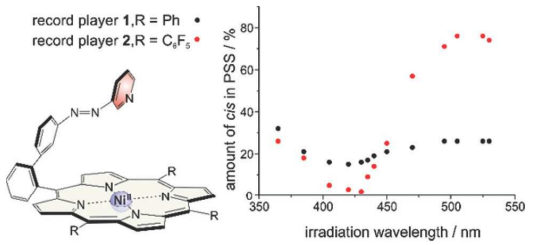

Fig. 7 Switching properties of *meso* phenyl (**1**) and *meso* pentafluorophenyl (**2**) substituted record players.

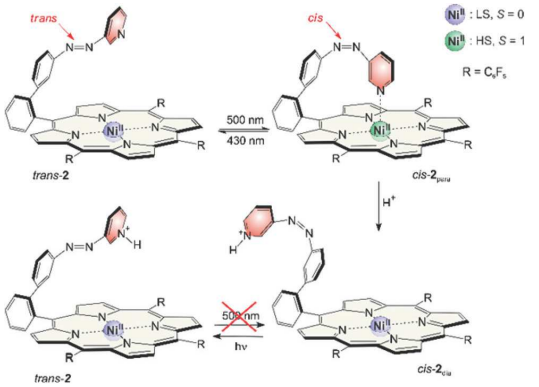

Fig. 8 Photo switching between *trans*-**2** and *cis*-$\mathbf{2}_{para}$ was achieved with 500 and 430 nm (top). After conversion into the respective protonated forms, photo conversion is only possible from the *cis* to the *trans* configuration (bottom).

Table 3 Record player **2** as a molecular digital logic gate (truth table)

Input *hν*	Input pH	Output *hν* & pH
500 nm	OH^-	para
500 nm	H^+	dia
430 nm	OH^-	dia
430 nm	H^+	dia

the isomerisation if it is indirectly induced by irradiation into a porphyrin absorption band (Soret or Q band) (Fig. 8).

Magnetic states and photo switching can be manipulated by changing the pH value. Addition of acids (<1% TFA) converts *cis*-**2** to a protonated form which is completely diamagnetic. Photo induced back-isomerisation is possible with any wavelength. Protonated *trans*-**2** does not isomerise to the *cis* configuration (*e.g.* by irradiation into the Q band).

Assuming light (430/500 nm) and pH (high/low) as input and the magnetic state (dia-/paramagnetic) as output, record player **2** can viewed as a molecular logic gate (truth table see Table 3). The molecule is extremely robust (several thousand switching cycles), and the spin state allows a nondestructive readout. Assuming 500 nm light, pH high and paramagnetic spin state as digital 1 the molecule corresponds to an AND gate.

2.3 Methods for magnetic measurements

Beside the photochromism the magnetic properties are the second important (and probably the most interesting) features of the record player **2**. The LD-CISSS approach is based on the assumption that the nickel complex is completely diamagnetic in *trans* and completely paramagnetic in *cis* configuration. However, one can essentially assume that the *trans* isomer should exhibit at least some residual paramagnetism because of intermolecular coordination, and the *cis* form might not be 100% paramagnetic because of incomplete binding of the azo-

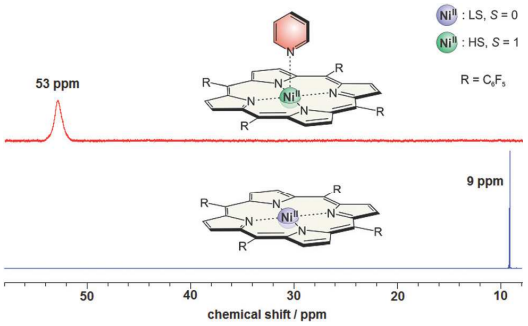

Fig. 9 ^{1}H NMR spectra of Ni-TPPF$_{20}$ with (red) and without (blue) pyridine (500 MHz, acetonitrile, 300 K).

pyridine arm. To quantify the paramagnetism of a Ni-porphyrin the chemical shifts of the pyrrole protons in ^{1}H NMR spectra were investigated. Diamagnetic Ni-TPPF$_{20}$ gives rise to a shift of about 8.9 (+/−0.4) ppm depending on the solvent while the proton signals of a paramagnetic complex appear at 53 (+/−0.4) ppm. This fact is shown in Fig. 9. By addition of pyridine a paramagnetic complex is formed which leads to a downfield shift of 44 ppm (from 8.9 to 53 ppm). The maximum shift only depends on the solvent (+/−0.4 ppm) but not on the nature of the axial ligand (see ESI†). The magnetic moment of the high-spin species (2.9 B.M.) was confirmed by Evans measurements.[33,41]

Because of the fast ligand exchange a time average of the pyrrole signals of dia- and paramagnetic Ni-porphyrin molecules is observed. The chemical shift δ is a linear function of the mole fraction of paramagnetic nickel (amount of paramagnetic nickel divided by the total amount of nickel):

$$\chi_{para} = \frac{\delta - \delta_{dia}}{\delta_{para} - \delta_{dia}} \quad (1)$$

χ_{para}, mole fraction of paramagnetic Ni-porphyrin; δ_{para}, paramagnetic shift of pyrrole protons (53 ppm); δ_{dia}, diamagnetic shift of pyrrole protons (8.9 ppm); δ, observed shift of pyrrole protons [ppm].

There is formation of square pyramidal complexes as well. However, square pyramidal and square bipyramidal complexes exhibit approximately the same paramagnetic shifts which can be shown by titration experiments (see ESI†).

2.4 Intermolecular coordination

Dilution series of *trans*-**2** show a concentration dependence of the chemical shifts of the pyrrole signals (Fig. 10). A concentrated solution gives rise to a slightly downfield shift indicating paramagnetism due to intermolecular coordination. The magnitude of this effect strongly depends on the solvent. Polar (coordinating) solvents like acetonitrile and DMSO suppress intermolecular coordination while nonpolar solvents like cyclohexane have no effect. There is a linear correlation between the average paramagnetic shift (δ_{para}) and the concen-

View Article Online
Dalton Transactions Paper

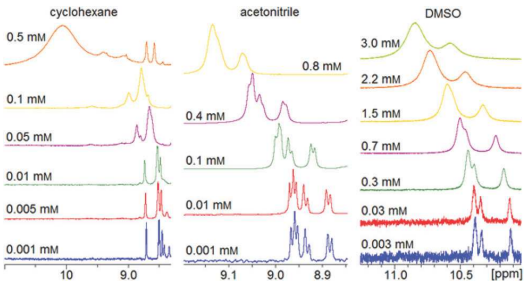

Fig. 10 ^{1}H NMR spectra of record player **2** in *trans* configuration in different solvents (500 MHz, 300 K). The downfield shift and signal broadening indicates intermolecular coordination.

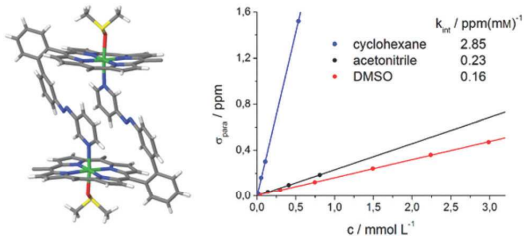

Fig. 11 Crystal structure of *trans*-**2** shows formation of dimers and a sixfold coordination sphere of Ni^{2+} complemented by one axial DMSO molecule (left). The pentafluorophenyl groups at the porphyrin rings are omitted for clarity. For details see ESI Fig. S4.† The linear correlation between paramagnetic shift of pyrrole signals (δ_{para}) and concentration of *trans*-**2** (right) confirms that there is also intermolecular coordination in solution.

tration (Fig. 11). The slope (k_{int}) is a solvent specific parameter representing the tendency for the formation of paramagnetic aggregates.

The crystal structure of *trans*-**2** (crystallized from DMSO) provides information for the mode of interaction, and the strong solvent dependence of intermolecular coordination. *trans*-**2** forms head to tail dimers (Fig. 11). The remaining axial coordination sites are complemented with DMSO. We interpret the reduced intermolecular coordination in DMSO, acetonitrile, methanol, and THF by competition of dimer (or oligomer) formation and coordination by the solvent. For most applications a low degree of intermolecular aggregation (small k_{int}, Fig. 13) is advantegeous. For a efficient LD-CISSS the *trans* configuration should be as diamagnetic as possible in solution. From the k_{int} value for cyclohexane (2.85 ppm mM^{-1}) a mole fraction of 6.5% paramagnetic species in a 1 mM solution due to intermolecular coordination can be derived. In DMSO (0.4%) this effect is negligible.

2.5 Intramolecular coordination

NMR signals of *cis* record player **2** do not show any concentration dependence. But we found that pyrrole signals have

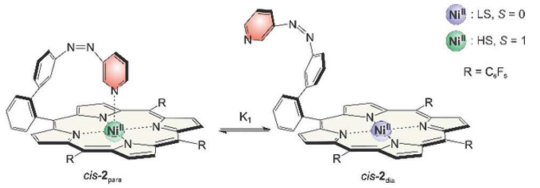

Fig. 12 Equilibrium of the magnetic conformers *cis*-2_{para} (left) and *cis*-2_{dia} (right).

Table 4 Mole fraction of paramagnetic *cis*-**2** (% *cis*-2_{para}) relative to the total amount of *cis*-**2** (equilibrium see Fig. 12), calculated from the average ^{1}H NMR chemical shifts of the pyrrole protons

Solvent	Shift of pyrrole proton/ppm	% *cis*-2_{para}
Acetone	42	75
Acetonitrile	44	80
Benzene	46	84
Cyclohexane	46	84
Dichloromethane	37	64
DMSO	49	91
Methanol	47	86
Pentafluoro benzonitrile	45	82
Tetrachloromethane	43	77
Tetrahydrofuran	50	93
Toluene	46	84

different chemical shifts depending on the solvent (Table 4). The maximum shift δ_{max} (eqn (1)) of 53 ppm was confirmed by addition of pyridine-d_5. However, in non-coordinating solvents such as cyclohexane or benzene the chemical shift of the pyrrole protons is lower (46 ppm) which indicates that the *cis* isomer is not completely paramagnetic. Obviously there is a fast equilibrium between the intramolecularly coordinated paramagnetic species (*cis*-2_{para}) and a non-coordinated diamagnetic form (*cis*-2_{dia}). The two species are magnetic conformers (Fig. 12).

In DMSO and tetrahydrofuran the proportions of *cis*-2_{para} (91 and 93%) are quite close to the maximum value. The properties of these polar solvents obviously favor the paramagnetic conformer. Previous studies on the association constants of axial ligands to Ni-porphyrins could give a hint why this is the case. Binding of the first axial ligand (K_1) is less exergonic than association of the second (K_2) (except for very strong ligands). DMSO and THF are not sufficiently strong ligands to efficiently bind to the square planar Ni-porphyrin (K_1 is small). However, intramolecular coordination of the azopyridine in the *cis*-isomer activates the sixth binding site sufficiently to bind a weak ligand such as DMSO.[33] Hence, upon addition of a solvent molecule the square bipyramidal complex is formed (K_2) which is now stabilized and which cannot directly convert into its diamagnetic form. Note that DMSO also complements the sixth binding site in the X-ray structure of *trans*-**2**. It is striking that the same solvents giving rise to a large downfield pyrrole shift in *cis*-**2** also favor the conversion of *trans*-**2** to *cis*-**2** upon irradiation at 495 nm (see Table 2).

2.6 Temperature dependence of NMR shifts

The high upfield shift of NMR signals of the paramagnetic complex is mainly due to the hyperfine contact shift.[42–44] Isotropic shifts ($\delta_{para} = \delta_{obs} - \delta_{dia}$) can be determined accurately comparing *cis*-**2** with the corresponding diamagnetic zinc derivative. Temperature dependence of chemical shifts show Curie behavior with a reasonable good fit. The slopes correlate with the magnitude of the hyperfine coupling. For the *ortho* pyridine protons the interaction is strongest. At 300 K the signals are already at about 100 ppm. Signals vanish at lower temperatures because they become too broad, and relaxation is too fast. All other shifts are shown in Fig. 13. Some intercepts differ significantly from Curie law which can be explained by the presence of a second spin species namely the diamagnetic *cis*-$\mathbf{2}_{dia}$. This seems reasonable taking into account that measurements are performed in dichloromethane in which the amount of diamagnetic *cis* isomer is high (36%).

From temperature dependent NMR measurements thermodynamic parameters ΔH and ΔS can be determined as well. The intramolecular association constant K_1 (see Fig. 12) can be calculated directly from the observed pyrrole proton shifts in ^{1}H NMR spectra (ESI†). Temperature dependence of K_1 gives ΔH and ΔS by the Gibbs free enthalpy relation. The experimental values are in good agreement with the calculated (B3LYP/def2TZVP//PBE/SVP) energies which again confirms that the used level of theory is suitable for the investigated complexes (Table 5).

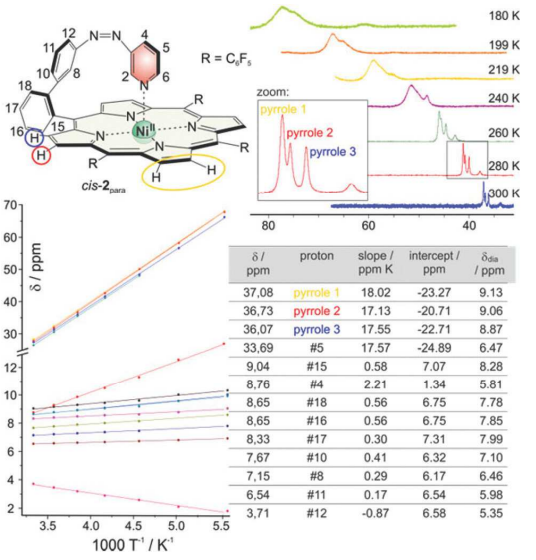

δ / ppm	proton	slope / ppm K	intercept / ppm	δ_{dia} / ppm
37,08	pyrrole 1	18.02	-23.27	9.13
36,73	pyrrole 2	17.13	-20.71	9.06
36,07	pyrrole 3	17.55	-22.71	8.87
33,69	#5	17.57	-24.89	6.47
9,04	#15	0.58	7.07	8.28
8,76	#4	2.21	1.34	5.81
8,65	#18	0.56	6.75	7.78
8,65	#16	0.56	6.75	7.85
8,33	#17	0.30	7.31	7.99
7,67	#10	0.41	6.32	7.10
7,15	#8	0.29	6.17	6.46
6,54	#11	0.17	6.54	5.98
3,71	#12	-0.87	6.58	5.35

Fig. 13 Temperature dependence of chemical shifts of *cis*-**2** in ^{1}H NMR spectra (500 MHz, dichloromethane-d_2). Shifts of the pyrrole protons as a function of temperature are shown top right. The table bottom right shows the chemical shifts of all protons (except those of *ortho* pyridine #2 and #6) at 300 K (δ), the slopes and intercepts of the corresponding Curie plots (bottom left) and the diamagnetic shifts of the corresponding zinc derivative (δ_{dia}).[18]

Table 5 Association constants K_1 (300 K), experimental (exp., DMSO-d_6) and calculated (calc., B3LYP/def2TZVP//PBE/SVP) and thermodynamic parameters ΔH (kcal mol^{-1}) and ΔS (cal mol^{-1} T^{-1}) for the intramolecular coordination of *cis*-**1** and *cis*-**2** (Fig. 12)

	cis-**1**	*cis*-**2**
K_1 (300 K)	0.0616	7.4674
ΔH (exp.)	−1.19 (±0.09)	−3.95 (±0.13)
ΔH (calc.)	−0.25	−3.26
ΔS (exp.)	−9.52 (±0.28)	−9.18 (±0.43)
$\Delta G_{300\ K}$ (exp.)	1.67 (±0.17)	−1.20 (±0.26)

The values for the association constant (7.47 at 300 K), enthalpy (−3.95 kcal mol^{-1}) and entropy (−9.18 cal mol^{-1} T^{-1}) of *cis*-**2** are in good agreement with values obtained for free pyridine and azopyridine ligands.[22–24] Binding enthalpy is smaller compared to pyridines which is compensated by a smaller entropy. As expected the binding enthalpy for the *meso* phenyl substituted record player **1** is much lower (−1.19 kcal mol^{-1}) whereas entropy is almost equal (−9.52 cal mol^{-1} K^{-1}). The thermodynamic data above explain why the phenyl substituted record player *cis*-**1** is not paramagnetic. Even though the geometry is suitable for coordination the binding is endergonic (ΔG = 1.67 kcal mol^{-1}). Coordination of the azopyridine "tonearm" in electron deficient *cis*-**2**, however, is clearly exergonic (ΔG = −1.20 kcal mol^{-1}).

2.7 Structure and molecular dynamics

Record player *cis*-$\mathbf{2}_{para}$ does not exhibit symmetry (C_1). However, the NMR spectra are rather in agreement with a time averaged C_s symmetry. The fact that there are only three pyrrole proton signals in *cis*-**2** (Fig. 10 and 13) can be explained by the fast conversion of the two respective enantiomers. The ^{19}F NMR spectra add more evidence for this process. *cis*-**2** exhibits four signals for *ortho* fluorine (1 : 2 : 2 : 1), two signals for *para* fluorine (1 : 2) and three signals for *meta* fluorine (1 : 2 : 3) atoms (Fig. 14).

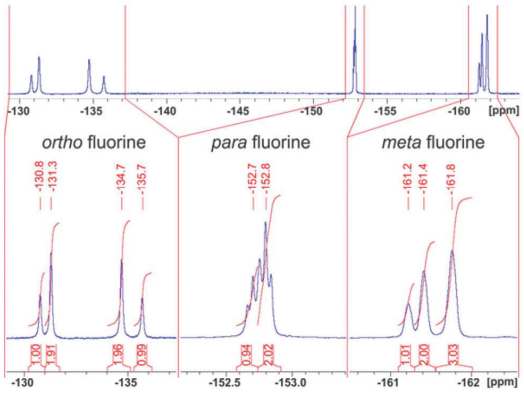

Fig. 14 ^{19}F-NMR spectra of *cis*-**2** (500 MHz, dichloromethane, 300 K).

View Article Online
Dalton Transactions Paper

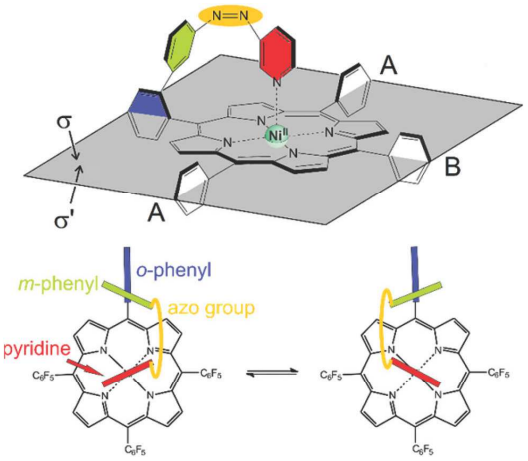

Fig. 15 Top: Record player *cis*-$\mathbf{2}_{para}$ has two symmetry non-equivalent sides σ and σ′. Neither of the *meso* substituents (pentafluorophenyl and "tone arm") rotate around the porphyrin plane on the NMR time scale at 300 K. For the sake of clarity the fluorine atoms at the *meso* positions A and B are omitted. Bottom: top view on the conversion between the two enantiomers of *cis*-**2**. The conformational equilibrium is fast on the NMR time scale at 300 K.

Information about the dynamic behavior of *cis*-**2** can be derived from the signal pattern. Since more than three *ortho* fluorine signals are observed the rotation of the pentafluorophenyl groups in *meso* position of the porphyrin must be hindered. Hence the molecule has two sides (σ and σ′) with chemical non-equivalent fluorine atoms. *cis*-**2** as shown in Fig. 12 has C_1 symmetry which should exhibit six *ortho* fluorine signals. The fact that there are only four signals and that the ratio given by the integrals is 1 : 2 : 2 : 1 indicates that the two *meso* substituents A must be equal. (Fig. 15) This is the case if *cis*-**1** is in equilibrium with its enantiomer and conversion is faster than NMR time scale. The conversion is only a reorientation to a different conformation and therefore should not need much activation energy (Fig. 15). However, racemisation can only proceed *via* a (short-lived) decoordinated (diamagnetic) state. ^{19}F signals of *meta* and *para* fluorine are in agreement with this hypothesis.

3. Conclusions

We present the rational design of a molecule whose spin state can be switched with visible light at room temperature in homogenous solution. Our approach is based on a three-part system: a photoswitchable azopyridine unit, a Ni-porphyrin, and a tether that connects the latter two building blocks ("record player" or "photodissociable ligand" design). Upon irradiation the azopyridine reversibly changes configuration which leads to coordination/decoordination of the pyridine to the Ni ion. The change of coordination number in turn switches the spin state of the Ni^{2+} between low-spin (diamagnetic) and high-spin (paramagnetic). We coined our approach light-driven coordination-induced spin state switching (LD-CISSS). To find a system with high switching efficiency, a number of systems differing in tether structure, and position of attachment were evaluated *in silico* by DFT calculations. Among 36 candidates three structures were identified as potentially operative, and worthwhile being synthesized. One of the three structures was actually prepared, and thoroughly investigated. While the basic properties have been published recently,[18] we here present a detailed experimental and computational study of the system. DFT calculations and experiments reveal that both, geometry and electronic requirements have to be accurately met to obtain an efficient system. The tether has to be constructed in such a way that the pyridine nitrogen lone pair is placed exactly perpendicular to the porphyrin plane, and at a distance of 2.25 to 2.35 Å. Moreover, the Ni-porphyrin must be electron poor. The "record player" compound with phenyl substituents at the *meso* positions exhibits no spin state switching, whereas the corresponding system with three pentafluorophenyl substituents is highly efficient. According to DFT calculations, and corresponding NMR experiments, electron withdrawing substituents at the porphyrin *meso* positions strongly improve the coordination of the pyridine to the Ni ion, which is a prerequisite for the spin change. Switching efficiency also strongly depends on the solvent. Weakly coordinating solvents prevent intermolecular coordination, and concomitantly improve intramolecular binding. The mole fraction of paramagnetic *cis*-**2** in DMSO is 91% and 93% in THF. Thermal isomerisation of the *cis* isomer back to the thermodynamically more stable *trans* form is slowed down considerably as well in weakly coordinating solvents. Thermal half-life of the high-spin *cis* isomer in DMSO is extraordinarily long (400 days at 20 °C). So DMSO seems to be the solvent of choice. Considering the extreme long-term switching stability (more than 20 000 cycles with no detectable side products) and the fact that it can be switched with visible light, combined with the above mentioned properties, "record player" **2** is superior to conventional azobenzenes in most aspects. Spin state switching is inhibited at low pH. If light (500/430 nm) and pH (low/high) is used as input, and the magnetic state (dia/paramagnetic) as output the molecule can be used as a logic gate (AND gate). The fact that the magnetic state can be used as output has the advantage that it provides means for a non-destructive readout (orthogonal to light and pH).

Room temperature switchable molecular magnets provide the potential for a number of interesting applications such as information storage[45,46] and processing,[47] sensor applications,[48] switchable contrast agents for MRI[49–51] or light induced magnetic levitation.[41] Further improvement based on the detailed information provided above should be possible. However, the mechanism of the unusual energy transfer from the porphyrin unit to the azopyridine ligand has yet to be elucidated.

Acknowledgements

This work has been supported by the Deutsche Forschungsgemeinschaft within the Sonderforschungsbereich 677 "Function by Switching".

Notes and references

1 M. P. Shores, C. M. Klug and S. R. Fiedler, *Spin-Crossover Materials: Properties and Applications*, ed. M. A. Halcrow, John Wiley & Sons, Ltd., 1st edn, 2013, ch. 10, pp. 281–301.
2 C. Gandolfi, G. G. Morgan and M. Albrecht, *Dalton Trans.*, 2012, **41**, 3726–3730.
3 P. N. Martinho, Y. Ortin, B. Gildea, C. Gandolfi, G. McKerr, B. O'Hagan, M. Albrecht and G. G. Morgan, *Dalton Trans.*, 2012, **41**, 7461–7463.
4 M. P. Shores, C. M. Klug and S. R. Fiedler, *Spin-Crossover Materials*, ed. M. A. Halcrow, 2013, pp. 281–301.
5 R. N. Muller, L. Vander Elst and S. Laurent, *J. Am. Chem. Soc.*, 2003, **125**, 8405–8407.
6 C. Rajadurai, M. Ruben and D. Kruk, *EP* 2 072 062 A1, 2009.
7 G. M. Clore and J. Iwahara, *Chem. Rev.*, 2009, **109**, 4108–4139.
8 A. R. Rocha, V. M. Garcia-suarez, S. W. Bailey, C. J. Lambert, J. Ferrer and S. Sanvito, *Nat. Mater.*, 2005, **4**, 335–339.
9 K. Hamachi, K. Matsuda, T. Itoh and H. Iwamura, *Bull. Chem. Soc. Jpn.*, 1998, **71**, 2937.
10 M. M. Paquette, B. O. Patrick and N. L. Frank, *J. Am. Chem. Soc.*, 2011, **133**, 10081–10093.
11 A. Bannwarth, S. O. Schmidt, G. Peters, F. D. Sönnichsen, W. Thimm, R. Herges and F. Tuczek, *Eur. J. Inorg. Chem.*, 2012, **2012**, 2776–2783.
12 Y. Hasegawa, S. Kume and H. Nishihara, *Dalton Trans.*, 2009, 280–284.
13 R. K. Wilson and S. Brooker, *Dalton Trans.*, 2013, **42**, 12075–12078.
14 N. Tanifuji, M. Irie and K. Matsuda, *J. Am. Chem. Soc.*, 2005, **127**, 13344–13353.
15 X. Ge, C. Manzano, R. Berndt, L. T. Anger, F. Köhler and R. Herges, *J. Am. Chem. Soc.*, 2009, **131**, 6096–6098.
16 T. G. Gopakumar, F. Matino, H. Naggert, A. Bannwarth, F. Tuczek and R. Berndt, *Angew. Chem., Int. Ed.*, 2012, **51**, 6262–6266.
17 T. G. Gopakumar, M. Bernien, H. Naggert, F. Matino, C. F. Hermanns, A. Bannwarth, S. Mühlenberend, A. Krüger, D. Krüger, F. Nickel, W. Walter, R. Berndt, W. Kuch and F. Tuczek, *Chem. – Eur. J.*, 2013, **19**, 15702–15709.
18 S. Venkataramani, U. Jana, M. Dommaschk, F. D. Sönnichsen, F. Tuczek and R. Herges, *Science*, 2011, **331**, 445–448.
19 D. Achey and G. J. Meyer, *Inorg. Chem.*, 2013, **52**, 9574–9582.
20 T. J. Lotz and T. A. Kaden, *J. Chem. Soc., Chem. Commun.*, 1977, 15–16.
21 Y. Song, R. E. Haddad, S.-L. Jia, S. Hok, M. M. Olmstead, D. J. Nurco, N. E. Schore, J. Zhang, J.-G. Ma, K. M. Smith, S. Gazeau, J. Pécaut, J.-C. Marchon, C. J. Medforth and J. A. Shelnutt, *J. Am. Chem. Soc.*, 2005, **127**, 1179–1192.
22 S. Thies, C. Bornholdt, F. Köhler, F. D. Sönnichsen, C. Näther, F. Tuczek and R. Herges, *Chem. – Eur. J.*, 2010, **16**, 10074–10083.
23 S. Thies, H. Sell, C. Bornholdt, C. Schütt, F. Köhler, F. Tuczek and R. Herges, *Chem. – Eur. J.*, 2012, **18**, 16358–16368.
24 S. Thies, H. Sell, C. Schütt, C. Bornholdt, C. Näther, F. Tuczek and R. Herges, *J. Am. Chem. Soc.*, 2011, **133**, 16243–16250.
25 H. K. Hombrecher and K. Lüdtke, *Tetrahedron*, 1993, **49**, 9489–9494.
26 K. H. Neumann and F. Vogtle, *J. Chem. Soc., Chem. Commun.*, 1988, 520–522.
27 C. A. Hunter and L. D. Sarson, *Tetrahedron Lett.*, 1996, **37**, 699–702.
28 H. Sugimoto, K. Kuramoto and S. Inoue, *J. Chem. Soc., Perkin Trans. 1*, 2002, 1826–1830.
29 L. J. Esdaile, P. Jensen, J. C. McMurtrie and D. P. Arnold, *Angew. Chem., Int. Ed.*, 2007, **46**, 2090–2093.
30 M. V. Peters, R. Goddard and S. Hecht, *J. Org. Chem.*, 2006, **71**, 7846–7849.
31 A. M. G. Silva, A. C. Tom'e, M. G. P. M. S. Neves, A. M. S. Silva and J. A. S. Cavaleiro, *J. Org. Chem.*, 2005, **70**, 2306–2314.
32 A. M. G. Silva, P. S. S. Lacerda, A. C. Tom'e, M. G. P. M. S. Neves, A. M. S. Silva, J. A. S. Cavaleiro, E. A. Makarova and E. A. Lukyanets, *J. Org. Chem.*, 2006, **71**, 8352–8356.
33 F. Matino, G. Schull, U. Jana, F. Köhler, R. Berndt and R. Herges, *Chem. Commun.*, 2010, **46**, 6780–6782.
34 A. A. Starikova, R. M. Minyaev, A. G. Starikov and V. I. Minkin, *Eur. J. Inorg. Chem.*, 2013, **2013**, 4203–4219.
35 D. Kim, Y. O. Su and T. G. Spiro, *Inorg. Chem.*, 1986, **25**, 3988–3993.
36 S. Grimme, J. Antony, S. Ehrlich and H. Krieg, *J. Chem. Phys.*, 2010, **132**, 154104.
37 F. A. Walker, E. Hui and J. M. Walker, *J. Am. Chem. Soc.*, 1975, **97**, 2390–2397.
38 S. J. Cole, G. C. Curthoys, E. A. Magnusson and J. N. Phillips, *Inorg. Chem.*, 1972, **11**, 1024–1028.
39 R. J. W. Le Fevre and J. Northcott, *J. Chem. Soc.*, 1953, 867–870.
40 E. R. Talaty and J. C. Fargo, *Chem. Commun.*, 1967, 65–66.
41 D. F. Evans, *J. Chem. Soc.*, 1959, 2003–2005.
42 J. A. Happe and R. L. Ward, *J. Chem. Phys.*, 1963, **39**, 1211–1218.
43 C. Belle, C. Bougault, M.-T. Averbuch, A. Durif, J.-L. Pierre, J.-M. Latour and L. Le Pape, *J. Am. Chem. Soc.*, 2001, **123**, 8053–8066.
44 I. Bertini, P. Turano and A. J. Vila, *Chem. Rev.*, 1993, **93**, 2833–2932.

45 L. Wei, K. Padmaja, W. J. Youngblood, A. B. Lysenko, J. S. Lindsey and D. F. Bocian, *J. Org. Chem.*, 2003, **69**, 1461–1469.
46 K. L. Kompa and R. D. Levine, *Proc. Natl. Acad. Sci. U. S. A.*, 2001, **98**, 410–414.
47 K. Szacilowski, *Chem. Rev.*, 2008, **108**, 3481–3548.
48 J. M. Perez, L. Josephson, T. O'Loughlin, D. Hogemann and R. Weissleder, *Nat. Biotechnol.*, 2002, **20**, 816–820.
49 Christian-Albrechts-Universität and Universitätsklinikum S.-H., *WO* 2012/022299, patent pending.
50 R. Herges, *Nachr. Chem.*, 2011, **59**, 817–821.
51 R. B. Lauffer, *Chem. Rev.*, 1987, **87**, 901–927.

Rational Design of a Room Temperature Molecular Spin Switch. The Light-Driven Coordination Induced Spin State Switch (LD-CISSS) Approach.

M. Dommaschk, C. Schütt, S. Venkataramani, U. Jana, C. Näther, F. Sönnichsen, R. Herges

Table of Contents

I. Association Constants and Thermodynamic Parameters

I.1 Association of pyridine to Ni-TPP

The association constant (K) of pyridine to Ni-TPP was determined by temperature dependent ^{1}H NMR spectroscopy. Calculation of K can be simplified to a pseudo first order kinetic because of the excess of pyridine as the solvent (eq S1 and S2). The paramagnetic shift (δ_{para}) of the pyrrole protons of Ni-TPP in pure pyridine is not the maximum shift (δ_{max}). Because of a very low association constant there is always an equilibrium between the square bipyramidal paramagnetic complex and the square planar diamagnetic complex. To determine the association constant, the pyrrole shift (δ_{py}) has to be compared with the maximum shift which was obtained by NMR measurement of Ni-TPP in (the much stronger ligand) pure piperidine (δ_{pip}) (equation 3). From temperature dependence of the association constant the thermodynamic parameters ΔH and ΔS are calculated by Gibbs free enthalpy relation (equation S4).

$$Ni\text{-}TPP + 2\ Pyridine \leftrightharpoons Ni\text{-}TPP(Py)_2 \quad \text{(eq S1)}$$

$$Ni\text{-}TPP_{dia} \leftrightharpoons Ni\text{-}TPP_{para} \quad \text{(eq S2)}$$

$$K = \frac{[Ni\text{-}TPP_{para}]}{[Ni\text{-}TPP_{dia}]} = \frac{\delta_{py} - \delta_{dia}}{\delta_{max} - \delta_{py}} \quad \text{(eq S3)}$$

$$\Delta G = \Delta H - T\Delta S = -RT\ln(K) \quad \text{(eq S4)}$$

K: association constant
δ_{py}: shift of pyrrole protons in pure pyridine [ppm]
δ_{dia}: diamagnetic shift of pyrrole protons [ppm] (9 ppm)
δ_{max}: maximum paramagnetic shift of pyrrole protons [ppm]

Table S1. Determination of association constant of pyridine to Ni-TPP.

T / K	T^{-1} / K^{-1}	δ_{py} / ppm	δ_{max} / ppm	Ni-TPP_{para} / %	Ni-TPP_{dia} / %	K	ln(K)
300	0,00333	22,11	51,22	0,31052	0,68948	0,45036	-0,79771
310	0,00323	18,96	48,70	0,25088	0,74912	0,33490	-1,09392
320	0,00313	16,74	45,37	0,21281	0,78719	0,27035	-1,30805
330	0,00303	15,18	43,14	0,18102	0,81898	0,22103	-1,50946

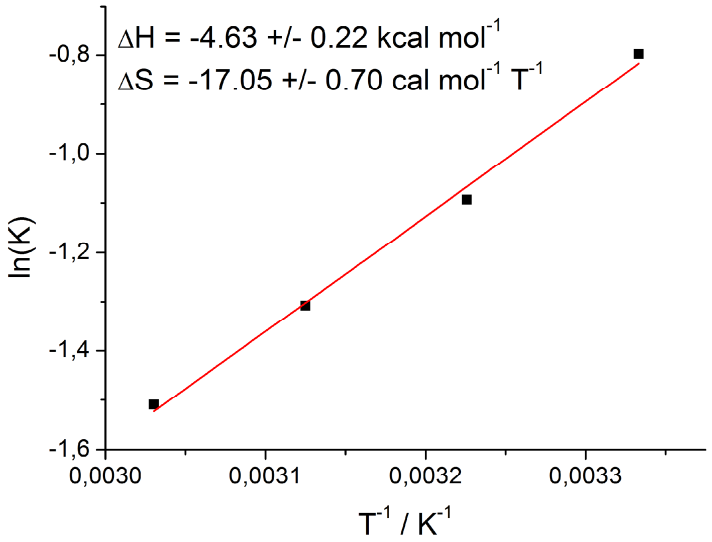

Figure S1. Gibbs free enthalpy plot for determination of thermodynamic parameters ΔH and ΔS for the association of pyridine to Ni-TPP.

I.2 Intramolecular association of record player 1 and 2

To determine the thermodynamic parameters ΔH and ΔS for the intramolecular coordination, the association constant (K_1) was measured as a function of temperature in DMSO. K_1 (Figure 14, equation S5) can be calculated from the pyrrole protons shifts of the *cis* isomer of the record player molecule. The maximum shift δ_{max} which is crucial to calculate the cis_{para}/cis_{dia} ratio (see eq. 1 and eq. S5), was measured differently for the record players **1** and **2**. For *cis*-**2** the value was obtained by an analogous experiment in pure pyridine. For *cis*-**1** this is not possible because association is too weak. Therefore we supposed the shifts obtained for Ni-TPP in piperidine to be the maximum shift δ_{max}. ΔH and ΔS were obtained by Gibbs free enthalpy plots (eq. S4, Figure S2 and S3).

$$cis_{dia} \leftrightharpoons cis_{para} \tag{S5}$$

$$K_1 = \frac{cis_{para}}{cis_{dia}} = \frac{\delta - \delta_{dia}}{\delta_{max} - \delta} \tag{S6}$$

K_1: association constant
δ_{para}: paramagnetic shift of pyrrole protons [ppm]
δ_{dia}: diamagnetic shift of pyrrole protons [ppm] (9 ppm)
δ_{max}: maximum paramagnetic shift of pyrrole protons [ppm]
δ: absolute chemical shift of pyrrole protons [ppm]

Table S2 Determination of intramolecular association constant of record player **2**. The maximum shift (σ_{max}) was found by measurement in pure pyridine.

T / K	T^{-1} / K^{-1}	δ / ppm	δ_{max} / ppm	*cis*-**2**$_{para}$ / %	*cis*-**2**$_{dia}$ / %	K	ln(K)
300	0,00333	48,42	53,69	0,8819	0,1181	7,4674	2,0106
310	0,00323	45,94	51,95	0,8600	0,1400	6,1429	1,8153
320	0,00313	43,46	50,45	0,8300	0,1700	4,8824	1,5856
330	0,00303	41,16	49,03	0,8000	0,2000	4,0000	1,3863
340	0,00294	38,93	47,49	0,7775	0,2225	3,4952	1,2514

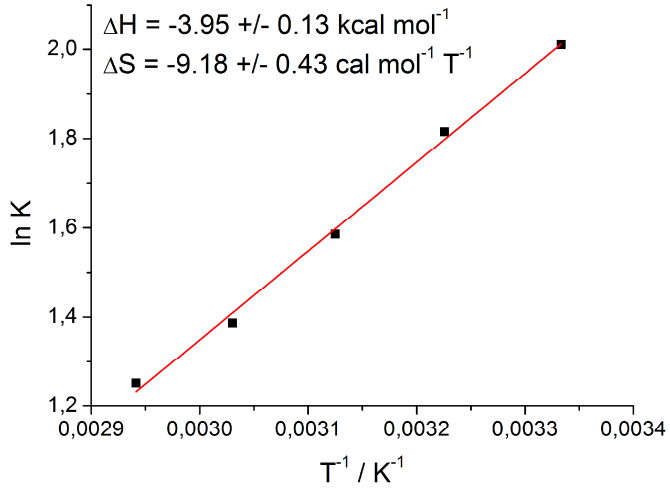

Figure S2. Gibbs free enthalpy plot for determination of thermodynamic parameters ΔH and ΔS for the intramolecular association of *cis*-**2**.

Table S3. Determination of intramolecular association constant of record player **1**. The maximum shift (δ_{max}) was found by measurement of Ni-TPP in pure piperidine (see Table S1).

T / K	T^{-1} / K^{-1}	δ / ppm	δ_{max} / ppm	*cis*-**1**$_{para}$ / %	*cis*-**1**$_{dia}$ / %	K	ln(K)
300	0,00333	11,45	51,22	0,0580	0,9420	0,0616	-2,7870
310	0,00323	11,13	48,70	0,0537	0,9464	0,0567	-2,8701
320	0,00313	10,87	45,37	0,0514	0,9486	0,0542	-2,9150
330	0,00303	10,66	43,14	0,0486	0,9514	0,0511	-2,9738

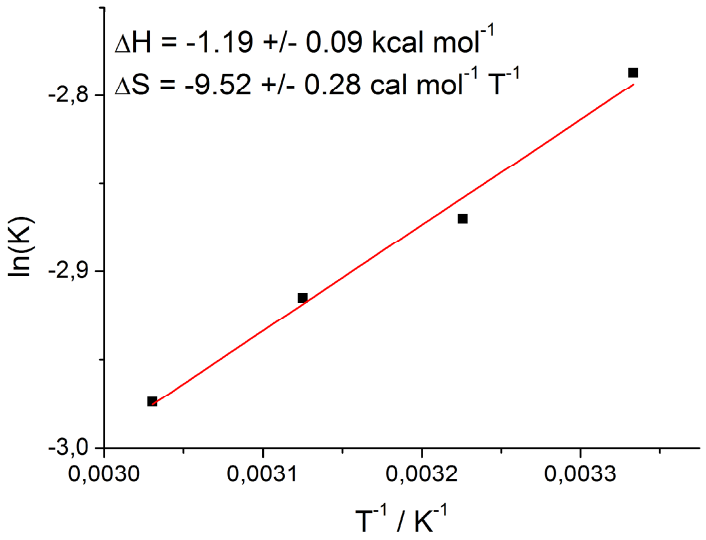

Figure S3. Gibbs free enthalpy plot for determination of thermodynamic parameters ΔH and ΔS for the intramolecular association of *cis*-**1**.

II. Single Crystal X-ray Analysis

Data collection was performed using an Imaging Plate Diffraction System (IPDS-1) from STOE with Mo-Kα radiation (λ = 0.71073 Å). The structure was solved with direct methods using SHELXS-97 and structure refinement was performed against F^2 using SHELXL-97. All non-hydrogen atoms except the disordered C atoms of lower occupancy) were refined anisotropic. The C-H H atoms were positioned with idealized geometry and refined isotropic with $U_{iso}(H) = 1.2 \cdot U_{eq}(C)$ (1.5 for methyl H atoms) using a riding model. One of the phenyl rings is disordered and was refined using a split model with restraints (SAME and FLAT). The site with lower occupancy was refined only isotropic. There are three additional solvate DMSO molecules in the asymmetric unit of which two are disordered and therefore, were also refined using split model. Selected crystal data and details on the structure refinement are given in Table S4 and an ORTEP plot is presented in Figure S4.

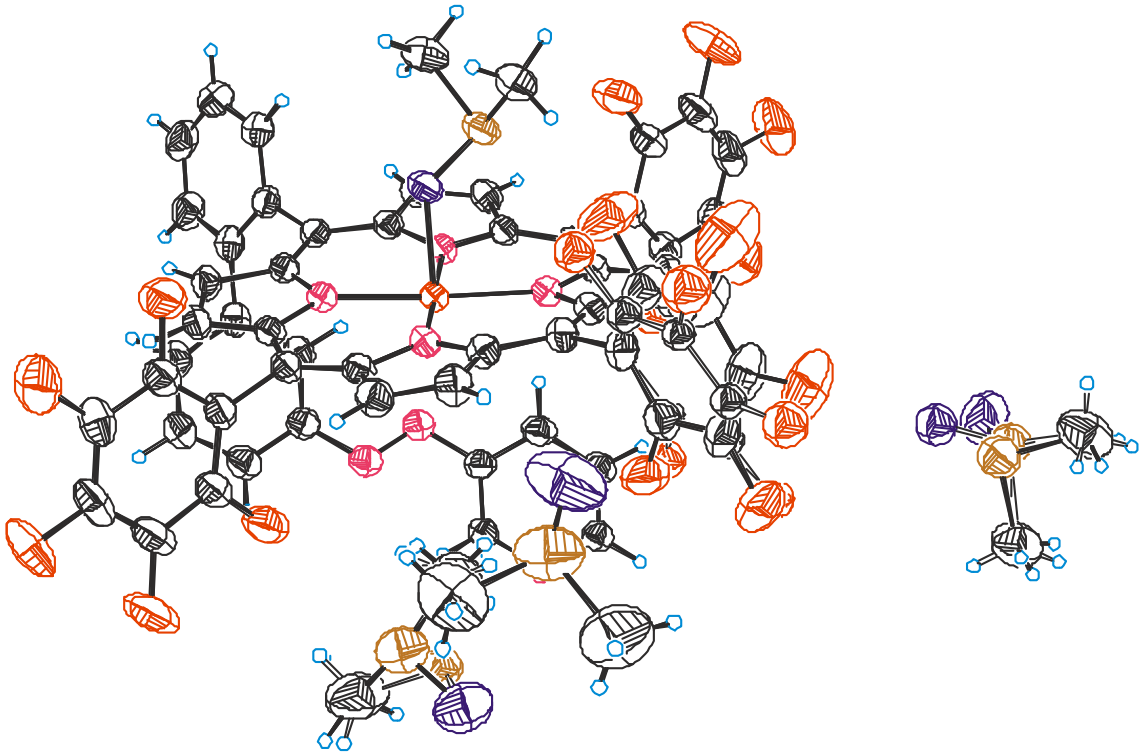

Figure S4. View of the asymmetric unit with displacement ellipsoids drawn at the 50% probability level.

Table S4. Crystal data and structure refinement for herges93.

Identification code	herges93	
Empirical formula	C126 H88 F30 N14 Ni2 O8 S8	
Formula weight	2870.00	
Temperature	200(2) K	
Wavelength	0.71073 Å	
Crystal system	triclinic	
Space group	P-1	
Unit cell dimensions	a = 14.3795(4) Å	α = 99.054(3)°.
	b = 14.9693(5) Å	β = 97.777(3)°.
	c = 16.9457(6) Å	γ = 117.019(2)°.
Volume	3119.06(17) $Å^3$	
Z	1	
Density (calculated)	1.528 Mg/m^3	
Absorption coefficient	0.544 mm^{-1}	
F(000)	1460	
Crystal size	? x ? x ? mm^3	
Theta range for data collection	1.63 to 25.00°.	
Index ranges	-17<=h<=17, -17<=k<=17, -19<=l<=20	
Reflections collected	27602	
Independent reflections	10894 [R(int) = 0.0463]	
Completeness to theta = 25.00°	99.2 %	
Refinement method	Full-matrix least-squares on F^2	
Data / restraints / parameters	10894 / 40 / 899	
Goodness-of-fit on F^2	1.057	
Final R indices [I>2sigma(I)]	R1 = 0.0484, wR2 = 0.1015	
R indices (all data)	R1 = 0.0676, wR2 = 0.1092	
Largest diff. peak and hole	0.395 and -0.386 $e.Å^{-3}$	

III. Thermal half-life

The thermal half-life was determined in DMSO, dichloromethane and chloroform by integration in ^{1}HNMR (Figure S5). The NMR samples were stored at 20 °C and kept in the dark.

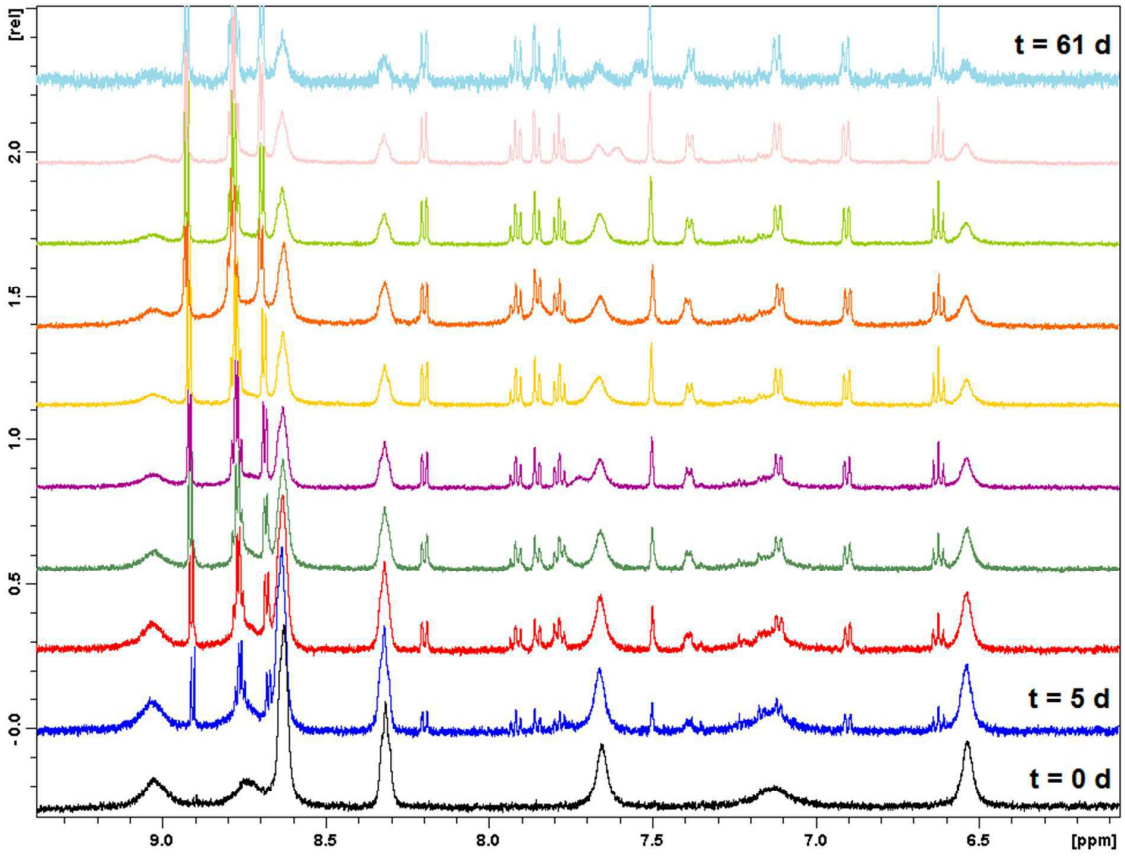

Figure S5. ^{1}H NMR spectra for determination of thermal half-life of *cis*-**2** in dichloromethane. The time between each measurement are 7 d beginning with the second spectrum (blue).

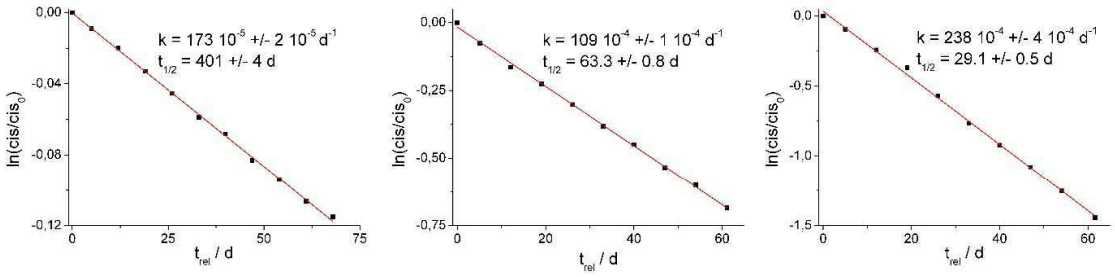

Figure S6. Linear plots for determination of the thermal half-life in DMSO (left), dichloromethane (middle) and chloroform (right).

IV. Computational Details

IV.1 Formation Enthalpies of Ni-TPP and Ni-TPPF20 complexes with pyridine

The geometry optimizations of the Ni-TPP and Ni-$TPPF_{20}$ complexes were performed at the PBE/DZP level of density functional theory. Single point energies were calculated at the optimized geometries using several functionals and basis sets. The calculated relative energies are compared with the corresponding experimentally determined ΔH values.

Table S5. Calculated enthalpies for the formation of the five coordinate (ΔH 1 Py) and six coordinate (ΔH 2 Py) complexes of Ni-TPP with pyridine.

Functional	Basis set	E_{abs} Pyridine (s) [Hartree]	E_{abs} Ni-TPP (s) [Hartree]	E_{abs} Ni-TPP · 1 Py (t) [Hartree]	E_{abs} Ni-TPP · 2 Py (t) [Hartree]	ΔH 1 Py [kcal/mol]	ΔH 2 Py [kcal/mol]
PBE	**SVP**	-247.7907293	-3416.8668675	-3664.6603572	-3912.4695187	**-1.73**	**-13.30**
PBE	**def2TZVP**	-248.0572139	-3419.0707883	-3667.1175150	-3915.1846324	**6.58**	**0.37**
PBE	**6-31G***	-247.9678670	-3418.2081610	-3666.1732030	-3914.1577327	**1.77**	**-8.68**
PBE	**6-31+G***	-247.9785310	-3418.2997021	-3666.2707783	-3914.2630143	**4.68**	**-3.92**
PBE	**6-311G***	-248.0184093	-3418.7028732	-3666.7192797	-3914.7554118	**1.26**	**-9.86**
B3LYP	**SVP**	-247.7907293	-3419.4665420	-3667.5878432	-3915.7044097	**-10.25**	**-17.54**
B3LYP	**def2TZVP**	-248.3773050	-3421.7070133	-3670.0874379	-3918.4682745	**-1.96**	**-4.17**
B3LYP	**6-31G***	-248.2842171	-3420.8212213	-3669.1173750	-3917.4114208	**-7.49**	**-13.66**
B3LYP	**6-31+G***	-248.2951273	-3420.9105850	-3669.2105602	-3917.5123502	**-3.04**	**-7.22**
B3LYP	**6-311G***	-248.3373511	-3421.3312805	-3669.6809926	-3918.0289152	**-7.76**	**-14.39**
B97D	**SVP**	-247.9229869	-3418.7190885	-3666.6649946	-3914.6239832	**-14.38**	**-36.97**
B97D	**def2TZVP**	-248.1885201	-3420.9173742	-3669.1158535	-3917.3323060	**-6.25**	**-23.78**
B97D	**6-31G***	-248.0970082	-3420.0365205	-3668.1516344	-3916.2830653	**-11.36**	**-32.96**
B97D	**6-31+G***	-248.1069197	-3420.1217110	-3668.2412745	-3916.3797896	**-7.93**	**-27.76**
B97D	**6-311G***	-248.1499864	-3420.5531952	-3668.7215460	-3916.9067779	**-11.52**	**-33.64**
B97D3	**SVP**	-247.9440954	-3418.8973575	-3666.8599549	-3914.8383211	**-11.61**	**33.12**
B97D3	**def2TZVP**	-248.2096286	-3421.0956432	-3669.3108138	-3917.5466439	**-3.48**	**-19.92**
B97D3	**6-31G***	-248.1181167	-3420.2147895	-3668.3465948	-3916.4974032	**-8.59**	**-29.10**
B97D3	**6-31+G***	-248.1280282	-3420.2999800	-3668.4362348	-3916.5941275	**-5.16**	**-23.90**
B97D3	**6-311G***	-248.1710949	-3420.7314642	-3668.9165063	-3917.1211159	**-8.75**	**-29.78**
B97-1	**SVP**	-248.0317295	-3418.8220858	-3666.8766852	-3914.9252599	**-14.35**	**-24.92**
B97-1	**def2TZVP**	-248.2991793	-3421.0304714	-3669.3397158	-3917.6480896	**-6.32**	**-12.09**
B97-1	**6-31G***	-248.2095684	-3420.1665399	-3668.3939938	-3916.6183326	**-11.22**	**-20.49**
B97-1	**6-31+G***	-248.2189648	-3420.2487233	-3668.4795083	-3916.7113422	**-7.42**	**-15.49**
B97-1	**6-311G***	-248.2599643	-3420,6570655	-3668.9363520	-3917.2124179	**-12.12**	**-22.23**
M06	**SVP**	-247.9089681	-3417.9229487	-3665.8559487	-3913.7932292	**-15.08**	**-32.85**
M06	**def2TZVP**	-248.1790803	-3420.1538082	-3668.3439753	-3916.5441810	**-6.96**	**-20.21**
M06	**6-31G***	-248.0926932	-3419.3195391	-3667.4318013	-3915.5508647	**-12.28**	**-28.83**
M06	**6-31+G***	-248.1014735	-3419.4028278	-3667.5189665	-3915.6445340	**-9.20**	**-24.32**
M06	**6-311G***	-248.1393864	-3419.7744237	-3667.9343651	-3916.1031842	**-12.90**	**-31.37**
Experiment[1]						**-**	**-4.63 (± 0.22)**

Functional	Basis set	E_{abs} Pyridine (s) [Hartree]	E_{abs} Ni-TPP (s) [Hartree]	E_{abs} Ni-TPP · 1 Py (t) [Hartree]	E_{abs} Ni-TPP · 2 Py (t) [Hartree]	ΔH 1 Py [kcal/mol]	ΔH 2 Py [kcal/mol]
M06L	**SVP**	-248.0687614	-3419.1855020	-3667.2846714	-3915.3841936	**-19.08**	**-38.38**
M06L	**def2TZVP**	-248.3337423	-3421.3753539	-3669.7278725	-3918.0857184	**-11.78**	**-26.91**
M06L	**6-31G***	-248.2464260	-3420.5291092	-3668.8025191	-3917.0778657	**-16.93**	**-35.08**
M06L	**6-31+G***	-248.2520476	-3420.5927651	-3668.8656084	-3917.1442481	**-13.05**	**-29.74**
M06L	**6-311G***	-248.2948281	-3421.0047018	-3669.3281490	-3917.6549322	**-17.96**	**-38.01**
MN12L	**SVP**	-247.8521535	-3417.2579922	-3665.1132325	-3912.9996023	**-1.94**	**-23.41**
MN12L	**def2TZVP**	-248.1287599	-3419.6102290	-3667.7244417	-3915.8768738	**9.13**	**-5.73**
MN12L	**6-31G***	-248.0452923	-3418.7643711	-3666.8061492	-3914.8831520	**2.21**	**-17.69**
MN12L	**6-31+G***	-248.0525888	-3418.8478387	-3666.8926905	-3914.9753716	**4.86**	**-14.03**
MN12L	**6-311G***	-248.0837359	-3419.2500896	-3667.3272279	-3915.4442915	**4.14**	**-16.77**
MN12SX	**SVP**	-247.8661294	-3417.5000714	-3665.3818463	-3913.2772225	**-9.82**	**-28.17**
MN12SX	**def2TZVP**	-248.1687256	-3420.0148446	-3668.1852527	-3916.3746919	**-1.06**	**-14.05**
MN12SX	**6-31G***	-248.0796822	-3419.1437864	-3667.2350185	-3915.3415381	**-7.25**	**-24.09**
MN12SX	**6-31+G***	-248.0884745	-3419.2245312	-3667.3192706	-3915.4322110	**-3.93**	**-19.28**
MN12SX	**6-311G***	-248.1235963	-3419.6362946	-3667.7695159	-3915.9223955	**-6.04**	**-24.42**
TPSSh	**SVP**	-248.1262254	-3419.6494978	-3667.7920901	-3915.9351659	**-10.27**	**-20.84**
TPSSh	**def2TZVP**	-248.3895921	-3421.8318714	-3670.2251587	-3918.6237402	**-2.32**	**-7.96**
TPSSh	**6-31G***	-248.3013587	-3420.9770688	-3669.2903030	-3917.6065766	**-7.45**	**-16.81**
TPSSh	**6-31+G***	-248.3100135	-3421.0560251	-3669.3725370	-3917.6955463	**-4.08**	**-12.23**
TPSSh	**6-311G***	-248.3510699	-3421.4627812	-3669.8264166	-3918.1938041	**-7.88**	**-18.12**
Experiment[1]						-	**-4.6 (± 0.2)**

Table S6. Deviation from the experimental value of the calculated enthalpies for the formation of the six coordinate complexes of Ni-TPP with pyridine in kcal*mol^{-1}.

	SVP	**def2TZVP**	**6-31G***	**6-31+G***	**6-311G***
TPSSh	16.24	3.36	12.21	7.63	13.52
MN12SX	23.57	9.45	19.49	14.68	19.82
MN12L	18.81	1.13	13.09	9.43	12.17
M06L	33.78	22.31	30.48	25.14	33.41
M06	28.25	15.61	24.23	19.72	26.77
B97-1	20.32	7.49	15.89	10.89	17.63
B97D3	28.52	15.32	24.50	19.30	25.18
B97D	32.37	19.18	28.36	23.16	29.04
B3LYP	12.94	-0.43	9.06	2.62	9.79
PBE	8.70	-4.97	4.08	-0.68	5.26

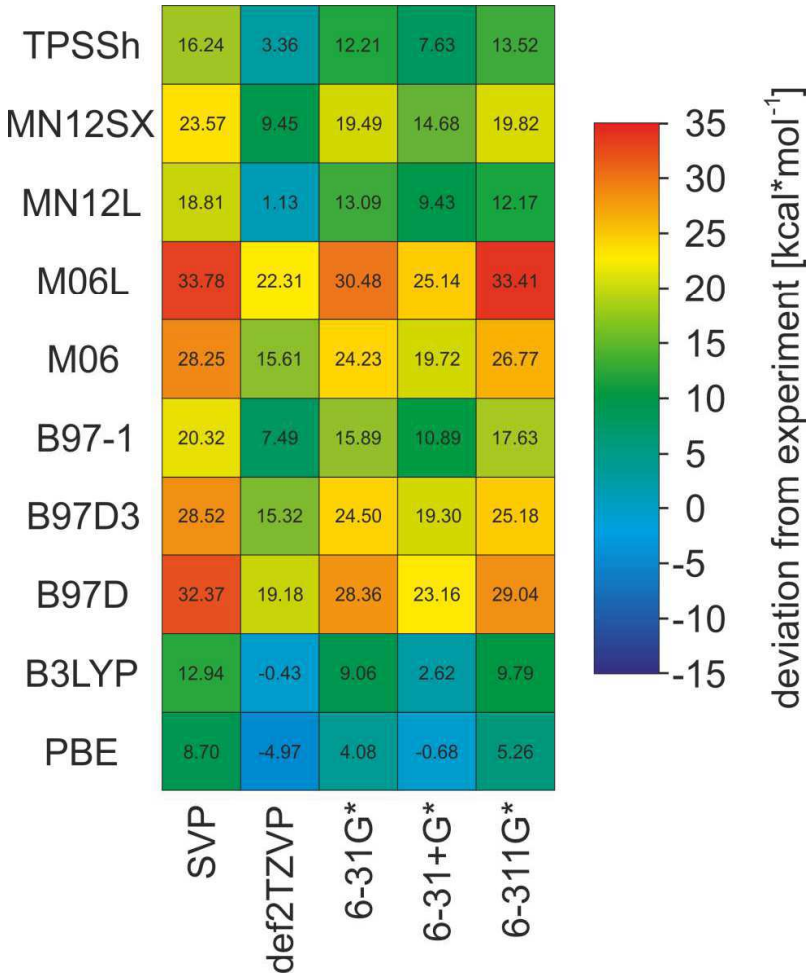

Figure S7. Colour coded representation of the deviation of theoretically calculated and experimentally determined values for the formation of the six coordinate complex of Ni-TPP with two pyridine molecules at different levels of theory. The exact values are given in kcal*mol^{-1}.

The smallest deviation from the experimental value is observed at the MN12L/def2TZVP (overestimated by 1.13 kcal*mol^{-1}), at the PBE/6-31+G* (underestimated by 0.68 kcal*mol^{-1}) and at the B3LYP/def2TZVP (underestimated by 0.43 kcal*mol^{-1}) level of density functional theory. Although there is no experimentally derived value for the complex formation enthalpy of the five coordinate complex of pyridine with Ni-TPP the calculated values at the MN12L/def2TZVP and the PBE/6-31+G* level of theory seem to be largely underestimated.

Table S7. Calculated enthalpies for the formation of the five coordinate (ΔH 1 Py) and six coordinate (ΔH 2 Py) complexes of Ni-$TPPF_{20}$ with pyridine.

Functional	Basis set	E_{abs} Pyridine (s) [Hartree]	E_{abs} Ni-$TPPF_{20}$ (s) [Hartree]	E_{abs} Ni-$TPPF_{20}$ · 1 Py (t) [Hartree]	E_{abs} Ni-$TPPF_{20}$ · 2 Py (t) [Hartree]	ΔH 1 Py [kcal/mol]	ΔH 2 Py [kcal/mol]
PBE	**SVP**	-247.7907293	-5398.2561063	-5646.0562612	-5893.8700228	**-5.91**	**-20.37**
PBE	**def2TZVP**	-248.0572139	-5402.8912268	-5650.9448704	-5899.0159446	**2.24**	**-6.46**
PBE	**6-31G***	-247.9678670	-5401.0661947	-5649.0374536	-5897.0259916	**-2.13**	**-15.10**
PBE	**6-31+G***	-247.9785310	-5401.3249080	-5649.3035868	-5897.2999247	**-0.09**	**-11.27**
PBE	**6-311G***	-248.0184093	-5402.2065906	-5650.2303544	-5898.2710974	**-3.36**	**-17.37**
B3LYP	**SVP**	-247.7907293	-5402.5030745	-5650.6322531	-5898.7535772	**-15.20**	**-25.47**
B3LYP	**def2TZVP**	-248.3773050	-5407.1878216	-5655.5762203	-5903.9610289	**-6.96**	**-11.67**
B3LYP	**6-31G***	-248.2842171	-5405.3401985	-5653.6438962	-5901.9421489	**-12.22**	**-21.03**
B3LYP	**6-31+G***	-248.2951273	-5405.5853926	-5653.8939606	-5902.1998376	**-8.43**	**-15.18**
B3LYP	**6-311G***	-248.3373511	-5406.4969677	-5654.8551831	-5903.2078326	**-13.09**	**-22.69**
B97D	**SVP**	-247.9229869	-5400.8449421	-5648.7990261	-5896.7633224	**-19.51**	**-45.44**
B97D	**def2TZVP**	-248.1885201	-5405.4729934	-5653.6797152	-5901.9006561	**-11.42**	**-31.77**
B97D	**6-31G***	-248.0970082	-5403.6333071	-5651.7562737	-5899.8924453	**-16.29**	**-40.86**
B97D	**6-31+G***	-248.1069197	-5403.8638296	-5651.9924009	-5900.1356356	**-13.59**	**-36.37**
B97D	**6-311G***	-248.1499864	-5404.7973107	-5652.9744939	-5901.1649089	**-17.07**	**-42.44**
B97D3	**SVP**	-247.9440954	-5401.0140187	-5648.9852364	-5896.9683011	**-17.02**	**-41.47**
B97D3	**def2TZVP**	-248.2096286	-5405.6420700	-5653.8659255	-5902.1056348	**-8.93**	**-27.80**
B97D3	**6-31G***	-248.1181167	-5403.8023837	-5651.9424840	-5900.0974239	**-13.79**	**-36.90**
B97D3	**6-31+G***	-248.1280282	-5404.0329062	-5652.1786112	-5900.3406142	**-11.09**	**-32.41**
B97D3	**6-311G***	-248.1710949	-5404.9663873	-5653.1607042	-5901.3698875	**-14.57**	**-38.47**
B97-1	**SVP**	-248.0317295	-5401.3914598	-5649.4537321	-5897.5068438	**-19.17**	**-32.58**
B97-1	**def2TZVP**	-248.2991793	-5406.0335369	-5654.3504409	-5902.6626377	**-11.12**	**-19.29**
B97-1	**6-31G***	-248.2095684	-5404.2325759	-5652.4672857	-5900.6955988	**-15.78**	**-27.54**
B97-1	**6-31+G***	-248.2189648	-5404.4537805	-5652.6929486	-5900.9287006	**-12.68**	**-23.21**
B97-1	**6-311G***	-248.2599643	-5405.3452003	-5653.6326550	-5901.9131734	**-17.25**	**-30.15**
M06	**SVP**	-247.9089681	-5400.5139687	-5648.4558475	-5896.3985664	**-20.65**	**-41.83**
M06	**def2TZVP**	-248.1790803	-5405.1162430	-5653.3150886	-5901.5199375	**-12.40**	**-28.57**
M06	**6-31G***	-248.0926932	-5403.4156060	-5651.5362555	-5899.6606404	**-17.54**	**-37.43**
M06	**6-31+G***	-248.1014735	-5403.6300767	-5651.7562956	-5899.8868309	**-15.53**	**-33.76**
M06	**6-311G***	-248.1393864	-5404.4115854	-5652.5811008	-5900.7553256	**-18.91**	**-40.77**
M06L	**SVP**	-248.0687614	-5402.0397616	-5650.1467109	-5898.2508189	**-23.96**	**-46.14**
M06L	**def2TZVP**	-248.3337423	-5406.6038731	-5654.9640963	-5903.3259196	**-16.62**	**-34.24**
M06L	**6-31G***	-248.2464260	-5404.9308296	-5653.2113125	-5901.4910196	**-21.37**	**-42.26**
M06L	**6-31+G***	-248.2520476	-5405.1035487	-5653.3854141	-5901.6681649	**-18.71**	**-37.98**
M06L	**6-311G***	-248.2948281	-5405.9736862	-5654.3053239	-5902.6366285	**-23.10**	**-45.99**
MN12L	**SVP**	-247.8521535	-5399.3201561	-5647.1816918	-5895.0733352	**-5.89**	**-30.67**
MN12L	**def2TZVP**	-248.1287599	-5404.1015468	-5652.2210231	-5900.3776348	**5.83**	**-11.65**
MN12L	**6-31G***	-248.0452923	-5402.3872746	-5650.4346608	-5898.5164173	**-1.31**	**-24.20**
MN12L	**6-31+G***	-248.0525888	-5402.5903480	-5650.6421335	-5898.7295185	**0.50**	**-21.33**
MN12L	**6-311G***	-248.0837359	-5403.4250803	-5651.5086005	-5899.6307526	**0.14**	**-23.97**
Experiment						**-5.3 (± 0.1)[1]**	**-11.2 (± 0.5)[1]**

Functional	Basis set	E_{abs} Pyridine (s) [Hartree]	E_{abs} Ni-$TPPF_{20}$ (s) [Hartree]	E_{abs} Ni-$TPPF_{20}$ · 1 Py (t) [Hartree]	E_{abs} Ni-$TPPF_{20}$ · 2 Py (t) [Hartree]	ΔH 1 Py [kcal/mol]	ΔH 2 Py [kcal/mol]
MN12SX	**SVP**	-247.8661294	-5399.4128008	-5647.3021828	-5895.2024524	**-14.59**	**-36.01**
MN12SX	**def2TZVP**	-248.1687256	-5404.5409211	-5652.7182271	-5900.9113245	**-5.38**	**-20.68**
MN12SX	**6-31G***	-248.0796822	-5402.7480843	-5650.8463954	-5898.9573695	**-11.69**	**-31.33**
MN12SX	**6-31+G***	-248.0884745	-5402.9530764	-5651.0560362	-5899.1731650	**-9.09**	**-27.07**
MN12SX	**6-311G***	-248.1235963	-5403.8161618	-5651.9572273	-5900.1147793	**-10.96**	**-32.27**
TPSSh	**SVP**	-248.1262254	-5402.6133303	-5650.7634505	-5898.9111366	**-14.99**	**-28.46**
TPSSh	**def2TZVP**	-248.3895921	-5407.2502970	-5655.6509960	-5904.0534318	**-6.97**	**-15.03**
TPSSh	**6-31G***	-248.3013587	-5405.4493352	-5653.7696028	-5902.0898919	**-11.87**	**-23.74**
TPSSh	**6-31+G***	-248.3100135	-5405.6662364	-5653.9910398	-5902.3180590	**-9.28**	**-19.95**
TPSSh	**6-311G***	-248.3510699	-5406.5633806	-5654.9349936	-5903.3068560	**-12.89**	**-25.94**
Experiment						**-5.3 (± 0.1)[1]**	**-11.2 (± 0.5) [1]**

Table S8. Deviation from the experimental value of the calculated enthalpies for the formation of the five coordinate complexes of Ni-$TPPF_{20}$ with pyridine in kcal*mol^{-1}.

	SVP	**def2TZVP**	**6-31G***	**6-31+G***	**6-311G***
TPSSh	9.69	1.67	6.57	3.98	7.59
MN12SX	9.29	0.08	6.39	3.79	5.66
MN12L	0.59	-11.13	-3.99	-5.80	-5.44
M06L	18.66	11.32	16.07	13.41	17.80
M06	15.35	7.10	12.24	10.23	18.90
B97-1	13.87	5.82	10.48	7.38	11.95
B97D3	11.72	3.63	8.49	5.79	9.27
B97D	14.21	6.12	10.99	8.29	11.77
B3LYP	9.90	1.66	6.92	3.13	7.79
PBE	0.61	-7.54	-3.17	-5.21	-1.94

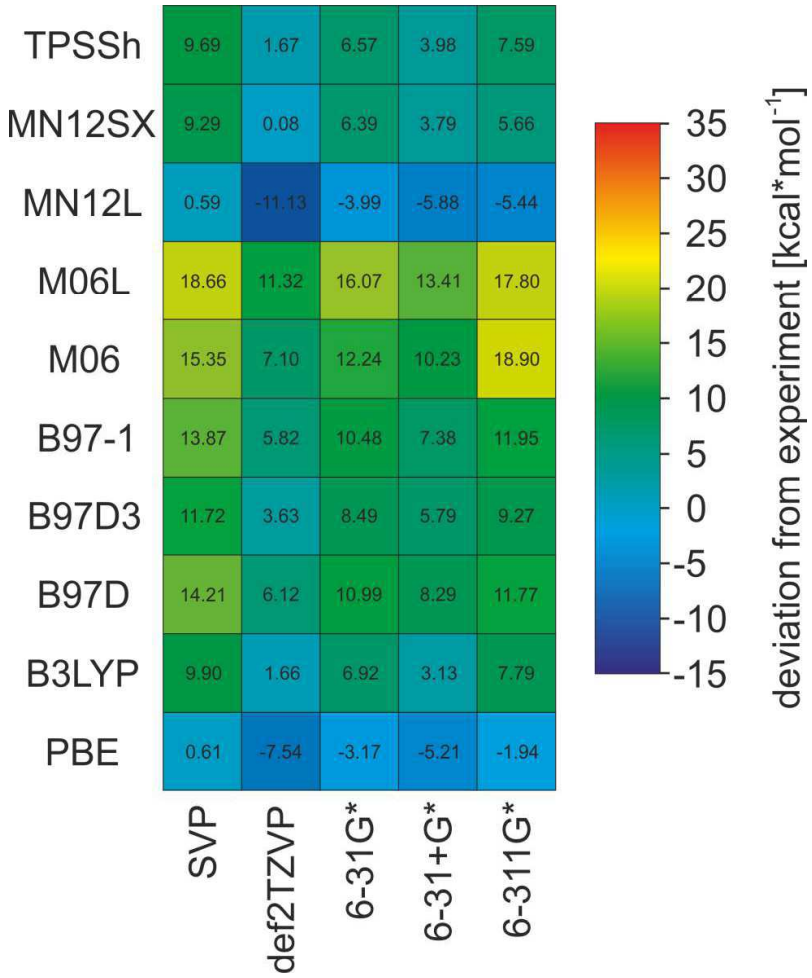

Figure S8. Colour coded representation of the deviation of theoretically calculated and experimentally determined values for the formation of the five coordinate complex of Ni-$TPPF_{20}$ with one pyridine molecule at different levels of theory. The exact values are given in kcal*mol^{-1}.

The smallest deviation from the experimental value is obtained at the MN12SX/def2TZVP (overestimated by 0.08 kcal*mol^{-1}), the B3LYP/def2TZVP (overestimated by 1.66 kcal*mol^{-1}) and at the TPPSh/def2TZVP (overestimated by 1.67 kcal*mol^{-1}) level of density functional theory. It should be noted that the values calculated at the MN12L/SVP (overestimated by 0.59 kcal*mol^{-1}) and the PBE/SVP (overestimated by 0.61 kcal*mol^{-1}) level of theory are also in very good agreement with the experimentally derived value, however fail largely in case of the six coordinated complex. Therefore both are not a reliable method to calculate complex formation enthalpies of Ni(II) porphyrins in general.

Table S9. Deviation from the experimental value of the calculated enthalpies for the formation of the six coordinate complexes of Ni-$TPPF_{20}$ with pyridine in kcal*mol^{-1}.

	SVP	def2TZVP	6-31G*	6-31+G*	6-311G*
TPSSh	17.26	3.83	12.54	8.75	14.74
MN12SX	24.81	9.48	20.13	15.87	21.07
MN12L	19.47	0.45	13.00	10.13	12.77
M06L	34.94	23.04	31.06	26.78	34.79
M06	30.63	17.37	26.23	22.56	29.57
B97-1	21.38	8.09	16.34	12.01	18.95
B97D3	30.27	16.60	25.70	21.21	27.27
B97D	34.24	20.57	29.66	25.17	31.24
B3LYP	14.27	0.47	9.83	3.98	11.49
PBE	9.17	-4.74	3.90	0.07	6.17

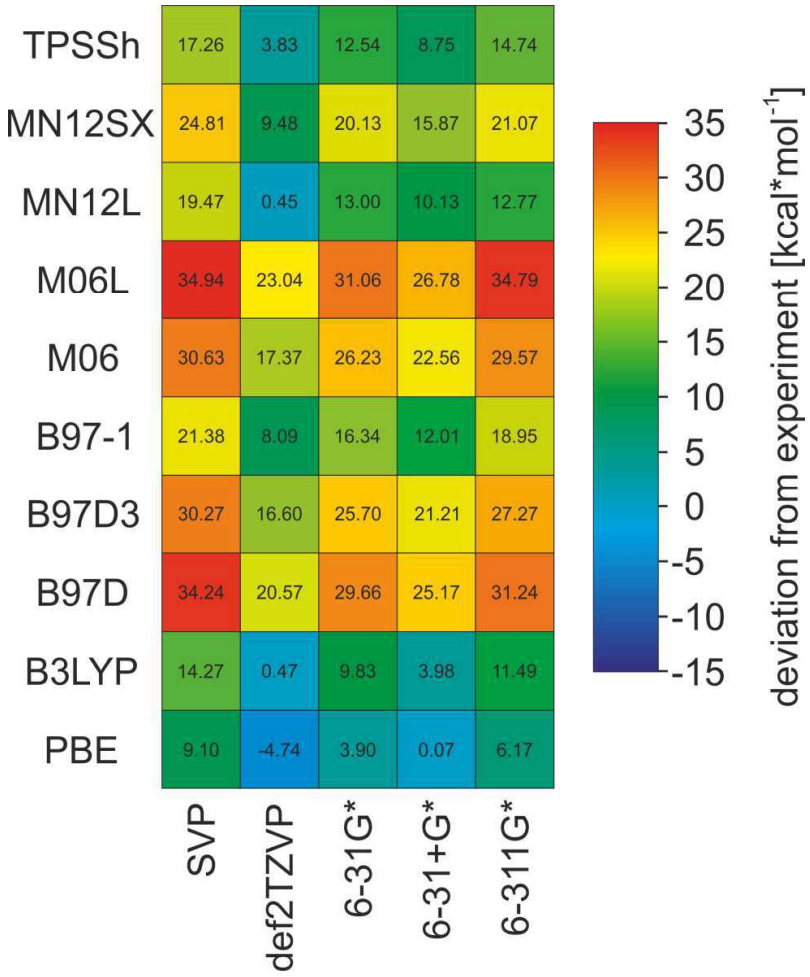

Figure S9. Colour coded representation of the deviation of theoretically calculated and experimentally determined values for the formation of the six coordinate complex of Ni-$TPPF_{20}$ with two pyridine molecules at different levels of theory. The exact values are given in kcal*mol^{-1}.

The smallest deviation from the experimental value is observed at the PBE/6-31+G* (overestimated by 0.07 kcal*mol^{-1}), MN12L/def2TZVP (overestimated by 0.45 kcal*mol^{-1}) and at the B3LYP/def2TZVP

(overestimated by 0.45 kcal*mol^{-1}) level of density functional theory. However, PBE/6-31+G* as well as the MN12L/def2TZVP level of theory fail largely in the prediction of the complex formation enthalpies of the five coordinated complex and therefore cannot be applied as a general method to calculate complex formations enthalpies of Ni(II) porphyrins.

In summary B3LYP/def2TZVP//PBE/DZP obviously is the level of choice since the complex formation energy of the 5- and 6-coordinate complexes are both in good agreement with experiment.

IV.2 Record player design

Density functional theory calculations (B3LYP/6-31G*) were performed on 36 different structures that looked promising based on geometry and synthesizability. The structures are presented in figure S10. For obvious reasons the structures were coined “record players” because the porphyrin resembles a disk, the azopyridine works like a tone arm by placing the pyridine nitrogen lone pair (needle) onto the nickel ion.

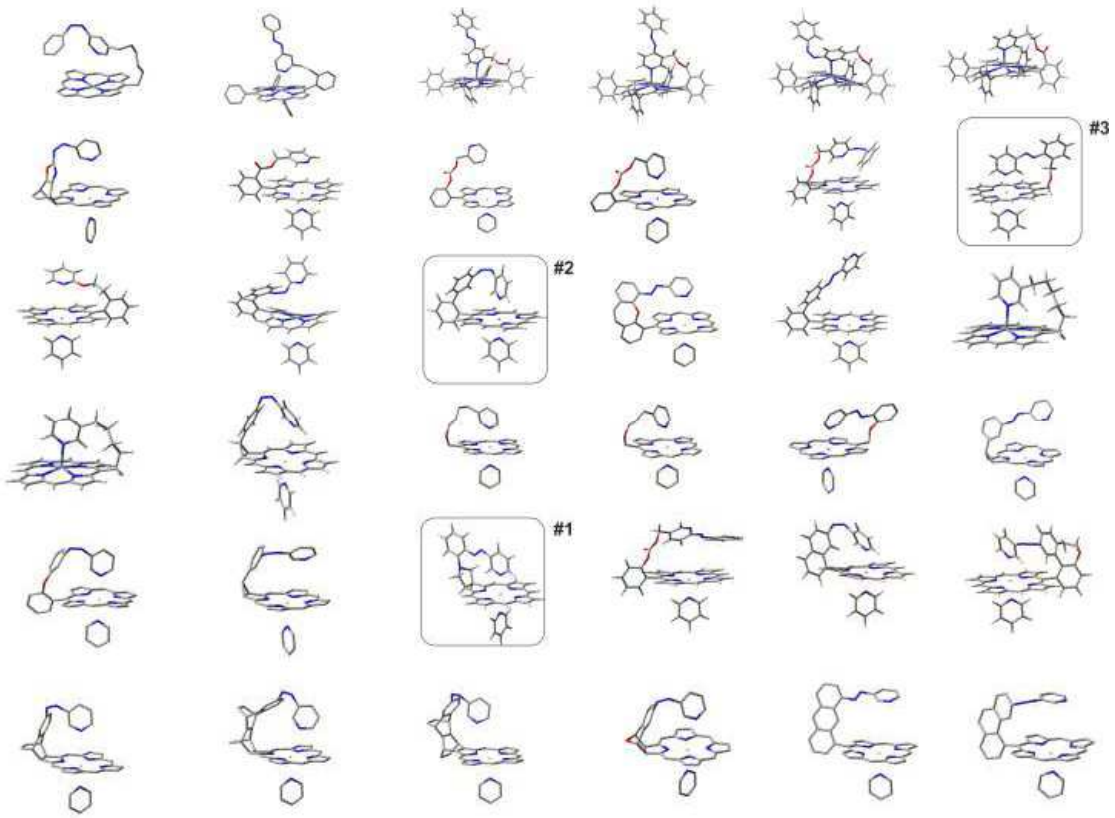

Figure S10. Potential candidates for a light-driven coordination-induced spin state switch (LD-CISSS). The structures were optimized at the B3LYP/6-31G* level of density functional theory and ranked according to an optimal N-Ni distance and a minimal deviation from orthogonal binding of the pyridine unit to the porphyrin plane. The three most promising candidates are highlighted.

IV.3 Energy difference of *cis*$_{para}$ and *cis*$_{dia}$

The energies of the coordinated and uncoordinated record players **1** and **2** were calculated at the B3LYP/def2TZVP//PBE/SVP level of theory. The calculated values for ΔH (*cis*-**1**: -0.25 and *cis*-**2**: -3.26 kcal mol^{-1} see Figure S11) are in good agreement with the experimental data. (*cis*-**1**: -1.19 and *cis*-**2**: -3.95 kcal mol^{-1} see Figure S2 and S3).

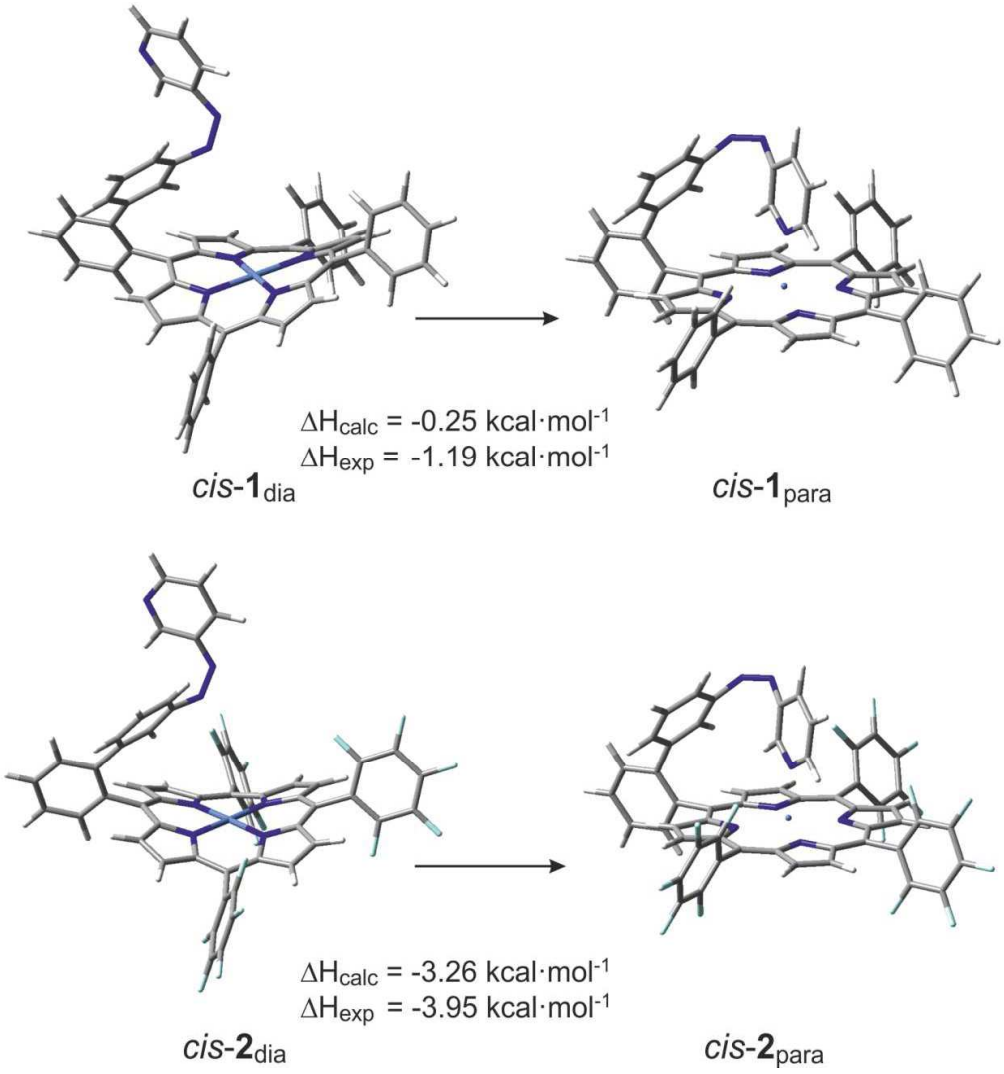

Figure S11. Calculated enthalpies (B3LYP/def2TZVP//PBE/SVP) of the intramolecular coordination of the magnetic conformers of *cis*-**1** and *cis*-**2**.

V. Ni-TPPF$_{20}$ maximum shift and titration with piperidine

The maximum chemical shift of octahedral, paramagnetic Ni-TPPF$_{20}$ pyrrole protons was observed with pyridine (green), *N*-methylimidazole (yellow) and piperdine (blue) as axial ligands (Figure S12). The Ligands were add to a 2 mM solution of Ni-TPPF$_{20}$ in acetone. Addition was discontinued as no further shift was observed. The spin density distribution in the porphyrin plane seems to be similar for all octahedral complexes independent of the nature of the axial ligand.

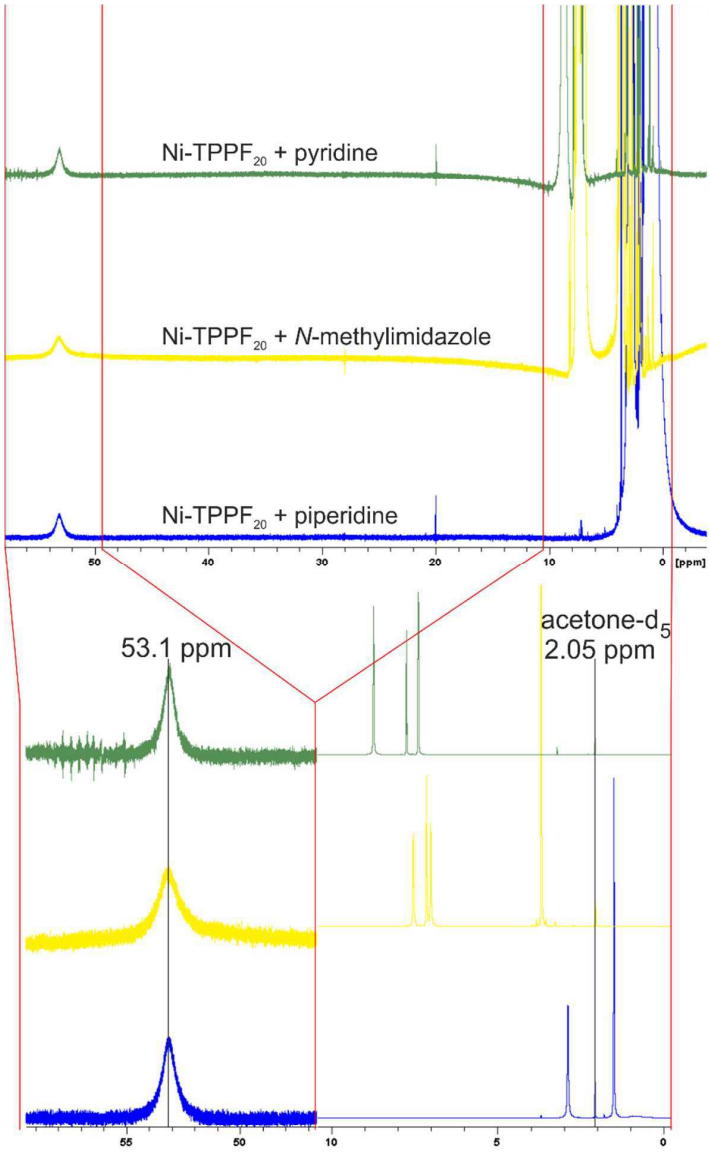

Figure S12. ^{1}H NMR spectra (acetone-d$_6$, 300 K) of Ni-TPPF$_{20}$ with an excess of pyridine-d$_5$ (green), methylimidazole (yellow) and piperidine (blue). All three axial ligands gives rise to the same chemical shift of the pyrrole protons signal at 53.1 ppm with respect to the acetone-d$_5$ signal at 2.05 ppm.

To figure out the maximum chemical shift (δ_{max}) of the square pyramidal complex, Ni-TPPF$_{20}$ was titrated with piperidine. The advantage over pyridine is the much higher association constant of the first ligand (K_1). The square pyramidal complex is formed with much less equivalents and can therefore

be observed more accurate. The shift of the pyrrole protons in ^{1}H NMR was observed indicating the amount of paramagnetic nickel(II). The titration (Figure S13) was evaluated using nonlinear fitting. The following binding model was assumed:

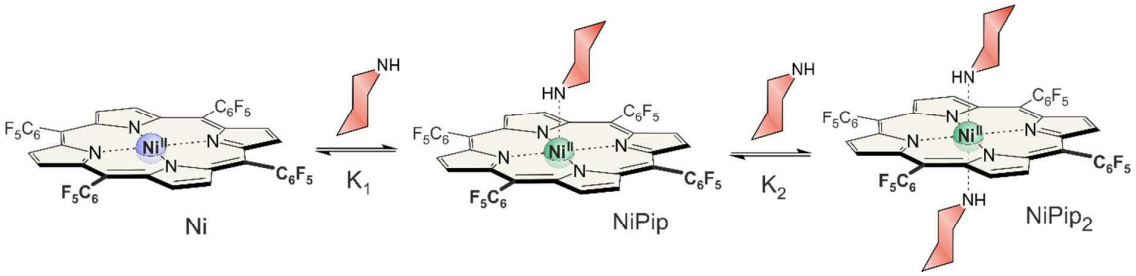

Figure S13. Binding model for the association of piperdine to Ni-TPPF$_{20}$.

$$K_1 = \frac{[NiPip]}{[Ni][Pip]} \qquad \text{(eq S7)}$$

$$K_2 = \frac{[NiPip_2]}{[NiPip][Pip]} \qquad \text{(eq S8)}$$

Table S10. Experimental ([Ni-TPPF$_{20}$], [Pip] and δ measured) and calculated values (δ calculated, [Ni], [NiPip] and [NiPip$_2$]) for the complex concentrations of Ni, NiPip and NiPip$_2$ in the titration series of Ni-TPPF$_{20}$ with piperidine.

[Ni-TPPF$_{20}$] mol L^{-1}	[Pip] mol L^{-1}	δ measured ppm	δ calculated ppm	[Ni] mol L^{-1}	[NiPip] mol L^{-1}	[NiPip$_2$] mol L^{-1}
9.230E-03	0.000E+00	8.58	8.58	9.230E-03	0.000E+00	0.000E+00
9.116E-03	6.691E-04	11.58	11.44	8.539E-03	5.769E-04	8.894E-08
9.005E-03	1.322E-03	14.30	14.23	7.878E-03	1.126E-03	3.675E-07
8.487E-03	4.361E-03	26.80	26.83	5.055E-03	3.427E-03	5.300E-06
8.297E-03	5.481E-03	31.28	31.03	4.170E-03	4.117E-03	9.276E-06
7.940E-03	7.576E-03	37.40	37.62	2.832E-03	5.087E-03	2.085E-05
7.612E-03	9.499E-03	41.89	41.95	1.985E-03	5.591E-03	3.592E-05
7.311E-03	1.127E-02	44.75	44.66	1.468E-03	5.791E-03	5.213E-05
7.239E-03	1.102E-01	53.16	53.19	8.167E-05	6.113E-03	1.044E-03
7.169E-03	2.072E-01	53.45	53.45	3.679E-05	5.354E-03	1.778E-03
7.100E-03	3.023E-01	53.55	53.54	2.209E-05	4.749E-03	2.329E-03
6.966E-03	4.871E-01	53.59	53.59	1.104E-05	3.866E-03	3.089E-03
6.837E-03	6.652E-01	53.60	53.61	6.778E-06	3.258E-03	3.573E-03
6.593E-03	1.002E+00	53.61	53.61	3.403E-06	2.477E-03	4.113E-03
6.153E-03	1.609E+00	53.62	53.61	1.427E-06	1.673E-03	4.479E-03

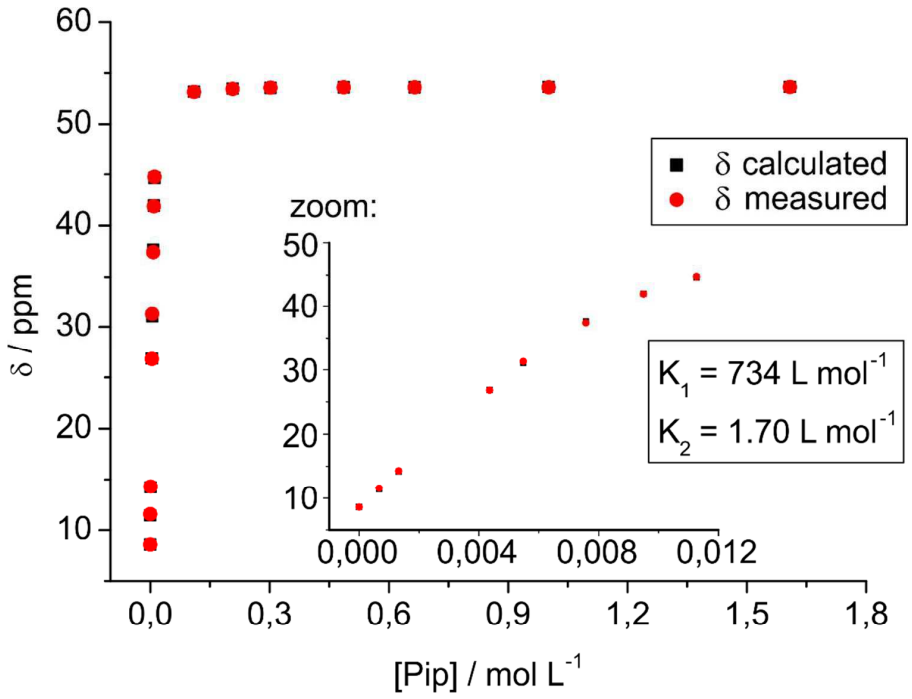

Figure S14. Measured (500 MHz, 298 K) and calculated values for the chemical shifts of the titration series.

The values of the maximum shifts are δ_{max}(NiPip) = 53.7 ppm and δ_{max}(NiPip$_2$) = 53.6 ppm. This small difference is within the accuracy of the method and can be neglected. Note that the chemical shifts in the titration series were observed at 298 K which gives rise to a slightly higher paramagnetic shifts than the experiments performed at 300 K.

Lit:

1. S. Thies, C. Bornholdt, F. Köhler, F.D. Sönnichsen, C. Näther, F. Tuczek and R. Herges, *Chem. Eur. J.* **2010** , *16*, 10074–10083.

4 Photoswitching of MRI Contrasts

The efficiency of a CA is quantified by its relaxivity (section 1.3). The value for free Gd(III) in water is $R_1 = 9\,\mathrm{mM^{-1}s^{-1}}$.[26] In clinically applied CAs the Gd(III) is complexed by a multidentate ligand which restricts the accessibility of water to the paramagnetic center. Therefore, the relaxivities of Gd(III) CAs are significantly lower, e.g. $R_1 = 3.83\,\mathrm{mM^{-1}s^{-1}}$ for Gd-DOTA (**1**, Figure 1.4).[25] Ni(II) has intrinsically lower values. The relaxivity of free Ni(II) in water is $R_1 = 0.78\,\mathrm{mM^{-1}s^{-1}}$. Similar to Gd(III) the values decrease upon complex formation with chelating agents. The Ni-EDTA (ethylenediaminetetraacetic acid) complex exhibits a relaxivity of $R_1 = 0.11\,\mathrm{mM^{-1}s^{-1}}$.[26] Conventional Gd(III)-based MRI CAs are administered as a $0.5\,\mathrm{mol\,l^{-1}}$ aqueous solution.[135] (except of Gadobutrol which is administered as $1.00\,\mathrm{mol\,l^{-1}}$ solution because of good physicochemical properties)[136] In 95% of all applications extracellular CAs are used. They have a half-life of approximately 90 min and are discharged via the kidney.[136] Extracellular CAs are highly hydrophilic molecules and therefore exclusively propagate in the in the blood plasma and the interstitial (room between the cells, Figure 4.1). The distribution volume is $0.25\,\mathrm{l\,kg^{-1}}$.[136,137] During the first pass through the vascular system 50% of the CA molecules are transfered to the interstitial. After 4-5 cycles the CA is uniformly distributed in the extracellular space. Consequently, the concentration during a MRI examination is $0.4 - 1.2\,\mathrm{mmol\,l^{-1}}$.[136] To prove that a Ni-porphyrin is applicable as a CA, MR images should exhibit a significant effect at this concentration.

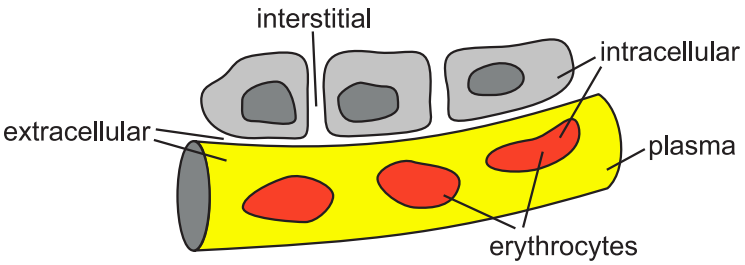

Figure 4.1: Sketch of a blood vessel to clarify the terms interstitial, plasma, erythrocytes, extracellular and intracellular.[137]

4.1 Photoswitchable Magnetic Resonance Imaging Contrast by Improved Light-Driven Coordination-Induced Spin State Switch

Marcel Dommaschk, Morten Peters, Florian Gutzeit, Christian Schütt, Christian Näther, Frank D. Sönnichsen, Sanjay Tiwari, Christian Riedel, Susann Boretius and Rainer Herges

J. Am. Chem. Soc. **2015**, *137*, 7552-7555.
DOI:10.1021/jacs.5b00929

Summary

RPs with different pyridine derivatives as axial ligand were synthesized and characterized. Electron donating substituents at the *para* pyridine position (R', Figure 4.2) increase the intramolecular coordination. The amount of diamagnetic *cis* isomer is drastically reduced. Surprisingly, the stronger association gives rise to improved PSSs upon irradiation with 500 nm (up to >95% *cis* isomer) although the UV-vis spectrum remains unchanged. This fact underlines the involvement of the coordination in the isomerization process. 100,000 switching cycles were performed without any sign of fatigue. The relaxivities of the investigated RPs were determined in DMSO. The parent system **7** can be switched between $R_1 = 0.03\,\mathrm{mM^{-1}s^{-1}}$ (*trans* isomer) and $R_1 = 0.16\,\mathrm{mM^{-1}s^{-1}}$ (*cis* isomer). This relative difference is higher than of any activatable Gd CA. Although the absolute value of the MRI active *cis* isomer is smaller by the factor 24 compared to Gd-DOTA (**1**) (Figure 1.4),[25] the effect is significant and can be visualized by MRI. Even the improved switching of the RP derivatives **8** and **9** caused by the electron donating substituents at the *para* pyridine position (Me and OMe) can be monitored (Figure 4.2).

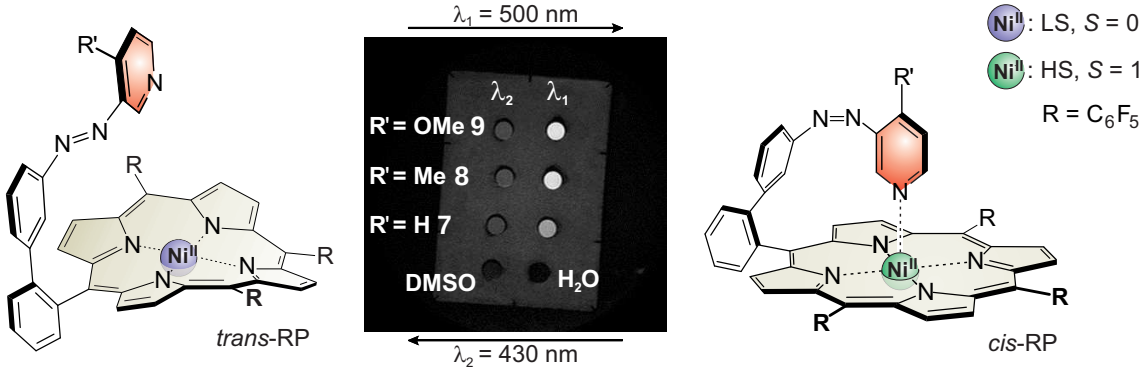

Figure 4.2: MRI contrast switching (3 T) with the RPs (3 mmol l^{-1}) is more efficient with an electron-donating substituent at the *para* pyridine position (R').

To prove that an *in vivo* application may be possible, the contrast switching was directly observed by MRI. For this purpose the irradiation of RP **7** was performed inside a MRI scanner by using an optical fiber. The switching of the MRI contrast over time was clearly visible and monitored in a sequence of MR images. It is the first example of a fully reversible photoswitching of MRI contrast.

JACS
JOURNAL OF THE AMERICAN CHEMICAL SOCIETY
Communication
pubs.acs.org/JACS

Photoswitchable Magnetic Resonance Imaging Contrast by Improved Light-Driven Coordination-Induced Spin State Switch

Marcel Dommaschk,[†] Morten Peters,[†] Florian Gutzeit,[†] Christian Schütt,[†] Christian Näther,[‡] Frank D. Sönnichsen,[†] Sanjay Tiwari,[§] Christian Riedel,[§] Susann Boretius,[§] and Rainer Herges*[,†]

[†]Otto-Diels-Institut für Organische Chemie, Christian-Albrechts-Universität, Otto-Hahn-Platz 4, 24098 Kiel, Germany
[‡]Institut für Anorganische Chemie, Christian-Albrechts-Universität, Otto-Hahn-Platz 6/7, 24098 Kiel, Germany
[§]Clinic for Radiology and Neuroradiology, Arnold Heller Straße 3, 24105 Kiel, Germany

Web-Enhanced Feature *Supporting Information*

ABSTRACT: We present a fully reversible and highly efficient on−off photoswitching of magnetic resonance imaging (MRI) contrast with green (500 nm) and violet-blue (435 nm) light. The contrast change is based on intramolecular light-driven coordination-induced spin state switch (LD-CISSS), performed with azopyridine-substituted Ni-porphyrins. The relaxation time of the solvent protons in 3 mM solutions of the azoporphyrins in DMSO was switched between 3.5 and 1.7 s. The relaxivity of the contrast agent changes by a factor of 6.7. No fatigue or side reaction was observed, even after >100 000 switching cycles in air at room temperature. Electron-donating substituents at the pyridine improve the LD-CISSS in two ways: better photostationary states are achieved, and intramolecular binding is enhanced.

Magnetic resonance imaging (MRI) is one of the most important noninvasive tools in diagnostic medicine. As opposed to other deep tissue imaging modalities such as computer tomography (CT) or positron emission spectroscopy (PET), no ionizing radiation is used in MRI examinations, and no radiation damage is induced. To date, >200 million doses of MRI contrast agents (CAs) have been administered to patients worldwide.[1] Commercially available CAs are mainly gadolinium-(III) chelate complexes.[2] With a spin of $S = {}^{7}/_{2}$, these molecules are highly paramagnetic and decrease the NMR relaxation time of surrounding water protons (or other NMR-active nuclei), which in turn leads to signal enhancement in MRI. The majority of clinically used Gd(III) chelates are strongly hydrophilic; therefore, after intravenous injection, the complexes stay mainly in the blood circuit, leading to high contrast of blood vessels. Since the MRI signal enhancement correlates with the concentration of CAs, they primarily increase anatomical contrast. Further physiological information could be obtained by using responsive or "smart" CAs whose relaxivity (capability of reducing the relaxation time of surrounding nuclei) is controlled by metabolic parameters. The design of responsive CAs reporting on parameters such as temperature, pH, or biochemical markers is a subject of intensive research because they are potentially capable of visualizing the site of a disease in a magnetic resonance image. Research in this field started in the mid-1990s. Most of the approaches since then have been based on Gd(III) complexes whose relaxivity is controlled by controlling water coordination to the Gd^{3+} ion, which is the most efficient relaxation mechanism. A number of CAs were developed that respond to proteins and enzymes,[3] carbohydrates,[4] pH values,[5] and ions like Ca^{2+},[6] Zn^{2+},[7] $Cu^{+/2+}$,[8] and K^{+}.[9] A less intensively investigated stimulus is light. Functionalization of Gd(III) chelates with photochromic spiropyrans gave rise to relaxivity changes of ∼20%.[10] Our approach to the design of responsive and particularly light-controlled CAs is different from the above methods. We are not controlling the access of the solvent molecules to the paramagnetic ion, but we are switching the spin state of transition metal ions between paramagnetic and diamagnetic. Whereas a Gd complex in the "off" state, with a completely filled coordination sphere blocking water access, still exhibits a residual relaxivity by outer-sphere relaxation (through-space magnetic dipole interaction), a diamagnetic transition metal complex with $S = 0$ is completely MRI silent. Thus, spin state switching offers the potential to achieve a higher efficiency in relaxivity control. Contrast switching is very important in interventional radiology (catheter-based surgery under imaging control).[11] The change in contrast so far is obtained by administering additional CAs each time this is required. After multiple injections, the CAs accumulate in the bloodstream to a level where they are harmful, and the contrast change is gradually lost. Light-sensitive CAs have the advantages that they need be administered only once and the contrast can be switched rapidly via an optical fiber.

Recently, we developed a very efficient system for switching the spin state of Ni^{2+} complexes between diamagnetic ($S = 0$) and paramagnetic ($S = 1$) with light of two different wavelengths.[12] We now present a systematic improvement of the effect and demonstrate that it can be used to switch MRI contrast on and off.

Addition of axial ligands to a solution of Ni-porphyrins results in a coordination-induced spin state switch (CISSS).[13] Upon increasing the coordination number (CN) from CN = 4 (no axial ligand, square planar, $S = 0$) to CN = 5 (one axial ligand, square pyramidal, $S = 1$) or CN = 6 (two axial ligands, square bipyramidal, $S = 1$), the Ni^{2+} ion is switched from diamagnetic (contrast off) to paramagnetic (contrast on). To achieve light-controlled addition and removal of axial ligands, we use a

Received: January 29, 2015
Published: April 27, 2015

DOI: 10.1021/jacs.5b00929
J. Am. Chem. Soc. 2015, 137, 7552−7555

photochromic azopyridine covalently attached to a Ni-porphyrin. The geometry is designed in such a way that the pyridine unit coordinates to the Ni ion if the azo group is in the *cis* configuration; however, intramolecular coordination is not possible in the *trans* form. Light of two different wavelengths is used to isomerize the azo group and to lift the pyridine ring up and down. For obvious reasons, we named this approach the "record player" design, and the process is called light-driven, coordination-induced spin state switch (LD-CISSS). To achieve maximum efficiency in MRI contrast switching, every step in the cascade of events must be optimized: photoisomerization → coordination change → spin switch → MRI contrast change.

Even a perfect photoconversion between *trans* and *cis* isomers does not imply a complete change in CN. Incomplete intramolecular binding in the *cis* form, and intermolecular coordination of the *trans* isomer, particularly at higher concentrations, limit the efficiency. Previous work on our prototype system showed that the intramolecular coordination of the *cis* configuration is not complete.[11a] Obviously, there is a nonbinding conformation of the *cis* isomer with the azopyridine unit pointing away from the porphyrin ring that is in fast equilibrium (on the NMR time scale) with the binding conformation (Figure 1).[11b,12] It is known that the association

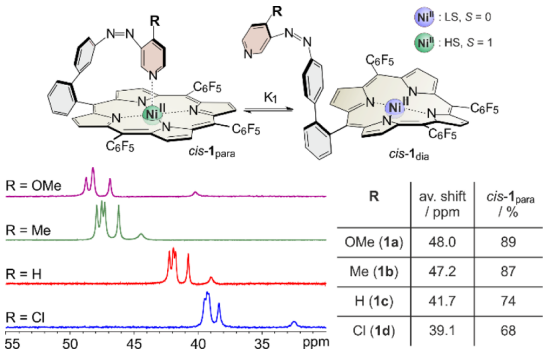

R	av. shift / ppm	*cis*-$\mathbf{1}_{para}$ / %
OMe (**1a**)	48.0	89
Me (**1b**)	47.2	87
H (**1c**)	41.7	74
Cl (**1d**)	39.1	68

Figure 1. Equilibrium between the coordinated *cis*-$\mathbf{1}_{para}$ and the non-coordinated form *cis*-$\mathbf{1}_{dia}$ (top). From the chemical shifts of the pyrrole protons (average shift) in acetone-d_6 (bottom left), the percentage of paramagnetic Ni^{2+} (*cis*-$\mathbf{1}_{para}$) was calculated (bottom right).

constant of 4-substituted pyridines follows a Hammett relationship.[13c] To improve the intramolecular coordination, we therefore introduced electron-donating groups (Me and OMe) at the 4-position of the pyridine unit (for syntheses, see the Supporting Information (SI)).

To quantify intramolecular binding, the chemical shifts of pyrrole protons in the ^{1}H NMR spectra of **1a–d** were compared. We previously showed that coordination and de-coordination of axial ligands in Ni-porphyrins is fast on the NMR time scale. The chemical shift of the pyrrole protons of record player **1c** in non-coordinating solvents is 8.9 and 53 ppm in pure pyridine-d_5 (complete axial coordination). Thus, the average chemical shift is an accurate measure of the ratio of diamagnetic and paramagnetic Ni-porphyrins in solution. Acetone-d_6 was chosen as the solvent for our experiments because of its low coordination power as an axial ligand and the high solubility of **1a–d** in acetone (Figure 1).

The amount of paramagnetic *cis* isomer (*cis*-$\mathbf{1}_{para}$) depends strongly on the 4-pyridine substituent (R). Electron-donating groups increase the amount of *cis*-$\mathbf{1}_{para}$ drastically (from 74% for R = H to 89% for R = OMe). Electron-withdrawing groups (R = Cl) have a contrary effect (Figure 1). Thus, the efficiency of switching to the paramagnetic state is strongly improved by introducing the OMe group at the 4-position of the pyridine.

Obviously the pyridine substituent affects the axial binding to the Ni-porphyrin, but we were surprised to observe an improved photochemical *trans*/*cis* conversion as well. Irradiation of the *trans* isomers with 500 nm light (Q-bands of *trans* azoporphyrin **1a–d**: 523 and 557 nm) is most efficient to convert the *trans* to the *cis* isomer. This is surprising because the $\pi-\pi^*$ excitation that induces *trans*/*cis* isomerization in azobenzenes and azopyridines has a much shorter wavelength (~320 nm). The isomerization mechanism in our azoporphyrins obviously is completely different from the usual azobenzene isomerization pathway. Recently, a theoretical investigation suggested an excitation of the porphyrin and a subsequent thermal isomerization of the azopyridine unit.[14] To determine the *trans*/*cis* conversion rate, we used ^{1}H NMR spectroscopy. The protons on the phenyl ring in a position *meta* to the azo group resonate between 6.5 and 6.8 ppm for all four derivatives. Signals for *cis* and *trans* isomer are well separated, so the *trans*/*cis* ratio could be determined by integration of the corresponding signals (see SI). Although the *cis* isomer has decreased ^{1}H relaxation times due to its paramagnetism, the integral is still representative of the amount of isomers, as demonstrated by comparison with external signals (see SI). Photochemical conversion of the *trans* to the *cis* isomer (Figure 2) follows the same trend as the coordination of the *cis*

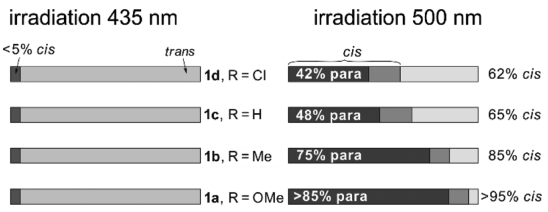

Figure 2. Photostationary states (% *cis* isomer) and percentage of paramagnetic Ni ions upon irradiation of solutions of **1a–d** in acetone-d_6 at 20 °C with 435 and 500 nm light. The *cis*/*trans* ratio and the percentage of paramagnetic Ni ions were determined by NMR spectroscopy (for details see text).

isomer (Figure 1). Upon irradiation with 500 nm light, the photostationary state increases from 62% (R = Cl) to >95% (R = OMe) conversion to the *cis* form. Back-reaction to the *trans* form upon irradiation with 435 nm light is quantitative within the detection limit of NMR (<5% remaining *cis*). Thus, overall conversion from the diamagnetic to the paramagnetic state improved considerably upon introduction of the methoxy substituent (**1a**, 85%) compared to the parent system (**1c**, 48%).

The systems were tested regarding their long-term switching stability. The methoxy-substituted derivative **1a** does not exhibit any fatigue after >100 000 switching cycles at room temperature under air (Figure 3). To test the stability of compounds **1a–c** in a biologically relevant environment, we treated them with a 10 mM solution of glutathione in acetonitrile/PBS buffer (1:1). We observed no reduction of the azo function and no degradation of the switching efficiency, which are requirements for in vivo applications.[15]

Crystals of the *cis* isomer of **1b** (R = Me) suitable for X-ray structure determination were obtained (Figure 4, left). The Ni center is complexed in a distorted octahedral coordination

DOI: 10.1021/jacs.5b00929
J. Am. Chem. Soc. 2015, 137, 7552–7555

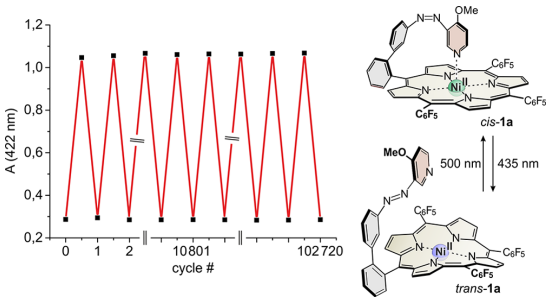

Figure 3. Long-term switching stability of **1a** (5.0 μM, MeCN, 20 °C) during alternating irradiation with 500 and 435 nm light. The UV–vis absorption at 422 nm is plotted as a function of the number of switching cycles.

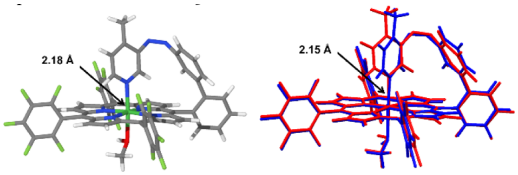

Figure 4. Crystal structure of *cis*-**1b** (left) and overlay of the crystal structure (red) and calculated structure (blue, PBE/SVP) (right).

geometry. The equatorial plane is formed by the porphyrin N-atoms with bond lengths ranging from 2.03 to 2.05 Å. The axial positions are occupied by the pyridine N-atom of the azopyridine and the O-atom of a methanol molecule, with longer distances of Ni–N = 2.18 Å and Ni–O = 2.27 Å. The Ni center is situated almost exactly in the porphyrin plane with a deviation of 0.08 Å. The X-ray structure is in good agreement with the DFT (PBE/SVP) optimized structure (Figure 4, right). The root-mean-square deviation is 0.31 Å (for details see SI).

The application of the record player molecules **1a–c** as light-switchable CAs was investigated by MRI (3 and 7 T) and independently by NMR relaxation time measurements (200 MHz NMR). Switching between the diamagnetic and paramagnetic states in a homogeneous solution of **1a–d** allows us to switch the relaxation time of the solvent protons and thus to switch MRI contrast using violet-blue and green light. Figure 5 shows the MRI contrast of 3 mM solutions of **1a–d** in DMSO after irradiation with 435 and 500 nm light. As expected, the increased rate of conversion to the paramagnetic state (**1c** < **1b** < **1a**) also leads to an increase of the signal in the MRI images (Figure 5). The diamagnetic *trans* state is MRI silent in all cases.

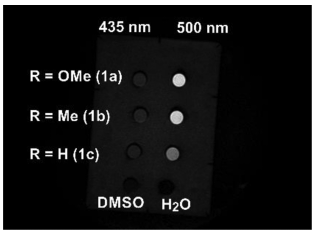

Figure 5. 3 T magnetic resonance image of 3 mM solutions of **1a–c** irradiated with 435 and 500 nm light. For details, see the SI.

The efficiency of paramagnetic ions for shortening the relaxation time of solvent protons, normalized by their concentration, is called relaxivity (R in mM^{-1} s^{-1}). R_1 and R_2 are the relaxivities corresponding to the longitudinal (T_1) and transverse (T_2) relaxation times. In the following we present results only for T_1 and R_1 because there are no significant differences to T_2 and R_2 in homogeneous solutions (see SI). The R_1 relaxivity was determined by relaxation time measurements at different CA concentrations. The experiments were performed with **1a–c** in a mixture of 99% DMSO-d_6 and 1% DMSO in a 200 MHz (4.7 T) NMR spectrometer (Table 1 and SI).

Table 1. Relaxivities of 1a–c in a Mixture of 99% DMSO-d_6 and 1% DMSO Measured in a 200 MHz NMR Spectrometer

	R_1/mM^{-1} s^{-1}	
R (compd)	at 500 nm	at 435 nm
MeO (**1a**)	0.159	0.045
Me (**1b**)	0.155	0.029
H (**1c**)	0.121	0.0.18

The relaxivity of the *trans* isomers (**1a–c**) after irradiation with 500 nm light increased by factors of 3.5, 5.3, and 6.7. Upon irradiation with 435 nm, the relaxivity drastically decreased again but was different from zero, probably due to some residual paramagnetism from intermolecular coordination. The absolute value of R_1 is lower by a factor of ~25 compared to that of standard Gd-CAs, mainly due to the lower magnetic moment (Ni(II), S = 1; Gd(III); S = 7/2). We determined relaxivity of gadobutrol in DMSO-d_6 to be 3.75 mM^{-1} s^{-1}, good agreement with the literature (see SI).[16] To realize the switching in a physiological medium, we attach glycerol dendrimers to the *meso*-pentafluorophenyl substituents by nucleophilic aromatic substitution. It was already shown that this concept is applicable for symmetric porphyrins.[13d] We performed cell tests and proved that the dendronized water-soluble Ni-porphyrin does not influence cell activity at physiologically relevant concentrations (see SI).

As a further step toward application of the switchable CAs, we performed the photoswitching in a MRI scanner to monitor the magnetic switching in situ. Light of 530 and 405 nm was applied by an optical fiber coupled to monochromatic LEDs (light intensity at the fiber outlet ~35 and 75 mW). A coaxial NMR tube with a 3 mM solution of record player **1c** in DMSO was irradiated. The on–off switching of the MRI constrast is shown in Figure 6 (right) (see also the accompanying video).

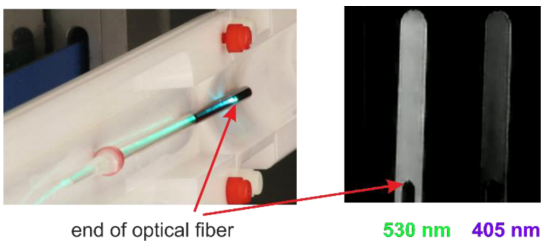

Figure 6. Experimental setup for the contrast switching in a 7 T MRI scanner (left). A 3 mM solution of **1c** was irradiated with 530 and 405 nm light, and MRI images were recorded after irradiation (right). A video that demonstrates MRI contrast switching is also available.

DOI: 10.1021/jacs.5b00929
J. Am. Chem. Soc. 2015, 137, 7552–7555

In summary, we have developed a highly efficient, light-responsive molecular magnetic switch. Green (500 nm) and violet-blue (435 nm) light was used to switch the relaxation time of solvent protons in a 3 mM solution by a factor of >2, and the relaxivity (R_1) of the contrast agent changes by a factor up to 6.7. The change in contrast is clearly visible in a clinical MRI scanner. Contrast control is based on a cascade of events that includes photoisomerization of an azopyridine ligand, coordination change at Ni^{2+}, spin switch, and MRI contrast change. The system was optimized in such a way that each step is close to quantitative. No side reaction or fatigue was detected after >100 000 switching cycles. The metastable *cis* form (contrast "on" state) has a half-life of >1 year at room temperature. Our light-driven coordination-induced spin state switch approach has the potential to provide the basis for the development of a number of interesting applications, including the design of temperature- or pH-responsive contrast agents for MRI. The latter would be useful to detect tumors because they exhibit a higher temperature and a lower pH than surrounding tissue.

■ ASSOCIATED CONTENT

Ⓢ Supporting Information

Experimental procedures and spectral data, details of computational studies, and crystallographic data. The Supporting Information is available free of charge on the ACS Publications website at DOI: 10.1021/jacs.5b00929.

Ⓦ Web-Enhanced Feature

A video that demonstrates MRI contrast switching is available in the online version of this paper.

■ AUTHOR INFORMATION

Corresponding Author

*rherges@oc.uni-kiel.de

Notes

The authors declare no competing financial interest.

■ ACKNOWLEDGMENTS

The authors gratefully acknowledge funding from the collaborative research center SFB 677 Function by Switching. High field MRI measurements were performed at the Molecular Imaging North Competence Center, CAU, Kiel.

■ REFERENCES

(1) (a) Kulaksiz, S.; Bau, M. *Appl. Geochem.* **2011**, *26*, 1877. (b) Hao, D.; Ai, T.; Goerner, F.; Hu, X.; Runge, V. M.; Tweedle, M. *J. Magn. Reson. Imaging* **2012**, *36*, 1060.

(2) (a) Aime, S.; Botta, M.; Fasano, M.; Terreno, E. *Acc. Chem. Res.* **1999**, *32*, 941. (b) Caravan, P.; Ellison, J. J.; McMurry, T. J.; Lauffer, R. B. *Chem. Rev.* **1999**, *99*, 2293.

(3) (a) Touti, F.; Maurin, P.; Hasserodt, J. *Angew. Chem., Int. Ed.* **2013**, *52*, 4654. (b) Louie, A. Y.; Huber, M. M.; Ahrens, E. T.; Rothbacher, U.; Moats, R.; Jacobs, R. E.; Fraser, S. E.; Meade, T. J. *Nat. Biotechnol.* **2000**, *18*, 321. (c) Duimstra, J. A.; Femia, F. J.; Meade, T. J. *J. Am. Chem. Soc.* **2005**, *127*, 12847. (d) Querol, M.; Chen, J. W.; Weissleder, R.; Bogdanov, A. *Org. Lett.* **2005**, *7*, 1719. (e) Giardiello, M.; Lowe, M. P.; Botta, M. *Chem. Commun.* **2007**, 4044. (f) Hanaoka, K.; Kikuchi, K.; Terai, T.; Komatsu, T.; Nagano, T. *Chem.—Eur. J.* **2008**, *14*, 987. (g) Mizukami, S.; Takikawa, R.; Sugihara, F.; Hori, Y.; Tochio, H.; Wälchli, M.; Shirakawa, M.; Kikuchi, K. *J. Am. Chem. Soc.* **2008**, *130*, 794.

(4) (a) Trokowski, R.; Zhang, S.; Sherry, A. D. *Bioconjugate Chem.* **2004**, *15*, 1431. (b) Aime, S.; Delli Castelli, D.; Fedeli, F.; Terreno, E. *J. Am. Chem. Soc.* **2002**, *124*, 9364.

(5) (a) Hall, J.; Häner, R.; Aime, S.; Botta, M.; Faulkner, S.; Parker, D.; de Sousa, A. S. *New J. Chem.* **1998**, *22*, 627. (b) Aime, S.; Crich, S. G.; Botta, M.; Giovenzana, G.; Palmisano, G.; Sisti, M. *Chem. Commun.* **1999**, 1577. (c) Zhang, S.; Wu, K.; Sherry, A. D. *Angew. Chem.* **1999**, *111*, 3382. (d) Lowe, M. P.; Parker, D.; Reany, O.; Aime, S.; Botta, M.; Castellano, G.; Gianolio, E.; Pagliarin, R. *J. Am. Chem. Soc.* **2001**, *123*, 7601. (e) Woods, M.; Kiefer, G. E.; Bott, S.; Castillo-Muzquiz, A.; Eshelbrenner, C.; Michaudet, L.; McMillan, K.; Mudigunda, S. D. K.; Ogrin, D.; Tircsó, G.; Zhang, S.; Zhao, P.; Sherry, A. D. *J. Am. Chem. Soc.* **2004**, *126*, 9248. (f) Tóth, E.; Bolskar, R. D.; Borel, A.; González, G.; Helm, L.; Merbach, A. E.; Sitharaman, B.; Wilson, L. J. *J. Am. Chem. Soc.* **2005**, *127*, 799. (g) De Leon-Rodriguez, L. M.; Lubag, A. J. M.; Malloy, C. R.; Martinez, G. V.; Gillies, R. J.; Sherry, A. D. *Acc. Chem. Res.* **2009**, *42*, 948.

(6) (a) Li, W.-h.; Fraser, S. E.; Meade, T. J. *J. Am. Chem. Soc.* **1999**, *121*, 1413. (b) Li, W.-h.; Parigi, G.; Fragai, M.; Luchinat, C.; Meade, T. J. *Inorg. Chem.* **2002**, *41*, 4018. (c) Dhingra, K.; Fousková, P.; Angelovski, G.; Maier, M. E.; Logothetis, N. K.; Tóth, E. *J. Biol. Inorg. Chem.* **2007**, *13*, 35. (d) Angelovski, G.; Fouskova, P.; Mamedov, I.; Canals, S.; Toth, E.; Logothetis, N. K. *ChemBioChem* **2008**, *9*, 1729. (e) Dhingra, K.; Maier, M. E.; Beyerlein, M.; Angelovski, G.; Logothetis, N. K. *Chem. Commun.* **2008**, 3444. (f) Mishra, A.; Fousková, P.; Angelovski, G.; Balogh, E.; Mishra, A. K.; Logothetis, N. K.; Tóth, E. *Inorg. Chem.* **2008**, *47*, 1370.

(7) (a) Hanaoka, K.; Kikuchi, K.; Urano, Y.; Nagano, T. *J. Chem. Soc., Perkin Trans. 2* **2001**, 1840. (b) Major, J. L.; Parigi, G.; Luchinat, C.; Meade, T. J. *Proc. Natl. Acad. Sci. U.S.A.* **2007**, *104*, 13881. (c) Major, J. L.; Boiteau, R. M.; Meade, T. J. *Inorg. Chem.* **2008**, *47*, 10788.

(8) Que, E. L.; Gianolio, E.; Baker, S. L.; Wong, A. P.; Aime, S.; Chang, C. J. *J. Am. Chem. Soc.* **2009**, *131*, 8527.

(9) Hifumi, H.; Tanimoto, A.; Citterio, D.; Komatsu, H.; Suzuki, K. *Analyst* **2007**, *132*, 1153.

(10) (a) Tu, C.; Louie, A. Y. *Chem. Commun.* **2007**, 1331. (b) Tu, C.; Osborne, E. A.; Louie, A. Y. *Tetrahedron* **2009**, *65*, 1241.

(11) (a) Herges, R.; Jansen, O.; Tuczek, F.; Venkatamarani, S. Molecular Switch. Patent WO 2012022299 A1, Feb 23, 2012. (b) Herges, R.; Jansen, O.; Tuczek, F.; Venkatamarani, S. Photosensitive metal porphyrin complexes with pendant photoisomerizable chelate arm as photochromic molecular switches undergoing photoinduced spin transition. Patent DE 102010034 A1, Feb 16, 2012.

(12) (a) Venkataramani, S.; Jana, U.; Dommaschk, M.; Sönnichsen, F. D.; Tuczek, F.; Herges, R. *Science* **2011**, *331*, 445. (b) Dommaschk, M.; Schütt, C.; Venkataramani, S.; Jana, U.; Nather, C.; Sonnichsen, F. D.; Herges, R. *Dalton Trans.* **2014**, *43*, 17395.

(13) (a) Thies, S.; Sell, H.; Bornholdt, C.; Schütt, C.; Köhler, F.; Tuczek, F.; Herges, R. *Chem.—Eur. J.* **2012**, *18*, 16358. (b) Thies, S.; Sell, H.; Schütt, C.; Bornholdt, C.; Näther, C.; Tuczek, F.; Herges, R. *J. Am. Chem. Soc.* **2011**, *133*, 16243. (c) Thies, S.; Bornholdt, C.; Köhler, F.; Sönnichsen, F. D.; Näther, C.; Tuczek, F.; Herges, R. *Chem.—Eur. J.* **2010**, *16*, 10074. (d) Dommaschk, M.; Gutzeit, F.; Boretius, S.; Haag, R.; Herges, R. *Chem. Commun.* **2014**, *50*, 12476.

(14) Alcover-Fortuny, G.; de Graaf, C.; Caballol, R. *Phys. Chem. Chem. Phys.* **2015**, *17*, 217.

(15) (a) Samanta, S.; McCormick, T. M.; Schmidt, S. K.; Seferos, D. S.; Woolley, G. A. *Chem. Commun.* **2013**, *49*, 10314. (b) Yang, Y.; Hughes, R. P.; Aprahamian, I. *J. Am. Chem. Soc.* **2014**, *136*, 13190. (c) Samanta, S.; Beharry, A. A.; Sadovski, O.; McCormick, T. M.; Babalhavaeji, A.; Tropepe, V.; Woolley, G. A. *J. Am. Chem. Soc.* **2013**, *135*, 9777. (d) Kosower, E. M.; Kanety-Londner, H. *J. Am. Chem. Soc.* **1976**, *98*, 3001.

(16) (a) Vogler, H.; Platzek, J.; Schuhmann-Giampieri, G.; Frenzel, T.; Weinmann, H.-J.; Radbüchel, B.; Press, W.-R. *Eur. J. Radiol.* **1995**, *21*, 1. (b) Fenchel, M.; Franow, A.; Martirosian, P.; Engels, M.; Kramer, U.; Stauder, N. I.; Helber, U.; Vogler, H.; Claussen, C. D.; Miller, S. *Br. J. Radiol.* **2007**, *80*, 884.

DOI: 10.1021/jacs.5b00929
J. Am. Chem. Soc. 2015, 137, 7552−7555

Photoswitchable MRI contrast by improved LD-CISSS.

Marcel Dommaschk, Morten Peters, Florian Gutzeit, Christian Schütt, Christian Näther, Frank D. Sönnichsen, Christian Riedel, Susann Boretius and Rainer Herges

Table of Contents

I Relaxivity and MRI measurements

The MR-image in Figure 6 and the supporting video were recorded with a 7 T MRI spectrometer (ClinScan 70/30 USR, Bruker Biospin, Germany) with a FLASH (Fast Low Angle Shot Magnetic Resonance) sequence (3D, TE/TR = 1.5/40 ms, flip angle ½ = 5/29°, spatial resolution 177x177 mm2, slice thic kness 1500 mm).

The MR-image in Figure 5 was measured with a 3 T MRI scanner (Achieva 3 T, Phillips, Best, Netherlands) with a T_1-weighted turbo spin echo sequence

Relaxivities (R_1 and R_2) of **1a**, **1b** and **1c** were determined via NMR spectroscopy (Bruker AC 200) in DMSO-d_6 + 1% DMSO. T_1-relaxation times (T_1) were determined by an inversion recovery pulse sequence. The integral of the DMSO signal was observed as a function of the delay time (Figure S1).

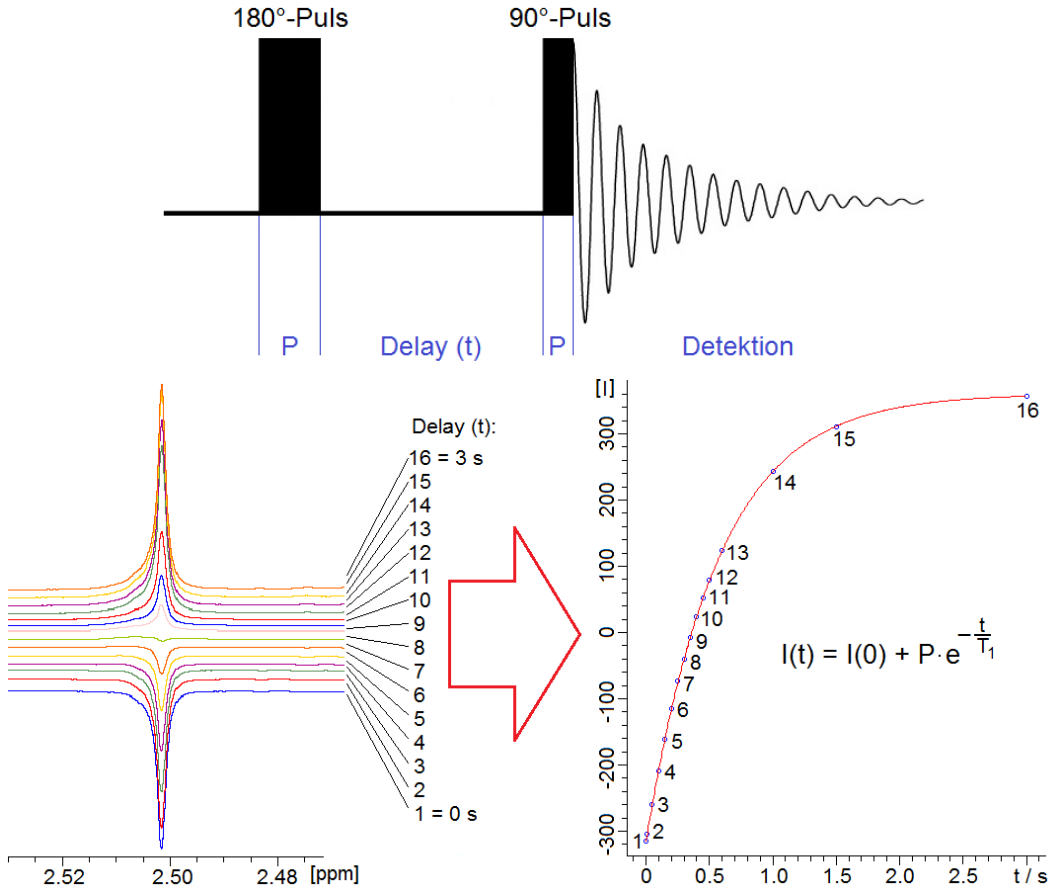

Figure S1: Inversion recovery pulse sequence (top) with the resulting DMSO signals (bottom left) and the exponential fitting for the calculation of T_1 (bottom right). The experiments were performed with 1% DMSO in DMSO-d_6.

T_2-relaxation times (T_2) were determined by a spin echo pulse sequence. The integral of the DMSO signal was observed as a function of the spin echo (n) with an echo time (τ) of 10 ms (Figure S2).

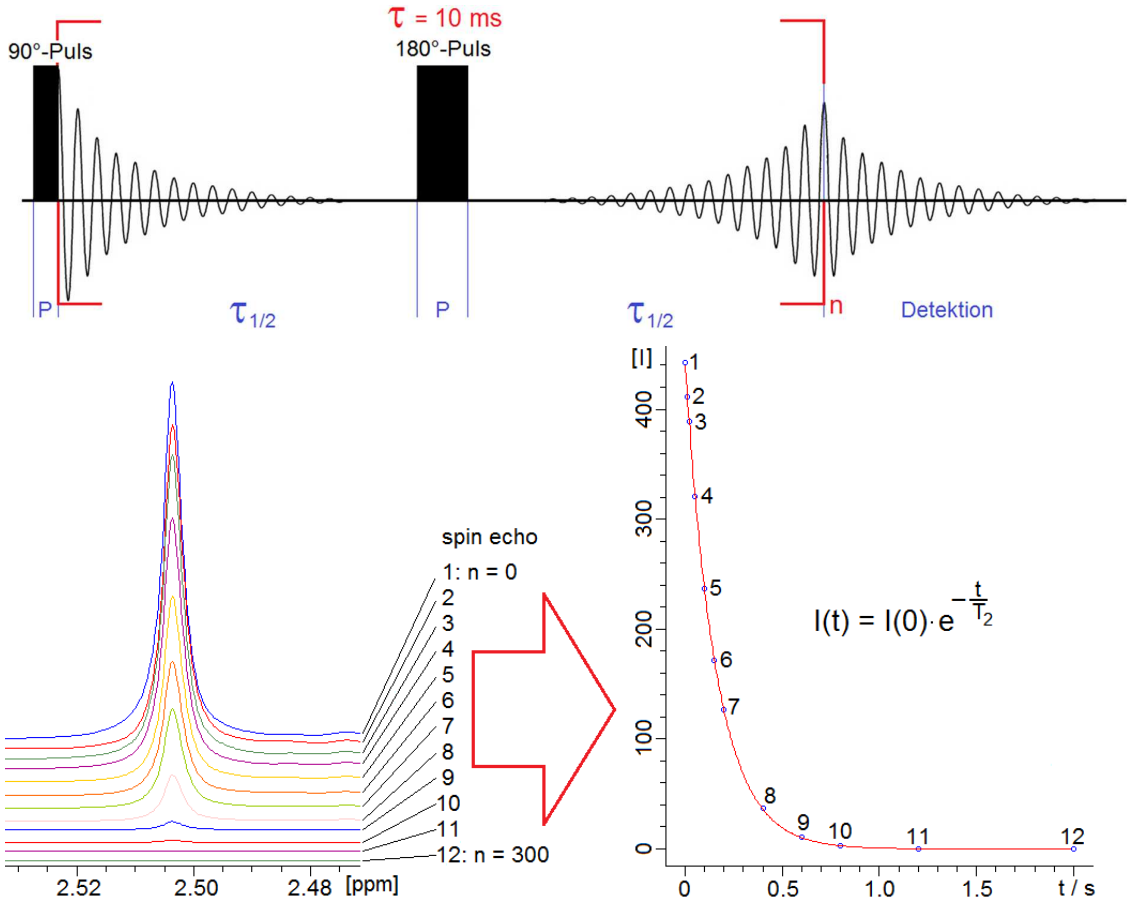

Figure S2: Spin echo pulse sequence (top) with the resulting DMSO signals (bottom left) and the exponential fitting for the calculation of T_2 (bottom right). The experiments were performed with 1% DMSO in DMSO-d_6.

The plot of the relaxation rate ($1/T_1$ or $1/T_2$) versus the concentration of a molecule shows a linear relation. The slope is defined as relaxivity (R_1 and R_2). The relaxivity of record players **1a**, **1b** and **1c** was determined after irradiation with green and blue light (Figure S3).

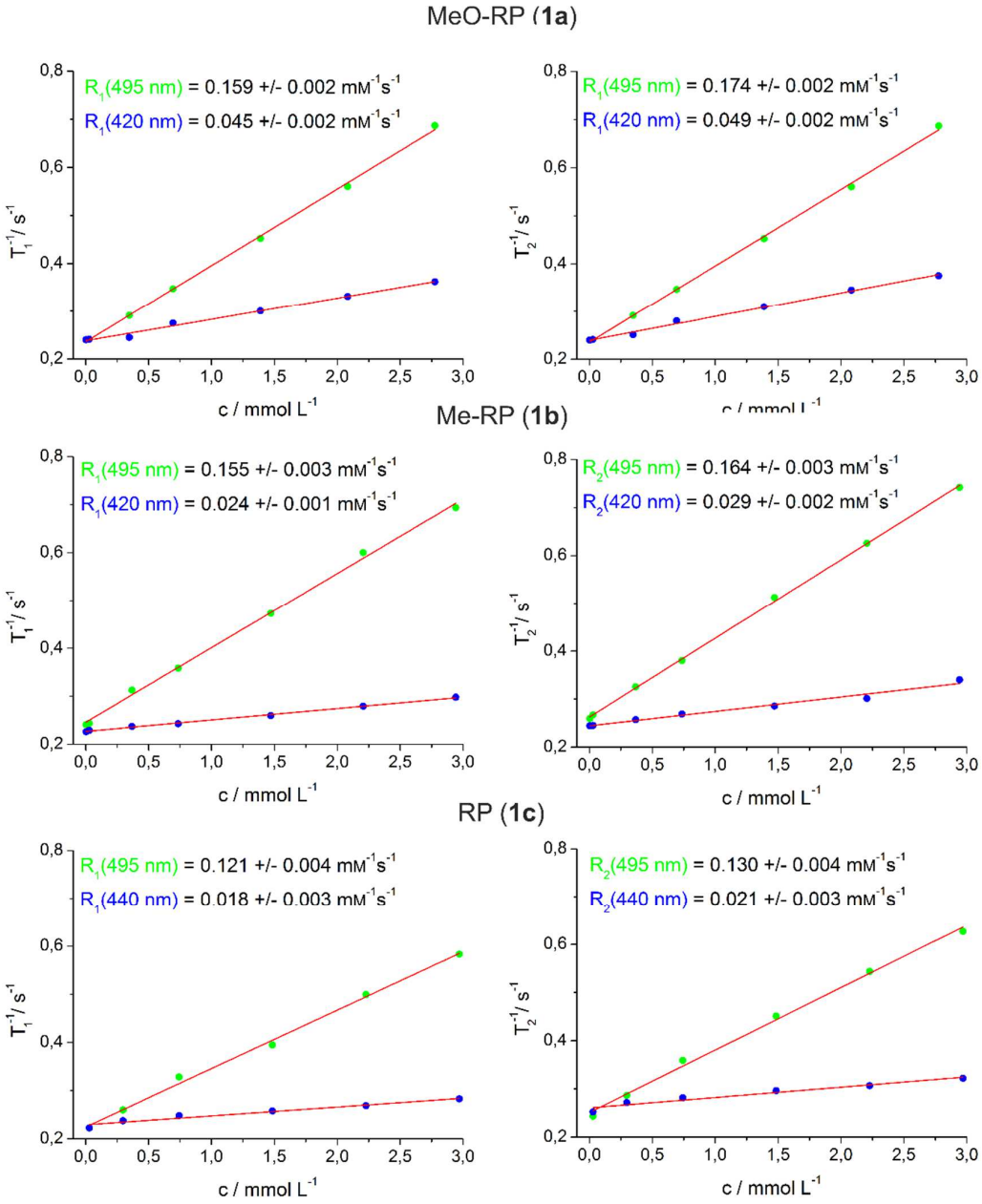

Figure S3: Relaxivity plots (R_1: left, R_2: right) for RPs **1a**, **1b** and **1c**. The relaxation rate (T_1^{-1}, T_2^{-1}) of 1% DMSO in DMSO-d_6 was measured.

Table S1: Relaxivities (R_1 and R_2) of RPs **1a**, **1b** and **17c** after irradiation with 495 nm.

RP	R_1 / mM^{-1}	R_2 / mM^{-1}
MeO-RP (**1a**)	0.159	0.174
Me-RP (**1b**)	0.155	0.164
RP (**1c**)	0.121	0.130

Table S2: Relaxivities (R_1 and R_2) of RPs **17c**, **17d** and **17f** after irradiation with 420 nm[a] or 440 nm[b].

RP	R_1 / mM^{-1}	R_2 / mM^{-1}
MeO-RP (**1a**)[a]	0.045	0.049
Me-RP (**1b**)[a]	0.024	0.029
RP (**1c**)[b]	0.018	0.021

To compare our values with clinically applied contrast agents, we determined the T_1-relaxivity (R_1) of gadobutrol, which is the MRI active Gd-complex in the commercially available Gadovist® (Figure S4). We used the same experimental setup (1% DMSO in DMSO-d_6) as for the record player molecules. We obtained a value of 3.75 mM^{-1}s^{-1} which is in good agreement with values obtained in water of this and similar complexes.[1, 2]

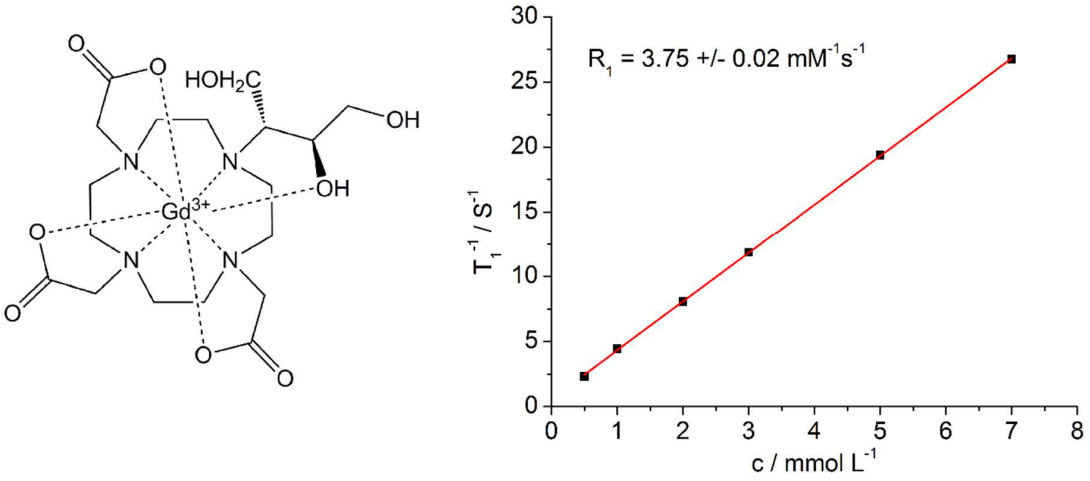

Figure S4: Gadobutrol (left) and its relaxivity plot (R_1). The relaxation rate (T_1^{-1}) of 1% DMSO in DMSO-d_6 was measured.

II Isomerization experiments monitored by UV-vis- and NMR-spectroscopy

The isomerization of RPs can be observed with NMR- and UV-vis spectroscopy. By integration of appropriate signals in ^{1}H-NMR spectrum the *cis-trans*-ratio can be determined.

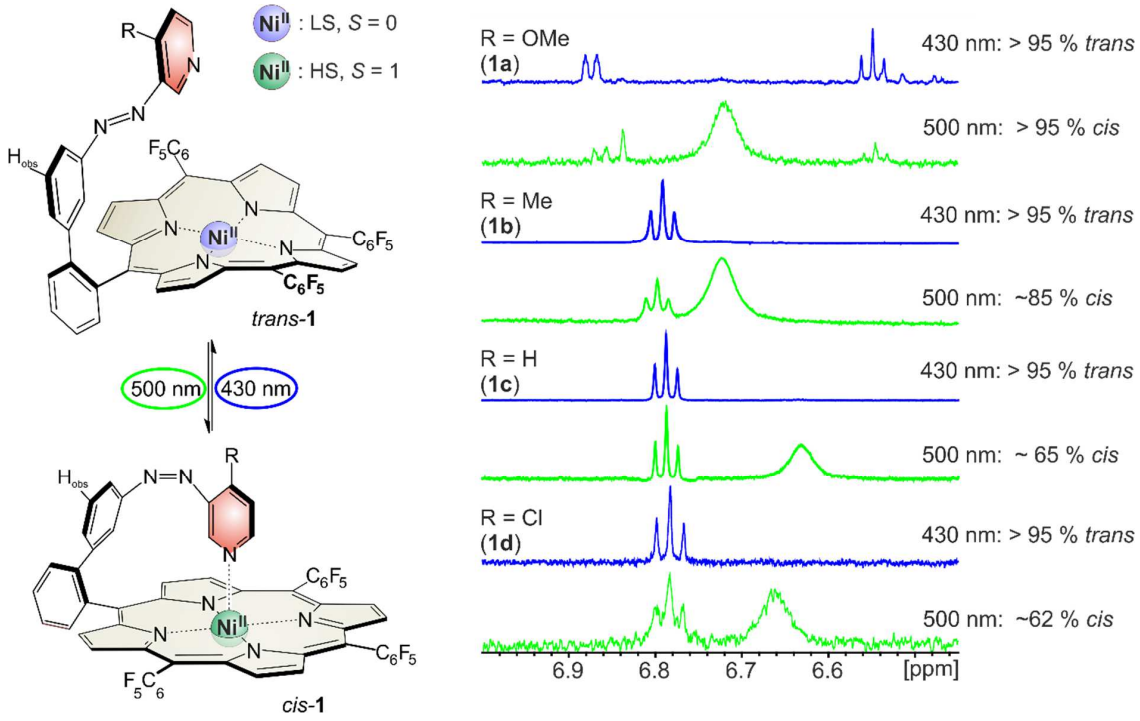

Figure S5: Photo stationary states at 500 and 430 nm of **1a-d** observed by ^{1}H-NMR spectroscopy in acetone-d$_6$. The sharp triplet belongs to H_{obs} of the *trans* isomers and the broad signal to H_{obs} of the *cis* isomers.

Since the protons of the paramagnetic species have drastically reduced relaxation times, it is important to check if the measured integral values represent the amount of the corresponding isomers. For this purpose they have to be compared with an external reference signal, e.g. a solvent signal. Figure S6 shows the ^{1}H NMR spectra of **1c** after irradiation with 430 nm and 500 nm. At 4.36 and 4.35 ppm the signals of the water traces (H_2O and HDO) show up. The water integral should be proportional to the overall integral of H_{obs} (*trans* and *cis*, see Figure S5). But this is not the case. The overall integral after irradiation with 500 nm (higher amount of paramagnetic *cis*-**1c**) is about 5% lower than the integral after irradiation with 430 nm with almost exclusively

diamagnetic *trans*-**1c**. However, the NMR integration underestimates the amount of *cis*-isomer only slightly (< 5%) and therefore is adequate.

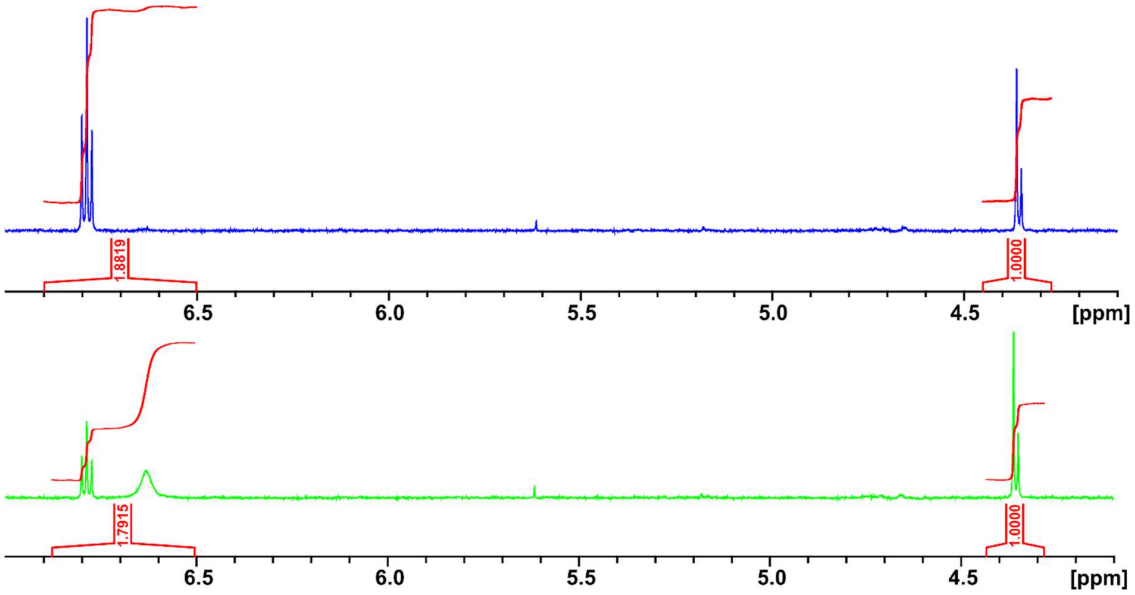

Figure S6: ^{1}H NMR spectrum of **1c** after irradiation with 430 nm (top) and 500 nm (bottom) in acetone-d_6. The overall integral of H_{obs} (*trans*-signal at 6.79 ppm and *cis*-signal at 6.62 ppm) is compared with the water signal (H_2O at 4.36 ppm and HDO at 4.35 ppm) as an external reference.

The UV-vis spectra also provide information about the isomerization. Very characteristic is the bathochromic shift of the Soret band from 405 (diamagnetic) to 421 nm. The absorption at the corresponding wavelengths (405 and 421 nm) provides a quantitative measure of the ratio of diamagnetic and paramagnetic Ni-porphyrin spezies. However, it does not represent the trans/cis ratio because the UV-spectra of the non-coordinated cis and the *trans*-isomer are almost undistiguishable. The porphyrin absorption bands of **1a-d** are almost completely identical. The only difference in the UV-vis spectra can be found between 280 and 350 nm which is due to the $\pi\pi^*$ absorption of the azopyridine. It is reasonable to assume that the substituent in the *para*-pyridine position only influences the azo function and not the porphyrin absorption. After irradiation with 500 nm the differences of UV-vis spectra are larger due to the different photo stationary states of **1a-d**. The λ_{max} of all bands seems to be identical.

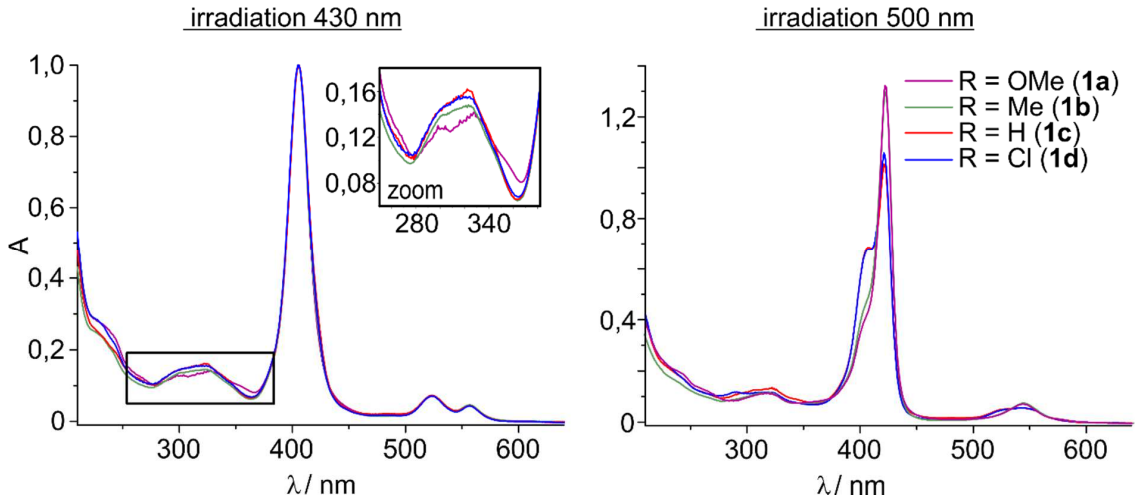

Figure S7: Photo stationary states at 430 nm (left) and 500 nm (right) of **1a-d** measured by UV-vis spectroscopy in acetonitrile.

III Test for stability to glutathione reduction

Compounds **1a**-**1c** (5.9 μM) were incubated (24 h, 27 ℃) in 1:1 acetonitrile: PBS (phosphate buffered saline 1x: 137 mM NaCl, 2 mM KCl, 8 mM Na_2PHO_4, 2 mM KH_2PO_4, pH = 7.4). Isomerization was observed before and after incubation. No reduction of the azo function and no degradation of the switching efficiency could be detected (Figure S8-S10).

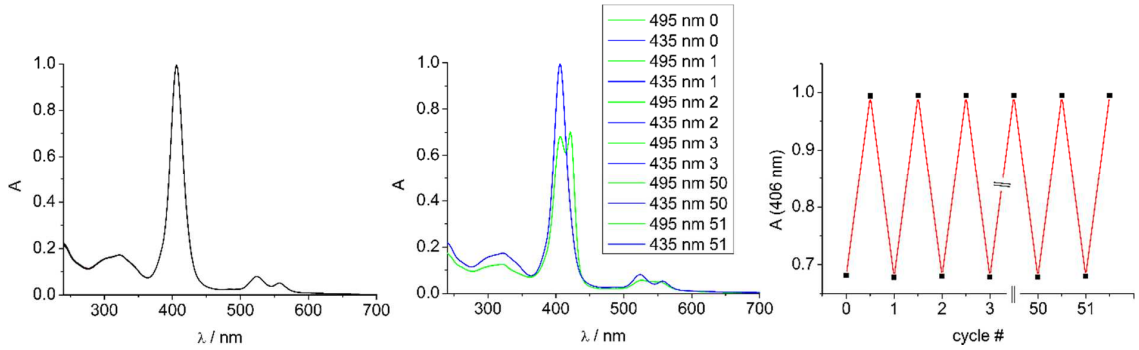

Figure S8: Overlay of 48 UV-vis spectra of **1c** (10 mM glutathione, acetonitrile:PBS = 1:1, 27 ℃) measured every 30 min (left). Switching experiment after 24 h glutathione incubation (middle: UV-vis spectra, right: switching cycles).

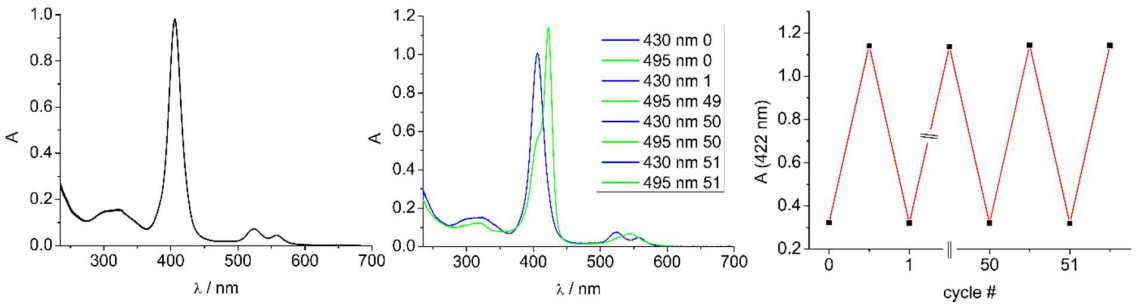

Figure S9: Overlay of 48 UV-vis spectra of **1b** (10 mM glutathione, acetonitrile:PBS = 1:1, 27 ℃) measured every 30 min (left). Switching experiment after 24 h glutathione incubation (middle: UV-vis spectra, right: switching cycles).

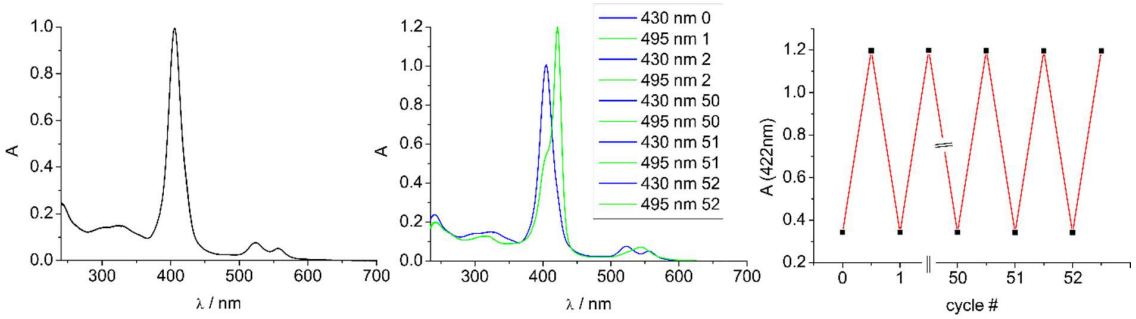

Figure S10: Overlay of 48 UV-vis spectra of **1a** (10 mM glutathione, acetonitrile:PBS = 1:1, 27 ℃) measured every 30 min (left). Switching experiment after 24 h glutathione incubation (middle: UV-vis spectra, right: switching cycles).

IV Synthesis

The porphyrins were prepared via a mixed aldehyde synthesis. Procedures for the parent system (R = H, compounds **1c**, **8c**, **10c** and **17c**) are already published.[3] For the required record player tone arms, we started from amino pyridines **4a**-**4f** which were obtained by reduction of the 3-nitropyridine derivatives **3a**-**3f**. Since **3e** and **3f** are not commercially available, these were synthesized by nitration of the corresponding 4-amino pyridines **2e** and **2f**. **2f** was also obtained by nucleophilic aromatic substitution with pyrrolidine and 4-chloro-3-nitropyridine with a yield of 96 % (experimental section).

Scheme 1. Synthetic route for 3-aminopyridines 4a-4f. Reduction of 3-nitropyridines was carried out with palladium on charcoal [a] or tin(II)chloride [b]. Commercially purchased molecules are labeled with cp.

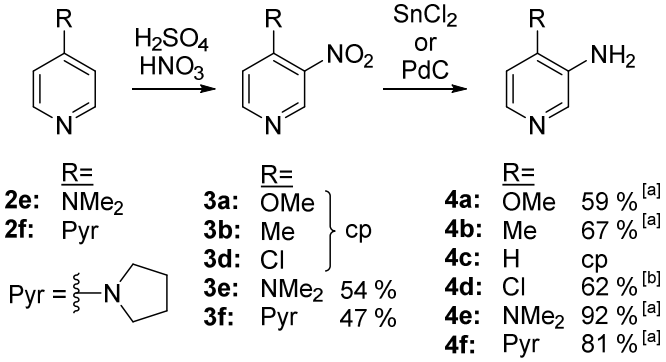

The 4-substituted 3-aminopyridines were utilized for condensation reactions with 1-bromo-3-nitrosobenzene (**7**) which was obtained by reduction of 1-bromo-3-nitrobenzene (**5**) and immediate oxidation of the hydroxylamine **6**. The bromo substituted azopyridines **8a-8f** were obtained in varying yields (Scheme 2).

Scheme 2. Syntheses of azopyridines 8a-8f by condensation reactions.

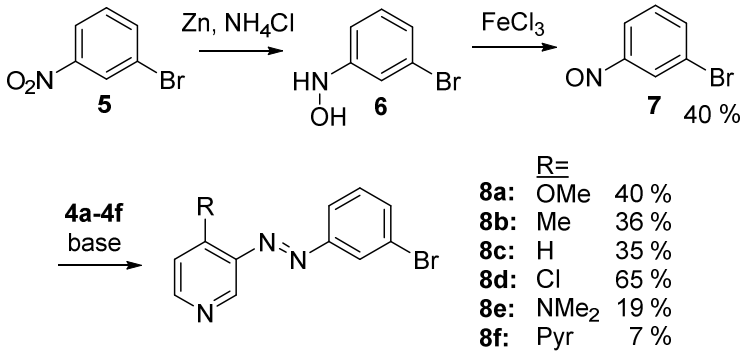

The yields of the condensation reactions increase with electron deficiency of the corresponding amine. This is probably due to the more facile deprotonation of the amino function in more electron deficient 3-aminopyridines. For the generation of larger quantities of the electron rich azo compounds, a different approach was chosen. Electron donating groups can be introduced by nucleophilic aromatic substitution. The electron deficient chloro derivative **8d**, which is obtained with the best yield, can be used as a precursor (Scheme 3).

Scheme 3. Synthesis of azopyridines 8a, 8e, 8f and 8g by nucleophilic aromatic substitution.

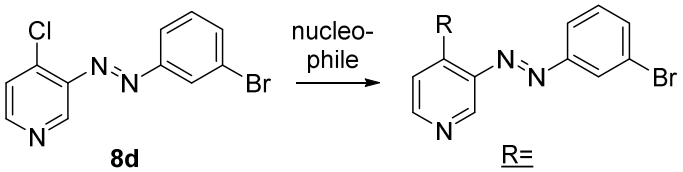

	R=	
8a:	OMe	97 %
8e:	NMe_2	65 %
8f:	Pyr	95 %
8g:	O^{i}Pr	91 %

The record player tone arms were completed by Suzuki cross coupling reaction of azopyridines **8a**-**8g** with the commercially available 2-formylphenyl boronic acid (**9**) (Scheme 4).

Scheme 4. Syntheses of record player tone arms 10a-10g by Suzuki cross coupling reactions.

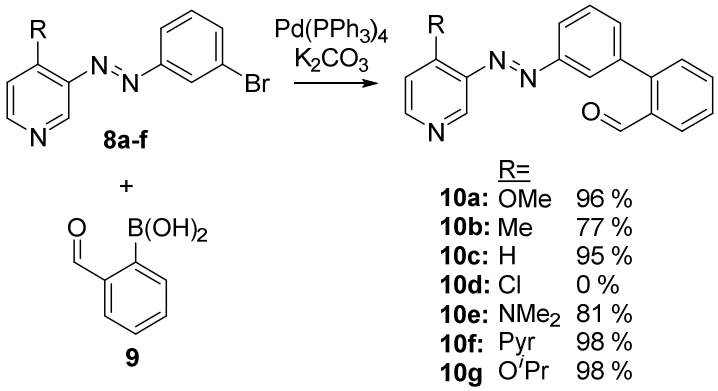

	R=	
10a:	OMe	96 %
10b:	Me	77 %
10c:	H	95 %
10d:	Cl	0 %
10e:	NMe_2	81 %
10f:	Pyr	98 %
10g	O^{i}Pr	98 %

The azopyridine **8d** showed an unprecedented reactivity. Instead of connecting the boronic acid **9** with the phenyl bromine, we observed reaction with the 4-chloropyridine (scheme 5) yielding the 4-phenylpyridine derivative **11**. The cross coupling reaction

with the electron more deficient aromatic halide seems to be preferred. To get access to the chlorine derivative **10d** we had to synthesize the iodinated azopyridine **14** analogue of the bromo derivative **8d** (Scheme 5). Although the 4-chloropyridine substituted record player is not expected to show an improved intramolecular coordination, it may be interesting for functionalization after the porphyrin formation.

Scheme 5. Cross coupling reaction between azopyridine 10d and boronic acid 9 (top) and synthetic route to obtain the chlorinated tone arm 10d (bottom).

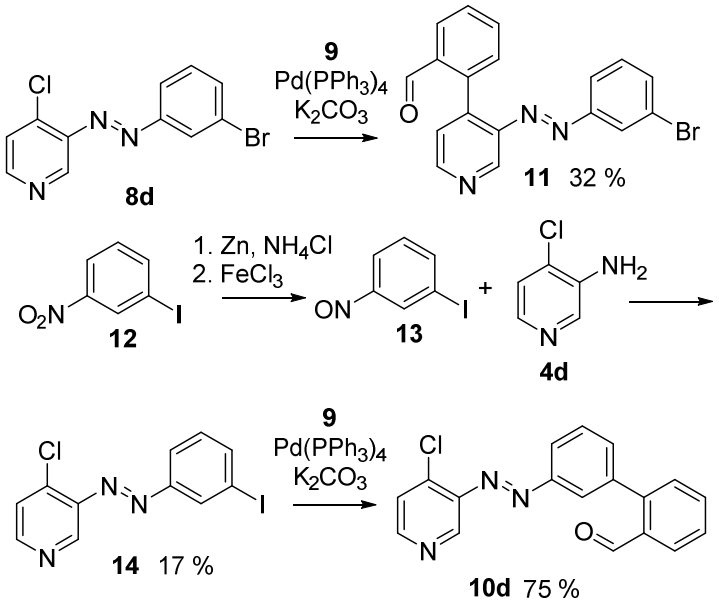

The aldehyde group of azopyridines **10a**-**10g** should react in a mixed aldehyde synthesis to form the desired metal free record player molecules (mf-RPs). Under Lewis acid conditions a macrocycle (MC) with pentafluorobenzaldehyde (**16**) and *meso*-pentafluorophenyl dipyrromethane (**15**) is formed. This MC is oxidized by *p*-chloranil to yield the mf-RP. The symmetric tetrakis-pentafluorophenyl porphyrin and the two-armed porphyrin are side products which cannot be avoided by this synthetic approach. The yields of mf-RPs (**17a**-**17g**) vary substantially and do not follow an obvious trend. The mf-Me-RP (**16d**) was obtained with by far the best yield (14 %). Formation of mf-O^{i}Pr-RP (**16f**) was not observed at all.

Scheme 6. Mixed aldehyde synthesis and nickel insertion to obtain mf-RPs 17a-17f and RPs 1a-1d.

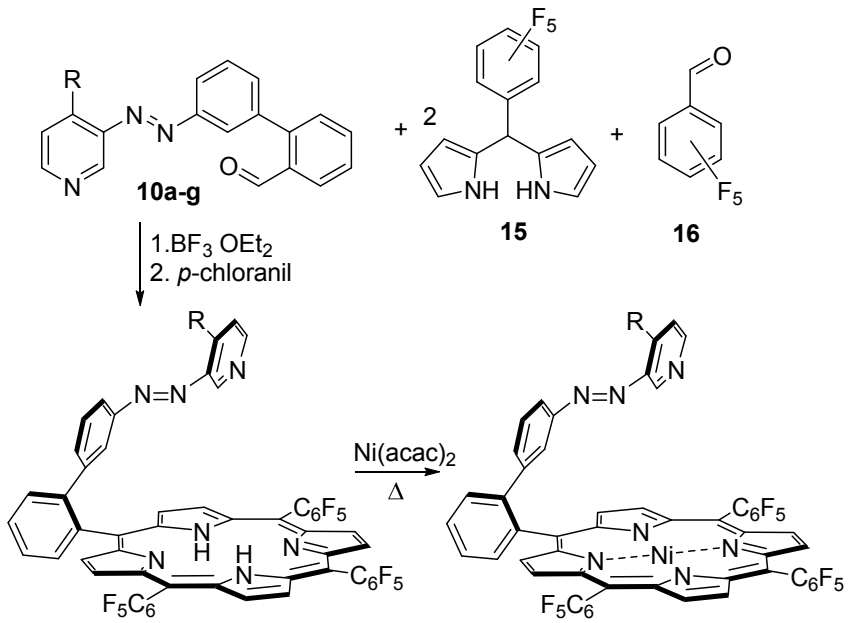

mf-RPs:	R=		RPs:	R=	
17a:	OMe	4.4 %	**1a:**	OMe	45 %
17b:	Me	14 %	**1b:**	Me	57 %
17c:	H	7.2 %	**1c:**	H	73 %
17d:	Cl	5.5 %	**1d:**	Cl	64 %
17e:	NMe_2	0.5 %	**1e:**	NMe_2	0 %
17f:	Pyr	1.1 %	**1f:**	Pyr	0 %
17g:	OiPr	0 %			

The yields of the nickel complexation decrease if the azopyridine substituent is more electron rich probably due to stability. The reaction conditions lead to decomposition of the 4-amino derivatives **17e** and **17f**. A low stability was already observed for the synthetic precursors (4-amino-3-phenylazo derivatives **8e** and **10e**). The low thermodynamic stability was indicated by high fragmentation in mass spectra and low decomposition temperatures (85.9 and 82.9 ℃, see e xperimental section). No method was found to insert the nickel in mf-RPs **17e** and **17f**.

V Analytical Equipment and Methods

NMR Spectroscopy

NMR spectra were measured in deuterated solvents (Deutero). The degree of deuteration is given in parentheses. ^{1}H NMR-spectra in reference to the following signals.

acetone-d_6 (99.8 %): δ = 2.05 ppm (quint)

chloroform-d (99.8 %): δ = 7.26 ppm (s)

dichloromethane-d_2 (99.6 %): δ = 5.32 ppm (t)

DMSO-d_6 (99.8 %): δ = 2.50 ppm (quint)

methanol-d_4 (99.8 %): δ = 3.35 ppm (quint)

water-d_2 (99.9 %): δ = 4.79 ppm (s)

The signal multiplicities are abbreviated as follows.

s: singlet, d: doublet, t: triplet, q: quartet, quint: quint, m: multiplet, br: broad signal

Measurements were performed by the following instruments:

Bruker AC 200 (^{1}H NMR: 200 MHz, ^{13}C NMR: 50 MHz, relaxation time measurement)

Bruker DRX 500 (^{1}H NMR: 500 MHz, ^{19}F NMR: 470 MHz, ^{13}C NMR: 125 MHz)

Bruker AV 600 (^{1}H NMR: 600 MHz, ^{13}C NMR: 150 MHz)

The atom labeling for NMR interpretation is always starting at the pyridine nitrogen. For the sake of clarity the aromatic protons have always the same number in each compound. Example:

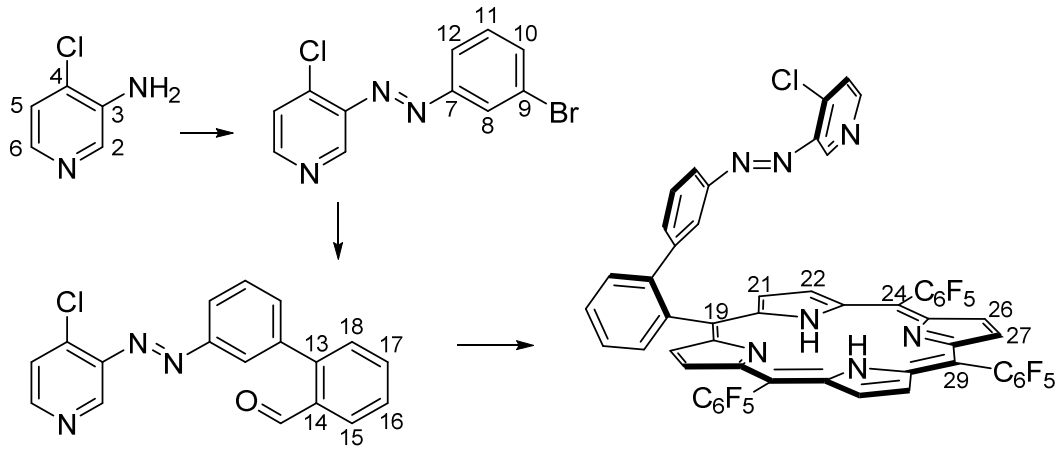

Figure S11. Numbering of the synthesized compounds.

Reference for all ^{19}F-NMR spectra is trichlorofluoromethane to the frequency of which the spectrometer is calibrated. Fluorine atoms are labeled as *o*-F, *m*-F und *p*-F (*ortho*-, *meta*- und *para*-fluorine) according to their position in the aromatic system. In case of asymmetric porphyrins there are to different *meso*-positions labelled as A and B (Figure S2). Due to the fact that the *meso*-phenyl rings do not rotate on the NMR time scale there are two different sides labelled as σ and σ' (Figure S2).

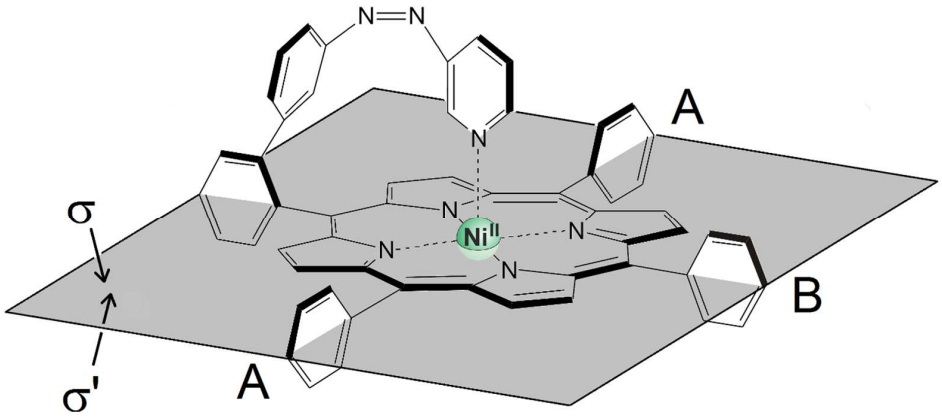

Figure S12. General structure of asymmetric porphyrins to explain the obtained ^{19}F NMR spectra. The fluorine atoms at the *meso*-positions A and B are now drawn for the sake of more clarity.

IR spectroscopy

Infrared spectra were measured on a Perkin-Elmer 1600 Series FT-IR spectrometer with an A531-G Golden-Gate-Diamond-ATR-unit. Signals were abbreviated with w, m, s and vs for weak, medium, strong and very strong intensities. Broad signals are additionally labeled with br.

UV-vis spectroscopy

The UV-vis spectra were measured on a Lambda 14 spectrometer (Perkin-Elmer) with a (Büchi) thermostat. Quartz cuvettes of 1 cm and 1 mm optical path length were used.

Elemental analysis

The amount of carbon, hydrogen and nitrogen in a compound was determined with a CHNSO-Elemental analyser Euro EA 3000 Series by co. Euro Vector.

Mass spectrometry

The high resolution (HR) mass spectra were measured with an APEX 3 FT-ICR with a 7.05 T magnet by co. Bruker Daltonics. Electron impact (EI) and chemical ionization (CI) mass spectra were measured with a MAT 8230 by co. Finnigan. Electron impact time of flight spectra (EI, TOF) were measured with an AccuTOF GCv4G mass spectrometer by JEOL.

Chromatography stationary phases

For column chromatography purifications silica gel (Merck, particle size 0.040-0.063 mm) was used. R_f values were determined by thin layer chromatography on Polygram® Sil G/UV_{254} (Macherey-Nagel, 0.2 mm particle size).

VI Experimental procedures

VI.1 General procedures

VI.1.1 Synthesis of 1-bromo-3-nitrosobenzene (7)

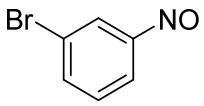

1-Bromo-3-nitrobenzene (**5**) (5.00 g, 24.8 mmol) was dissolved in ethanol (120 mL). An aqueous ammonium chloride solution (1.99 g, 37.2 mmol in 10 mL) was added. The mixture was warmed up to 40 ℃ until the disper sion changes into a clear solution. After cooling to room temperature zinc dust (4.86 g, 74.3 mmol) was added and the reaction mixture was stirred for 3 h. After filtration, the filtrate was added to an aqueous ice cooled solution of iron(III) chloride solution (hexa aquo complex, 4.69 g, 17.4 mmol in 240 mL) whereby a green solid precipitated. After 15 min stirring it was filtered off and washed with water. A mixture of 40 % 1-bromo-3-nitrosobenzene (9.92 mmol) and 60 % starting material (14.9 mmol) was obtained which was utilized for azo condensation reactions.

VI.1.2 Suzuki coupling with 2-formylphenyl boronic acid (9)

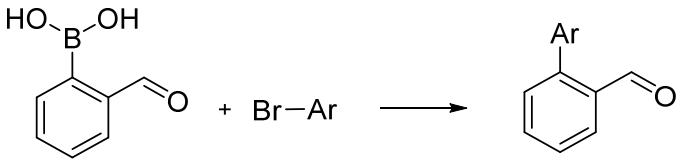

One equivalent of bromo aryl component **8a-f** was dissolved in a solvent mixture of toluene:ethanol:water = 65:20:15 under nitrogen atmosphere. 3.3 Equivalents potassium carbonate, 1.1 equivalents 2-formylphenyl boronic acid (**9**) and 2 mol% tetrakis(triphenylphosphin)palladium(0) were added. The mixture was stirred for 16 h at 90 ℃. Water was added and the mixture was extra cted three times with ethyl acetate. The combined organic layers were dried over magnesium sulfate and the solvent was removed under reduced pressure.

VI.2 Synthesis of 3-amino-4-chloropyridine (4d)

3-Nitro-4-chloropyridine (**3d**) (2.00 g, 12.6 mmol) was dissolved in ethanol (80 mL) and acetic acid (11.2 mL). Tin(II) chloride dihydrate (19.9 g, 88.4 mmol) was added and the mixture was stirred for 3 h at reflux. After cooling to room temperature, the mixture was poured into water and extracted three times with dichloromethane. The combined organic layers were dried over magnesium sulfate and the solvent was removed under reduced pressure. The product was obtained as a dark brown solid.

Yield: 1.00 g (7.76 mmol, 62 %)

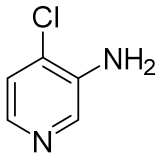

m.p.: 73.7 °C

FT-IR (layer): υ = 3396 (m), 3310 (m), 3197 (m), 1884 (w) 1635 (s), 1570 (m), 1557 (s), 1485 (s), 1415 (vs), 1328 (s), 1289 (m), 1244 (s), 1107 (m), 1057 (m), 943 (w), 897 (m), 839 (m), 818 (vs), 728 (m),690 (vs), 569 (vs) cm^{-1}.

^{1}H NMR (500 MHz, 300 K, $CDCl_3$, TMS): δ = 8.10 (s, 1H, *H*-2), 7.73 (d, ^{3}J = 5.3 Hz, 1H, *H*-6), 7.31 (d, ^{3}J = 5.3 Hz, 1H, *H*-5), 5.75 (s, br, 2H, *H*-N) ppm.

^{13}C NMR (125 MHz, 300 K, $CDCl_3$, TMS): δ = 142.1 (*C*3), 136.3 (*C*2, *C*6), 124.2 (*C*5), 125.6 (*C*4) ppm.

MS (EI, 70 eV): m/z (%) = 128 (100) $[M]^+$, 113 (6) $[M\text{-}NH_2]^+$.

MS (CI, isobutane): m/z (%) = 129 (100) $[M+H]^+$.

EA: (C_5H_5ClN)		C / %	H / %	N / %
	found:	46.77	3.84	21.83
	calc.:	46.71	3.92	21.79

VI.3 Synthesis of 3-(3-bromophenylazo)-4-chloropyridine (8d)

3-Amino-4-chloropyridine (**4d**) (1.00 g, 7.78 mmol) was dissolved in a mixture of pyridine (50 mL) and sodium hydroxide solution (40 %, 25 mL) and stirred at 80 °C. 1-Bromo-4-nitrosobenzene (**7**) (1.3 equivalent) obtained by general procedure V.1.1 dissolved in 30 mL pyridine was added. The mixture was stirred 3 h at 80 °C and afterwards over night at room temperature. Water was added and the mixture was extracted with toluene three times. The combined organic layers were dried over magnesium sulfate and the solvent was removed under reduced pressure. The crude product was purified by column chromatography (cyclohexane / ethyl acetate = 9:1, R_f = 0.19).The product was obtained as an orange solid.

Yield: 1.49 g (5.02 mmol, 65 %)

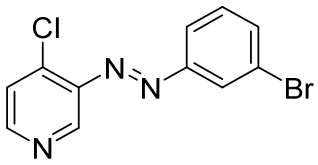

m.p.: 78.1 °C

FT-IR (layer): υ = 3083 (w), 1639 (w), 1558 (m), 1458 (m), 1393 (w), 1298 (w), 1189 (w), 1153 (w), 1084 (m), 996 (w), 930 (w), 909 (w), 886 (m), 825 (m), 788 (s), 731 (vs), 679 (s), 655 (m), 582 (m), 545 (m), 530 (m) cm^{-1}.

^{1}H NMR (500 MHz, 300 K, $CDCl_3$, TMS): δ = 8.76 (s, 1H, *H*-2), 8.53 (d, ^3J = 5.3 Hz, 1H, *H*-6), 8.07 (t, ^4J = 1.9 Hz, 1H, *H*-8), 7.91 (ddd, ^3J = 7.9 Hz, ^4J = 1.8, 1.0 Hz, 1H, *H*-12), 7.62 (ddd, ^3J = 7.9 Hz, ^4J = 1.9, 1.0 Hz, 1H, *H*-10), 7.49 (d, ^3J = 5.3 Hz, 1H, *H*-5), 7.39 (t, ^3J = 7.9 Hz, 1H, *H*-11) ppm.

^{13}C NMR (125 MHz, 300 K, $CDCl_3$, TMS): δ = 153.3 (*C*6), 151.9 (*C*5), 143.9 (*C*2, *C*3), 139.5 (*C*1), 134.7 (*C*9), 130.5 (*C*10), 125.5 (*C*4), 125.2 (*C*7), 123.4 (*C*11), 123.3 (*C*8) ppm.

MS (EI, 70 eV): m/z (%) = 297 (51) $[M]^+$, 183 (47) $[PhBrN_2]^+$, 155 (100) $[PhBr]^+$, 140 (15) $[PyClN_2]^+$, 112 (66) $[PyCl]^+$.

MS (CI, isobutane): m/z (%) = 298 (100) $[M+H]^+$.

UV-vis (MeCN): λ_{max} (lg ε) = 235 (4.133), 318 (4.221), 441 (2.736) nm.

EA: ($C_{11}H_7BrClN_3$)	C / %	H / %	N / %
found:	44.84	2.31	13.96
calc.:	44.55	2.38	14.17

VI.4 Synthesis of 3-(2-formylphenyl)phenylazo)-4-chloropyridine (11)

3-(3-Bromophenylazo)-4-chloropyridine (**8d**) (300 mg, 1.01 mmol) was used for a Suzuki coupling reaction according to general procedure V.1.2. The crude product was purified by column chromatography (cyclohexane / ethyl acetate = 9:1, R_f = 0.10). The product was obtained as a red solid.

Yield.: 118 mg (0.32 mmol, 32 %)

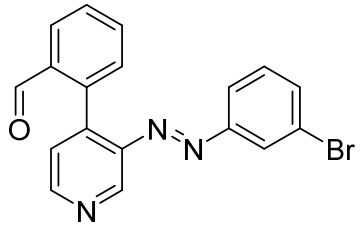

m.p.: 129.5 °C

FT-IR (layer): υ = 3040 (m), 3008 (w), 2861 (w), 2764 (w), 1688 (s), 1582 (m), 1539 (w), 1469 (m), 1395 (m), 1281 (w), 1243 (w), 1197 (s), 1149 (m), 1094 (m), 1062 (m), 962 (w), 930 (w), 849 (s), 758 (vs), 677 (s), 646 (s), 617 (m), 582 (m), 543 (s) cm^{-1}.

^{1}**H NMR** (600 MHz, 300 K, $CDCl_3$, TMS): δ = 9.80 (d, 1H, ^4J = 0.6 Hz, C*H*O), 8.84 (s, 1H, *H*-1), 8.69 (d, ^3J = 5.0 Hz, 1H, *H*-5), 7.96 (dd, ^3J = 7.8 Hz, ^4J = 1.2, 0.4 Hz, 1H, *H*-14), 7.63 (t, ^4J = 1.4 Hz, 1H, *H*-7), 7.59 (td, ^3J = 7.5 Hz, ^4J = 1.5 Hz, 1H, *H*-16), 7.51 (td, ^3J = 7.5 Hz, ^4J = 1.3 Hz, 1H, *H*-15), 7.45 (ddd, ^3J = 8.0 Hz, ^4J = 1.9, 1.0 Hz, 1H, *H*-11), 7.44 (ddd, ^3J = 8.0 Hz, ^4J = 1.9, 1.0 Hz, 1H, *H*-9), 7.37 (d, ^3J = 5.0 Hz, 1H, *H*-4), 7.31 (dd, ^3J = 7.6 Hz, ^4J = 1.3 Hz, 1H, *H*-17), 7.18 (t, ^3J = 8.0 Hz, 1H, *H*-10) ppm.

^{13}**C NMR** (150 MHz, 300 K, $CDCl_3$, TMS): = 190.6 (*C*HO), 153.2 (*C*6), 151.6 (*C*5), 144.6 (*C*2), 144.5 (*C*3), 138.7 (*C*12), 138.4 (*C*1), 134.5 (*C*9), 134.4 (*C*13), 133.5 (*C*16), 131.2 (*C*17), 130.5 (*C*10), 129.3 (*C*15), 128.1 (*C*14), 126.1 (*C*7), 125.4 (*C*4), 123.1 (*C*8), 122.2 (*C*11) ppm.

MS (EI, 70 eV): m/z (%) = 365 (17) $[M]^+$, 338 (57) $[M\text{-}N_2]^+$, 286 (100) $[M\text{-}Br]^+$,196 (90) $[M\text{-}BrPhN]^+$, 182 (92) $[M\text{-}BrPhN_2]^+$, 154 (34) $[PhBr]^+$.

MS (CI, isobutane): m/z (%) = 423 (5) $[M+^iBu]^+$,366 (89) $[M+H]^+$, 182 (100) $[M\text{-}BrPhN_2]^+$.

EA: ($C_{18}H_{12}BrN_3O$)		C / %	H / %	N / %
	found:	58.92	3.11	11.23
	calc.:	59.03	3.30	11.47

VI.5 Synthesis of 3-(3-iodophenylazo)-4-chloropyridine (14)

1-Iodo-3-nitrobenzene (**12**) (5.00 g, 20.1 mmol) was dissolved in ethanol (250 mL). An aqueous solution of ammonium chloride (1.61 g, 53.5 mmol in 30 mL) was added. The mixture was warmed up to 40 °C until the dispersion changes into a clear solution. After cooling to room temperature zinc dust (3.94 g, 60.3 mmol) was added and the mixture was stirred for 3 h. After filtration, the filtrate was poured into an aqueous ice cooled iron(III) chloride solution (hexa aquo complex, 3.80 g, 14.1 mmol in 185 mL) whereby a green solid precipitated. After 15 min stirring, the solid was filtered off and washed with water. The crude product was a mixture of 1-iodo-3-nitrosobenzene (**13**) and starting material **12** which was used for azo condensation without further purification.

3-Amino-4-chloropyridine (**4d**) (774 mg, 6.02 mmol) was dissolved in a mixture of pyridine (20 mL) and sodium hydroxide solution (25 %, 5 mL). The crude product of 1-iodo-3-nitrosobenzene (**13**) dissolved in pyridine (30 mL) was added. The reaction mixture was stirred for 1 h at 80 °C and overnight at room temperature. After addition of dichloromethane (200 mL) the phases were separated. The organic layer was washed with water twice and dried over sodium sulfate. The solvent was removed under reduced pressure. The crude product was purified by column chromatography (dichloromethane, R_f = 0,59). The product was obtained as an orange solid.

Yield: 350 mg (1.02 mmol, 17 %)

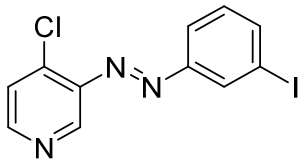

m.p.: 124.6 °C

FT-IR (layer): υ = 2324 (w), 1559 (m), 1455 (m), 1939 (m), 1350 (w), 1195 (w), 1150 (w), 1984 (m), 828 (m), 792 (m), 729 (m), 678 (m), 581 (m), 544 (m), 453 (m), 425 (m) cm^{-1}.

^{1}**H NMR** (500 MHz, 300 K, $CDCl_3$, TMS): δ = 8.78 (s, 1H, *H*-2), 8.57 (d, ^3J = 5.5 Hz, 1H, *H*-6), 8.30 (t, ^4J = 1.8 Hz, 1H, *H*-8), 7.98 (ddd, ^3J = 8.0 Hz, ^4J = 1.9 Hz, 1.1 Hz, 1H, *H*-12), 7.87 (ddd, ^3J = 7.8 Hz, ^4J = 1.7 Hz, 1.1 Hz, 1H, *H*-10), 7.53 (d, ^3J = 5.5 Hz, 1H, *H*-5), 6.71 (t, ^3J = 7.9 Hz, 1H, *H*-11) ppm.

^{13}C NMR (125 MHz, 300 K, $CDCl_3$, TMS): = 153.4 (*C*7), 148.9 (*C*3), 142.9 (*C*4), 124.0 (*C*10), 125.6 (*C*5), 130.9 (*C*8), 131.5 (*C*11), 139.6 (*C*2), 140.9 (*C*12), 151.8 (*C*6), 95.1 (*C*9) ppm.

MS (EI, TOF): m/z (%) = 342 (43) $[M]^+$, 230 (62) $[M\text{-}C_5H_3ClN]^+$, 202 (100) $[M\text{-}C_5H_3ClN_3]^+$, 76.0 (64) $[C_6H_4]^+$.

EA: ($C_{11}H_7IClN_3$)		C / %	H / %	N / %
	found:	39.91	2.02	11.98
	calc.:	39.46	2.05	12.23

VI.6 Synthesis of 3-(2-formylphenyl)phenylazo)-4-chloropyridine (10d)

3-(3-Iodophenylazo)-4-chloropyridine (**14**) (800 mg, 2.33 mmol) was used for a Suzuki coupling reaction according to general procedure V.1.2. The crude product was purified by column chromatography (cyclohexane / ethyl acetate = 4:1, R_f = 0.59). The product was obtained as an orange solid.

Yield.: 560 mg (1.74 mmol, 75 %)

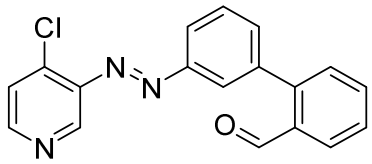

m.p.: 141.7 ℃

FT-IR (layer): υ = 3083 (w), 1687 (w), 1560 (w), 1455 (w), 1189 (m), 1070 (m), 954 (w), 903 (w), 822 (m), 775 (m), 704 (w), 543 (m), 491 (m), 424 (m), 459 (m) cm^{-1}.

^{1}H NMR (600 MHz, 300 K, $CDCl_3$, TMS): δ = 10.09 (s, 1H, C*H*O), 8.85 (s, 1H, *H*-2), 8.60 (d, ^3J = 5.5 Hz, 1H, *H*-6), 8.10 (d, ^3J = 7.9 Hz, 2H, H-12, *H*-15), 8.04 (s, 1H, *H*-8), 7.73 (td, ^3J = 7.6 Hz, ^4J = 1.3 Hz, 1H, *H*-17), 7.69 (t, ^3J = 7.9 Hz, 1H, *H*-11), 7.60-754 (m, 4H, *H*-18, *H*-16, *H*-10, *H*-5) ppm.

^{13}C NMR (150 MHz, 300 K, $CDCl_3$, TMS): = 191.9 (*C*HO), 152.6 (*C*7), 151.8 (*C*6), 144.7 (*C*13), 144.3 (*C*3), 143.8 (*C*4), 139.5 (*C*2), 139.3 (*C*9), 133.9 (*C*17), 133.8 (*C*14), 133.6 (*C*10), 130.9 (C18), 129.4 (C11), 128.4 (C16), 128.1 (C15), 125.6 (C5), 124.7 (*C*8), 123.4 (*C*12) ppm.

MS (EI, TOF): m/z (%) = 321 $[M]^+$, 181 $[M\text{-}C_5H_3N_2]^+$, 153 $[M\text{-}C_6H_4ClN_3O]^+$.

EA: ($C_{18}H_{12}ClN_3O$)		C / %	H / %	N / %
	found:	67.00	3.75	12.90
	calc.:	67.19	3.76	13.06

VI.7 Synthesis of mf-Cl-RP (17d)

3-(3-(2-Formylphenyl)phenylazo)-4-chloropyridine (**10d**) (500 mg, 1.56 mmol) and pentafluorobenzaldehyde (**16**) (305 mg, 1.56 mmol) were dissolved in chloroform (400 mL) under nitrogen atmosphere. Boron trifluoride in diethyl ether (390 µL, 3.13 mmol) was added. *meso*-Pentafluorophenyl dipyrromethane (**15**) (972 mg, 3.12 mmol) dissolved in 20 mL chloroform was added within 1 h by a syringe pump. After 5 h of stirring *p*-chloranil (805 mg, 3.27 mmol) was added and the mixture was stirred overnight under reflux. After addition of triethylamine (2 mL) stirring was continued for 30 min at room temperature. The mixture was successively filtered through Celite® and silica gel. The solvent was removed under reduced pressure. The crude product was purified by column chromatography (*n*-pentane / diethylether = 3:2, R_f = 0.43).

Yield: 94.0 mg (85.5 µmol, 5.5 %)

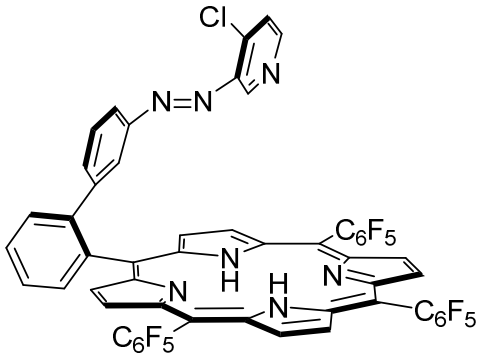

FT-IR (layer): υ = 2925 (w), 1687 (w), 2005 (w), 1516 (m), 1495 (m), 1398 (w), 1043 (w), 987 (m), 917 (m), 802 (m), 721 (m), 559 (w), 513 (w), 497 (w), 402 (m) cm^{-1}.
^{1}H NMR (500 MHz, 300 K, $CDCl_3$, TMS): δ = 8.88 (d, ^3J = 4.9 Hz, 2H, *H*-22), 8.75 (s, br, 4H, *H*-26, *H*-27), 8.65 (d, ^3J = 4.9 Hz, 2H, *H*-21), 8.28 (d, ^3J = 5.5 Hz, 1H, *H*-6), 8.19 (s, 1H, *H*-2), 8.10 (dd, ^3J = 7.6 Hz, ^4J = 1.0 Hz, 1H, *H*-15), 7.87 (td, ^3J = 7.7 Hz, ^4J = 1.0 Hz, 1H, *H*-17), 7.82 (dd, ^3J = 7.8 Hz, ^4J = 1.7 Hz, 1H, *H*-18), 7.72 (t, ^4J = 1.8 Hz,

1H, *H*-8), 7.70 (td, ^3J = 7.7 Hz, ^4J = 1.4 Hz, 1H, *H*-16), 7.23 (d, ^3J = 5.5 Hz, 1H, *H*-5), 7.05 (ddd, ^3J = 7.9 Hz, ^4J = 1.8 Hz, 1.1 Hz, 1H, *H*-10), 6.98 (ddd, ^3J = 7.8 Hz, ^4J = 1.7 Hz, 1.1 Hz, 1H, *H*-12), 6.49 (t, ^3J = 7.9 Hz, 1H, *H*-11), -2.93 (s, 2H, N*H*) ppm.
^{19}F NMR (470 MHz, 300 K, $CDCl_3$, $CFCl_3$): δ = -136.29 (d, ^3J = 24.4 Hz, 2F, A-*o*-*F*), -136.55 (d, ^3J = 26.0 Hz, 1F, B-*o*-*F*), -136.65 (d, ^3J = 27.0 Hz, 1F, B-*o'*-*F*), -136.72 (d, ^3J = 25.1 Hz, 2F, A-*o'*-*F*), -151.76 (t, ^3J = 20.6 Hz, 1F, B-*p*-*F*), -151.86 (t, ^3J = 20.3 Hz, 2F, A-*p*-*F*), -161.50 to -161.82 (m, 6F, A-*m*-*F*, B-*m*-*F*, A-*m'*-*F*, B-*m'*-*F*) ppm.
MS (HR): m/z (calc.) = 1100.137 (1100.138) $[M+H]^+$.

VI.8 Synthesis of Cl-RP (1d)

mf-Cl-RP (**17d**) (75 mg, 68 µmol) and nickel(II) acetylacetonate (205 mg, 801 µmol) were dissolved in toluene (100 mL) and stirred under reflux for 4 d. The solvent was removed under reduced pressure and the crude product was purified by column chromatography (n-pentane / diethylether = 3:2, R_f = 0.44).

Yield: 50.0 mg (43.2 µmol, 64%)

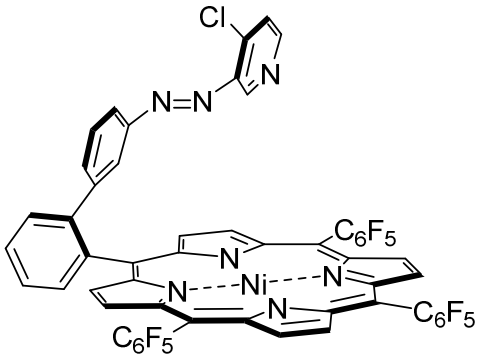

FT-IR (layer): υ = 2926 (w), 1518 (m), 1560 (w), 1491 (w), 1348 (w), 1165 (w), 1059 (m), 988 (s), 939 (m), 801 (w), 763 (m), 704 (w), 556 (w), 513 (w), 449 (w) cm^{-1}.
^{1}H NMR (500 MHz, 300 K, DMSO-d_6, TMS): *δ* = 10.60 (s, br, 4H, *H*-26,*H*-27), 10.53 (s, br, 2H, *H*-22), 10.33 (s, br, 2H, *H*-21), 8.49 (s, br, 1H, *H*-6), 8.27 (d, ^3J = 7.1 Hz, 1H, *H*-15), 8.09 (s, br, 1H, *H*-2), 8.02 (t, ^3J = 7.8 Hz, 1H, *H*-17), 7.93 (d, ^3J = 7.8 Hz, 1H, *H*-18), 7.89 (t, ^3J = 7.4 Hz, 1H, *H*-16), 7.53 (d, ^3J = 4.5 Hz, 1H, *H*-5), 7.42 (s, 1H, *H*-8), 7.23 (d, ^3J = 7.9 Hz, 1H, *H*-10), 7.14 (d, ^3J = 7.9 Hz, 1H, *H*-12), 6.88 (t, ^3J = 7.9 Hz, 1H, *H*-11) ppm.

^{19}F NMR (470 MHz, 300 K, $CDCl_3$, $CFCl_3$): δ = -136.34 (d, ^3J = 23.7 Hz, 2F, A-*o*-*F*), -136.61 (d, ^3J = 23.9 Hz, 1F, B-*o*-*F*), -136.81 (d, ^3J = 23.9 Hz, 1F, B-*o'*-*F*), -136.94 (d, ^3J = 23.7 Hz, 2F, A-*o'*-*F*), -151.81 (t, ^3J = 20.7 Hz, 1F, B-*p*-*F*), -151.89 (t, ^3J = 20.4 Hz, 2F, A-*p*-*F*), -161.35 to -161.66 (m, 6F, A-*m*-*F*, B-*m*-*F*, A-*m'*-*F*, B-*m'*-*F*) ppm.

MS (HR): m/z (calc.) = 1178.070 (1178.073) $[M+H]^+$.

VI.9 Synthesis of 3-amino-4-methylpyridine dihydrochloride (4b)

3-Nitro-4-methylpyridine (**3b**) (1.50 g, 10.9 mmol) was dissolved in dimethylformamide (120 mL). Palladium on charcoal (10 %, 150 mg) was added and the mixture was stirred in a flask with baffles under hydrogen atmosphere overnight. After filtration through Celite®, the solvent was removed under reduced pressure. The crude product was dissolved in a minimum volume of concentrated hydrochloric acid. By addition of an excess of tetrahydrofuran a pale yellow solid precipitated which was filtered off and washed with tetrahydrofuran.

Yield: 1.32 g (7.30 mmol, 67 %)

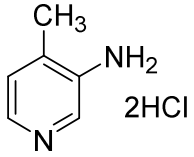

m.p.: 164.8 °C

FT-IR (layer): υ = 3085 (w), 2796 (m), 2734 (m), 2518 (s), 1648 (s), 1561 (s), 1526 (vs), 1493 (s), 1385 (m), 1353 (m), 1164 (vs), 1122 (m), 1045 (w), 971 (m), 857 (m), 799 (vs), 716 (m), 565 (w), 500 (w), 453 (s) cm^{-1}.

^{1}H NMR (500 MHz, 300 K, D_2O): δ = 8.02 (d, ^4J = 0.8 Hz, 1H, *H*-2), 7.94 (dd, ^3J = 5.8 Hz, ^4J = 0.8 Hz, 1H, *H*-6), 7.63 (d, ^3J = 5.8 Hz, 1H, *H*-5), 2.39 (s, 3H, C*H*$_3$) ppm. NH_2 does not appear in ^{1}H NMR-Spektrum because of H/D-exchange.

^{13}C NMR (125 MHz, 300 K, D_2O): δ = 145.5 (*C*3), 143.1 (*C*4), 129.4 (*C*6), 127.6 (*C*5), 125.0 (*C*2), 17.4 (*C*H_3) ppm.

MS (EI, TOF): m/z (%) = 108 (100) $[M-2HCl]^+$.

EA: ($C_6H_8N_2O$*2HCl)	C / %	H / %	N / %
found:	39.80	5.40	15.31
calc.:	39.80	5.57	15.47

VI.10 Synthesis of 3-(3-bromophenylazo)-4-methylpyridine (8b)

3-Amino-4-methylpyridine dihydrochloride (**4b**) (2.01 g, 11.1 mmol) was dissolved in a mixture of toluene (30 mL) and potassium hydroxide solution (60 %, 25 mL) at 100 °C. 1-Bromo-3-nitrosobenzene (**7**) (0.9 equivalents) obtained by general procedure V.1.1 was added and the mixture was stirred overnight at 100 °C. The mixture was poured onto ice and extracted three times with ethyl acetate. The combined organic layers were dried over magnesium sulfate and the solvent was removed under reduced pressure. The crude product was purified by column chromatography (cyclohexane / ethyl acetate = 8:2, R_f (cyclohexane / ethyl acetate = 1:1) = 0.32)

Yield: 974 mg (3.53 mmol, 36 %)

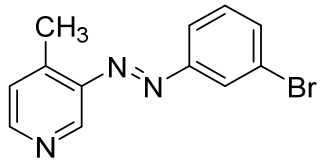

m.p.: 62.1 °C

FT-IR (layer): υ = 3036 (w), 3005 (w), 2920 (w), 1592 (s), 1477 (s), 1456 (m), 1417 (s), 1377 (m), 1202 (m), 1144 (m), 1061 (m), 914 (m), 858 (s), 823 (s), 781 (vs), 728 (s), 699 (s), 678 (vs), 653 (s), 581 (s), 559 (m), 527 (s) cm^{-1}.

^{1}H NMR (500 MHz, 300 K, $CDCl_3$, TMS): δ = 8.71 (s, 1H, *H*-2), 8.51 (d, ^3J = 5.0 Hz, 1H, *H*-6), 8.01 (t, ^4J = 1.9 Hz, 1H, *H*-8), 7.88 (ddd, ^3J = 8.0 Hz, ^4J = 1.8, 1.0 Hz, 1H, *H*-12), 7.60 (ddd, ^3J = 7.9 Hz, ^4J = 1.9, 1.0 Hz, 1H, *H*-10), 7.40 (t, ^3J = 7.9 Hz, 1H, *H*-11), 7.27 (d, ^3J = 5.0 Hz, 1H, *H*-5), 2.70 (s, 3H, CH_3) ppm.

^{13}C NMR (125 MHz, 300 K, $CDCl_3$, TMS): δ = 153.5 (*C*7), 153.0 (*C*6), 146.2 (*C*3), 145.9 (*C*4), 137.8 (*C*2), 134.1 (*C*10), 130.5 (*C*11), 126.1 (*C*5), 124.7 (*C*8), 123.4 (*C*12), 123.2 (*C*9), 17.2 (*C*H_3) ppm.

MS (EI, 70 eV): m/z (%) = 276 (89) $[M]^+$, 182 (40) $[PhBrN_2]^+$, 154 (100) $[PhBr]^+$, 120 (46) $[M\text{-}BrPh]^+$.

MS (CI, Isobutane): m/z (%) = 277 (100) $[M+H]^+$.

UV-vis (MeCN): λ_{max} (lg ε) = 232 (4.106), 316 (4.117), 439 (2.633) nm.

EA: ($C_{12}H_{10}BrN_3$)		C / %	H / %	N / %
	found:	51.92	3.62	14.88
	calc.:	52.20	3.65	15.22

VI.11 Synthesis of 3-(2-formylphenyl)phenylazo)-4-methylpyridine (10b)

3-(3-Bromophenylazo)-4-methylpyridine (**8b**) (974 mg, 3.53 mmol) was used for a Suzuki coupling reaction according to general procedure V.1.2. The crude product was purified by column chromatography (cyclohexane / ethyl acetate = 1:1, R_f = 0.31). The product was obtained as an orange solid.

Yield: 822 mg (2.73 mmol, 77 %)

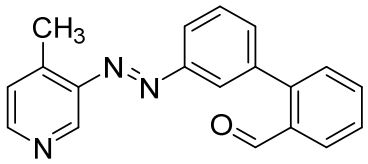

m.p.: 115.3 °C

FT-IR (layer): υ = 3026 (w), 2860 (w), 1686 (s), 1594 (s), 1477 (w), 1391 (m), 1252 (m), 1194 (m), 1102 (m) 1068 (w), 929 (w), 903 (m), 845 (m), 805 (m), 754 (vs), 727 (m), 697 (m), 648 (m), 577 (m), 543 (m), 529 (w) cm^{-1}.

^{1}H NMR (500 MHz, 300 K, $CDCl_3$, TMS): δ = 9.96 (s, 1H, C*H*O), 8.68 (s, 1H, *H*-2), 8.43 (d, ^3J = 5.0 Hz, 1H, *H*-6), 7.97 (dd, ^3J = 7.8 Hz, ^4J = 0.9 Hz, 1H, *H*-15), 7.92 (dt, ^3J = 8.1 Hz, ^4J = 1.3 Hz, 1H, *H*-12), 7.86 (t, ^4J = 1.4 Hz, 1H, *H*-8), 7.59 (td, ^3J = 7.5 Hz, ^4J = 1.3 Hz, 1H, *H*-17), 7.55 (t, ^3J = 7.8 Hz, 1H, *H*-11), 7.46 (t, ^3J = 7.5 Hz, 1H, *H*-16), 7.44-7.41 (m, 2H, *H*-18, *H*-10), 7.21 (d, ^3J = 4.9 Hz, 1H, *H*-5), 2.62 (s, 3H, CH_3) ppm.

^{13}C NMR (125 MHz, 300 K, $CDCl_3$, TMS): δ = 191.8 (*C*O), 152.5 (*C*7), 150.7 (*C*6), 146.3 (*C*4), 145.8 (*C*3), 144.7 (*C*13), 138.9 (*C*9), 137.7 (*C*2), 133.7 (*C*17), 133.7 (*C*14), 132.8 (*C*10), 130.7 (*C*18), 129.2 (*C*11), 128.2 (*C*16), 127.8 (*C*15), 126.1 (*C*5), 124.1 (*C*8), 123.0 (*C*12), 17.1 (*C*H_3) ppm.

MS (EI, 70 eV): m/z (%) = 301 (100) $[M]^+$, 181 (61) $[M\text{-}CH_3PyN_2]^+$, 153 (78) $[Ph_2]^+$.

MS (CI, isobutane): m/z (%) = 302 (100) $[M+H]^+$.

UV-vis (MeCN): λ_{max} (lg ε) = 212 (4.311), 232 (4.404), 316 (4.244), 455 (2.581) nm.

EA: ($C_{19}H_{15}N_3O$)		C / %	H / %	N / %
	found:	75.74	4.89	13.24
	calc.:	75.73	5.02	13.94

VI.12 Synthesis of mf-Me-RP (17b)

3-(3-(2-Formylphenyl)phenylazo)-4-methylpyridine (**10b**) (600 mg, 1.99 mmol) and pentafluorobenzaldehyde (**16**) (390 mg, 1.99 mmol) were dissolved in chloroform (230 mL) under nitrogen atmosphere. Boron trifluoride diethyl ether (420 µL, 3.34 mmol) was added. *meso*-Pentafluorophenyl dipyrromethane (**15**) (1.24 g, 3.98 mmol) dissolved in 20 mL chloroform was added within 1 h by a syringe pump. After 5 h of stirring *p*-chloranil (1.03 g, 4.18 mmol) was added and the mixture was stirred overnight at reflux. After addition of triethylamine (2 mL) stirring was continued for 30 min at room temperature. The solvent was removed under reduced pressure. The crude product was purified by column chromatography (chloroform, R_f = 0.18).

Yield: 300 mg (278 µmol, 14 %)

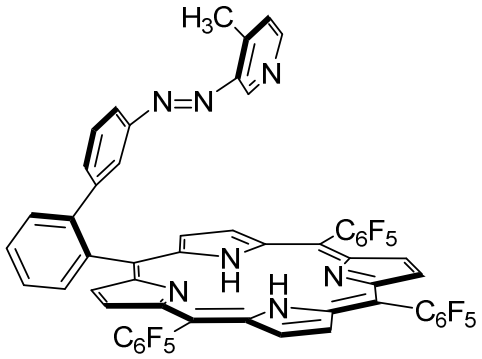

^{1}H NMR (500 MHz, 300 K, acetone-d_6, TMS): δ = 9.11 (s, br, 4H, *H*-26, *H*-27), 9.03 (d, ^3J = 4.1 Hz, 2H, *H*-22), 8.96 (d, ^3J = 4.3 Hz, 2H, *H*-21), 8.19 (dd, ^3J = 7.5 Hz, ^4J = 1.0 Hz, 1H, *H*-15), 8.16 (d, ^3J = 4.7 Hz, 1H, *H*-6), 7.91 (td, ^3J = 7.7 Hz, ^4J = 1.3 Hz, 1H, *H*-17), 7.90 (s, 1H, *H*-2), 7.85 (dd, ^3J = 7.9 Hz, ^4J = 1.2 Hz, 1H, *H*-18), 7.76 (td, ^3J = 7.5 Hz, ^4J = 1.5 Hz, 1H, *H*-16), 7.50 (t, ^4J = 1.8 Hz, 1H, *H*-8), 7.21 (ddd, ^3J = 7.9 Hz, ^4J = 1.8, 1.2 Hz, *H*-10), 7.06 (d, ^3J = 4.7 Hz, 1H, *H*-5), 6.95 (ddd, ^3J = 7.9 Hz, ^4J = 1.8, 1.1 Hz, 1H, *H*-12), 6.63 (t, ^3J = 7.9 Hz, 1H, *H*-11), 1.75 (s, 3H, CH_3), -2.92 (s, br, 2H, *H*-N) ppm.
^{19}F NMR (470 MHz, 300 K, CD_2Cl_2, $CFCl_3$): δ = -139.62 (dd, ^3J = 23.4 Hz, ^4J = 4.5 Hz, 2F, A-*o*-*F*), -139.86 (dd, ^3J = 23.5 Hz, ^4J = 5.8 Hz, 1F, B-*o*-*F*), -140.00 (dd, ^3J = 24.1 Hz, ^4J = 6.2 Hz, 1F, B-*o'*-*F*), -140.10 (dd, ^3J = 24.1 Hz, ^4J = 5.5 Hz, 2F, A-*o'*-*F*), -155.65 (t, ^3J = 20.2 Hz, 2F, A-*p*-*F*), -155.74 (t, ^3J = 20.1 Hz, 1F, B-*p*-*F*), -164.43 to -164.78 (m, 6F, A-*m*-*F*, A-*m'*-*F*, B-*m*-*F*, B-*m'*-*F*) ppm.
MS (HR): m/z (calc.) = 1080.194 (1080.192) $[M+H]^+$.

VI.13 Synthesis of Me-RP (1b)

mf-Me-RP (**17b**) (300 mg, 278 µmol) and nickel(II) acetylacetonate (714 mg, 2.78 mmol) were dissolved in toluene (120 mL) and stirred under reflux for 4 d. The solvent was removed under reduced pressure and the crude product was purified by column chromatography (chloroform, R_f (chloroform / ethanol = 95:5) = 0.40).

Yield: 180 mg (158 µmol, 57 %)

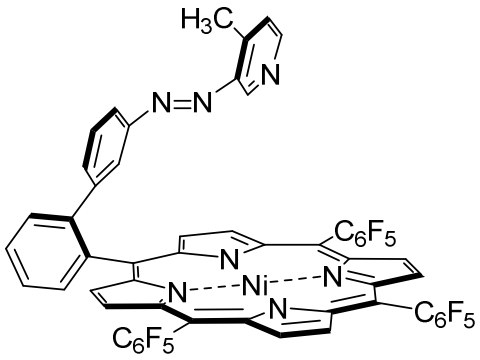

^{1}H NMR (600 MHz, 298 K, acetone-d_6, TMS): δ = 9.15-9.13 (m, 4H, *H*-26, *H*-27), 9.06 (d, ^3J = 4.9 Hz, 2H, *H*-22), 9.01 (d, ^3J = 4.9 Hz, 2H, *H*-21), 8.34 (s, br, 1H, *H*-6), 8.31 (dd, ^3J = 7.4 Hz, ^4J = 0.9 Hz, 1H, *H*-15), 8.12 (s, br, 1H, *H*-2), 8.00 (td, ^3J = 7.7 Hz, ^4J = 1.2 Hz, 1H, *H*-17), 7.91 (dd, ^3J = 7.9 Hz, ^4J = 1.0 Hz, 1H, *H*-18), 7.88 (td, ^3J = 7.6 Hz, ^4J = 1.3 Hz, 1H, *H*-16), 7.43 (t, ^4J = 1.7 Hz, 1H, *H*-8), 7.17 (ddd, ^3J = 7.9 Hz, ^4J = 1.7, 1.2 Hz, *H*-12), 7.13 (ddd, ^3J = 8.0 Hz, ^4J = 1.8, 1.1 Hz, 1H, *H*-10), 7.11 (d, ^3J = 4.6 Hz, 1H, *H*-5), 6.80 (t, ^3J = 7.9 Hz, 1H, *H*-11), 1.77 (s, 3H, C*H*$_3$) ppm.

^{19}F NMR (470 MHz, 300 K, CD_2Cl_2, $CFCl_3$): δ = -137.33 (dd, ^3J = 23.9 Hz, ^4J = 5.0 Hz, 2F, A-*o*-*F*), -137.64 (dd, ^3J = 23.5 Hz, ^4J = 6.2 Hz, 1F, B-*o*-*F*), -137.81 (dd, ^3J = 23.8 Hz, ^4J = 5.9 Hz, 1F, B-*o'*-*F*), -138.04 (dd, ^3J = 23.6 Hz, ^4J = 5.7 Hz, 2F, A-*o'*-*F*), -152.85 (t, ^3J = 21.7 Hz, 1F, B-*p*-*F*), -152.98 (t, ^3J = 19.9 Hz, 1F, B-*p*-*F*), -162.36 to -162.56 (m, 6F, A-*m*-*F*, A-*m'*-*F*, B-*m*-*F*, B-*m'*-*F*) ppm.

MS (EI, 70 eV): m/z (%) = 1135 (100) $[M]^+$, 1015 (12) $[M\text{-}C_6H_6N_3]^+$, 568 (6) $[M]^{2+}$.

MS (CI, isobutane): m/z (%) = 1136 (100) $[M+H]^+$.

MS (HR): m/z (calc.) = 1136.113 (1136.112) $[M+H]^+$.

VI.14 Synthesis of 3-amino-4-methoxypyridine (4a)

3-Nitro-4-methoxypyridine (**3a**) (2.15 g, 14.0 mmol) was dissolved in dimethylformamide (105 mL). Palladium on charcoal (10 %, 215 mg) was added and the mixture was stirred in a flask with baffles under hydrogen atmosphere overnight. The mixture was filtered through Celite® and the solvent was removed under reduced pressure. The crude product was dissolved in half concentrated hydrochloric acid and washed with chloroform. The acetic layer was alkalized with sodium hydroxide solution (25 %) and extracted three times with chloroform. The combined organic layers were dried over magnesium sulfate and the solvent was removed under reduced pressure.

Yield: 1.02 g (8.22 mmol, 59 %)

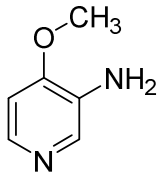

m.p.: 66.2 °C

FT-IR (layer): υ = 3402 (w), 3329 (w), 3169 (m), 3093 (m), 2935 (w), 2841 (w), 1574 (s), 1510 (s), 1426 (s), 1302 (s), 1283 (s), 2133 (s), 1181 (s), 1021 (vs), 936 (w), 908 (w), 888 (m), 854 (m), 807 (vs), 766 (s), 747 (s), 592 (s) 521 (s) cm^{-1}.

^{1}H NMR (500 MHz, 300 K, $CDCl_3$, TMS): δ = 8.06 (s, 1H, *H*-2), 7.90 (d, ^{3}J = 5.7 Hz, 1H, *H*-6), 6.72 (d, ^{3}J = 5.7 Hz, 1H, *H*-5), 4.09 (s, br, 2H, *H*-N), 3.89 (s, 3H, C*H*$_3$) ppm.

^{13}C NMR (125 MHz, 300 K, $CDCl_3$, TMS): δ = 154.2 (*C*4), 138.4 (*C*6), 134.1 (*C*3), 132.9 (*C*2), 105.7 (*C*5), 55.7 (*C*H$_3$) ppm.

MS (EI, 70 eV): m/z (%) = 124 (100) $[M]^+$, 109 (39) $[M\text{-}NH_2]^+$.

MS (CI, isobutane): m/z (%) = 125 (100) [M+H].

EA: ($C_6H_8N_2O$)		C / %	H / %	N / %
	found:	58.11	6.63	22.81
	calc.:	58.05	6.50	22.57

VI.15 Synthesis of 3-(3-bromophenylazo)-4-methoxypyridine (8a)

A. 3-Amino-4-methoxypyridine (**4a**) (1.85 g, 14.9 mmol) was dissolved in a mixture of toluene (30 mL) and potassium hydroxide solution (60 %, 25 mL) at 100 °C. 1-Bromo-3-nitrosobenzene (**7**) (0.67 equivalents) obtained by general procedure V.1.1 was added and it was stirred overnight at 100 °C. The m ixture was poured onto water and extracted three times with ethyl acetate. The combined organic layers were dried over magnesium sulfate and the solvent was removed under reduced pressure. The crude product was purified by column chromatography (ethyl acetate, R_f = 0.38).

Yield: 1.17 g (4.00 mmol, 40 %)

B. Sodium (2.00 g, 87.0 mmol) was dissolved in methanol (100 mL). 3-(3-bromophenylazo)-4-chloropyridine (**8d**) (1.05 g, 3.54 mmol) was added. The mixture was stirred overnight at 50 °C. The majority of the solvent was removed under reduced pressure. The residue was poured into water and extracted three times with ethyl acetate. The combined organic layers were dried over magnesium sulfate and the solvent was removed under reduced pressure. The crude product was purified by column chromatography (ethyl acetate, R_f = 0.38).

Yield: 1.00 g (3.43 mmol, 97 %)

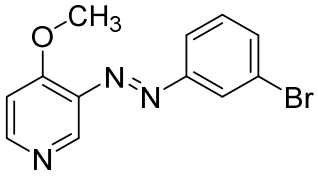

m.p.: 102.0 °C

FT-IR (layer): ϖ = 2975 (w), 1569 (s), 1493 (s), 1444 (s), 1300 (s), 1276 (vs), 1195 (s), 1087 (w), 1063 (m), 1019 (vs), 935 (m), 871 (m), 852 (m), 816 (s), 785 (vs), 754 (s), 704 (m), 677 (s), 653 (m), 587 (s), 567 (m), 544 (m), 520 (m) cm^{-1}.

^{1}H NMR (500 MHz, 300 K, $CDCl_3$): δ = 8.58 (s, 1H, *H*-2), 8.48 (d, ^3J = 5.8 Hz, 1H, *H*-6), 7.95 (t, ^4J = 1.9 Hz, 1H, *H*-8), 7.81 (ddd, ^3J = 8.0 Hz, ^4J = 1.8, 1.0 Hz, 1H, *H*-12), 7.53 (ddd, ^3J = 8.0 Hz, ^4J = 1.8, 1.0 Hz, 1H, *H*-10), 7.33 (t, ^3J = 8.0 Hz, 1H, *H*-11), 6.96 (d, ^3J = 5.8 Hz, 1H, *H*-5), 4.00 (s, 3H, CH_3) ppm.

^{13}C NMR (125 MHz, 300 K, $CDCl_3$): δ = 162.1 (*C*4), 153.8 (*C*7), 153.2 (*C*6), 138.8 (*C*2), 137.9 (*C*3), 134.0 (*C*10), 130.5 (*C*11), 124.6 (*C*8), 123.4 (*C*12), 123.2 (*C*9), 108.0 (*C*5), 56.2 (*C*H_3) ppm.

MS (EI, 70 eV): m/z (%) = 291 (59) $[M]^+$, 155 (78) $[BrPh]^+$, 136 (70) $[M\text{-}BrPh]^+$, 108 (100) $[M\text{-}BrPhN_2]^+$.

MS (CI, isobutane): m/z (%) = 292 (100) $[M+H]^+$, 136 (17) $[M\text{-}BrPh]^+$, 108 (14) $[M\text{-}BrPhN_2]^+$.

UV / Vis (Toluol): λ_{max} (lg ε) = 336 (4.095), 449 (2.766) nm.

EA: ($C_{12}H_{10}BrN_3O$)		C / %	H / %	N / %
	found:	48.82	3.50	14.01
	calc.:	49.34	3.45	14.38

VI.16 Synthesis of 3-(3-(2-formylphenyl)phenylazo)-4-methoxypyridine (10a)

3-(3-Bromophenylazo)-4-methoxypyridine (**8a**) (917 mg, 3.14 mmol) was used for a Suzuki coupling reaction according to general procedure V.1.2. The crude product was purified by column chromatography (ethyl acetate, R_f = 0.35). The product was obtained as an orange solid.

Yield: 950 mg (3.00 mmol, 96 %)

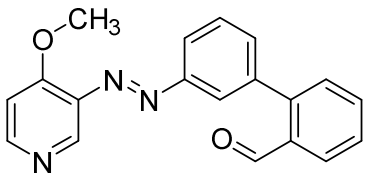

m.p.: 133.7 °C

FT-IR (layer): υ = 3058 (w), 2992 (w), 2949 (w), 2893 (w), 2842 (w), 2755 (w), 1694 (s), 1575 (s), 1487 (m), 1460 (m), 1395 (m), 1303 (m), 1269 (s), 1189 (s), 1120 (w), 1019 (vs), 906 (m), 827 (s), 800 (s), 765 (vs), 697 (vs), 650 (m), 576 (m), 557 (m), 534 (s) cm^{-1}.

^{1}H NMR (500 MHz, 300 K, $CDCl_3$, TMS): δ = 9.97 (s, 1H, C*H*O), 8.50 (s, 1H, *H*-2), 8.50 (d, ^3J = 5.8 Hz, 1H, *H*-6), 7.99 (dd, ^3J = 7.9 Hz, ^4J = 1.3 Hz, 1H, *H*-15), 7.94 (ddd, ^3J = 7.9 Hz, ^4J = 1.8, 1.2 Hz, 1H, *H*-12), 7.87 (t, ^4J = 1.8 Hz, 1H, *H*-8), 7.61 (dt, ^3J = 7.5 Hz,

^4J = 1.3 Hz, 1H, *H*-17), 7.57 (t, ^3J = 7.8 Hz, 1H, *H*-11), 7.48 (tt, ^3J = 7.6 Hz, ^3J = 0.9 Hz, 1H, *H*-16), 7.44 (dd, ^3J = 7.6 Hz, ^4J = 1.1 Hz, 1H, *H*-18), 7.42 (ddd, ^3J = 7.6 Hz, ^4J = 1.8, 1.2 Hz, 1H, *H*-10), 7.01 (d, ^3J = 5.8 Hz, 1H, *H*-5), 4.01 (s, 3H, CH_3) ppm.

^{13}C NMR (125 MHz, 300 K, $CDCl_3$, TMS): δ = 191.9 (*C*O), 162.4 (*C*4), 152.8 (*C*7), 152.2 (*C6*), 144.8 (*C*13), 139.0 (*C*9), 138.3 (*C*3), 138.2 (*C*2), 133.7 (*C*14), 133.7 (*C*17), 133.0 (*C*10), 130.8 (*C*18), 129.3 (*C*11), 128.3 (*C*16), 127.9 (*C*15), 123.8 (*C*8), 123.5 (*C*12), 108.2 (*C*5), 56.3 (*C*H_3) ppm.

MS (EI, 70 eV): m/z (%) = 317 (100) $[M]^+$, 210 (12) $[M\text{-}MeOPy]^+$, 181 (52) $[M\text{-}MeO\text{-}Py\text{-}N_2]^+$, 153 (72) $[Ph_2]^+$, 136 (18) $[MeOPyN_2]^+$, 108 (43) $[MeOPy]^+$.

MS (CI, isobutane): m/z (%) = 318 (79) $[M+H]^+$, 198 (100) [M-MeOPyN+H].

UV / Vis (MeCN): λ_{max} (lg ε) = 233 (4.419), 326 (4.112), 442 (2.938) nm.

EA: ($C_{19}H_{15}N_3O_2$)

	C / %	H / %	N / %
found:	71.84	4.81	12.81
calc.:	71.91	4.76	13.24

VI.17 Synthesis of mf-MeO-RP (17a)

3-(3-(2-Formylphenyl)phenylazo)-4-methylpyridine (**10a**) (590 mg, 1.86 mmol) and penta-fluorobenzaldehyde (**16**) (365 mg, 1.86 mmol) were dissolved in chloroform (200 mL) under nitrogen atmosphere. Boron trifluoride diethyl ether (397 µL, 3.16 mmol) was added. *meso*-Pentafluorophenyl dipyrromethane (**16**) (1.16 g, 3.72 mmol) dissolved in 20 mL chloroform was added within 30 min by a syringe pump. After 5 h of stirring *p*-chloranil (961 mg, 3.91 mmol) was added and the mixture was stirred overnight at reflux. After addition of triethylamine (1 mL) stirring was continued for 30 min at room temperature. The solvent was removed under reduced pressure. The crude product was purified by column chromatography (chloroform, R_f (chloroform / ethanol = 97:3) = 0.22).

Yield: 89.0 mg (81.3 µmol, 4.4 %)

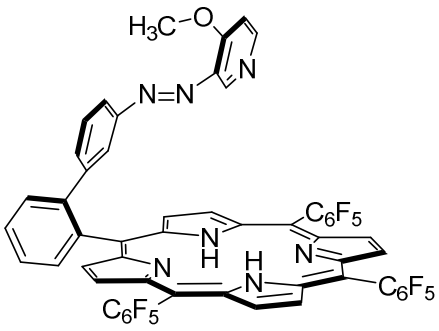

^{1}H NMR (500 MHz, 300 K, CD_2Cl_2, TMS): δ = 9.01 (d, ^{3}J = 4.7 Hz, 2H, *H*-21), 8.89 (m, 4H, *H*-26, *H*-27), 8.78 (d, ^{3}J = 4.7 Hz, 2H, *H*-22), 8.39 (d, ^{3}J = 5.8 Hz, 1H, *H*-6), 8.22 (dd, ^{3}J = 7.5 Hz, ^{4}J = 1.1 Hz, 1H, *H*-15), 8.16 (s, 1H, *H*-2), 7.99 (td, ^{3}J = 8.0 Hz, ^{4}J = 1.2 Hz, 1H, *H*-17), 7.96 (dd, ^{3}J = 8.0 Hz, ^{4}J = 2.0 Hz, 1H, *H*-18), 7.89 (t, ^{4}J = 1.8 Hz, 1H, *H*-8), 7.81 (td, ^{3}J = 7.3 Hz, ^{4}J = 1.9 Hz, 1H, *H*-16), 6.98 (ddd, ^{3}J = 7.9 Hz, ^{4}J = 2.0, 1.1 Hz, 1H, *H*-10), 6.88 (d, ^{3}J = 5.8 Hz, 1H, *H*-5), 6.85 (ddd, ^{3}J = 7.8 Hz, ^{4}J = 1.8, 1.1 Hz, 1H, *H*-12), 6.35 (t, ^{3}J = 7.9 Hz, 1H, *H*-11), 3.78 (s, 3H, C*H*$_3$), -2.95 (s, 2H, *H*-N) ppm.

^{19}F NMR (470 MHz, 300 K, CD_2Cl_2, $CFCl_3$): δ = -137.27 (dd, ^{3}J = 23.8 Hz, ^{4}J = 6.7 Hz, 2F, A-*o*-*F*), -137.57 (dd, ^{3}J = 23.9 Hz, ^{4}J = 7.0 Hz, 1F, B-*o*-*F*), -137.67 (dd, ^{3}J = 24.1 Hz, ^{4}J = 7.2 Hz, 1F, B-*o'*-*F*), -137.78 (dd, ^{3}J = 23.6 Hz, ^{4}J = 6.4 Hz, 2F, A-*o'*-*F*), -152.98 (t, ^{3}J = 20.3 Hz, 1F, B-*p*-*F*), -153.04 (t, ^{3}J = 20.8 Hz, 2F, A-*p*-*F*), -162.50 to -162.74 (m, 6F, A-*m*-*F*, A-*m'*-*F*, B-*m*-*F*, B-*m'*-*F*) ppm.

MS (EI, 70 eV): m/z (%) = 1095 (100) $[M]^{+}$, 548 (12) $[M]^{2+}$.

VI.18 Synthesis of MeO-RP (1a)

mf-MeO-RP (**17a**) (130 mg, 119 µmol) and nickel(II) acetylacetonate (366 mg, 1.42 mmol) were dissolved in toluene (120 mL) and stirred at reflux for 5 d. The solvent was removed under reduced pressure and the crude product was purified by column chromatography (chloroform, R_f (chloroform / ethanol = 90:10) = 0.40).

Yield: 61.0 mg (52.9 µmol, 45 %)

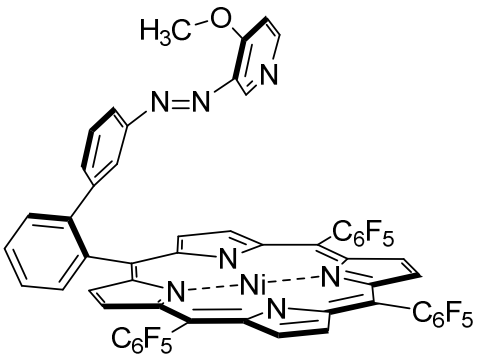

^{1}H NMR (600 MHz, 300 K, acetone-d_6, TMS): δ = 9.13 (s, 4H, *H*-26, *H*-27), 9.05 (d, ^3J = 4.7 Hz, 2H, *H*-22), 9.00 (d, ^3J = 4.7 Hz, 2H, *H*-21), 8.42 (d, ^3J = 5.9 Hz, 1H, *H*-6), 8.28 (dd, ^3J = 7.6 Hz, ^4J = 0.9 Hz, 1H, *H*-15), 8.11 (s, 1H, *H*-2), 8.01 (td, ^3J = 8.0 Hz, ^4J = 1.0 Hz, 1H, *H*-17), 7.91 (dd, ^3J = 8.0 Hz, ^4J = 1.0 Hz, 1H, *H*-18), 7.87 (td, ^3J = 7.5 Hz, ^4J = 1.3 Hz, 1H, *H*-16), 7.75 (t, ^4J = 1.7 Hz, 1H, *H*-8), 7.13 (d, ^3J = 5.9 Hz, 1H, *H*-5), 7.05 (ddd, ^3J = 7.8 Hz, ^4J = 1.8, 1.0 Hz, 1H, *H*-12), 6.87 (ddd, ^3J = 7.9 Hz, ^4J = 1.6, 1.1 Hz, 1H, *H*-10), 6.55 (t, ^3J = 7.9 Hz, 1H, *H*-11), 3.83 (s, 3H, CH_3) ppm.
^{19}F NMR (470 MHz, 300 K, CD_2Cl_2, $CFCl_3$): δ = -139.38 (d, ^3J = 23.4 Hz, 2F, A-*o*-*F*), -139.69 (d, ^3J = 23.1 Hz, 1F, B-*o*-*F*), -139.92 (d, ^3J = 23.4 Hz, 1F, B-*o'*-*F*), -140.09 (d, ^3J = 23.1 Hz, 2F, A-*o'*-*F*), -155.72 (t, ^3J = 20.1 Hz, 2F, A-*p*-*F*), -155.76 (t, ^3J = 19.2 Hz, 1F, B-*p*-*F*), -162.25 (td, ^3J = 21.8 Hz, ^4J = 6.1 Hz, 2F, A-*m*-*F*), -164.44 to -164.68 (m, 4F, A-*m'*-*F*, B-*m*-*F*, B-*m'*-*F*) ppm.
MS (EI, 70 eV): m/z (%) = 1150 (100) $[M]^+$, 1030 (12) $[M\text{-}C_6H_6N_2O]^+$, 576 (11) $[M]^{2+}$.
MS (HR): m/z (calc.) = 1152.107 (1152.107) $[M+H]^+$.

VI. 19 Synthesis of 3-(3-bromphenylazo)-4-isopropoxypyridine (8g)

Sodium (1.00 g, 43.7 mmol) was dissolved in 150 mL isopropanol at 60 ℃. 3-(3-Bromphenylazo)-4-chloropyridine (**8d**) (200 mg, 0.674 mmol) was added. The mixture was stirred 1.5 h at 60 ℃. The mixture was poured into water (300 mL) and extracted three times with ethyl acetate. The combined organic layers were dried over magnesium sulfate and the solvent was removed under reduced pressure. The crude product was purified by column chromatography (ethylacetat, R_f = 0.36). The product was obtained as an orange solid

Yield: 197 mg (0.615 mmol, 91 %)

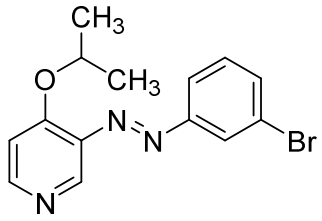

m.p.: 72.0 ℃

FT-IR (layer): υ = 3105 (w), 2984 (w), 2930 (w), 1582 (s), 1563 (m), 1486 (m), 1461 (m), 1387 (w), 1302 (s), 1272 (vs), 1191 (s), 1105 (s), 1062 (m), 946 (vs), 881 (m), 836 (w), 815 (vs), 786 (vs), 754 (w), 704 (m), 678 (s), 653 (w), 586 (w), 538 (m) cm^{-1}.

^{1}H NMR (500 MHz, 300 K, $CDCl_3$, TMS): δ = 8.62 (s, 1H, *H*-2), 8.48 (d, ^3J = 5.9 Hz, 1H, *H*-6), 8.02 (t, ^4J = 1.9 Hz, 1H, *H*-8), 7.87 (ddd, ^3J = 8.0 Hz, ^4J = 1.8, 1.0 Hz, 1H, *H*-12), 7.59 (ddd, ^3J = 8.0 Hz, ^4J = 2.0, 1.0 Hz, 1H, *H*-10), 7.39 (t, ^3J = 8.0 Hz, 1H, *H*-11), 6.98 (d, ^3J = 5.9 Hz, 1H, *H*-5), 4.83 (sept, ^3J = 6.1 Hz, 1H, C*H*), 1.47 (d, ^3J = 6.1 Hz, 6H, CH_3) ppm.

^{13}C NMR (125 MHz, 300 K, $CDCl_3$, TMS): δ = 160.8 (*C*4), 153.9 (*C*7), 153.1 (*C*6), 139.5 (*C*2), 138.7 (*C*3), 133.9 (*C*10), 130.5 (*C*11), 125.1 (*C*8), 123.3 (*C*12), 123.2 (*C*9), 110 (*C*5), 72.2 (*C*H), 22.0 (*C*H_3) ppm.

MS (EI, TOF): m/z (%) = 319 (5) $[M]^+$, 182 (10) $[BrPhN_2]^+$, 155 (72) $[BrPh]^+$, 149 (100) $[M\text{-}BrPhN]^+$.

EA: ($C_{12}H_{10}BrN_3O$)		C / %	H / %	N / %
	found:	52.52	4.41	13.12
	calc.:	52.78	4.41	13.31

VI. 20 Synthesis of 3-(3-(2-formylphenyl)phenylazo)-4-isopropoxypyridine (10g)

3-(3-Bromphenylazo)-4-isopropoxypyridine (**8g**) (473 mg, 1.48 mmol) was utilized for a Suzuki coupling reaction according to general procedure V.1.2. The crude product was purified by column chromatography (ethyl acetate, R_f = 0.26). The product was obtained as an orange solid.

Yield: 500 mg (1.45 mmol, 98 %)

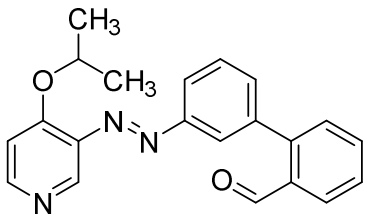

m.p.: 134.8 °C

FT-IR (layer): ῡ = 2985 (w), 2835 (w), 2746 (w), 1694 (vs), 1581 (s), 1563 (s), 1485 (s), 1389 (w), 1302 (m), 1270 (s), 1198 (s), 1140 (w), 1103 (s), 1066 (w), 949 (s), 907 (w), 877 (w), 827 (s), 801 (m), 762 (vs), 694 (s), 650 (m), 576 (w), 527 (m) cm^{-1}.

^{1}H NMR (500 MHz, 300 K, $CDCl_3$): δ = 10.05 (s, 1H, C*H*O), 8.65 (s, 1H, *H*-2), 8.49 (d, ^3J = 5.9 Hz, 1H, *H*-6), 8.06 (dd, ^3J = 7.8 Hz, ^4J = 1.4 Hz, 1H, *H*-15), 7.99 (ddd, ^3J = 8.0 Hz, ^4J = 1.9, 1.1 Hz, 1H, *H*-12), 7.94 (t, ^4J = 1.8 Hz, 1H, *H*-8), 7.68 (td, ^3J = 7.5 Hz, ^4J = 1.4 Hz, 1H, *H*-17), 7.62 (t, ^3J = 7.7 Hz, 1H, *H*-11), 7.55-7.51 (m, 2H, H-16, *H*-18), 7.49 (ddd, ^3J = 7.6 Hz, ^4J = 1.7, 1.2 Hz, 1H, *H*-10), 6.99 (d, ^3J = 5.9 Hz, 1H, *H*-5), 4.84 (sept, ^3J = 6.1 Hz, 1H, C*H*), 1.47 (d, ^3J = 6.1 Hz, 6H, CH_3) ppm.

^{13}C NMR (125 MHz, 300 K, $CDCl_3$): δ = 192.1 (*C*HO), 160.7 (*C*4), 153.0 (*C*6), 153.0 (*C*7), 145.1 (*C*13), 139.6 (*C*2), 139.0 (*C*3, *C*9), 133.9 (*C*14), 133.8 (*C*17), 132.8 (*C*10), 130.9 (*C*18), 129.3 (*C*11), 128.3 (*C*16), 128.0 (*C*15), 124.6 (*C*8), 123.0 (*C*12), 110.1 (*C*5), 72.2 (*C*H), 22.0 (*C*H_3) ppm.

MS (EI, TOF): m/z (%) = 345 (6) $[M]^+$, 153 (100) $[Ph_2]^+$, 149 (93) $[M\text{-}HOCPh_2N]^+$.

EA: ($C_{19}H_{15}N_3O_2$)		C / %	H / %	N / %
	found:	72.07	5.59	12.38
	calc.:	72.03	5.54	12.17

VI. 21 Synthesis of 3-nitro-4-*N*,*N*-dimethylaminopyridine (3e)

4-*N*,*N*-Dimethylaminopyridine (**2e**) (5.48 g, 44.9 mmol) was dissolved in concentrated sulfuric acid (100 mL) at 0 °C. A mixture of nitric acid (5.3 mL) and sulfuric acid (100 mL) was added slowly at 0 °C. After stirring for 3 h at room temperature, the mixture was poured onto ice and neutralized with sodium carbonate solution. The aqueous layer was extracted three times with chloroform. The combined organic layers were dried over magnesium sulfate and the solvent was removed under reduced pressure. The crude product was purified by column chromatography (ethyl acetate, R_f = 0.35). The product was obtained as a yellow solid.

Yield: 4.04 g (24.2 mmol, 54 %)

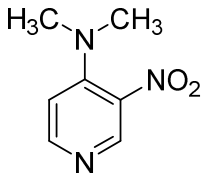

m.p.: 158.0 °C

FT-IR (layer): υ = 3296 (w), 2914 (w), 1601 (s), 1537 (s), 1498 (s) 1465 (s) 1385 (m), 1344 (s), 1303 (m), 1263 (s), 1219 (vs), 1166 (s), 1042 (s), 960 (s), 851 (s), 813 (vs), 760 (s), 679 (m), 658 (m), 588 (m), 561 (s), 548 (s), 534 (s) cm^{-1}.

^{1}H NMR (500 MHz, 300 K, $CDCl_3$, TMS): δ = 8.76 (s, 1H, *H*-2), 8.26 (d, ^3J = 6.2 Hz, 1H, *H*-6), 6.78 (d, ^3J = 6.2 Hz, 1H, *H*-5), 2.98 (s, 6H, C*H*$_3$) ppm.

^{13}C NMR (125 MHz, 300 K, $CDCl_3$, TMS): δ = 151.1 (*C*6), 149.2 (*C*4), 148.0 (*C*2), 135.0 (*C*3), 110.7 (*C*5), 41.6 (*C*H_3) ppm.

MS (EI, 70 eV): m/z (%) = 167 (48) $[M]^+$, 150 (84) $[M\text{-}O]^+$, 122 (55) $[M\text{-}N(Me)_2]^+$, 119 (100) $[M\text{-}NO_2]^+$, 105 (31) $[M\text{-}N(Me)_2\text{-}O]^+$.

MS (CI, isobutane): m/z (%) = 168 (100) $[M+H]^+$.

EA: ($C_7H_9N_3O_2$)		C / %	H / %	N / %
	found:	50.54	5.63	25.66
	calc.:	50.29	5.43	25.14

VI. 22 Synthesis of 3-amino-4-*N*,*N*-dimethylaminopyridine dihydrochloride (4e)

3-Nitro-4-*N*,*N*-dimethylaminopyridine (**3e**) (1.00 g, 5.98 mmol) was dissolved in dimethylformamide (100 mL). Palladium on charcoal (10 %, 100 mg) was added and the mixture was stirred in a chicane flask under hydrogen atmosphere overnight. After filtration through Celite®, the solvent was removed under reduced pressure. The crude product was dissolved in a minimum volume of tetrahydrofuran. By addition of concentrated hydrochloric acid a brown solid precipitated which was filtered off and washed with tetrahydrofuran.

Yield: 1.15 g (5.50 mmol, 92 %)

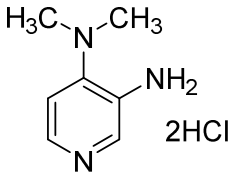

m.p.: 203.3 °C

FT-IR (layer): υ = 2703 (m), 2580 (s), 1650 (s), 1596 (m), 1557 (vs), 1484 (s), 1424 (s), 1391 (s), 1313 (w), 1280 (s), 1204 (s), 1148 (w), 1110 (m), 1082 (w), 1054 (m), 990 (w), 889 (m), 821 (vs), 725 (s), 703 (w), 549 (w), 504 (w), 433 (m) cm^{-1}.

^{1}H NMR (500 MHz, 300 K, $CDCl_3$, TMS): δ = 7.93 (s, 1H, *H*-2), 7.88 (d, ^{3}J = 5.3 Hz, 1H, *H*-6), 6.71 (d, ^{3}J = 5.3 Hz, 1H, *H*-5), 3.90 (s, br, 2H, *H*-N), 2.66 (s, 6H, CH_3) ppm.

^{13}C NMR (125 MHz, 300 K, $CDCl_3$, TMS): δ = 146.8 (*C*4), 140.7 (*C*6), 136.9 (*C*2), 136.5 (*C*3), 112.8 (*C*5), 41.6 (*C*H_3) ppm.

MS (EI, 70 eV): m/z (%) = 137 (100) $[M\text{-}2HCl]^+$, 122 (45) $[M\text{-}2HCl\text{-}CH_3]^+$, 107 (8) $[M\text{-}2HCl\text{-}2CH_3]^+$.

MS (CI, isobutane): m/z (%) = 138 (100) $[M+H]^+$.

EA: ($C_7H_{13}N_3Cl_2$)		C / %	H / %	N / %
	found:	40.00	6.23	19.93
	calc.:	40.02	6.24	20.00

VI. 23 Synthesis of 3-(3-bromphenylazo)-4-*N*,*N*-dimethylaminopyridine (8e)

3-Amino-4-*N*,*N*-dimethylaminopyridine (**4e**) (1.99 g, 14.5 mmol) was dissolved in a mixture of pyridine (50 mL) and sodium hydroxide solution (40 %, 15 mL) and warmed up to 40 °C. 1-Bromo-3-nitrosobenzene (**7**) (1.4 equivalents) obtained by general procedure V.1.1 was added. After 6 h of stirring at 40 °C the mixture was poured into water and extracted three times with dichloromethane. The combined organic layers were dried over magnesium sulfate and the solvent was removed under reduced pressure. The crude product was purified by column chromatography (ethyl acetate, R_f = 0.11). The product was obtained as an orange-red solid.

Yield: 558 mg (1.84 mmol, 19 %)

Dimethylammonium chloride (864 mg, 10.6 mmol) was dissolved in a mixture of acetonitrile (135 mL) and triethylamine (15 mL). 3-(3-Bromphenylazo)-4-chloropyridine (**8d**) (315 mg, 1.06 mmol) was added and the mixture was stirred for 6 h at 40 °C. The solvent was removed under reduced pressure and the crude product was purified by column chromatography (ethyl acetate, R_f = 0.11). The product was obtained as an orange-red solid.

Yield: 210 mg (688 µmol, 65 %)

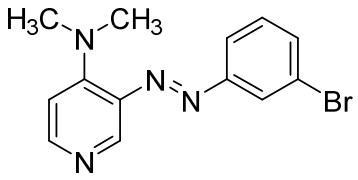

m.p.: 85.9 °C (decomposition)

FT-IR (layer): ῡ = 2919 (m), 2814 (m), 1589 (vs), 1521 (s), 1506 (s), 1464 (s), 1404 (s), 1366 (s), 1289 (vs), 1228 (m), 1200 (vs), 1171 (vs), 1130 (s), 1064 (vs), 994 (m), 954 (s), 937 (m), 919 (m), 870 (m), 807 (s), 793 (vs), 755 (s), 743 (s), 677 (vs) cm^{-1}.

^{1}H NMR (500 MHz, 300 K, $CDCl_3$, TMS): δ = 8.46 (s, 1H, *H*-2), 8.12 (d, ^3J = 6.2 Hz, 1H, *H*-6), 7.84 (t, ^4J = 1.9 Hz, 1H, *H*-8), 7.73 (ddd, ^3J = 8.0 Hz, ^4J = 1.8, 1.1 Hz, 1H, *H*-12), 7.50 (ddd, ^3J = 8.0 Hz, ^4J = 1.8, 1.1 Hz, 1H, *H*-10), 7.32 (t, ^3J = 8.0 Hz, 1H, *H*-11), 6.68 (d, ^3J = 6.2 Hz, 1H, *H*-5), 3.22 (s, 6H, C*H*$_3$) ppm.

^{13}C NMR (125 MHz, 300 K, $CDCl_3$, TMS): δ = 153.6 (*C*7), 152.9 (*C*4), 149.2 (*C*6), 138.2 (*C*2), 136.9 (*C*3), 133.3 (*C*10), 130.6 (*C*11), 124.5 (*C*8), 123.2 (*C*12), 123.0 (*C*9), 110.4 (*C*5), 43.9 (*C*H_3) ppm.

MS (EI, 70 eV): m/z (%) = 304 (10) $[M]^+$, 134 (100) $[C_7H_8N_3]^+$.

MS (CI, isobutane): m/z (%) = 361 (5) $[M+C_4H_9]^+$, 305 (92) $[M+H]^+$, 134 (31) $[C_7H_8N_3]^+$.

EA: ($C_{13}H_{13}N_4Br$)		C / %	H / %	N / %
	found:	50.79	4.16	17.90
	calc.:	51.16	4.29	18.36

VI. 24 Synthesis of 3-(3-(2-formylphenyl)phenylazo)-4-*N*,*N*-dimethylamino-pyridine (10e)

3-(3-Bromphenylazo)-4-*N*,*N*-dimethylaminopyridine (**8e**) (387 mg, 1.27 mmol) was utilized for a Suzuki coupling reaction according to general procedure V.1.2. The crude product was purified by column chromatography (dichloromethane / methanol = 49:1, R_f = 0.35). The product was obtained as an orange solid.

Yield: 340 mg (1.03 mmol, 81 %)

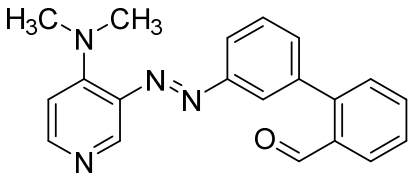

m.p.: 82.8 °C (decomposition)

FT-IR (layer): ῡ = 2882 (m), 1686 (s), 1593 (vs), 1528 (s), 1514 (s), 1435 (s), 1408 (w), 1394 (w), 1369 (w), 1288 (m), 1256 (m), 1194 (s), 1167 (s), 1121 (m), 1069 (s), 959 (s), 900 (w), 825 (m), 801 (m), 758 (vs), 721 (s), 698 (s), 647 (m), 540 (vs) cm^{-1}.

^{1}H NMR (500 MHz, 300 K, $CDCl_3$): δ = 10.03 (s, 1H, C*H*O), 8.55 (s, 1H, *H*-2), 8.19 (d, ^3J = 6.1 Hz, 1H, *H*-6), 8.04 (ddd, ^3J = 7.8 Hz, ^4J = 1.4, 0.4 Hz, 1H, *H*-15), 7.91 (ddd, ^3J = 8.0 Hz, ^4J = 1.9, 1.1 Hz, 1H, *H*-12), 7.82 (t, ^4J = 1.9 Hz, 1H, *H*-8), 7.66 (td, ^3J = 7.5 Hz, ^4J = 1.4 Hz, 1H, *H*-17), 7.60 (t, ^3J = 7.8 Hz, 1H, *H*-11), 7.52 (tt, ^3J = 7.5 Hz, ^4J = 1.1 Hz, 1H, *H*-16), 7.50 (dd, ^3J = 7.7 Hz, ^4J = 1.2 Hz, 1H, *H*-18), 7.45 (ddd, ^3J = 7.5 Hz, ^4J = 1.9, 1.1 Hz, 1H, *H*-10), 6.70 (d, ^3J = 6.1 Hz, 1H, *H*-5), 3.24 (s, 6H, C*H*$_3$) ppm.

^{13}C NMR (125 MHz, 300 K, $CDCl_3$): δ = 192.0 (*C*HO), 152.7 (*C*7), 152.6 (*C*4), 150.7 (*C*6), 145.0 (*C*13), 139.3 (*C*2), 138.8 (*C*9), 137.2 (*C*3), 133.8 (*C*17), 133.7 (*C*14), 131.9 (*C*10), 130.8 (*C*18), 129.3 (*C*11), 128.2 (*C*16), 127.9 (*C*15), 123.9 (*C*8), 122.8 (*C*12), 110.3 (*C*5), 43.7 (*C*H$_3$) ppm.

MS (EI, 70 eV): m/z (%) = 330 (11) $[M]^+$, 277 (19) $[M\text{-}C_3H_3N]^+$, 134 (100) $[C_7H_8N_3]^+$.

MS (CI, isobutane): m/z (%) = 387 (5) $[M+C_4H_9]^+$, 331 (100) $[M+H]^+$, 279 (20) $[M\text{-}C_3H_3N+2H]$, 138 (43) $[C_7H_{12}N_2]^+$, 134 (16) $[C_7H_8N_3]^+$.

VI.25 Synthesis of mf-NMe$_2$-RP (17e)

3-(3-(2-Formylphenyl)phenylazo)-4-*N*,*N*-dimethylamino-pyridine (**10e**) (600 mg, 1.81 mmol) and pentafluorobenzaldehyde (**16**) (355 mg, 1.81 mmol) were dissolved in chloroform (250 mL) under nitrogen atmosphere. Boron trifluoride diethyl ether (345 µL, 2.75 mmol) was added. *meso*-Pentafluorophenyl dipyrromethane (**15**) (1.16 g, 3.72 mmol) dissolved in 30 mL chloroform was added within 60 min by a syringe pump. After 6 h of stirring *p*-chloranil (906 mg, 3.68 mmol) was added and the mixture was stirred overnight at 55 °C. After addition of triet hylamine (4 mL) stirring was continued for 15 min at room temperature. The mixture was filtered through silica gel and the solvent was removed under reduced pressure. The crude product was purified by two column chromatographies (1st: chloroform / triethylamine / methanol = 100:5:2, R_f (chloroform / triethylamine / methanol = 17:2:1) = 0.61) (2nd: ethyl acetate).

Yield: 10.0 mg (9.02 µmol, 0.5 %)

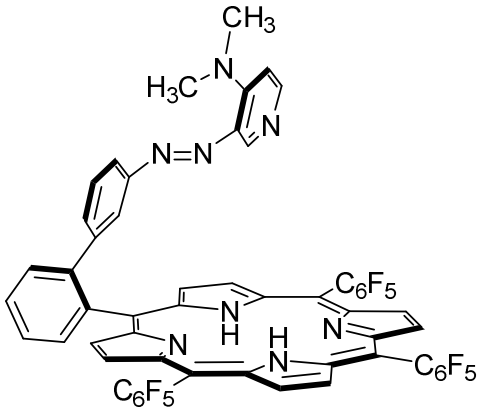

FT-IR (layer): υ = 3319 (w), 2924 (m), 2854 (m), 1650 (w), 1592 (m), 1517 (s), 1497 (s), 1436 (m), 1401 (m), 1350 (m), 1260 (m), 1076 (s), 1041 (s), 1024 (s), 987 (vs), 935 (m), 917 (vs), 862 (w), 801 (vs), 757 (s), 737 (s), 696 (m), 662 (w) cm^{-1}.

^{1}H NMR (500 MHz, 300 K, CD_2Cl_2): δ = 9.01 (d, ^3J = 4.8 Hz, 2H, *H*-21), 8.90 (m, 4H, *H*-26, *H*-27), 8.77 (d, ^3J = 4.8 Hz, 2H, *H*-22), 8.22 (dd, ^3J = 7.5 Hz, ^4J = 1.1 Hz, 1H, *H*-15), 8.00 (s, 1H, *H*-2), 7.98 (d, ^3J = 6.1 Hz, 1H, *H*-6), 7.98 (td, ^3J = 7.5 Hz, ^4J = 1.3 Hz, 1H, *H*-17), 7.95 (dd, ^3J = 7.8 Hz, ^4J = 1.6 Hz, 1H, *H*-18), 7.81 (td, ^3J = 7.4 Hz, ^4J = 1.7 Hz, 1H, *H*-16), 7.67 (t, ^4J = 1.8 Hz, 1H, *H*-8), 6.97 (ddd, ^3J = 7.9 Hz, ^4J = 1.9, 1.1 Hz, 1H, *H*-10), 6.92 (ddd, ^3J = 7.8 Hz, ^4J = 1.7, 1.1 Hz, 1H, *H*-12), 6.47 (d, ^3J = 6.1 Hz, 1H, *H*-5), 6.46 (t, ^3J = 7.9 Hz, 1H, *H*-11), 2.56 (s, 6H, C*H*$_3$), -2.94 (s, 2H, *H*-N) ppm.

^{19}F NMR (470 MHz, 300 K, CD_2Cl_2, $CFCl_3$): δ = -137.34 (dd, ^3J = 24.0 Hz, ^4J = 7.6 Hz, 2F, A-*o*-*F*), -137.59 to -137.68 (m, 2F, B-*o*-*F*, B-*o'*-*F*), -137.75 (dd, ^3J = 23.6 Hz, ^4J = 7.6 Hz, 2F, A-*o'*-*F*), -152.93 (t, ^3J = 20.5 Hz, 1F, B-*p*-*F*), -152.97 (t, ^3J = 20.5 Hz, 2F, A-*p*-*F*), -162.49 to -162.67 (m, 6F, A-*m*-*F*, A-*m'*-*F*, B-*m*-*F*, B-*m'*-*F*) ppm.
MS (HR): m/z (calc.) = 1109.219 (1109.217) $[M+H]^+$.

VI. 26 Synthesis of 3-nitro-4-*N*-pyrrolidinopyridine (3f)

4-*N*-Pyrrolidinopyridine (**2f**) (665 mg, 4.49 mmol) was dissolved in concentrated sulfuric acid (10 mL) at 0 °C. A mixture of nitric acid (0.53 mL) and sulfuric acid (10 mL) was added slowly at 0 °C. After stirring for 3 h at room temperature, the mixture was poured onto ice and neutralized with sodium carbonate solution. The aqueous layer was extracted three times with chloroform. The combined organic layers were dried over magnesium sulfate and the solvent was removed under reduced pressure. The crude product was purified by column chromatography (dichloromethane / methanol = 9:1, R_f = 0.80). The product was obtained as a yellow solid.

Yield: 404 mg (2.09 mmol, 47 %)

3-Nitro-4-chloropyridin (**3d**) (5.00 g, 31.5 mmol) was suspended in 7 mL water. Pyrrolidine (13.0 mL, 158 mmol) was slowly added under vigorous stirring. The orange solution was heated to 130 °C in the microwave oven for 30 min. Dichloromethane (125 mL) was added. The organic layer was washed with saturated sodium carbonate solution. The organic layer was dried over magnesium sulfate and the solvent was removed under reduced pressure. The crude product was purified by column chromatography (dichloromethane / methanol = 95:5, R_f = 0.62). The product was obtained as a yellow solid.

Yield: 5.86 g (30.3 mmol, 96 %)

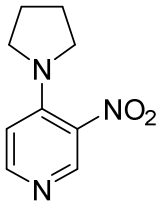

m.p.: 78.5 °C

FT-IR (layer): υ = 3394 (w), 2970 (w), 2880 (w), 1596 (s), 1528 (s), 1495 (vs), 1467 (s) 1340 (m), 1237 (s), 1206 (s), 1040 (m), 969 (s), 932 (m), 845 (s), 802 (s), 753 (s), 694 (m), 641 (m) 588 (s), 543 (s) cm^{-1}.

^{1}H NMR (500 MHz, 300 K, $CDCl_3$, TMS): δ = 8δ = 8.68 (s, 1H, *H*-2), 8.19 (d, ^{3}J = 6.2 Hz, 1H, *H*-6), 6.66 (d, ^{3}J = 6.2 Hz, 1H, *H*-5), 3.26-3.23 (m, 4H, NCH_2), 2.00-1.98 (m, 4H, NCH_2CH_2) ppm.

^{13}C NMR (125 MHz, 300 K, $CDCl_3$, TMS): δ = 150.9 (C6), 147.6 (*C*2), 145.6 (*C*4), 134.6 (*C*3), 110.1 (*C*5), 50.2 (NCH_2), 25.5 (NCH_2CH_2) ppm.

MS (EI, 70 eV): m/z (%) = 193 (26) $[M]^+$, 176 (100) $[M-O]^+$, 146 (93) $[M-NO_2]^+$.

MS (CI, isobutane): m/z (%) = 194 (100) $[M+H]^+$.

EA: ($C_9H_{11}N_3O_2$)		C / %	H / %	N / %
	found:	55.61	5.69	21.92
	calc.:	55.95	5.74	21.75

VI. 27 Synthesis of 3-amino-4-*N*-pyrrolidinopyridine dihydrochloride (4f)

3-Nitro-4-*N*,*N*-dimethylaminopyridine (**3f**) (1.00 g, 5.18 mmol) was dissolved in dimethylformamide (100 mL). Palladium on charcoal (10 %, 100 mg) was added and the mixture was stirred in a buffled flask under hydrogen atmosphere overnight. After filtration through Celite®, the solvent was removed under reduced pressure. The crude product was dissolved in a minimum volume of tetrahydrofuran. By addition of concentrated hydrochloric acid a orange solid precipitated which was filtered off and washed with tetrahydrofuran.

Yield: 986 g (4.18 mmol, 81 %)

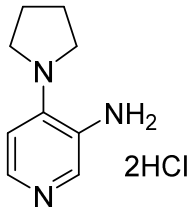

m.p.: 236.7 ℃

FT-IR (layer): υ = 3085 (w), 3052 (w), 2797 (w), 2519 (m), 1649 (s), 1561 (s), 1536 (s), 1493 (m), 1455 (m), 1353 (m), 1290 (w), 1180 (m), 1164 (s), 1122 (w), 1056 (w), 1046 (w), 971 (w), 858 (m), 799 (vs), 716 (m), 565 (w), 499 (w), 454 (s) cm^{-1}.

^{1}H NMR (500 MHz, 300 K, $CDCl_3$, TMS): δ = 7.77 (s, 1H, *H*-2), 7.75 (d, ^{3}J = 5.4 Hz, 1H, *H*-6), 6.46 (d, ^{3}J = 5.4 Hz, 1H, *H*-5), 3.65 (s, br, 2H, *H*-N), 3.19-3.16 (m, 4H, NCH_2), 1.82-1.80 (m, 4H, NCH_2CH_2) ppm.

^{13}C NMR (125 MHz, 300 K, $CDCl_3$, TMS): δ = 141.7 (*C*4), 141.3 (*C*6), 137.8 (*C*2), 133.7 (*C*3), 110.2 (*C*5) 49.5 (NCH_2), 24.8 (NCH_2CH_2) ppm.

MS (EI, 70 eV): m/z (%) = 163 (100) $[M]^+$, 134 (26) $[M\text{-}NCH_3]^+$, 120 (63) $[M\text{-}NC_2H_5]^+$.

MS (CI, isobutane): m/z (%) = 164 (100) $[M+H]^+$.

EA: ($C_9H_{15}N_3Cl_2$)		C / %	H / %	N / %
	found:	45.74	6.31	17.47
	calc:	45.78	6.40	17.79

VI. 28 Synthesis of 3-(3-bromphenylazo)-4-*N*-pyrrolidinopyridine (8f)

A. 3-Amino-4-*N*-pyrrolidinopyridine (**4f**) (1.32 g, 6.81 mmol) was dissolved in a mixture of pyridine (15 mL) and sodium hydroxide solution (25 %, 6 mL) and warmed up to 80 °C. 1-Bromo-3-nitrosobenzene (**7**) (1.5 equivalents) obtained by general procedure V.1.1 was added. After 1 h of stirring at 80 °C the mixture was poured into water and extracted three times with dichloromethane. The combined organic layers were dried over magnesium sulfate and the solvent was removed under reduced pressure. The crude product was purified by column chromatography (ethyl acetate, R_f = 0.11). The product was obtained as an orange-red solid.

Yield: 148 mg (0.45 mmol, 6.6 %)

B. 3-(3-Bromphenylazo)-4-chloropyridine (**8d**) (664 mg, 2.24 mmol) was dissolved in 60 mL acetonitrile. Pyrrolidine (920 µL, 11.2 mmol) was added drop wise and the mixture was stirred overnight. The solvent was removed under reduced pressure. The residue was dissolved in dichloromethane. The organic layer was successively washed with a saturated solution of sodium carbonate and brine. Afterwards it was dried over magnesium sulfate and the solvent was removed under reduced pressure. The crude product was purified by column chromatography (ethyl acetate, R_f = 0.11). The product was obtained as an orange-red solid.

Yield: 704 mg (2.13 mmol, 95 %)

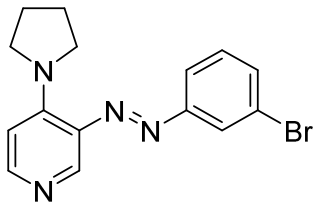

m.p.: 100.8 °C (decomposition)

FT-IR (layer): ῡ = 2967 (m), 2866 (m), 1592 (s), 1524 (s), 1501 (s), 1452 (s), 1423 (m), 1408 (m), 1346 (m), 1281 (s), 1196 (vs), 1159 (m), 1058 (s), 969 (s), 933 (m), 868 (m), 810 (m), 782 (vs), 699 (m), 677 (s), 640 (m), 586 (m), 546 (s) cm^{-1}.

^{1}H NMR (500 MHz, 300 K, $CDCl_3$, TMS): δ = 8.50 (s, 1H, *H*-2), 8.01 (d, ^3J = 6.1 Hz, 1H, *H*-6), 7.74 (t, ^4J = 1.8 Hz, 1H, *H*-8), 7.60 (ddd, ^3J = 7.9 Hz, ^4J = 1.8, 1.0 Hz, 1H, *H*-12), 7.41 (ddd, ^3J = 7.9 Hz, ^4J = 1.9, 1.0 Hz, 1H, *H*-10), 7.24 (t, ^3J = 7.9 Hz, 1H,

H-11), 6.46 (d, ^{3}J = 6.1 Hz, 1H, *H*-5), 3.53 (t, ^{3}J = 6.3 Hz, 4H, NC*H*$_2$), 1.93-1.90 (m, 4H, NCH$_2$C*H*$_2$) ppm.

^{13}C NMR (125 MHz, 300 K, $CDCl_3$, TMS): δ = 153.8 (*C*7), 150.4 (*C*6), 149.3 (*C*4), 138.9 (*C*2), 135.8 (*C*3), 132.6 (*C*10), 130.4 (*C*11), 124.9 (*C*8), 123.0 (*C*9), 122.1 (*C*12), 110.1 (*C*5), 51.6 (NCH$_2$), 25.6 (NCH$_2$*C*H$_2$) ppm.

MS (EI, 70 eV): m/z (%) = 330 (3) $[M]^+$, 160 (100) $[M\text{-}NPhBr]^+$, 105 (9) $[PhN_2]^+$.

MS (CI, isobutane): m/z (%) = 389 (16) $[M+H+^{i}Bu]^+$, 331 (100) $[M+H]^+$.

EA: ($C_{15}H_{15}BrN_4$)		C / %	H / %	N / %
	found:	54.13	4.49	16.36
	calc.:	54.39	4.56	16.92

VI. 29 Synthesis of 3-(3-(2-Formylphenyl)phenylazo)-4-*N*-pyrrolidino-pyridine (10f)

3-(3-Bromphenylazo)-4-*N*-pyrrolidinopyridine (**8f**) (600 mg, 1.81 mmol) was used for a Suzuki coupling reaction according to general procedure V.1.2. The crude product was purified by column chromatography (dichloromethane / methanol = 95:5, R_f = 0.27). The product was obtained as an orange solid.

Yield: 637 mg (1.78 mmol, 98 %)

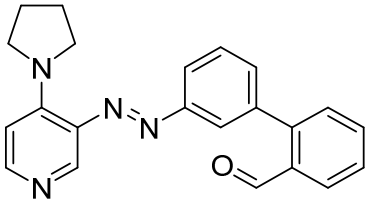

^{1}H NMR (500 MHz, 300 K, $CDCl_3$): δ = 10.04 (d, ^4J = 0.8 Hz, 1H, OCH), 8.62 (s, 1H, *H*-2), 8.12 (d, ^3J = 6.1 Hz, 1H, *H*-6), 8.03 (ddd, ^3J = 7.8 Hz, ^4J = 1.5, 0.6 Hz, 1H, *H*-15), 7.85 (ddd, ^3J = 8.0 Hz, ^4J = 1.9, 1.1 Hz, 1H, *H*-12), 7.77 (t, ^4J = 1.8 Hz, 1H, *H*-8), 7.65 (td, ^3J = 7.5 Hz, ^4J = 1.5 Hz, 1H, *H*-17), 7.58 (t, ^3J = 7.7 Hz, 1H, *H*-11), 7.51 (td, ^3J = 7.7 Hz, ^4J = 1.3 Hz, 1H, *H*-16), 7.50 (dd, ^3J = 7.6 Hz, ^4J = 1.3 Hz, 1H, *H*-18), 7.43 (ddd, ^3J = 7.5 Hz, ^4J = 1.8, 1.1 Hz, 1H, *H*-10), 6.59 (d, ^3J = 6.1 Hz, 1H, *H*-5), 3.65 (t, ^3J = 6.4 Hz, 4H, NCH_2), 2.01-1.99 (m, 4H, NCH_2CH_2) ppm.

^{13}C NMR (125 MHz, 300 K, $CDCl_3$): δ = 192.0 (*C*HO), 152.8 (*C*7), 150.4 (*C*6), 149.4 (*C*4), 145.1 (*C*13), 138.9 (*C*2), 138.7 (*C*9), 136.0 (*C*3), 133.8 (*C*14), 133.7 (*C*17), 131.4 (*C*10), 130.7 (*C*18), 129.3 (*C*11), 128.1 (*C*15), 127.8 (*C*16), 124.1 (*C*8), 122.5 (*C*12), 110.1 (*C*5), 51.7 (NCH_2), 25.7 (NCH_2CH_2) ppm.

MS (EI, 70 eV): m/z (%) = 356) $[M]^+$ (11), 160 (100) $[M\text{-}NPhPhCHO]^+$.

MS (CI, isobutane): m/z (%) = 357 (33) $[M+H]^+$, 198 (20) $[M\text{-}PyPyN+H]^+$, 164 (100) $[M\text{-}NPhPhCO+2H]^+$.

VI.30 Synthesis of mf-Pyr-RP (17f)

3-(3-(2-Formylphenyl)phenylazo)-4-*N*-pyrrolidinopyridine (**10f**) (817 mg, 2.29 mmol) and pentafluorobenzaldehyde (**16**) (449 mg, 2.29 mmol) were dissolved in chloroform (400 mL) under nitrogen atmosphere. Boron trifluoride diethyl ether (432 µL, 3.44 mmol) was added. *meso*-Pentafluorophenyl dipyrromethane (**15**) (1.43 g, 4.58 mmol) dissolved in 50 mL chloroform was added within 60 min by a syringe pump. After 6 h of stirring *p*-chloranil (1.14 g, 4.64 mmol) was added and the mixture was stirred overnight at 55 °C. After addition of triet hylamine (1 mL) stirring was continued for 30 min at room temperature. The mixture was filtered through celite® and the solvent was removed under reduced pressure. The residue was dissolved in a minimum volume of chloroform and filtered through silica gel. The solvent was removed and the crude product was purified by column chromatography (cyclohexane / ethyl acetate = 6:4, R_f = 0.13).

Yield: 28.8 mg (25.4 µmol, 1.1 %)

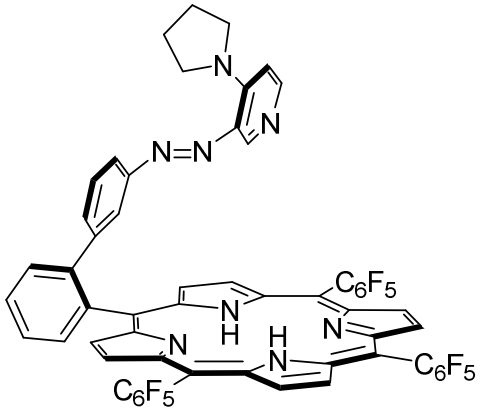

FT-IR (layer): υ = 2984 (w), 2838 (w), 2746 (w), 1694 (w), 1649 (w), 1581 (w), 1516 (m), 1485 (s), 1390 (w), 1301 (m), 1270 (m), 1199 (m), 1109 (w), 1076 (w), 1043 (w), 985 (s), 950 (m), 917 (s), 877 (w), 826 (m), 801 (s), 757 (vs), 695 (m), 651 (m), 576 (w), 528 (m) cm^{-1}.

^{1}H NMR (500 MHz, 300 K, acetone-d_6): δ = 9.11 (s, br, 4H, *H*-26, *H*-27), 9.01 (d, ^3J = 4.1 Hz, 2H, *H*-22), 8.96 (d, ^3J = 4.1 Hz, 2H, *H*-21), 8.18 (dd, ^3J = 7.6 Hz, ^4J = 1.2 Hz, 1H, *H*-15), 7.91 (td, ^3J = 7.7 Hz, ^4J = 1.3 Hz, 1H, *H*-17), 7.89 (s, 1H, *H*-2), 7.84 (dd, ^3J = 7.8 Hz, ^4J = 1.2 Hz, 1H, *H*-18), 7.79 (d, ^3J = 6.3 Hz, 1H, *H*-6), 7.76 (td, ^3J = 7.6 Hz, ^4J = 1.4 Hz, 1H, *H*-16), 7.61 (t, ^4J = 1.8 Hz, 1H, *H*-8), 6.88 (ddd, ^3J = 8.0 Hz, ^4J = 1.6,

1.1 Hz, *H*-10), 6.75 (ddd, ^{3}J = 8.1 Hz, ^{4}J = 1.9, 1.1 Hz, 1H, *H*-12), 6.43 (d, ^{3}J = 6.3 Hz, 1H, *H*-5), 6.35 (t, ^{3}J = 8.1 Hz, 1H, *H*-11), 3.21 (t, ^{3}J = 6.6 Hz, 4H, NCH_2), 1.62-1.60 (m, 4H, NCH_2CH_2), -3.04 (s, 2H, *H*-N) ppm.

^{19}F NMR (470 MHz, 300 K, CD_2Cl_2, $CFCl_3$): δ = -139.65 (dd, ^{3}J = 23.2 Hz, ^{5}J = 5.5 Hz, 2F, A-*o*-*F*), -139.85 (dd, ^{3}J = 23.9 Hz, ^{5}J = 5.6 Hz, 1F, B-*o*-*F*), -140.00 (dd, ^{3}J = 23.9 Hz, ^{5}J = 5.6 Hz, 1F, B-*o'*-*F*), -140.10 (dd, ^{3}J = 24.1 Hz, ^{5}J = 5.7 Hz, 2F, A-*o'*-*F*), -155.68 (t, ^{3}J = 20.3 Hz, 2F, A-*p*-*F*), -155.76 (t, ^{3}J = 20.4 Hz, 1F, B-*p*-*F*), -164.48 (td, ^{3}J = 21.9 Hz, ^{5}J = 6.7 Hz, 2F, A-*m*-*F*), -164.65 to -164.78 (m, 4F, A-*m'*-*F*, B-*m*-*F*, B-*m'*-*F*) ppm.

MS (HR): m/z (calc.) = 1135.237 (1135.235) $[M+H]^+$.

VII Crystal structure data

Table S3: Crystal data and structure refinement for herges88.

Identification code	herges88	
Empirical formula	$C_{65}H_{38}F_{15}N_7NiO_2$	
Formula weight	1292.73	
Temperature	200(2) K	
Wavelength	0.71073 Å	
Crystal system	triclinic	
Space group	P-1	
Unit cell dimensions	a = 12.415(2) Å	α= 66.98(3)°.
	b = 15.100(3) Å	β= 75.68(3)°.
	c = 17.541(5) Å	γ = 72.77(2)°.
Volume	2858.2(11) $Å^3$	
Z	2	
Density (calculated)	1.502 Mg/m^3	
Absorption coefficient	0.442 mm^{-1}	
F(000)	1312	
Crystal size	0.3 x 0.3 x 0.2 mm^3	
Theta range for data collection	2.48 to 26.03°.	
Index ranges	-15<=h<=15, -18<=k<=18, -21<=l<=21	
Reflections collected	28094	
Independent reflections	10845 [R(int) = 0.0486]	
Completeness to theta = 26.03°	96.2 %	
Refinement method	Full-matrix least-squares on F^2	
Data / restraints / parameters	10845 / 13 / 824	
Goodness-of-fit on F^2	1.036	
Final R indices [I>2sigma(I)]	R1 = 0.0434, wR2 = 0.1102	
R indices (all data)	R1 = 0.0582, wR2 = 0.1173	
Extinction coefficient	0.0060(11)	
Largest diff. peak and hole	0.338 and -0.428 $e.Å^{-3}$	

Comments:

All non-hydrogen atoms except three C atoms of the disordered toluene molecule were refined anisotropic. The C-H H atoms were positioned with idealized geometry (methyl H atoms allowed to rotate but not to tip) and refined isotropic with $U_{iso}(H) = 1.2 \cdot U_{eq}(C)$ (1.5 for methyl H atoms) using a riding model. The methanol O-H H atoms were located in difference map, their bond length set to ideal values and afterwards they were refined isotropic with $U_{iso}(H) = 1.5 \cdot U_{eq}(C)$ using a riding model. The structure contains one additional methanol and one toluene molecule. The toluene molecule is disordered in two orientations and was refined using a split model and restraints.

Table S4: Atomic coordinates (x 10^4) and equivalent isotropic displacement parameters ($Å^2$x 10^3). U(eq) is defined as one third of the trace of the orthogonalized U_{ij} tensor.

	x	y	z	U(eq)
Ni(1)	-194(1)	-541(1)	-2695(1)	21(1)
N(1)	728(1)	-1923(1)	-2635(1)	25(1)
N(2)	1199(1)	24(1)	-3381(1)	23(1)
N(3)	-1126(1)	865(1)	-2825(1)	23(1)
N(4)	-1621(1)	-1071(1)	-2120(1)	24(1)
C(1)	342(2)	-2778(1)	-2255(1)	26(1)
C(2)	1279(2)	-3612(2)	-2281(1)	32(1)
C(3)	2217(2)	-3251(2)	-2676(1)	33(1)
C(4)	1869(2)	-2191(1)	-2903(1)	27(1)
C(5)	2590(2)	-1539(2)	-3359(1)	27(1)
C(6)	2264(2)	-509(1)	-3583(1)	26(1)
C(7)	3037(2)	147(2)	-4010(1)	32(1)
C(8)	2436(2)	1063(2)	-4036(1)	30(1)
C(9)	1283(2)	989(1)	-3646(1)	24(1)
C(10)	397(2)	1771(1)	-3523(1)	25(1)
C(11)	-728(2)	1716(1)	-3154(1)	24(1)
C(12)	-1654(2)	2545(1)	-3100(1)	29(1)
C(13)	-2602(2)	2191(2)	-2743(1)	29(1)
C(14)	-2266(2)	1138(1)	-2564(1)	24(1)
C(15)	-3003(2)	489(1)	-2176(1)	25(1)
C(16)	-2701(2)	-535(1)	-1975(1)	25(1)
C(17)	-3493(2)	-1177(2)	-1605(1)	32(1)
C(18)	-2878(2)	-2101(2)	-1533(2)	33(1)
C(19)	-1708(2)	-2037(1)	-1853(1)	25(1)
C(20)	-786(2)	-2823(1)	-1909(1)	27(1)
C(21)	3808(2)	-1977(2)	-3636(1)	32(1)
C(22)	4133(2)	-1985(2)	-4454(2)	41(1)
C(23)	5240(3)	-2430(2)	-4719(2)	52(1)
C(24)	6013(3)	-2867(2)	-4168(2)	59(1)
C(25)	5712(2)	-2864(2)	-3361(2)	52(1)
C(26)	4606(2)	-2412(2)	-3082(2)	36(1)
C(27)	4315(2)	-2416(2)	-2202(2)	37(1)
C(28)	4385(3)	-3296(2)	-1530(2)	49(1)
C(29)	4126(3)	-3293(2)	-715(2)	59(1)
C(30)	3805(3)	-2416(2)	-554(2)	48(1)
C(31)	3734(2)	-1540(2)	-1223(2)	36(1)
C(32)	4010(2)	-1531(2)	-2041(2)	35(1)
N(5)	3510(2)	-615(1)	-1075(1)	37(1)
N(6)	2525(2)	-227(1)	-820(1)	33(1)
C(33)	1583(2)	-649(2)	-755(1)	28(1)
C(34)	1212(2)	-497(2)	-1491(1)	27(1)
N(7)	293(2)	-775(1)	-1505(1)	26(1)
C(35)	-277(2)	-1226(2)	-756(1)	31(1)
C(36)	33(2)	-1382(2)	1(1)	35(1)
C(37)	984(2)	-1089(2)	23(1)	30(1)
C(38)	1361(2)	-1250(2)	825(2)	40(1)
C(41)	687(2)	2756(1)	-3783(1)	27(1)
C(42)	965(2)	3325(2)	-4613(2)	36(1)
C(43)	1250(2)	4217(2)	-4839(2)	49(1)
C(44)	1268(2)	4571(2)	-4230(2)	55(1)
C(45)	988(2)	4038(2)	-3400(2)	49(1)
C(46)	703(2)	3140(2)	-3182(2)	36(1)

Table S4 continued: Atomic coordinates (x 10^4) and equivalent isotropic displacement parameters (Å^{2}x 10^3). U(eq) is defined as one third of the trace of the orthogonalized U_{ij} tensor.

	x	y	z	U(eq)
F(42)	962(1)	3011(1)	-5233(1)	48(1)
F(43)	1514(2)	4747(1)	-5654(1)	72(1)
F(44)	1551(2)	5436(1)	-4444(2)	90(1)
F(45)	997(2)	4373(1)	-2791(2)	75(1)
F(46)	452(1)	2636(1)	-2366(1)	48(1)
C(51)	-4241(2)	944(1)	-1975(1)	27(1)
C(52)	-4967(2)	1307(2)	-2561(2)	43(1)
C(53)	-6102(2)	1745(2)	-2401(2)	49(1)
C(54)	-6552(2)	1809(2)	-1625(2)	41(1)
C(55)	-5866(2)	1452(2)	-1023(2)	45(1)
C(56)	-4724(2)	1030(2)	-1201(2)	37(1)
F(52)	-4560(2)	1250(2)	-3332(1)	93(1)
F(53)	-6765(2)	2122(2)	-3008(2)	104(1)
F(54)	-7652(1)	2237(1)	-1462(1)	63(1)
F(55)	-6301(2)	1532(2)	-270(1)	90(1)
F(56)	-4076(2)	701(2)	-598(1)	76(1)
C(61)	-1064(2)	-3825(2)	-1585(1)	29(1)
C(62)	-1194(2)	-4385(2)	-740(2)	43(1)
C(63)	-1452(3)	-5300(2)	-448(2)	56(1)
C(64)	-1599(3)	-5669(2)	-1011(2)	51(1)
C(65)	-1486(2)	-5133(2)	-1850(2)	44(1)
C(66)	-1215(2)	-4223(2)	-2128(2)	36(1)
F(62)	-1063(2)	-4038(1)	-179(1)	71(1)
F(63)	-1578(3)	-5822(2)	374(1)	99(1)
F(64)	-1851(2)	-6555(1)	-739(1)	79(1)
F(65)	-1618(2)	-5504(1)	-2394(1)	71(1)
F(66)	-1110(2)	-3724(1)	-2952(1)	60(1)
O(1)	-646(2)	-412(1)	-3919(1)	39(1)
C(71)	-1502(3)	-830(3)	-3984(2)	65(1)
O(2)	-1228(2)	1325(1)	-5122(1)	64(1)
C(72)	-1402(3)	2336(2)	-5245(2)	66(1)
C(81)	-5265(6)	4482(3)	-2942(4)	98(2)
C(82)	-6290(5)	4264(3)	-2456(5)	105(2)
C(83)	-6421(5)	4017(3)	-1597(5)	110(2)
C(84)	-5594(4)	3939(2)	-1211(3)	118(2)
C(85)	-4562(4)	4146(2)	-1689(3)	94(2)
C(86)	-4405(4)	4426(3)	-2526(4)	96(2)
C(87)	-5071(9)	4744(5)	-3843(5)	186(4)
C(81')	-5453(17)	4240(30)	-2042(11)	88(12)
C(83')	-6010(30)	4370(30)	-3296(11)	77(10)
C(85')	-4290(30)	4740(40)	-3376(10)	115(17)

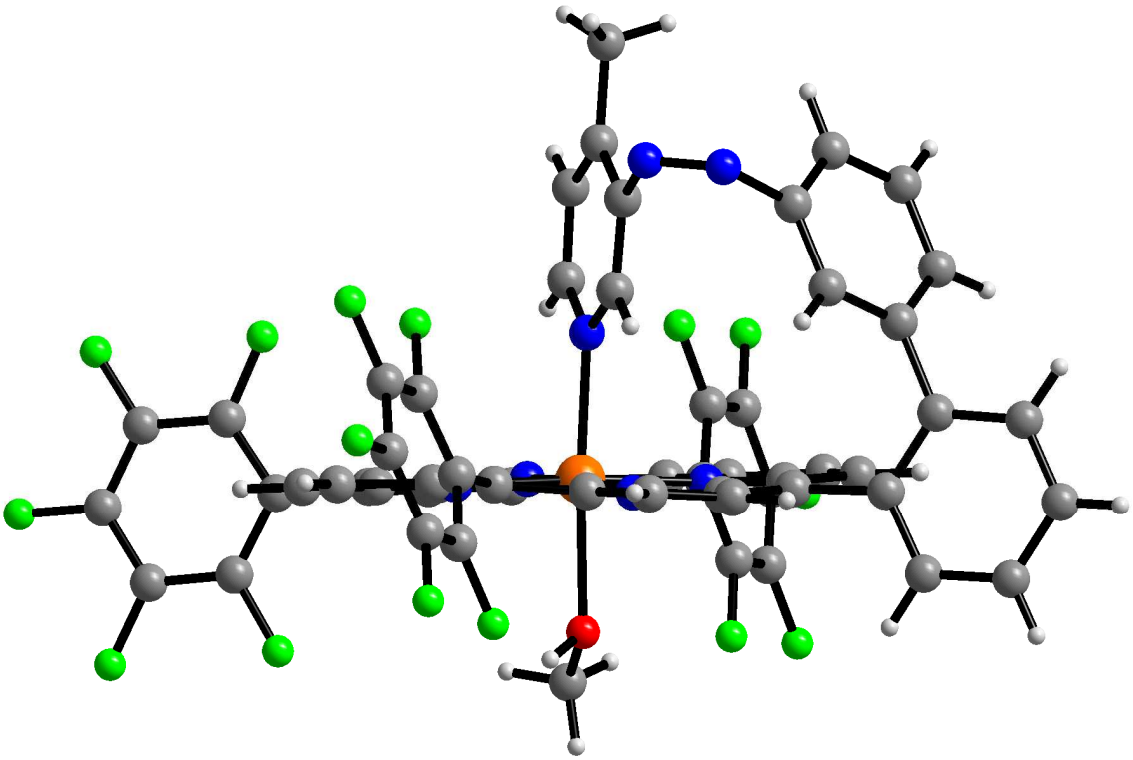

Table S5: Bond lengths [Å] and angles [°].

Ni(1)-N(4)	2.0298(18)	Ni(1)-N(2)	2.0508(18)
Ni(1)-N(1)	2.0376(17)	Ni(1)-N(7)	2.1825(19)
Ni(1)-N(3)	2.0477(16)	Ni(1)-O(1)	2.2737(17)
N(4)-Ni(1)-N(1)	90.60(7)	N(3)-Ni(1)-N(7)	93.75(7)
N(4)-Ni(1)-N(3)	89.99(7)	N(2)-Ni(1)-N(7)	92.83(7)
N(1)-Ni(1)-N(3)	176.72(7)	N(4)-Ni(1)-O(1)	86.86(7)
N(4)-Ni(1)-N(2)	174.60(7)	N(1)-Ni(1)-O(1)	86.56(7)
N(1)-Ni(1)-N(2)	89.78(7)	N(3)-Ni(1)-O(1)	90.26(7)
N(3)-Ni(1)-N(2)	89.32(7)	N(2)-Ni(1)-O(1)	87.79(7)
N(4)-Ni(1)-N(7)	92.56(7)	N(7)-Ni(1)-O(1)	175.95(6)
N(1)-Ni(1)-N(7)	89.44(7)		

Table S5 continued: Bond lengths [Å] and angles [°].

N(1)-C(4)	1.367(3)	C(31)-C(32)	1.386(3)
N(1)-C(1)	1.370(2)	C(31)-N(5)	1.454(3)
N(2)-C(6)	1.372(3)	N(5)-N(6)	1.244(3)
N(2)-C(9)	1.374(2)	N(6)-C(33)	1.451(3)
N(3)-C(14)	1.365(3)	C(33)-C(34)	1.390(3)
N(3)-C(11)	1.372(2)	C(33)-C(37)	1.392(3)
N(4)-C(16)	1.367(3)	C(34)-N(7)	1.335(3)
N(4)-C(19)	1.376(2)	N(7)-C(35)	1.348(3)
C(1)-C(20)	1.392(3)	C(35)-C(36)	1.386(3)
C(1)-C(2)	1.447(3)	C(36)-C(37)	1.391(3)
C(2)-C(3)	1.348(3)	C(37)-C(38)	1.500(3)
C(3)-C(4)	1.443(3)	C(41)-C(42)	1.387(3)
C(4)-C(5)	1.402(3)	C(41)-C(46)	1.395(3)
C(5)-C(6)	1.401(3)	C(42)-F(42)	1.346(3)
C(5)-C(21)	1.502(3)	C(42)-C(43)	1.376(3)
C(6)-C(7)	1.446(3)	C(43)-F(43)	1.350(3)
C(7)-C(8)	1.352(3)	C(43)-C(44)	1.376(5)
C(8)-C(9)	1.442(3)	C(44)-F(44)	1.338(3)
C(9)-C(10)	1.402(3)	C(44)-C(45)	1.373(5)
C(10)-C(11)	1.399(3)	C(45)-F(45)	1.353(3)
C(10)-C(41)	1.501(3)	C(45)-C(46)	1.385(3)
C(11)-C(12)	1.444(3)	C(46)-F(46)	1.338(3)
C(12)-C(13)	1.345(3)	C(51)-C(52)	1.377(3)
C(13)-C(14)	1.444(3)	C(51)-C(56)	1.381(3)
C(14)-C(15)	1.400(3)	C(52)-F(52)	1.349(3)
C(15)-C(16)	1.397(3)	C(52)-C(53)	1.378(4)
C(15)-C(51)	1.501(3)	C(53)-F(53)	1.349(3)
C(16)-C(17)	1.444(3)	C(53)-C(54)	1.366(4)
C(17)-C(18)	1.351(3)	C(54)-F(54)	1.340(3)
C(18)-C(19)	1.439(3)	C(54)-C(55)	1.363(4)
C(19)-C(20)	1.400(3)	C(55)-F(55)	1.336(3)
C(20)-C(61)	1.505(3)	C(55)-C(56)	1.384(3)
C(21)-C(22)	1.394(3)	C(56)-F(56)	1.336(3)
C(21)-C(26)	1.397(4)	C(61)-C(66)	1.381(3)
C(22)-C(23)	1.392(4)	C(61)-C(62)	1.385(3)
C(23)-C(24)	1.369(5)	C(62)-F(62)	1.343(3)
C(24)-C(25)	1.374(4)	C(62)-C(63)	1.378(4)
C(25)-C(26)	1.402(3)	C(63)-F(63)	1.340(3)
C(26)-C(27)	1.493(3)	C(63)-C(64)	1.378(4)
C(27)-C(28)	1.386(4)	C(64)-F(64)	1.338(3)
C(27)-C(32)	1.397(3)	C(64)-C(65)	1.369(4)
C(28)-C(29)	1.388(4)	C(65)-F(65)	1.341(3)
C(29)-C(30)	1.385(4)	C(65)-C(66)	1.381(3)
C(30)-C(31)	1.379(4)	C(66)-F(66)	1.337(3)
C(4)-N(1)-C(1)	106.53(16)	N(1)-C(4)-C(5)	125.47(17)
C(6)-N(2)-C(9)	106.67(16)	N(1)-C(4)-C(3)	109.88(18)
C(14)-N(3)-C(11)	106.04(15)	C(5)-C(4)-C(3)	124.62(19)
C(16)-N(4)-C(19)	106.11(16)	C(6)-C(5)-C(4)	125.23(19)
N(1)-C(1)-C(20)	124.61(18)	C(6)-C(5)-C(21)	117.33(18)
N(1)-C(1)-C(2)	109.53(18)	C(4)-C(5)-C(21)	117.44(17)
C(20)-C(1)-C(2)	125.86(18)	N(2)-C(6)-C(5)	125.87(18)
C(3)-C(2)-C(1)	107.10(18)	N(2)-C(6)-C(7)	109.63(17)
C(2)-C(3)-C(4)	106.96(19)	C(5)-C(6)-C(7)	124.33(19)

Table S5 continued: Bond lengths [Å] and angles [°].

C(8)-C(7)-C(6)	106.86(19)	F(64)-C(64)-C(63)	120.1(3)
C(7)-C(8)-C(9)	107.38(18)	C(65)-C(64)-C(63)	120.3(2)
N(2)-C(9)-C(10)	125.14(18)	F(65)-C(65)-C(64)	119.8(2)
N(2)-C(9)-C(8)	109.44(17)	F(65)-C(65)-C(66)	120.7(2)
C(10)-C(9)-C(8)	125.37(18)	C(64)-C(65)-C(66)	119.4(2)
C(11)-C(10)-C(9)	126.16(18)	F(66)-C(66)-C(65)	117.6(2)
C(11)-C(10)-C(41)	116.60(17)	F(66)-C(66)-C(61)	120.20(19)
C(9)-C(10)-C(41)	117.20(18)	C(65)-C(66)-C(61)	122.2(2)
N(3)-C(11)-C(10)	124.70(17)	C(37)-C(33)-N(6)	120.81(19)
N(3)-C(11)-C(12)	109.89(18)	N(7)-C(34)-C(33)	123.27(19)
C(10)-C(11)-C(12)	125.35(18)	C(34)-N(7)-C(35)	116.50(18)
C(13)-C(12)-C(11)	107.01(17)	C(34)-N(7)-Ni(1)	120.52(14)
C(12)-C(13)-C(14)	106.85(18)	C(35)-N(7)-Ni(1)	122.95(15)
N(3)-C(14)-C(15)	124.94(17)	N(7)-C(35)-C(36)	123.2(2)
N(3)-C(14)-C(13)	110.20(17)	C(35)-C(36)-C(37)	120.8(2)
C(15)-C(14)-C(13)	124.85(19)	C(36)-C(37)-C(33)	115.4(2)
C(16)-C(15)-C(14)	126.31(18)	C(36)-C(37)-C(38)	122.9(2)
C(16)-C(15)-C(51)	116.98(17)	C(33)-C(37)-C(38)	121.7(2)
C(14)-C(15)-C(51)	116.69(17)	C(42)-C(41)-C(46)	116.32(19)
N(4)-C(16)-C(15)	125.02(18)	C(42)-C(41)-C(10)	123.21(19)
N(4)-C(16)-C(17)	110.19(17)	C(46)-C(41)-C(10)	120.46(19)
C(15)-C(16)-C(17)	124.76(19)	F(42)-C(42)-C(43)	117.5(2)
C(18)-C(17)-C(16)	106.68(19)	F(42)-C(42)-C(41)	120.13(19)
C(17)-C(18)-C(19)	107.25(18)	C(43)-C(42)-C(41)	122.4(2)
N(4)-C(19)-C(20)	124.08(18)	F(43)-C(43)-C(42)	120.4(3)
N(4)-C(19)-C(18)	109.77(17)	F(43)-C(43)-C(44)	119.7(2)
C(20)-C(19)-C(18)	126.14(18)	C(42)-C(43)-C(44)	119.8(3)
C(1)-C(20)-C(19)	127.45(18)	F(44)-C(44)-C(45)	120.0(3)
C(1)-C(20)-C(61)	116.70(18)	F(44)-C(44)-C(43)	120.2(3)
C(19)-C(20)-C(61)	115.81(18)	C(45)-C(44)-C(43)	119.8(2)
C(22)-C(21)-C(26)	119.6(2)	F(45)-C(45)-C(44)	120.8(2)
C(22)-C(21)-C(5)	119.1(2)	F(45)-C(45)-C(46)	119.4(3)
C(26)-C(21)-C(5)	121.2(2)	C(44)-C(45)-C(46)	119.8(2)
C(23)-C(22)-C(21)	120.6(3)	F(46)-C(46)-C(45)	117.9(2)
C(24)-C(23)-C(22)	119.6(3)	F(46)-C(46)-C(41)	120.19(19)
C(23)-C(24)-C(25)	120.8(2)	C(45)-C(46)-C(41)	121.9(2)
C(24)-C(25)-C(26)	120.8(3)	C(52)-C(51)-C(56)	115.8(2)
C(21)-C(26)-C(25)	118.7(2)	C(52)-C(51)-C(15)	121.47(19)
C(21)-C(26)-C(27)	122.1(2)	C(56)-C(51)-C(15)	122.7(2)
C(25)-C(26)-C(27)	119.2(2)	F(52)-C(52)-C(51)	119.4(2)
C(28)-C(27)-C(32)	118.7(2)	F(52)-C(52)-C(53)	117.8(2)
C(28)-C(27)-C(26)	120.9(2)	C(51)-C(52)-C(53)	122.8(2)
C(32)-C(27)-C(26)	120.4(2)	F(53)-C(53)-C(54)	119.9(2)
C(27)-C(28)-C(29)	120.4(2)	F(53)-C(53)-C(52)	120.3(2)
C(30)-C(29)-C(28)	121.0(3)	C(54)-C(53)-C(52)	119.7(2)
C(31)-C(30)-C(29)	118.5(3)	F(54)-C(54)-C(55)	120.2(2)
C(30)-C(31)-C(32)	121.2(2)	F(54)-C(54)-C(53)	120.3(2)
C(30)-C(31)-N(5)	119.6(2)	C(55)-C(54)-C(53)	119.5(2)
C(32)-C(31)-N(5)	118.7(2)	F(55)-C(55)-C(54)	119.5(2)
C(31)-C(32)-C(27)	120.1(2)	F(55)-C(55)-C(56)	120.6(3)
N(6)-N(5)-C(31)	120.40(19)	C(54)-C(55)-C(56)	119.9(2)
N(5)-N(6)-C(33)	119.40(17)	F(56)-C(56)-C(51)	119.5(2)
C(34)-C(33)-C(37)	120.8(2)	F(56)-C(56)-C(55)	118.2(2)
C(34)-C(33)-N(6)	117.96(19)	C(51)-C(56)-C(55)	122.3(2)

Table S5 continued: Bond lengths [Å] and angles [°].

F(64)-C(64)-C(65)	119.6(3)	F(62)-C(62)-C(61)	119.7(2)
C(66)-C(61)-C(62)	116.7(2)	C(63)-C(62)-C(61)	122.3(2)
C(66)-C(61)-C(20)	120.8(2)	F(63)-C(63)-C(64)	120.0(2)
C(62)-C(61)-C(20)	122.53(19)	F(63)-C(63)-C(62)	120.8(3)
F(62)-C(62)-C(63)	118.0(2)	C(64)-C(63)-C(62)	119.2(2)
O(1)-C(71)	1.434(3)	O(2)-C(72)	1.411(3)
C(81)-C(82)	1.395(8)	C(84)-C(81')	1.328(17)
C(81)-C(86)	1.401(7)	C(84)-C(85)	1.3937
C(81)-C(87)	1.447(9)	C(85)-C(86)	1.339(7)
C(82)-C(83')	1.382(14)	C(86)-C(85')	1.361(15)
C(82)-C(83)	1.383(8)	C(86)-C(81')	1.407(13)
C(82)-C(81')	1.390(13)	C(87)-C(83')	1.41(3)
C(83)-C(84)	1.317(7)	C(87)-C(85')	1.42(3)
C(82)-C(81)-C(86)	117.7(6)	C(85)-C(86)-C(85')	178(2)
C(82)-C(81)-C(87)	122.1(7)	C(85)-C(86)-C(81)	120.5(6)
C(86)-C(81)-C(87)	120.2(7)	C(85')-C(86)-C(81)	58.1(13)
C(83')-C(82)-C(83)	170.3(16)	C(85)-C(86)-C(81')	58.6(7)
C(83')-C(82)-C(81')	118.2(14)	C(85')-C(86)-C(81')	119.9(14)
C(83)-C(82)-C(81')	56.7(7)	C(81)-C(86)-C(81')	62.1(8)
C(83')-C(82)-C(81)	56.2(12)	C(83')-C(87)-C(85')	110.0(10)
C(83)-C(82)-C(81)	119.3(5)	C(83')-C(87)-C(81)	54.4(9)
C(81')-C(82)-C(81)	62.6(8)	C(85')-C(87)-C(81)	55.8(9)
C(84)-C(83)-C(82)	122.4(6)	C(84)-C(81')-C(82)	121.0(11)
C(83)-C(84)-C(81')	59.7(7)	C(84)-C(81')-C(86)	121.1(11)
C(83)-C(84)-C(85)	118.8(4)	C(82)-C(81')-C(86)	117.5(11)
C(81')-C(84)-C(85)	59.1(6)	C(82)-C(83')-C(87)	125.8(19)
C(86)-C(85)-C(84)	121.2(3)	C(86)-C(85')-C(87)	125.4(19)

Table S6: Anisotropic displacement parameters ($Å^2 x\ 10^3$) for herges87. The anisotropic displacement factor exponent takes the form: $-2\pi^2[\ h^2\ a^{*2}U^{11} + ...\ + 2\ h\ k\ a^*\ b^*\ U^{12}\ ]$

	U^{11}	U^{22}	U^{33}	U^{23}	U^{13}	U^{12}
Ni(1)	18(1)	21(1)	27(1)	-10(1)	0(1)	-6(1)
N(1)	21(1)	24(1)	30(1)	-11(1)	1(1)	-7(1)
N(2)	20(1)	22(1)	26(1)	-9(1)	0(1)	-6(1)
N(3)	18(1)	23(1)	29(1)	-11(1)	-1(1)	-7(1)
N(4)	20(1)	23(1)	32(1)	-11(1)	-2(1)	-7(1)
C(1)	29(1)	21(1)	29(1)	-10(1)	-2(1)	-8(1)
C(2)	31(1)	23(1)	42(1)	-13(1)	-2(1)	-7(1)
C(3)	28(1)	26(1)	42(1)	-14(1)	0(1)	-3(1)
C(4)	23(1)	24(1)	32(1)	-13(1)	-2(1)	-3(1)
C(5)	22(1)	29(1)	31(1)	-14(1)	0(1)	-5(1)
C(6)	20(1)	28(1)	29(1)	-11(1)	3(1)	-8(1)
C(7)	21(1)	31(1)	39(1)	-11(1)	4(1)	-9(1)
C(8)	25(1)	28(1)	35(1)	-8(1)	2(1)	-11(1)
C(9)	23(1)	24(1)	27(1)	-6(1)	-3(1)	-10(1)
C(10)	25(1)	23(1)	26(1)	-7(1)	-2(1)	-9(1)
C(11)	24(1)	21(1)	27(1)	-9(1)	-4(1)	-6(1)
C(12)	29(1)	22(1)	37(1)	-11(1)	-3(1)	-6(1)
C(13)	24(1)	26(1)	38(1)	-16(1)	-3(1)	-2(1)
C(14)	21(1)	24(1)	29(1)	-13(1)	-4(1)	-3(1)
C(15)	18(1)	31(1)	28(1)	-14(1)	-2(1)	-6(1)
C(16)	17(1)	31(1)	29(1)	-13(1)	-1(1)	-8(1)
C(17)	20(1)	35(1)	43(1)	-16(1)	1(1)	-11(1)
C(18)	28(1)	32(1)	43(1)	-14(1)	1(1)	-15(1)
C(19)	23(1)	25(1)	30(1)	-11(1)	-1(1)	-11(1)
C(20)	29(1)	25(1)	29(1)	-9(1)	-2(1)	-12(1)
C(21)	26(1)	25(1)	41(1)	-14(1)	5(1)	-8(1)
C(22)	36(1)	43(1)	41(1)	-18(1)	8(1)	-10(1)
C(23)	44(2)	55(2)	49(2)	-23(1)	15(1)	-9(1)
C(24)	36(2)	55(2)	63(2)	-20(1)	16(1)	4(1)
C(25)	30(1)	53(2)	59(2)	-18(1)	0(1)	6(1)
C(26)	26(1)	32(1)	46(1)	-14(1)	2(1)	-5(1)
C(27)	22(1)	37(1)	47(1)	-14(1)	-4(1)	-3(1)
C(28)	51(2)	36(1)	54(2)	-16(1)	-2(1)	-4(1)
C(29)	74(2)	39(1)	47(2)	-6(1)	-3(1)	-8(1)
C(30)	50(2)	49(1)	42(1)	-15(1)	-1(1)	-12(1)
C(31)	22(1)	39(1)	47(1)	-15(1)	-6(1)	-9(1)
C(32)	25(1)	35(1)	45(1)	-12(1)	-6(1)	-7(1)
N(5)	31(1)	44(1)	41(1)	-16(1)	-6(1)	-14(1)
N(6)	32(1)	39(1)	36(1)	-15(1)	-6(1)	-13(1)
C(33)	28(1)	27(1)	34(1)	-15(1)	-4(1)	-8(1)
C(34)	23(1)	32(1)	30(1)	-13(1)	-2(1)	-9(1)
N(7)	24(1)	26(1)	29(1)	-11(1)	-2(1)	-6(1)
C(35)	28(1)	35(1)	32(1)	-10(1)	-1(1)	-14(1)
C(36)	37(1)	38(1)	30(1)	-10(1)	0(1)	-14(1)
C(37)	32(1)	29(1)	30(1)	-13(1)	-4(1)	-6(1)
C(38)	46(2)	44(1)	32(1)	-15(1)	-7(1)	-11(1)
C(41)	21(1)	22(1)	38(1)	-9(1)	-4(1)	-6(1)
C(42)	24(1)	30(1)	45(1)	-7(1)	0(1)	-5(1)
C(43)	29(1)	24(1)	68(2)	1(1)	7(1)	-5(1)
C(44)	32(1)	26(1)	104(2)	-22(1)	6(1)	-13(1)
C(45)	36(1)	39(1)	86(2)	-39(1)	-4(1)	-11(1)

Table S6: Anisotropic displacement parameters ($Å^2 x\ 10^3$) for herges87. The anisotropic displacement factor exponent takes the form: $-2\pi^2[\ h^2\ a^{*2}U^{11} + ... + 2\ h\ k\ a^*\ b^*\ U^{12}\ ]$

	U^{11}	U^{22}	U^{33}	U^{23}	U^{13}	U^{12}
C(46)	28(1)	32(1)	50(1)	-17(1)	-2(1)	-10(1)
F(42)	51(1)	52(1)	33(1)	-8(1)	1(1)	-16(1)
F(43)	54(1)	40(1)	78(1)	14(1)	14(1)	-13(1)
F(44)	70(1)	34(1)	165(2)	-35(1)	8(1)	-29(1)
F(45)	63(1)	74(1)	124(2)	-70(1)	-6(1)	-23(1)
F(46)	54(1)	57(1)	45(1)	-24(1)	-6(1)	-21(1)
C(51)	20(1)	28(1)	35(1)	-14(1)	-1(1)	-6(1)
C(52)	28(1)	66(2)	41(1)	-31(1)	-5(1)	0(1)
C(53)	27(1)	66(2)	62(2)	-31(1)	-18(1)	3(1)
C(54)	20(1)	39(1)	64(2)	-24(1)	2(1)	-3(1)
C(55)	39(2)	50(1)	41(1)	-25(1)	10(1)	-2(1)
C(56)	32(1)	44(1)	34(1)	-16(1)	-5(1)	-2(1)
F(52)	51(1)	172(2)	54(1)	-68(1)	-21(1)	27(1)
F(53)	49(1)	172(2)	98(2)	-77(2)	-45(1)	37(1)
F(54)	22(1)	61(1)	100(1)	-39(1)	4(1)	3(1)
F(55)	66(1)	131(2)	51(1)	-50(1)	10(1)	20(1)
F(56)	53(1)	125(2)	44(1)	-45(1)	-19(1)	18(1)
C(61)	27(1)	25(1)	37(1)	-11(1)	-1(1)	-10(1)
C(62)	55(2)	42(1)	35(1)	-10(1)	-3(1)	-23(1)
C(63)	70(2)	43(1)	45(2)	4(1)	-4(1)	-29(1)
C(64)	51(2)	29(1)	69(2)	-12(1)	2(1)	-19(1)
C(65)	45(2)	37(1)	60(2)	-28(1)	1(1)	-18(1)
C(66)	40(1)	32(1)	39(1)	-13(1)	1(1)	-14(1)
F(62)	118(2)	74(1)	36(1)	-15(1)	-9(1)	-50(1)
F(63)	161(3)	79(1)	48(1)	18(1)	-10(1)	-72(2)
F(64)	94(2)	35(1)	106(2)	-11(1)	0(1)	-40(1)
F(65)	90(1)	66(1)	86(1)	-47(1)	-1(1)	-41(1)
F(66)	96(1)	59(1)	37(1)	-15(1)	-7(1)	-40(1)
O(1)	48(1)	38(1)	34(1)	-10(1)	-10(1)	-12(1)
C(71)	83(3)	82(2)	50(2)	-21(2)	-15(2)	-45(2)
O(2)	90(2)	47(1)	45(1)	-14(1)	-8(1)	-5(1)
C(72)	90(3)	51(2)	68(2)	-25(2)	-31(2)	-12(2)
C(81)	120(5)	50(2)	123(4)	-33(3)	-38(4)	1(3)
C(82)	88(4)	55(2)	187(6)	-45(3)	-67(4)	4(2)
C(83)	85(4)	57(3)	185(7)	-43(3)	-30(4)	-1(2)
C(84)	123(5)	73(3)	173(6)	-55(3)	-38(5)	-10(3)
C(85)	84(4)	74(3)	141(5)	-55(3)	-36(3)	-1(2)
C(86)	81(3)	57(2)	164(5)	-55(3)	-42(3)	6(2)
C(87)	282(13)	125(6)	154(7)	-44(5)	-57(7)	-36(6)

Table S7: Hydrogen coordinates (x 10^4) and isotropic displacement parameters ($Å^2$x 10^3).

	x	y	z	U(eq)
H(2)	1240	-4287	-2060	39
H(3)	2966	-3623	-2785	39
H(7)	3818	-32	-4230	38
H(8)	2721	1647	-4269	36
H(12)	-1603	3214	-3282	35
H(13)	-3350	2563	-2631	35
H(17)	-4292	-986	-1443	38
H(18)	-3164	-2684	-1311	40
H(22)	3593	-1684	-4834	49
H(23)	5457	-2430	-5277	63
H(24)	6767	-3176	-4347	71
H(25)	6259	-3173	-2987	62
H(28)	4611	-3906	-1628	59
H(29)	4170	-3902	-260	70
H(30)	3638	-2417	5	58
H(32)	3992	-921	-2493	42
H(34)	1632	-180	-2010	33
H(35)	-923	-1447	-746	37
H(36)	-408	-1694	510	42
H(38A)	706	-1291	1273	59
H(38B)	1681	-697	753	59
H(38C)	1943	-1866	971	59
H(1O1)	-801	165	-4262	59
H(71A)	-1338	-1542	-3675	98
H(71B)	-1501	-712	-4574	98
H(71C)	-2252	-522	-3746	98
H(1O2)	-765	1150	-5503	96
H(72A)	-2016	2507	-4818	99
H(72B)	-1612	2734	-5803	99
H(72C)	-698	2468	-5199	99
H(82)	-6891	4284	-2712	126
H(82A)	-7036	4206	-2168	126
H(83)	-7133	3900	-1273	132
H(84)	-5698	3744	-618	142
H(84A)	-4866	3830	-1028	177
H(84B)	-5858	3321	-975	177
H(84C)	-6161	4445	-1018	177
H(85)	-3959	4088	-1417	113
H(86)	-3705	4587	-2840	115
H(86A)	-3781	4332	-2259	115
H(87A)	-4305	4872	-4066	279
H(87B)	-5640	5338	-4087	279
H(87C)	-5137	4199	-3987	279
H(87D)	-4981	4963	-4437	223
H(83')	-6482	4184	-3526	92
H(85')	-3623	4980	-3683	138

VIII Computational details

The structure of porphyrin **1b** was optimized at the PBE/SVP level of density functional theory using TURBOMOLE 6.3.[4] The calculated structure was superimposed by the crystal structure of **1b** using the program Mercury CSD 3.3.1.[5] The RMSD (route main square deviation) is 0.31 Å.

Table S8. Cartesian coordinates of the optimized structure (PBE/SVP) of reocord player **1b** in *cis* configuration.

Ni	-0.5108310	0.1170407	-0.4887039
N	0.0395675	-1.8552560	-0.4542278
N	1.1985273	0.5701573	-1.5639373
N	-1.1495198	2.0704106	-0.7335511
N	-2.3112437	-0.3583516	0.3886412
C	-0.6817358	-2.8948070	0.0792798
C	0.0269184	-4.1502123	-0.1174986
H	-0.3168921	-5.1386041	0.2111820
C	1.1792471	-3.8467420	-0.7930959
H	1.9561923	-4.5370705	-1.1423692
C	1.1795296	-2.4047839	-0.9935425
C	2.2086271	-1.6998515	-1.6644030
C	2.1931418	-0.3099179	-1.9313188
C	3.2680522	0.4061316	-2.6010110
H	4.1843211	-0.0491005	-2.9966826
C	2.9032541	1.7284529	-2.6280529
H	3.4663627	2.5706043	-3.0489140
C	1.6029321	1.8148836	-1.9827816
C	0.8667583	3.0154289	-1.8267275
C	-0.4201574	3.1187138	-1.2483213
C	-1.1840094	4.3514920	-1.1502305
H	-0.8531691	5.3386388	-1.4959473
C	-2.3818335	4.0277730	-0.5646863
H	-3.2163436	4.6998213	-0.3286626
C	-2.3450171	2.5985844	-0.3034891
C	-3.3870909	1.8734020	0.3194888
C	-3.3616226	0.4945537	0.6327955
C	-4.4558540	-0.2265655	1.2623830
H	-5.4191848	0.2062920	1.5596696
C	-4.0457657	-1.5302739	1.3853183
H	-4.6098120	-2.3741977	1.8016370
C	-2.7043090	-1.5992351	0.8285971
C	-1.9494850	-2.7877005	0.7009081
C	3.3860624	-2.5060407	-2.1377589
C	3.4954600	-2.8442057	-3.5032836
H	2.7353471	-2.4640517	-4.2053098

C	4.5315236	-3.6686702	-3.9678163
H	4.5931222	-3.9221912	-5.0388708
C	5.4753121	-4.1788296	-3.0628904
H	6.2887759	-4.8338015	-3.4158061
C	5.3857574	-3.8450688	-1.7033496
H	6.1351880	-4.2268295	-0.9903550
C	4.3604467	-3.0020776	-1.2253542
C	4.3079524	-2.6308069	0.2209472
C	4.0277590	-3.5916928	1.2181810
H	3.8874967	-4.6460879	0.9315919
C	3.8940699	-3.2042342	2.5604413
H	3.6651882	-3.9603940	3.3294793
C	4.0217922	-1.8578420	2.9312957
H	3.9061443	-1.5453759	3.9813289
C	4.3428434	-0.9010933	1.9459656
C	4.5184378	-1.2934556	0.6056911
H	4.7831989	-0.5330573	-0.1457655
N	4.6371773	0.4478791	2.3152514
N	3.7698439	1.2281569	2.7700801
C	2.3686248	0.9851976	2.7403243
C	1.7169369	0.5953254	1.5483127
H	2.2970790	0.3192352	0.6558971
N	0.3826845	0.6032047	1.4085722
C	-0.3679230	0.9822912	2.4642953
H	-1.4588370	0.9777574	2.3184381
C	0.1956068	1.3805731	3.6829866
H	-0.4677086	1.6921863	4.5060785
C	1.5893315	1.4081694	3.8508326
C	2.2524703	1.8514932	5.1229599
H	1.5439787	2.3862851	5.7887751
H	3.1206065	2.5080004	4.8914661
H	2.6603064	0.9804533	5.6859985
C	1.4836376	4.2787056	-2.3354448
C	1.5550129	4.5557819	-3.7140089
C	2.1089812	5.7504759	-4.2030062
C	2.6089153	6.7010829	-3.2968596
C	2.5558371	6.4500881	-1.9152290
C	1.9944436	5.2484774	-1.4514042
F	1.0774037	3.6723894	-4.5985597
F	2.1563981	5.9925768	-5.5159898
F	3.1315965	7.8414836	-3.7489667
F	3.0378633	7.3514622	-1.0557580
F	1.9503318	5.0398219	-0.1310812
C	-4.6248125	2.6328146	0.6736977
C	-5.6383907	2.8456784	-0.2780002
C	-6.7998827	3.5734352	0.0297737
C	-6.9558209	4.1084804	1.3202654
C	-5.9601924	3.9079712	2.2918410
C	-4.8105387	3.1725400	1.9589192
F	-5.5087999	2.3456001	-1.5134719
F	-7.7504960	3.7609903	-0.8888101

F	-8.0504559	4.8057956	1.6253506
F	-6.1135552	4.4197507	3.5158849
F	-3.8746283	2.9940703	2.9002194
C	-2.5680758	-4.0500392	1.2092921
C	-2.6278298	-4.3361895	2.5859605
C	-3.1866300	-5.5310281	3.0700491
C	-3.7062618	-6.4686195	2.1615711
C	-3.6697200	-6.2050184	0.7814460
C	-3.1057030	-5.0029208	0.3232516
F	-2.1366772	-3.4629839	3.4723462
F	-3.2219490	-5.7847356	4.3813454
F	-4.2330868	-7.6087650	2.6098806
F	-4.1712458	-7.0940757	-0.0798587
F	-3.0849751	-4.7756485	-0.9964084
O	-1.4396952	-0.1833285	-2.5275566
H	-1.4898882	0.7718911	-2.7554769
C	-2.7205845	-0.7779097	-2.7345222
H	-2.6722666	-1.8054440	-2.3207890
H	-2.9533969	-0.8428794	-3.8237904
H	-3.5364739	-0.2218907	-2.2164778

IX Cell toxicity test with water soluble Ni-porphyrin

Methods

XTT assay: To assess the effect of Ni-porphyrin on cell vitality XTT colorimetric assays were performed on human squamous carcinoma cells (A431) and compared with the toxicity of conventional very well tolerated current MRI and x-ray contrast media. After 24 h baseline growth cells were treated either with Ni-porphyrin, Gd-DTPA (MRI contrast agent, Magnograf®, Jenapharm GmbH, Germany), or iomeprol (iodinated x-ray contrast medium, Imeron® 300, Bracco Imaging, Germany) at concentrations of 1, 10, 100, 250, 500, 1000, 3000, and 5000 µM. Only vital cells are able to convert 2,3-Bis-(2-methoxy-4-nitro-5-sulfophenyl)-2H-tetrazolium-5-carboxanilide salt (XTT) to an orange-colored formazan product which was quantified by spectrophotometric readout at 450 nm and expressed as percentage of the signal of untreated cells. Each measurement was performed in three independent replicates.

Results

In comparison to Gd-DTPA and iomeprol significant differences in toxicity were observed only at concentration of 5 mM.

Discussion

While there are some indications that the Ni containing agents are more toxic at very high concentrations compared to extremely well tolerated current contrast agents, at a 1 mM concentration no difference was observed. Thus, further evaluation of the value of this new type of contrast agents in animal systems can be performed. And of course, as the next step further derivatives being even more efficient as contrast agents and being even less toxic can be undergone.

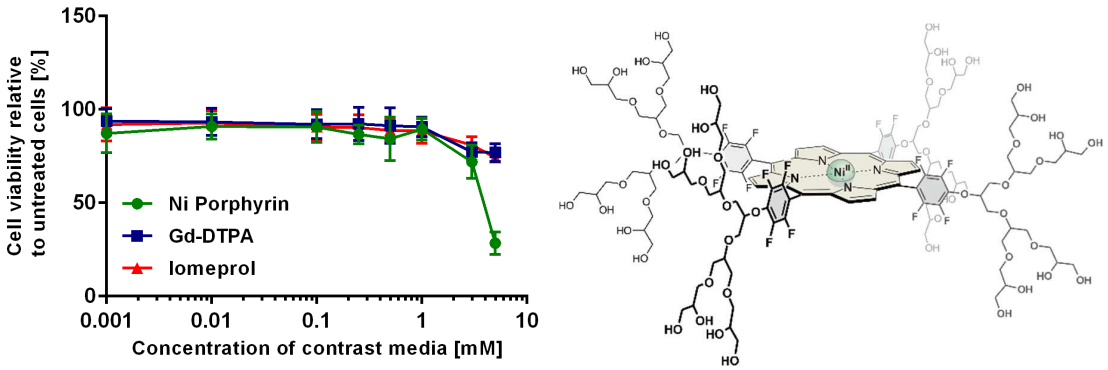

Figure S13: Assay of A431 cells treated with various concentrations of Ni porphyrin, Gd-DTPA, and Iomeprol for 24 h (left). Utilized water soluble Ni-porphyrin (right).

(1) Vogler, H.; Platzek, J.; Schuhmann-Giampieri, G.; Frenzel, T.; Weinmann, H.-J.; Radbüchel, B.; Press, W.-R. *Eur. J. Radiol.* **1995**, *21*, 1–10.

(2) Fenchel, M.; Franow, A.; Martirosian, P.; Engels, M.; Kramer, U.; Stauder, N. I.; Helber, U.; Vogler, H.; Claussen, C. D.; Miller, S. *Brit. J. Radiol.* **2007**, *80*, 884–892.

(3) Venkataramani, S.; Jana, U.; Dommaschk, M.; Sönnichsen, F. D.; Tuczek, F.; Herges, R. *Science* **2011**, *331*, 445–448.

(4) TURBOMOLE V6.3 **2011** a development of University of Karlsruhe and Forschungszentrum Karlsruhe GmbH, **1989-2007**, TURBOMOLE GmbH, since **2007**; available from http://www.turbomole.com.

(5) Mercury CSD 2.0 - New Features for the Visualization and Investigation of Crystal Structures, Macrae, C. F.; Bruno, I. J.; Chisholm, J. A.; Edgington, P. R.; McCabe, P.; Pidcock, E.; Rodriguez-Monge, L.; Taylor, R.; Van de Streek, J.; Wood, P. A.; *J. Appl. Cryst.* **2008**, *41*, 466-470.

5 Improved LD-CISSS

The association of a pyridine derivative to a Ni-porphyrin can be enhanced in two ways. Either the pyridine is functionalized with electron-donating groups (section 4.1), or the electron deficiency of the porphyrin is increased by electron-withdrawing *meso* substituents. Since three out of four *meso* positions of the RP are already occupied with pentafluorphenyl groups, the last possibility for a further coordination enhancement is the introduction of electron-withdrawing substituents to the tether. So far, all RPs have been obtained by a strictly linear synthesis. The aldehyde of the photochromic moiety **10**-**10**c (prepared in three to five steps, depending on the *para* pyridine substituent) is utilized with (pentafluorophenyl)dipyrromethane (**11**) and pentafluorobenzaldehyde (**12**) to form a porphyrin (LINDSEY mixed aldehyde approach, Figure 5.1).[138,139] Besides the RP **7**-**7**c (A_3B porphyrin) there is also formation of A_4 prophyrin ($NiTPPF_{20}$, **3**) and *trans*-A_2B_2 prophyrin. However, the linear RP synthesis involves many steps including the low yielding porphyrin formation (2-7%) as the last one. Hence, the majority of the prior synthesized photochromic moiety is wasted. For an efficient functionalization of the RP tether a different, preferably convergent, synthetic approach has to be applied.

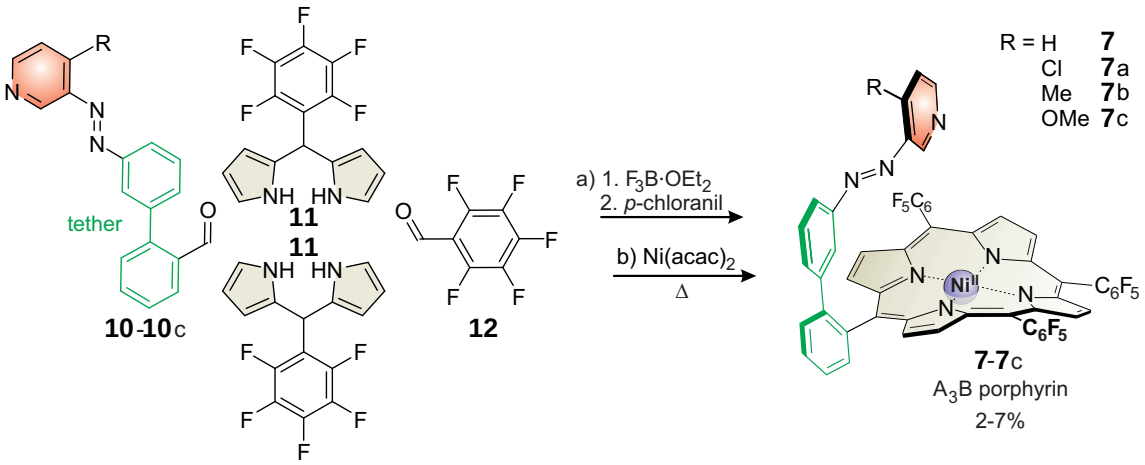

Figure 5.1: The preparation of the RPs (**7**-**7**c) via mixed aldehyde synthesis (a) and Ni insertion (b) has poor yields of 2-7% (section 4.1).

5.1 Synthesis of Functionalized Perfluorinated Porphyrins for Improved Spin Switching

Marcel Dommaschk, Christian Näther and Rainer Herges

J. Org. Chem. **2015**, *80*, 8496-8500.
DOI:10.1021/acs.joc.5b01524

Summary

This work reports on a novel synthetic strategy for the preparation of RPs. The aim is the introduction of substituents to the RP tether, or more precisely the perfluorination of the phenyl moiety that is bound to the porphyrin. In the recently applied synthetic approaches the metal free RPs are prepared by the mixed aldehyde synthesis. The complete subunit of tether plus azopyridine had to be used as an aldehyde building block. This is a strictly linear synthetic approach. Even a very small modification of the target molecule requires to start the synthesis from scratch. The presented convergent strategy improves the overall yields of the RPs and allows an easier functionalization. The innovation is to introduce the photochromic ligand after the porphyrin formation. For this purpose the mono iodo Ni-porphyrin **14** ($NiTPPF_{19}I$) was synthesized. Apart from the iodo substituent the *meso* phenyl groups are perfluorinated. The iodo substituent can be utilized for a Suzuki cross coupling reaction with the boronic pinacol ester of the photochromic ligand **13**. The novel RP **15** is more electron-deficient than the parent system **7** which results in an enhanced intramolecular coordination. The fraction of paramagnetic *cis* isomer increases by 15% (Figure 5.2). The novel convergent synthetic approach is not limited to the preparation of RPs. Basically, every perfluorinated *meso*-*o*-phenyl substituted porphyrin is accessible.

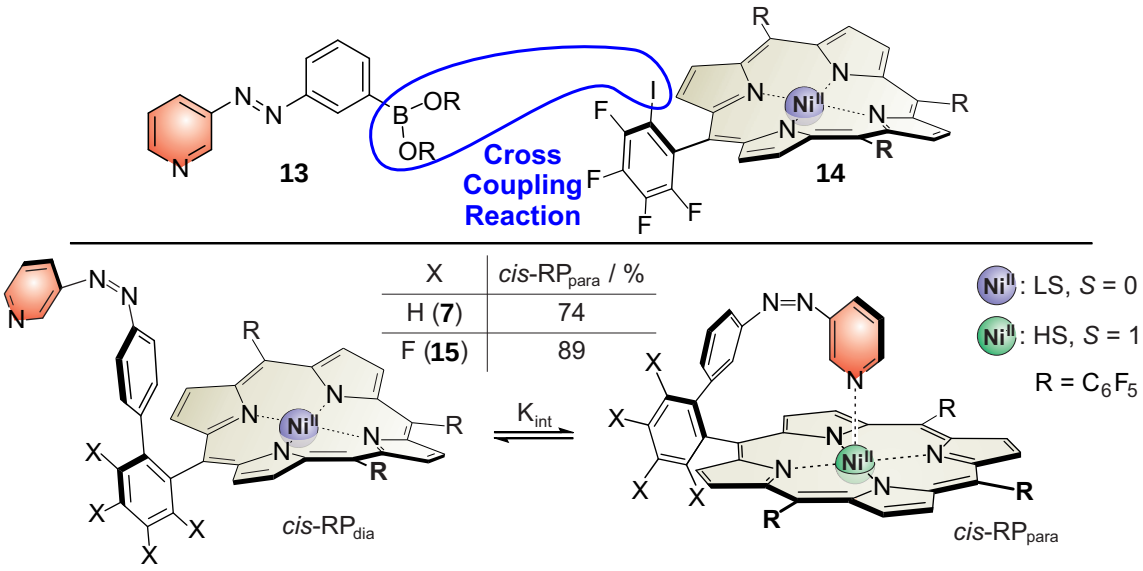

Figure 5.2: Formation of RP **15** by cross coupling reaction of **14** and **13** (top). By the electron-deficient tether the equilibrium between the magnetic conformers *cis*-RP_{dia} and *cis*-RP_{para} is shifted towards the paramagnetic form (bottom) (acetone, 300 K).

JOC The Journal of Organic Chemistry
Brief Communication
pubs.acs.org/joc

Synthesis of Functionalized Perfluorinated Porphyrins for Improved Spin Switching

M. Dommaschk,[†] C. Näther,[‡] and R. Herges*,[†]

[†]Otto-Diels-Institut für Organische Chemie, Christian-Albrechts-Universität, Otto-Hahn-Platz 4, 24098 Kiel, Germany
[‡]Institut für Anorganische Chemie, Christian-Albrechts-Universität, Otto-Hahn-Platz 6/7, 24098 Kiel, Germany

Supporting Information

ABSTRACT: We have established a method to synthesize perfluorinated *meso*-phenylporphyrins with one phenyl group bearing a substituent in the *ortho* position. These novel electron-deficient porphyrins are interesting for model enzymes, catalysis, photodynamic therapy, and electron transfer. The key step is the synthesis of an iodine-substituted porphyrin and its Suzuki cross coupling with boronic acid derivatives. We applied the novel strategy to synthesize a highly electron-deficient, azopyridine-substituted Ni–porphyrin that undergoes an improved ligand-driven coordination-induced spin-state switch.

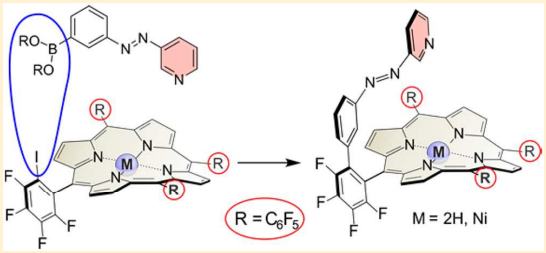

Nickel–porphyrins are known to change their spin state upon coordination of axial ligands, which is also known as a coordination-induced spin-state switch (CISSS).[1,2] Ni–porphyrins without axial ligands and square planar geometry are always diamagnetic (low spin, LS, $S = 0$). Upon axial coordination of ligands, square-pyramidal and octahedral complexes are formed which are paramagnetic (high spin, HS, $S = 1$). The process is fully reversible and can be controlled by light (LD-CISSS) using photochromic azopyridines as free ligands (photo-dissociable ligands, PDL)[3] or azopyridines covalently attached to the Ni–porphyrin (record player, RP concept) (Figure 1).[4] The systems are designed in such a way

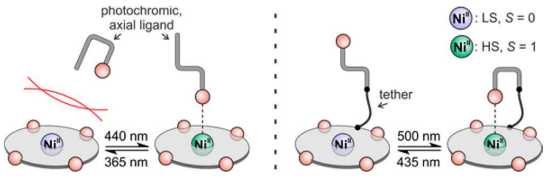

Figure 1. Spin-state switching using PDLs (left) and the RP concept (right).

that only one of the two azopyridine configurations coordinates to the Ni ion (*trans* isomer for PDL, *cis* isomer for RP), whereas the other isomer does not. Consequently, isomerization of the azo group changes the coordination number and thereby switches the spin state of the nickel.

The switching efficiency (diamagnetic to paramagnetic) depends on the association constants of the axial ligands to the porphyrin. Generally, a strong coordination of the binding isomer is advantageous to achieve a high conversion to the high spin state. It is known that electron-deficient porphyrins exhibit a higher association constant to axial ligands.[2] For the realization of the PDL concept, therefore, *meso*-tetrakis-(pentafluorophenyl)nickel(II)porphyrin (Ni–$TPPF_{20}$, **1**) was used as the square-planar Ni complex. Ni–$TPPF_{20}$ is one of the most electron-deficient porphyrins.[3] The RP concept is also based on *meso*-tetraarylporphyrins; however, one of the *ortho* positions of the aryl groups is equipped with an azopyridine unit as the switching ligand (Figure 2). So far, the synthesis of

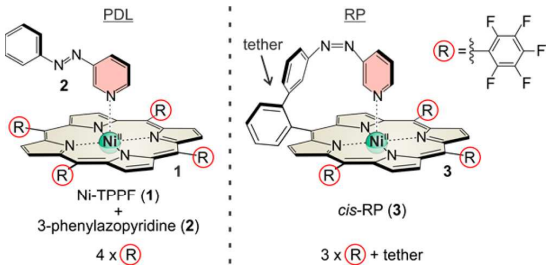

Figure 2. Association of the axial ligand to the Ni–porphyrin by untethered free 3-phenylazopyridine (**2**) (PDL concept, left) and by intramolecular coordination (RP concept, right).

RP systems has been performed via the "mixed aldehyde synthesis". Consequently, in previous designs, only three of the four *meso* positions are substituted with electron-withdrawing pentafluorophenyl groups (Figure 2), which give rise to an incomplete intramolecular coordination. Only 74% of *cis*-RP **3**

Received: July 3, 2015
Published: August 24, 2015

DOI: 10.1021/acs.joc.5b01524
J. Org. Chem. 2015, 80, 8496–8500

is in the paramagnetic, coordinated form (300 K, acetone-d_6), and 26% remain noncoordinating and diamagnetic.

Perfluorination of the fourth *meso* position, to which the tether is attached, should enhance the intramolecular association. Thus, we developed a novel strategy to prepare porphyrins with three pentafluorophenyl substituents and one *ortho*-substituted tetrafluorophenyl substituent. With an iodine at this position, aryl substituents such as azopyridines can be introduced using cross-coupling reactions. A further advantage of this strategy compared to the mixed aldehyde approach is the fact that the yields are considerably higher with respect to the functional unit, which should be introduced.

The starting material is the commercially available 1,2,3,4-tetrafluorobenzene (**4**). It is known that metalation of **4** is possible with *n*-butyllithium (*n*-BuLi).[5] The metalated species **5** is well characterized.[6] At temperatures higher than −40 °C, lithium fluoride is eliminated and an aryne is formed. At lower temperatures, **5** is stable and can react with electrophiles. We were able to obtain the formylated product **6** by addition of ethyl formate (Scheme 1) in analogy to the reaction of the

Scheme 1. Synthesis of 9

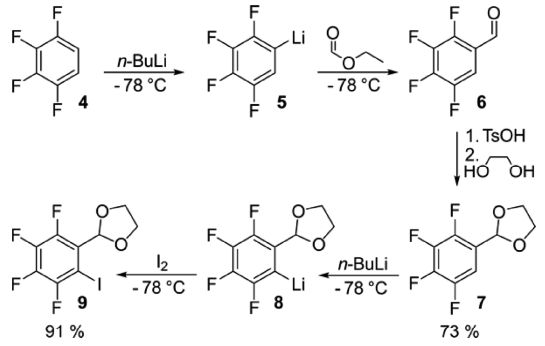

regioisomer 1,2,4,5-tetrafluorobenzene.[7] Formylation with dimethylformamide (DMF) failed because the aryne formation is faster than the reaction with DMF. The lithiation/formylation sequence is the first one-pot preparation of 2,3,4,5-tetrafluorobenzaldehyde (**6**) from commercially available 1,2,3,4-tetrafluorobenzene (**4**). Thus far, it has been obtained by Grignard reaction from the less accessible 1-bromo-2,3,4,5-tetrafluorobenzene[8] or by Swern oxidation of the corresponding benzylic alcohol.[9] 2,3,4,5-Tetrafluorobenzaldehyde (**6**) rapidly oxidizes under air to the corresponding carboxylic acid. To prevent oxidation and to allow metalation, the crude aldehyde was immediately protected with ethylene glycol yielding 2-(2,3,4,5-tetrafluorophenyl)-1,3-dioxolane (**7**) with an overall yield of 73% over three steps from 1,2,3,4-tetrafluorobenzene (Scheme 1). Compound **7** was metalated with *n*-BuLi in analogy to the corresponding carboxylic acid.[10] Addition of iodine gave the 2-(2-iodo-3,4,5,6-tetrafluorophenyl)-1,3-dioxolane (**9**) with a yield of 91% (Scheme 1). A structural analysis of **9** is available in the Supporting Information.

Deprotection of dioxolane **9** to the corresponding aldehyde was achieved quantitatively with AcOH/HCl. The (iodo, tetrafluorophenyl) tris(pentafluorophenyl) porphyrin **14** was prepared by the mixed aldehyde synthesis also known as the Lindsey method (Scheme 2).[11] To reduce the number of

Scheme 2. Synthesis of the Porphyrin Mixtures 13−15 and the Corresponding Nickel Derivatives 1, 16, and 17

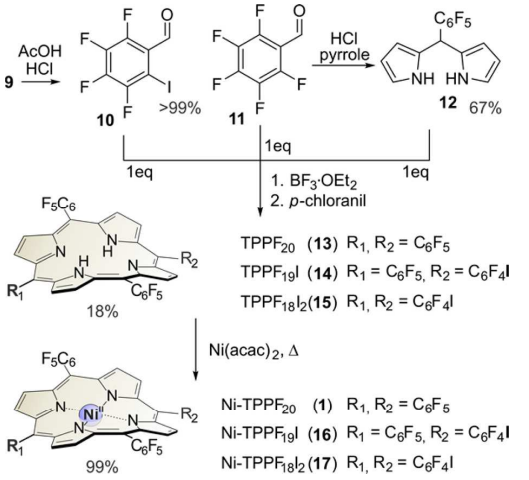

possible products from 6 to 3, prefabricated *meso*-(pentafluorophenyl)dipyrromethane (**12**) (synthesized from pentafluorobenzaldehyde (**11**) and pyrrole) was used instead of pyrrole as one of the three components.[12] The resulting porphyrins $TPPF_{20}$ (**13**), $TPPF_{19}I$ (**14**), and $TPPF_{18}I_2$ (**15**) cannot be separated and therefore are used as a mixture. The yields correspond to the statistical product distribution of 1:2:1. The porphyrin mixture was metalated quantitatively with nickel(II) acetylacetonate ($Ni(acac)_2$) yielding a Ni−porphyrin mixture of Ni−$TPPF_{20}$ (**1**), Ni−$TPPF_{19}I$ (**16**), and Ni−$TPPF_{18}I_2$ (**17**).

The porphyrin mixtures **13−15** and the corresponding Ni compounds **1**, **16**, and **17** were used for Suzuki cross-coupling reactions[13] with pinacol boronic ester **19** to prepare record player molecules **20** and **21** (Scheme 3). Compound **19** was synthesized by a Miyaura borylation reaction[14] with the brominated phenylazopyridine **18** as starting material.[4] Note

Scheme 3. Miyaura Borylation of Phenylazopyridine 18 Yields Pinacol Boronic Ester 19, Which Is Utilized for Suzuki Cross-Coupling Reaction with Porphyrins 14 and 16 To Prepare the Record Players 20 and 21

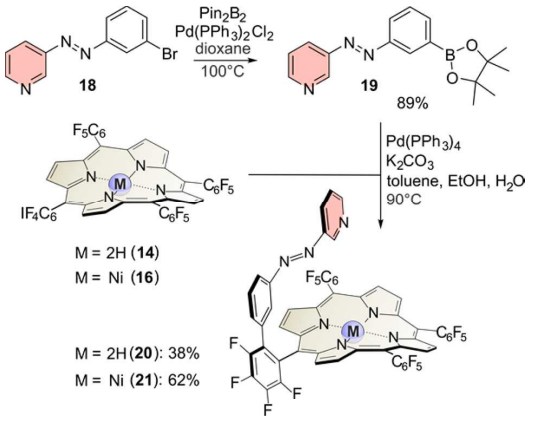

DOI: 10.1021/acs.joc.5b01524
J. Org. Chem. 2015, 80, 8496−8500

The Journal of Organic Chemistry Brief Communication

that separation of the porphyrins is not possible before the cross-coupling reaction.

The improved coordination of perfluorinated RP **21** (compared to the parent system **3**) can be observed by NMR spectroscopy. The intramolecular association was quantified by the ^{1}H NMR shift of the pyrrole protons. The maximum shift (100% paramagnetic complex) for **3** and **21** is identical (~53 ppm). The latter was measured by addition of an excess of an axial ligand (pyridine-d_5). The diamagnetic shift (~9 ppm) is known from the *trans* isomer and the corresponding Zn–porphyrin.[4] The equilibrium between the paramagnetic and diamagnetic conformer is faster than the ^{1}H NMR time scale. Hence, an average shift is observed that is directly proportional to the amount of the paramagnetic complex. By irradiation with light of 500 nm 61% of the *cis*-isomer was obtained, which is the same percentage as for the parent system **3**. Hence, the perfluorination does not influence the photochromism. As expected, the pyrrole protons of the perfluorinated RP **21** (X = F) resonate at lower fields as those of the parent system **3** (X = H) (Figure 3). The average shift rises from 41.7 to 48.2 ppm

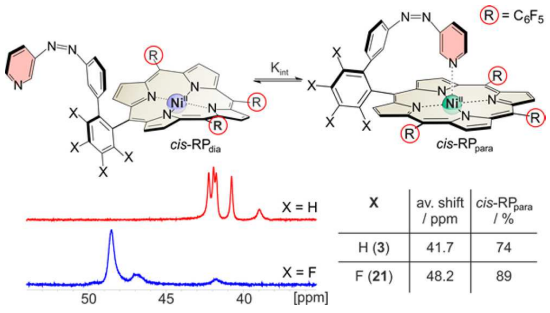

X	av. shift / ppm	*cis*-RP$_{para}$ / %
H (3)	41.7	74
F (21)	48.2	89

Figure 3. Equilibrium between the dia- (*cis*-RP$_{dia}$) and paramagnetic (*cis*-RP$_{para}$) conformations of the perfluorinated RP **21** (X = F) and of the parent system **3** (X = H). Average shift is the average chemical shift of the four pyrrole protons; *cis*-RP$_{para}$ is the percentage of the paramagnetic *cis* isomer relative to the total amount of *cis* isomer.

(acetone-d_6), which corresponds to 15% higher percentage of the paramagnetic *cis* isomer (*cis*-RP$_{para}$). The overall switching efficiency (diamagnetic to paramagnetic) has increased from 45% to 54%.

In summary, we present a novel, modular approach to prepare highly electron-deficient functionalized porphyrins. Key intermediates are the porphyrins TPPF$_{19}$I (**14**) and Ni–TPPF$_{19}$I (**16**). Cross-coupling reactions were used to functionalize these porphyrins as demonstrated by the synthesis of perfluorinated RP **21**, a Ni–porphyrin that exhibits an improved LD-CISSS. Our approach provides access to a number of perfluorinated mono *meso*-*o*-phenyl-functionalized porphyrins which have not been described so far and which are difficult to prepare by the established mixed aldehyde synthesis. TPPF$_{19}$I (**14**) is a suitable building block to tether various functional groups, particularly axial ligands. Besides spin switching, metalated derivatives of such porphyrins are of broad interest as model enzymes[15] and for catalysis,[16] photodynamic therapy (PDT),[17] and electron-transfer processes.[18]

EXPERIMENTAL SECTION

General Experimental Methods. Tetrahydrofuran was dried and distilled from sodium/benzophenone. All compounds were characterized using ^{1}H, ^{13}C and, if possible, ^{19}F NMR spectroscopy. The signals were assigned using 2D spectroscopy. For ^{1}H and ^{13}C NMR signal assignment we performed HSQC and HMBC. For ^{19}F signal assignment we applied ^{19}F COSY.

Synthesis of 2-(2,3,4,5-Tetrafluorophenyl)-1,3-dioxolane (7). 1,2,3,4-Tetrafluorobenzene (**4**) (10.0 g, 7.09 mL, 66.6 mmol) was mixed with tetrahydrofuran (200 mL) and cooled to −78 °C. *n*-Buthyllithium (30 mL, 75.0 mmol, 2.5 M in hexane) was slowly added, and the reaction mixture was stirred for another 1 h at −78 °C. Ethyl formate (27 mL, 333 mmol) was slowly added, and the mixture was allowed to warm to room temperature overnight. Diethyl ether (500 mL) was added. The organic layer was washed with water three times and dried over magnesium sulfate, and the solvent was removed under reduced pressure. Crude product of 2,3,4,5-tetrafluorobenzaldehyde (**3**) (12.4 g) was obtained as a pale yellow liquid. The crude product was mixed with benzene (500 mL) and ethylene glycol (12.4 g, 200 mmol). *p*-Toluenesulfonic acid monohydrate (111 mg, 0.583 mmol) was added, and the benzene water mixture was removed by azeotropic distillation. The residue was treated with triethylamine (2 mL) and diethyl ether (200 mL). The organic layer was successively washed with saturated sodium carbonate, diluted sodium carbonate solution, and water. The organic phase was dried over magnesium sulfate, and the solvent was removed under reduced pressure. The crude product (11.8 g yellow liquid) was purified by vacuum distillation (bp 105 °C, 0.7 mbar) to obtain 2-(2,3,4,5-tetrafluorophenyl)-1,3-dioxolane (**7**) (10.8 g, 48.6 mmol, 73%) as a colorless liquid. n^{20}_D = 1.4561. FT-IR: ν = 2892 (m), 1635 (w), 1524 (s), 1488 (vs), 1406 (m) 1371 (m), 1265 (w), 1194 (w), 1134 (s), 1103 (w), 1030 (s), 973 (s), 946 (vs), 868 (m), 757 (m), 708(m), 616 (m), 560 (w), 499 (w) cm^{-1}. ^{1}H NMR (500 MHz, 300 K, $CDCl_3$): δ = 7.04 (m, 1H, Ar-*H*), 5.90, (s, 1H, C*H*O$_2$), 4.02–3.91 (m, 4H, C*H*$_2$) ppm. ^{13}C NMR (125 MHz, 300 K, $CDCl_3$): δ = 147.1 (dddd, ^1J = 247 Hz, ^2J = 10.2 Hz, ^3J = 3.7 Hz, ^4J = 1.9 Hz, C5), 146.1 (dddd, ^1J = 250 Hz, ^2J = 10.9 Hz, ^3J = 3.8 Hz, ^4J = 1.7 Hz, C2), 141.0 (dddd, ^1J = 255 Hz, ^2J = 16.8, 12.2 Hz, ^3J = 3.3 Hz, C4), 140.7 (dddd, ^1J = 254 Hz, ^2J = 16.5, 12.3 Hz, ^3J = 3.6 Hz, C3), 122.3 (dddd, ^2J = 11.6 Hz, ^3J = 5.9, 3.9 Hz, ^4J = 0.7 Hz, C1), 109.0 (dt, ^2J = 20.5 Hz, ^3J = 3.7 Hz, C6), 97.7 (m, CHO_2), 65.6 (s, CH_2) ppm. ^{19}F NMR (470 MHz, 300 K, $CDCl_3$): δ = −139.14 (ddd, ^3J = 20.9 Hz, ^5J = 13.1 Hz, ^4J = 2.4 Hz, 1F, *F*-5), −145.00 (ddd, ^3J = 20.3 Hz, ^5J = 13.1 Hz, ^4J = 3.9 Hz, 1F, *F*-2), −154.92 (td, ^3J = 20.1 Hz, ^4J = 3.9 Hz, 1F, *F*-4), −153.73 (td, ^3J = 19.9 Hz, ^4J = 2.4 Hz, 1F, *F*3) ppm. MS (EI, TOF): *m*/*z* = 222 (67) [M]$^+$, 203 (45) [M − F]$^+$, 178 (100) [M − C_2H_4O]$^+$. HRMS (EI, TOF-Q) *m*/*z*: [M]$^+$ calcd for $C_9H_6F_4O_2$ 222.0304, found 222.0305.

Synthesis of 2-(2-Iodo-3,4,5,6-tetrafluorophenyl)-1,3-dioxolane (9). 2-(2,3,4,5-Tetrafluorophenyl)-1,3-dioxolane (**7**) (9.29 g, 41.8 mmol) was mixed with tetrahydrofuran (150 mL) and cooled to −78 °C. *n*-Buthyllithium (18.4 mL, 46.0 mmol, 2.5 M in hexane) was added within 1 h whereby the solution became pale red. The mixture was stirred for another 1 h at −78 °C. Iodine (11.7 g, 46.0 mmol) was dissolved in tetrahydrofuran (50 mL) and slowly added with a syringe pump within 1.5 h. Finally, the color of iodine did not disappear upon addition. The reaction mixture was allowed to warm to room temperature and added to diethyl ether (300 mL). The organic layer was washed with diluted sodium carbonate and saturated sodium thiosulfate and once again with diluted sodium carbonate solution. Than it was dried over magnesium sulfate, and the solvent was removed under reduced pressure. A pale yellow solid was obtained which was dissolved in a minimum amount of dichloromethane. By addition of pentane the product **9** precipitated as a fluffy, colorless solid (13.2 g, 37.9 mmol, 91%). Crystals for structure analysis were obtained by vapor diffusion of pentane in a saturated solution of **9** in dichloromethane. Mp: 128.3 °C. FT-IR: ν = 2909 (m), 1627 (w), 1506 (s), 1470 (m), 1395 (m), 1353 (w), 1337 (m), 1270 (w), 1170 (w), 1148 (s), 1094 (m), 1070 (m), 1017 (w), 994 (m), 964 (s), 950 (vs), 925 (s), 809 (s), 753 (m), 724 (m), 652 (w), 624 (s), 617 (m),

DOI: 10.1021/acs.joc.5b01524
J. Org. Chem. 2015, 80, 8496–8500

The Journal of Organic Chemistry Brief Communication

519 (w) cm^{-1}. ^1H NMR (500 MHz, 300 K, $CDCl_3$): δ = 6.06 (s, 1H, CHO_2), 4.18−3.96 (m, 4H, CH_2) ppm. ^{13}C NMR (125 MHz, 300 K, $CDCl_3$): δ = 147.2 (dddd, ^1J = 242 Hz, ^2J = 11.0 Hz, ^3J = 4.3 Hz, ^4J = 2.0 Hz, *C*3), 146.8 (dddd, ^1J = 257 Hz, ^2J = 11.1 Hz, ^3J = 3.9 Hz, ^4J = 2.0 Hz, *C*6), 141.0 (dddd, ^1J = 255 Hz, ^2J = 17.3, 12.3 Hz, ^3J = 3.7 Hz, *C*5), 140.3 (dddd, ^1J = 259 Hz, ^2J = 19.7, 12.8 Hz, ^3J = 3.9 Hz, *C*4), 122.9 (dm, ^2J = 9.6 Hz, *C*1), 105.1 (dd, ^3J = 4.6 Hz, ^4J = 2.3 Hz, CH), 78.5 (dt, ^2J = 24.9 Hz, ^3J = 3.3 Hz, *C*2), 66.2 (d, ^5J = 1.2 Hz, CH_2) ppm. ^{19}F NMR (470 MHz, 300 K, $CDCl_3$): δ = −113.04 (ddd, ^3J = 23.3 Hz, ^5J = 9.8 Hz, ^4J = 3.9 Hz, 1F, *F*-3), −140.52 (ddd, ^3J = 20.3 Hz, ^5J = 9.8 Hz, ^4J = 5.2 Hz, 1F, *F*-6), −151.29 (td, ^3J = 21.5 Hz, ^4J = 5.2 Hz, 1F, *F*-4), −153.73 (td, ^3J = 19.9 Hz, ^4J = 3.9 Hz, 1F, *F*-5) ppm. MS (EI, TOF): *m*/*z* = 348 (100) $[M]^+$, 303 (31) $[M - C_2H_4O]^+$, 275 (6) $[M - C_3H_5O_2]^+$, 221 (20) $[M - I]^+$. Anal. Calcd for $C_9H_5F_4O_2I$: C, 31.06; H, 1.45. Found: C, 31.21; H, 1.47.

Synthesis of 2-Iodo-3,4,5,6-tetrafluorophenylbenzaldehyde (10). 2-(2-Iodo-3,4,5,6-tetrafluorophenyl)-1,3-dioxolane (**9**) (1.01 g, 2.90 mmol) was dissolved in acetic acid (25 mL). After dropwise addition of concentrated hydrochloric acid (6 mL), the mixture was stirred for 3 h. Ethyl acetate (200 mL) was added. The organic layer was washed with water and saturated sodium carbonate solution and dried over magnesium sulfate. The solvent was removed under reduced pressure. The obtained aldehyde (883 mg, 2.90 mmol, > 99%) is sensitive to oxidation and therefore was directly used for the porphyrin synthesis. ^1H NMR (500 MHz, 300 K, $CDCl_3$): δ = 10.05 (s, 1H, C*H*) ppm. ^{13}C NMR (125 MHz, 300 K, $CDCl_3$): δ = 188.1 (m, CH), 149.2 (dddd, ^1J = 267 Hz, ^2J = 11.1 Hz, ^3J = 3.7 Hz, ^4J = 2.4 Hz, *C*3), 147.9 (dddd, ^1J = 245 Hz, ^2J = 11.1 Hz, ^3J = 4.4 Hz, ^4J = 1.5 Hz, *C*6), 144.0 (dddd, ^1J = 267 Hz, ^2J = 19.7, 12.7 Hz, ^3J = 3.9 Hz, *C*5), 140.9 (dddd, ^1J = 259 Hz, ^2J = 16.2, 12.5 Hz, ^3J = 3.3 Hz, *C*4), 119.9 (dd, ^2J = 7.2 Hz, ^3J = 3.8 Hz, *C*1), 78.4 (dd, ^2J = 25.5 Hz, ^3J = 4.7 Hz, *C*2) ppm. ^{19}F NMR (470 MHz, 300 K, $CDCl_3$): δ = −113.29 (ddd, ^3J = 23.1 Hz, ^5J = 10.6 Hz, ^4J = 4.8 Hz, 1F, *F*-3), −142.84 (ddd, ^3J = 19.8 Hz, ^5J = 10.6 Hz, ^4J = 8.7s Hz, 1F, *F*-6), −143.89 (ddd, ^3J = 23.1, 19.1 Hz, ^4J = 8.7 Hz, 1F, *F*-4), −152.45 (td, ^3J = 19.5 Hz, ^4J = 4.8 Hz, 1F, *F*-5) ppm.

Synthesis of 3-(3-(Pinacol boronic ester)phenylazo)pyridine (19). A solution of 3-(3-bromophenylazo)pyridine (**18**) (1.00 g, 3.82 mmol) and potassium acetate (748 mg, 7.62 mmol) in dioxane (40 mL) was dried over molecular sieves (3 Å) by heating to 120 °C for 4 h. Bis(pinacolato)diboron (1.07 g, 4.20 mmol) and bis-(triphenylphosphine)palladium(II) dichloride (140 mg, 0.20 FT-IRded and the solution was kept at 100 °C overnight without stirring. After cooling the molecular sieve and all solid components were filtered off. The volume of the filtrate was doubled with water and extracted twice with dichloromethane. The combined organic layers were dried over magnesium sulfate and the solvent was removed under reduced pressure. The crude product was purified by column chromatography (cyclohexane/ethyl acetate =6:4, R_f = 0.15). The product was obtained as an orange solid (1.05 g, 3.40 mmol, 89%). Mp: 86.6 °C. FT-IR (layer): ν = 2975 (m), 1422 (m), 1356 (s), 1333 (s), 1273 (w), 1213 (w), 1139 (s), 1064 (m), 967 (w), 918 (w), 851 (m), 817 (s), 698 (vs), 676 (m), 618 (w), 566 (w), 538 (m), 512 (w) cm^{-1}. ^1H NMR (500 MHz, 300 K, $CDCl_3$): δ = 9.21 (dd, ^4J = 2.3, ^5J = 0.5 Hz, 1H, *H*-2), 8.70 (dd, ^3J = 4.7 Hz, ^4J = 1.6 Hz 1H, *H*-6), 8.37 (m, 1H, *H*-8), 8.14 (ddd, ^3J = 8.2 Hz, ^4J = 2.3, 1.6 Hz, 1H, *H*-4), 8.02 (ddd, ^3J = 7.9 Hz, ^4J = 2.3, 1.2 Hz, 1H, *H*-12), 7.95 (dt, ^3J = 7.3 Hz, ^4J = 1.2 Hz, 1H, *H*-10), 7.54 (t, ^3J = 7.6 Hz, 1H, *H*-11), 7.45 (ddd, ^3J = 8.2, 4.7 Hz, ^5J = 0.5 Hz, 1H, *H*-5), 1.38 (s, 12H, CH_3) ppm. ^{13}C NMR (125 MHz, 300 K, $CDCl_3$): δ = 152.1 (*C*7), 151.7 (*C*6), 148.1 (*C*3), 147.5 (*C*2), 138.2 (*C*10), 130.7 (*C*9), 129.7 (*C*8), 128.8 (*C*11), 127.1 (*C*4), 125.6 (*C*12), 124.1 (*C*5), 25.1 (CH_3) ppm. MS (EI, TOF): *m*/*z* = 319 (29) $[M]^+$, 203 (100) $[PhBPin]^+$. Anal. Calcd for $C_{17}H_{20}BN_3O_2$: C, 66.04; H, 6.52; N, 13.59. Found: C, 65.71; H, 6.80; N, 13.52.

Synthesis of Metal-Free Record Player 20. 2-Iodo-3,4,5,6-tetrafluorophenylbenzaldehyde (**10**) (883 mg, 2.90 mmol) and pentafluorophenylbenzaldehyde (**11**) (568 mg, 2.90 mmol) were dissolved in dichloromethane (700 mL) under nitrogen atmosphere. Boron trifluoride diethyl etherate (280 μL, 0.50 mmol) was added dropwise. Pentafluorophenyl dipyrromethane (**12**) (1.81 g, 5.81 mmol) dissolved in dichloromethane (100 mL) was added, and the mixture was stirred for 14 h. *p*-Chloranil (1.50 g, 6.09 mmol) was added, and the mixture was stirred under reflux for 4 h. The solvent was removed under reduced pressure, and the crude product was purified by column chromatography (cyclohexane/chloroform = 1:1, R_f = 0.45). The mixture of three porphyrins (**13**−**15**) was obtained as a purple solid (555 mg, 513 μmol, 18% assuming a 1:2:1 porphyrin mixture). HRMS (EI, TOF-Q) *m*/*z*: $[M]^+$ calcd for $C_{44}H_{10}F_{20}N_4$ 974.059, found 974.055; $[M]^+$ calcd for $C_{44}H_{10}F_{19}IN_4$ 1081.964, found 1081.961; $[M]^+$ calcd for $C_{44}H_{10}F_{18}I_2N_4$ 1189.871, found 1189.866. The metal-free porphyrin mixture (**13**−**15**) (229 mg, 212 μmol), pinacol boronic ester **19** (157 mg, 0.51 mmol), and tetrakis-(triphenylphosphine)palladium(0) (∼10 mg) were dissolved in a toluene (6.5 mL)/ethanol (2 mL) mixture under nitrogen atmosphere. Potassium carbonate (232 mg, 1.68 mmol) dissolved in 1.5 mL of water was added, and the mixture was stirred overnight at 80 °C. Water (50 mL) was added, and the aqueous layer was extracted twice with dichloromethane. The combined organic layers were dried over magnesium sulfate, and the solvent was removed under reduced pressure. The crude product was purified by column chromatography (cyclohexane/ethyl acetate = 7:3, R_f = 0.15). The product was obtained as a purple solid (46 mg, 40.4 μmol, 38% assuming a 1:2:1 porphyrin mixture as starting material). Mp: 216.2 °C. FT-IR (layer): ν = 3316 (w), 1651 (w), 1516 (s), 1495 (s), 1391 (m), 1080 (w), 1066 (m), 1043 (m), 1026 (w), 987 (vs), 917 (vs), 801 (s), 768 (m), 754 (s), 722 (m), 700 (s), 645 (w) cm^{-1}. ^1H NMR (500 MHz, 300 K, acetone-d_6): δ = 9.51 (s, br, 2H, *H*-Por), 9.36 (s, br, 2H, *H*-Por), 9.32−9.27 (m, 4H, *H*-Por), 8.64 (s, 1H, NC*H*), 8.60 (d, ^3J = 4.5 Hz, 1H, NC*H*), 7.78 (t, ^4J = 1.7 Hz, 1H, N_2CCH), 7.50 (d, ^3J = 8.1 Hz, 1H, NCHCHC*H*), 7.44 (dm, ^3J = 7.9 Hz, 1H, N_2CCH), 7.30 (dd, ^3J = 8.1, 4.5 Hz, 1H, NCHC*H*), 7.01 (ddd, ^3J = 7.9 Hz, ^4J = 2.0, 1.1 Hz, 1H, $N_2CCHCHCH$), 7.54 (t, ^3J = 7.9 Hz, 1H, N_2CCHCH), −3.01 (s, 2H, *H*-N) ppm. ^{13}C NMR (125 MHz, 300 K, acetone-d_6): δ = 152.8 (NCH), 151.0 ($N_2C(CH)_2$), 148.0 ($NCHCN_2$), 147.2 (NCH), 133.9 (N_2CCHCH), 133.6 (N_2CHC), 129.4 (N_2CCHCH), 127.0 (NCHCHCH), 124.8 (NCHCH), 124.5 (N_2CCHC), 123.9 ($N_2CCHCHCH$) ppm, C atoms of the porphyrin and of the perfluorinated *meso* phenyl substituents cannot be assigned. ^{19}F NMR (470 MHz, 300 K, acetone-d_6): δ = −137.19 (ddd, ^3J = 23.2 Hz, ^5J = 11.9 Hz, ^4J = 3.5 Hz, 1F, *F*-*o*′-C), −139.72 (dd, ^3J = 23.8 Hz, ^5J = 7.9 Hz, 2F, *F*-*o*′-A), −139.82 to −139.94 (m, 4F, *F*-*o*-A, *F*-*o*-B, *F*-*o*′-B), −142.78 (ddd, ^3J = 22.2 Hz, ^5J = 11.9 Hz, ^4J = 3.1 Hz, 1F, *F*-*m*-C), −155.44 (t, ^3J = 20.5 Hz, 2F, *F*-*p*-A), −155.49 (t, ^3J = 20.2 Hz, 1F, *F*-*p*-B), −156.80 (td, ^3J = 21.0 Hz, ^4J = 3.5 Hz, 1F, *F*-*p*-C), −159.23 (td, ^3J = 21.8 Hz, ^4J = 3.1 Hz, 1F, *F*-*m*′-C), −164.18 (td, ^3J = 22.2 Hz, ^5J = 8.0 Hz, 2F, *F*-*m*′-A), −164.46 to −164.61 (m, 4F, *F*-*m*-A, *F*-*m*-B, *F*-*m*′-B) ppm. HRMS (EI, TOF-Q) *m*/*z*: $[M]^+$ calcd for $C_{55}H_{18}F_{19}N_7$ 1137.1320, found 1137.1350.

Synthesis of Record Player 21. The metal-free porphyrin mixture (150 mg, 139 μmol) and nickel(II) acetylacetonate (360 mg, 1.40 mmol) were dissolved in toluene (30 mL) and stirred under reflux for 4 d. The solvent was removed under reduced pressure, and the crude product was purified by column chromatography (cyclohexane/ethyl acetate = 3:1, R_f = 0.30). The mixture of three Ni−porphyrins (**1**, **16**, and **17**) was obtained as a purple solid (156 mg, 137 μmol, 99% assuming a 1:2:1 Ni−porphyrin mixture). HRMS (EI, TOF-Q) *m*/*z*: $[M]^+$ calcd for $C_{44}H_8F_{20}N_4Ni$ 1029.978, found 1029.974; $[M]^+$ calcd for $C_{44}H_8F_{19}IN_4Ni$ 1137.884, found 1137.880; $[M]^+$ calcd for $C_{44}H_8F_{18}I_2N_4Ni$ 1245.790, found 1245.785. The Ni−porphyrin mixture (**1**, **16**, **17**) (156 mg, 137 μmol), pinacol boronic ester **19** (103 mg, 333 μmol), and tetrakis(triphenylphosphine)-palladium(0) (∼10 mg) were dissolved in a toluene (6.5 mL)/ethanol (2 mL) mixture under nitrogen atmosphere. Potassium carbonate (151 mg, 1.09 mmol) dissolved in 1.5 mL of water was added, and the mixture was stirred overnight at 80 °C. Water (50 mL) was added, and the aqueous layer was extracted twice with dichloromethane. The combined organic layers were dried over magnesium sulfate, and the solvent was removed under reduced pressure. The crude product was purified by column chromatography (cyclohexane/ethyl acetate = 2:1, R_f = 0.20). The product was obtained as a purple solid (49.2 mg, 41.9

DOI: 10.1021/acs.joc.5b01524
J. Org. Chem. 2015, 80, 8496−8500

μmol, 62% assuming a 1:2:1 Ni−porphyrin mixture as starting material). Mp: 209.0 °C. FT-IR (layer): ν = 2980 (w), 1652 (w), 1518 (s), 1486 (s), 1346 (m), 1079 (m), 1061 (m), 1025 (w), 985 (vs), 937 (vs), 800 (m), 760 (s), 732 (w), 701 (s), 644 (m) cm^{-1}. ^1H NMR (500 MHz, 300 K, acetone-d_6): δ = 9.60 (s, br, 2H, *H*-Por), 9.41 (s, br, 6H, *H*-Por), 9.28 (s, br, 1H, NC*H*), 9.21 (s, br, NC*H*), 9.15 (s, br, NCHCHC*H*), 7.53 (s, 1H, N_2CC*H*), 7.44 (d, ^3J = 7.9 Hz, 1H, NCHC*H*), 7.27 (d, ^3J = 7.9 Hz, 1H, N_2CC*H*), 7.06 (d, ^3J = 7.9 Hz, 1H, N_2CCHCHC*H*), 6.81 (t, ^3J = 7.9 Hz, 1H, N_2CCHC*H*) ppm. ^{13}C NMR (125 MHz, 300 K, acetone-d_6): δ = 152.0 (N_2C), 134.0 (N_2CCH), 133.1 (N_2CCHC), 129.9 (N_2CCHCH), 124.2 (N_2CCH), 124.0 (N_2CCHCHCH) ppm, C atoms of the pyridine, porphyrin, and the perfluorinated *meso* aryl substituents are not detectable because of the low concentration and slight paramagnetism due to intermolecular coordination. ^{19}F NMR (470 MHz, 300 K, acetone-d_6): δ = −136.97 (dd, ^3J = 21.2 Hz, ^5J = 10.8 Hz, 1F, *F*-*o*′-C), −139.59 to −139.69 (m, 3F, *F*-*o*′-A, *F*-*o*′-B), −139.96 to −140.06 (m, 3F, *F*-*o*-A, *F*-*o*-B), −142.76 (dd, ^3J = 21.6 Hz, ^5J = 10.8 Hz, 1F, *F*-*m*-C), −155.60 (t, ^3J = 20.4 Hz, 2F, *F*-*p*-A), −155.63 (t, ^3J = 20.4 Hz, 1F, *F*-*p*-B), −156.92 (t, ^3J = 21.5 Hz, 1F, *F*-*p*-C), −159.07 (t, ^3J = 21.3 Hz, 1F, *F*-*m*′-C), −164.13 (td, ^3J = 21.6 Hz, ^5J = 7.5 Hz, 2F, *F*-*m*′-A), −164.42 (td, ^3J = 22.3 Hz, ^5J = 7.8 Hz, 1F, *F*-*m*′-B), −164.46 to −164.59 (m, 3F, *F*-*m*-A, *F*-*m*-B) ppm. UV−vis (MeCN): λ_{max} (lg ε) = 311 (4.547), 403 (5.390), 523 (4.234), 556 (4.125) nm. HRMS (EI, TOF-Q) *m*/*z*: $[M]^+$ calcd for $C_{55}H_{16}F_{19}N_7Ni$ 1193.0517, found 1193.0528.

■ ASSOCIATED CONTENT

Supporting Information

The Supporting Information is available free of charge on the ACS Publications website at DOI: 10.1021/acs.joc.5b01524. CCDC-1409964 contains the supplementary crystallographic data for compound **9**. These data can be obtained free of charge from the Cambridge Crystallographic Data Centre via http://www.ccdc.cam.ac.uk/data_request/cif.

^1H, ^{13}C, ^{19}F, and 2D NMR spectra of new compounds and crystal structure data for 2-(2-iodo-3,4,5,6-tetraphenyl)-1,3-dioxolane (**9**) (PDF)

X-ray cystallographic data for compound **9** (CIF)

■ AUTHOR INFORMATION

Corresponding Author

*E-mail: rherges@oc.uni-kiel.de.

Notes

The authors declare no competing financial interest.

■ ACKNOWLEDGMENTS

The authors gratefully acknowledge funding from the Collaborative Research Center SFB 677 Function by Switching and a scholarship from the Fonds der Chemischen Industrie for M.D.

■ REFERENCES

(1) (a) Caughey, W. S.; Deal, R. M.; McLees, B. D.; Alben, J. O. *J. Am. Chem. Soc.* **1962**, *84*, 1735−1736. (b) Dommaschk, M.; Gutzeit, F.; Boretius, S.; Haag, R.; Herges, R. *Chem. Commun.* **2014**, *50*, 12476−12478.

(2) (a) McLees, B. D.; Caughey, W. S. *Biochemistry* **1968**, *7*, 642−652. (b) Walker, F. A.; Hui, E.; Walker, J. M. *J. Am. Chem. Soc.* **1975**, *97*, 2390−2397. (c) Bütje, K.; Nakamoto, K. *Inorg. Chim. Acta* **1990**, *167*, 97−108. (d) Song, Y.; Haddad, R. E.; Jia, S.-L.; Hok, S.; Olmstead, M. M.; Nurco, D. J.; Schore, N. E.; Zhang, J.; Ma, J.-G.; Smith, K. M.; Gazeau, S.; Pécaut, J.; Marchon, J.-C.; Medforth, C. J.; Shelnutt, J. A. *J. Am. Chem. Soc.* **2005**, *127*, 1179−1192. (e) Thies, S.; Bornholdt, C.; Köhler, F.; Sönnichsen, F. D.; Näther, C.; Tuczek, F.; Herges, R. *Chem. - Eur. J.* **2010**, *16*, 10074−10083.

(3) (a) Thies, S.; Sell, H.; Schütt, C.; Bornholdt, C.; Näther, C.; Tuczek, F.; Herges, R. *J. Am. Chem. Soc.* **2011**, *133*, 16243−16250. (b) Thies, S.; Sell, H.; Bornholdt, C.; Schütt, C.; Köhler, F.; Tuczek, F.; Herges, R. *Chem. - Eur. J.* **2012**, *18*, 16358−16368.

(4) (a) Venkataramani, S.; Jana, U.; Dommaschk, M.; Sönnichsen, F. D.; Tuczek, F.; Herges, R. *Science* **2011**, *331*, 445−448. (b) Dommaschk, M.; Schütt, C.; Venkataramani, S.; Jana, U.; Näther, C.; Sönnichsen, F. D.; Herges, R. *Dalton Trans.* **2014**, *43*, 17395−17405. (c) Dommaschk, M.; Peters, M.; Gutzeit, F.; Schütt, C.; Näther, C.; Sönnichsen, F. D.; Tiwari, S.; Riedel, C.; Boretius, S.; Herges, R. *J. Am. Chem. Soc.* **2015**, *137*, 7552−7555.

(5) Harper, R. J.; Soloski, E. J.; Tamborski, C. *J. Org. Chem.* **1964**, *29*, 2385−2389.

(6) Kottke, T.; Sung, K.; Lagow, R. J. *Angew. Chem.* **1995**, *107*, 1612−1614.

(7) (a) Krebs, F. C.; Jensen, T. *J. Fluorine Chem.* **2003**, *120*, 77−84. (b) Leroy, J.; Schöllhorn, B.; Syssa-Magalé, J.-L.; Boubekeur, K.; Palvadeau, P. *J. Fluorine Chem.* **2004**, *125*, 1379−1382.

(8) Belf, L.; Buxton, M.; Tilney-Bassett, J. *Tetrahedron* **1967**, *23*, 4719−4727.

(9) Vedejs, E.; Erdman, D. E.; Powell, D. R. *J. Org. Chem.* **1993**, *58*, 2840−2845.

(10) (a) Richardson, R. D.; Zayed, J. M.; Altermann, S.; Smith, D.; Wirth, T. *Angew. Chem., Int. Ed.* **2007**, *46*, 6529−6532. (b) Sarwar, M. G.; Dragisic, B.; Dimitrijevic, E.; Taylor, M. S. *Chem. - Eur. J.* **2013**, *19*, 2050−2058.

(11) (a) Lindsey, J. S.; Schreiman, I. C.; Hsu, H. C.; Kearney, P. C.; Marguerettaz, A. M. *J. Org. Chem.* **1987**, *52*, 827−836. (b) Lindsey, J. S.; Wagner, R. W. *J. Org. Chem.* **1989**, *54*, 828−836.

(12) Rohand, T.; Dolusic, E.; Ngo, T. H.; Maes, W.; Dehaen, W. *ARKIVOC* **2007**, 307−324.

(13) Miyaura, N.; Suzuki, A. *J. Chem. Soc., Chem. Commun.* **1979**, 866−867.

(14) Ishiyama, T.; Murata, M.; Miyaura, N. *J. Org. Chem.* **1995**, *60*, 7508−7510.

(15) (a) Kumar, D.; Tahsini, L.; Visser, S. P. d.; Kang, H. Y.; Kim, S. J.; Nam, W. *J. Phys. Chem. A* **2009**, *113*, 11713−11722. (b) Rebelo, S. L.; Pereira, M. M.; Monsanto, P. V.; Burrows, H. D. *J. Mol. Catal. A: Chem.* **2009**, *297*, 35−43. (c) Sainna, M. A.; Kumar, S.; Kumar, D.; Fornarini, S.; Crestoni, M. E.; de Visser, S. P. *Chem. Sci.* **2015**, *6*, 1516−1529.

(16) (a) Cunningham, I. D.; Basaleh, A.; Gazzaz, H. A. *Dalton Trans.* **2012**, *41*, 9158−9160. (b) Baran, J. D.; Grönbeck, H.; Hellman, A. *J. Am. Chem. Soc.* **2014**, *136*, 1320−1326. (c) Castro, K. A. D. F.; Simoes, M. M. Q.; Neves, M. G. P. M. S.; Cavaleiro, J. A. S.; Wypych, F.; Nakagaki, S. *Catal. Sci. Technol.* **2014**, *4*, 129−141.

(17) (a) Samaroo, D.; Vinodu, M.; Chen, X.; Drain, C. M. *J. Comb. Chem.* **2007**, *9*, 998−1011. (b) Králová, J.; Bríza, T.; Moserová, I.; Dolenský, B.; Vašek, P.; Poucková, P.; Kejík, Z.; Kaplánek, R.; Martásek, P.; Dvorák, M.; Král, V. *J. Med. Chem.* **2008**, *51*, 5964−5973.

(18) (a) Gobeze, H. B.; Das, S. K.; D'Souza, F. *J. Phys. Chem. C* **2014**, *118*, 16660−16671. (b) Das, S. K.; Song, B.; Mahler, A.; Nesterov, V. N.; Wilson, A. K.; Ito, O.; D'Souza, F. *J. Phys. Chem. C* **2014**, *118*, 3994−4006.

DOI: 10.1021/acs.joc.5b01524
J. Org. Chem. 2015, 80, 8496−8500

Synthesis of functionalized perfluorinated porphyrins for improved spin switching (LD-CISSS).

Marcel Dommaschk, C. Näther, Rainer Herges*

Table of Contents

I Analytical methods

IR spectroscopy

Infrared spectra were measured on a FT-IR spectrometer with an ATR unit. Signals were abbreviated with w, m, s and vs for weak, medium, strong and very strong intensities.

UV-vis spectroscopy

The UV-vis spectra were measured on a two-beam spectrometer with a thermostat (T = 20 °C). Quartz cuvettes of 1 cm optical path length were used.

Chromatography stationary phases

For column chromatography purifications silica gel (particle size 0.040-0.063 mm) was used. R_f values were determined by thin layer chromatography on Polygram® Sil G/UV_{254} (0.2 mm particle size).

NMR spectroscopy

NMR spectra were measured in deuterated solvents. The degree of deuteration is given in parentheses. ^{1}H NMR-spectra in reference to the following signals.

acetone-d_6 (99.8 %): δ = 2.05 ppm (quint)
chloroform-d (99.8 %): δ = 7.26 ppm (s)

All assignments of ^{1}H and ^{13}C nuclei were confirmed by the 2D methods HSQC and HMBC. The signal multiplicities are abbreviated as follows.
s: singlet, d: doublet, t: triplet, q: quartet, quint: quint, m: multiplet, br: broad signal
Reference for all ^{19}F-NMR spectra is trichlorofluoromethane to the frequency of which the spectrometer is calibrated. Fluorine atoms are labeled as *o*-F, *m*-F und *p*-F (*ortho*-, *meta*- und *para*-fluorine) according to their position in the aromatic system.

For the asymmetric porphyrins there are three different *meso*-positions labelled as A, B and C (Figure S2). Due to the fact that the *meso*-phenyl rings do not rotate on the NMR time scale there are two different sides labelled as σ (same side as the azo pyridine) and σ' (opposite side as the azo pyridine). E.g. the fluorine marked in figure S2 is abbreviated *F-m*'-C.

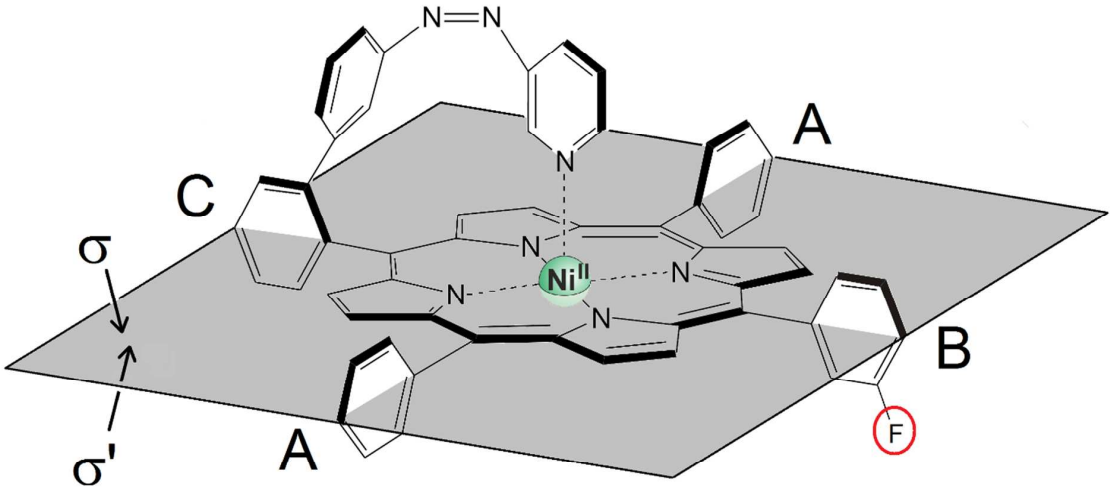

Figure S1. General structure of asymmetric porphyrins to explain the signals of ^{19}F NMR spectra. The fluorine atoms at the *meso*-positions A, B and C are now drawn for the sake of more clarity, except for the *F-m*'-B as an example for the nomenclature.

Spectra of 2-(2,3,4,5-tetrafluorophenyl)-1,3-dioxolane (7)

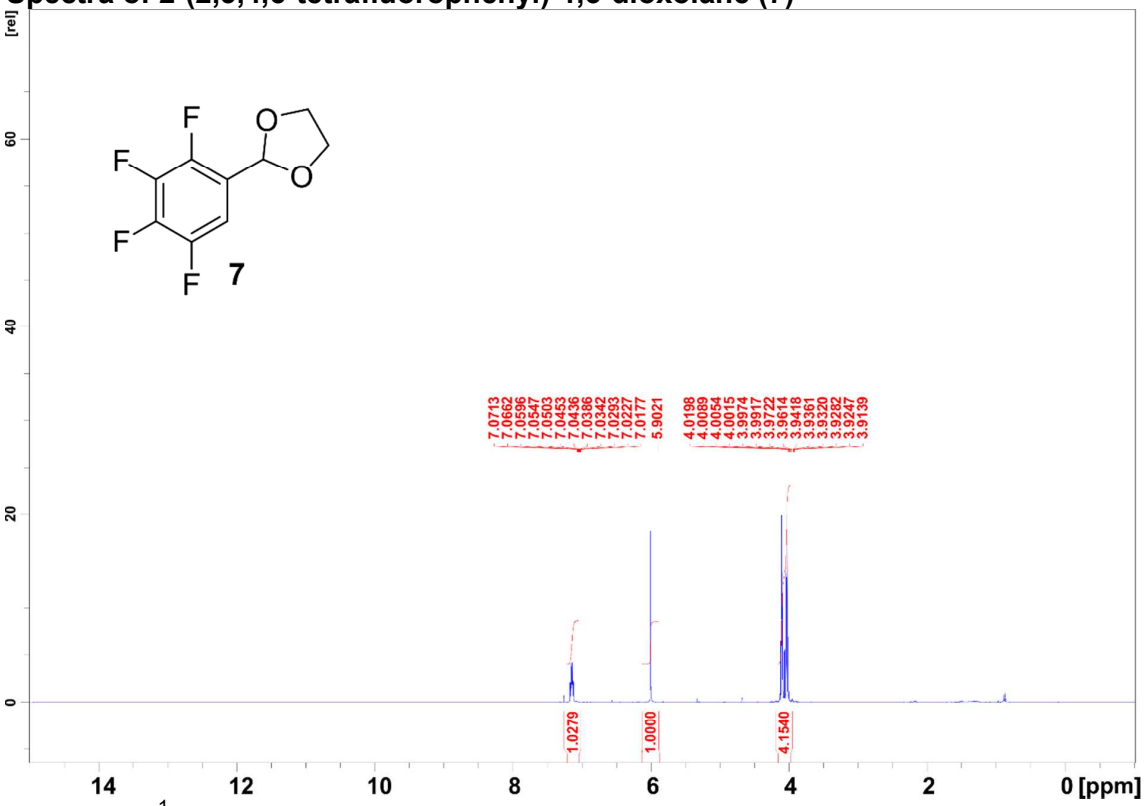

Figure S2. ^{1}H NMR (500 MHz, $CDCl_3$) spectrum of **7**.

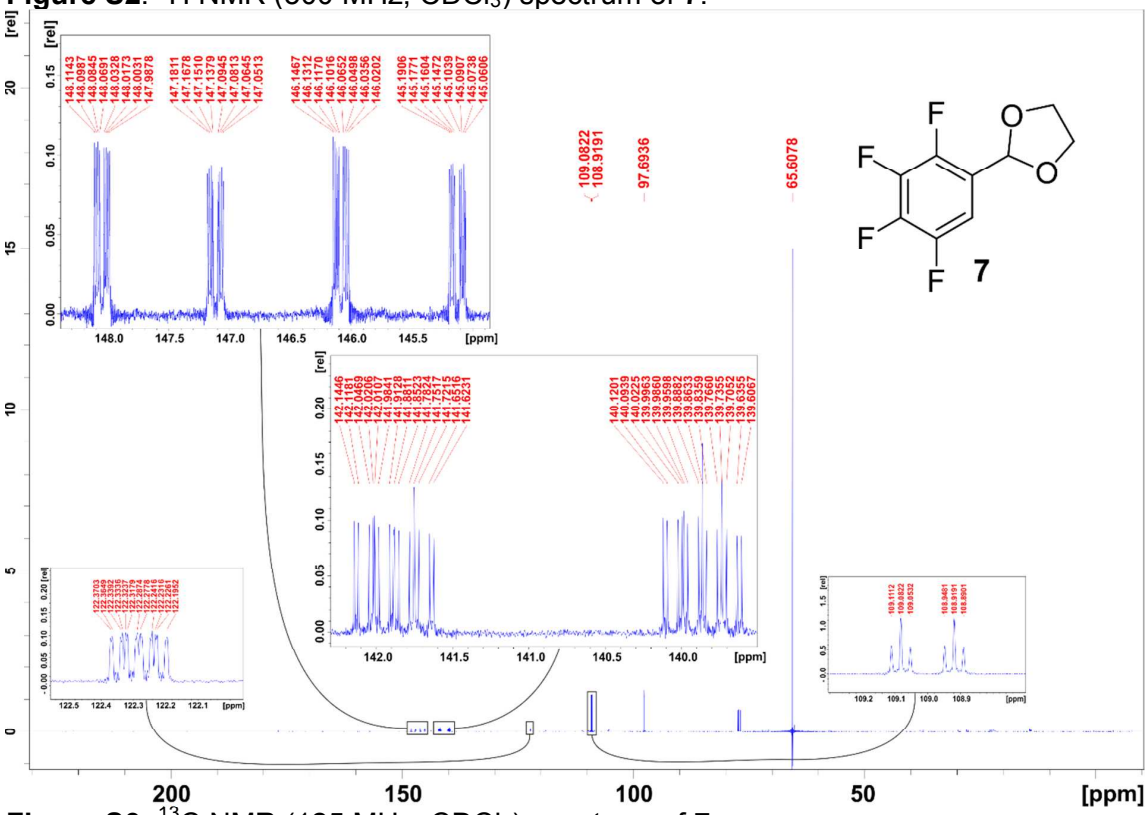

Figure S3. ^{13}C NMR (125 MHz, $CDCl_3$) spectrum of **7**.

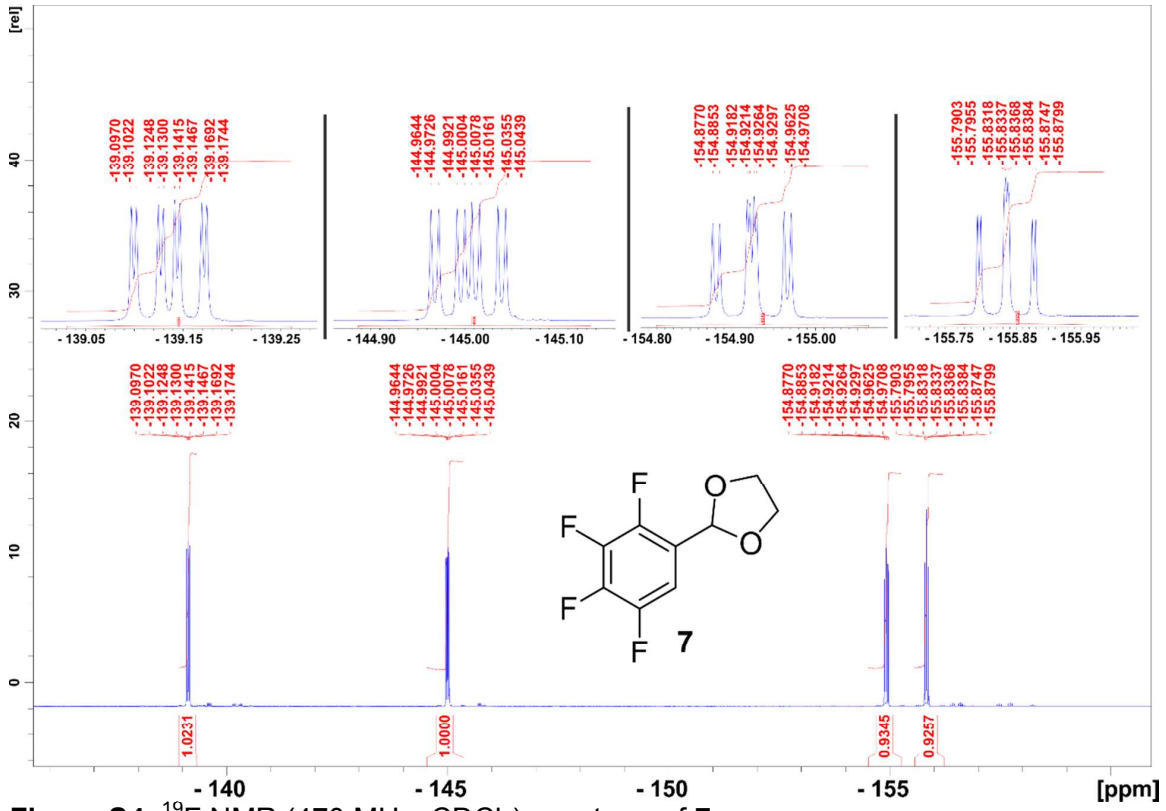

Figure S4. ^{19}F NMR (470 MHz, $CDCl_3$) spectrum of **7**.

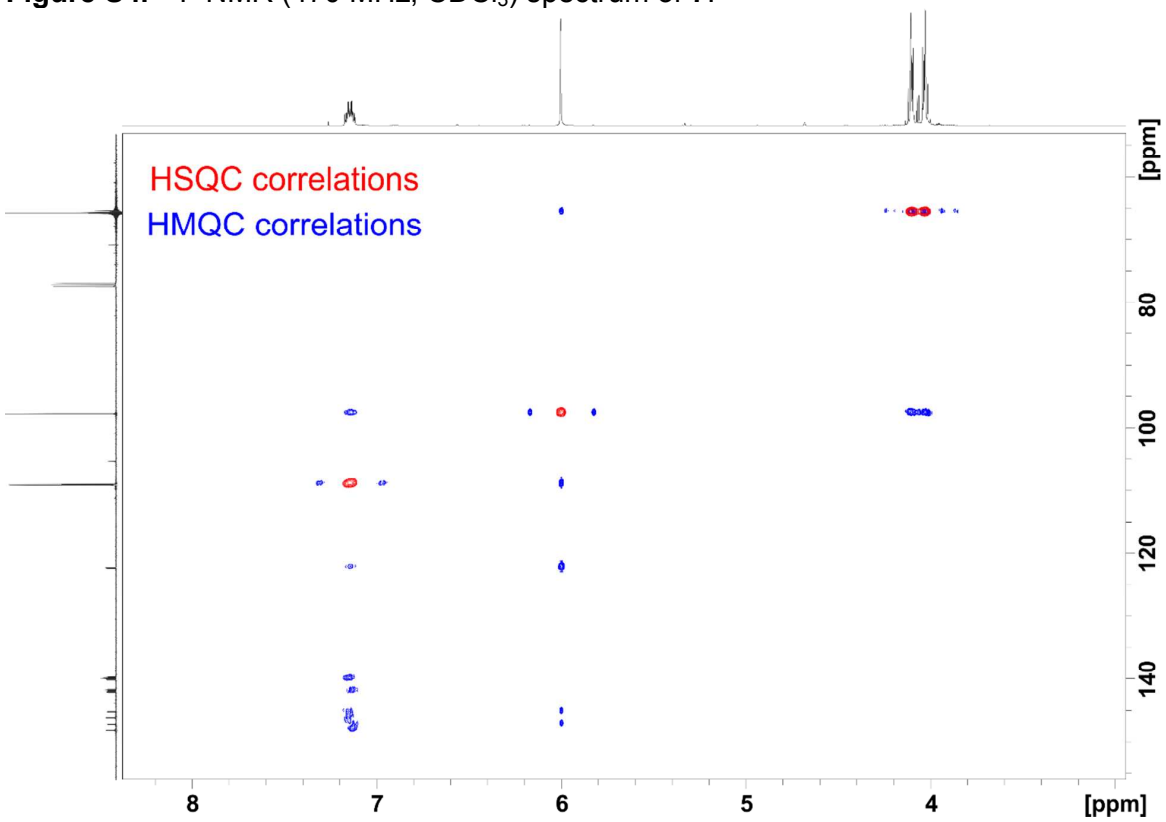

Figure S5. 2D spectra (HSQC: red, HMQC: blue) of **7**.

Spectra of 2-(2-iodo-3,4,5,6-tetrafluorophenyl)-1,3-dioxolane (9)

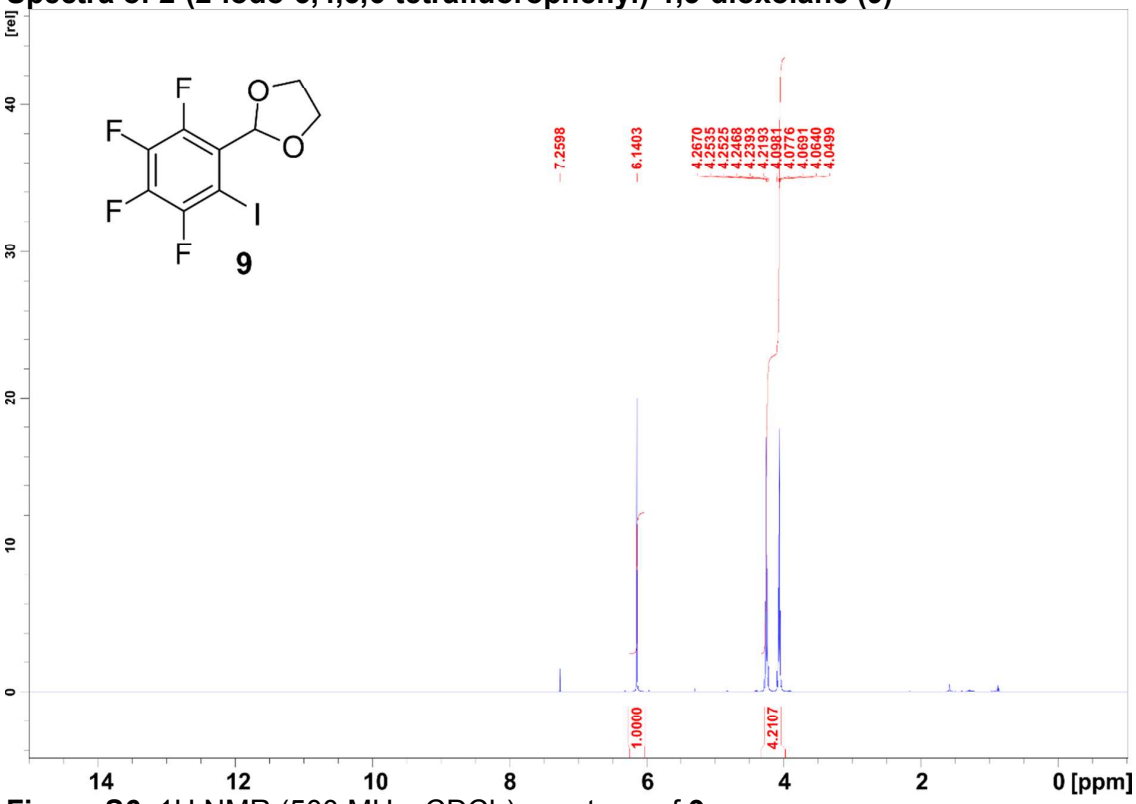

Figure S6. 1H NMR (500 MHz, $CDCl_3$) spectrum of **9**.

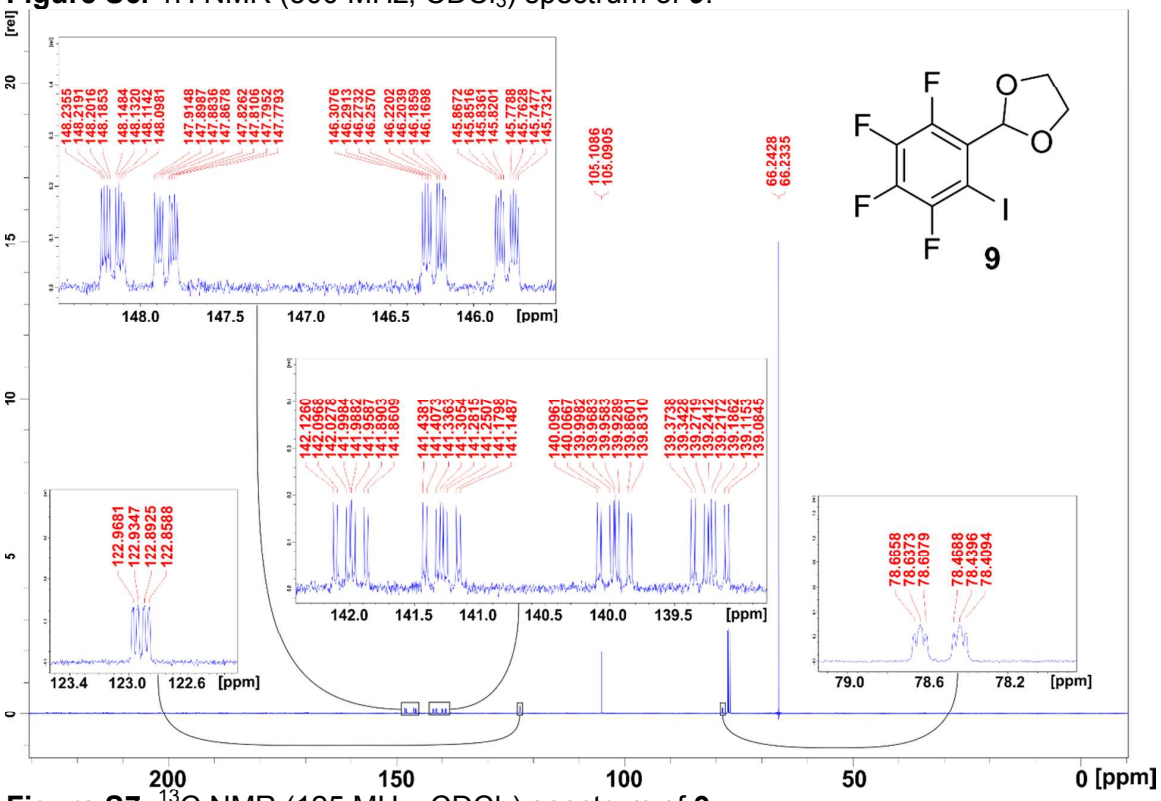

Figure S7. ^{13}C NMR (125 MHz, $CDCl_3$) spectrum of **9**.

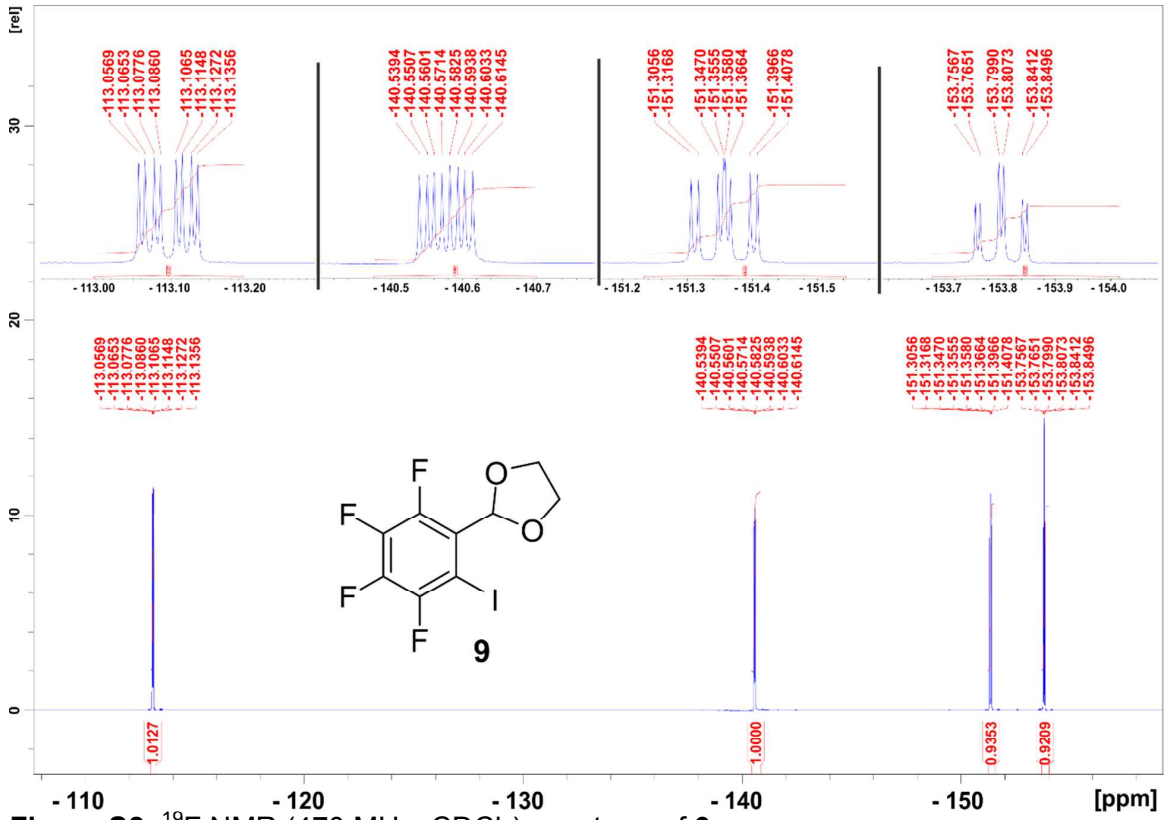

Figure S8. ^{19}F NMR (470 MHz, $CDCl_3$) spectrum of **9**.

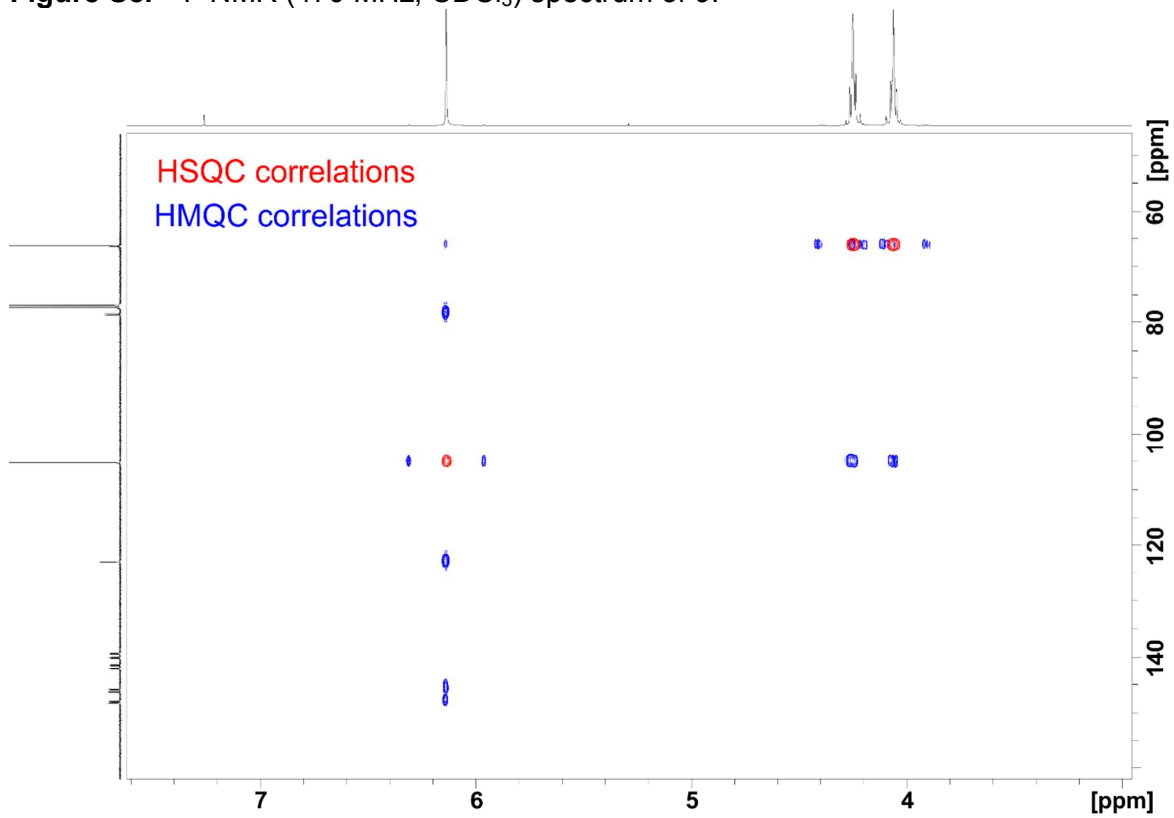

Figure S9. 2D spectra (HSQC: red, HMQC: blue) of **9**.

Spectra of 2-iodo-3,4,5,6-tetrafluorophenylbenzaldehyde (10)

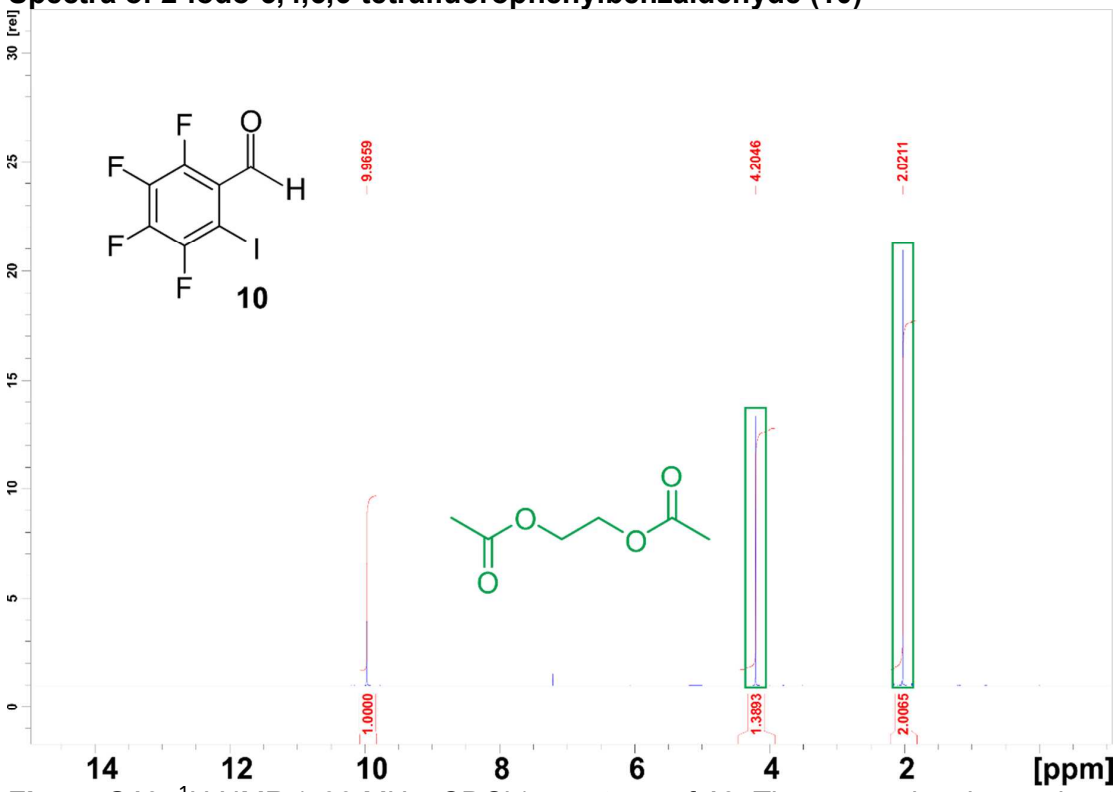

Figure S10. ^{1}H NMR (500 MHz, $CDCl_3$) spectrum of **10**. The green signals are due to residues of acetylated ethylene glycol from the acidic deprotection.

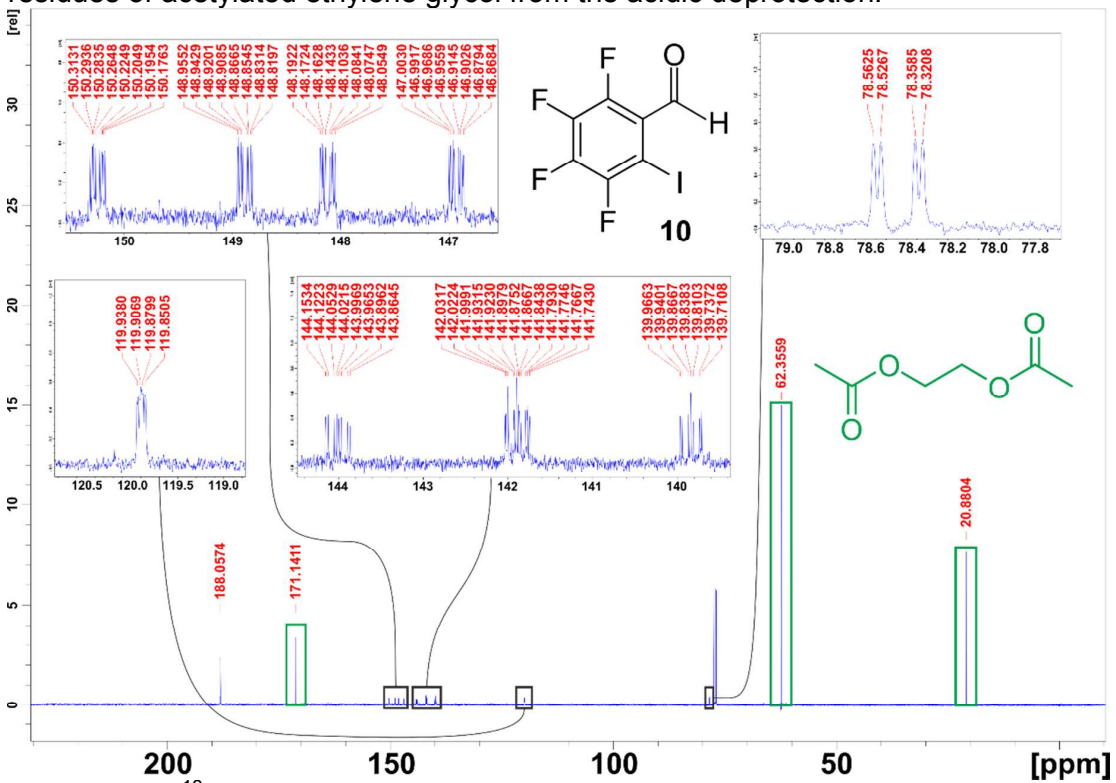

Figure S11. ^{13}C NMR (125 MHz, $CDCl_3$) spectrum of **10**. The green signals are due to residues of acetylated ethylene glycol from the acidic deprotection.

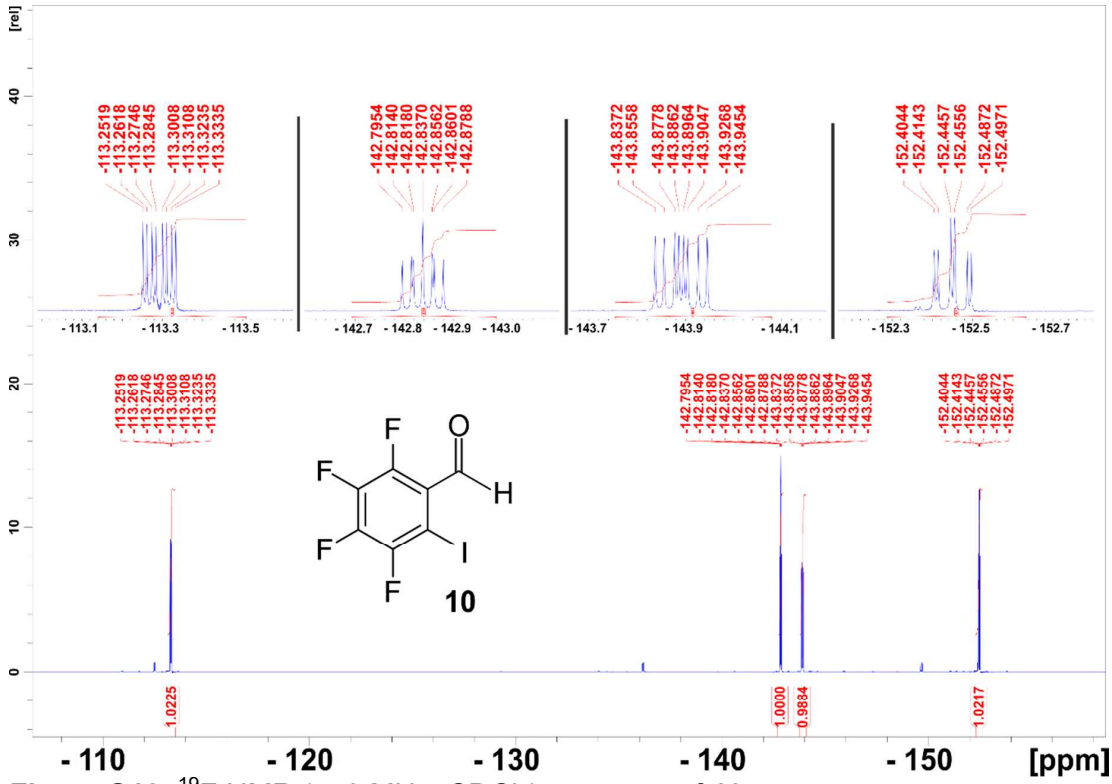

Figure S12. ^{19}F NMR (470 MHz, $CDCl_3$) spectrum of **10**.

Spectra of 3-(3-(pinacol boronic ester)phenylazo)pyridine (19)

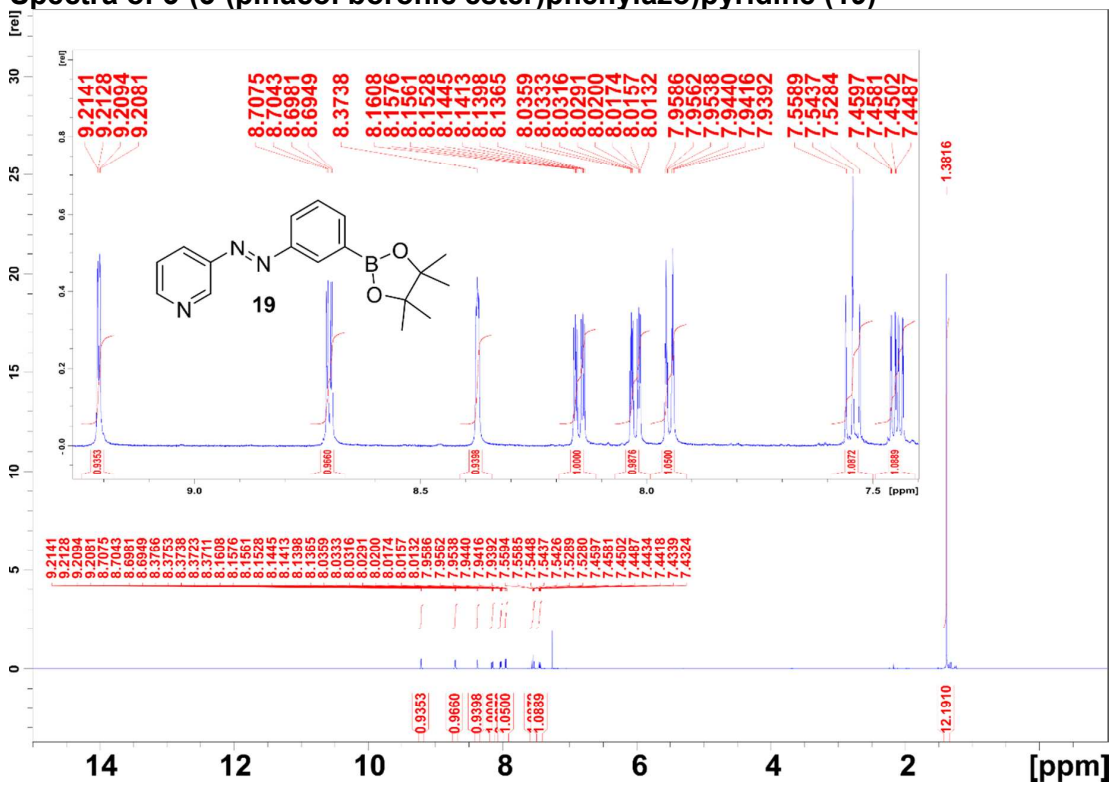

Figure S13. ^{1}H NMR (500 MHz, $CDCl_3$) spectrum of **19**.

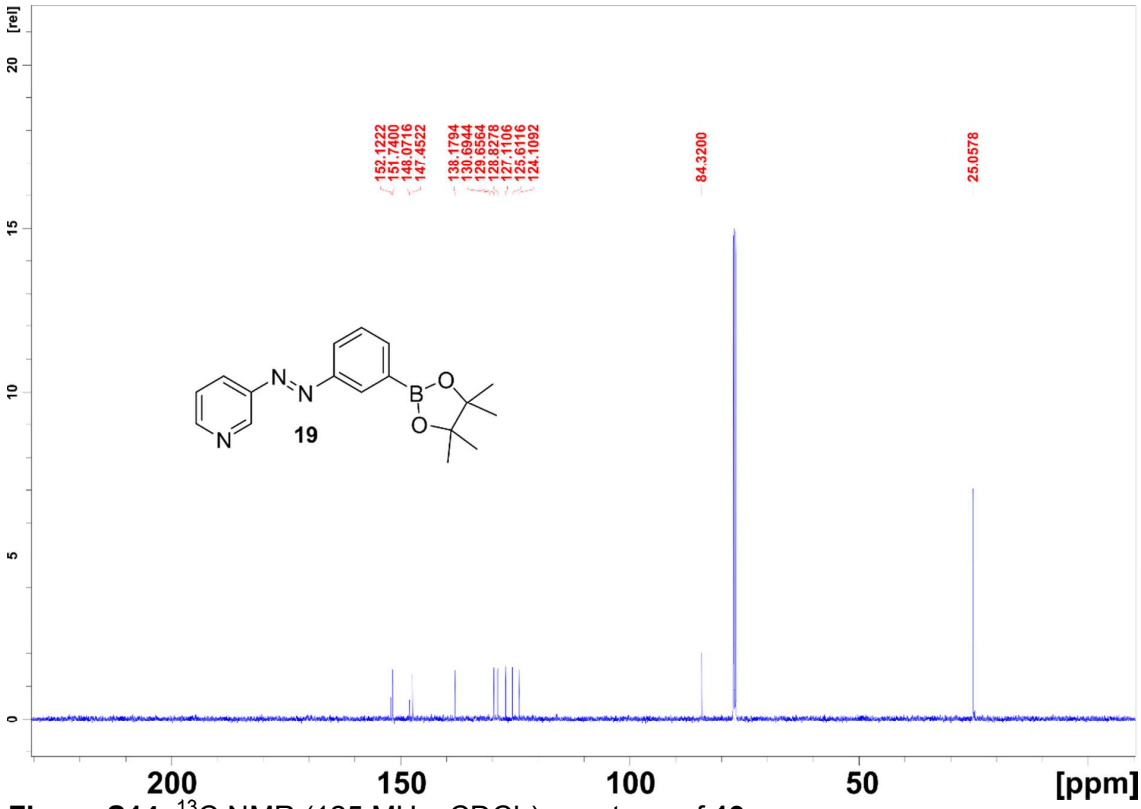

Figure S14. ^{13}C NMR (125 MHz, $CDCl_3$) spectrum of **19**.

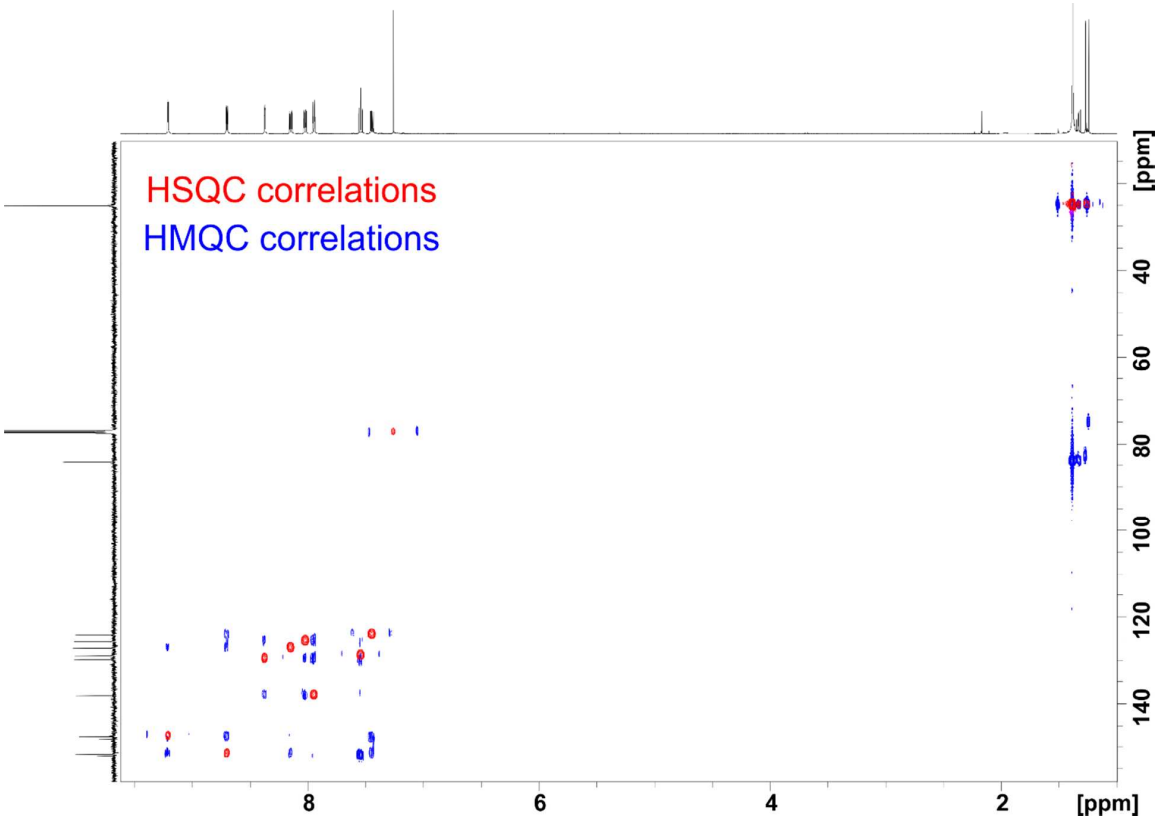

Figure S15. 2D spectra (HSQC: red, HMQC: blue) of **19**.

Spectra of metal free RP 20

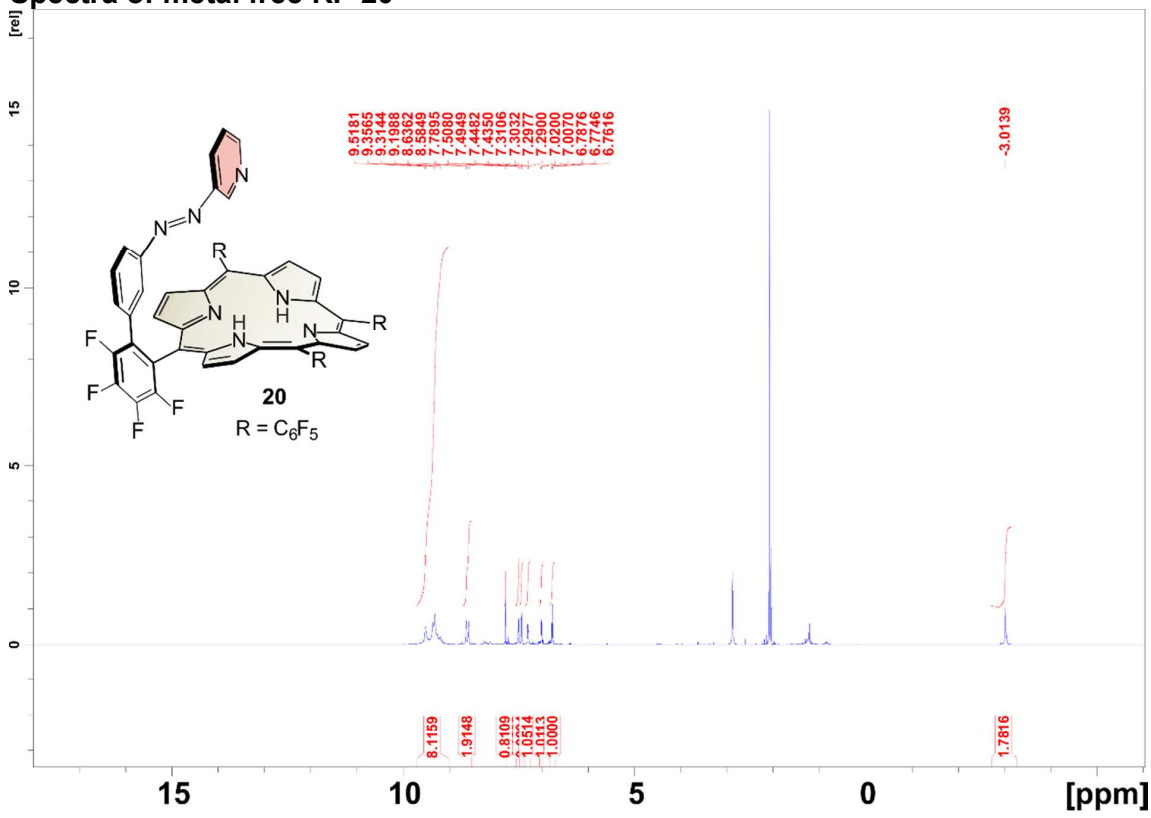

Figure S16. ^{1}H NMR (500 MHz, acetone-d_6) spectrum of **20** with ~10 % *cis* isomer.

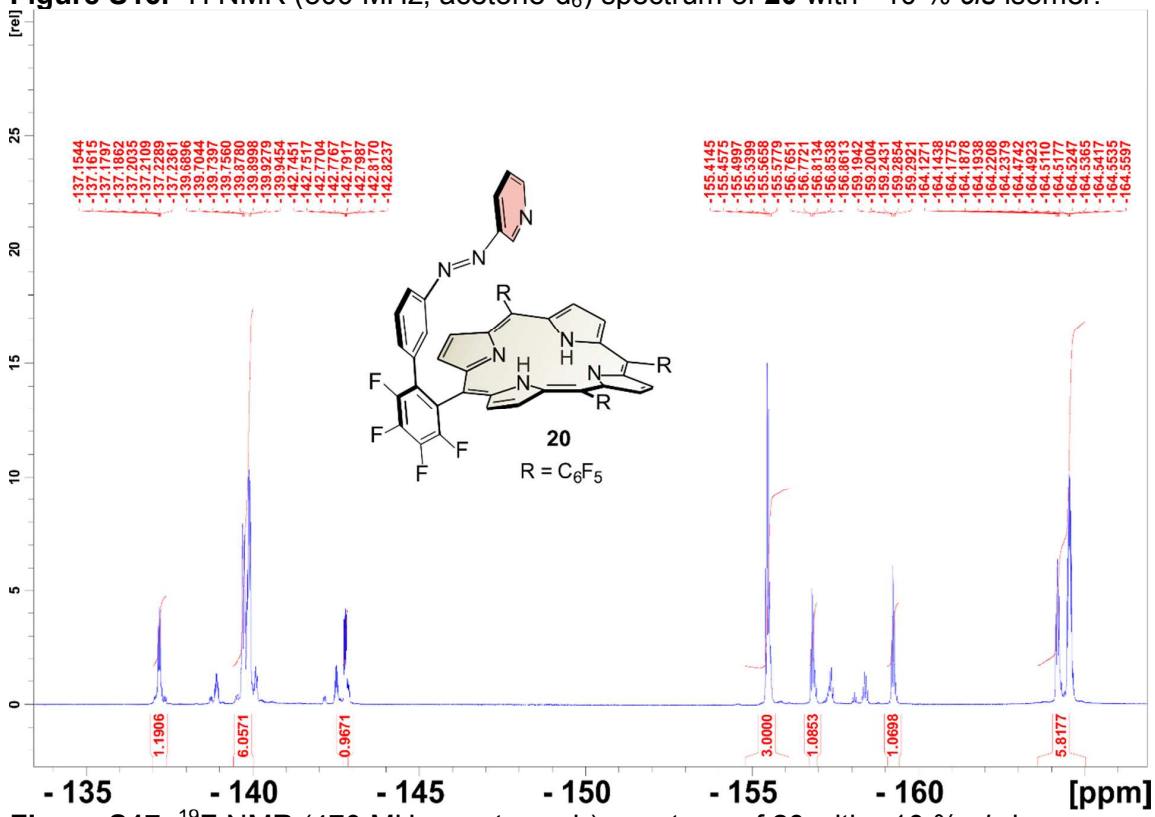

Figure S17. ^{19}F NMR (470 MHz, acetone-d_6) spectrum of **20** with ~10 % *cis* isomer.

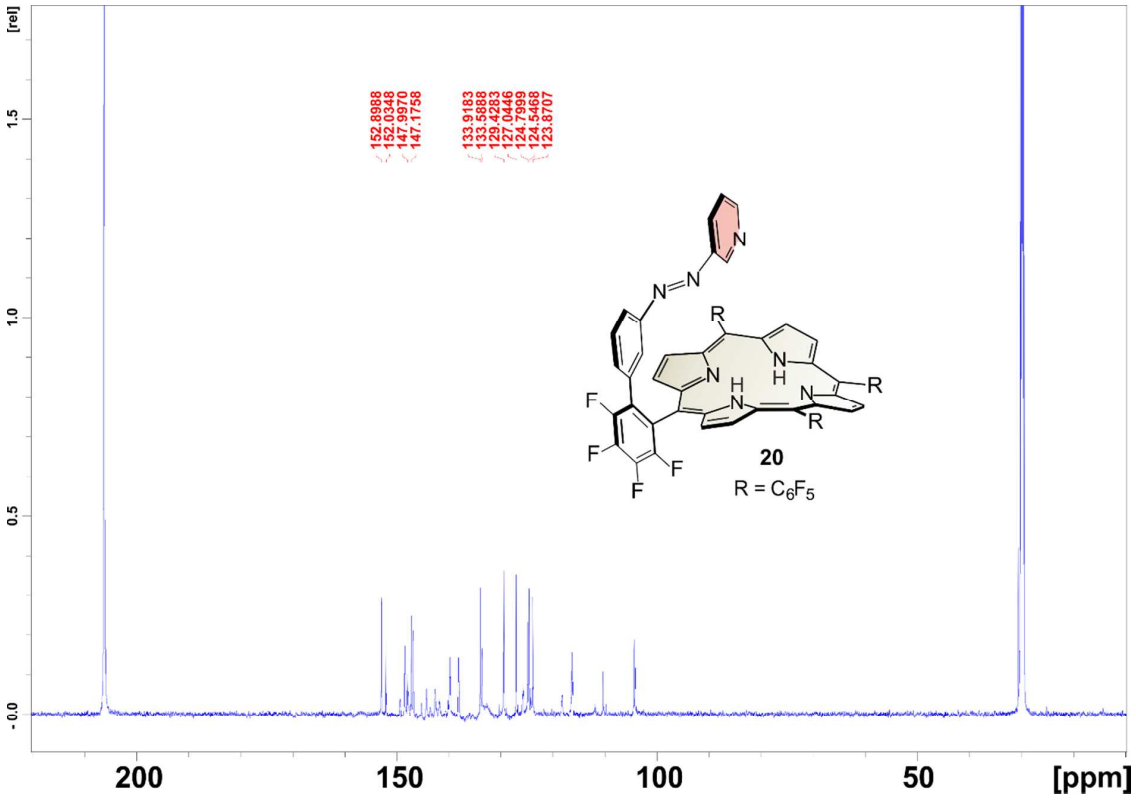

Figure S18. ^{13}C NMR (125 MHz, acetone-d_6) spectrum of **20** with ~10 % *cis* isomer. The C atoms of the porphyrin cannot be assigned due to the strong signal broadened caused by the molecular dynamic of the porphyrin. The 19 different C atoms at the aryl *meso* positions cannot be assigned due to high signal splitting (to ^{1}J, ^{2}J, ^{3}J and ^{4}J couling to the ^{19}F atoms) and the resulting low intensity and signal overlapping.

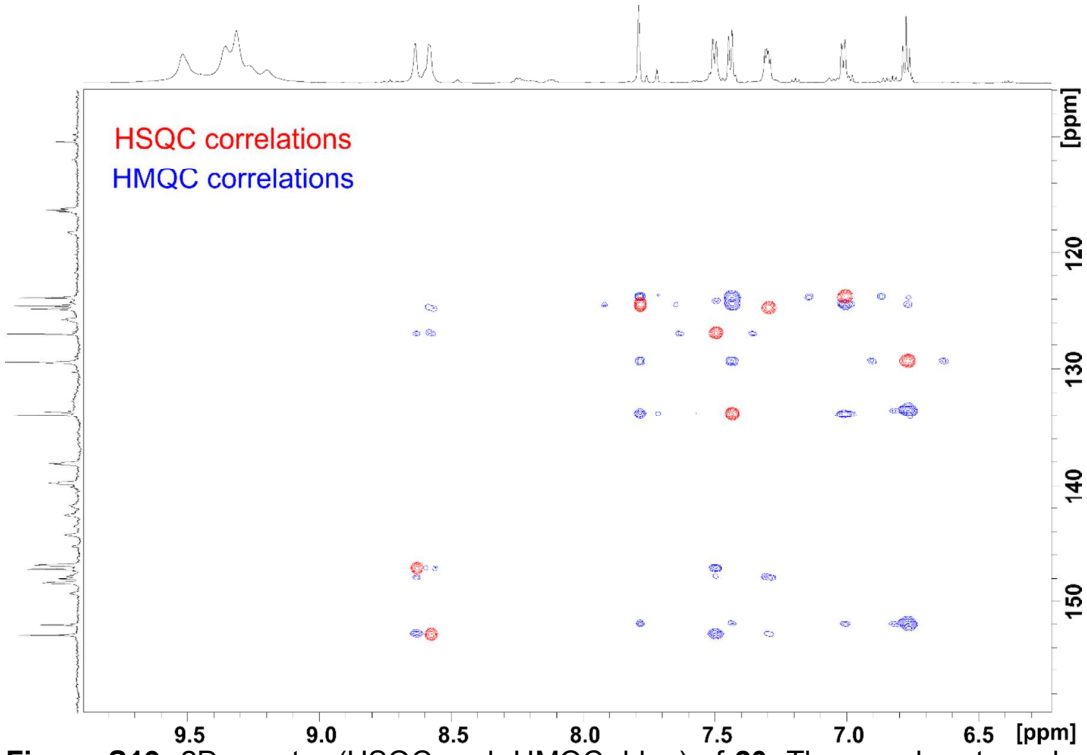

Figure S19. 2D spectra (HSQC: red, HMQC: blue) of **20**. The pyrrol protons do not show any correlation due to the signal broadening caused by the molecular dynamic.

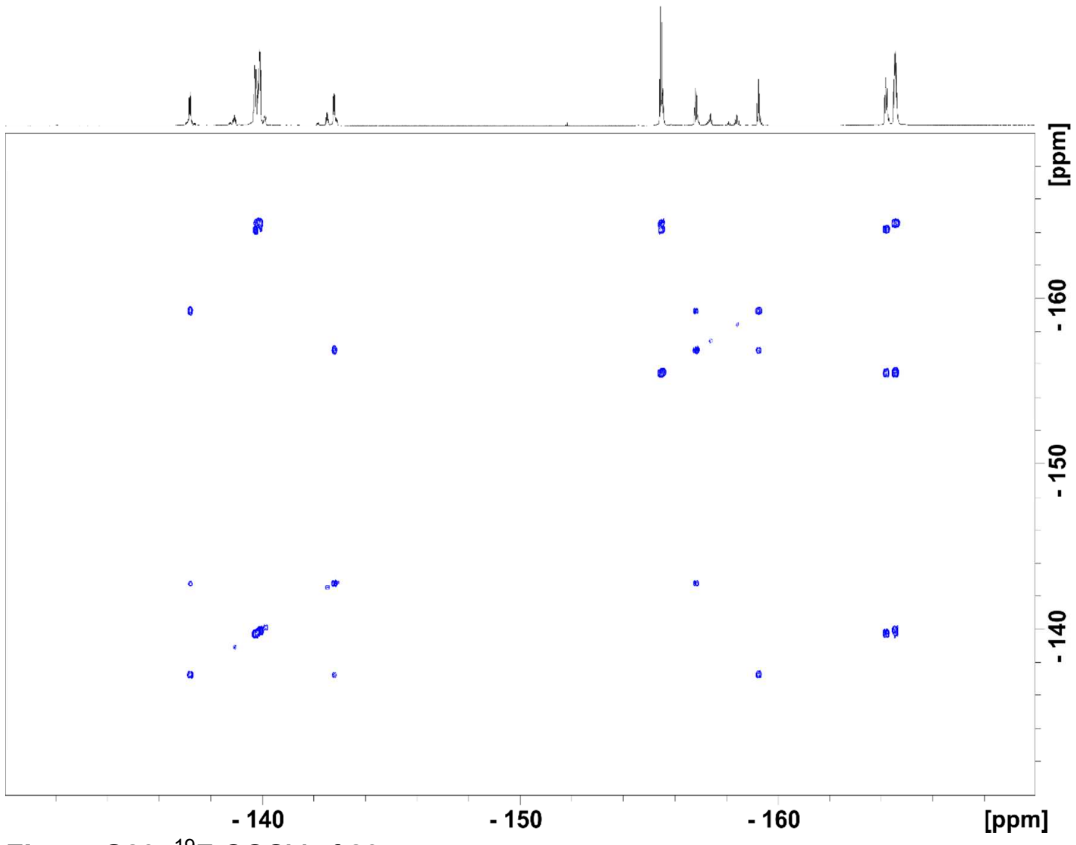

Figure S20. ^{19}F COSY of **20**.

Spectra of RP 21

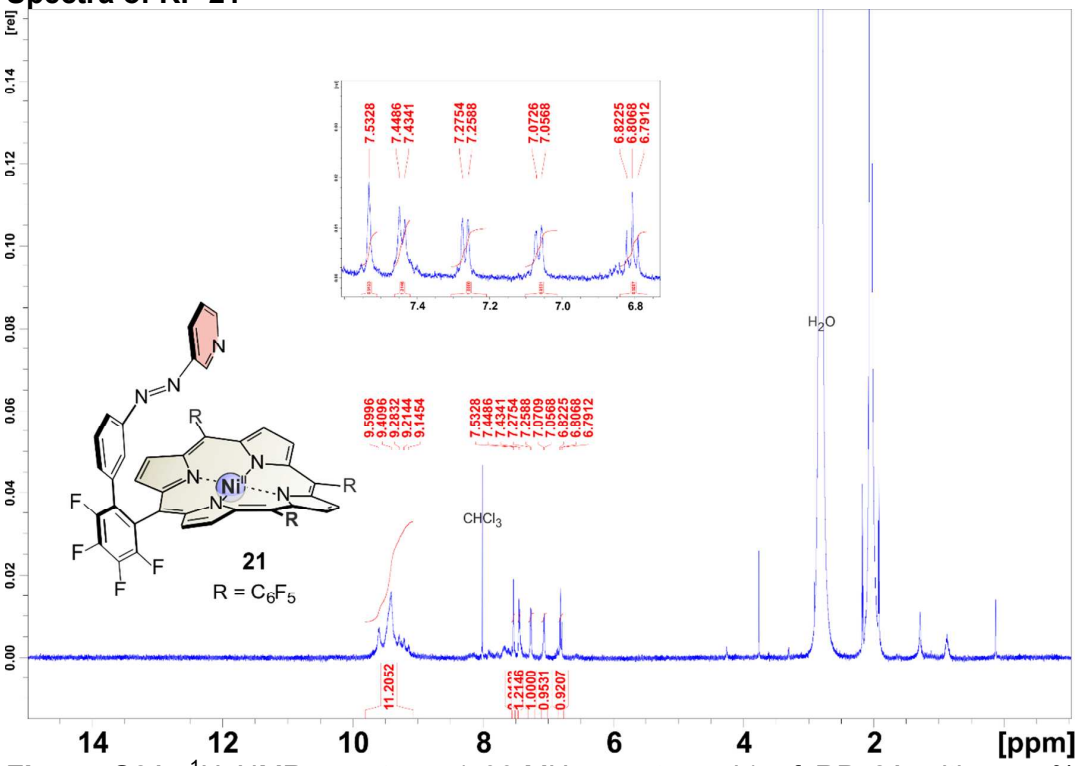

Figure S21. ^{1}H NMR spectrum (500 MHz, acetone-d_6) of RP **21** with < 5 % cis isomer. The low concentration is necessary to reduce paramagnetism due to intermolecular coordination. Even so the *ortho* and *meta* pyridine protons are shifted to > 9 ppm.

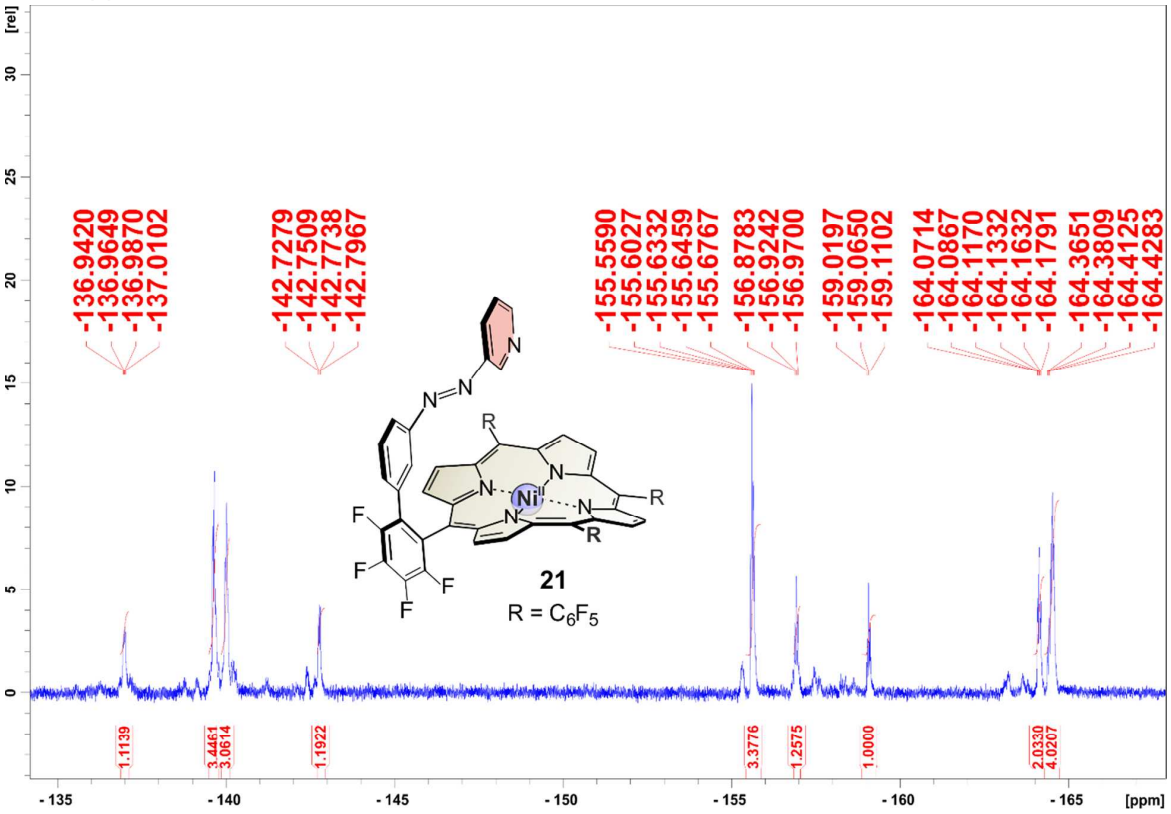

Figure S22. ^{19}F NMR spectrum (470 MHz, acetone-d_6) of RP **21** with < 5 % cis isomer.

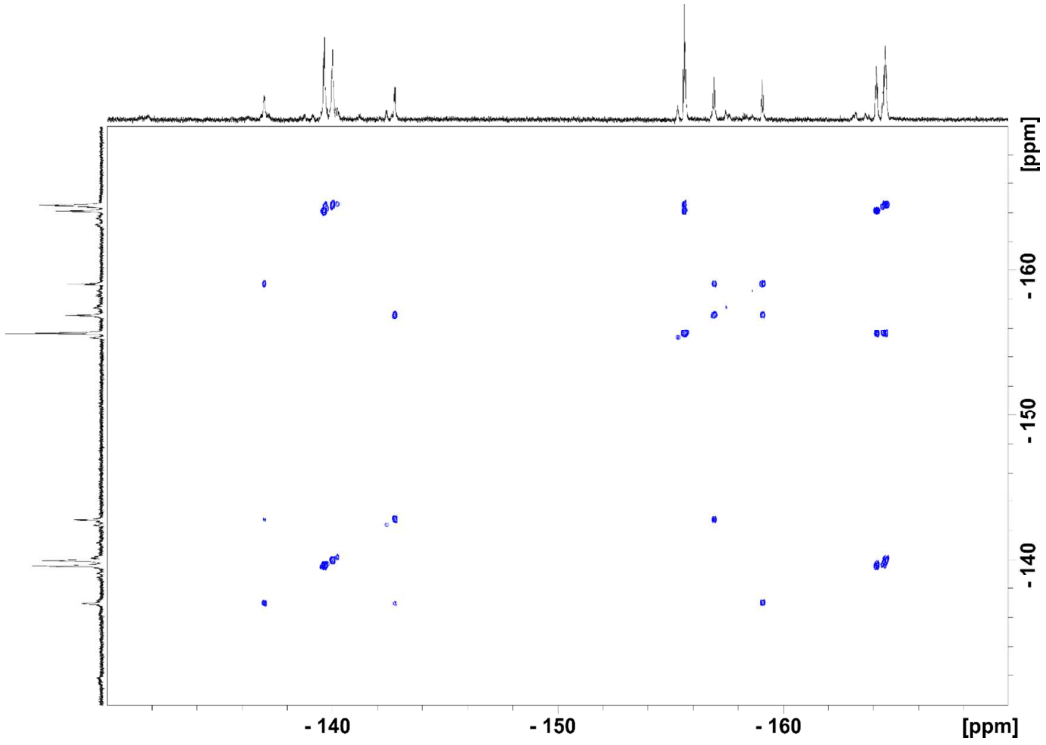

Figure S23. ^{19}F COSY of **21**.

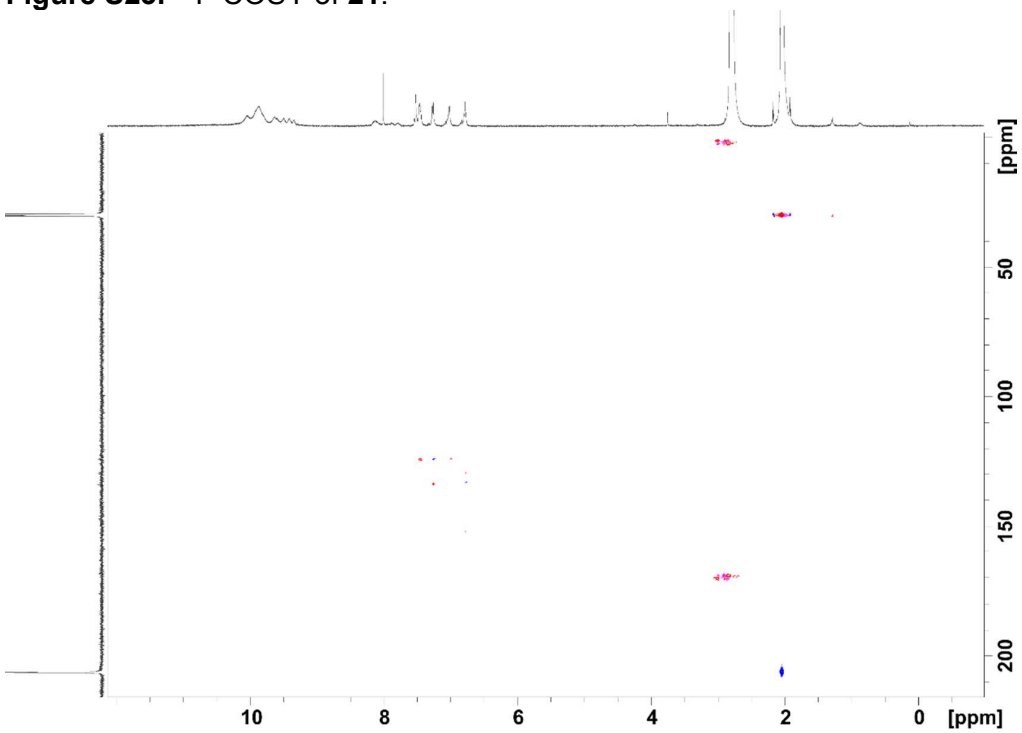

Figure S24. 2D spectra (HSQC: red, HMQC: blue) of **21**. Only very few correlations are observed because of the low concentration of the porphyrin and slight amount of paramagnetic species due to intermolecular coordination. Higher concentrations

gives rise to more intermolecular coordination and more paramagnetism which is not beneficial for the signal intensities.

II UV-vis spectroscopy

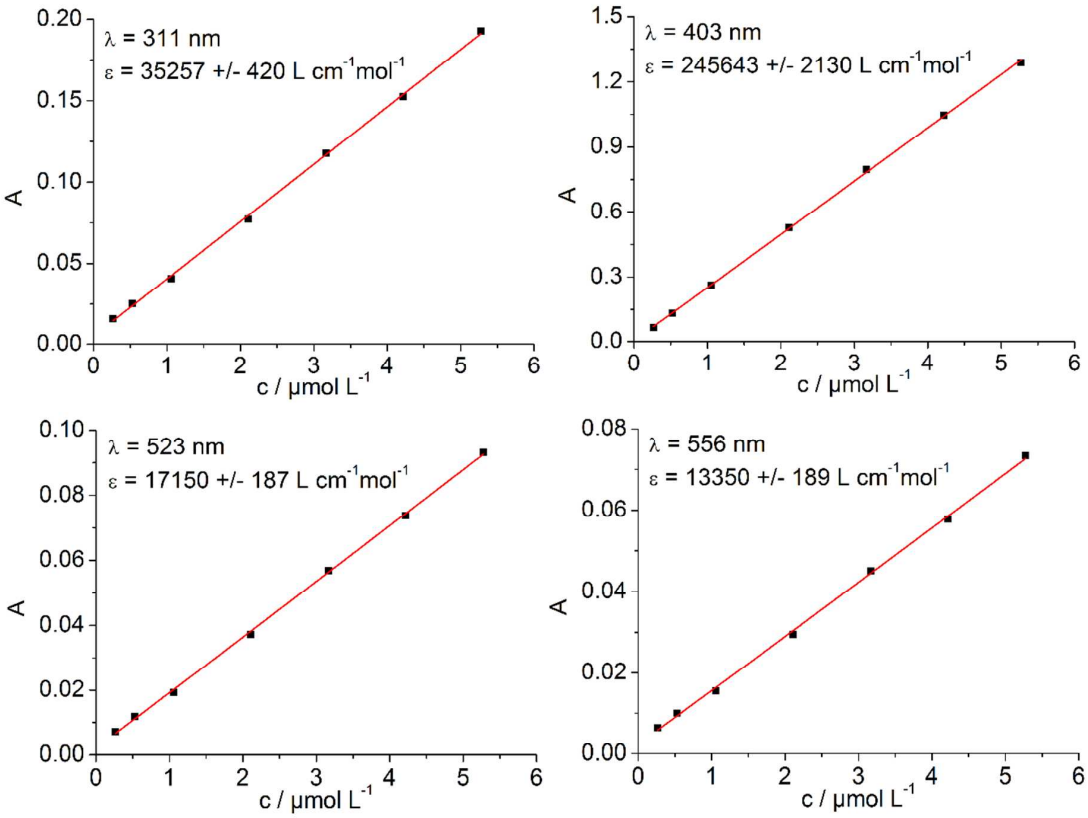

Figure S25. Plots for the extinction coefficients of the absorption maxima (λ = 311, 403, 523 and 556 nm) of RP **21**.

Ni-TPPF$_{20}$ (**1**) and 3-phenylazopyridine (**2**) were obtained as presented previously.[1-3] Their extinction coefficients were measured in acetonitrile (Figure S18 and Figure S19) for a quantitative comparison with RP **21**.

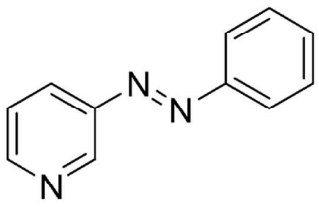

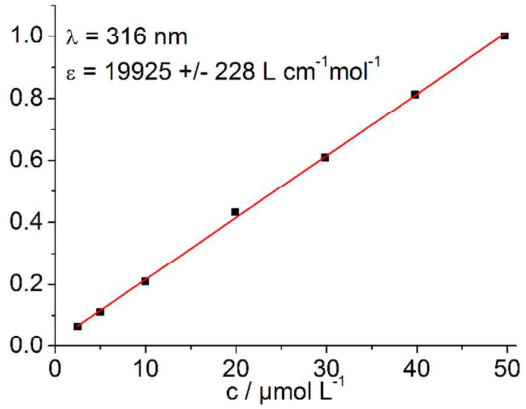

Figure S26. Plots for the extinction coefficient of the absorption maxima (λ = 316 nm) 3-phenylazopyridine (**2**).

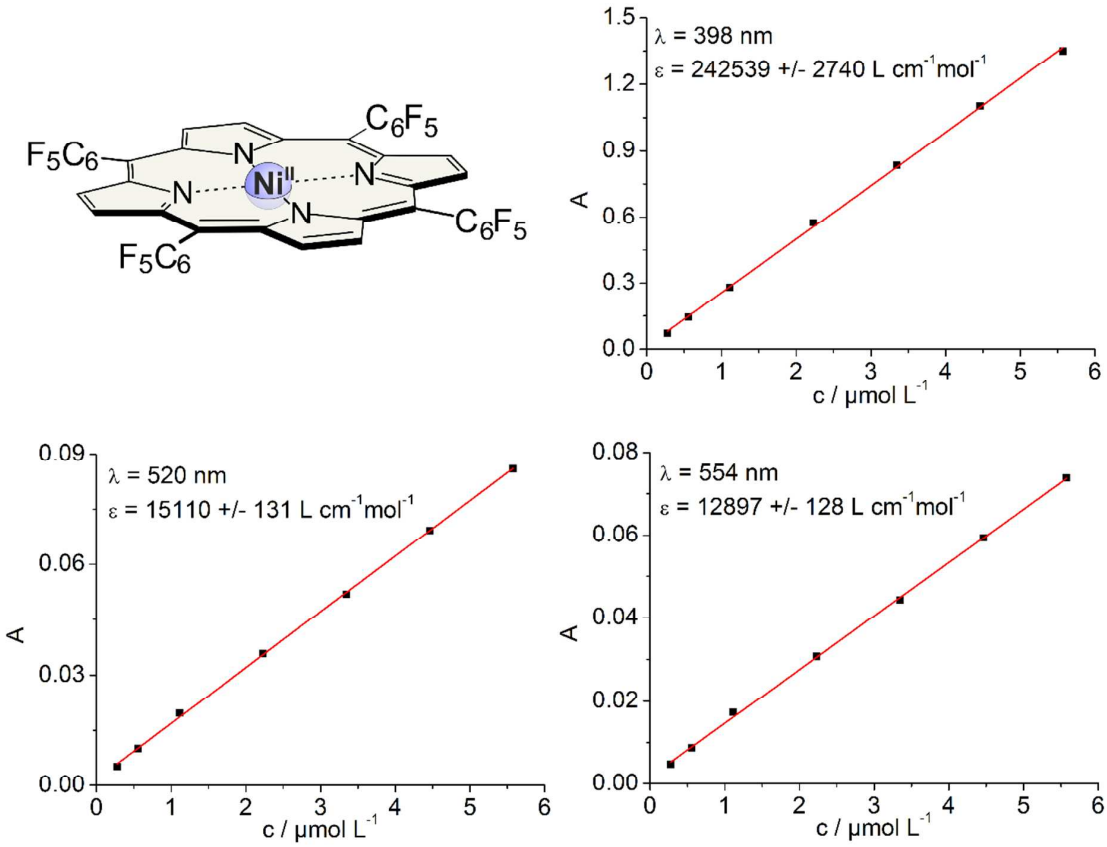

Figure S27. Plots for the extinction coefficients of the absorption maxima (λ = 398, 520 and 554 nm) of Ni-TPPF$_{20}$ (**1**).

Photochrosim of the RP 21

An interesting aspect of the RP molecules is the unusual photochromism. Irradiation into the Q band of the porphyrin induces the isomerization of the azo group from *trans* to the *cis*-configuration, a process which is unprecedented in the literature. The corresponding mechanism is not yet fully understood.[4] To investigate if there is any electronic coupling between the aromatic system of the porphyrin and the phenylazopyridine, the UV-vis sprectrum of the RP **21** was compared to the UV-vis spectrum of the separated compounds (Ni-TPPF$_{20}$, **1** and 3-phenylazopyridine, **2**). The sum of the UV-vis spectra of the separated units (**1** and **2**) is almost equivalent to the UV-vis spectrum of RP **21**. (the extinction coefficients for **1**, **2** and **21** were measured in acetonitrile, see SI). The bands of the porphyrin (Soret and Q bands)

and the azopyridine ($\pi\pi^*$ band) are clearly separated. No additional absorption bands are arising from the covalent bonding between both moieties (Figure 4). The $\pi\pi^*$ band of the azo group in **21** exhibits a very small hypsochromic shift of 5 nm and the Soret band is shifted 5 nm to longer wavelengths. This suggests that both units are separated chromophores with a very weak configuration interaction between the two π systems.

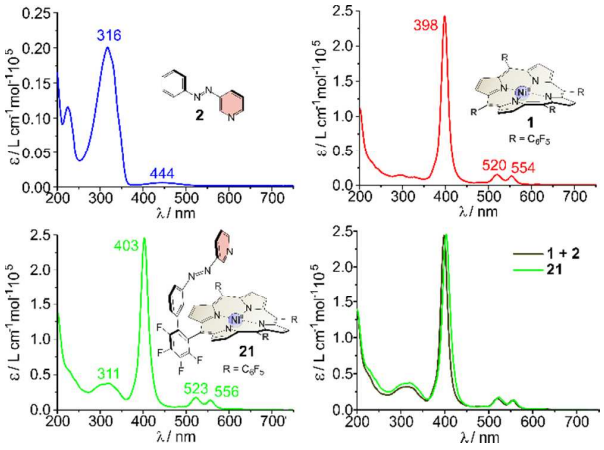

Figure S28. UV-vis spectra of 3-phenylazopyridine (**2**) (top left), Ni-TPPF$_{20}$ (**1**) (top right), perfluorinated RP **21** (bottom left) and an overlay of **21** and the sum of **1** +**2** (bottom right).

III Crystal structure of compound 9

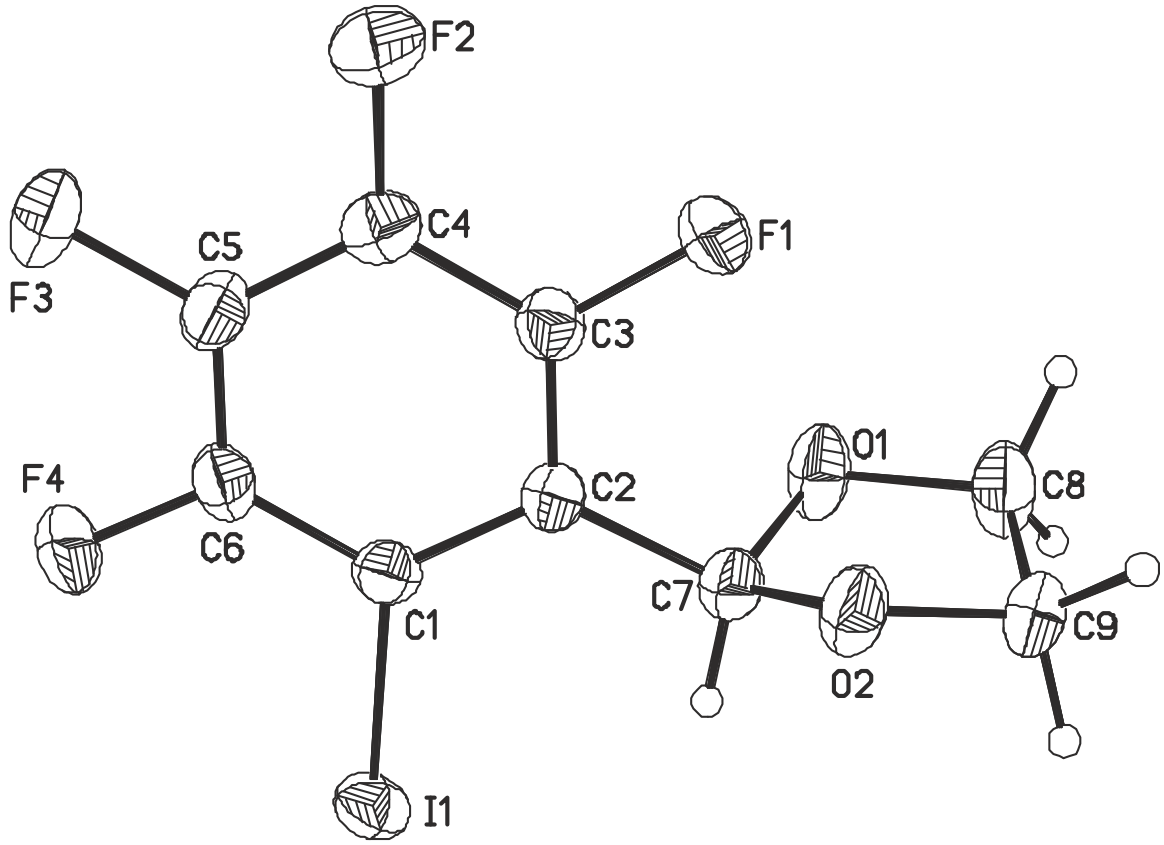

Figure S29. Thermal ellipsoid plot (50% probability) of compound **9**.

2-(2-Iodo-3,4,5,6-tetrafluorophenyl)-1,3-dioxolane (**9**) crystalizes in the monoclinic space $P2_1/n$. We obtained a crystal structure of high quality (R1 = 0.0203, wR2 = 0.0484). All non-hydrogen atoms were refined anisotropic. The C-H H atoms were positioned with idealized geometry and refined isotropic with $U_{iso}(H) = 1.2 \cdot U_{eq}(C)$ (1.5 for methyl H atoms) using a riding model. A numerical absorption correction was performed (Tmin/max: 0.4523/0.6626). The NMR spectra (page 6 and 7) match perfectly with the crystal structure. The ^{13}C NMR spectrum shows signals with interesting but very complicated splitting pattern up to dddd. Hence, very high concentrations are necessary to measure these signals.

(1) Dommaschk, M.; Gutzeit, F.; Boretius, S.; Haag, R.; Herges, R. *Chem. Commun.* **2014**, *50*, 12476–12478.

(2) Thies, S.; Sell, H.; Bornholdt, C.; Schütt, C.; Köhler, F.; Tuczek, F.; Herges, R. *Chem. Eur. J.* **2012**, *18*, 16358–16368.

(3) Lindsey, J. S.; Wagner, R. W. *J. Org. Chem.* **1989**, *54*, 828–836.

(4) Alcover-Fortuny, G.; de Graaf, C.; Caballol, R. *Phys. Chem. Chem. Phys.* **2015**, *17*, 217–225.

6 Water Soluble Ni-Porphyrins

A paramagnetic molecule is only useful for MRI if it is applicable in water. Hence, an approach must be found which enables the water solubilization of the RPs. This is challenging because porphyrins are highly hydrophobic macrocycles. Furthermore, it is known that water coordinates to the electron deficient Ni-porphyrins as axial ligands. This would prevent the function as a photoswitchable contrast agent for two reasons: 1. The aqua ligands block the binding sites for the intramolecular coordination. 2. The aqua complex of the Ni(II)-porphyrin is already paramagnetic. Therefore a Ni-porphyrin must be found which is completely diamagnetic in water but still a good acceptor for nitrogen-based ligands.
The most established water soluble porphyrins bear ionic groups at the aromatic *meso* substituents.[140–142] These groups can have a tremendous influence on the electronic properties of the porphyrin. In case of Ni-porphyrins the *meso* substituents influence the affinity of the Ni(II) to accept axial ligands directly. Therefore, cationic groups give rise to highly electron-deficient Ni-porphyrins which are always paramagnetic in water due to the formation of the diaquo complex.[114,115] In contrast to that, anionic groups give rise to highly electron-rich porphyrins which do not accept any kind of axial ligand.[142] These effects are intrinsic properties of the ionic substituents that can only be avoided by using neutral strongly hydrophilic substituents instead.

6.1 Coordination-Induced Spin State Switch (CISSS) in water

Marcel Dommaschk, Florian Gutzeit, Susann Boretius, Rainer Haag and Rainer Herges

Chem. Commun. **2014**, 12476-12479.
DOI:10.1039/c4cc05525j

Summary

We investigated symmetric porphyrins that are water soluble and non-ionic as model systems for RPs. The perfluorinated porphyrins $TPPF_{20}$ and Ni-$TPPF_{20}$ (**3**) were functionalized with 2nd generation glycerol dendrimers. The introduction of the alkoxy groups to the *para* position of the *meso* pentafluorophenyl substituent is regioselective and almost quantitative. The reaction proceeds according to a nucleophilic aromatic substitution mechanism. The dendrimers have two effects. They provide water solubility by the high number of hydrophilic hydroxy groups. Furthermore, the electron-donating alkoxy substituent is regulating the electronic properties of the Ni-porphyrin. The investigations of Ni-$TPPF_{20}$ (**3**) and the RP **7** in water-containing solvent mixtures have shown that these Ni-porphyrins are too electron-deficient. They tend to form paramagnetic diaquo complexes. The replacement of one fluorine atom at each of the four phenyl groups with one alkoxy groups reduces the electron-deficiency of the Ni-porphyrin. The resulting dendronized Ni-porphyrin **16** exhibits excellent properties. It is highly water soluble and not too electron-deficient which means that water is not coordinating to the Ni(II). But it is electron-deficient enough to accept nitrogen-based axial ligands like piperidine. (Figure 6.1).

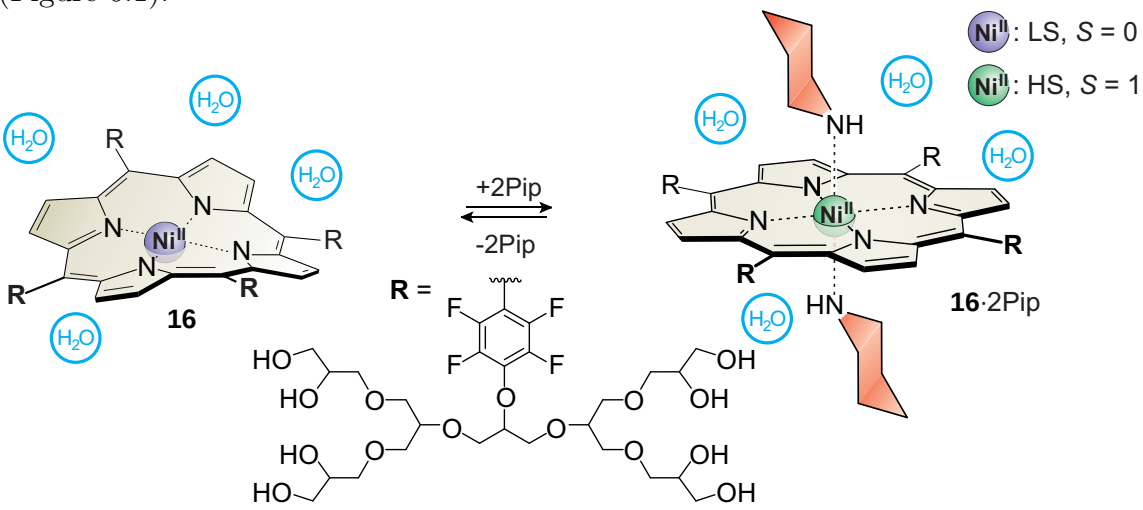

Figure 6.1: The dendronized Ni-porphyrin **16** undergoes a CISSS in water upon addition of piperidine.

The dendronized Ni-porphyrin **16** is the first Ni-complex which keeps a square planar geometry (diamagnetic) in the presence of water and adapts an octahedral geometry (paramagnetic) upon addition of nitrogen-based ligands. This is the proof of principle for a CISSS in water. Hence, a LD-CISSS with a water soluble RP should be possible as well.

ChemComm

COMMUNICATION

View Article Online
View Journal | View Issue

Coordination-Induced Spin-State-Switch (CISSS) in water†

Marcel Dommaschk,[a] Florian Gutzeit,[a] Susann Boretius,[b] Rainer Haag[c] and Rainer Herges*[a]

Cite this: *Chem. Commun.*, 2014, 50, 12476

Received 17th July 2014,
Accepted 27th August 2014

DOI: 10.1039/c4cc05525j

www.rsc.org/chemcomm

We present a non-ionic water-soluble porphyrin that does not exhibit measurable aggregation even at high concentrations in water. The spin state of the corresponding nickel(II) complex changes from completely diamagnetic (low-spin) to paramagnetic (high-spin) upon addition of a strong axial ligand. This leads to a strongly reduced NMR relaxation time of the water protons even at low concentrations of the complex.

Ni-porphyrins are of strong interest for spin switching in solution.[1–6] Square planar complexes are diamagnetic (low-spin, $S = 0$) while square pyramidal and square bipyramidal (distorted octahedral) complexes are paramagnetic (high-spin, $S = 1$). The transition between the two spin states was coined Coordination Induced Spin-State-Switch (CISSS). Until now this process was limited to organic solutions because porphyrins with the required electronic properties are not soluble in water. We present here the first dendronized porphyrin which undergoes a CISSS in water.

Most of the known water-soluble porphyrins bear solubilizing groups in the *meso* position. They are either anionic Ph-SO_3^- (**TPPS**),[7,8] Ph-COO^- (**TPPC**),[9–12] or cationic Ph-NMe_3^+ (**TAPP**),[13,14] Py-Me^+ (*o*-, *m*-, *p*-**TMPyP**)[8,15,16] or tetrafluoro-Ph-NMe_3^+ (**TAPPF$_{16}$**)[17,18] or they are equipped with neutral hydrophilic groups. None of the corresponding ionic Ni-porphyrins provides the required electronic environment for a CISSS (Fig. 1). Ni(II) complexes of **TPPS**, **TPPC**, and **TAPP** do not coordinate even strong axial ligands in water because they are too electron rich, whereas *o*-, *m*-, *p*-**TMPyP** and **TAPPF$_{16}$** are so electron deficient that even water is coordinating.[17–20] So far there is no known Ni-porphyrin that is completely diamagnetic in water (no coordination of water as the axial ligand) but which is still sufficiently reactive for binding stronger ligands such as piperidine or 1-methylimidazole.

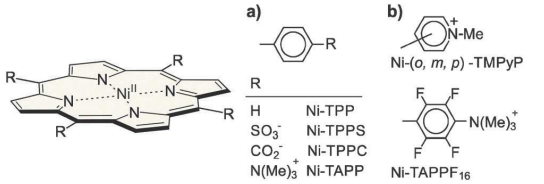

Fig. 1 Ni-tetraphenylporphyrin TPP and some water-soluble derivatives. (a) Electron rich porphyrins which do not bind axial ligands in water (diamagnetic). (b) Electron deficient porphyrins which bind water (partially paramagnetic in water).

Non-ionic water-soluble porphyrins are gaining interest because they possess advantages in photooxygenation and photodynamic therapy (PDT).[21,22] Water solubility was achieved by substitution with ethylene glycols,[23,24] carbohydrates,[25–28] and polyhydroxyamides.[29] Griesbeck *et al.* synthesized water-soluble TPP derivatives decorated with polyols.[30] Our approach is based on a different kind of polyols namely the dendritic glycerol. It has been shown that these groups are suitable for water solubilisation of organic compounds.[31–33] In addition it has been demonstrated that oligoglycerol dendrons can provide sufficient shielding to prevent aggregation of planar perylene dye molecules and enhance their quantum yields to almost 100%.[34,35]

We report here on the functionalisation of the established porphyrins TPPF$_{20}$ (**1**)[36] and Ni-TPPF$_{20}$ (**2**)[5] with the second generation glycerol (G[2.0]-OH), and we present the properties of the corresponding water-soluble porphyrins. TPPF$_{20}$ (**1**) instead of TPP was chosen as the starting material because it is substantially more electron deficient, which is necessary to achieve axial coordination. Moreover, it is known that amines, alcoholates and thiolates can be introduced into the *para*-phenyl position by nucleophilic aromatic substitution which is a simple and efficient way of functionalisation.[17,18,25,27,28] The second generation glycerol (G[2.0]-OH) was synthesised according to a procedure of Haag *et al.* as described previously.[32] The reaction scheme of the functionalisation procedure

[a] *Otto-Diels-Institute of Organic Chemistry, Christian-Albrechts-Universität zu Kiel, Otto-Hahn-Platz 4, 24118 Kiel, Germany. E-mail: rherges@oc.uni-kiel.de*
[b] *Department of Diagnostic Radiology, Christian-Albrechts-Universität zu Kiel, Arnold-Heller-Str. 3, 24105 Kiel, Germany*
[c] *Institute of Chemistry and Biochemistry, Freie Universität Berlin, Takustr. 3, 14195 Berlin, Germany*

† Electronic supplementary information (ESI) available. See DOI: 10.1039/c4cc05525j

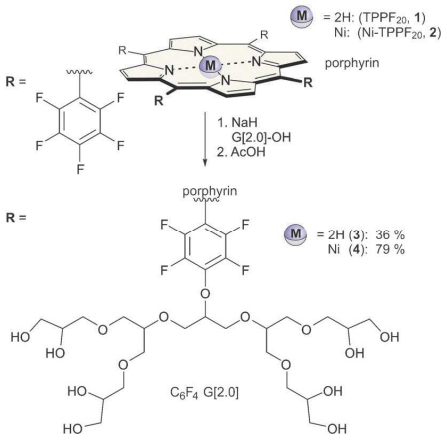

Fig. 2 Syntheses of the glycerol functionalised porphyrins **3** and **4**. Experimental details are given in the ESI.†

is shown in Fig. 2. Deprotection of the 32 alcohol functions was achieved quantitatively with acetic acid (Fig. 2).

In contrast to many other water-soluble porphyrins[8,14,28,37] the glycerol functionalised derivatives **3** and **4** do not exhibit aggregation or excimer formation which is probably due to the large steric hindrance of the polyols.[34,35] Solutions of **3** and **4** perfectly follow the Lambert–Beer law up to a concentration of 50 μm. NMR experiments do not show any changes in the line shape suggesting that there is no aggregation even at concentrations of 0.8 mM (see ESI†).

Compound **4** in water exhibits a Soret band at 409 nm, which is indicative of a diamagnetic low-spin state. Addition of piperidine gives rise to a new band at 428 nm due to axial coordination and the associated spin state switch to the high-spin triplet state (Fig. 3).

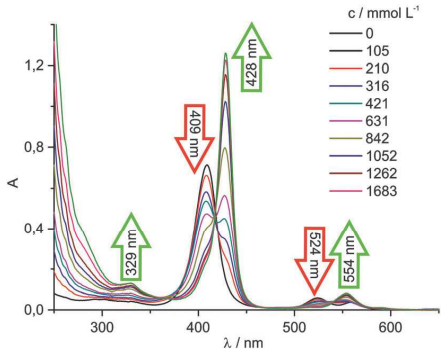

Fig. 3 UV-Vis spectra (top) of titration series of piperidine to Ni-porphyrin **4** (4.05 μm, 20 °C) in water. Association constants for addition of one piperidine ligand (K_1 = 0.48 L mol^{-1}), and the association of a second piperidine ligand (K_2 = 14.7 L mol^{-1}) were determined from the UV-visible data (see ESI†). The green arrows correspond to increasing absorption upon increasing piperidine concentration.

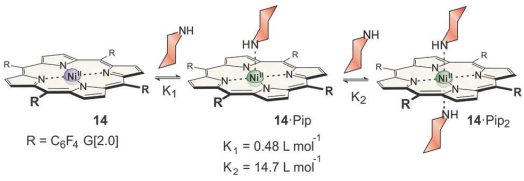

Fig. 4 Formation of the square pyramidal (**4**·Pip) and the square bipyramidal complexes (**4**·Pip$_2$).

The titration experiment reveals very low values for the association constants (K_1, K_2) (Fig. 4, for details see the ESI†) compared to the values for Ni-TPPF$_{20}$ (**2**) obtained in organic solution by similar experiments.[3–5] Water is an adverse solvent for axial coordination because it reduces the donor strength of ligands by hydrogen bonding. Nevertheless, the association constants obtained for piperidine are higher than those for many alkyl- and aryl-substituted Ni-porphyrins in organic solution.[38–42] Except for very strong donor ligands, and very electron poor porphyrins, K_1 is known to be much smaller than K_2.[17,41,42] Spin change occurs upon binding of the first axial ligand which in turn activates the second axial binding site. Usually, the predominant species, therefore, is the 2 : 1, square bipyramidal complex. This is in agreement with our findings: K_2 is approximately 30 times larger than K_1 (see ESI†).

Both magnetic species exhibit different ^{1}H NMR spectra, and their relative ratio can be quantified using ^{1}H NMR spectroscopy. Ligand exchange is fast on the NMR time scale, and an averaged shift of high-spin and low-spin species is observed at room temperature. Particularly, the chemical shift of the pyrrole protons is an excellent indicator of the ratio of high and low-spin Ni(II) in solution.[2–5] In pure complex **4** these protons resonate at 9.1 ppm, which is typical for a completely diamagnetic Ni-porphyrin. Upon addition of piperidine (~1000 eq.), the corresponding peak is shifted downfield to 52.7 ppm which is the chemical shift of the pure triplet Ni-porphyrin. Hence, the molecule has almost completely switched to the high-spin state (Fig. 5).

Paramagnetic metal ions are known to decrease the proton relaxation time of the surrounding water molecules.[43] Gd^{3+} complexes (7 unpaired electrons), therefore, are widely used

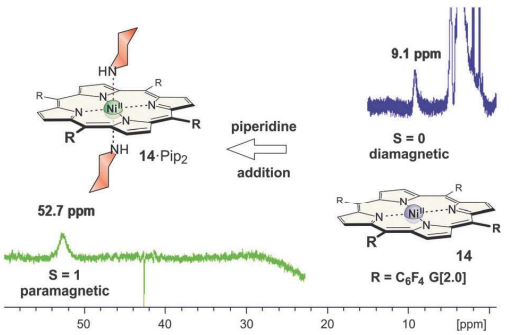

Fig. 5 NMR spectra (D_2O, 500 MHz, T = 300 K) of Ni-porphyrin **4** (0.8 mM) before (blue) and after (green) addition of piperidine.

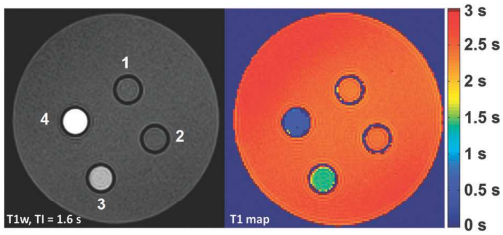

Fig. 6 MR images of 4 different solutions: 1. **4** (2 mM in water), 2. water, 3. water + 20% piperidine and 4. **4** (2 mM in water + 20% piperidine). For details see ESI.†

as contrast agents in magnetic resonance imaging (MRI).[44] Ni-porphyrin **4** in water is diamagnetic and inactive as a MRI contrast agent which is shown by 7 T MR images (note that nickel salts such as $NiCl_2{\cdot}6H_2O$ are paramagnetic). Upon addition of piperidine as a strong axial ligand the complex changes to the paramagnetic state ($S = 1$) and the contrast is turned on (Fig. 6). In a 2 mM solution in water the relaxation rate thereby rises from 0.71 s^{-1} (water + 20% piperidine) to 1.96 s^{-1} (factor ~2.8). The relaxivity (effectiveness in reducing the relaxation time of water protons, r_1) of the paramagnetic complex **4**·Pip_2 (0.63 mM^{-1} s^{-1}) is slightly lower than r_1 of Ni^{2+} salts (aquo complex: 0.78 mM^{-1} s^{-1}) but is much higher than for other nickel complexes (*e.g.* EDTA complex: 0.11 mM^{-1} s^{-1}). The MR images demonstrate that porphyrins such as **4** could be viewed as a first step towards the development of responsive contrast agents.[45,46]

A neutral, water-soluble, oligoglycerol dendron substituted Ni-porphyrin was synthesised whose spin state was switched from completely diamagnetic (low-spin) to paramagnetic (high-spin) by addition of piperidine. Both, the Ni-porphyrin and the free base are easily accessible in a two-step procedure from commercially available starting materials. No aggregation or excimer formation was observed even at high concentrations in water. The hydrophilic Ni-porphyrin complex is an excellent candidate for spin switching in water. The longitudinal relaxivity r_1 of the paramagnetic state which is unusually high for an $S = 1$ complex (0.63 mM^{-1} s^{-1}) and the spin switching mechanism could provide a basis for responsive contrast agents for MRI. The metal-free porphyrin should be suitable for applications such as photooxidation or photodynamic therapy in physiological environments.

Notes and references

1 S. Venkataramani, U. Jana, M. Dommaschk, F. D. Sönnichsen, F. Tuczek and R. Herges, *Science*, 2011, **331**, 445–448.
2 R. Herges, *Nachr. Chem.*, 2011, **59**, 817–821.
3 S. Thies, H. Sell, C. Schütt, C. Bornholdt, C. Näther, F. Tuczek and R. Herges, *J. Am. Chem. Soc.*, 2011, **133**, 16243–16250.
4 S. Thies, H. Sell, C. Bornholdt, C. Schütt, F. Köhler, F. Tuczek and R. Herges, *Chem. – Eur. J.*, 2012, **18**, 16358–16368.
5 S. Thies, C. Bornholdt, F. Köhler, F. D. Sönnichsen, C. Näther, F. Tuczek and R. Herges, *Chem. – Eur. J.*, 2010, **16**, 10074–10083.
6 F. Matino, G. Schull, U. Jana, F. Köhler, R. Berndt and R. Herges, *Chem. Commun.*, 2010, **46**, 6780–6782.
7 E. B. Fleischer, J. M. Palmer, T. S. Srivastava and A. Chatterjee, *J. Am. Chem. Soc.*, 1971, **93**, 3162–3167.
8 R. F. Pasternack, P. R. Huber, P. Boyd, G. Engasser, L. Francesconi, E. Gibbs, P. Fasella, G. Cerio Venturo and L. d. Hinds, *J. Am. Chem. Soc.*, 1972, **94**, 4511–4517.
9 J. Turay, P. Hambright and N. Datta-Gupta, *J. Inorg. Nucl. Chem.*, 1978, **40**, 1687–1688.
10 F. R. Longo, M. G. Finarelli and J. B. Kim, *J. Heterocycl. Chem.*, 1969, **6**, 927–931.
11 N. Datta-Gupta and T. J. Bardos, *J. Heterocycl. Chem.*, 1966, **3**, 495–502.
12 T. Fujimoto, H. Umekawa and N. Nishino, *Chem. Lett.*, 1992, 37–40.
13 M. Krishnamurthy, *Indian J. Chem.*, 1977, **15B**, 964.
14 K. Kano, M. Takei and S. Hashimoto, *J. Phys. Chem.*, 1990, **94**, 2181–2187.
15 P. Hambright and E. B. Fleischer, *Inorg. Chem.*, 1970, **9**, 1757–1761.
16 R. Fiel, J. Howard, E. Mark and N. Gupta, *Nucleic Acids Res.*, 1979, **6**, 3093–3118.
17 T. La, R. A. Richards, R. S. Lu, R. Bau and G. M. Miskelly, *Inorg. Chem.*, 1995, **34**, 5632–5640.
18 T. La, R. Richards and G. M. Miskelly, *Inorg. Chem.*, 1994, **33**, 3159–3163.
19 M. Ravikant, D. Reddy and T. K. Chandrashekar, *J. Chem. Soc., Dalton Trans.*, 1991, 2103–2108.
20 K. Bütje and K. Nakamoto, *Inorg. Chim. Acta*, 1990, **167**, 97–108.
21 M. Ethirajan, Y. Chen, P. Joshi and R. K. Pandey, *Chem. Soc. Rev.*, 2011, **40**, 340–362.
22 R. Bonnett, *Chem. Soc. Rev.*, 1995, **24**, 19–33.
23 P. Mineo, E. Scamporrino and D. Vitalini, *Macromol. Rapid Commun.*, 2002, **23**, 681–687.
24 V. Villari, P. Mineo, E. Scamporrino and N. Micali, *Chem. Phys.*, 2012, **409**, 23–31.
25 J. a. P. Tomé, M. G. Neves, A. C. Tomé, J. A. Cavaleiro, A. F. Mendonça, I. N. Pegado, R. Duarte and M. L. Valdeira, *Bioorg. Med. Chem.*, 2005, **13**, 3878–3888.
26 A. G. Griesbeck, M. A. Miranda and J. Uhlig, *Photochem. Photobiol. Sci.*, 2011, **10**, 1431–1435.
27 D. Samaroo, M. Vinodu, X. Chen and C. M. Drain, *J. Comb. Chem.*, 2007, **9**, 998–1011.
28 D. Oulmi, P. Maillard, C. Vever-Bizet, M. Momenteau and D. Brault, *Photochem. Photobiol.*, 1998, **67**, 511–518.
29 J. E. Bradshaw, K. A. Gillogly, L. J. Wilson, K. Kumar, X. Wan, M. F. Tweedle, G. Hernandez and R. G. Bryant, *Inorg. Chim. Acta*, 1998, **275–276**, 106–116.
30 A. G. Griesbeck, M. Schäfer and J. Uhlig, *Adv. Synth. Catal.*, 2008, **350**, 2104–2108.
31 C. Kordel, C. S. Popeney and R. Haag, *Chem. Commun.*, 2011, **47**, 6584–6586.
32 M. Wyszogrodzka and R. Haag, *Chem. – Eur. J.*, 2008, **14**, 9202–9214.
33 M. Wyszogrodzka, K. Möws, S. Kamlage, J. Wodzinska, B. Plietker and R. Haag, *Eur. J. Org. Chem.*, 2008, 53–63.
34 T. Heek, C. Fasting, C. Rest, X. Zhang, F. Würthner and R. Haag, *Chem. Commun.*, 2010, **46**, 1884–1886.
35 T. Heek, F. Würthner and R. Haag, *Chem. – Eur. J.*, 2013, **19**, 10911–10921.
36 G. R. Geier III and J. S. Lindsey, *Tetrahedron*, 2004, **60**, 11435–11444.
37 R. R. Das, R. F. Pasternack and R. A. Plane, *J. Am. Chem. Soc.*, 1970, **92**, 3312–3316.
38 B. D. McLees and W. S. Caughey, *Biochemistry*, 1968, **7**, 642–652.
39 S. J. Cole, G. C. Curthoys, E. A. Magnusson and J. N. Phillips, *Inorg. Chem.*, 1972, **11**, 1024–1028.
40 F. A. Walker, E. Hui and J. M. Walker, *J. Am. Chem. Soc.*, 1975, **97**, 2390–2397.
41 D. Kim, Y. O. Su and T. G. Spiro, *Inorg. Chem.*, 1986, **25**, 3988–3993.
42 Y. Song, R. E. Haddad, S.-L. Jia, S. Hok, M. M. Olmstead, D. J. Nurco, N. E. Schore, J. Zhang, J.-G. Ma, K. M. Smith, S. Gazeau, J. Pécaut, J.-C. Marchon, C. J. Medforth and J. A. Shelnutt, *J. Am. Chem. Soc.*, 2005, **127**, 1179–1192.
43 R. B. Lauffer, *Chem. Rev.*, 1987, **87**, 901–927.
44 H. Gries, *Top. Curr. Chem.*, 2002, **221**, 1–24.
45 G. Angelowski and I. Mamedov, *Curr. Inorg. Chem.*, 2011, **1**, 76–90.
46 C. Tu, E. A. Osborne and A. Y. Louie, *Ann. Biomed. Eng.*, 2011, **39**, 1335–1348.

Coordination-Induced Spin-State-Switch (CISSS) in water

Marcel Dommaschk, Florian Gutzeit, Susann Boretius, Rainer Haag and Rainer Herges

Table of Contents

I. Analytical equipment

NMR Spectroscopy

NMR spectra were measured in deuterated solvents (Deutero). The degree of deuteration is given in parentheses. ^{1}H NMR-spectra in reference to the following signals.

acetone-d_6 (99.8 %): δ = 2.0549 ppm (quintet)

chloroform-d (99.8 %): δ = 7.2600 ppm (s)

methanol-d_4 (99.8 %): δ = 3.3500 ppm (quintet)

water-d_2 (99.9 %): δ = 4.7900 ppm (s)

Reference for all ^{19}fluorine-NMR-spectra is trichloro fluoromethane to the frequency of which the spectrometer is calibrated. Fluorine atoms are labeled as *o*-F, *m*-F und *p*-F (*ortho*-, *meta*- und *para*-fluorine) according to their position in the aromatic system.

The signal multiplicities are abbreviated as follows.

s: singlet, d: doublet, t: triplet, q: quartet, quint: quintet, m: multiplet, br: broad signal

Measurements were performed with a Bruker DRX 500 (^{1}H NMR: 500 MHz, ^{19}F NMR: 470 MHz) and a Bruker AV 600 (^{1}H NMR: 600 MHz)

IR spectroscopy

Infrared spectra were measured on a Perkin-Elmer 1600 Series FT-IR spectrometer with a A531-G Golden-Gate-Diamond-ATR-unit. Signals were abbreviated with w, m, s and vs for weak, medium, strong and very strong intensities. Broad signals are additionally labeled with br.

UV-Vis spectroscopy

The UV-Vis spectra were measured on a Lambda 14 spectrometer (Perkin-Elmer) with a (Büchi) thermostat. Quartz cuvettes of 1 cm and 1 mm optical path length were used.

Elemental analysis

The amount of carbon, hydrogen and nitrogen in a compound was determined with a CHNSO-Elementaranalysator Euro EA 3000 Series by co. Euro Vector. The dendronized porphyrins were not examined by this method because of the low amount of obtained substance.

Mass spectrometry

The high resolution (HR) mass spectra were measured with an APEX 3 FT-ICR with a 7.05 T magnet by co. Bruker Daltonics. Electron impact (EI) and chemical ionisation (CI) mass spectra were measured with a MAT 8230 by co. Finnigan.

Chromatography stationary phases

For column chromatography purifications silica gel (Merck, particle size 0.040-0.063 mm) was used. R_f values were determined by thin layer chromatography on Polygeram® Sil G/UV$_{254}$ (Macherey-Nagel, 0.2 mm particle size).

II. Syntheses

II.1 Synthesis of *meso*-tetrakis(pentafluorophenyl)porphyrin (1)

Freshly destilled pyrrole (700 µL, 10.1 mmol), pentafluoro benzaldehyde (1.91 g, 9.72 mmol) and boron trifluoride diethyl etherate (150 µL, 1.19 mmol) were stirred in dichloromethane (400 mL) for 40 h under nitrogen atmosphere at 37 °C. After addition of *p*-chloranil (1.90 g, 7.73 mmol) stirring at 37 °C was continued for 3 h. The solvent was removed under reduced pressure. The black crude product was purified by column chromatography (hexane/chloroform = 3:2, R_f = 0.45).

Yield: 870 mg (0.89 mmol, 37 %, Lit.: 25 %)[1]

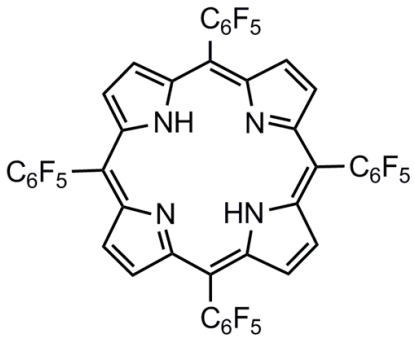

^{1}H NMR (500 MHz, 300 K, $CDCl_3$): δ = 8.92 (s, 8H, *H*-Ar), -2.91 (s, 2H, N-*H*) ppm.

^{19}F NMR (470 MHz, 300 K, $CDCl_3$) δ = -136.50 (dd, ^3J = 23.4 Hz, ^5J = 8.4 Hz, *o*-F), -151.21 (t, ^3J = 20.7 Hz, *p*-F), -161.32 (td, ^3J = 22.3 Hz, ^5J = 8.4 Hz, *m*-F) ppm.

MS (EI, 70 eV): m/z (%) = 974 (100) $[M]^+$, 955 (12) $[M\text{-}F]^+$, 487 (33) $[M]^{2+}$, 478 (4) $[M\text{-}F]^{2+}$.

MS (CI, isobutane): m/z (%) = 975 (100) $[M+H]^+$.

EA: ($C_{44}H_{10}F_{20}N_4$)		C / %	H / %	N / %
	found:	54.10	0.94	5.65
	calc.:	54.23	1.03	5.75

II.2 Synthesis of *meso*-tetrakis(pentafluorophenyl)nickel(II)porphyrin (2)

Porphyrin **1** (503 mg, 0.516 mmol) and nickel(II)acetylacetonate (1.33 g, 5.15 mmol) were stirred under reflux for 4 d in toluene (100 mL). The solvent was removed under reduced pressure and the crude product was purified by column chromatography (chloroform, $R_f = 0.78$).

Yield: 518 mg (0.502 mmol, 97 %)

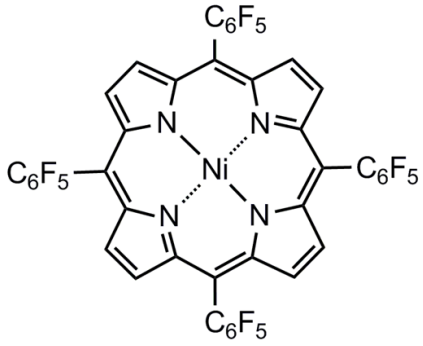

^{1}H NMR (500 MHz, 300 K, $CDCl_3$): δ = 8.79 (s, 8H, *H*-Ar) ppm.

^{19}F NMR (470 MHz, 300 K, $CDCl_3$) δ = -136.62 (dd, ^3J = 23.0 Hz, ^5J = 8.4 Hz, *o*-F), -151.29 (t, ^3J = 21.0 Hz, *p*-F), -161.32 (td, ^3J = 22.0 Hz, ^5J = 8.4 Hz, *m*-F) ppm.

MS (EI, 70 eV): m/z (%) = 1030 (100) $[M]^+$, 1011 (9) $[M\text{-}F]^+$, 515 (29) $[M]^{2+}$.

EA: ($C_{44}H_8F_{20}N_4Ni$)		C / %	H / %	N / %
	found:	50.90	0.85	5.26
	calc.:	51.25	0.78	5.69

II.3 Synthesis of glycerol functionalised porphyrin 5

Sodium hydride (15 mg, 375 µmol) (60 % dispersion in mineral oil) was suspended in dry tetrahydrofuran (5 mL) under nitrogen atmosphere. [G2.0]-OH (83.4 mg, 120 µmol) was dissolved in tetrahydrofuran (3 mL) and slowly added to the sodium hydride suspension. The suspension was stirred for 50 min. $TPPF_{20}$ (**1**) (19.5 mg, 20 µmol) was added and stirring was continued for 7 d. The reaction was quenched with water and diethyl ether (200 mL) was added. The organic layer was washed with 200 mL of 0.1 M hydrochloric acid and dried over magnesium sulphate. The solvent was removed under reduced pressure. The crude product was purified by column chromatography (silica gel, dichloromethane / methanol = 98 : 2, R_f = 0.06). The product was obtained as a red, viscous oil.

Yield: 26.2 mg (7.12 µmol, 36 %)

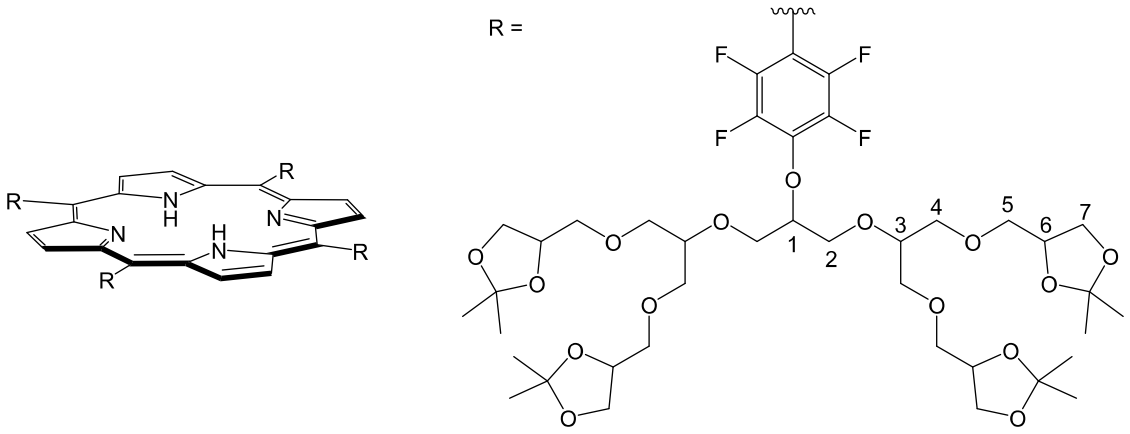

FT-IR (layer): υ = 2986 (m), 2873 (m), 1696 (w), 1649 (w), 1494 (s), 1479 (s), 1430 (m), 1370 (s), 1255 (s), 1212 (s), 1144 (s), 1050 (vs), 983 (vs), 921 (s), 841 (s), 806 (m), 773 (m), 757 (s), 727 (w), 636 (w), 516 (m), 463 (m), 416 (m) cm^{-1}.

^{1}H NMR (600 MHz, acetone-d_6, 300 K): δ = 9.29 (s, 8H, *H*-Ar), 5.04-4.97 (m, 4H, *H*-1), 4.32-4.25 (m, 16H, *H*-6), 4.23-4.17 (m, 16H, *H*-2), 4.09-4.03 (m, 16H, H_a-7), 3.89-3.84 (m, 8H, *H*-3), 3.83-3.48 (m, 80H, H-4, H-5, H_b-7), 1.37-1.26 (m, 96H, CH_3), -2.85 (s, 2H, *H*-N) ppm.

^{19}F NMR (470 MHz, acetone-d_6, 300 K): δ = -141.9 (m, 8F, *o*-F), -157.1 (m, 8F, *m*-F) ppm.

MS (HR): m/z (calc.) = 1227.533 (1227.543) $[M+3H]^{3+}$

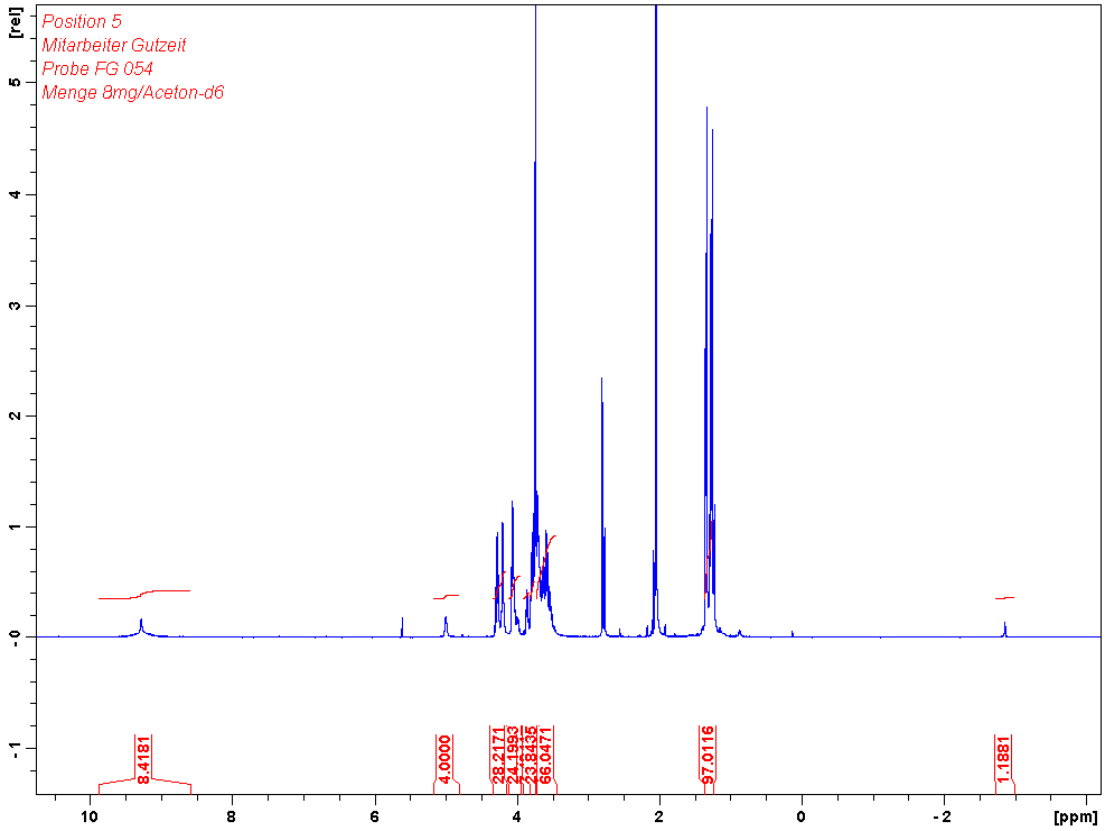

Fig S1 ^{1}H NMR spectrum of **5** in acetone-d_6.

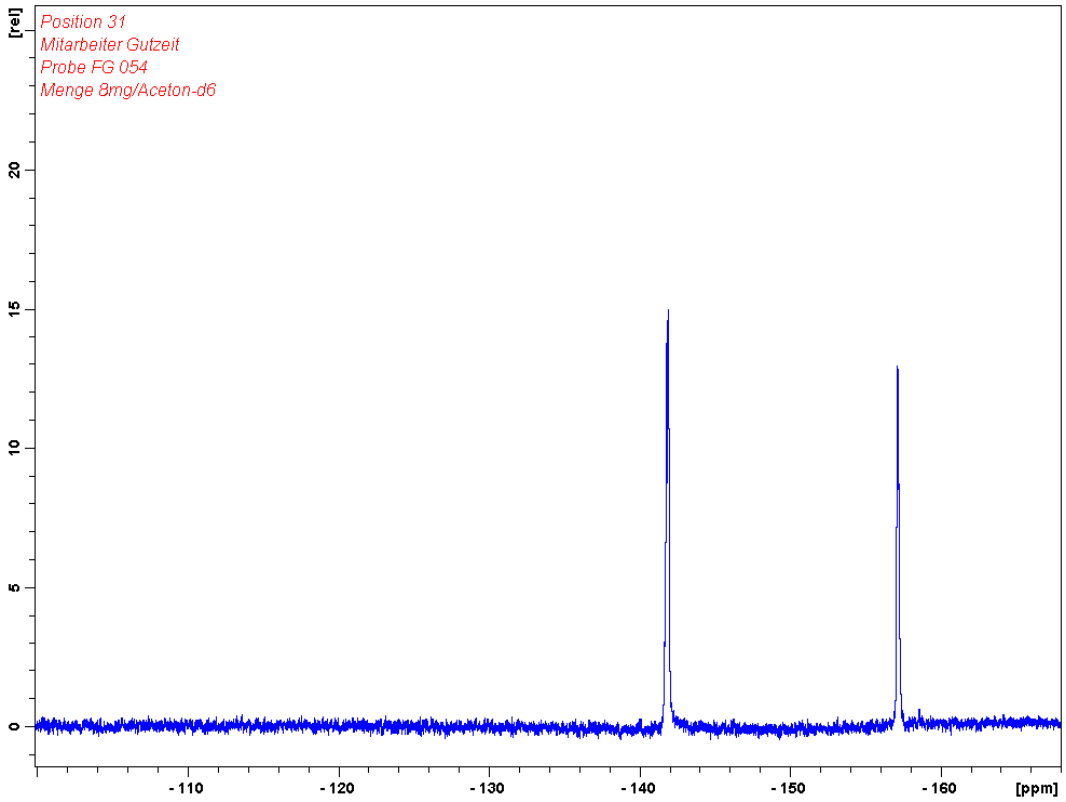

Fig S2 ^{19}F NMR spectrum of **5** in acetone-d_6.

II.4 Synthesis of glycerol functionalised porphyrin 3

Acetal protected porphyrin **5** (17.3 mg, 4.7 µmol) was dissolved in a mixture of 0.3 mL of acetic acid, 1 mL of methanol and 0.5 mL of water and stirred for 4 d at 40 °C. The solvent was removed under reduced pressure. The product was obtained as a red, viscous oil.

Yield: 16.4 mg (4.73 µmol, quant.)

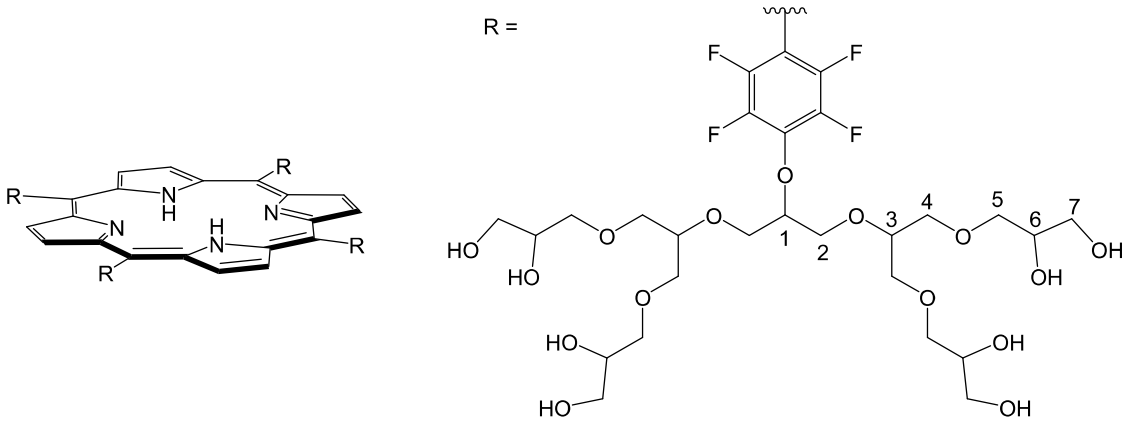

FT-IR (layer): υ = 3321 (br, m), 2873 (m), 1650 (w), 1493 (s), 1478 (s), 1429 (m), 1401 (m), 1352 (m), 1250 (m), 1045 (vs), 981 (vs), 909 (s), 866 (m), 807 (m), 772 (m), 756 (s), 571 (m) cm^{-1}.

^{1}H NMR (500 MHz, methanol-d_4, 300 K): δ = 9.47-8.91 (m, br, 8H, *H*-Ar), 5.03 (q, ^3J = 4.7 Hz, 4H, *H*-1) 4.27-4.08 (m, 16H, *H*-2), 3.96-3.46 (m, 120H, *H*-3, *H*-4, *H*-5, *H*-6, *H*-7) ppm.

HN- and HO-protons are not found because of deuterium exchange.

^{19}F NMR (470 MHz, methanol-d_4, 300 K): δ = -142.1 (m, 8F, *o*-F), -157.7 (m, 8F, *m*-F) ppm.

UV-Vis (MeOH): λ_{max} (lg ε) = 409 (5.4333), 504 (4.2900), 581 (3.7672) nm.

UV-Vis (H_2O): λ_{max} (lg ε) = 419 (5.3973), 509 (4.2509), 582 (3.7672) nm.

MS (HR): m/z (calc.) = 1014.044 (1014.043) $[M+3H]^{3+}$

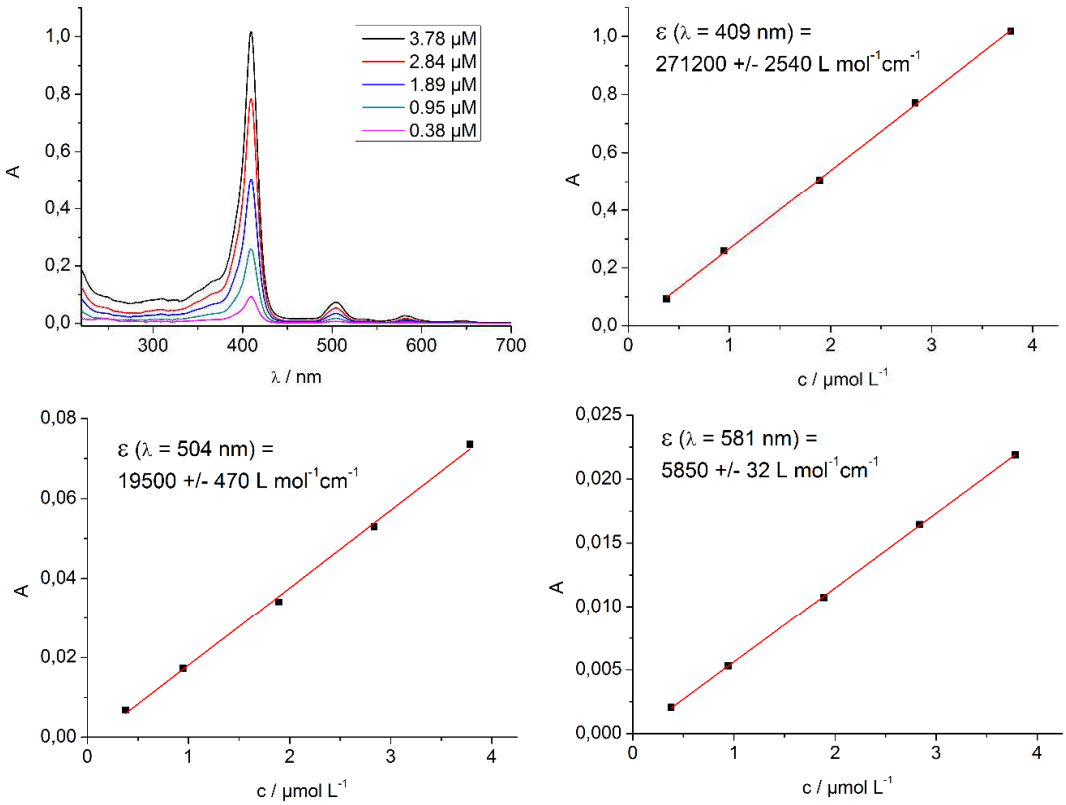

Fig S3 UV-Vis spectra (top left) and extinction coefficients of **3** in methanol.

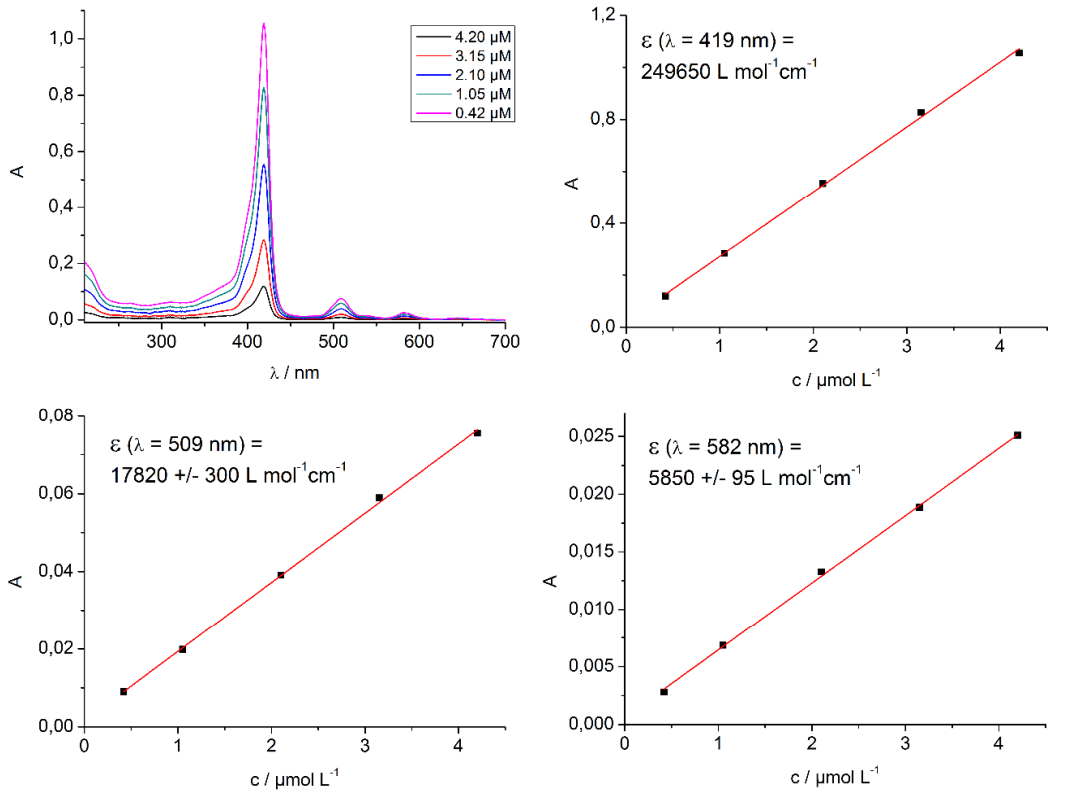

Fig S4 UV-vis spectra (top left) and extinction coefficients of **3** in water.

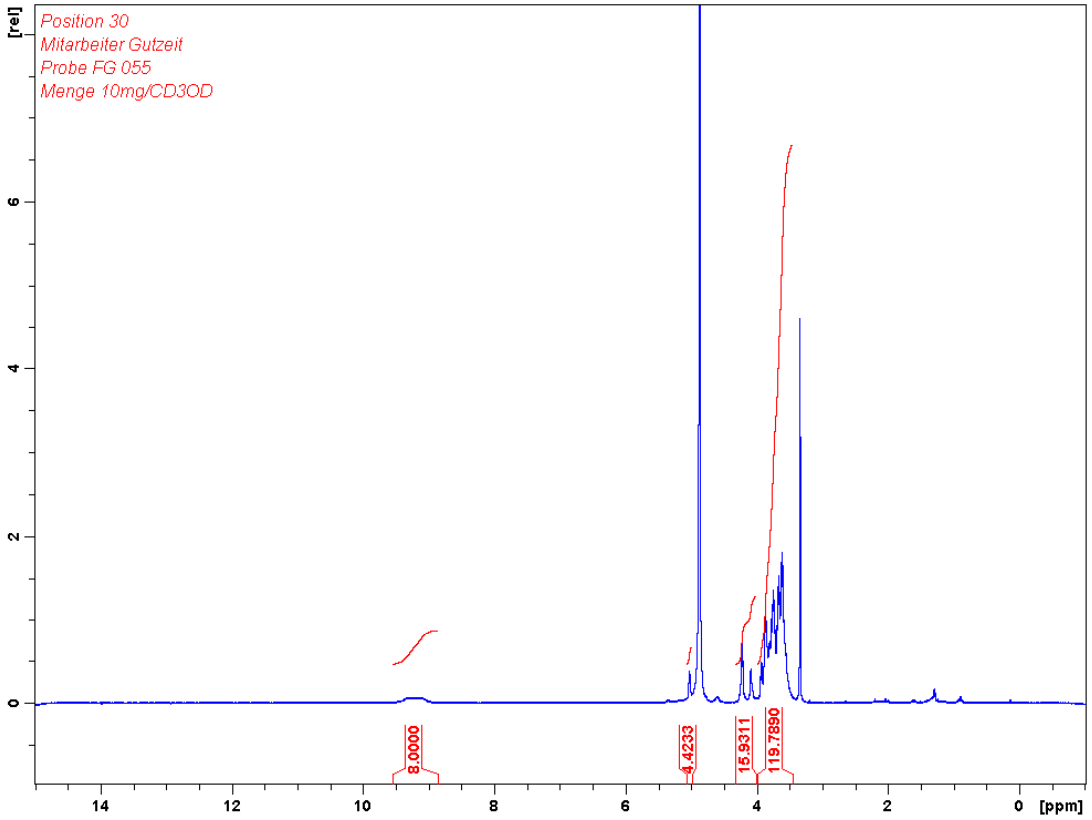

Fig S5 ^{1}H NMR spectrum of **3** in methanol-d_4.

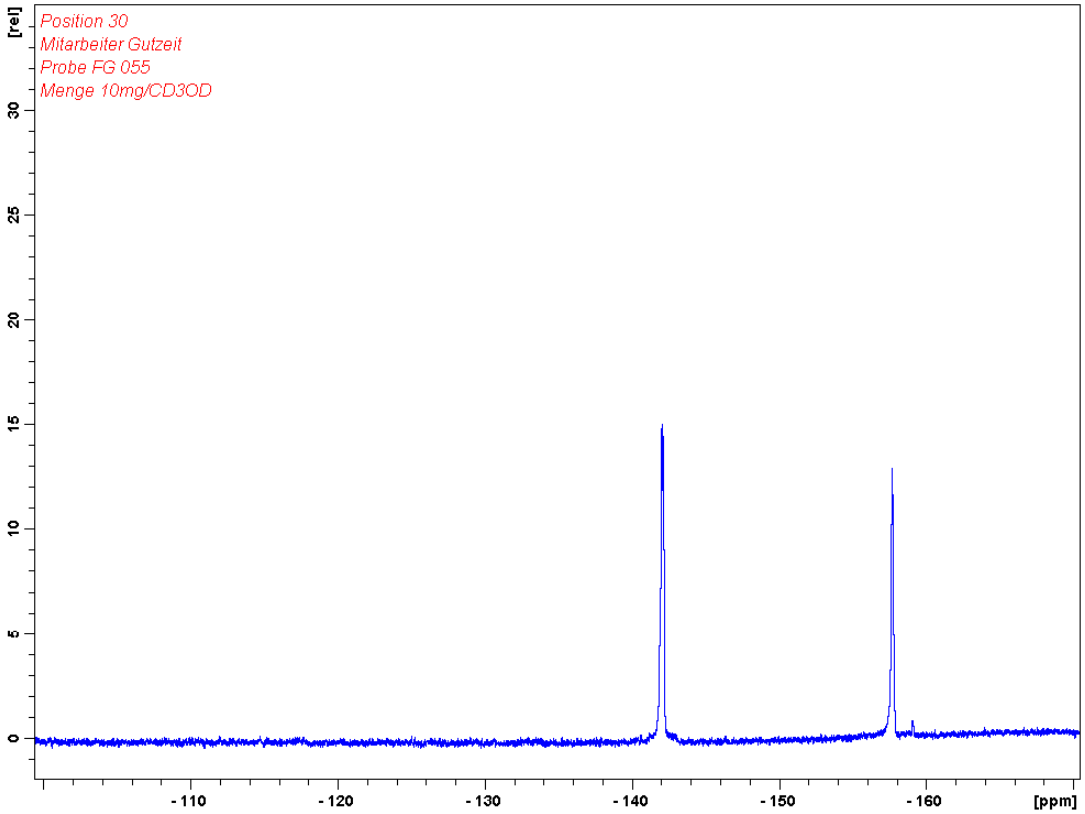

Fig S6 ^{19}F NMR spectrum of **3** in methanol-d_4.

II.5 Synthesis of glycerol functionalised Ni-porphyrin 6

Sodium hydride (15 mg, 375 µmol) (60 % dispersion in mineral oil) was suspended in 5 mL of dry tetrahydrofuran under nitrogen atmosphere. [G2.0]-OH (85.7 mg, 123 µmol) was dissolved in 3 mL of tetrahydrofuran and slowly added to the sodium hydride suspension. The suspension was stirred for 1 h. Ni-$TPPF_{20}$ (**2**) (21.1 mg, 20.5 µmol) was added and the mixture was stirred for 5 d. The reaction was quenched with water and added to 100 mL of diethyl ether. The organic layer was washed with 100 mL of 0.1 M hydrochloric acid and dried over magnesium sulphate. The solvent was removed under reduced pressure. The crude product was purified by column chromatography (silica gel, dichloromethane / methanol = 97 : 3, R_f = 0.1). The product was obtained as a red, viscous oil.

Yield: 60.1 mg (16.1 µmol, 79 %)

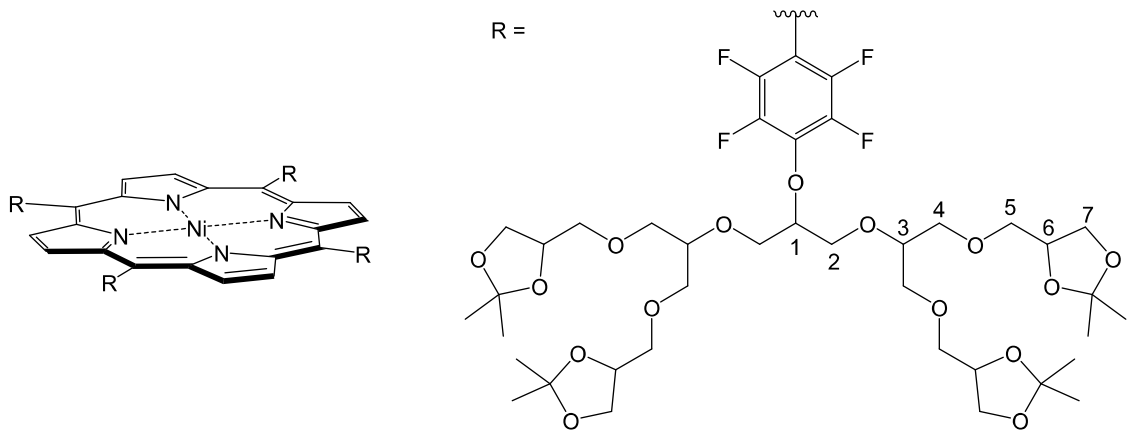

FT-IR (layer): υ = 2987 (m), 2876 (m), 1650 (w), 1490 (s), 1427 (w), 1370 (m), 1258 (m), 1214 (m), 1147 (s), 1080 (vs), 984 (s), 947 (s), 842 (m), 763 (m), 667 (w), 514 (w), 463 (w) cm^{-1}.

^{1}H NMR (600 MHz, acetone-d_6, 300 K): δ = 9.17 (s, 8H, *H*-Ar), 4.99-4.92 (m, 4H, *H*-1), 4.30-4.24 (m, 16H, *H*-6), 4.20-4.15 (m, 16H, *H*-2), 4.07-4.02 (m, 16H, H_a-7), 3.85-3.81 (m, 8H, *H*-3), 3.80-3.51 (m, 80H, H-4, H-5, H_b-7), 1.35-1.25 (m, 96H, CH_3) ppm.

^{19}F NMR (470 MHz, acetone-d_6, 300 K): δ = -141.9 (m, 8F, *o*-F), -157.0 (m, 8F, *m*-F) ppm.

MS (HR): m/z (calc.) = 1246.173 (1227.178) $[M+3H]^{3+}$

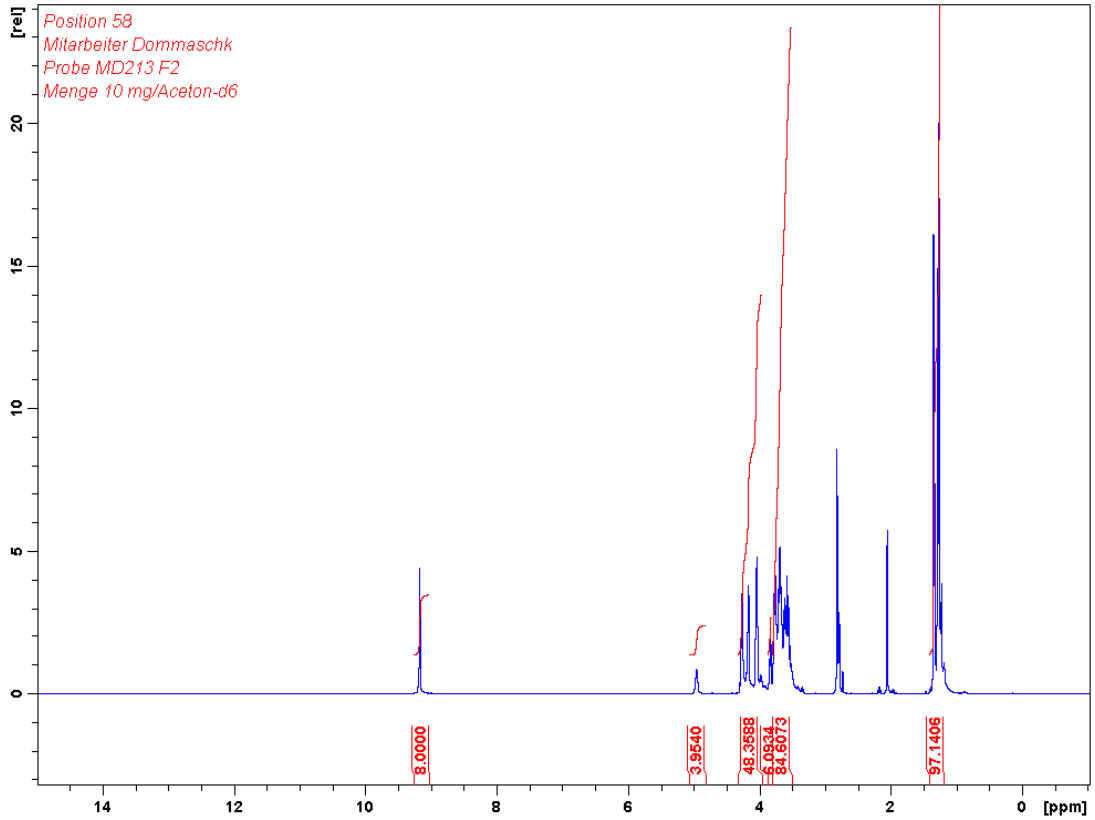

Fig S7 ^{1}H NMR spectrum of **6** in acetone-d_6.

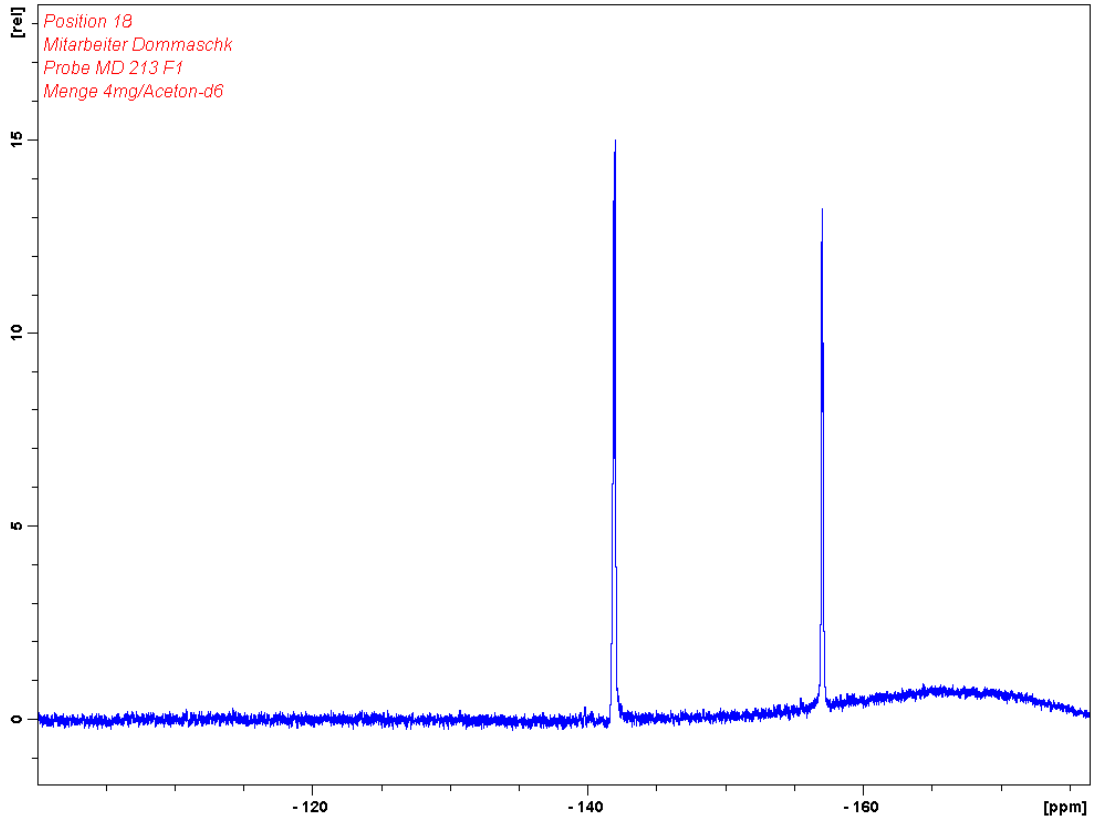

Fig S8 ^{19}F NMR spectrum of **6** in acetone-d_6.

II.6 Synthesis of glycerol functionalised Ni-porphyrin 4

Acetal protected porphyrin **6** (60.1 mg, 16.1 µmol) was dissolved in a mixture of 1.00 mL of acetic acid, 2 mL of methanol and 1.00 mL of water and stirred for 4 d at 40 °C. The solvent was removed under reduced pressure. The product was obtained as a red, viscous oil.

Yield: 49.8 mg (16.1 µmol, quant.)

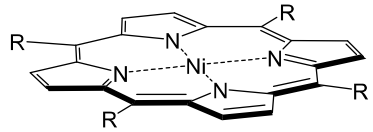

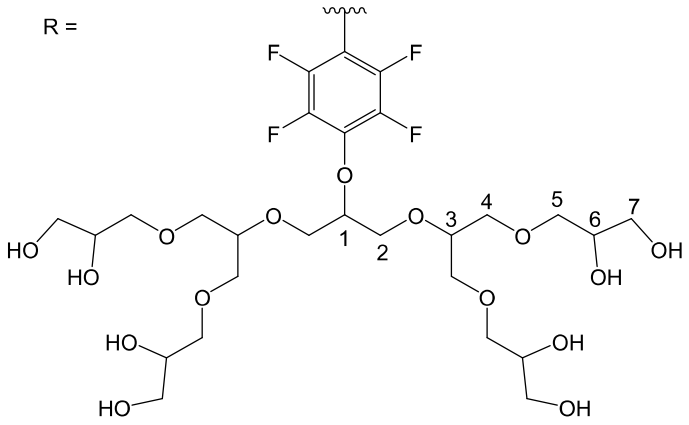

FT-IR (layer): υ = 3368 (br, m), 2921 (s), 1648 (m), 1484 (s), 1347 (m), 1070 (vs), 980 (vs), 945 (s), 854 (m), 762 (s), 705 (m), 617 (s), 543 (s), 487 (s), 442 (vs), 420 (vs), 411 (s) cm^{-1}.

^{1}H NMR (500 MHz, methanol-d_4, 300 K): δ = 9.58 (s, 8H, *H*-Ar), 4.95 (p, ^{3}J = 4.7 Hz, 4H, *H*-1), 4.20-4.05 (m, 16H, *H*-2), 3.88-3.43 (m, 120H, *H*-3, *H*-4, *H*-5, *H*-6, *H*-7) ppm.

HO-protons are not found because of deuterium exchange.

^{19}F NMR (470 MHz, methanol-d_4, 300 K): δ = -142.2 (m, 8F, *o*-F), -157.7 (m, 8F, *m*-F) ppm.

UV-Vis (MeOH): λ_{max} (lg ε) = 401 (5.3625), 520 (4.1867), 554 (4.0554) nm.

UV-Vis (H_2O): λ_{max} (lg ε) = 409 (5.2483), 524 (4.1824), 559 (4.0013) nm.

MS (HR): m/z (calc.) = The mass peak is not found due to high fragmentation during electrospray ionisation.

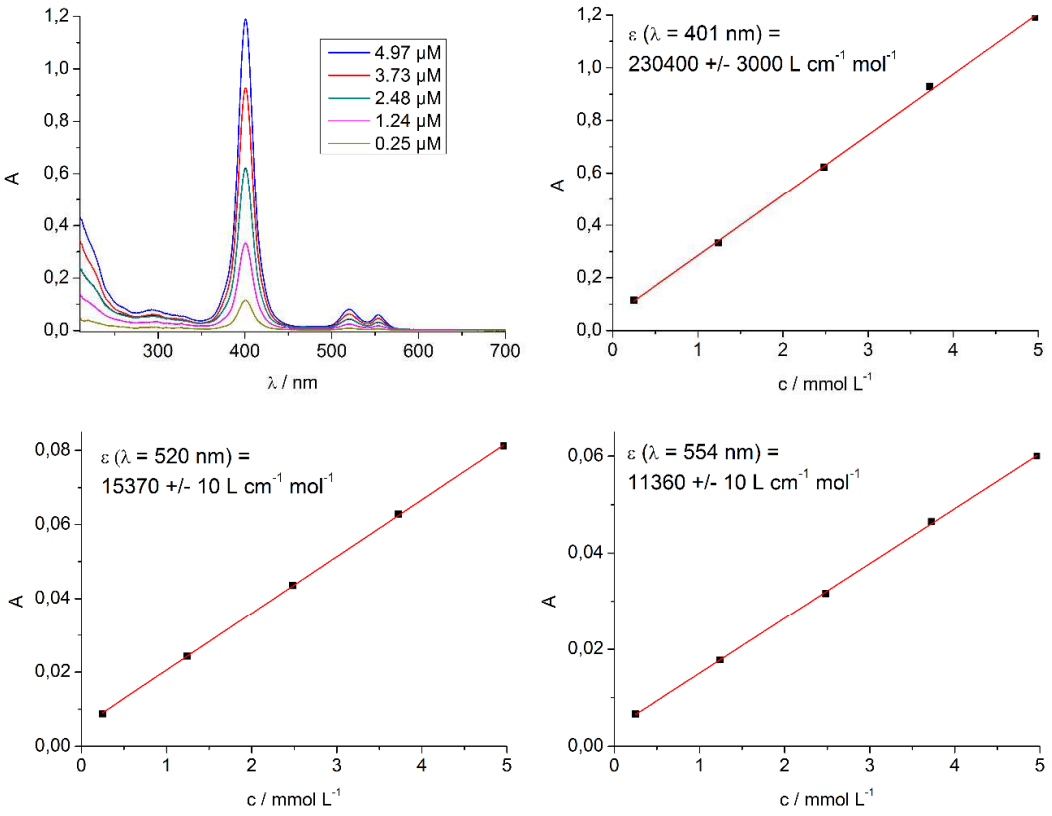

Fig S9 UV-vis spectra (top left) and extinction coefficients of **4** in methanol.

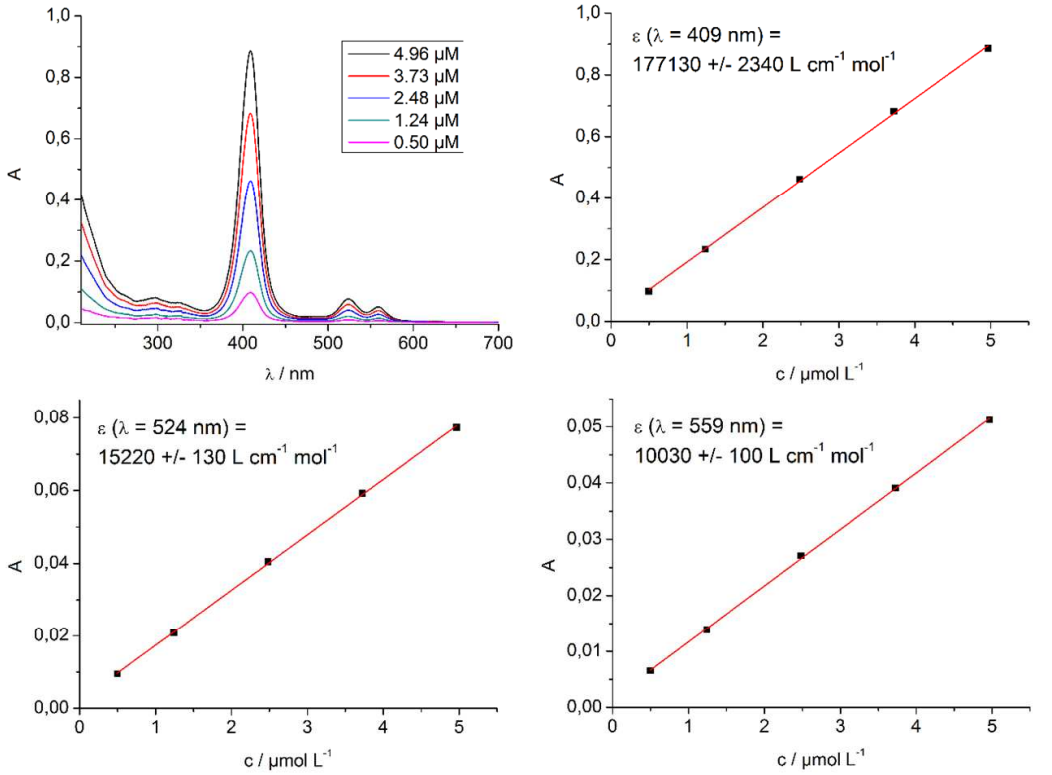

Fig S10 UV-vis spectra (top left) and extinction coefficients of **4** in water.

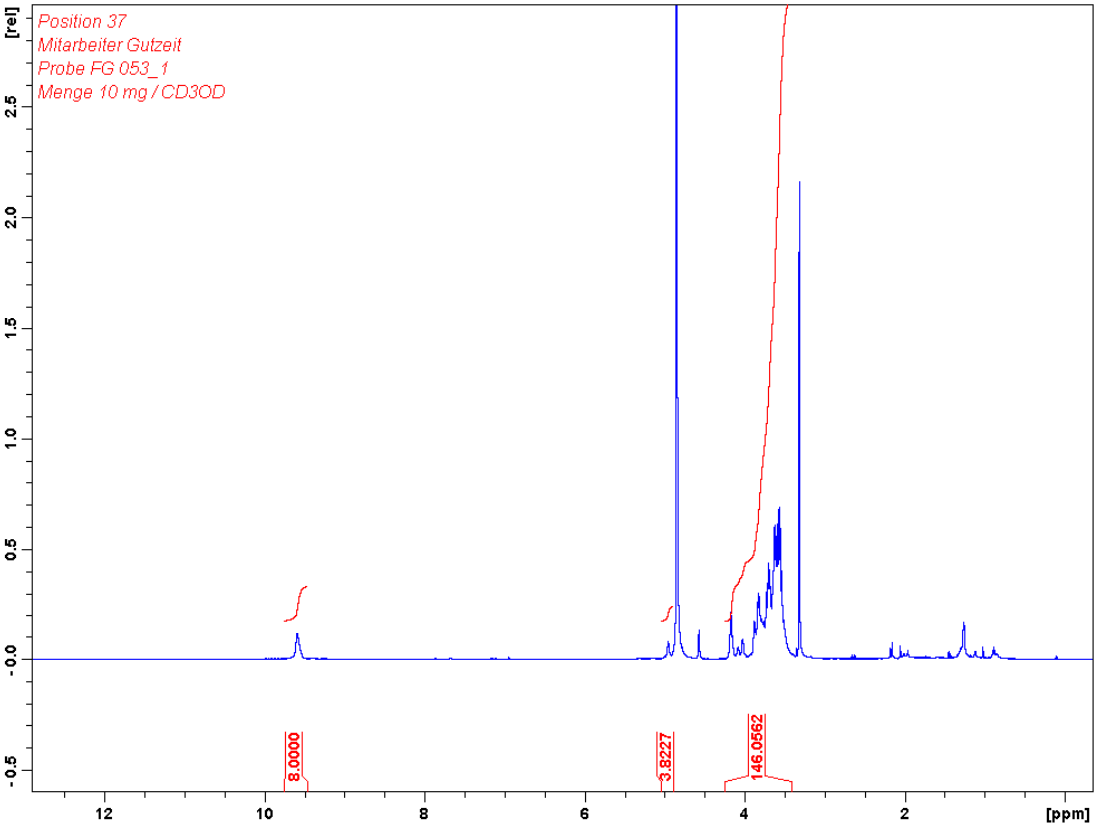

Fig S11 ^{1}H NMR spectrum of **4** in methanol-d_4.

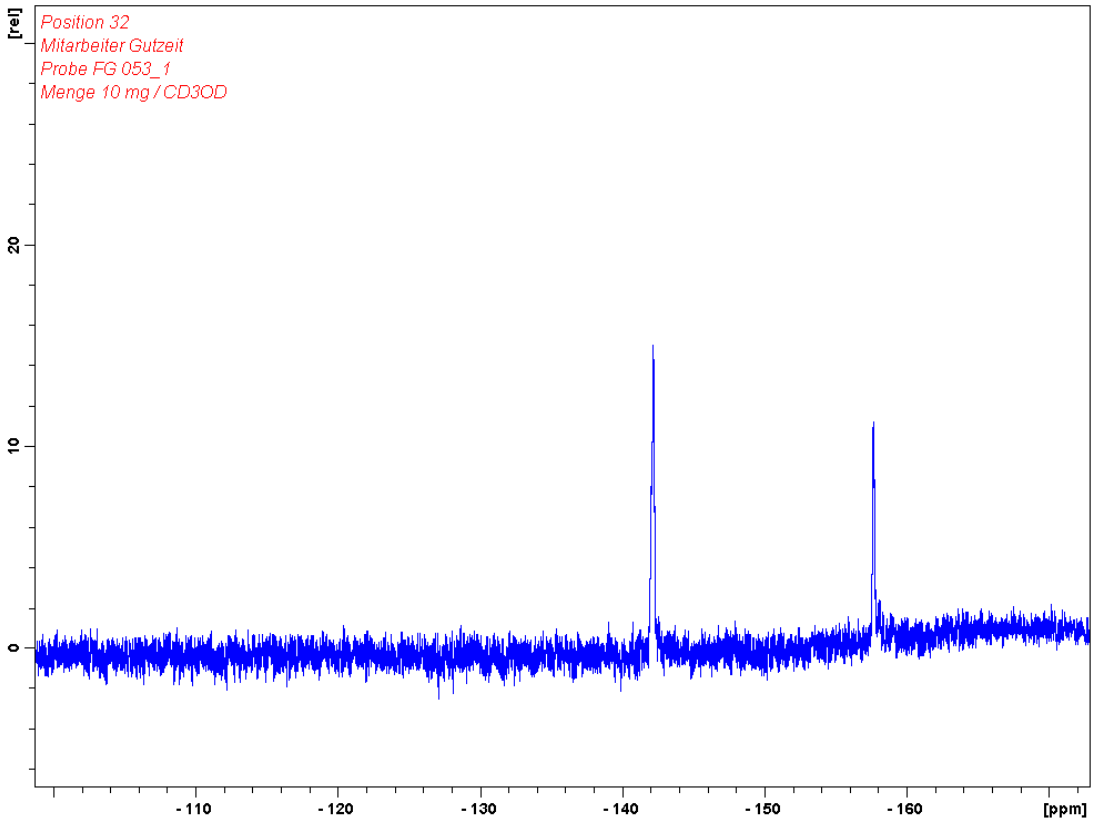

Fig S12 ^{19}F NMR spectrum of **4** in methanol-d_4.

Tab S1 Overview of absorption maxima and extinction coefficients of water soluble glycerol substituted porphyrins **12** and **14**.

Compound (solvent)	λ_{max} (ε) / nm (L cm^{-1} mol^{-1})		
3 (MeOH)	409 (271200)	504 (19500)	581 (5850)
3 (H_2O)	419 (249650)	509 (17820)	582 (5850)
4 (MeOH)	401 (230400)	520 (15370)	554 (11360)
4 (H_2O)	409 (177130)	524 (15220)	559 (10030)

III. UV-vis titration

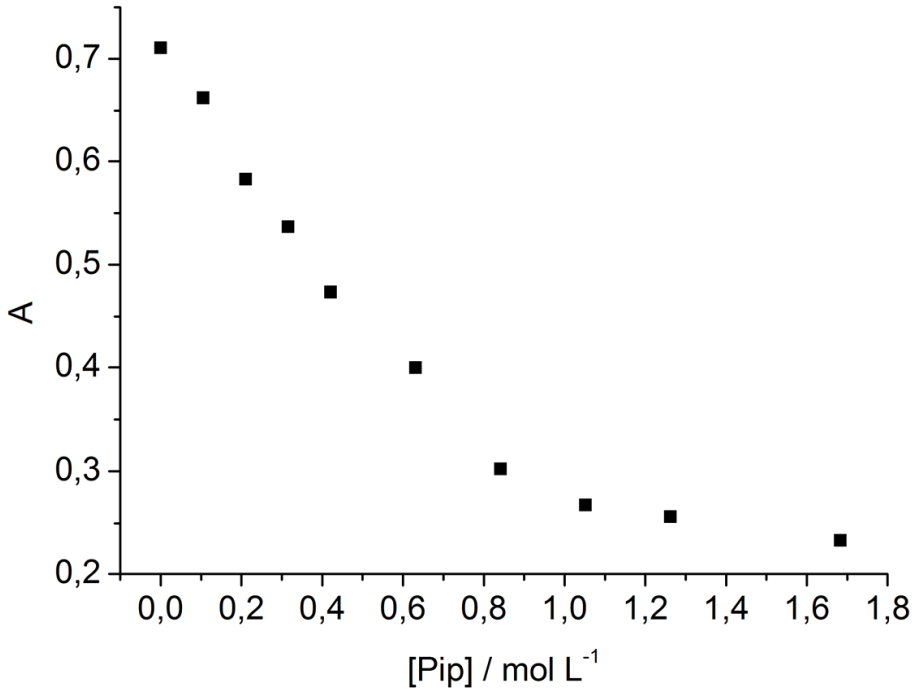

Fig S13 UV-Vis titration of Ni-porphyrin **4** with piperidine. The concentration of the aqueous solution of the porphyrin was 4.05 μmol L^{-1}.

At least two complex formation reactions have to be considered (Fig. S14):

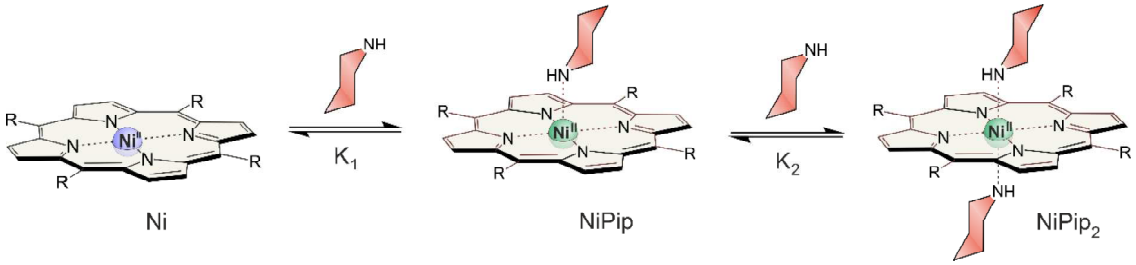

Fig S14 Formation of the square pyramidal and the square bipyramidal complexes upon titration with piperidine.

Formation of square pyramidal paramagnetic complex: $K_1 = \frac{[NiPip]}{[Ni][Pip]} = 0.481$ (eq 1)

Formation of square bipyramidal paramagnetic complex: $K_2 = \frac{[NiPip_2]}{[NiPip][Pip]} = 14.662$ (eq 2)

The paramagnetic complexes NiPip and $NiPip_2$ cannot be observed separately. Assuming their absorption wavelengths and extinction coefficients are almost equal, the overall concentration of paramagnetic Ni-complexes (NiPip and $NiPip_2$) and diamagnetic Ni-complex (Ni) can be estimated from the decreasing absorption at 409 nm by nonlinear fitting (SSQ = 0.005).[2] Piperidine is a strong base (pK_a = 11.12). For the calculation of K_1 and K_2 the concentration of the free base ($[Pip]_{eff}$) was considered using the formula for strong bases:

$$[Pip]_{eff} = [Pip] - [PipH^+] = [Pip] - \left(-\frac{K_B}{2} + \sqrt{\frac{K_B^2}{4} + K_B c_0} \right) \qquad \text{(eq 3)}$$

Tab. S2 Results of the titration series.

[Pip]	$[Pip]_{eff}$	A (409 nm)	[Ni]	[NiPip]	$[NiPip_2]$
mol L^{-1}	mol L^{-1}		mol L^{-1}	mol L^{-1}	mol L^{-1}
0.000	0.000	0.71064	4.050E-06	0.000E+00	0.000E+00
0.105	0.086	0.66223	3.704E-06	1.531E-07	1.930E-07
0.210	0.183	0.58275	3.059E-06	2.690E-07	7.215E-07
0.316	0.282	0.53681	2.389E-06	3.237E-07	1.337E-06
0.421	0.382	0.47362	1.833E-06	3.362E-07	1.881E-06
0.631	0.583	0.39976	1.102E-06	3.088E-07	2.640E-06
0.842	0.786	0.30235	7.066E-07	2.670E-07	3.076E-06
1.052	0.990	0.26764	4.833E-07	2.300E-07	3.337E-06
1.262	1.194	0.25638	3.484E-07	2.000E-07	3.502E-06
1.683	1.604	0.2325	2.034E-07	1.569E-07	3.690E-06

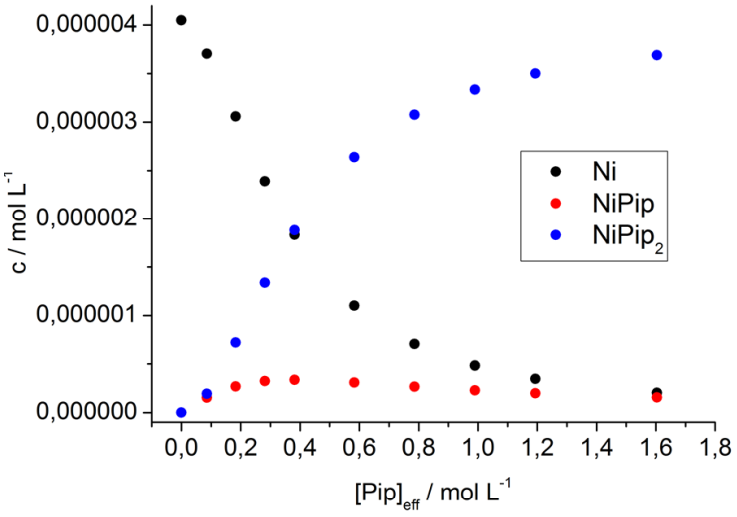

Fig S15 Concentrations of the complexes Ni, NiPip and $NiPip_2$ as a function of added piperidine in the titration experiment.

The values for K_1 and K_2 are small compared to the corresponding association constants in organic solution obtained by similar experiments.[3-5] The ligand seems to be drastically decreased in its donor strength because of hydrogen bonding.

IV. Aggregation investigation

The glycerol functionalised porphyrins **3** and **4** do not exhibit aggregation or excimer formation which is probably due to the large steric hindrance of the polyols. Solutions of **3** and **4** perfectly follow the Lambert-Beer law up to a concentration of 50 µM (Fig. S16).

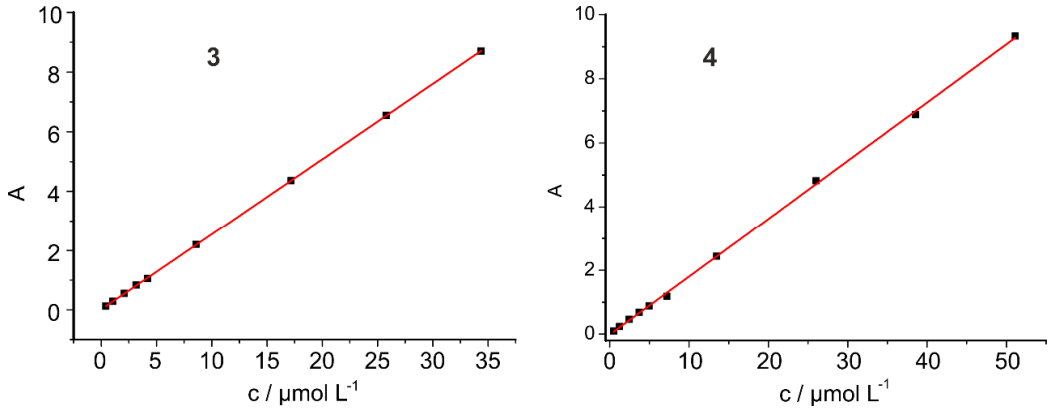

Fig. S16 Absorption of solutions of **3** (λ = 419 nm) and **4** (λ = 409 nm) in water as a function of molar concentration perfectly follows the Lambert-Beer law up to a concentration of 35 or 50 µM.

To investigate the aggregation of **3** and **4** at higher concentrations, NMR spectra at different concentrations were measured (Fig S17).

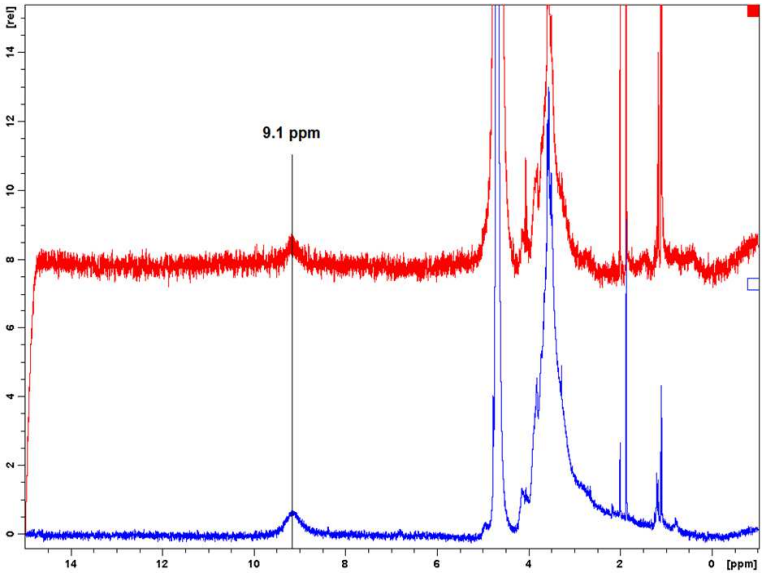

Fig S17 ^{1}H NMR spectra of 0.8 mM (blue) and 0.08 mM (red) solutions of water soluble porphyrin **4**. The signal of pyrrole protons do not exhibit a downfield shift or broadening at higher concentrations which proves that there is no aggregation.

V. Relaxation time experiments

Longitudinal relaxation times (T_1) were measured in water using an inversion recovery spin echo sequence (2D, TE/TR=6.3/3000 ms, 24 inversion times (TI 50 - 2000 ms), spatial resolution 300 x 300 µm^2, slice thickness 700 µm) at a 7 T MRI spectrometer (ClinScan 70/30 USR, Bruker Biospin, Germany). Relaxation follows first order exponential decay:

$$I(t) = I_0 + Pe^{\left(-\frac{t}{T_1}\right)} \qquad \text{(eq 4)}$$

I (t): Intensity

I_0: Intensity after 180 ° pulse

P: Pre-exponential factor

T_1: Relaxation time

To determine the effect of the coordination induced spin state switch (CISSS) on the relaxation time four samples were investigated:

1. 2 mM solution of **4**
2. Water
3. Water + piperidine (20 %)
4. 2 mM solution of **4** + piperidine (20 %)

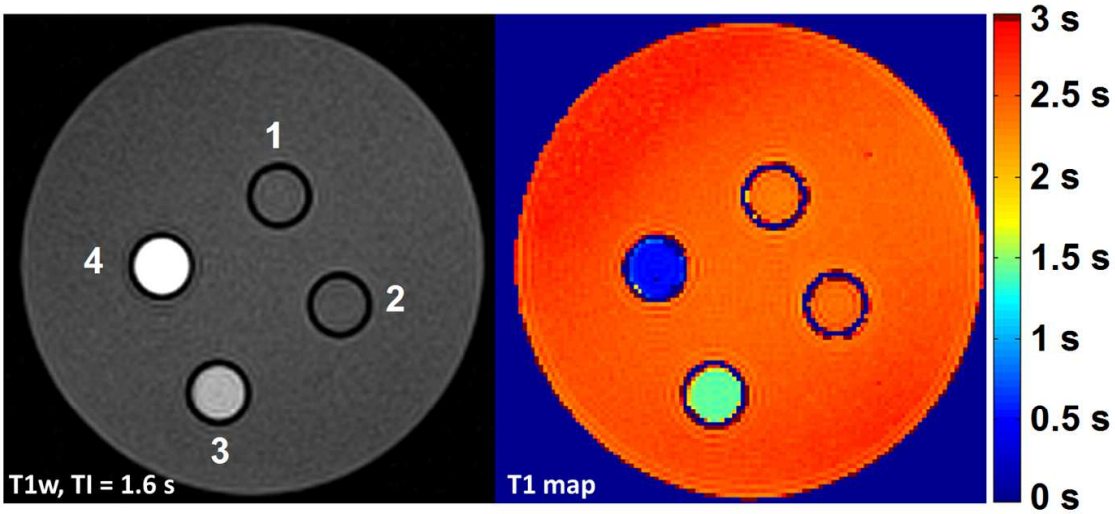

Fig S18 MR images of 1. **14** (2 mM in water), 2. Water, 3. Water + 20 % piperidine and 4. **14** (2 mM in water + 20 % piperidine).

Tab. S3 Relaxation times (T_1) and relaxation rates (T_1^{-1}) of the observed samples. Times and errors were determined from MR images (Fig. 7).

Samples	T_1 / ms	T_1^{-1} / s^{-1}
1. 2 mM solution of **4**	2350 +/- 38	0.426
2. Water	2410 +/- 45	0.415
3. Water + piperidine (20 %)	1415 +/- 13	0.707
4. 2 mM solution of **4** + piperidine (20 %)	510 +/- 13	1.961

From the relaxation time of the 2 mM solution **4**·Pip_2 the relaxivity is estimated to be 0.627 $mM^{-1}s^{-1}$ (eq 5)

$$T_1^{-1} = T_s^{-1} + R_1[c] \qquad \text{(eq 5)}$$

T_1^{-1}: relaxation rate (1,961 s^{-1})

T_s^{-1}: relaxation rate of solution without paramagnetic substance (0,707 s^{-1})

R_1: T_1 relaxivity / $(mmol)^{-1}s^{-1}$ or $mM^{-1}s^{-1}$

$[c]$: concentration of paramagnetic substance (2 mmol)

Literature

1 J. S. Lindsey and R. W. Wagner, *J. Org. Chem.*, 1989, **54**, 828–836.

2 S. del Piero, A. Melchior, P. Polese, R. Portanova and M. Tolazzi, *Annali di Chimica*, 2006, **96**, 29–49.

3 S. Thies, C. Bornholdt, F. Köhler, F. D. Sönnichsen, C. Näther, F. Tuczek and R. Herges, *Chem. Eur. J.*, 2010, **16**, 10074–10083.

4 S. Thies, H. Sell, C. Bornholdt, C. Schütt, F. Köhler, F. Tuczek and R. Herges, *Chem. Eur. J.*, 2012, **18**, 16358–16368.

5 S. Thies, H. Sell, C. Schütt, C. Bornholdt, C. Näther, F. Tuczek and R. Herges, *J. Am. Chem. Soc.*, 2011, **133**, 16243–16250.

7 Novel Ni-platforms for the CISSS

For *in vivo* applications of photoswitchable molecules some practical aspects have to be considered. Light can be applied from outside the body (performed for the treatment of dermal cancer with photodynamic therapy) or by optical fibers e.g. during catheter based interventions.[143] However, blood supported tissue is not transparent at the absorption wavelengths of Ni-porphyrins. Blood consists of roughly 55% plasma (mainly water) and 45% erythrocytes (cells) which contain the oxygen-transporting agent hemoglobin.[144,145] This protein is a tetramer of four subunits containing Fe-porphyrin as prosthetic group. The blood hemoglobin concentration is an important physiological parameter, e.g. for blood donations. For a healthy human being the value should be $12 - 18\,\mathrm{g\,l^{-1}}$ dl^{-1} which is equivalent to $7 - 12\,\mathrm{mmol\,l^{-1}}$.[146–148] The penetration depth of light through such a dense solution is very low, for the required switching wavelengths 435 nm and 500 nm less than 1 mm.[149] Consequently, an efficient photoswitching of Ni-porphyrins under *in vivo* conditions cannot be realized. Figure 7.1 shows the penetration depth of light into tumor.

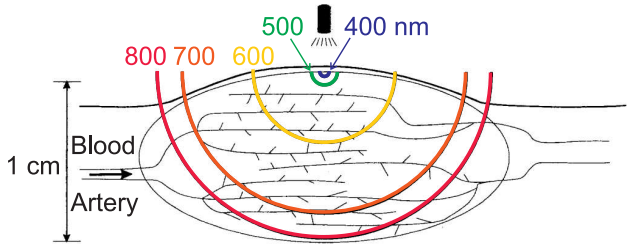

Figure 7.1: Penetration depth of light into a tumor.[143]

For efficient photoswitching under *in vivo* conditions a molecule must be addressable by light within the bio-optical window (between 650 nm and 800 nm) which is the region with the highest penetration depth.[143,149] So far the CISSS and LD-CISSS were exclusively proved for porphyrins as square planar Ni-platforms. To obtain longer switching wavelengths, Ni-complexes with bathochromic absorptions have to be considered.

7.1 Coordination-Induced Spin State Switching with Nickel Chlorin and Nickel Isobacteriochlorin

Marcel Dommaschk, Vanessa Thoms, Christian Schütt, Christian Näther, Rakesh Puttreddy, Kari Rissanen and Rainer Herges

Inorg. Chem. **2015**, *54*, 9390-9392.
DOI:10.1021/acs.inorgchem.5b01756

Summary

The electron-deficient Ni-chlorin **17** and Ni-isobacteriochlorin **18** were synthesized and investigated regarding their applicability as square planar Ni-platforms for a CISSS. The compounds were prepared by cycloaddition of *N*-methyl azomethine ylide to Ni-TPPF$_{20}$ (**3**). Similar macrocycles are known to exhibit bathochromically shifted absorption bands compared to the corresponding porphyrins which could be confirmed. The absorption maxima of the longest wavelength Q bands are 613 nm for **17** and 596 nm for **18**. The association constant of axial ligands is the most important parameter for the CISSS. Therefore, the coordination of pyridine to all three compounds (**3**, **17** and **18**) was investigated by NMR titrations. A tremendous increase of the association constant from porphyrin to chlorin to isobacteriochlorin was observed. The improvement is most pronounced for the coordination of the first pyridine which is the key step for the CISSS. K_1 rises from 8 l mol^{-1} (Ni-porphyrin **3**) to 91 l mol^{-1} (Ni-chlorin **17**) to 441 l mol^{-1} (Ni-isobacteriochlorin **18**). Hence, the novel Ni-macrocycles are superior Ni-platforms. Crystal structures were obtained for all three paramagnetic bis(pyridine) complexes. The increased binding strength reflects in a shorter pyridine-Ni(II) bond length in solid state.

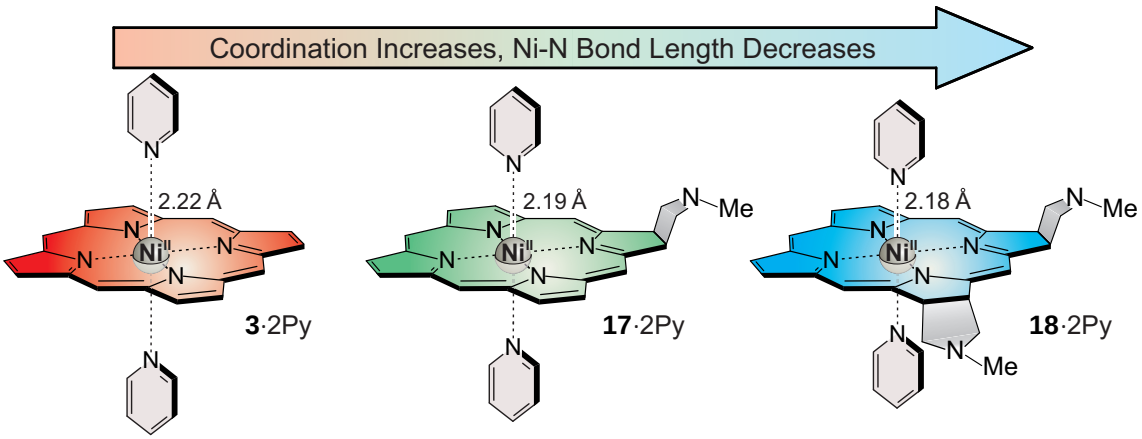

Figure 7.2: The axial association of pyridine to the Ni(II) increases from Ni-TPPF$_{20}$ (**3**) to Ni-TPCF$_{20}$ (**17**) to Ni-TPIBF$_{20}$ (**18**) which is also reflected in shorter pyridine-Ni(II) bond (Ni-N).

The results demonstrate that magnetic switching by the CISSS is not limited to Ni-porphyrins. The presented Ni-chlorin and Ni-isobacteriochlorin platforms exhibit superior absorption and association properties. Furthermore, they can be the basis for novel RP designs. Instead of the methyl group an appropriate photochromic ligand could be attached to the pyrrolidine.

Inorganic Chemistry
Communication
pubs.acs.org/IC

Coordination-Induced Spin-State Switching with Nickel Chlorin and Nickel Isobacteriochlorin

Marcel Dommaschk,[†] Vanessa Thoms,[†] Christian Schütt,[†] Christian Näther,[‡] Rakesh Puttreddy,[§] Kari Rissanen,[§] and Rainer Herges*[,†]

[†]Otto-Diels-Institut für Organische Chemie, Christian-Albrechts-Universität, Otto-Hahn-Platz 4, D-24098 Kiel, Germany
[‡]Institut für Anorganische Chemie, Christian-Albrechts-Universität, Otto-Hahn-Platz 6/7, 24098 Kiel, Germany
[§]Department of Chemistry, Nanoscience Center, University of Jyvaskyla, P.O. Box 35, 40014 Jyvaskyla, Finland

Supporting Information

ABSTRACT: We present the first coordination-induced spin-state switching with nickel chlorin and nickel isobacteriochlorin. The spin-state switching was monitored by UV−vis spectroscopy and NMR titration experiments. The association constants (K_1 and K_2) and thermodynamic parameters (ΔH and ΔS) of the coordination of pyridine were determined. The first X-ray analyses of a paramagnetic nickel chlorin and a nickel isobacteriochlorin provide further information about the structure of the octahedral complexes. Nickel chlorin and even more pronounced nickel isobacteriochlorin exhibit stronger coordination of axial ligands compared to the corresponding nickel porphyrin and thus provide the basis for more efficient spin-switching systems.

Nickel(II) can exist in two different spin states ($S = 0$ and 1). The spin state of nickel complexes in solution is known to depend on the coordination number and geometry. A frequently used method to control the spin state is the addition of ligands to a square-planar nickel complex ($S = 0$).[1−4] Axial-ligand coordination gives rise to the formation of square-pyramidal and octahedral complexes and converts the nickel(II) to the $S = 1$ state.[5−7] This process was coined coordination-induced spin-state switching (CISSS).[8] Preconditions for the design of efficient spin-switching systems are rigid square-planar nickel complexes that allow strong coordination of axial ligands. Nickel porphyrins have proven to be suitable. With photochromic ligands, the coordination number and spin state can be controlled by irradiation with light (light-driven CISSS).[9−12] As previously shown, this process has been used to change the contrast in magnetic resonance imaging (MRI).[13,14] The square-planar complex is MRI-silent (contrast off), whereas the axial complexes are paramagnetic and active (contrast on). The CISSS approach provides the basis for the design of smart MRI contrast agents, which have a high potential for applications in functional medical imaging.

The nickel porphyrin systems that have been developed toward this end so far still suffer from drawbacks, mainly in view of medical applications. Axial coordination has to be improved, and the wavelength of light for addressing the systems in vivo has to be shifted toward the biooptical window (650−950 nm), where blood-supported tissue is transparent (penetration depth of up to 20 mm). To solve these problems, we explore the implementation of nickel chlorins and nickel isobacteriochlorins in CISSS systems because they are known to have bathochromic-shifted absorption bands compared to the corresponding porphyrins.

We started from *meso*-tetrakis(pentafluorophenyl)nickel porphyrin (Ni-TPPF$_{20}$, **1**), whose complex formation with pyridine is well investigated and which is a common platform for CISSS.[8,9,11] Chlorins and isobacteriochlorins can be prepared by the reduction of porphyrins. In the case of electron-deficient porphyrins, however, cycloaddition reactions are more convenient to convert β double bonds to C−C single bonds (Supporting Information). Hence, we applied the method of Cavaleiro et al. using *N*-methylglycine and formaldehyde in boiling toluene (Scheme 1).[15−17] The corresponding chlorin

Scheme 1. Formation of 2 and 3 by the 1,3-Dipolar Cycloaddition of 1 and an Azomethine Ylide Formed in Situ by the Reaction of *N*-Methylglycine and Formaldehyde

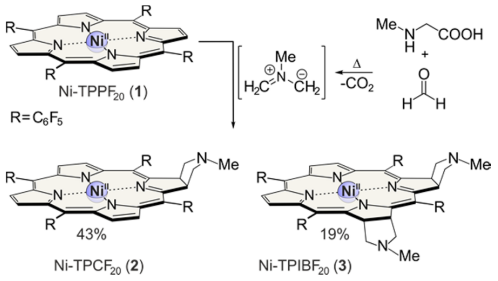

(Ni-TPCF$_{20}$, **2**) and isobacteriochlorin (Ni-TPIBF$_{20}$, **3**) were obtained with 43 and 19% yield (Supporting Information). No detectable amounts of bacteriochlorin and syn-configured isobacteriochlorin were observed, which confirms the selectivity of this reaction with the free base porphyrin.[16]

The nickel macrocycles **2** and **3** were investigated with UV−vis spectroscopy (Figure 1). The most bathochromic absorption bands (Q bands) were found at 554 nm for the porphyrin, at 596 nm for the nickel isobacteriochlorin **3**, and at 613 nm for the

Received: August 4, 2015
Published: September 24, 2015

DOI: 10.1021/acs.inorgchem.5b01756
Inorg. Chem. 2015, 54, 9390−9392

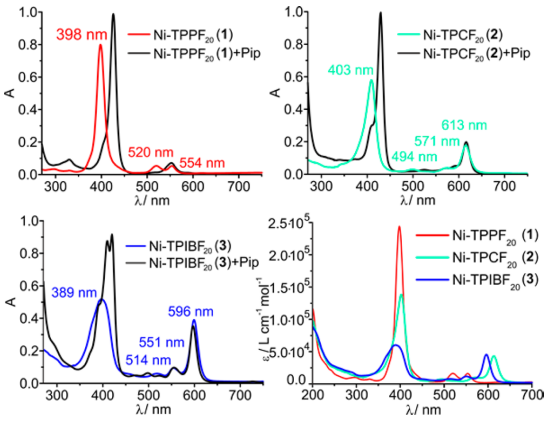

Figure 1. (top and bottom left) UV–vis spectra of compounds **1**–**3** in pure MeCN (red, green, and blue) and with an excess of piperidine in MeCN (black). (bottom right) Comparison of the extinction coefficients of compounds **1**–**3**.

nickel chlorin **2**. The latter absorption is close to the near-IR window and has a measurable absorption at >650 nm. An even larger bathochromic shift was observed for the metal-free chlorin (652 nm).[16] The extinction coefficients of the Soret bands are decreasing from **1** to **2** to **3**, in contrast to the more interesting Q bands, for which the order is in reverse (**3** to **2** to **1**). All three compounds exhibit a bathochromic shift of the Soret band upon the addition of piperidine, which is due to formation of the paramagnetic octahedral complex.[18]

The capability of a nickel complex to perform CISSS is quantified by the association constants. It is important to consider that there are two association processes. The coordination of the first axial ligand to form the paramagnetic square-pyramidal complex is described by the association constant K_1, and the coordination of the second ligand to form the octahedral complex is denoted as K_2 (Figure 2). Note that K_1 is the key parameter

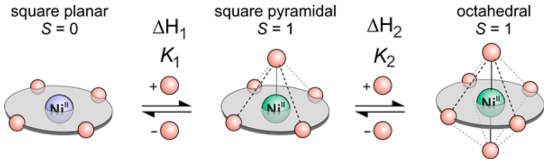

Figure 2. Formation of square-pyramidal and octahedral nickel complexes as described by the association constants (K_1 and K_2) and the complex formation enthalpies (ΔH_1 and ΔH_2).

because in this step the spin state of the nickel changes from $S = 0$ (singlet) to 1 (triplet). Whereas the two sides of **1** and **3** are homotopic, there are two different possibilities for the coordination of the first ligand to the nickel chlorin **2** (Scheme 1). According to our calculations, both 1:1 complexes (syn and anti to the pyrrolidine ring) are isoenergetic (ΔE = 0.13 kcal mol^{-1}; Supporting Information) because there is very little steric repulsion between the axial ligand and the pyrrolidine unit. Hence, we use the same binding model as that for the nickel porphyrin **1** and nickel isobacteriochlorin **3** (Figure 2).

The association constants of pyridine with the nickel porphyrin **1**, nickel chlorin **2**, and nickel isobacteriochlorin **3** were determined by ^{1}H NMR spectroscopy (toluene-d_8; see Supporting Information). Surprisingly, the key parameter for the spin switch, K_1, drastically increases with the number of saturated double bonds in the macrocycle (Table 1). The nickel

Table 1. Association Constants (K_1 and K_2; 300 K, Toluene-d_8) of Pyridine to 1,[8] 2, and 3[a]

	K_1 (L mol^{-1})	K_2 (L mol^{-1})
Ni-TPPF$_{20}$ (**1**)	7.8	20.5
Ni-TPCF$_{20}$ (**2**)	91.1	43.4
Ni-TPIBF$_{20}$ (**3**)	441.0	77.5

[a]All values and titration curves are given in the Supporting Information.

chlorin **2** binds pyridine 12 times stronger and the nickel isobacteriochlorin **3** even 57 times stronger than the nickel porphyrin **1**. Hence, nickel chlorins, and even more so nickel isobacteriochlorins, are better platforms for CISSS.

From temperature-dependent measurements of the association constants, the thermodynamic parameters (ΔH and ΔS) for complex formation were determined (Table 2). The entropies

Table 2. ΔH and ΔS Values for the Association of Pyridine to 1,[8] 2, and 3 Determined by the Temperature Dependence of the Association Constants (Supporting Information)

	ΔH_1 (kcal mol^{-1})	ΔS_1 (cal mol^{-1} K^{-1})	ΔH_2 (kcal mol^{-1})	ΔS_2 (cal mol^{-1} K^{-1})
Ni-TPPF$_{20}$ (**1**)	−5.3	−13.6	−6.0	−13.9
Ni-TPCF$_{20}$ (**2**)	−6.9	−14.1	−6.2	−13.0
Ni-TPIBF$_{20}$ (**3**)	−8.0	−14.6	−7.0	−14.9

ΔS_1 and ΔS_2 for all processes are almost equal (−13.6 to −14.9 cal mol^{-1} K^{-1}). Hence, the association enthalpies ΔH_1 and ΔH_2 exhibit the same trend as the association constants K_1 and K_2. The key parameter ΔH_1 for **1**–**3** increases more strongly than ΔH_2.

These trends are very well reproduced by quantum-chemical calculations. Previously, we have shown that the B3LYP/def2TZVP//PBE/SVP level of density functional theory (DFT) is a good compromise between the computational costs and accuracy for the calculation of binding energies in nickel porphyrins.[9,10] Table 3 compares the experimental and theoretical values for **1**–**3**. Obviously, this DFT level is also reliable for nickel chlorins and nickel isobacteriochlorins.

Table 3. Experimental (ΔH) and Theoretical (E_f) Values (B3LYP/def2TZVP//PBE/SVP) of Complex Formation Energies of 1–3 with Two Pyridine Ligands

	$\Delta H_1 + \Delta H_2$ (kcal mol^{-1})	E_f (kcal mol^{-1})
Ni-TPPF$_{20}$ (**1**)	−11.3	−10.8
Ni-TPCF$_{20}$ (**2**)	−13.1	−12.1
Ni-TPIBF$_{20}$ (**3**)	−15.0	−13.6

We were able to obtain single-crystal structures of the bis(pyridine) complexes of **1**–**3** (**1**·2Py, **2**·2Py, and **3**·2Py; Figure 3), which allows (for the first time) the direct comparison of the structures of paramagnetic nickel porphyrins and saturated analogues. As expected from the increasing binding energies in **1**–**3**, the coordinative Ni–N bond length decreases. The coordination sphere of the nickel ion in all three complexes is octahedral with tetragonal distortion (square-bipyramidal). Whereas the porphyrin unit in **1**·2Py is perfectly planar, slight

DOI: 10.1021/acs.inorgchem.5b01756
Inorg. Chem. 2015, 54, 9390–9392

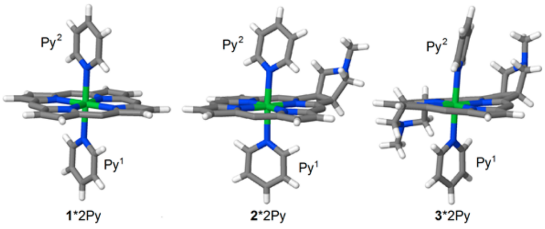

Figure 3. Single-crystal structure of octahedral complexes of the nickel porphyrin **1** (left), nickel chlorin **2** (middle), and nickel isobacteriochlorin **3** (right) with pyridine as the axial ligand. The C_6F_5 substituents at the meso positions were omitted.

ruffling is observed in chlorin **2**·2Py and is even more pronounced in isobacteriochlorin **3**·2Py, which is quantified by the maximum torsion angle between the four porphyrin nitrogen atoms (N_4 torsion; see Table 4). The axial pyridines are perfectly orthogonal

Table 4. Structural Parameters of 1·2Py, 2·2Py, and 3·2Py[a]

		Ni–N bond/Å		tilt	Py^1Py^2	N_4-	space-
		crystal	calc.	angle	twist	torsion	group
1·2Py	Py^1	2.223	2.205	0°	0°	0°	P-1
	Py^2	2.223	2.205	0°			
2·2Py	Py^1	2.185	2.191	0°	20°	1.4°	$P2_1/c$
	Py^2	2.199	2.198	10°			
3·2Py	Py^1	2.181	2.185	2°	27°	3.1°	P-1
	Py^2	2.192	2.185	10°			

[a]The overlay of calculated (PBE/SVP) and crystal structure is provided in the Supporting Information.

to the porphyrin plane in **1**·2Py. In **2**·2Py and **3**·2Py, one of the pyridines is 10° tilted, which is probably a packing effect. The suboptimal binding angle results in a slightly increased bond length (Table 4). In **1**·2Py, the pyridines (Py^1 and Py^2) are perfectly coplanar, whereas they are twisted in **2**·2Py and are even more pronounced in **3**·2Py. Interesting structural parameters are summarized in Table 4.

By crystallization in the absence of pyridine, we obtained single-crystal structures of the diamagnetic nickel porphyrin **1** and a linear coordination polymer of the nickel chlorin **2**. The structures are in good agreement with the calculated structures at the PBE/SVP level of DFT (Supporting Information).

In summary, we show that nickel chlorins and nickel isobacteriochlorins are superior as square-planar platforms for CISSS compared to the corresponding nickel porphyrins. The association constants with axial ligands increase with the number of double bonds that are replaced by single bonds (porphyrin < chlorin < isobacteriochlorin). A strong coordination of the axial ligand is important for the development of water-soluble systems because the coordination strength in water is reduced by hydrogen bonding to the ligand. Moreover, the absorption is shifted to longer wavelengths. The nickel chlorin **2** has a Q band at 613 nm, which extends into the biooptical window (650–950 nm). Nickel bacteriochlorins absorb at even longer wavelengths (~700 nm) and, therefore, are our next targets.[16] Further studies are devoted toward substitution of the pyrrolidine nitrogen with photochromic azopyridine switches to prepare spin switches that can be controlled with near-IR light.[10,12,13] These compounds are interesting candidates as functional MRI contrast agents with potential applications in functional imaging and interventional radiology.[19]

■ ASSOCIATED CONTENT

Supporting Information

The Supporting Information is available free of charge on the ACS Publications website at DOI: 10.1021/acs.inorgchem.5b01756.

Experimental details, full characterization of all new compounds, data evaluation of the titration experiments, computational details, and XRD data (PDF)

CCDC 1415585 (**1**), 1415586 (**1**·2Py), 1415587 (**2**), 1407134 (**2**·2Py), and 1415588 (**3**·2Py) (CIF)

■ AUTHOR INFORMATION

Corresponding Author

*E-mail: rherges@oc.uni-kiel.de. Phone: +49 431 880 2440.

Notes

The authors declare no competing financial interest.

■ ACKNOWLEDGMENTS

This work has been supported by the Deutsche Forschungsgemeinschaft within the SFB 677 "Function by Switching" and the Academy of Finland (Grants 263256 and 265328 to K.R.).

■ REFERENCES

(1) Caughey, W. S.; Deal, R. M.; McLees, B. D.; Alben, J. O. *J. Am. Chem. Soc.* **1962**, *84*, 1735–1736.
(2) Caughey, W. S.; Fujimoto, W. Y.; Johnson, B. P. *Biochemistry* **1966**, *5*, 3830–3843.
(3) Cole, S. J.; Curthoys, G. C.; Magnusson, E. A.; Phillips, J. N. *Inorg. Chem.* **1972**, *11*, 1024–1028.
(4) McLees, B. D.; Caughey, W. S. *Biochemistry* **1968**, *7*, 642–652.
(5) Kim, D.; Su, Y. O.; Spiro, T. G. *Inorg. Chem.* **1986**, *25*, 3988–3993.
(6) Song, Y.; Haddad, R. E.; Jia, S.-L.; Hok, S.; Olmstead, M. M.; Nurco, D. J.; Schore, N. E.; Zhang, J.; Ma, J.-G.; Smith, K. M.; Gazeau, S.; Pécaut, J.; Marchon, J.-C.; Medforth, C. J.; Shelnutt, J. A. *J. Am. Chem. Soc.* **2005**, *127*, 1179–1192.
(7) Bütje, K.; Nakamoto, K. *Inorg. Chim. Acta* **1990**, *167*, 97–108.
(8) Thies, S.; Bornholdt, C.; Köhler, F.; Sönnichsen, F. D.; Näther, C.; Tuczek, F.; Herges, R. *Chem. - Eur. J.* **2010**, *16*, 10074–10083.
(9) Thies, S.; Sell, H.; Bornholdt, C.; Schütt, C.; Köhler, F.; Tuczek, F.; Herges, R. *Chem. - Eur. J.* **2012**, *18*, 16358–16368.
(10) Dommaschk, M.; Schütt, C.; Venkataramani, S.; Jana, U.; Näther, C.; Sönnichsen, F. D.; Herges, R. *Dalton Trans.* **2014**, *43*, 17395–17405.
(11) Thies, S.; Sell, H.; Schütt, C.; Bornholdt, C.; Näther, C.; Tuczek, F.; Herges, R. *J. Am. Chem. Soc.* **2011**, *133*, 16243–16250.
(12) Venkataramani, S.; Jana, U.; Dommaschk, M.; Sönnichsen, F. D.; Tuczek, F.; Herges, R. *Science* **2011**, *331*, 445–448.
(13) Dommaschk, M.; Peters, M.; Gutzeit, F.; Schütt, C.; Näther, C.; Sönnichsen, F. D.; Tiwari, S.; Riedel, C.; Boretius, S.; Herges, R. *J. Am. Chem. Soc.* **2015**, *137*, 7552–7555.
(14) Dommaschk, M.; Gutzeit, F.; Boretius, S.; Haag, R.; Herges, R. *Chem. Commun.* **2014**, *50*, 12476–12478.
(15) Silva, A. M. G.; Tomé, A. C.; Neves, M. G. P. M. S.; Silva, A. M. S.; Cavaleiro, J. A. S. *Chem. Commun.* **1999**, 1767–1768.
(16) Silva, A. M. G.; Tomé, A. C.; Neves, M. G. P. M. S.; Silva, A. M. S.; Cavaleiro, J. A. S. *J. Org. Chem.* **2005**, *70*, 2306–2314.
(17) de Souza, J. M.; de Assis, F. F.; Carvalho, C. M.; Cavaleiro, J. A.; Brocksom, T. J.; de Oliveira, K. T. *Tetrahedron Lett.* **2014**, *55*, 1491–1495.
(18) Kaplan, W. A.; Scott, R. A.; Suslick, K. S. *J. Am. Chem. Soc.* **1990**, *112*, 1283–1285.
(19) Herges, R.; Jansen, O.; Tuczek, F.; Venkatamarani, S. Molecular Switch. Patent WO 2012022299 A1, Feb 23, 2012.

DOI: 10.1021/acs.inorgchem.5b01756
Inorg. Chem. 2015, 54, 9390–9392

Coordination Induced Spin State Switch with Ni-Chlorin and Ni-Isobacteriochlorin.

Marcel Dommaschk[†], Vanessa Thoms[†], Christian Schütt[†], Christian Näther[§], Rakesh Puttreddy[‡], Kari Rissanen[‡], Rainer Herges*[,†]

[†] Otto-Diels-Institut für Organische Chemie, Christian-Albrechts-Universität, Otto-Hahn-Platz 4, D-24098 Kiel, Germany

[§] Institut für Anorganische Chemie, Christian-Albrechts-Universität, Otto-Hahn-Platz 6/7, 24098 Kiel, Germany

[‡] University of Jyvaskyla, Department of Chemistry, Nanoscience Center, P. O. Box 35, 40014 University of Jyvaskyla, Finland

Table of Contents

I Synthesis of metal free chlorins

The double bonds of a metal free porphyrin can directly be reduced with diimide which is released from *p*-toluenesulfonylhydrazine (Scheme 1, a).[1-3] This method is not working well for electron deficient porphyrins. Furthermore the reaction conditions are very harsh so the porphyrins cannot contain sensitive functional groups. Another option is to treat a porphyrin with osmium tetraoxide to obtain vicinal dihydroxy compounds (Scheme 1, b).[4-8] The most recent approaches use the porphyrin double bond for a cycloaddition reaction. This is particular useful for electron deficient porphyins. [4+2] Cycloaddition with *o*-benzoquinodimethane[9] (Scheme 1, c) and pentacene[10] as well as [3+2] cycloaddition with nitrones[11, 12] (Scheme 1, d) and azomethine ylides[13-15] (Scheme 1, e) were already presented.

Scheme S1. Conversion of porphyrin to chlorin by treatment with *p*-toluenesulfonylhydrazine (a), oxidation with osmium tetraoxide (b) and cycloadditions with *o*-benzoquinodimethane (c), nitrons (d) and azomethine ylide (e).

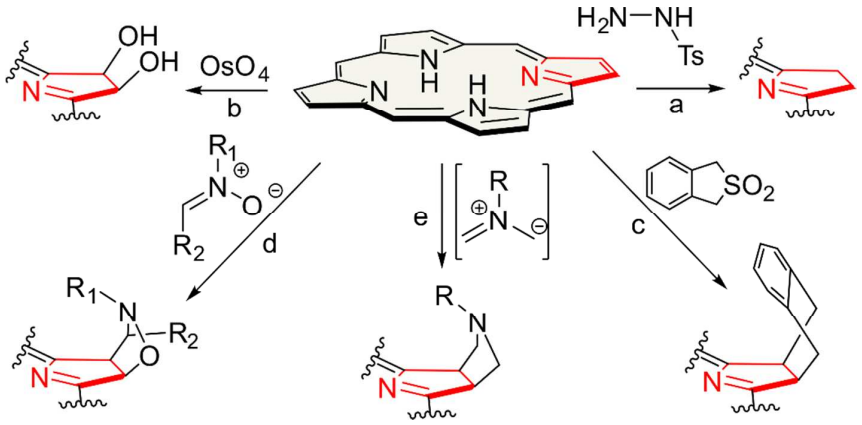

II Analytical Equipment and Methods

NMR Spectroscopy

NMR spectra were measured in deuterated solvents (Deutero). The degree of deuteration is given in parentheses. ^{1}H NMR-spectra in reference to the following signals.

acetone-d_6 (99.8 %): δ= 2.05 ppm (quint)

chloroform-d (99.8 %): δ = 7.26 ppm (s)

The signal multiplicities are abbreviated as follows.

s: singlet, d: doublet, t: triplet, q: quartet, quint: quint, m: multiplet, br: broad signal

Measurements were performed by the following instrument:

Bruker DRX 500 (^{1}H NMR: 500 MHz, ^{19}F NMR: 470 MHz)

Reference for all ^{19}F-NMR spectra is trichlorofluoromethane to the frequency of which the spectrometer is calibrated. Fluorine atoms are labeled as *o*-F, *m*-F and *p*-F (*ortho*-, *meta*- and *para*-fluorine) according to their position in the aromatic system. For the asymmetric porphyrins there are three different *meso*-positions labelled as A, B and C. ^{13}C NMR signals were not assigned. Due to the molecular dynamic of the Ni-macrocycles and the strong splitting of many signals (caused by ^1J, ^2J, ^3J, ^4J, and ^5J coupling with the ^{19}F cores) the intensities are very low and 2D correlation can hardly be observed.

IR spectroscopy

Infrared spectra were measured on a Perkin-Elmer 1600 Series FT-IR spectrometer with an A531-G Golden-Gate-Diamond-ATR-unit. Signals were abbreviated with w, m, s and vs for weak, medium, strong and very strong intensities. Broad signals are additionally labeled with br.

UV-vis spectroscopy

The UV-vis spectra were measured on a Lambda 14 spectrometer (Perkin-Elmer) with a (Büchi) thermostat (T = 20°C). Quartz cuvettes of 1 cm optical path length were used.

Mass spectrometry

High resolution mass spectra (HRMS) were measured by electron impact ionization and quadrupole time-of-flight mass analyser (EI, Q-TOF) with an AccuTOF GCv4G mass spectrometer by JEOL.

Chromatography stationary phases

For column chromatography purifications silica gel (Merck, particle size 0.040-0.063 mm) was used. R_f values were determined by thin layer chromatography on Polygram® Sil G/UV_{254} (Macherey-Nagel, 0.2 mm particle size).

III Experimental procedure and analysis for Ni-TPCF$_{20}$ (2) and Ni-TPIBF$_{20}$ (3)

meso-Tetrakis(pentafluorophenyl)nickel(II)porphyrin (Ni-TPPF$_{20}$, **1**) (250 mg, 242 μmol) was dissolved in toluene (100 mL). *N*-Methylglycin (86.3 mg, 969 μmol) and paraformaldehyde (72.6 mg, 2.42 mmol) were added and the mixture was under refux for 48 h. After 3, 6 and 27 h the addition of *N*-Methylglycin and paraformaldehyde was repeated. The solvent was removed under reduced pressure and the crude product was purified by column chromatography (silica gel, 0.040-0.063 mm, dichloromethane → dichloromethane / methanol 50:1).

Ni-TPCF$_{20}$ (**2**)
Yield: 113 mg (104 μmol, 43%) dark green crystals
R_f (dichloromethane / methanol 50:1) = 0.33

Ni-TPIBF$_{20}$ (**3**)
Yield: 55.2 mg (48.2 μmol, 19%) blue crystals
R_f (dichloromethane / methanol 50:1) = 0.12

Analytical details for Ni-TPCF$_{20}$ (**2**)

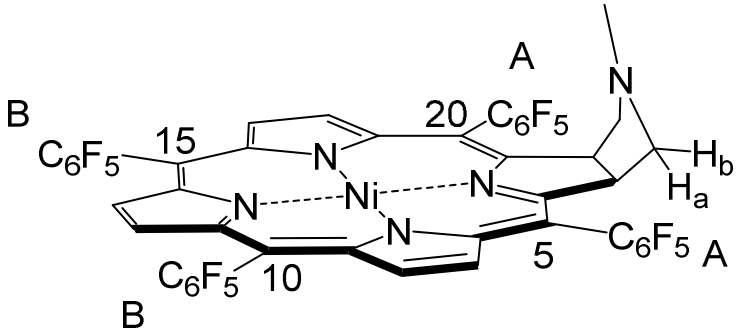

m.p.: 387.5°C

FT-IR (layer): υ = 2920 (w), 1650 (w), 1586 (w), 1516 (s), 1488 (s), 1343 (m), 1312 (m), 1203 (w), 1160 (w), 1054 (m), 984 (vs), 950 (s), 859 (m), 826 (m), 765 (s), 739 (m), 701 (m), 667 (w), 584 (w) 489 (w) cm^{-1}.

^{1}H NMR (500 MHz, 300 K, $CDCl_3$, TMS): δ = 8.38 (d, ^{3}J = 5.0 Hz, 2H, *H*-8, *H*-17), 8.26 (s, 2H, *H*-12, *H*-13), 8.02 (d, ^{3}J = 5.0 Hz, 2H, *H*-7, *H*-18), 4.94 (t, ^{3}J = 5.4 Hz, 2H, *H*-2, *H*-3), 3.08 (m, 2H, H_a), 2.51 (m, 2H, H_b), 2.32 (s, 3H, CH_3) ppm.

^{19}F NMR (470 MHz, 300 K, acetone-d_6): δ = -137.94 (d, ^{3}J = 23.6 Hz, 2F, B-*m*-F_2), -139.19 (d, ^{3}J = 23.6 Hz, 2F, B-*m*-F_1), -140.50 (d, ^{3}J = 23.8 Hz, 2F, A-*m*-F_2), -140.85 (d, ^{3}J = 23.5 Hz, 2F, A-*m*-F_1), -154.47 (t, ^{3}J = 20.5 Hz, 2F, B-*p*-F), -155.69 (t, ^{3}J = 20.5 Hz, 2F, A-*p*-F), -162.23 (t, ^{3}J = 22.1 Hz, 2F, B-*m*-F_2), -162.69 (s, br, 2F, B-*m*-F_1), -164.21 (t, ^{3}J = 22.2 Hz, 2F, A-*m*-F_2), -164.32 (t, ^{3}J = 22.1 Hz, 2F, A-*m*-F_1) ppm.

HRMS (EI, TOF-Q) m/z: $[M]^+$ Calcd for $C_{47}H_{15}F_{20}N_5Ni$ 1087.036; Found 1087.037.

UV-vis (MeCN): λ_{max} (lg ε) = 403 (5.134), 494 (3.765), 571 (3.925), 613 (4.629) nm.

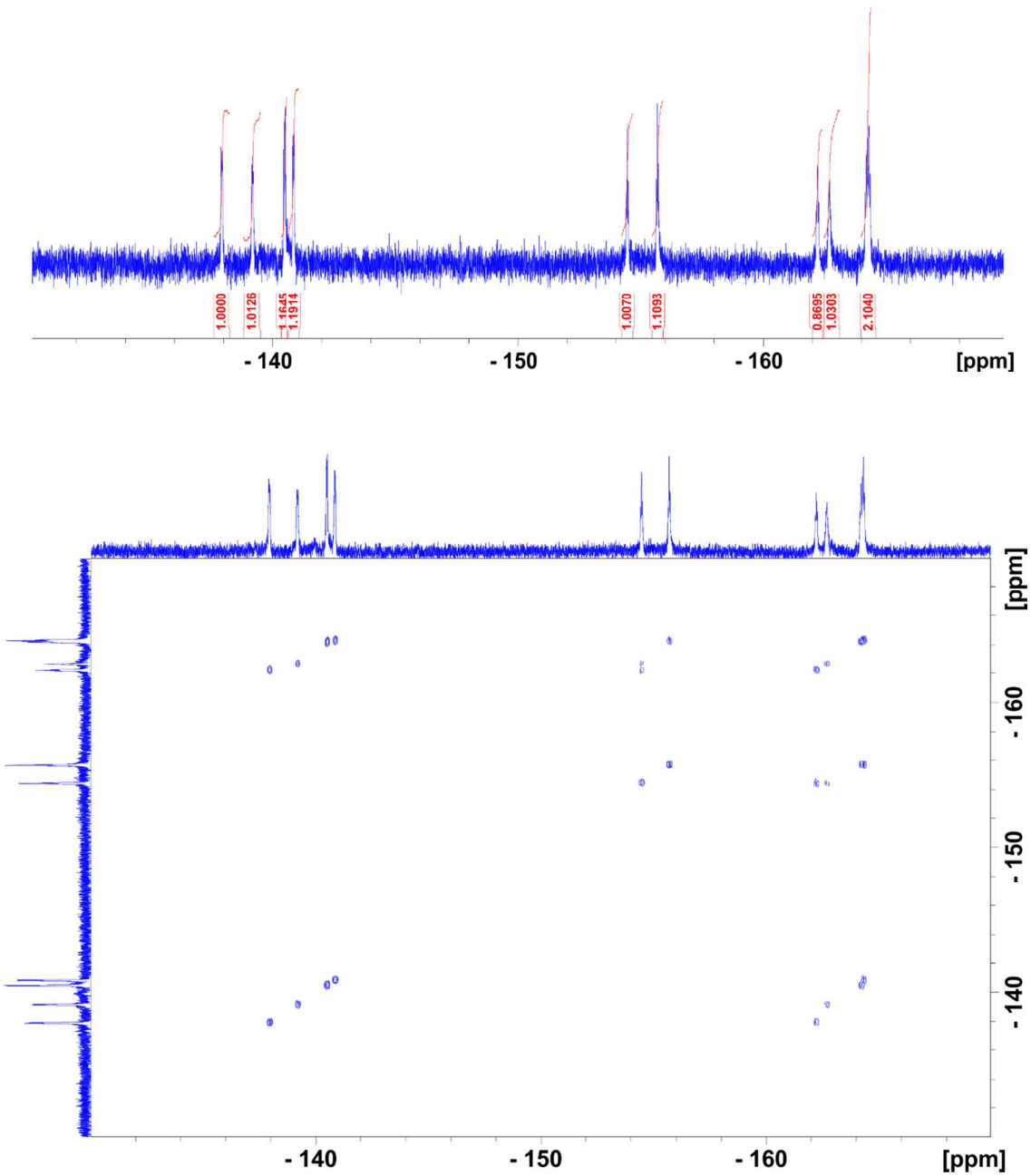

Figure S1. ^{19}F-NMR spectrum (top) and ^{19}F-COSY (bottom) of Ni-TPCF$_{20}$ (**2**).

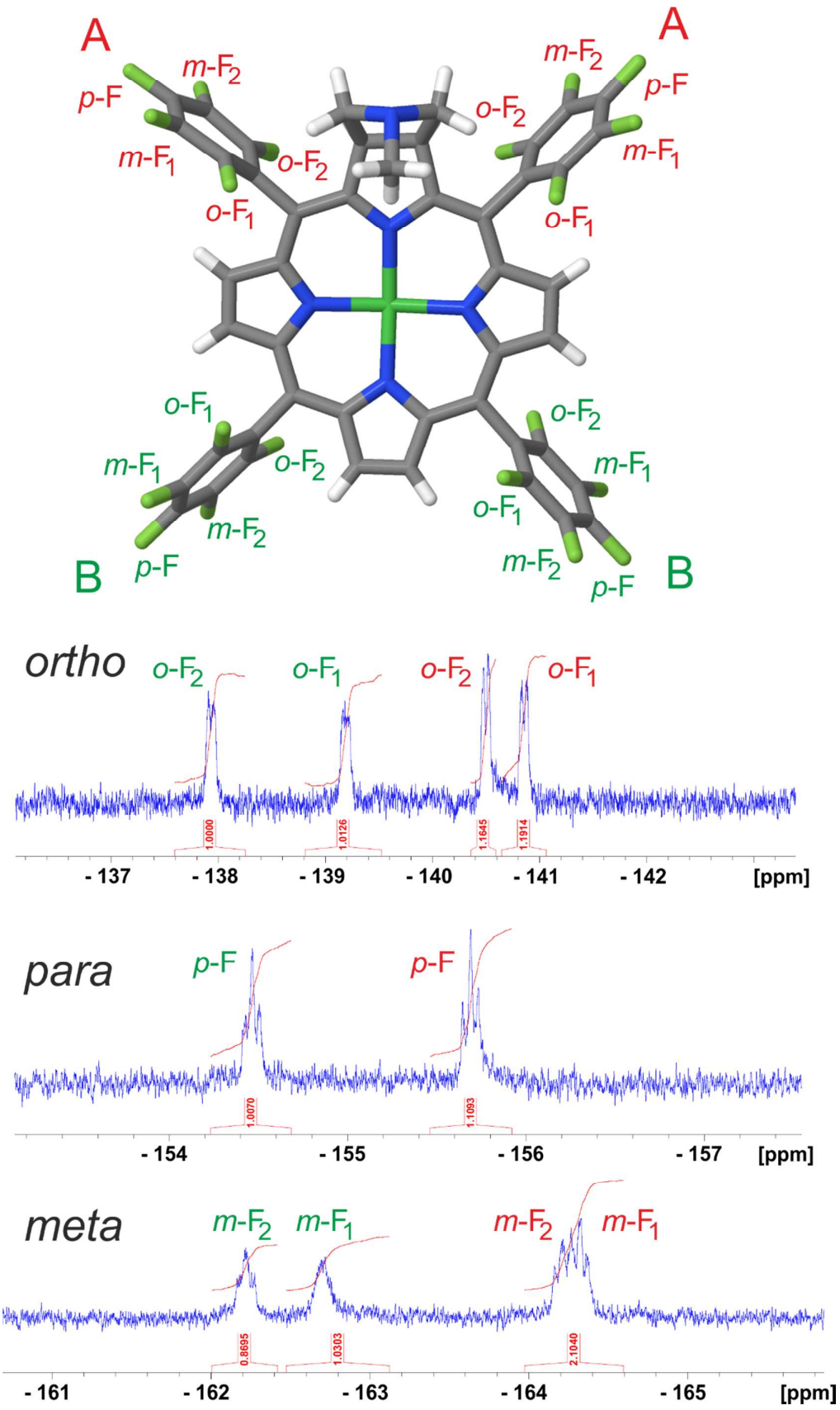

Figure S2. Assignment of all fluorine atoms of Ni-TPCF$_{20}$ (**2**).

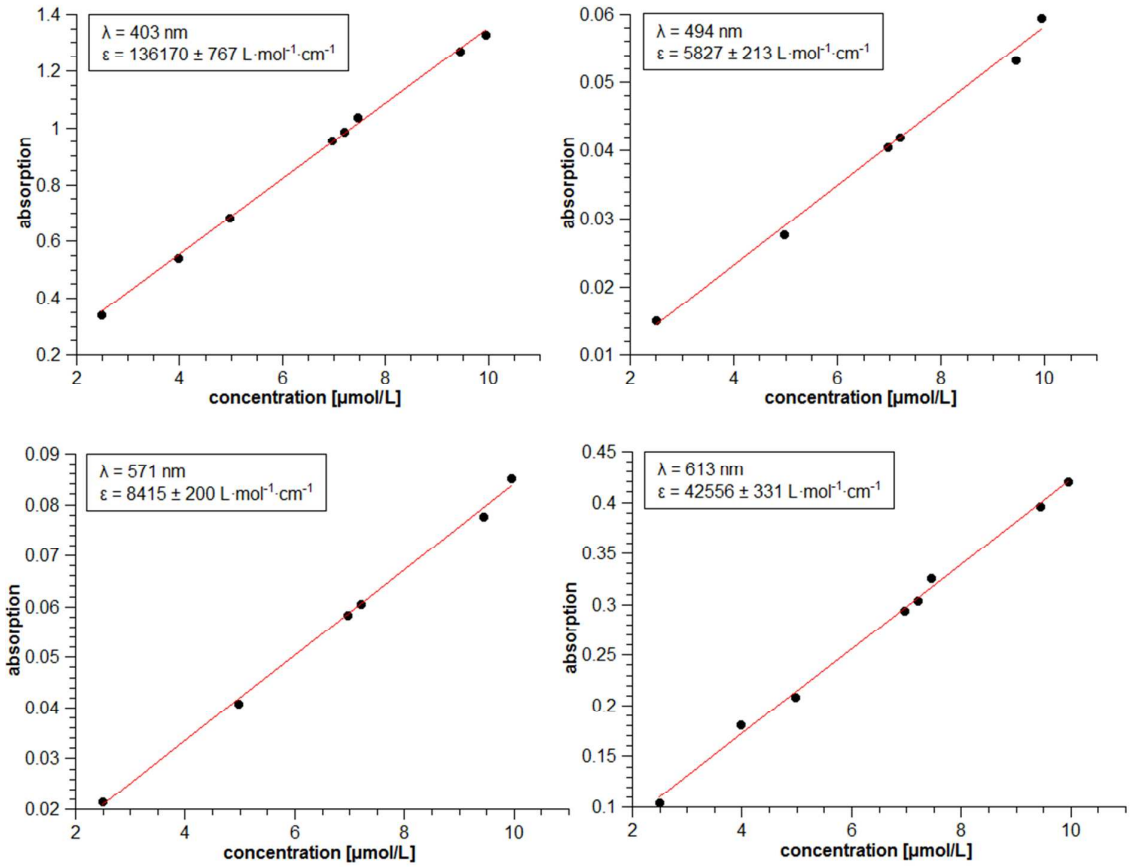

Figure S3. Linear regression for determination of extinction coefficients of Ni-TPCF$_{20}$ (**2**) in acetonitrile. Plot of the absorption at 403 nm (top left), 494 nm (top right), 571 nm (bottom left) and 613 nm (bottom right) over the concentration.

Analytical details for Ni-TPIBF$_{20}$ (**3**)

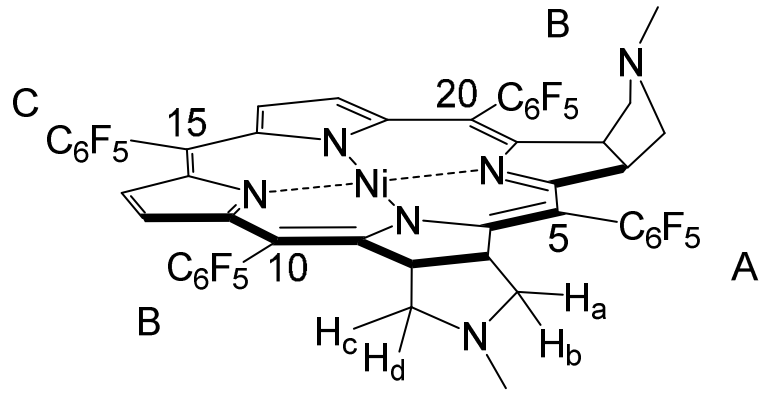

FT-IR (layer): υ = 2923 (m), 1652 (w), 1562 (w), 1519 (s), 1490(s), 1369 (m), 1294 (w), 1266 (w), 1147 (m), 986 (vs), 850 (w), 796 (w), 772 (w), 742 (m), 698 (w) cm^{-1}.

^{1}H NMR (500 MHz, 300 K, $CDCl_3$, TMS): δ = 7.74 (s, br, 2H, *H*-13, *H*-16), 7.31 (s, br, 2H, *H*-12, *H*-17), 4.37 (m, 2H, *H*-2, *H*-8), 4.28 (m, 2H, *H*-3, *H*-7), 2.87 (m, 2H, H_c), 2.73 (m, 2H, H_a), 2.35-2.25 (m, 4H, H_b, H_d), 2.22 (s, 6H, CH_3) ppm.

^{19}F NMR (470 MHz, 300 K, acetone-d_6): δ = -137.54 (dd, ^{3}J = 24.1 Hz, ^{5}J = 6.6 Hz, 2F, C-*o*-F), -138.06 (dd, ^{3}J = 23.8 Hz, ^{5}J = 6.4 Hz, 2F, B-*o*-F_2), -140.63 (dd, ^{3}J = 23.8 Hz, ^{5}J = 7.8 Hz, 2F, B-*o*-F_1), -141.25 (dd, ^{3}J = 23.6 Hz, ^{5}J = 7.1 Hz, 2F, A-*o*-F), -154.49 (t, ^{3}J = 20.6 Hz, 1F, C-*p*-F), -156.08 (t, ^{3}J = 20.5 Hz, 2F, B-*p*-F), -156.47 (t, ^{3}J = 20.5 Hz, 1F, A-*p*-F), -161.94 (td, ^{3}J = 22.4 Hz, ^{5}J = 6.6 Hz, 2F, C-*m*-F), -163.40 (td, ^{3}J = 22.2 Hz, ^{5}J = 7.4 Hz, 2F, B-*m*-F_1), -163.59 (td, ^{3}J = 22.2 Hz, ^{5}J = 7.8 Hz, 2F, B-*m*-F_2), -164.47 (td, ^{3}J = 22.0 Hz, ^{5}J = 7.1 Hz, 2F, A-*m*-F) ppm.

HRMS (EI, TOF-Q) m/z: $[M]^+$ Calcd for $C_{50}H_{22}F_{20}N_6Ni$ 1144.094; Found 1144.095.

UV-vis (MeCN): λ_{max} (lg ε) = 389 (4.775), 514 (3.715), 551 (3.986), 596 (4.667) nm.

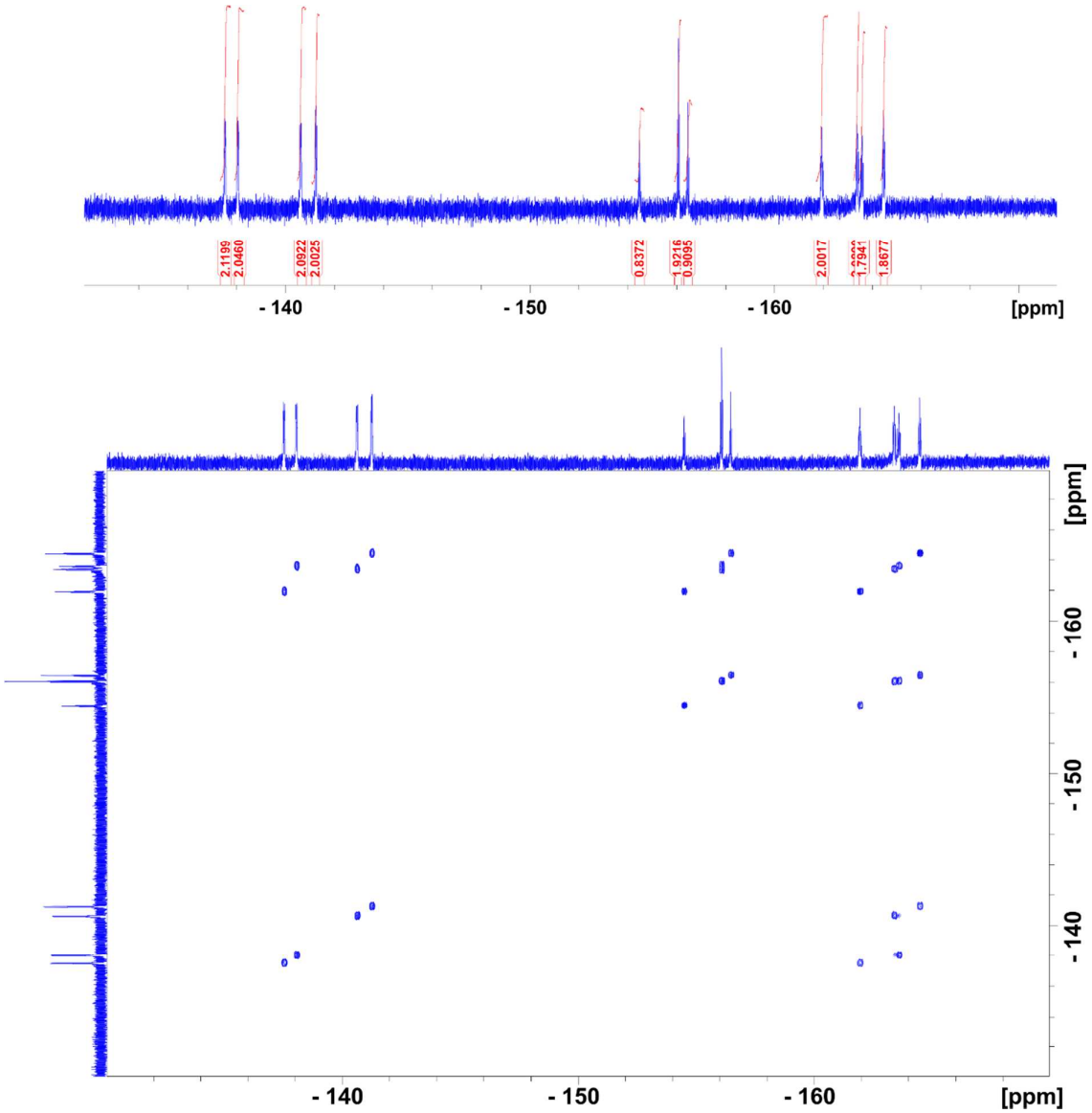

Figure S4. ^{19}F-NMR spectrum (top) and ^{19}F-COSY (bottom) of Ni-TPIBF$_{20}$ (**3**).

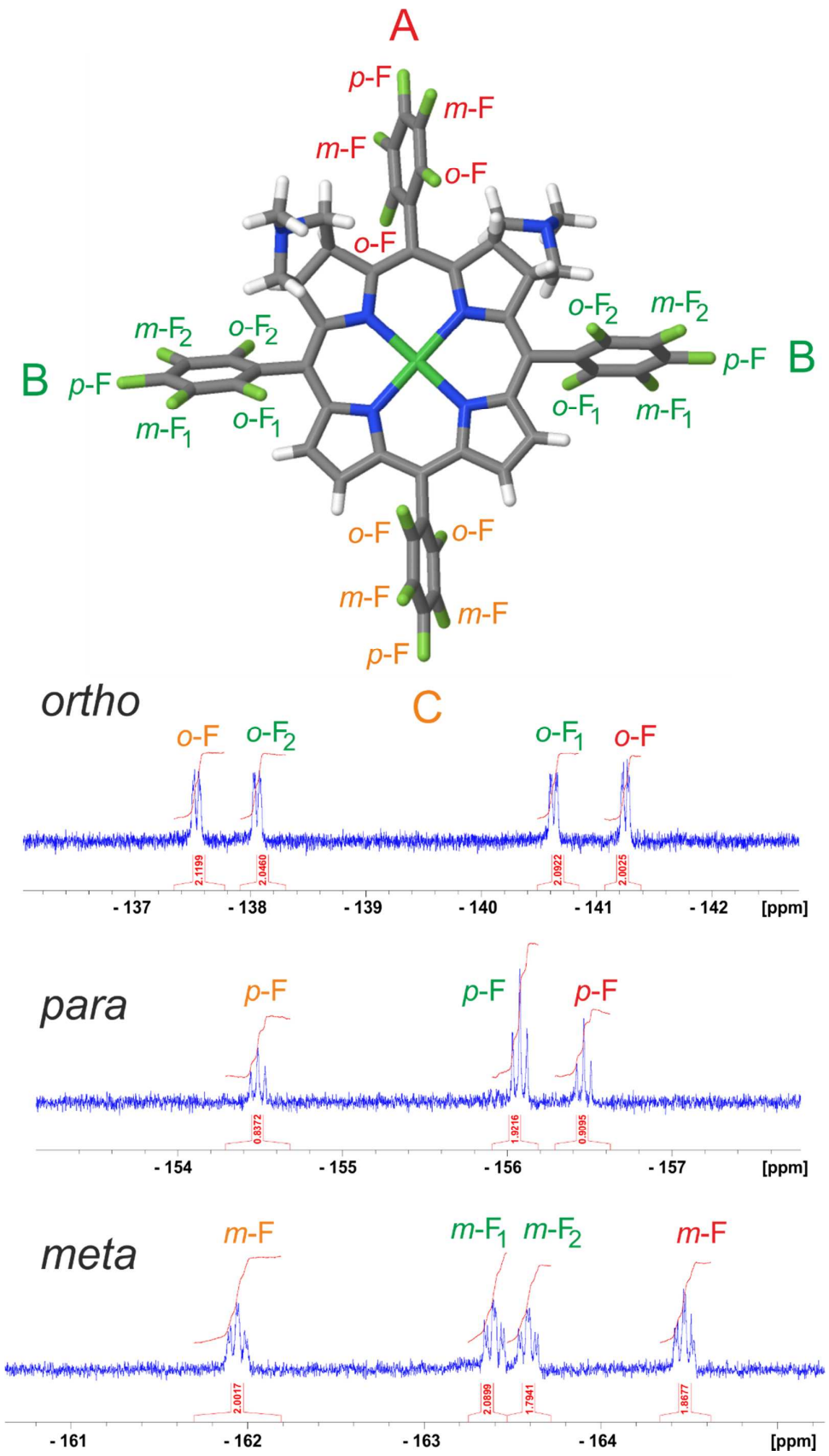

Figure S5. Assignment of all fluorine atoms of Ni-TPIBF$_{20}$ (**3**).

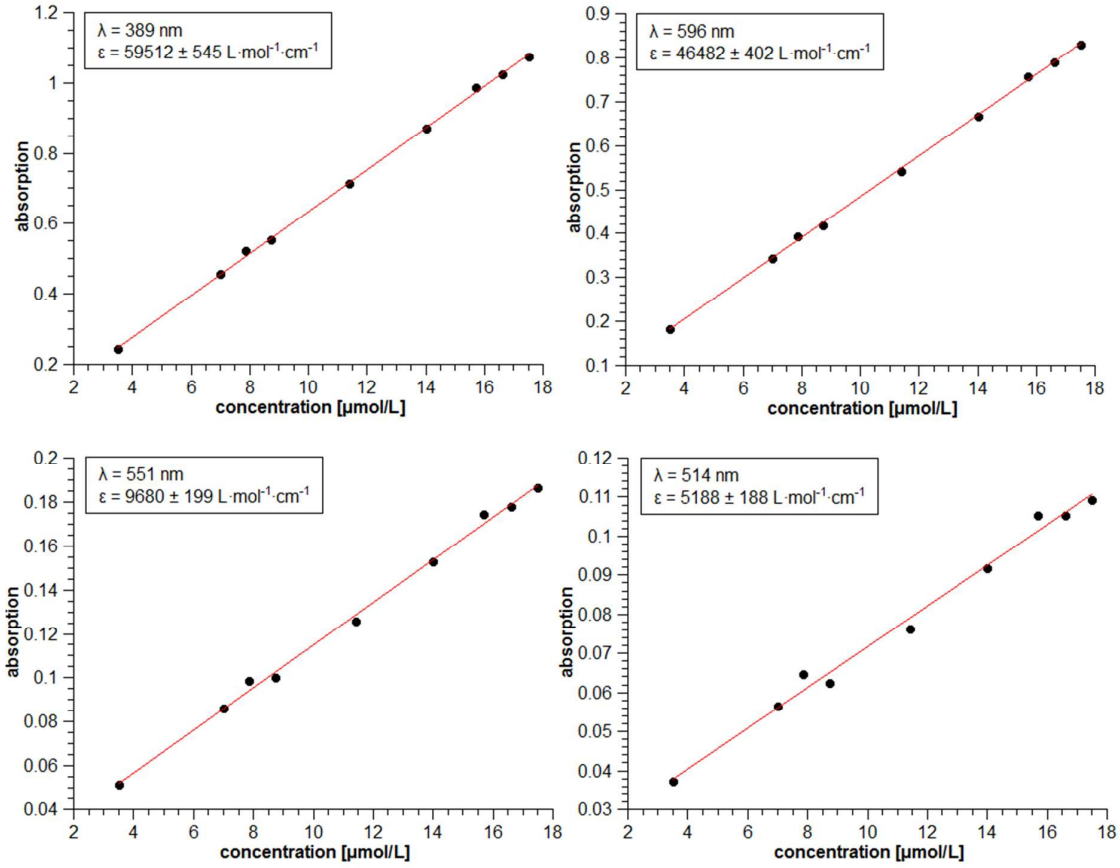

Figure S6. Linear regression for determination of extinction coefficients of Ni-TPIBF$_{20}$ (**3**) in acetonitrile. Plot of the absorption at 389 nm (top left), 514 nm (top right), 551 nm (bottom left) and 596 nm (bottom right) over the concentration.

IV Titration experiments

The association constants were determined by ^{1}H-NMR titration experiments in toluene-d_8. The average chemical shift of the signal of the pyrrole protons was measured as a function of the pyridine concentration. Association constants (K_1 and K_2) were obtained from the titration curves using nonlinear fitting based on classical Newton-Raphson method with the excel add-in EST (Equilibrium Speciation tool).[16] The thermodynamic parameter were determined from the temperature dependence (300, 310, 320 and 330 K) of the association constants. The results for Ni-chlorin **2** (Figures S7 and S8, Tables S1 and S2) and Ni-isobacteriochlorin **3** (Figures S9 and S10, Tables S3 and S4) are summarized beneath.

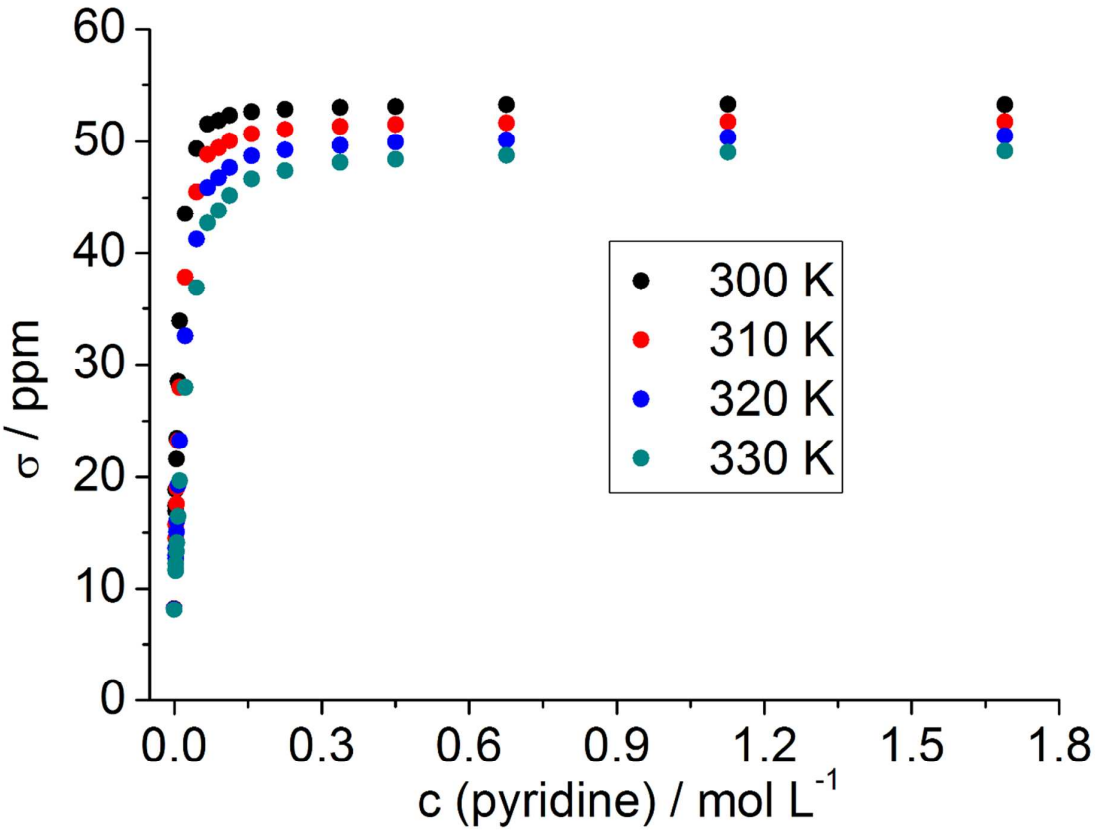

Figure S7. Titration curves for Ni-TPCF$_{20}$ (**2**) in toluene-d_8 with pyridine.

Table S1. Results of ^{1}H-NMR titration experiments (toluene-d_8) of Ni-TPCF$_{20}$ (2) with pyridine ($\sigma_{measured}$) compared to the values obtained by nonlinear fitting with EST (σ EST). The mean square error (MSE) is between 0.014 and 0.065 ppm.

c	300 K		310 K		320 K		330 K	
	δ measured	δ EST	δ measured	δ EST	δ measured	δ EST	δ measured	δ EST
mol L^{-1}	ppm	ppm	ppm	ppm	ppm	ppm	ppm	ppm
0.0000	8.23	8.23	8.18	8.18	8.15	8.15	8.09	8.09
0.0027	16.98	16.92	14.47	14.43	12.69	12.51	11.58	11.31
0.0029	17.47	17.56	15.75	14.89	12.96	12.85	11.75	11.57
0.0034	18.87	18.79	15.81	15.78	13.60	13.52	12.23	12.07
0.0045	21.60	21.67	17.61	17.92	15.02	15.15	13.30	13.32
0.0052	23.47	23.25	19.04	19.13	16.13	16.09	14.09	14.04
0.0079	28.48	28.71	23.24	23.51	19.30	19.57	16.50	16.78
0.0113	33.89	33.89	27.95	28.03	23.25	23.35	19.67	19.88
0.0225	43.54	43.41	37.83	37.75	32.57	32.43	27.97	27.95
0.0451	49.34	49.47	45.49	45.56	41.25	41.31	36.89	37.10
0.0676	51.55	51.28	48.83	48.32	45.87	45.09	42.68	41.58
0.0901	51.88	52.03	49.44	49.57	46.76	46.97	43.82	44.01
0.1126	52.32	52.41	50.05	50.23	47.66	48.02	45.18	45.45
0.1577	52.65	52.77	50.68	50.86	48.71	49.09	46.64	46.98
0.2253	52.86	52.97	51.07	51.23	49.24	49.75	47.40	47.96
0.3379	53.03	53.08	51.32	51.45	49.65	50.15	48.13	48.57
0.4505	53.11	53.12	51.50	51.53	49.94	50.29	48.41	48.80
0.6758	53.26	53.15	51.67	51.58	50.13	50.40	48.75	48.97
1.1263	53.30	53.17	51.77	51.61	50.37	50.46	49.03	49.07
1.6895	53.27	53.17	51.77	51.62	50.50	50.48	49.13	49.10
MSE		0.0165		0.0688		0.0913		0.1218

Table S2. Results for the association constants (K_1 and K_2, toluene-d_8) for Ni-TPCF$_{20}$ (2) with pyridine.

T	T^{-1}	K_1	K_2	ln K1	lnK2
K	K^{-1}	L mol^{-1}	L mol^{-1}		
300	0.003333	91.081	43.382	4.511749	3.770045
310	0.003226	59.584	32.096	4.087387	3.468731
320	0.003125	42.753	21.951	3.755439	3.088813
330	0.00303	31.574	17.351	3.452334	2.85365

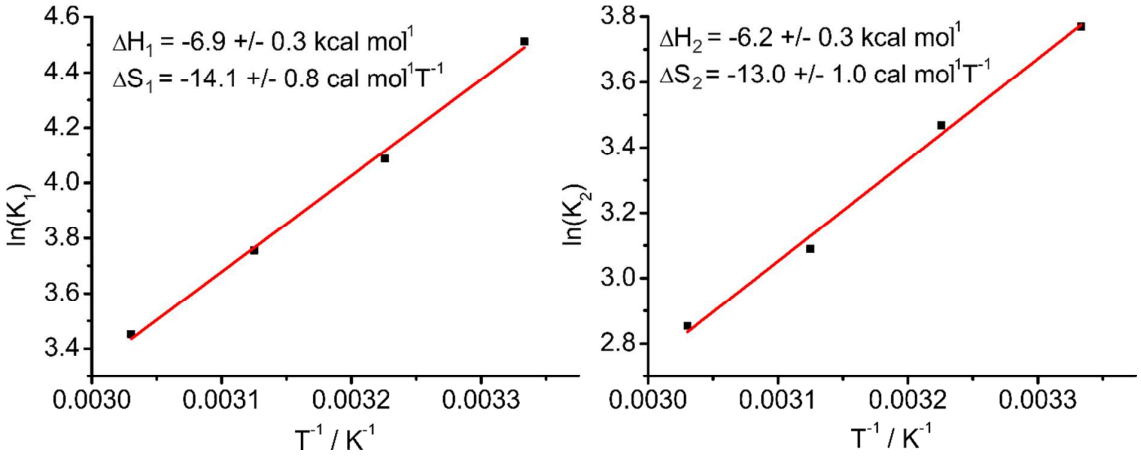

Figure S8. Linear plot for the determination of the thermodynamic parameter (ΔH and ΔS) of the two coordination processes of pyridine to Ni-TPCF$_{20}$ (**2**).

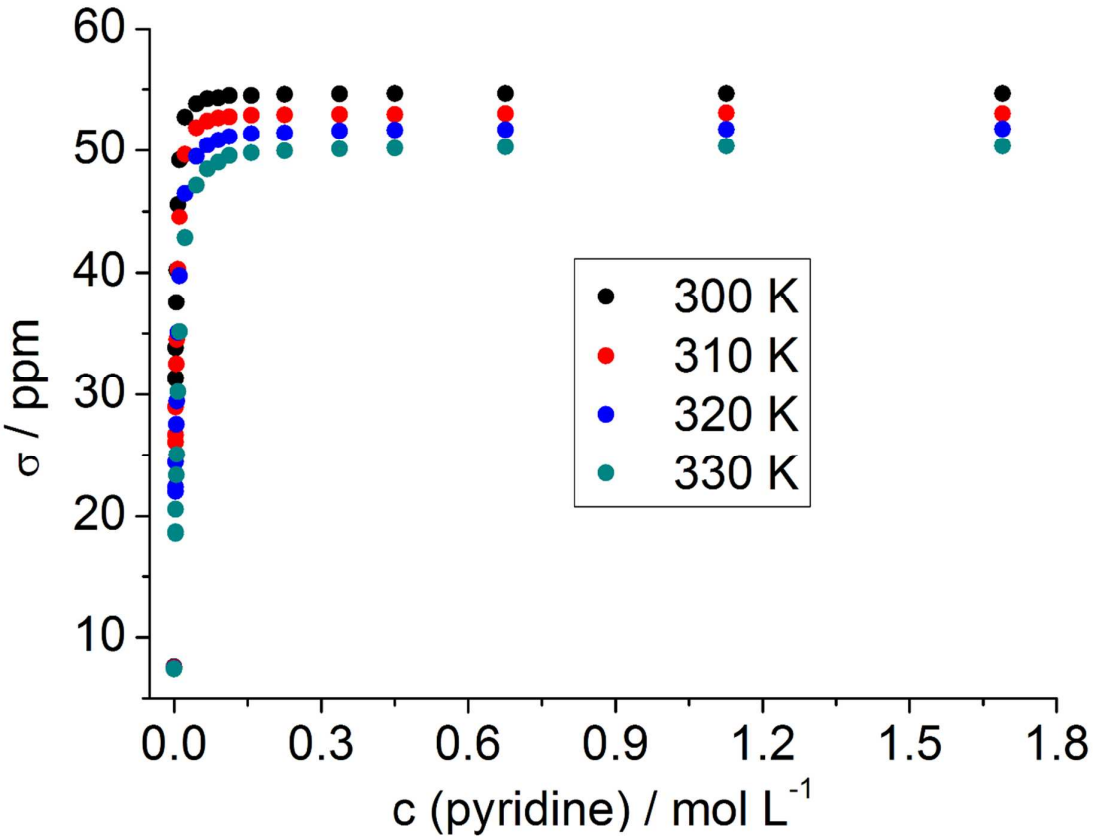

Figure S9. Titration curves for Ni-TPIBF$_{20}$ (**3**) in toluene-d$_8$ with pyridine.

Table S3. Results of ^{1}H-NMR titration experiments (toluene-d_8) of Ni-TPIBF$_{20}$ (3) with pyridine ($\sigma_{measured}$) compared to the values obtained by nonlinear fitting with EST (σ EST). The mean square error (MSE) is between 0.014 and 0.065 ppm.

c	300 K		310 K		320 K		330 K	
	$\delta_{measured}$	δ EST	$\delta_{measured}$	δ EST	$\delta_{measured}$	δ EST	$\delta_{measured}$	δ EST
mol L^{-1}	ppm	ppm	ppm	ppm	ppm	ppm	ppm	ppm
0.0000	7.62	7.62	7.56	7.56	7.50	7.50	7.47	7.47
0.0027	30.53	31.28	25.79	26.09	21.68	22.00	18.32	18.51
0.0029	31.72	31.35	26.83	26.67	22.56	22.36	19.04	18.71
0.0034	33.86	33.84	28.74	28.94	24.20	24.41	20.41	20.56
0.0045	38.15	37.56	32.73	32.52	27.77	27.55	23.48	23.35
0.0052	40.15	40.19	34.69	34.49	29.60	29.45	25.10	25.07
0.0079	45.48	45.58	40.30	40.27	35.17	35.08	30.34	30.20
0.0113	48.91	49.20	44.35	44.50	39.63	39.76	34.90	35.14
0.0225	52.71	52.72	49.59	49.65	46.21	46.48	42.54	42.81
0.0451	54.10	53.84	51.90	51.87	49.66	49.51	47.22	47.14
0.0676	54.41	54.26	52.48	52.43	50.62	50.42	48.68	48.47
0.0901	54.52	54.31	52.70	52.67	51.01	50.85	49.31	49.02
0.1126	54.58	54.50	52.81	52.77	51.22	51.13	49.64	49.58
0.1577	54.63	54.51	52.92	52.89	51.40	51.38	49.96	49.79
0.2253	54.65	54.61	52.97	52.92	51.51	51.45	50.15	49.95
0.3379	54.67	54.63	53.00	52.98	51.57	51.61	50.26	50.13
0.4505	54.67	54.67	53.02	52.98	51.59	51.67	50.30	50.18
0.6758	54.68	54.66	53.02	53.02	51.61	51.69	50.33	50.27
1.1263	54.68	54.66	53.03	53.10	51.62	51.74	50.34	50.33
1.6895	54.68	54.68	53.03	53.03	51.62	51.76	50.35	50.35
MSE		0.0651		0.0142		0.0253		0.0289

Table S4. Results for the association constants (K_1 and K_2, toluene-d_8) for Ni-TPIBF$_{20}$ (3) with pyridine.

T	T^{-1}	K_1	K_2	ln K1	lnK2
K	K^{-1}	L mol^{-1}	L mol^{-1}		
300	0.00333	441	78	6.09	4.35
310	0.00323	297	49	5.69	3.90
320	0.00313	201	35	5.30	3.55
330	0.00303	129	26	4.86	3.27

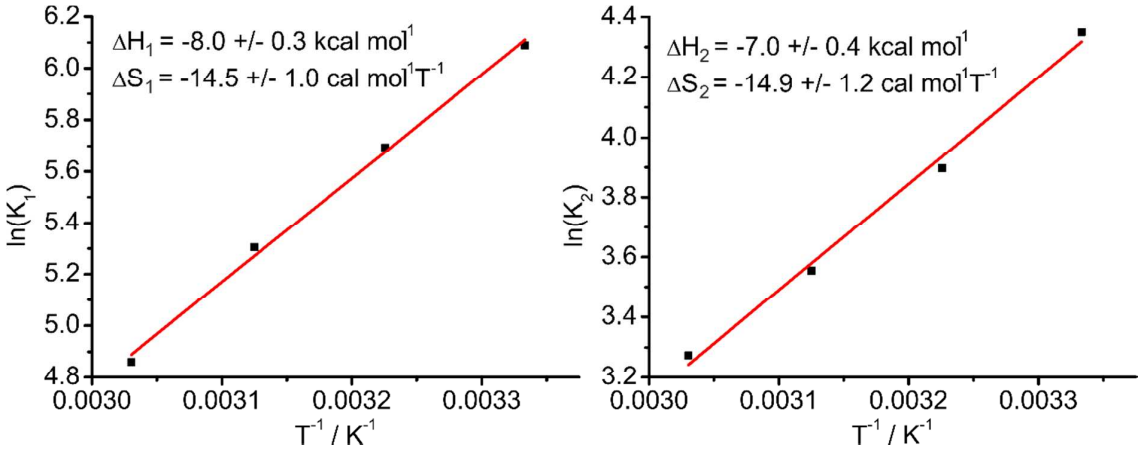

Figure S10. Linear plot for the determination of the thermodynamic parameter (ΔH and ΔS) of the two coordination processes of pyridine to Ni-TPIBF$_{20}$ (**3**).

V Computational Details

V.1 Comparison of Calculated and Crystal Structures

The calculations have been conducted using Turbomole 6.6.[17] The crystal structure data (see section VI) was used as starting geometry for the optimizations at the PBE/SVP level of theory. The optimized structures of Ni-$TPPF_{20}$ (**1**)as well as the six coordinate complexes of Ni-$TPPF_{20}$ (**1**·2Py), Ni-$TPCF_{20}$ (**2**·2Py) and Ni-$TPIBF_{20}$ (**3**·2Py) with two pyridine (Py) ligands were superimposed by the corresponding crystal structure using the program Mercury CSD 3.3.1.[18]

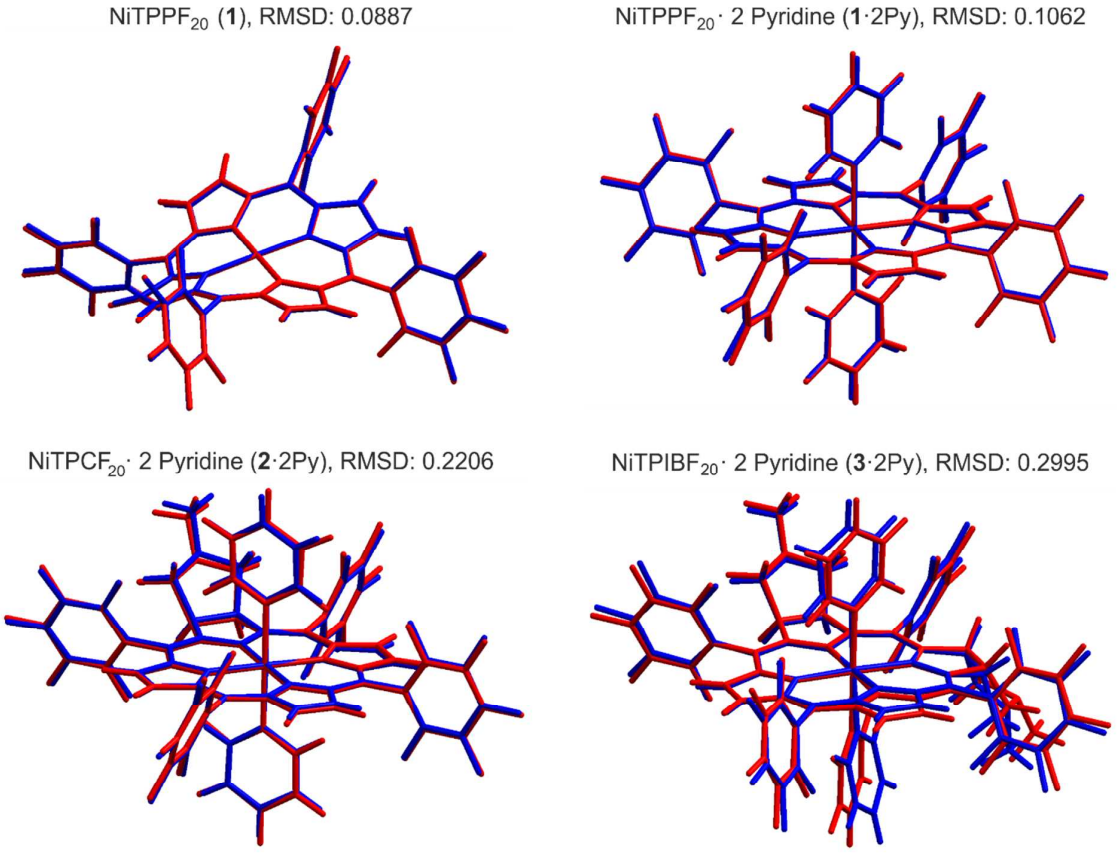

Figure S11. Overlay of the calculated (PBE/SVP, red) and crystal structures (blue) for the bare Ni-$TPPF_{20}$ (**1**, top left), the six coordinate complexes of two pyridine ligands with Ni-$TPPF_{20}$ (**1**·2Py, top right), Ni-$TPCF_{20}$ (**2**·2Py, bottom left) and Ni-$TPIBF_{20}$ (**3**·2Py, bottom right). The root mean square deviation (RMSD) is given in each case. Note that the calculated structures are in good agreement with the crystal structures.

V.2 Calculated Complex Formation Energies of Pyridine with Ni-TPPF$_{20}$ (1), Ni-TPCF$_{20}$ (2) and Ni-TPIBF$_{20}$ (3)

Single point energies at the B3LYP/def2TZVP level of theory were performed on the optimized geometries. The complex formation energies of the six coordinate complex of **1**, **2** and **3** with two pyridine (Py) ligands (ΔE_f) were compared to the corresponding experimentally determined (ΔH_{exp}) values.

Table S5. Calculated (B3LYP/def2TZVP//PBE/SVP) energies for the formation of the six coordinate complexes (ΔE_f) of 1, 2 and 3 with two pyridine (Py) molecules, analogous to the following equation: ΔE_f : Ni-TPPF$_{20}$(singlet) + 2 Pyridine → Ni-TPPF$_{20}$ · 2 Pyridine(triplet).

#	E_{abs} Py [a.u.]	E_{abs} Porphyrin (singlet) [a.u.]	E_{abs} Porphyrin · 2 Py (triplet) [a.u.]	ΔE_f 2 Py [kcal/mol]	$\Delta H_{exp.}$ 2 Py [kcal/mol]
1	-248.22217588	-5405.27403340	-5901.73564811	**-10.8**	**-11.3**
2	-248.22217588	-5578.49182805	-6074.95551590	**-12.1**	**-13.1**
3	-248.22217588	-5751.70855669	-6248.17453228	**-13.6**	**-15.0**

The calculated ΔE_f predicts the same trend as the experimentally derived association constants (ΔH_{exp}, see Figure S2). Both values increases with the number of double bonds that are replaced by single bonds (**1** < **2** < **3**).

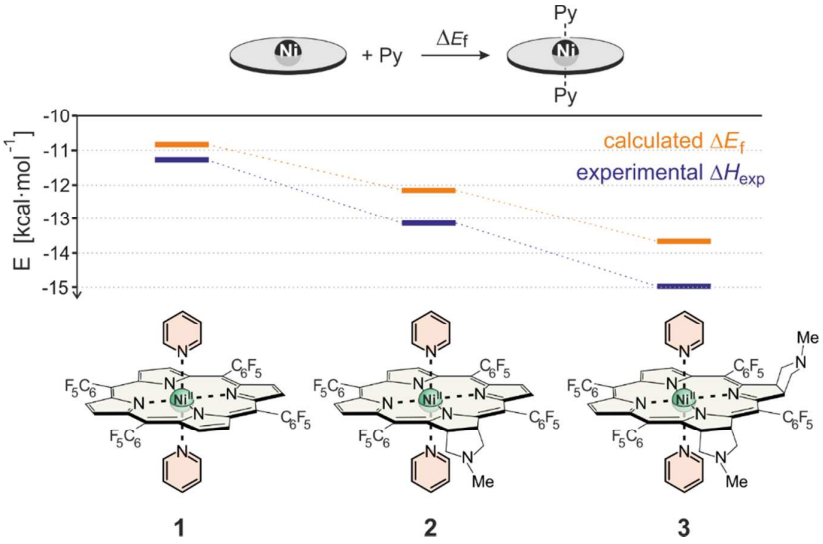

Figure S12. Calculated (B3LYP/def2TZVP//PBE/SVP) complex formation energies (ΔE_f, orange bars, kcal·mol^{-1}) of two pyridine molecules to Ni-TPPF$_{20}$ (**1**), Ni-TPCF$_{20}$ (**2**) and Ni-TPIBF$_{20}$ (**3**). The definition of ΔE_f is given on top. The experimental derived association energies (ΔH_{exp}) for the 1:2 complexes of the corresponding porphyrine with two pyridine molecules are given as blue bars. Note that the experimental and calculated association energies are in good agreement.

V.3 Orbital Energy Levels of NiTPP, $NiTPPF_{20}$, $NiTPCF_{20}$ and $NiTPIBF_{20}$

Single point energies at the B3LYP/def2TZVP level of theory were performed on PBE/SVP optimized geometries using Gaussian 09.D01 to calculate the orbital energy levels of $NiTPPF_{20}$ (**1**), $NiTPCF_{20}$ (**2**) and $NiTPIBF_{20}$ (**3**).[17] The energy levels of NiTPP are given for comparison.

Table S6. Calculated (B3LYP/def2TZVP//PBE/SVP) energies of the dz^2 and the dx^2-y^2 orbitals as well as energy difference (ΔE) of the dz^2 and the dx^2-y^2 of 1, 2, 3 and NiTPP.

#	E_{abs} [eV] dz^2	E_{abs} [eV] dx^2-y^2	ΔE [eV]
NiTPP	-6.41	-1.34	**5.06**
$NiTPPF_{20}$	-7.13	-2.09	**5.04**
$NiTPCF_{20}$	-7.13	-2.13	**5.00**
$NiTPIBF_{20}$	-7.12	-2.16	**4.96**

Substitution of the phenyl rings in *meso*-position with pentafluorophenyl groups leads to an overall decrease in energy for the dz^2 and the dx^2-y^2 orbitals as well as a smaller energy difference (ΔE) compared to NiTPP. The calculated ΔE further decreases with the number of added pyrrolidine moieties (**1** > **2** > **3**) which is in good agreement with the stronger coordination of pyridine to **3** > **2** > **1** observed in the experiment.

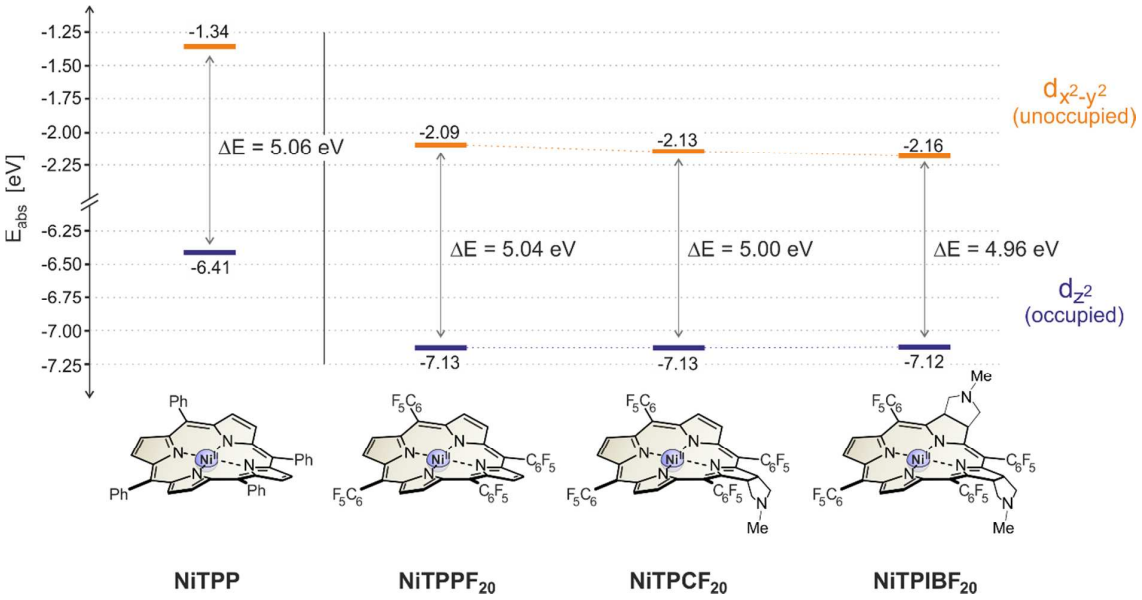

Figure S13. Calculated (B3LYP/def2TZVP//PBE/SVP) energy gaps between the occupied dz^2 and the unoccupied dx^2-y^2 orbitals (ΔE, eV) of NiTPP, $NiTPPF_{20}$ (**1**), $NiTPCF_{20}$ (**2**) and $NiTPIBF_{20}$ (**3**). Substitution of the phenyl rings in *meso*-position with pentafluorophenyl groups leads to an overall decrease in energy for the dz^2 and

the dx^2-y^2. After addition of pyrrolidine moieties the energy level of the dz^2 is almost constant whereas the dx^2-y^2 orbital further decreases in energy in the order **1** > **2** > **3**.

V.4 Coordination Isomers of one Pyridine with $NiTPCF_{20}$ (2)

Whereas the two sides of $NiTPPF_{20}$ (**1**) and $NiTPIBF_{20}$ (**3**) are homotopic, there are two different possibilities (*syn* and *anti* to the pyrrolidine ring) for the coordination of the first ligand to the $NiTPCF_{20}$ (**2**) (Figure S4). According to our calculations both 1:1 complexes are isoenergetic (ΔE = 0.13 kcal·mol^{-1}) since there is very little steric repulsion between the axial ligand and the pyrrolidine moiety. Thus, the affinity of pyridine to $NiTPCF_{20}$ (**1**) is not influenced by the direction of the pyridine coordination.

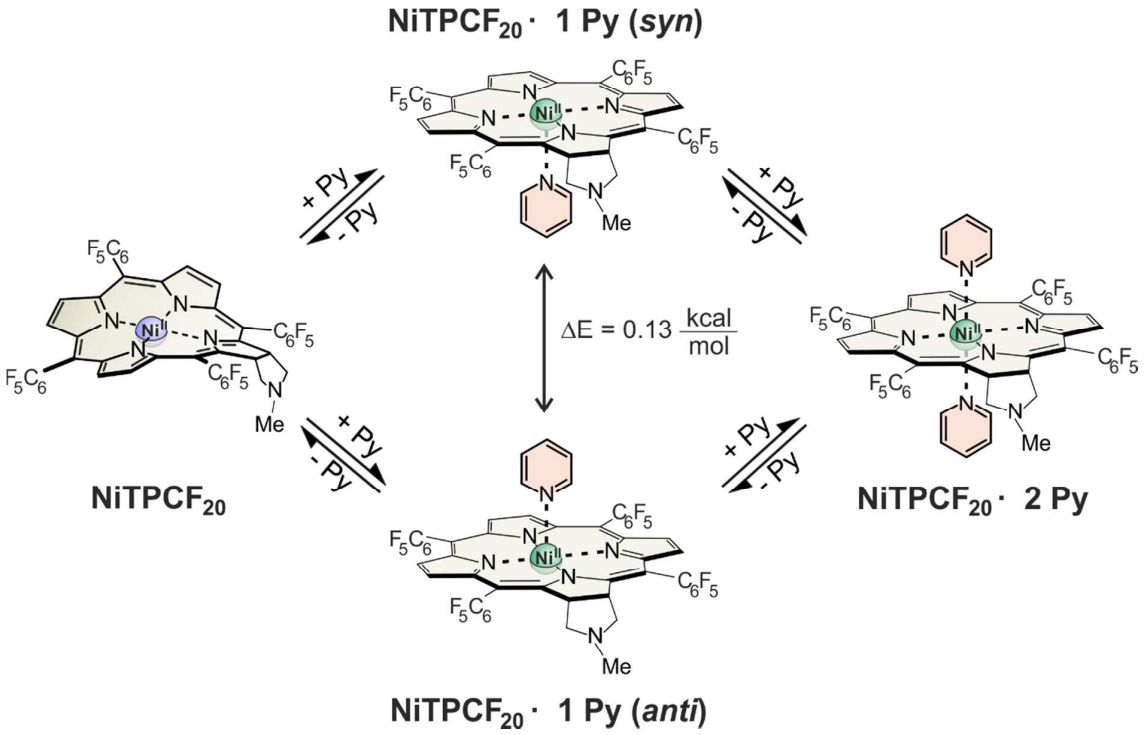

Figure S14. The calculated (B3LYP/def2TZVP//PBE/SVP) structures of the *syn* (top) and the *anti* (bottom) coordination isomers of one pyridine molecule and $NiTPCF_{20}$ (**2**) are isoenergetic. Hence, the first coordination of pyridine to $NiTPCF_{20}$ (**2**) is not sterically hindered by the pyrrolidine moiety.

V.5 XYZ Coordinates of the PBE/SVP optimized Ligand and Complexes

Table S7. XYZ Coordinates of the PBE/SVP optimized pyridine.

$E_{PBE/SVP}$ = -247.7806069479 Hartree
NImag = 0

C	-1.146920	0.000000	-0.919580
C	-1.205890	0.000000	0.485050
C	0.000000	0.000000	1.202610
C	1.205890	0.000000	0.485050
C	1.146920	0.000000	-0.919580
N	0.000000	0.000000	-1.617530
H	0.000000	0.000000	2.305570
H	-2.080280	0.000000	-1.514700
H	-2.179000	0.000000	1.003240
H	2.179000	0.000000	1.003240
H	2.080280	0.000000	-1.514700
C	-1.146920	0.000000	-0.919580

Table S8. XYZ Coordinates of the PBE/SVP optimized Ni-$TPPF_{20}$ (1).

$E_{PBE/SVP}$ = -5398.246215777 Hartree
NImag = 0

Ni	0.000000	0.000000	0.000000
N	-1.656490	-1.004720	0.025630
C	-2.912310	-0.544530	0.389420
C	-3.865360	-1.630320	0.418550
H	-4.918670	-1.539390	0.708470
C	-3.201000	-2.745610	-0.014690
H	-3.590870	-3.763010	-0.138970
C	-1.827750	-2.352000	-0.232080
C	-0.804090	-3.259920	-0.539860
C	-1.179290	-4.654030	-0.913390
C	-1.006950	-5.737690	-0.029720
C	-1.390370	-7.043790	-0.376680
C	-1.962830	-7.285410	-1.637380
C	-2.151990	-6.222890	-2.537600
C	-1.760880	-4.925260	-2.168040
F	-0.476950	-5.539210	1.181960
F	-1.221430	-8.050160	0.483790
F	-2.327610	-8.520800	-1.977590
F	-2.696220	-6.451150	-3.734440
F	-1.951720	-3.935100	-3.044750
N	-1.004720	1.656490	-0.025630
C	-0.544530	2.912310	-0.389420
C	-1.630320	3.865360	-0.418550
H	-1.539390	4.918670	-0.708470
C	-2.745610	3.201000	0.014690
H	-3.763010	3.590870	0.138970
C	-2.352000	1.827750	0.232080
C	-3.259920	0.804090	0.539860
C	-4.654030	1.179290	0.913390
C	-5.737690	1.006950	0.029720
C	-7.043790	1.390370	0.376680
C	-7.285410	1.962830	1.637380
C	-6.222890	2.151990	2.537600
C	-4.925260	1.760880	2.168040
F	-5.539210	0.476950	-1.181960
F	-8.050160	1.221430	-0.483790
F	-8.520800	2.327610	1.977590

F	-6.451150	2.696220	3.734440
F	-3.935100	1.951720	3.044750
N	1.004720	-1.656490	-0.025630
C	0.544530	-2.912310	-0.389420
C	1.630320	-3.865360	-0.418550
H	1.539390	-4.918670	-0.708470
C	2.745610	-3.201000	0.014690
H	3.763010	-3.590870	0.138970
C	2.352000	-1.827750	0.232080
C	3.259920	-0.804090	0.539860
C	4.654030	-1.179290	0.913390
C	5.737690	-1.006950	0.029720
C	7.043790	-1.390370	0.376680
C	7.285410	-1.962830	1.637380
C	6.222890	-2.151990	2.537600
C	4.925260	-1.760880	2.168040
F	5.539210	-0.476950	-1.181960
F	8.050160	-1.221430	-0.483790
F	8.520800	-2.327610	1.977590
F	6.451150	-2.696220	3.734440
F	3.935100	-1.951720	3.044750
N	1.656490	1.004720	0.025630
C	2.912310	0.544530	0.389420
C	3.865360	1.630320	0.418550
H	4.918670	1.539390	0.708470
C	3.201000	2.745610	-0.014690
H	3.590870	3.763010	-0.138970
C	1.827750	2.352000	-0.232080
C	0.804090	3.259920	-0.539860
C	1.179290	4.654030	-0.913390
C	1.006950	5.737690	-0.029720
C	1.390370	7.043790	-0.376680
C	1.962830	7.285410	-1.637380
C	2.151990	6.222890	-2.537600
C	1.760880	4.925260	-2.168040
F	0.476950	5.539210	1.181960
F	1.221430	8.050160	0.483790
F	2.327610	8.520800	-1.977590
F	2.696220	6.451150	-3.734440
F	1.951720	3.935100	-3.044750

Table S9. XYZ Coordinates of the PBE/SVP optimized Ni-TPPF$_{20}$ · 2 Pyridine (1·2Py).

$E_{PBE/SVP}$ = -5893.838811042 Hartree
NImag = 0

Ni	0.000000	0.000000	0.000000
N	0.827580	-1.859870	0.328070
C	1.117500	-2.810900	-0.619610
C	1.665340	-3.999850	0.015490
H	1.994290	-4.910140	-0.500680
C	1.686210	-3.748080	1.362470
H	2.022050	-4.419720	2.161830
C	1.162300	-2.402420	1.544530
C	1.014350	-1.765580	2.800750
C	0.493060	-0.465940	3.009700
C	0.395310	0.181150	4.309820
H	0.710690	-0.252330	5.266890
C	-0.141210	1.423690	4.091880
H	-0.353150	2.202600	4.834710
C	-0.370200	1.530040	2.658900
C	-0.909370	2.670170	2.014020
N	0.025290	0.374870	2.029730
C	1.439230	-2.536140	4.009110
C	2.798030	-2.798340	4.272590
C	3.206880	-3.536890	5.395880
C	2.239560	-4.030230	6.287720
C	0.876900	-3.780830	6.053760
C	0.493090	-3.040120	4.923450
F	3.740760	-2.339830	3.441410
F	4.502420	-3.769840	5.624020
F	2.612680	-4.735830	7.355930
F	-0.039380	-4.255230	6.901940
F	-0.812050	-2.825790	4.723230
C	-1.269040	3.837620	2.873080
C	-2.421450	3.828140	3.679920
C	-2.774860	4.929390	4.477260
C	-1.960580	6.074960	4.471090
C	-0.800410	6.110880	3.678470
C	-0.469610	4.995490	2.892200
F	-3.217370	2.750890	3.692790
F	-3.876730	4.902490	5.230750
F	-2.288110	7.128600	5.219220
F	-0.026670	7.198980	3.680920
F	0.643610	5.049960	2.147700
N	2.013980	0.872510	-0.208320
C	2.952420	0.264110	-0.959830
H	2.659390	-0.681720	-1.442690
C	4.240180	0.788370	-1.139800
H	4.965290	0.247740	-1.768350
C	4.572270	1.998080	-0.512970
H	5.575090	2.440190	-0.633900
C	3.596710	2.632980	0.269030
H	3.799650	3.586240	0.782260
C	2.334620	2.035050	0.392760
H	1.546040	2.512280	0.995590
N	-0.827580	1.859870	-0.328070
C	-1.117500	2.810900	0.619610
C	-1.665340	3.999850	-0.015490
H	-1.994290	4.910140	0.500680
C	-1.686210	3.748080	-1.362470
H	-2.022050	4.419720	-2.161830
C	-1.162300	2.402420	-1.544530

C	-1.014350	1.765580	-2.800750
C	-0.493060	0.465940	-3.009700
C	-0.395310	-0.181150	-4.309820
H	-0.710690	0.252330	-5.266890
C	0.141210	-1.423690	-4.091880
H	0.353150	-2.202600	-4.834710
C	0.370200	-1.530040	-2.658900
C	0.909370	-2.670170	-2.014020
N	-0.025290	-0.374870	-2.029730
C	-1.439230	2.536140	-4.009110
C	-2.798030	2.798340	-4.272590
C	-3.206880	3.536890	-5.395880
C	-2.239560	4.030230	-6.287720
C	-0.876900	3.780830	-6.053760
C	-0.493090	3.040120	-4.923450
F	-3.740760	2.339830	-3.441410
F	-4.502420	3.769840	-5.624020
F	-2.612680	4.735830	-7.355930
F	0.039380	4.255230	-6.901940
F	0.812050	2.825790	-4.723230
C	1.269040	-3.837620	-2.873080
C	2.421450	-3.828140	-3.679920
C	2.774860	-4.929390	-4.477260
C	1.960580	-6.074960	-4.471090
C	0.800410	-6.110880	-3.678470
C	0.469610	-4.995490	-2.892200
F	3.217370	-2.750890	-3.692790
F	3.876730	-4.902490	-5.230750
F	2.288110	-7.128600	-5.219220
F	0.026670	-7.198980	-3.680920
F	-0.643610	-5.049960	-2.147700
N	-2.013980	-0.872510	0.208320
C	-2.952420	-0.264110	0.959830
H	-2.659390	0.681720	1.442690
C	-4.240180	-0.788370	1.139800
H	-4.965290	-0.247740	1.768350
C	-4.572270	-1.998080	0.512970
H	-5.575090	-2.440190	0.633900
C	-3.596710	-2.632980	-0.269030
H	-3.799650	-3.586240	-0.782260
C	-2.334620	-2.035050	-0.392760
H	-1.546040	-2.512280	-0.995590

Table S10. XYZ Coordinates of the PBE/SVP optimized Ni-TPCF$_{20}$ (2).

$E_{PBE/SVP}$ = -5571.159258200 Hartree
NImag = 0

C	-1.165680	-0.637090	3.438710
N	-0.126880	-0.246920	2.609740
C	-0.783620	-0.512660	4.822630
C	0.477520	0.028300	4.836760
C	0.894170	0.138640	3.461800
C	-2.462800	-0.962080	3.004370
C	-2.868220	-0.716200	1.689830
C	-4.245580	-0.662310	1.265500
C	-4.246180	-0.121720	0.003020
C	-2.864100	0.079930	-0.358890
N	-2.031220	-0.277170	0.670770
Ni	-0.104790	-0.222110	0.676190
N	1.820710	-0.224690	0.704540
C	2.660710	-0.622360	-0.308570
C	4.035500	-0.599960	0.133880
C	4.031690	-0.083270	1.404800
C	2.649250	0.111020	1.766210
C	-2.434130	0.445400	-1.655130
C	-1.128920	0.245450	-2.075670
C	0.979570	-0.496710	-2.085140
N	-0.080390	-0.158650	-1.275560
C	2.254550	-0.837590	-1.646690
C	2.216870	0.398290	3.063330
H	-5.105380	0.094260	-0.643470
H	-5.105430	-0.953950	1.880560
H	4.887480	0.097960	2.066310
H	4.901660	-0.910040	-0.461220
H	-1.415530	-0.772560	5.679730
H	1.092690	0.286110	5.706780
C	-3.470080	-1.449650	3.990690
C	3.219880	0.854350	4.069100
C	-3.456660	0.930430	-2.629970
C	3.250040	-1.328160	-2.643670
C	3.089930	-2.595960	-3.238280
C	4.004840	-3.102610	-4.175110
C	5.119730	-2.328950	-4.538620
C	5.303330	-1.055860	-3.973120
C	4.368510	-0.570880	-3.044230
F	2.032120	-3.352470	-2.919760
F	3.828100	-4.309480	-4.715970
F	5.999070	-2.801080	-5.420990
F	6.354930	-0.314640	-4.328890
F	4.552830	0.664060	-2.557710
C	3.774900	-0.018560	5.023740
C	4.726130	0.420080	5.959870
C	5.139650	1.763490	5.947970
C	4.606170	2.655180	5.002350
C	3.657670	2.192930	4.075170
F	3.404070	-1.303080	5.051830
F	5.239410	-0.428300	6.853700
F	6.038900	2.193350	6.832650
F	4.999360	3.930530	4.993970
F	3.164160	3.061550	3.188180
C	-4.047620	0.078020	-3.581030
C	-5.004670	0.538420	-4.499610
C	-5.395440	1.888310	-4.468530
C	-4.829840	2.762440	-3.524850

C	-3.871740	2.276250	-2.619560
F	-3.686460	-1.211200	-3.637620
F	-5.541410	-0.292410	-5.395920
F	-6.300360	2.341540	-5.335300
F	-5.201540	4.044060	-3.499480
F	-3.343030	3.131270	-1.738710
C	-4.053240	-0.591760	4.942760
C	-4.996860	-1.054440	5.874560
C	-5.380100	-2.406540	5.856760
C	-4.822830	-3.282700	4.910340
C	-3.879400	-2.797350	3.989640
F	-3.713030	0.701120	4.976670
F	-5.531230	-0.220270	6.769460
F	-6.272740	-2.859310	6.736580
F	-5.188730	-4.566100	4.895640
F	-3.363490	-3.653150	3.102640
C	-0.737150	0.322580	-3.530690
H	-1.469810	-0.207720	-4.168270
C	0.646370	-0.361160	-3.560070
H	0.594070	-1.364980	-4.032640
C	1.545000	0.602710	-4.385560
H	2.222790	1.179030	-3.697290
H	2.187260	0.074620	-5.124030
C	-0.468290	1.731160	-4.107090
H	-0.155110	2.436000	-3.284240
H	-1.357800	2.172510	-4.607360
N	0.593410	1.472470	-5.065890
C	1.168120	2.637010	-5.702250
H	1.932390	2.322430	-6.446600
H	0.377750	3.201690	-6.244150
H	1.664230	3.341860	-4.976360

Table S11. XYZ Coordinates of the PBE/SVP optimized Ni-TPCF$_{20}$ · 1 Pyridine (*syn*).

$E_{PBE/SVP}$ = -5818.951239038 Hartree
NImag = 0

Ni	-0.620640	-0.416720	-0.091710
F	-3.408720	0.582740	-4.678580
F	-4.681810	0.033890	-7.008440
F	-3.547070	-4.551900	-6.560390
F	-2.283970	-4.017630	-4.221830
F	3.654360	0.381380	-3.235250
F	6.074250	-0.062540	-4.393530
F	7.515020	-2.295330	-3.741990
F	6.517230	-4.096260	-1.936560
F	4.089620	-3.672960	-0.791400
F	2.022210	-1.595680	4.930220
F	3.056970	-0.744050	7.293410
F	3.066080	1.925870	7.905570
F	2.044590	3.743620	6.134720
F	1.012770	2.899680	3.764130
F	-7.718360	-1.518660	3.874470
F	-8.869130	0.945390	3.580220
F	-5.086860	2.444480	1.168870
N	-2.569390	-0.672050	-0.724820
N	1.339420	-0.598380	0.694570
N	0.018690	-1.269810	-1.843730
N	-1.314080	-0.055810	1.805430
N	-0.425910	1.535060	-0.678970
N	5.151490	0.926770	1.526830
C	-3.715100	-0.431580	0.001620
C	-4.889200	-0.634550	-0.818520
H	-5.928580	-0.528930	-0.484230
C	-4.436800	-1.004910	-2.061300
H	-5.037290	-1.267710	-2.940540
C	-2.990870	-1.020650	-1.988260
C	-2.143730	-1.395000	-3.060430
C	-0.746000	-1.522060	-2.973110
C	0.103760	-1.959870	-4.061110
H	-0.233500	-2.225190	-5.070080
C	1.314300	-1.534830	-2.197340
C	2.454740	-1.376080	-1.359080
C	2.447360	-0.948710	-0.027050
C	3.729050	-0.804080	0.780720
H	4.232580	-1.786900	0.882210
C	3.224370	-0.281630	2.144430
H	3.483880	-0.976680	2.967970
C	1.717890	-0.218470	1.954170
C	0.860900	0.181900	2.981450
C	-0.559700	0.221290	2.912440
C	-1.409220	0.544830	4.043150
H	-1.063160	0.780170	5.056790
C	-2.703800	0.470530	3.594800
H	-3.625440	0.642180	4.164200
C	-2.634380	0.100290	2.196460
C	-3.755330	-0.058780	1.365260
C	-5.101530	0.202740	1.962040
C	-5.799680	-0.794880	2.665850
C	-7.071080	-0.555800	3.214290
C	-7.663310	0.709310	3.062160
C	-6.985490	1.725090	2.365740
C	-5.716350	1.459910	1.825990
C	-2.800940	-1.698100	-4.368100

C	-2.854670	-3.007400	-4.886600
C	-3.506880	-3.300070	-6.096470
C	-4.128390	-2.265830	-6.816490
C	-4.091000	-0.949970	-6.325030
C	-3.428320	-0.681640	-5.116250
C	3.785320	-1.640860	-1.988120
C	4.549880	-2.780110	-1.677250
C	5.810250	-3.009730	-2.254310
C	6.323410	-2.087400	-3.182110
C	5.581100	-0.942130	-3.518030
C	4.329520	-0.735230	-2.918550
C	1.471160	0.623980	4.274290
C	2.010550	-0.284120	5.204040
C	2.556010	0.140260	6.427720
C	2.560700	1.509460	6.744380
C	2.032500	2.441950	5.835070
C	1.498050	1.989840	4.617990
C	0.641380	1.937980	-1.400990
H	1.386680	1.166130	-1.653660
C	0.803430	3.263830	-1.822520
H	1.692400	3.541010	-2.410520
C	-0.178590	4.207730	-1.486730
C	-1.289010	3.783460	-0.741670
C	-1.375580	2.439230	-0.357340
H	-2.233960	2.067020	0.225500
C	4.735920	0.271990	0.297160
H	5.614520	-0.156370	-0.232820
H	4.226200	0.982900	-0.416640
C	3.951400	1.073720	2.335850
H	3.291510	1.918170	1.982610
H	4.217680	1.281740	3.395060
C	5.945490	2.122060	1.359560
H	5.398850	2.948670	0.821510
H	6.865580	1.888090	0.779590
H	6.259590	2.511220	2.353150
F	-4.753560	-2.531980	-7.963960
F	-7.548920	2.927750	2.223850
F	-5.257100	-2.005310	2.824770
H	-0.081360	5.259030	-1.803810
H	-2.090420	4.482180	-0.455150
C	1.386080	-1.981830	-3.575340
H	2.297490	-2.283360	-4.105580

Table S12. XYZ Coordinates of the PBE/SVP optimized Ni-TPCF$_{20}$ · 1 Pyridine (*anti*).

$E_{PBE/SVP}$ = -5818.950762296 Hartree
NImag = 0

Ni	-0.586550	-0.084470	-0.191530
F	-3.353600	1.355930	-4.933540
F	-4.600410	0.783570	-7.270910
F	-3.415170	-3.787170	-6.796130
F	-2.177200	-3.228410	-4.449530
F	3.774170	1.232870	-3.494470
F	6.191640	0.751990	-4.639580
F	7.591500	-1.505810	-3.986390
F	6.550430	-3.298370	-2.195490
F	4.118180	-2.839600	-1.068150
F	2.095960	-0.839630	4.667300
F	3.145880	-0.021200	7.035710
F	3.177130	2.641720	7.676900
F	2.162870	4.485870	5.929180
F	1.118070	3.675990	3.553370
F	-7.597720	-0.697250	3.605910
F	-8.790200	1.750380	3.344060
F	-5.049090	3.337650	0.928670
N	-2.497290	0.110170	-0.959230
N	1.413310	0.166160	0.460070
N	0.092160	-0.461630	-2.089590
N	-1.234810	0.772050	1.557370
N	-0.751350	-2.037400	0.412470
N	5.196490	1.788130	1.275820
C	-3.637010	0.426210	-0.252870
C	-4.810340	0.276840	-1.085660
H	-5.844700	0.467010	-0.773920
C	-4.363720	-0.135810	-2.317010
H	-4.966030	-0.357500	-3.206090
C	-2.921940	-0.229770	-2.224650
C	-2.076120	-0.607640	-3.296070
C	-0.675330	-0.701790	-3.219160
C	0.178280	-1.047760	-4.336690
H	-0.160430	-1.262940	-5.357160
C	1.392750	-0.659490	-2.467610
C	2.532840	-0.521500	-1.624950
C	2.524260	-0.130660	-0.281320
C	3.808910	0.037150	0.516010
H	4.339750	-0.933240	0.598840
C	3.303800	0.525210	1.892500
H	3.586780	-0.176580	2.703150
C	1.794010	0.551850	1.717290
C	0.939700	0.963040	2.743500
C	-0.478070	1.056560	2.661210
C	-1.321410	1.482070	3.762930
H	-0.973990	1.765700	4.763500
C	-2.613650	1.449540	3.303880
H	-3.529280	1.712170	3.847870
C	-2.549910	1.004640	1.927330
C	-3.672260	0.837930	1.099640
C	-5.018300	1.091880	1.700430
C	-5.697650	0.076340	2.396230
C	-6.969380	0.284160	2.953490
C	-7.583040	1.541250	2.818030
C	-6.926270	2.575070	2.128790
C	-5.654100	2.340450	1.579310
C	-2.727590	-0.917090	-4.605420

C	-2.758240	-2.227780	-5.121740
C	-3.395840	-2.532940	-6.336000
C	-4.023600	-1.508720	-7.065000
C	-4.005610	-0.190730	-6.578160
C	-3.357080	0.090240	-5.364230
C	3.863320	-0.790910	-2.252300
C	4.605680	-1.945190	-1.944620
C	5.865090	-2.196870	-2.512560
C	6.400440	-1.278850	-3.432490
C	5.679700	-0.120150	-3.768370
C	4.428110	0.110180	-3.175450
C	1.556480	1.391280	4.038010
C	2.094090	0.469940	4.955660
C	2.647960	0.876520	6.181380
C	2.664210	2.242030	6.513030
C	2.139710	3.188130	5.615690
C	1.597370	2.753590	4.395510
C	0.220120	-2.933910	0.137730
H	1.101770	-2.555560	-0.405580
C	4.782250	1.145550	0.038350
H	5.665410	0.745910	-0.506480
H	4.246940	1.852600	-0.658250
C	4.001990	1.893700	2.099690
H	3.318930	2.728020	1.769860
H	4.276240	2.087900	3.159540
C	5.959710	3.005730	1.120580
H	5.387730	3.827920	0.604020
H	6.878080	2.803710	0.525980
H	6.276600	3.383890	2.117580
F	-4.636090	-1.786320	-8.216630
C	0.127610	-4.279100	0.517290
F	-7.511740	3.767930	2.000800
F	-5.133150	-1.132580	2.538070
C	-1.851700	-2.451830	1.076130
H	-2.620920	-1.690640	1.282570
C	-2.021860	-3.779370	1.489020
H	-2.939380	-4.065300	2.026670
C	-1.014920	-4.713840	1.205740
H	-1.119000	-5.766330	1.516630
H	0.947760	-4.970950	0.269490
C	1.466660	-1.032570	-3.867580
H	2.384260	-1.249180	-4.427240

Table S13. XYZ Coordinates of the PBE/SVP optimized Ni-TPCF$_{20}$ · 2 Pyridine (2·2Py).

$E_{PBE/SVP}$ = -6066.754572686 Hartree
NImag = 0

Ni	-0.537710	-0.224420	-0.126150
F	-3.329130	0.977170	-4.797160
F	-4.597580	0.402720	-7.122050
F	-3.430210	-4.172130	-6.641150
F	-2.172600	-3.612460	-4.306160
F	3.779660	0.847250	-3.348370
F	6.199810	0.391880	-4.502490
F	7.624570	-1.852290	-3.856590
F	6.607860	-3.658770	-2.066380
F	4.172860	-3.228710	-0.932360
F	2.123650	-1.207800	4.810160
F	3.166780	-0.378870	7.177540
F	3.183700	2.285690	7.813250
F	2.161160	4.120980	6.060720
F	1.122200	3.300800	3.685910
F	-7.609470	-1.064480	3.745010
F	-8.779820	1.392370	3.470440
F	-5.012170	2.941080	1.067020
N	-2.488900	-0.246230	-0.830230
N	1.451280	-0.196250	0.593490
N	0.126560	-0.853050	-1.972490
N	-1.227550	0.395060	1.716140
N	-0.725890	-2.320550	0.509390
N	-0.324640	1.863130	-0.755950
N	5.236020	1.392810	1.423280
C	-3.626940	0.040590	-0.114080
C	-4.801930	-0.137970	-0.943620
H	-5.840790	0.014730	-0.625660
C	-4.350190	-0.540230	-2.177020
H	-4.953030	-0.787080	-3.059360
C	-2.902930	-0.598810	-2.091890
C	-2.050540	-0.984620	-3.160740
C	-0.647230	-1.100130	-3.091030
C	0.203570	-1.493350	-4.199000
H	-0.135350	-1.736440	-5.213310
C	1.422460	-1.079310	-2.335250
C	2.561050	-0.922710	-1.485350
C	2.556700	-0.513940	-0.142880
C	3.839910	-0.352830	0.661750
H	4.364590	-1.325920	0.751750
C	3.330420	0.144740	2.035770
H	3.605790	-0.556730	2.849100
C	1.819980	0.184710	1.852990
C	0.957500	0.587490	2.880020
C	-0.465950	0.663630	2.814750
C	-1.312680	1.039960	3.935730
H	-0.966580	1.292680	4.945330
C	-2.607690	0.997950	3.482350
H	-3.524430	1.220140	4.042550
C	-2.542750	0.594400	2.090060
C	-3.660870	0.436800	1.247670
C	-5.007590	0.694850	1.843650
C	-5.698050	-0.312900	2.539540
C	-6.970050	-0.091070	3.091580
C	-7.572400	1.170690	2.949420
C	-6.903840	2.197160	2.259910
C	-5.632280	1.947810	1.717230

C	-2.708940	-1.297690	-4.466110
C	-2.750990	-2.610120	-4.977590
C	-3.400070	-2.916160	-6.185670
C	-4.029360	-1.891920	-6.913030
C	-4.001200	-0.572570	-6.430680
C	-3.341270	-0.290890	-5.223270
C	3.892490	-1.182690	-2.113150
C	4.648190	-2.328900	-1.808120
C	5.909140	-2.564840	-2.379850
C	6.431960	-1.639720	-3.299820
C	5.697910	-0.488230	-3.632540
C	4.445850	-0.274680	-3.035670
C	1.573580	1.018680	4.174310
C	2.115190	0.102250	5.094630
C	2.665380	0.514460	6.320270
C	2.673950	1.880580	6.649360
C	2.144870	2.821780	5.749730
C	1.605890	2.381590	4.530210
C	0.237400	-3.222880	0.235680
H	1.123150	-2.849580	-0.303090
C	0.739730	2.268710	-1.476840
H	1.483140	1.497510	-1.733970
C	0.912170	3.594630	-1.898790
H	1.803120	3.867050	-2.486400
C	-0.064540	4.543470	-1.563020
C	-1.176070	4.121470	-0.819070
C	-1.264510	2.775120	-0.437420
H	-2.125390	2.411360	0.145660
C	4.823670	0.747410	0.187160
H	5.706580	0.341830	-0.353860
H	4.296590	1.458040	-0.513530
C	4.037810	1.508250	2.241160
H	3.362760	2.346480	1.903710
H	4.307760	1.705660	3.301540
C	6.005720	2.605320	1.266140
H	5.439690	3.428130	0.742630
H	6.926190	2.396800	0.676930
H	6.319150	2.987650	2.262650
F	-4.653160	-2.171000	-8.058750
C	0.143030	-4.572090	0.605480
F	-7.478390	3.395410	2.126890
F	-5.144950	-1.525010	2.686860
C	-1.824720	-2.741530	1.166730
H	-2.593380	-1.982320	1.378950
C	-2.005540	-4.071400	1.572500
H	-2.926450	-4.356100	2.105370
C	-1.002290	-5.008630	1.287410
H	-1.111020	-6.062930	1.591400
H	0.962460	-5.264400	0.355680
H	0.037270	5.594950	-1.878920
H	-1.975610	4.822250	-0.531630
C	1.492320	-1.491380	-3.727160
H	2.405390	-1.748440	-4.277870

Table S14. XYZ Coordinates of the PBE/SVP optimized Ni-TPIBF$_{20}$ (3).

$E_{PBE/SVP}$ = -5744.070646963 Hartree
NImag = 0

C	-1.781360	-0.310640	3.240730
N	-0.723770	0.032050	2.400560
C	-1.420100	-0.080110	4.611360
C	-0.155840	0.461480	4.601760
C	0.284400	0.456380	3.232380
C	-3.054940	-0.692320	2.801940
C	-3.444520	-0.527190	1.466120
C	-4.810270	-0.532530	1.022440
C	-4.814320	0.008390	-0.245120
C	-3.443740	0.271420	-0.582910
N	-2.608960	-0.061560	0.453450
Ni	-0.679470	-0.002520	0.471660
N	1.266010	-0.100890	0.514570
C	2.053290	-0.526520	-0.518270
C	2.082340	0.216560	1.588970
C	-3.009450	0.706230	-1.864040
C	-1.701610	0.579740	-2.272250
C	0.391280	-0.195600	-2.288870
N	-0.655250	0.115920	-1.479520
C	1.650050	-0.636730	-1.852880
C	1.639970	0.617400	2.834750
H	-5.673150	0.190560	-0.902550
H	-5.668490	-0.847320	1.628330
H	-2.063420	-0.266490	5.478890
H	0.439680	0.786830	5.462020
C	-4.065340	-1.167270	3.791320
C	2.640620	1.104230	3.828770
C	-4.039580	1.194320	-2.829190
C	2.619930	-1.138910	-2.873800
C	2.423080	-2.396710	-3.479210
C	3.315510	-2.917230	-4.431050
C	4.442900	-2.166220	-4.803590
C	4.662100	-0.902090	-4.230990
C	3.748490	-0.405680	-3.288500
F	1.352960	-3.131010	-3.152100
F	3.105410	-4.115530	-4.978930
F	5.301090	-2.650890	-5.699510
F	5.726390	-0.181850	-4.590680
F	3.980450	0.817020	-2.782010
C	3.022400	0.359530	4.961930
C	3.956590	0.843210	5.892180
C	4.540840	2.105330	5.693060
C	4.194860	2.866880	4.564610
C	3.255370	2.360080	3.652260
F	2.513310	-0.863240	5.165590
F	4.298360	0.111720	6.955590
F	5.427300	2.576960	6.569230
F	4.753430	4.064070	4.373480
F	2.954340	3.104990	2.581270
C	-4.613980	0.345130	-3.793120
C	-5.590740	0.797810	-4.694710
C	-6.010800	2.138030	-4.639420
C	-5.457880	3.009450	-3.685870
C	-4.482710	2.530230	-2.795010
F	-4.217490	-0.931800	-3.877900
F	-6.114900	-0.030020	-5.601870
F	-6.931640	2.584870	-5.493460

F	-5.855960	4.283070	-3.639210
F	-3.965570	3.383010	-1.904950
C	-4.670830	-0.298220	4.719100
C	-5.611460	-0.756450	5.656490
C	-5.975430	-2.113590	5.664980
C	-5.399630	-3.000190	4.739800
C	-4.456300	-2.520370	3.816470
F	-4.357160	1.001990	4.727520
F	-6.161940	0.088290	6.532160
F	-6.866790	-2.561540	6.549300
F	-5.747860	-4.289030	4.747820
F	-3.922800	-3.387870	2.950980
C	-1.270230	0.772230	-3.703360
H	-1.998130	0.324600	-4.406440
C	0.095600	0.053280	-3.756710
H	0.030660	-0.914590	-4.299060
C	1.037800	1.048690	-4.491990
H	1.726940	1.543500	-3.753180
H	1.671350	0.559490	-5.264270
C	-0.941810	2.215660	-4.145840
H	-0.618400	2.831290	-3.257640
H	-1.806840	2.732380	-4.615990
N	0.127140	2.005270	-5.108550
C	0.752730	3.199570	-5.631080
H	1.509430	2.925780	-6.399040
H	-0.010690	3.843650	-6.120310
H	1.271100	3.813600	-4.840620
C	3.549200	-0.010100	1.273630
H	4.082810	0.961470	1.195610
C	3.485010	-0.729300	-0.090540
H	4.198770	-0.294210	-0.811310
C	4.308440	-0.999990	2.203080
H	5.101710	-0.507910	2.807690
H	3.588360	-1.483650	2.917910
C	3.907090	-2.178770	0.239170
H	4.352140	-2.709590	-0.630900
H	3.015830	-2.776900	0.586820
N	4.894530	-1.971710	1.285490
C	5.414340	-3.168640	1.908860
H	5.875370	-3.826870	1.139840
H	6.204470	-2.899550	2.644030
H	4.627990	-3.765720	2.452330

Table S15. XYZ Coordinates of the PBE/SVP optimized Ni-TPIBF$_{20}$ · 2 Pyridine (3·2Py).

$E_{PBE/SVP}$ = -6239.668465040 Hartree
NImag = 0

Ni	0.626170	0.319830	0.128880
N	-1.400860	0.870860	0.334760
N	0.049310	-1.556000	-0.662130
N	2.618270	-0.190410	-0.100280
N	1.208560	2.139110	0.933040
C	-1.842240	2.083300	0.818770
C	-3.358580	2.189550	0.747620
H	-3.789910	2.343800	1.757350
C	-3.782270	0.821770	0.162620
H	-4.434970	0.266850	0.866110
C	-2.453780	0.103760	-0.028690
C	-2.391130	-1.219680	-0.528560
C	-1.228240	-1.978350	-0.801740
C	-1.310280	-3.411330	-1.308860
H	-1.846590	-3.451550	-2.278750
C	0.176880	-3.810040	-1.466260
H	0.414680	-4.073550	-2.516500
C	0.921890	-2.552190	-1.044130
C	2.310280	-2.470000	-1.046340
C	3.102360	-1.347160	-0.634830
C	4.547080	-1.302740	-0.712780
H	5.194540	-2.090390	-1.117120
C	4.932570	-0.086210	-0.195450
H	5.951690	0.306560	-0.091850
C	3.719570	0.597500	0.189960
C	3.671110	1.871690	0.797090
C	2.502870	2.574710	1.162420
C	2.483870	3.868980	1.804390
H	3.365390	4.445500	2.111650
C	1.157890	4.212360	1.950620
H	0.749200	5.124050	2.403700
C	0.384820	3.123570	1.392060
C	-1.046210	3.109810	1.316120
C	-3.928030	3.232810	-0.246690
H	-4.295340	4.156400	0.252120
H	-3.127650	3.540160	-0.978530
C	-4.561990	1.173300	-1.130100
H	-3.875580	1.107420	-2.023290
H	-5.420970	0.493550	-1.322310
N	-5.029510	2.528720	-0.887520
C	-5.618660	3.197220	-2.025030
H	-5.991870	4.200610	-1.723130
H	-4.897400	3.340690	-2.880060
H	-6.485220	2.611370	-2.404250
C	-1.895450	-4.459020	-0.327070
H	-1.899600	-4.043350	0.721850
H	-2.940010	-4.752370	-0.571660
N	-1.000120	-5.596180	-0.468790
C	0.345670	-5.047610	-0.549310
H	1.050310	-5.803290	-0.960040
H	0.742530	-4.727630	0.456250
C	-1.186050	-6.657450	0.493600
H	-0.495100	-7.499380	0.267700
H	-2.227050	-7.045740	0.434880
H	-0.998000	-6.332610	1.557100
C	-1.751310	4.344290	1.784030
C	-1.723050	5.526860	1.018890

C	-2.420210	6.682330	1.407950
C	-3.168680	6.670240	2.597290
C	-3.209610	5.509460	3.387720
C	-2.495730	4.370930	2.978140
F	-1.043810	5.558770	-0.134010
F	-2.389630	7.785080	0.654110
F	-3.843220	7.758500	2.972140
F	-3.921730	5.499180	4.518280
F	-2.565200	3.275860	3.748930
C	-3.706590	-1.892620	-0.769740
C	-4.217200	-2.091910	-2.065900
C	-5.464170	-2.696140	-2.295030
C	-6.239150	-3.112090	-1.198260
C	-5.758910	-2.930630	0.110520
C	-4.503090	-2.334830	0.303390
F	-3.505180	-1.690670	-3.132100
F	-5.925700	-2.864950	-3.536770
F	-7.429090	-3.678220	-1.398030
F	-6.495580	-3.326370	1.151450
F	-4.065770	-2.183570	1.565430
C	3.074840	-3.683290	-1.473440
C	3.141540	-4.102410	-2.815320
C	3.872790	-5.236140	-3.207820
C	4.575750	-5.974090	-2.240760
C	4.530130	-5.582550	-0.891880
C	3.783720	-4.450850	-0.527480
F	2.483480	-3.423860	-3.766660
F	3.913870	-5.608690	-4.490560
F	5.282980	-7.046460	-2.600410
F	5.191180	-6.288930	0.030090
F	3.744420	-4.115410	0.767660
C	4.981900	2.538110	1.062540
C	5.754140	2.206640	2.189280
C	7.002780	2.803690	2.429430
C	7.496390	3.757840	1.523250
C	6.743140	4.110020	0.390490
C	5.496090	3.500850	0.176630
F	5.303190	1.298920	3.065590
F	7.721920	2.474370	3.506010
F	8.682940	4.328870	1.736510
F	7.219560	5.013560	-0.470450
F	4.797920	3.846420	-0.913980
N	0.616250	1.184690	-1.877570
C	-0.333130	0.867740	-2.781060
H	-1.097380	0.141740	-2.458410
C	-0.369910	1.416720	-4.070730
H	-1.170720	1.121300	-4.767020
C	0.623370	2.334400	-4.443750
H	0.626230	2.785680	-5.449720
C	1.613140	2.662690	-3.506280
H	2.417890	3.376220	-3.743260
C	1.570770	2.066170	-2.238040
H	2.331500	2.304860	-1.478820
N	0.605840	-0.558150	2.129690
C	-0.454070	-1.255610	2.585980
H	-1.312640	-1.351970	1.901890
C	-0.490820	-1.837810	3.860950
H	-1.385310	-2.396570	4.179050
C	0.620800	-1.690580	4.703710
H	0.627050	-2.135020	5.712710
C	1.722920	-0.963090	4.231880

H	2.622100	-0.814670	4.850110
C	1.672860	-0.415680	2.941880
H	2.522330	0.159210	2.541040

VI Crystal structure data

VI.1 Ni-TPPF$_{20}$·2pyridine (1·2Py).

Table S16. Crystal data and structure refinement for Ni-TPPF$_{20}$·2pyridine (1·2Py).

Identification code	herges100 (Sample No 5)	
Empirical formula	$C_{69}H_{33}F_{20}N_9Ni$	
Formula weight	1426.75	
Temperature	170(2) K	
Wavelength	0.71073 Å	
Crystal system	Triclinic	
Space group	P-1	
Unit cell dimensions	a = 9.6240(3) Å	α= 106.463(3)°.
	b = 12.9847(4) Å	β= 101.692(3)°.
	c = 13.0914(5) Å	γ = 96.436(3)°.
Volume	1511.10(9) Å^3	
Z	1	
Density (calculated)	1.568 Mg/m^3	
Absorption coefficient	0.436 mm^{-1}	
F(000)	718	
Crystal size	0.3 x 0.3 x 0.2 mm^3	
Theta range for data collection	1.663 to 27.003°.	
Index ranges	-11<=h<=12, -16<=k<=16, -16<=l<=16	
Reflections collected	21978	
Independent reflections	6599 [R(int) = 0.0367]	
Completeness to theta = 25.242°	99.8 %	
Refinement method	Full-matrix least-squares on F^2	
Data / restraints / parameters	6599 / 0 / 367	
Goodness-of-fit on F^2	1.052	
Final R indices [I>2sigma(I)]	R1 = 0.0361, wR2 = 0.1052	
R indices (all data)	R1 = 0.0403, wR2 = 0.1073	
Extinction coefficient	n/a	
Largest diff. peak and hole	0.303 and -0.521 e.Å^{-3}	

Comments

All non-hydrogen atoms were refined anisotropic. The H atoms were positioned with idealized geometry and refined isotropic with $U_{iso}(H) = 1.2\ U_{eq}(C)$ using a riding model. There are two additional pyridine molecules in cavities of the structure, of which one is located on a center of inversion. Both of these molecules are disordered and no reasonable split model can be found. Therefore, the data were corrected using SQUEEZE in Platon. The potential volume for the solvent of 451.9 Å^3 and the total electron count of 119.2 is in very good agreement with 3 molecules pyridine in the unit cell.

Table S17. Atomic coordinates (x 10^4) and equivalent isotropic displacement parameters (Å^{2}x 10^3) for herges100. U(eq) is defined as one third of the trace of the orthogonalized U^{ij} tensor.

	x	y	z	U(eq)
Ni(1)	5000	5000	5000	27(1)
N(1)	5718(1)	3653(1)	5290(1)	30(1)
C(1)	5689(2)	2689(1)	4522(1)	31(1)
C(2)	6320(2)	1949(1)	5048(1)	36(1)
C(3)	6711(2)	2486(1)	6140(1)	36(1)
C(4)	6334(2)	3559(1)	6286(1)	30(1)
C(5)	6561(2)	4382(1)	7300(1)	30(1)
C(6)	6243(2)	5431(1)	7455(1)	30(1)
C(7)	6576(2)	6286(1)	8506(1)	34(1)
C(8)	6128(2)	7174(1)	8314(1)	34(1)
C(9)	5494(2)	6873(1)	7145(1)	30(1)
C(10)	4882(2)	7565(1)	6611(1)	31(1)
N(2)	5592(1)	5814(1)	6645(1)	29(1)
C(11)	7236(2)	4122(1)	8311(1)	31(1)
C(12)	8645(2)	3941(1)	8514(1)	34(1)
C(13)	9292(2)	3725(1)	9451(1)	38(1)
C(14)	8545(2)	3707(1)	10240(1)	40(1)
C(15)	7152(2)	3892(1)	10078(1)	39(1)
C(16)	6507(2)	4073(1)	9115(1)	34(1)
F(11)	9443(1)	3997(1)	7797(1)	44(1)
F(12)	10654(1)	3555(1)	9603(1)	51(1)
F(13)	9180(1)	3526(1)	11166(1)	56(1)
F(14)	6426(1)	3879(1)	10843(1)	52(1)
F(15)	5130(1)	4209(1)	8971(1)	43(1)
C(21)	4851(2)	8679(1)	7327(1)	34(1)
C(22)	3893(2)	8856(1)	7994(1)	40(1)
C(23)	3913(2)	9873(2)	8708(1)	47(1)
C(24)	4904(2)	10747(1)	8760(1)	48(1)
C(25)	5861(2)	10609(1)	8111(1)	47(1)
C(26)	5823(2)	9582(1)	7403(1)	40(1)
F(21)	2920(1)	8014(1)	7963(1)	58(1)
F(22)	2990(2)	10010(1)	9358(1)	70(1)
F(23)	4935(2)	11736(1)	9454(1)	69(1)
F(24)	6838(2)	11464(1)	8180(1)	70(1)
F(25)	6775(1)	9476(1)	6779(1)	58(1)
N(31)	7178(1)	5620(1)	4858(1)	36(1)
C(31)	7719(2)	5080(2)	4034(2)	49(1)
C(32)	9061(2)	5427(2)	3907(2)	62(1)
C(33)	9895(3)	6376(2)	4638(2)	71(1)
C(34)	9363(3)	6924(2)	5470(2)	80(1)
C(35)	8008(2)	6528(2)	5557(2)	62(1)

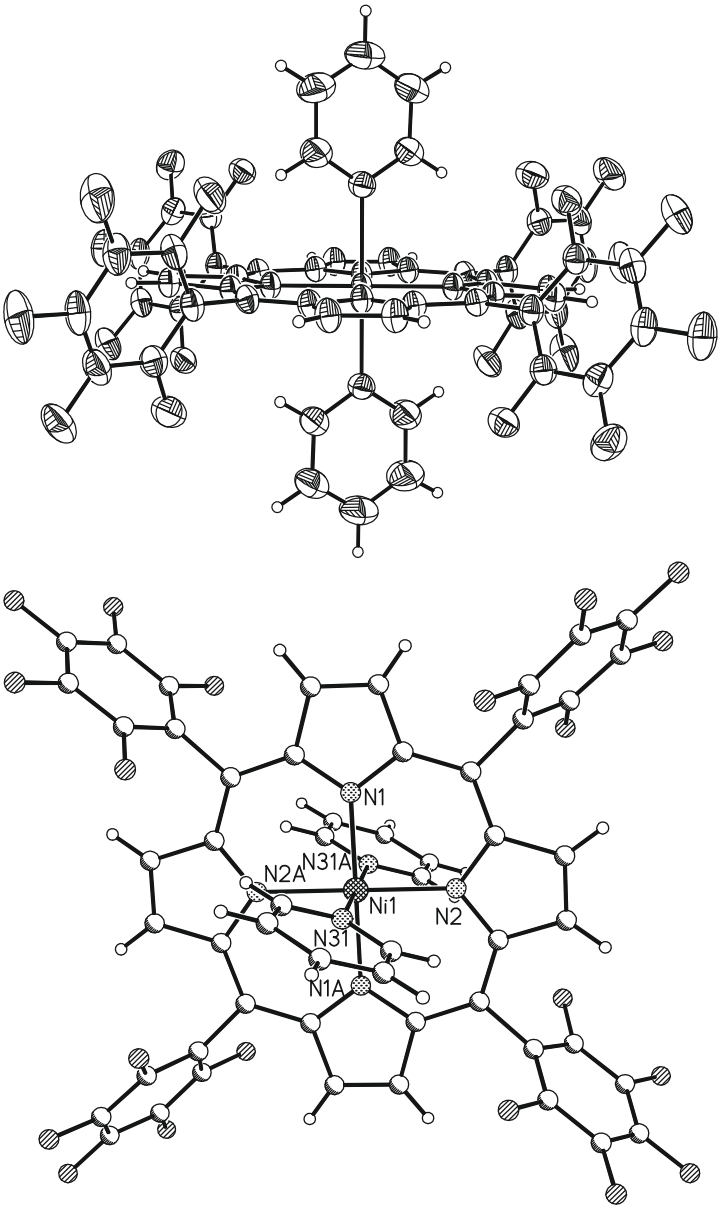

Table S18. Bond lengths [Å] and angles [°].

Ni(1)-N(2)	2.0392(11)	Ni(1)-N(1A)	2.0548(11)
Ni(1)-N(2A)	2.0392(11)	Ni(1)-N(31)	2.2228(13)
Ni(1)-N(1)	2.0548(11)	Ni(1)-N(31A)	2.2229(13)
N(2)-Ni(1)-N(2A)	180.00(10)	N(1)-Ni(1)-N(31)	89.94(5)
N(2)-Ni(1)-N(1)	89.97(5)	N(1A)-Ni(1)-N(31)	90.06(5)
N(2A)-Ni(1)-N(1)	90.03(5)	N(2)-Ni(1)-N(31A)	90.19(5)
N(2)-Ni(1)-N(1A)	90.03(5)	N(2A)-Ni(1)-N(31A)	89.81(5)
N(2A)-Ni(1)-N(1A)	89.97(5)	N(1)-Ni(1)-N(31A)	90.06(5)
N(1)-Ni(1)-N(1A)	180.0	N(1A)-Ni(1)-N(31A)	89.94(5)
N(2)-Ni(1)-N(31)	89.81(5)	N(31)-Ni(1)-N(31A)	180.0
N(2A)-Ni(1)-N(31)	90.19(5)		

Symmetry transformations used to generate equivalent atoms: A: -x+1,-y+1,-z+1

Table S19. Bond lengths [Å] and angles [°].

N(1)-C(1)	1.3586(18)	C(14)-F(13)	1.3388(17)
N(1)-C(4)	1.3638(17)	C(14)-C(15)	1.373(2)
C(1)-C(10A)	1.400(2)	C(15)-F(14)	1.3358(18)
C(1)-C(2)	1.4502(19)	C(15)-C(16)	1.383(2)
C(2)-C(3)	1.352(2)	C(16)-F(15)	1.3391(19)
C(3)-C(4)	1.4489(19)	C(21)-C(26)	1.383(2)
C(4)-C(5)	1.4062(19)	C(21)-C(22)	1.387(2)
C(5)-C(6)	1.3972(19)	C(22)-F(21)	1.343(2)
C(5)-C(11)	1.4967(19)	C(22)-C(23)	1.381(2)
C(6)-N(2)	1.3650(17)	C(23)-F(22)	1.341(2)
C(6)-C(7)	1.4504(19)	C(23)-C(24)	1.376(3)
C(7)-C(8)	1.346(2)	C(24)-F(23)	1.3398(18)
C(8)-C(9)	1.4480(19)	C(24)-C(25)	1.368(3)
C(9)-N(2)	1.3680(18)	C(25)-F(24)	1.341(2)
C(9)-C(10)	1.398(2)	C(25)-C(26)	1.383(2)
C(10)-C(1A)	1.400(2)	C(26)-F(25)	1.3397(19)
C(10)-C(21)	1.4915(19)	N(31)-C(35)	1.322(2)
C(11)-C(12)	1.387(2)	N(31)-C(31)	1.343(2)
C(11)-C(16)	1.390(2)	C(31)-C(32)	1.379(3)
C(12)-F(11)	1.3392(17)	C(32)-C(33)	1.370(3)
C(12)-C(13)	1.377(2)	C(33)-C(34)	1.350(4)
C(13)-F(12)	1.3387(19)	C(34)-C(35)	1.386(3)
C(13)-C(14)	1.376(2)	F(13)-C(14)-C(15)	120.27(15)
C(1)-N(1)-C(4)	106.84(11)	F(13)-C(14)-C(13)	120.18(15)
N(1)-C(1)-C(10A)	125.35(13)	C(15)-C(14)-C(13)	119.55(14)
N(1)-C(1)-C(2)	109.99(12)	F(14)-C(15)-C(14)	119.71(14)
C(10A)-C(1)-C(2)	124.65(13)	F(14)-C(15)-C(16)	120.63(15)
C(3)-C(2)-C(1)	106.59(13)	C(14)-C(15)-C(16)	119.65(14)
C(2)-C(3)-C(4)	106.84(12)	F(15)-C(16)-C(15)	117.77(14)
N(1)-C(4)-C(5)	124.88(12)	F(15)-C(16)-C(11)	119.79(13)
N(1)-C(4)-C(3)	109.74(12)	C(15)-C(16)-C(11)	122.44(15)
C(5)-C(4)-C(3)	125.38(13)	C(26)-C(21)-C(22)	116.42(14)
C(6)-C(5)-C(4)	126.19(13)	C(26)-C(21)-C(10)	121.72(14)
C(6)-C(5)-C(11)	116.61(12)	C(22)-C(21)-C(10)	121.79(14)
C(4)-C(5)-C(11)	117.19(12)	F(21)-C(22)-C(23)	118.18(15)
N(2)-C(6)-C(5)	125.47(13)	F(21)-C(22)-C(21)	119.58(14)
N(2)-C(6)-C(7)	109.62(12)	C(23)-C(22)-C(21)	122.24(16)
C(5)-C(6)-C(7)	124.90(13)	F(22)-C(23)-C(24)	120.05(16)
C(8)-C(7)-C(6)	107.10(12)	F(22)-C(23)-C(22)	120.65(18)
C(7)-C(8)-C(9)	106.82(13)	C(24)-C(23)-C(22)	119.29(16)
N(2)-C(9)-C(10)	125.33(13)	F(23)-C(24)-C(25)	120.06(17)
N(2)-C(9)-C(8)	109.81(12)	F(23)-C(24)-C(23)	119.66(17)
C(10)-C(9)-C(8)	124.85(13)	C(25)-C(24)-C(23)	120.27(15)
C(9)-C(10)-C(1A)	126.17(13)	F(24)-C(25)-C(24)	119.75(15)
C(9)-C(10)-C(21)	116.05(12)	F(24)-C(25)-C(26)	120.82(17)
C(1A)-C(10)-C(21)	117.78(12)	C(24)-C(25)-C(26)	119.42(16)
C(6)-N(2)-C(9)	106.64(11)	F(25)-C(26)-C(21)	119.81(14)
C(12)-C(11)-C(16)	115.90(13)	F(25)-C(26)-C(25)	117.85(15)
C(12)-C(11)-C(5)	121.83(13)	C(21)-C(26)-C(25)	122.34(16)
C(16)-C(11)-C(5)	122.25(13)	C(35)-N(31)-C(31)	116.21(16)
F(11)-C(12)-C(13)	117.28(14)	N(31)-C(31)-C(32)	123.24(19)
F(11)-C(12)-C(11)	120.17(13)	C(33)-C(32)-C(31)	119.3(2)
C(13)-C(12)-C(11)	122.53(14)	C(34)-C(33)-C(32)	117.9(2)
F(12)-C(13)-C(14)	120.12(14)	C(33)-C(34)-C(35)	120.0(2)
F(12)-C(13)-C(12)	120.00(15)	N(31)-C(35)-C(34)	123.3(2)
C(14)-C(13)-C(12)	119.87(15)		

Table 20. Anisotropic displacement parameters ($Å^2 x\ 10^3$) . The anisotropic displacement factor exponent takes the form: $-2\pi^2[h^2 a^{*2} U^{11} + ... + 2 h k a^* b^* U^{12}]$

	U^{11}	U^{22}	U^{33}	U^{23}	U^{13}	U^{12}
Ni(1)	32(1)	24(1)	23(1)	4(1)	7(1)	7(1)
N(1)	36(1)	26(1)	25(1)	5(1)	7(1)	7(1)
C(1)	37(1)	27(1)	29(1)	5(1)	9(1)	9(1)
C(2)	48(1)	28(1)	32(1)	7(1)	10(1)	12(1)
C(3)	45(1)	30(1)	31(1)	9(1)	8(1)	12(1)
C(4)	35(1)	29(1)	28(1)	8(1)	8(1)	7(1)
C(5)	34(1)	30(1)	27(1)	7(1)	8(1)	6(1)
C(6)	32(1)	30(1)	27(1)	7(1)	6(1)	6(1)
C(7)	39(1)	34(1)	26(1)	5(1)	4(1)	9(1)
C(8)	41(1)	30(1)	26(1)	2(1)	7(1)	7(1)
C(9)	35(1)	28(1)	26(1)	4(1)	7(1)	6(1)
C(10)	37(1)	28(1)	28(1)	5(1)	10(1)	8(1)
N(2)	35(1)	27(1)	24(1)	3(1)	6(1)	8(1)
C(11)	37(1)	28(1)	27(1)	5(1)	6(1)	9(1)
C(12)	38(1)	31(1)	32(1)	7(1)	9(1)	7(1)
C(13)	38(1)	32(1)	38(1)	7(1)	1(1)	10(1)
C(14)	54(1)	33(1)	29(1)	9(1)	2(1)	11(1)
C(15)	53(1)	34(1)	29(1)	9(1)	12(1)	8(1)
C(16)	39(1)	32(1)	30(1)	6(1)	8(1)	8(1)
F(11)	40(1)	54(1)	42(1)	15(1)	16(1)	13(1)
F(12)	41(1)	55(1)	53(1)	14(1)	0(1)	19(1)
F(13)	76(1)	56(1)	34(1)	18(1)	0(1)	20(1)
F(14)	71(1)	56(1)	38(1)	19(1)	26(1)	16(1)
F(15)	40(1)	52(1)	40(1)	13(1)	15(1)	15(1)
C(21)	44(1)	30(1)	27(1)	6(1)	9(1)	11(1)
C(22)	42(1)	34(1)	39(1)	6(1)	11(1)	8(1)
C(23)	56(1)	47(1)	40(1)	5(1)	20(1)	21(1)
C(24)	75(1)	31(1)	34(1)	0(1)	12(1)	17(1)
C(25)	75(1)	26(1)	36(1)	6(1)	14(1)	2(1)
C(26)	58(1)	32(1)	31(1)	7(1)	17(1)	9(1)
F(21)	53(1)	49(1)	67(1)	5(1)	29(1)	2(1)
F(22)	74(1)	69(1)	67(1)	0(1)	41(1)	23(1)
F(23)	113(1)	35(1)	52(1)	-5(1)	28(1)	20(1)
F(24)	115(1)	32(1)	56(1)	5(1)	32(1)	-11(1)
F(25)	77(1)	45(1)	50(1)	5(1)	36(1)	-3(1)
N(31)	36(1)	36(1)	39(1)	12(1)	12(1)	6(1)
C(31)	47(1)	52(1)	46(1)	9(1)	18(1)	4(1)
C(32)	56(1)	71(1)	62(1)	18(1)	30(1)	6(1)
C(33)	52(1)	80(2)	82(2)	24(1)	31(1)	-4(1)
C(34)	58(1)	73(2)	87(2)	0(1)	27(1)	-20(1)
C(35)	54(1)	57(1)	61(1)	-3(1)	25(1)	-7(1)

Table S21. Hydrogen coordinates (x 10^4) and isotropic displacement parameters ($Å^2 x\ 10^3$).

	x	y	z	U(eq)
H(2)	6437	1228	4695	44
H(3)	7148	2212	6703	43
H(7)	7026	6229	9200	41
H(8)	6212	7866	8844	41
H(31)	7147	4426	3515	58
H(32)	9405	5013	3317	74
H(33)	10818	6640	4563	86
H(34)	9918	7581	5996	95
H(35)	7658	6930	6150	74

VI.2 Ni-TPCF$_{20}$·2 pyridine (2·2Py)

Table S22. Crystal data and structure refinement for Ni-TPCF$_{20}$·2 pyridine (2·2Py).

Identification code	2·2Py	
Empirical formula	$C_{196}H_{100}F_{60}N_{26}Ni_3$	
Formula weight	4135.14	
Temperature	120 K	
Wavelength	1.54184 Å	
Crystal system	Monoclinic	
Space group	$P2_1/c$	
Unit cell dimensions	a = 20.4208(3) Å	α= 90°.
	b = 16.22196(18) Å	β= 94.1895(13)°.
	c = 26.4999(4) Å	γ = 90°.
Volume	8755.0(2) Å^3	
Z	2	
Density (calculated)	1.569 Mg/m^3	
Absorption coefficient	1.516 mm^{-1}	
F(000)	4164	
Crystal size	0.42 x 0.04 x 0.03 mm^3	
Theta range	3.34 to 66.75°.	
Index ranges	-23<=h<=24, -19<=k<=13, -29<=l<=31	
Reflections collected	27157	
Independent reflections	15394 [R(int) = 0.0412]	
Completeness	99.06 %	
Refinement method	Full-matrix least-squares on F^2	
Data / restraints / parameters	15394 / 24 / 1320	
Goodness-of-fit on F^2	1.060	
Final R indices [I>2sigma(I)]	R1 = 0.0809, wR2 = 0.2223	
R indices (all data)	R1 = 0.0943, wR2 = 0.2349	
Largest diff. peak and hole	1.209 and -0.494 e.Å^{-3}	

Comments

The data collection was performed at 120 K using Agilent Super-Nova dual source wavelength diffractometer with an Atlas CCD detector using multilayer optics monochromatized Cu- Kα (λ = 1.54184 Å) radiation. The data collection and reduction were performed using the program *CrysAlisPro*. The intensities were corrected for absorption using Gaussian face index absorption correction method. Hydrogen atoms are included in the calculated positions for carbons with isotropic displacement parameters 1.2 or 1.5 times the isotropic equivalent of their carrier atoms. Constraints (EADP) and restraints (ISOR) are used where appropriate, and for high thermal movement atoms.

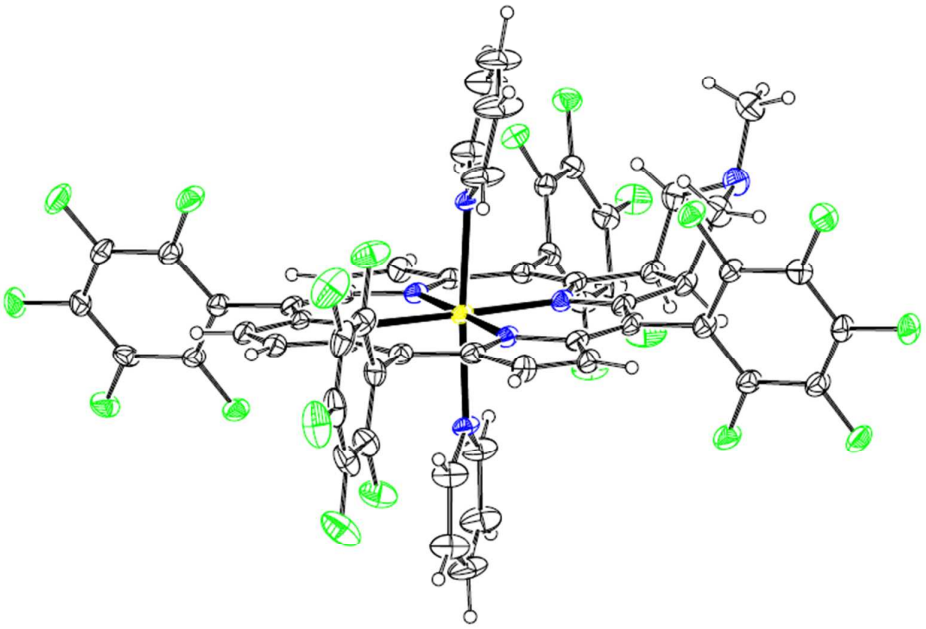

Table S23. Anisotropic Displacement Parameters ($Å^2 \times 10^3$) for Ni-TPCF$_{20}$ · 2 pyridine (2·2Py). The Anisotropic displacement factor exponent takes the form: $-2\pi^2[h^2a^{*2}U_{11}+2hka^*b^*U_{12}+\ldots]$.

Atom	U_{11}	U_{22}	U_{33}	U_{23}	U_{13}	U_{12}
Ni1	42.2(4)	18.4(3)	17.3(3)	0.1(2)	0.0(3)	-1.3(3)
F1	83(2)	29.4(13)	38.3(14)	-0.7(11)	-12.4(14)	-9.1(13)
F2	73.6(19)	56.4(17)	35.9(15)	-10.8(13)	-16.2(13)	-8.8(15)
F3	56.6(16)	68.9(19)	23.8(12)	1.1(12)	-7.6(11)	22.1(14)
F4	80(2)	35.0(13)	34.2(14)	9.7(11)	2.8(13)	17.1(13)
F5	70.1(17)	24.1(11)	33.0(13)	0.4(9)	-5.3(12)	1.6(11)
F6	51.1(15)	41.7(14)	37.4(14)	-11.7(11)	3.0(11)	-3.8(12)
F7	52.5(15)	48.3(15)	40.9(14)	-7.2(12)	9.7(12)	10.6(12)
F8	57.0(17)	53.7(17)	61.0(18)	2.7(14)	29.2(15)	-5.5(14)
F9	76(2)	36.4(15)	82(2)	-6.3(14)	31.8(18)	-19.1(14)
F10	70.7(18)	30.0(13)	54.7(17)	-8.2(12)	24.5(14)	-4.1(12)
F11	86(2)	30.3(13)	38.4(14)	-0.7(11)	-13.0(14)	0.0(13)
F12	79(2)	48.5(16)	31.8(14)	-9.8(12)	-15.7(13)	-1.2(15)
F13	50.9(14)	59.1(16)	20.6(11)	7.4(11)	-2.2(10)	3.2(12)
F14	68.5(18)	35.9(14)	40.4(15)	12.9(11)	-0.8(13)	1.7(12)
F15	64.8(17)	32.5(13)	35.1(13)	1.1(10)	-4.8(12)	-9.9(12)
F16	80(2)	37.2(15)	74(2)	6.4(14)	21.4(18)	6.0(15)
F17	74(2)	79(2)	91(3)	22(2)	32(2)	36(2)
F18	41.8(16)	115(3)	66(2)	35(2)	5.2(14)	-7.6(18)
F19	89(3)	73(2)	67(2)	5.4(18)	10.1(19)	-48(2)
F20	95(2)	39.9(15)	58.1(19)	-5.2(13)	21.6(17)	-18.1(16)
N1	41.3(18)	20.7(15)	23.1(16)	0.9(12)	0.3(13)	-2.0(13)
N2	40.0(18)	26.7(16)	20.4(15)	0.1(12)	1.3(13)	-1.5(13)
N3	45.3(19)	23.0(15)	17.9(15)	1.6(12)	4.1(13)	0.0(14)
N4	41.9(18)	23.3(15)	21.1(15)	1.1(12)	0.1(13)	-1.9(13)
N5	58(2)	19.7(15)	23.7(16)	-1.2(12)	4.6(15)	-2.2(15)
N6	54(2)	19.9(15)	25.9(17)	-1.5(13)	-1.6(15)	0.4(14)
N7	54(2)	45(2)	41(2)	6.1(17)	-1.1(18)	3.0(19)
C1	45(2)	19.0(17)	33(2)	1.7(15)	-2.8(17)	-5.3(16)
C2	45(2)	23.4(18)	35(2)	3.6(16)	-3.5(18)	-4.6(17)
C3	52(2)	22.6(18)	30(2)	1.7(15)	-8.4(18)	-2.9(17)
C4	46(2)	18.3(16)	24.5(19)	-1.7(14)	-3.0(16)	-1.0(16)
C5	51(2)	20.4(17)	20.2(18)	-1.6(14)	-4.1(16)	-0.6(16)
C6	49(2)	23.9(18)	18.2(17)	-1.2(14)	0.8(16)	1.5(16)

C7	58(3)	36(2)	18.3(18)	4.8(16)	1.7(17)	6.7(19)
C8	49(2)	44(2)	24(2)	6.1(17)	7.1(18)	4(2)
C9	47(2)	26.3(18)	20.5(19)	1.8(14)	5.4(16)	3.4(17)
C10	46(2)	29.6(19)	21.7(19)	1.0(15)	5.3(16)	2.1(17)
C11	47(2)	23.4(18)	23.6(19)	-1.8(14)	1.1(16)	0.1(16)
C12	47(2)	32(2)	27(2)	0.6(16)	0.6(17)	-3.9(18)
C13	48(2)	36(2)	23.1(19)	-0.6(16)	-0.5(17)	-7.9(18)
C14	46(2)	24.9(18)	23.0(19)	0.1(15)	1.3(16)	-5.5(17)
C15	45(2)	28.5(19)	20.1(18)	-0.5(15)	0.2(16)	-4.4(17)
C16	46(2)	20.6(17)	21.1(18)	1.7(14)	0.8(16)	-3.2(16)
C17	48(2)	33(2)	22.1(19)	3.9(16)	-1.1(17)	-2.0(18)
C18	45(2)	43(2)	25(2)	8.7(17)	5.2(17)	-1.0(19)
C19	45(2)	24.2(18)	27(2)	1.4(15)	4.5(17)	-1.7(16)
C20	43(2)	23.6(18)	31(2)	1.2(15)	1.6(17)	-3.9(16)
C21	40(2)	42(2)	28(2)	11.2(17)	-1.9(17)	-0.6(19)
C22	51(3)	41(2)	42(3)	15(2)	4(2)	4(2)
C23	49(3)	64(3)	46(3)	20(2)	5(2)	19(3)
C24	38(2)	85(4)	38(3)	22(3)	-1(2)	0(3)
C25	58(3)	67(3)	31(2)	14(2)	-9(2)	-22(3)
C26	59(3)	44(3)	27(2)	3.9(18)	0.8(19)	-9(2)
C27	47(2)	30(2)	22.3(19)	0.4(15)	-0.3(17)	3.7(17)
C28	49(2)	28(2)	22.9(19)	-2.2(15)	-0.8(17)	5.6(17)
C29	54(3)	34(2)	29(2)	5.2(17)	7.1(18)	14.8(19)
C30	47(2)	50(3)	19.7(19)	1.3(17)	-0.9(17)	14(2)
C31	53(3)	45(3)	24(2)	-9.0(18)	-4.6(18)	0(2)
C32	58(3)	32(2)	27(2)	-0.2(17)	-5.0(19)	-0.5(19)
C33	41(2)	32(2)	20.8(18)	9.0(15)	3.2(16)	6.1(17)
C34	59(3)	25.5(19)	32(2)	2.7(16)	16.2(19)	1.6(19)
C35	60(3)	29(2)	45(3)	8.6(18)	16(2)	-3(2)
C36	49(2)	37(2)	35(2)	10.1(18)	10.3(19)	4.0(19)
C37	46(2)	40(2)	21.3(19)	3.1(16)	4.6(17)	10.2(19)
C38	44(2)	33(2)	23.2(19)	0.7(15)	-1.5(16)	4.4(17)
C39	41(2)	37(2)	22.5(19)	1.6(16)	4.0(16)	-3.0(18)
C40	57(3)	32(2)	25(2)	0.1(16)	0.7(18)	1.4(19)
C41	50(2)	43(2)	27(2)	-5.9(18)	0.7(18)	-1(2)
C42	43(2)	45(2)	17.4(18)	5.3(16)	3.4(16)	0.0(19)
C43	45(2)	34(2)	30(2)	9.8(17)	9.2(17)	-2.0(18)
C44	40(2)	33(2)	23.6(19)	0.8(16)	3.9(16)	-6.3(17)
C45	68(3)	42(3)	62(3)	-8(2)	20(3)	-2(2)
C46	86(4)	44(3)	70(4)	-8(3)	25(3)	3(3)
C47	134(6)	24(2)	41(3)	-5(2)	11(3)	-4(3)
C48	98(5)	33(3)	64(4)	-1(2)	29(3)	-17(3)
C49	76(3)	34(2)	50(3)	-5(2)	21(3)	-7(2)
C50	89(4)	36(3)	58(3)	-2(2)	26(3)	2(3)
C51	106(5)	44(3)	75(4)	-10(3)	29(4)	8(3)
C52	155(7)	28(3)	68(4)	-4(3)	26(4)	15(3)
C53	179(8)	23(2)	57(4)	5(2)	42(4)	0(3)
C54	133(6)	26(2)	42(3)	0(2)	33(3)	-1(3)
C55	55(3)	50(3)	34(2)	6(2)	0(2)	5(2)
C56	59(3)	50(3)	43(3)	14(2)	7(2)	1(2)
C57	62(3)	47(3)	58(3)	4(2)	-2(3)	9(2)
Ni2	37.8(5)	15.5(4)	22.8(4)	-1.0(3)	-4.3(4)	0.4(3)
F21	73(2)	38.5(15)	81(2)	-12.3(15)	35.7(18)	-1.4(14)
F22	110(3)	40.2(17)	116(3)	-26.9(19)	52(3)	8.0(19)
F23	98(2)	17.5(12)	71(2)	-7.7(12)	-0.7(18)	0.4(13)
F24	91(3)	34.3(16)	117(3)	-7.3(17)	37(2)	-24.6(17)
F25	70(2)	41.5(16)	109(3)	-20.0(17)	46(2)	-12.7(15)
F26	45.9(14)	52.0(16)	43.1(15)	8.6(12)	0.3(11)	-5.2(12)
F27	42.7(14)	57.3(17)	44.6(15)	4.7(12)	-11.6(12)	9.3(12)

F28	65.9(18)	74(2)	29.3(14)	11.6(13)	-9.8(13)	6.2(16)
F29	62.0(18)	87(2)	39.3(16)	15.7(15)	5.0(13)	-4.3(17)
F30	45.1(15)	83(2)	41.9(15)	9.0(15)	-6.8(12)	-4.3(15)
N8	38.4(17)	17.7(14)	22.5(15)	-0.9(12)	-2.6(13)	-1.8(13)
N9	38.3(17)	14.9(14)	25.8(16)	-1.5(12)	-7.2(13)	0.2(12)
N10	38.8(18)	23.5(16)	40(2)	0.6(14)	2.0(15)	-0.1(14)
N11	88(7)	57(6)	72(7)	-16(5)	-18(6)	25(6)
C58	36.2(19)	18.3(17)	30(2)	2.2(14)	0.1(16)	-3.9(15)
C59	51(2)	23.8(19)	34(2)	5.6(16)	-2.4(19)	-8.3(18)
C60	75(3)	23.3(19)	27(2)	4.7(16)	6(2)	-2(2)
C61	41(2)	20.4(18)	29(2)	3.1(15)	-1.4(16)	1.7(16)
C62	42(2)	25.4(19)	27(2)	2.0(15)	-6.1(16)	0.2(16)
C63	42(2)	25.5(19)	28(2)	-2.6(15)	-6.8(16)	0.5(16)
C64	49(2)	29(2)	32(2)	-6.7(17)	-11.6(18)	0.7(18)
C65	48(2)	22.8(18)	34(2)	-6.7(16)	-6.6(18)	2.4(17)
C66	34.4(19)	20.6(17)	33(2)	-4.9(15)	-1.1(16)	-0.2(15)
C67	36(2)	19.6(17)	30(2)	-3.5(14)	1.3(16)	-0.6(15)
C68	77(8)	56(6)	48(6)	-10(5)	-7(5)	5(6)
C69	78(8)	54(6)	51(6)	-8(5)	-5(6)	13(6)
C70	82(12)	71(13)	110(16)	-56(11)	-15(11)	37(8)
C71	49(2)	20.3(17)	27(2)	-2.3(15)	-6.7(17)	1.1(16)
C72	48(2)	45(2)	27(2)	-1.8(18)	-5.7(18)	1(2)
C73	52(3)	49(3)	32(2)	1.4(19)	3.2(19)	4(2)
C74	54(3)	39(2)	26(2)	1.8(17)	-10.0(18)	6(2)
C75	46(2)	28(2)	36(2)	-3.6(17)	-8.2(18)	7.8(18)
C76	44(2)	25.9(18)	28(2)	-2.3(15)	-2.4(17)	1.3(17)
C77	36(2)	20.7(18)	27.0(19)	-2.0(14)	-4.6(15)	2.7(15)
C78	48(2)	26(2)	46(3)	-2.2(18)	9(2)	-1.9(18)
C79	62(3)	31(2)	57(3)	-14(2)	12(2)	8(2)
C80	69(3)	17.2(19)	45(3)	-3.3(17)	-7(2)	0.9(19)
C81	60(3)	27(2)	57(3)	-3(2)	7(2)	-11(2)
C82	49(3)	29(2)	53(3)	-9.4(19)	9(2)	-4.4(19)
C83	50(3)	48(3)	47(3)	9(2)	7(2)	2(2)
C84	67(4)	58(3)	61(3)	13(3)	16(3)	-1(3)
C85	44(3)	69(4)	81(4)	7(3)	16(3)	-8(3)
C86	47(3)	98(5)	80(5)	-6(4)	-4(3)	-12(3)
C87	40(3)	73(4)	54(3)	-7(3)	-1(2)	-8(2)
C98	114(15)	68(14)	114(15)	-33(10)	-21(11)	38(10)
C99	54(7)	160(19)	46(7)	-47(9)	-13(6)	30(9)
C100	66(9)	180(20)	54(8)	10(10)	25(7)	30(11)
C101	62(8)	124(15)	122(15)	-8(12)	32(9)	9(9)
C102	73(8)	67(8)	97(11)	-29(8)	-31(8)	33(7)
N14	109(8)	98(8)	87(7)	-17(6)	-45(6)	27(6)
N12	84(4)	101(5)	101(5)	-16(4)	0(4)	0(4)
C88	105(6)	73(5)	98(6)	-9(4)	-5(5)	-8(4)
C89	136(7)	62(4)	111(6)	5(4)	-31(5)	4(5)
C90	92(6)	77(5)	162(10)	-17(6)	-36(7)	-6(5)
C91	101(7)	83(6)	163(11)	-40(7)	27(7)	-23(5)
C92	115(7)	102(7)	105(7)	-21(6)	3(6)	-11(6)
N13	89(4)	65(4)	103(5)	-5(3)	9(4)	-10(3)
C93	75(4)	53(4)	127(7)	14(4)	3(4)	0(3)
C94	111(6)	84(6)	92(6)	21(5)	11(5)	15(5)
C95	129(8)	103(7)	85(6)	-21(5)	13(5)	21(6)
C96	162(9)	53(4)	89(6)	-11(4)	32(6)	-1(5)
C97	104(6)	62(4)	85(5)	-4(4)	25(4)	-13(4)
C59A	51(2)	23.8(19)	34(2)	5.6(16)	-2.4(19)	-8.3(18)
C60A	75(3)	23.3(19)	27(2)	4.7(16)	6(2)	-2(2)

Table S24. List of Bond lengths [Å]* for Ni-TPCF$_{20}$ · 2 pyridine (2·2Py).

Bond type	Bond length	Bond type	Bond length	Bond type	Bond length	Bond type	Bond length
Ni1—N1	2.059 (4)	N9—C63	1.364 (5)	N5—C45	1.362 (7)	C100—C101	1.3900
Ni1—N2	2.096 (4)	N9—C66	1.364 (5)	N5—C49	1.311 (6)	C101—C102	1.3900
Ni1—N3	2.049 (3)	N10—C83	1.318 (6)	N6—C50	1.353 (7)	C102—N14	1.3900
Ni1—N4	2.043 (3)	N10—C87	1.339 (7)	N6—C54	1.314 (6)	N12—C88	1.310 (12)
Ni1—N5	2.185 (3)	N11—C68	1.463 (15)	N7—C55	1.463 (6)	N12—C92	1.328 (13)
Ni1—N6	2.199 (3)	N11—C69	1.463 (16)	N7—C56	1.462 (7)	C88—C89	1.402 (13)
F1—C32	1.341 (5)	N11—C70	1.51 (2)	N7—C57	1.451 (7)	C89—C90	1.402 (16)
F2—C31	1.341 (5)	C58—C59	1.464 (6)	C1—C2	1.434 (6)	C90—C91	1.331 (16)
F3—C30	1.336 (5)	C58—C67^{i}	1.400 (6)	C1—C20	1.407 (6)	C91—C92	1.396 (15)
F4—C29	1.337 (5)	C58—C59A	1.464 (6)	C2—C3	1.355 (6)	N13—C93	1.349 (11)
F5—C28	1.323 (5)	C59—C60	1.417 (6)	C3—C4	1.434 (6)	N13—C97	1.344 (10)
F6—C38	1.332 (5)	C59—C69	1.735 (13)	C4—C5	1.414 (6)	C93—C94	1.353 (13)
F7—C37	1.338 (5)	C60—C61	1.457 (6)	C5—C6	1.386 (6)	C94—C95	1.385 (13)
F8—C36	1.336 (6)	C60—C68	1.755 (14)	C5—C27	1.489 (6)	C95—C96	1.343 (13)
F9—C35	1.344 (6)	C61—C62	1.395 (6)	C6—C7	1.461 (6)	C96—C97	1.339 (12)
F10—C34	1.347 (5)	C61—C60A	1.457 (6)	C7—C8	1.353 (7)	C59A—C60A	1.417 (6)
F11—C40	1.344 (5)	C62—C63	1.403 (6)	C8—C9	1.445 (6)		
F12—C41	1.320 (5)	C62—C71	1.503 (5)	C9—C10	1.404 (6)		
F13—C42	1.337 (5)	C63—C64	1.453 (6)	C10—C11	1.393 (6)		
F14—C43	1.342 (5)	C64—C65	1.369 (6)	C10—C33	1.493 (6)		
F15—C44	1.332 (5)	C65—C66	1.442 (6)	C11—C12	1.508 (6)		
F16—C22	1.344 (6)	C66—C67	1.393 (6)	C12—C13	1.518 (6)		
F17—C23	1.352 (7)	C67—C58^{i}	1.400 (6)	C12—C55	1.543 (7)		
F18—C24	1.332 (6)	C67—C77	1.503 (5)	C13—C14	1.504 (6)		
F19—C25	1.338 (7)	C71—C72	1.395 (7)	C13—C56	1.550 (7)		
F20—C26	1.334 (6)	C71—C76	1.392 (6)	C80—C81	1.354 (8)		
N1—C1	1.373 (6)	C72—C73	1.377 (7)	C81—C82	1.376 (7)		
N1—C4	1.365 (5)	C73—C74	1.364 (7)	C83—C84	1.378 (8)		
N2—C11	1.363 (6)	C74—C75	1.368 (7)	C84—C85	1.355 (9)		
N2—C14	1.350 (5)	C75—C76	1.373 (6)	C85—C86	1.381 (10)		
N3—C6	1.379 (5)	C77—C78	1.373 (6)	C86—C87	1.371 (9)		
N3—C9	1.358 (6)	C77—C82	1.384 (6)	C98—C99	1.3900		
N4—C16	1.355 (5)	C78—C79	1.391 (6)	C98—N14	1.3900		
N4—C19	1.376 (6)	C79—C80	1.383 (8)	C99—C100	1.3900		

***Symmetry code(s): (i) -*x*, -*y*+1, -*z*.**

Table S25. List of Bond angles [°]*for Ni-TPCF$_{20}$ (2) 2Py

Bond type	Angle	Bond type	Angle	Bond type	Angle
N1—Ni1—N2	178.89 (13)	C57—N7—C55	111.6 (4)	N8—C61—C60	110.7 (3)
N1—Ni1—N5	91.39 (14)	C57—N7—C56	112.5 (4)	N8—C61—C62	125.4 (3)
N1—Ni1—N6	93.29 (13)	N1—C1—C2	109.8 (4)	N8—C61—C60A	110.7 (3)
N2—Ni1—N5	89.71 (14)	N1—C1—C20	124.8 (4)	C62—C61—C60	123.9 (4)
N2—Ni1—N6	85.61 (13)	C20—C1—C2	125.4 (4)	C62—C61—C60A	123.9 (4)
N3—Ni1—N1	89.69 (14)	C3—C2—C1	106.8 (4)	C61—C62—C63	127.0 (4)
N3—Ni1—N2	90.33 (14)	C2—C3—C4	107.3 (4)	C61—C62—C71	115.9 (3)
N3—Ni1—N5	90.06 (12)	N1—C4—C3	109.8 (4)	C63—C62—C71	117.0 (4)
N3—Ni1—N6	90.66 (13)	N1—C4—C5	124.8 (4)	N9—C63—C62	124.9 (4)
N4—Ni1—N1	89.72 (14)	C5—C4—C3	125.4 (4)	N9—C63—C64	109.5 (3)
N4—Ni1—N2	90.27 (13)	C4—C5—C27	117.3 (4)	C62—C63—C64	125.6 (4)
N4—Ni1—N3	178.90 (14)	C6—C5—C4	126.5 (4)	C65—C64—C63	106.4 (4)
N4—Ni1—N5	89.02 (13)	C6—C5—C27	116.3 (4)	C64—C65—C66	106.9 (3)
N4—Ni1—N6	90.31 (13)	N3—C6—C5	125.4 (4)	N9—C66—C65	109.7 (3)
N5—Ni1—N6	175.27 (14)	N3—C6—C7	108.8 (4)	N9—C66—C67	124.8 (4)
C1—N1—Ni1	126.6 (3)	C5—C6—C7	125.8 (4)	C67—C66—C65	125.5 (4)
C4—N1—Ni1	126.9 (3)	C8—C7—C6	106.7 (4)	C58^{i}—C67—C77	115.1 (3)
C4—N1—C1	106.4 (3)	C7—C8—C9	107.3 (4)	C66—C67—C58^{i}	127.7 (3)
C11—N2—Ni1	125.4 (3)	N3—C9—C8	109.9 (4)	C66—C67—C77	117.1 (3)
C14—N2—Ni1	125.1 (3)	N3—C9—C10	125.5 (4)	N11—C68—C60	102.5 (9)
C14—N2—C11	109.4 (3)	C10—C9—C8	124.6 (4)	N11—C69—C59	103.8 (8)
C6—N3—Ni1	126.6 (3)	C9—C10—C33	116.7 (3)	C72—C71—C62	121.2 (4)
C9—N3—Ni1	126.1 (3)	C11—C10—C9	127.8 (4)	C76—C71—C62	122.7 (4)
C9—N3—C6	107.2 (3)	C11—C10—C33	115.5 (4)	C76—C71—C72	116.0 (4)
C16—N4—Ni1	126.6 (3)	N2—C11—C10	124.8 (4)	F30—C72—C71	119.7 (4)
C16—N4—C19	106.4 (3)	N2—C11—C12	111.9 (3)	F30—C72—C73	118.1 (4)
C19—N4—Ni1	127.0 (3)	C10—C11—C12	123.4 (4)	C73—C72—C71	122.2 (4)
C45—N5—Ni1	120.3 (3)	C11—C12—C13	102.9 (4)	F29—C73—C72	120.3 (5)
C49—N5—Ni1	122.9 (3)	C11—C12—C55	115.6 (4)	F29—C73—C74	120.1 (4)
C49—N5—C45	116.6 (4)	C13—C12—C55	105.6 (4)	C74—C73—C72	119.6 (5)
C50—N6—Ni1	121.1 (3)	C12—C13—C56	103.6 (4)	F28—C74—C73	119.9 (4)
C54—N6—Ni1	122.1 (3)	C14—C13—C12	103.7 (3)	F28—C74—C75	119.8 (4)
C54—N6—C50	115.5 (4)	C14—C15—C39	117.3 (4)	C73—C74—C75	120.3 (4)
C56—N7—C55	103.8 (4)	C16—C15—C39	115.8 (4)	F27—C75—C74	120.0 (4)
F27—C75—C76	120.2 (4)	N4—C16—C15	125.0 (4)	N12—C92—C91	122.4 (11)
C74—C75—C76	119.8 (4)	N4—C16—C17	110.5 (4)	C97—N13—C93	116.1 (8)
F26—C76—C71	119.2 (4)	C15—C16—C17	124.5 (4)	N13—C93—C94	123.0 (8)
F26—C76—C75	118.7 (4)	C18—C17—C16	106.4 (4)	C93—C94—C95	118.5 (8)
C75—C76—C71	122.1 (4)	C17—C18—C19	107.3 (4)	C96—C95—C94	118.9 (9)
C78—C77—C67	122.8 (4)	N4—C19—C18	109.4 (4)	C97—C96—C95	119.8 (8)
C78—C77—C82	116.4 (4)	N4—C19—C20	125.2 (4)	C96—C97—N13	123.5 (8)

Bond type	Angle	Bond type	Angle	Bond type	Angle
C82—C77—C67	120.8 (4)	C20—C19—C18	125.4 (4)	C60A—C59A—C58	105.5 (3)
F21—C78—C77	119.4 (4)	C1—C20—C21	117.2 (4)	C59A—C60A—C61	105.6 (4)
F21—C78—C79	118.1 (4)	C19—C20—C1	126.7 (4)	F4—C29—C28	120.8 (4)
C77—C78—C79	122.4 (4)	C19—C20—C21	116.1 (4)	F4—C29—C30	119.2 (4)
F22—C79—C78	120.6 (5)	C22—C21—C20	121.8 (4)	C30—C29—C28	120.0 (4)
F22—C79—C80	120.5 (4)	C26—C21—C20	121.9 (4)	F3—C30—C29	119.8 (4)
C80—C79—C78	118.9 (4)	C26—C21—C22	116.1 (4)	F3—C30—C31	120.1 (4)
F23—C80—C79	119.8 (5)	F16—C22—C21	119.3 (4)	C31—C30—C29	120.1 (4)
F23—C80—C81	120.3 (5)	F16—C22—C23	118.4 (5)	F2—C31—C30	119.8 (4)
C81—C80—C79	119.9 (4)	C23—C22—C21	122.3 (5)	F2—C31—C32	120.6 (4)
F24—C81—C80	119.1 (4)	F17—C23—C22	119.6 (5)	C30—C31—C32	119.5 (4)
F24—C81—C82	120.7 (5)	F17—C23—C24	121.1 (5)	F1—C32—C27	119.7 (4)
C80—C81—C82	120.2 (5)	C22—C23—C24	119.3 (5)	F1—C32—C31	117.7 (4)
F25—C82—C77	120.0 (4)	F18—C24—C23	119.9 (6)	C31—C32—C27	122.6 (4)
F25—C82—C81	117.6 (4)	F18—C24—C25	120.0 (6)	C34—C33—C10	122.3 (4)
C81—C82—C77	122.2 (4)	C25—C24—C23	120.1 (5)	C34—C33—C38	115.8 (4)
N10—C83—C84	123.8 (5)	F19—C25—C24	119.4 (5)	C38—C33—C10	121.9 (4)
C85—C84—C83	119.5 (6)	F19—C25—C26	121.0 (6)	F10—C34—C33	119.4 (4)
C84—C85—C86	117.2 (6)	C24—C25—C26	119.6 (5)	F10—C34—C35	117.3 (4)
C87—C86—C85	120.4 (6)	F20—C26—C21	119.7 (4)	C35—C34—C33	123.3 (4)
N10—C87—C86	122.0 (6)	F20—C26—C25	117.8 (5)	F9—C35—C34	121.3 (4)
C99—C98—N14	120.0	C21—C26—C25	122.5 (5)	F9—C35—C36	119.7 (4)
C100—C99—C98	120.0	C28—C27—C5	121.6 (4)	C34—C35—C36	118.9 (4)
C101—C100—C99	120.0	C32—C27—C5	122.3 (4)	F8—C36—C35	119.4 (4)
C100—C101—C102	120.0	C32—C27—C28	116.1 (4)	F8—C36—C37	120.2 (4)
N14—C102—C101	120.0	F5—C28—C27	120.2 (4)	C37—C36—C35	120.4 (4)
C102—N14—C98	120.0	F5—C28—C29	118.1 (4)	F7—C37—C36	120.2 (4)
C88—N12—C92	117.9 (9)	C29—C28—C27	121.7 (4)	F7—C37—C38	120.7 (4)
N12—C88—C89	123.1 (10)	C91—C90—C89	118.0 (9)	C36—C37—C38	119.1 (4)
C90—C89—C88	118.1 (10)	C90—C91—C92	120.5 (11)	F6—C38—C33	119.0 (4)
F6—C38—C37	118.5 (4)	F12—C41—C42	120.2 (4)	N8—C58—C59A	110.3 (3)
C37—C38—C33	122.5 (4)	C42—C41—C40	118.7 (4)	C67^{i}—C58—C59	124.2 (4)
C40—C39—C15	121.5 (4)	F13—C42—C41	119.5 (4)	C67^{i}—C58—C59A	124.2 (4)
C44—C39—C15	121.7 (4)	F13—C42—C43	120.3 (4)	C58—C59—C69	112.7 (5)
C44—C39—C40	116.8 (4)	C43—C42—C41	120.1 (4)	C60—C59—C58	105.5 (3)
F11—C40—C39	119.9 (4)	F14—C43—C42	119.8 (4)	C60—C59—C69	105.2 (5)
F11—C40—C41	117.3 (4)	F14—C43—C44	120.3 (4)	C59—C60—C61	105.6 (4)
C39—C40—C41	122.7 (4)	C42—C43—C44	119.9 (4)	C59—C60—C68	103.7 (5)
F12—C41—C40	121.1 (4)	F15—C44—C39	120.1 (4)	C61—C60—C68	109.8 (5)
F15—C44—C43	118.1 (4)	N10—Ni2—N10^{i}	180.0	C68—N11—C70	110.2 (13)
C39—C44—C43	121.8 (4)	C58—N8—Ni2	125.5 (3)	C69—N11—C70	109.5 (13)

N5—C45—C46	122.9 (5)	C61—N8—Ni2	126.5 (2)	N8—C58—C59	110.3 (3)
Bond type	Angle	Bond type	Angle		
C45—C46—C47	117.6 (6)	C61—N8—C58	107.9 (3)		
C48—C47—C46	118.7 (5)	C63—N9—Ni2	126.5 (3)		
C47—C48—C49	120.5 (5)	C63—N9—C66	107.4 (3)		
N5—C49—C48	123.6 (5)	C66—N9—Ni2	126.1 (3)		
N6—C50—C51	123.7 (5)	C83—N10—Ni2	121.6 (3)		
C52—C51—C50	119.1 (6)	C83—N10—C87	117.1 (4)		
C53—C52—C51	118.2 (5)	C87—N10—Ni2	121.4 (3)		
C52—C53—C54	120.2 (6)	C68—N11—C69	103.3 (9)		
N6—C54—C53	123.3 (5)	N8—C58—C67^{i}	125.5 (3)		
N7—C55—C12	104.4 (4)				
N7—C56—C13	103.7 (4)				
N8^{i}—Ni2—N8	180.0				
N8—Ni2—N9^{i}	90.37 (12)				
N8—Ni2—N9	89.63 (12)				
N8^{i}—Ni2—N9	90.37 (12)				
N8^{i}—Ni2—N9^{i}	89.63 (12)				
N8^{i}—Ni2—N10	89.78 (13)				
N8^{i}—Ni2—N10^{i}	90.22 (13)				
N8—Ni2—N10^{i}	89.78 (13)				
N8—Ni2—N10	90.22 (13)				
N9—Ni2—N9^{i}	180.0				
N9^{i}—Ni2—N10	90.29 (13)				
N9^{i}—Ni2—N10^{i}	89.71 (13)				
N9—Ni2—N10^{i}	90.29 (13)				
N9—Ni2—N10	89.71 (13)				

*Symmetry code(s): (i) -*x*, -*y*+1, -*z*.

VI.3 Ni-TIBF$_{20}$·2 pyridine (3·2Py)

Table S26. Crystal data and structure refinement for Ni-TIBF$_{20}$·2 pyridine (3·2Py).

Identification code	herges98	
Empirical formula	$C_{60}H_{32}F_{20}N_8Ni$	
Formula weight	1303.64	
Temperature	170(2) K	
Wavelength	0.71073 Å	
Crystal system	Triclinic	
Space group	P-1	
Unit cell dimensions	a = 13.8902(6) Å	α= 78.967(4)°.
	b = 14.1867(6) Å	β= 88.714(4)°.
	c = 24.5324(11) Å	γ = 73.607(3)°.
Volume	4549.5(4) Å^3	
Z	3	
Density (calculated)	1.427 Mg/m^3	
Absorption coefficient	0.426 mm^{-1}	
F(000)	1968	
Crystal size	0.08 x 0.08 x 0.3 mm^3	
Theta range for data collection	1.525 to 25.004°.	
Index ranges	-16<=h<=16, -16<=k<=16, -29<=l<=29	
Reflections collected	35682	
Independent reflections	15899 [R(int) = 0.0626]	
Completeness to theta = 25.242°	96.6 %	
Refinement method	Full-matrix least-squares on F^2	
Data / restraints / parameters	15899 / 41 / 1247	
Goodness-of-fit on F^2	0.939	
Final R indices [I>2sigma(I)]	R1 = 0.0664, wR2 = 0.1432	
R indices (all data)	R1 = 0.1263, wR2 = 0.1663	
Extinction coefficient	n/a	
Largest diff. peak and hole	0.311 and -0.394 e.Å^{-3}	

Comments

All non-hydrogen atoms except those, which are disordered were refined anisotropic. The C-H H atoms were positioned with idealized geometry. There are two crystallographically independent molecules in the asymmetric unit, of which one is located on a center of inversion. Two pyridine rings as well as some C and N atoms of the 5-membered side rings are disordered and were refined using a split model. The molecule which is located on a center of inversion is disordered because of symmetry. Therefore, all C and N atoms of the side rings can only be occupied to 50%. There are no hints for super structure reflections and the disordering remain constant if structure is refined in space group P1.

Table S27. Atomic coordinates (x 10^4) and equivalent isotropic displacement parameters (Å^{2}x 10^3). U(eq) is defined as one third of the trace of the orthogonalized U^{ij} tensor.

	x	y	z	U(eq)
Ni(1)	6566(1)	1080(1)	1524(1)	46(1)
N(1)	5022(3)	1449(3)	1610(2)	49(1)
N(2)	6514(3)	-122(3)	1166(2)	48(1)
N(3)	8071(3)	775(3)	1407(2)	50(1)
N(4)	6630(3)	2233(3)	1897(2)	50(1)
C(1)	4442(4)	2295(3)	1791(2)	49(1)
C(2)	3339(4)	2472(3)	1677(2)	52(1)
C(3)	3300(3)	1508(4)	1487(2)	52(1)
C(4)	4398(3)	968(3)	1439(2)	49(1)
C(5)	4720(3)	69(3)	1240(2)	48(1)
C(6)	5692(3)	-436(3)	1118(2)	47(1)
C(7)	5915(3)	-1403(3)	912(2)	49(1)
C(8)	7058(3)	-1665(3)	831(2)	51(1)
C(9)	7348(3)	-816(3)	1011(2)	49(1)
C(10)	8310(3)	-741(3)	1010(2)	49(1)
C(11)	8653(3)	21(3)	1170(2)	50(1)
C(12)	9656(4)	103(4)	1114(2)	57(1)
C(13)	9690(4)	900(4)	1333(2)	58(1)
C(14)	8716(4)	1319(4)	1515(2)	53(1)
C(15)	8421(4)	2121(4)	1797(2)	52(1)
C(16)	7472(4)	2532(4)	1986(2)	51(1)
C(17)	7196(4)	3362(4)	2265(2)	54(1)
C(18)	6191(4)	3585(4)	2329(2)	52(1)
C(19)	5851(4)	2891(4)	2092(2)	50(1)
C(20)	4822(3)	2921(3)	2028(2)	48(1)
C(21)	2932(4)	3297(4)	1170(2)	64(1)
C(22)	2714(4)	1875(4)	926(2)	63(1)
N(5)	2193(4)	2927(4)	921(2)	55(1)
N(5')	2845(16)	2895(12)	688(7)	100(9)
C(23)	1914(5)	3490(5)	342(3)	91(2)
C(24)	5764(4)	-2307(4)	1317(2)	59(1)
N(6)	6607(3)	-3119(3)	1199(2)	60(1)
C(25)	7469(4)	-2711(4)	1182(2)	57(1)
C(26)	6742(5)	-4054(4)	1600(3)	81(2)
C(31)	4080(4)	3786(4)	2201(2)	50(1)
C(32)	3921(4)	4744(4)	1899(2)	58(1)
C(33)	3283(4)	5570(4)	2033(2)	64(1)
C(34)	2718(4)	5458(4)	2497(3)	66(2)
C(35)	2825(4)	4532(4)	2811(2)	63(1)
C(36)	3502(4)	3713(4)	2664(2)	54(1)
F(31)	4461(3)	4878(2)	1435(1)	74(1)
F(32)	3179(3)	6478(2)	1723(2)	94(1)
F(33)	2067(3)	6263(2)	2646(2)	93(1)
F(34)	2266(3)	4420(3)	3259(1)	91(1)
F(35)	3582(2)	2803(2)	2982(1)	70(1)
C(41)	3910(3)	-418(3)	1171(2)	49(1)
C(42)	3545(3)	-470(3)	660(2)	50(1)
C(43)	2825(4)	-937(4)	605(2)	54(1)
C(44)	2436(4)	-1368(4)	1078(2)	58(1)
C(45)	2760(4)	-1329(4)	1591(2)	58(1)
C(46)	3501(4)	-865(4)	1630(2)	51(1)
F(41)	3910(2)	-35(2)	190(1)	61(1)
F(42)	2496(2)	-972(2)	103(1)	69(1)
F(43)	1726(2)	-1823(2)	1024(1)	73(1)
F(44)	2366(2)	-1733(2)	2048(1)	72(1)

Table S28. Atomic coordinates (x 10^4) and equivalent isotropic displacement parameters ($Å^2$x 10^3). U(eq) is defined as one third of the trace of the orthogonalized U^{ij} tensor.

	x	y	z	U(eq)
F(45)	3824(2)	-871(2)	2143(1)	63(1)
C(51)	9113(4)	-1590(4)	861(2)	52(1)
C(52)	9312(4)	-1734(4)	330(2)	58(1)
C(53)	10059(5)	-2519(4)	203(3)	72(2)
C(54)	10634(4)	-3222(4)	628(3)	71(2)
C(55)	10443(4)	-3113(4)	1161(3)	66(2)
C(56)	9711(4)	-2314(4)	1277(2)	57(1)
F(51)	8781(2)	-1064(2)	-101(1)	74(1)
F(52)	10247(3)	-2625(3)	-326(2)	103(1)
F(53)	11363(3)	-4003(2)	512(2)	102(1)
F(54)	11009(3)	-3791(2)	1582(2)	92(1)
F(55)	9560(2)	-2236(2)	1810(1)	74(1)
C(61)	9198(3)	2654(3)	1858(2)	50(1)
C(62)	9900(4)	2325(4)	2290(2)	56(1)
C(63)	10613(4)	2810(4)	2349(2)	65(1)
C(64)	10611(4)	3656(4)	1973(3)	67(2)
C(65)	9928(4)	4008(4)	1541(2)	62(1)
C(66)	9229(4)	3490(4)	1491(2)	54(1)
F(61)	9895(2)	1519(2)	2685(1)	73(1)
F(62)	11289(3)	2478(3)	2772(2)	90(1)
F(63)	11287(2)	4154(2)	2033(2)	85(1)
F(64)	9921(3)	4841(2)	1166(2)	83(1)
F(65)	8563(2)	3860(2)	1052(1)	64(1)
N(71)	6241(3)	2139(3)	729(2)	51(1)
C(71)	5494(4)	2178(4)	385(2)	56(1)
C(72)	5167(4)	2923(4)	-79(2)	68(1)
C(73)	5641(5)	3667(5)	-196(2)	79(2)
C(74)	6434(5)	3624(5)	141(3)	84(2)
C(75)	6704(4)	2848(4)	600(2)	69(1)
N(72)	6811(3)	30(3)	2317(2)	62(1)
C(76)	6150(10)	-357(10)	2561(5)	75(3)
C(77)	6261(12)	-992(11)	3082(6)	102(6)
C(78)	7227(10)	-1233(10)	3348(6)	92(4)
C(79)	7983(10)	-950(11)	3068(5)	90(4)
C(80)	7762(9)	-256(9)	2564(5)	70(3)
C(76')	5981(8)	48(9)	2663(4)	60(3)
C(77')	6014(11)	-659(11)	3141(6)	91(5)
C(78')	6913(14)	-1463(12)	3246(7)	130(7)
C(79')	7735(13)	-1461(13)	2944(7)	119(5)
C(80')	7619(10)	-674(10)	2470(5)	79(3)
Ni(2)	15000	10000	5000	72(1)
N(81)	14933(4)	8822(4)	4642(2)	81(2)
N(82)	16308(4)	9124(3)	5422(2)	70(1)
C(81)	14169(5)	8806(4)	4295(2)	76(2)
C(82)	14315(6)	7822(6)	4155(3)	105(2)
C(83)	15246(5)	7202(6)	4446(3)	97(2)
C(84)	15580(5)	7859(5)	4749(2)	79(2)
C(85)	16433(5)	7571(4)	5087(2)	74(2)
C(86)	16790(5)	8141(5)	5394(2)	74(2)
C(87)	17722(5)	7777(5)	5731(2)	75(2)
C(88)	17780(5)	8610(5)	5981(2)	81(2)
C(89)	16887(5)	9417(4)	5772(2)	71(2)
C(90)	16651(5)	10369(5)	5901(2)	73(2)
C(91)	14307(11)	7624(11)	3554(6)	100(4)
C(92)	15827(11)	6648(13)	4000(6)	110(5)

Table S29. Atomic coordinates (x 10^4) and equivalent isotropic displacement parameters ($Å^2$x 10^3). U(eq) is defined as one third of the trace of the orthogonalized U^{ij} tensor.

	x	y	z	U(eq)
N(83')	15065(13)	6654(13)	3565(8)	96(5)
N(83)	15440(20)	7290(20)	3534(12)	92(8)
C(93)	15606(18)	6834(18)	3103(10)	169(8)
C(94)	18757(11)	7620(11)	5398(6)	95(4)
C(95)	18846(10)	8882(10)	5827(5)	81(3)
N(84)	19494(12)	7917(12)	5731(6)	70(4)
C(96)	20362(17)	8051(18)	5447(9)	89(6)
N(84')	19060(30)	8480(30)	5235(17)	132(12)
C(96')	19860(30)	8580(30)	5024(14)	86(9)
C(101)	17034(5)	6505(5)	5160(3)	80(2)
C(102)	17960(20)	6207(11)	4833(8)	76(6)
C(103)	18458(13)	5213(8)	4910(5)	92(6)
C(104)	18377(18)	4541(9)	5303(7)	98(6)
C(105)	17513(13)	4690(10)	5602(7)	90(5)
C(106)	16931(16)	5734(12)	5543(8)	89(8)
F(101)	18231(7)	6902(7)	4461(4)	95(3)
F(102)	19363(8)	5000(7)	4612(4)	122(3)
F(103)	18934(9)	3584(5)	5389(4)	114(3)
F(104)	17316(10)	4053(7)	6014(6)	146(5)
F(105)	16050(7)	5894(7)	5819(4)	114(3)
C(202)	17720(20)	6114(16)	4853(15)	91(13)
C(203)	18290(30)	5141(18)	5042(15)	190(20)
C(204)	17969(18)	4507(13)	5372(11)	87(8)
C(205)	17277(17)	4821(13)	5754(9)	82(7)
C(206)	16710(30)	5865(16)	5588(12)	99(11)
F(201)	17913(9)	6712(10)	4395(6)	93(4)
F(202)	18877(15)	4763(15)	4611(8)	175(8)
F(203)	18407(13)	3497(12)	5501(8)	165(8)
F(204)	16970(16)	4241(14)	6149(8)	161(8)
F(205)	16135(10)	6210(10)	6004(5)	107(5)
C(111)	17406(4)	10515(4)	6285(2)	71(2)
C(112)	17493(4)	10085(4)	6843(2)	67(1)
C(113)	18198(4)	10169(4)	7195(2)	68(1)
C(114)	18845(5)	10711(5)	7003(3)	77(2)
C(115)	18788(6)	11164(6)	6455(3)	94(2)
C(116)	18068(6)	11066(5)	6109(3)	89(2)
F(111)	16862(2)	9547(3)	7057(1)	75(1)
F(112)	18279(2)	9706(2)	7733(1)	72(1)
F(113)	19553(3)	10787(3)	7336(2)	96(1)
F(114)	19413(4)	11699(4)	6256(2)	130(2)
F(115)	18030(4)	11506(4)	5564(2)	122(1)
N(121)	14106(4)	9455(4)	5671(2)	76(1)
C(121)	13118(11)	9930(12)	5725(6)	97(4)
C(122)	12515(13)	9578(13)	6131(7)	114(5)
C(123)	12872(15)	8746(15)	6515(9)	106(7)
C(124)	13916(12)	8185(12)	6464(6)	93(4)
C(125)	14431(10)	8632(10)	6061(5)	80(3)
C(221)	13232(12)	9414(12)	5601(7)	83(4)
C(222)	12693(13)	8963(13)	5994(7)	92(4)
C(223)	13180(19)	8522(15)	6504(8)	80(6)
C(224)	14024(13)	8636(14)	6597(8)	100(5)
C(225)	14581(13)	9094(13)	6188(7)	91(4)

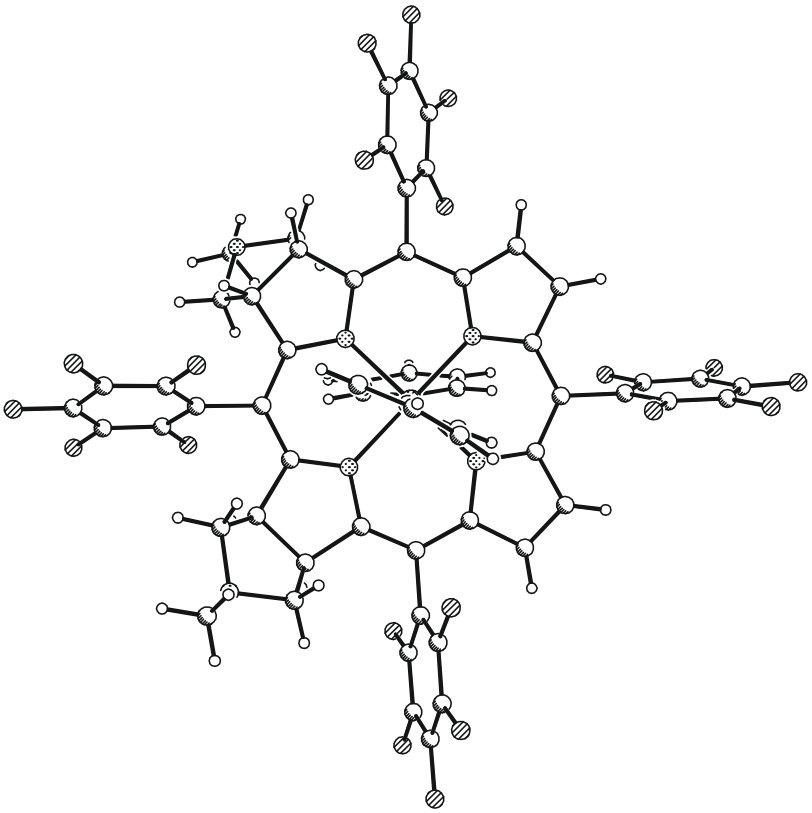

Table S30. Bond lengths [Å] and angles [°].

Ni(1)-N(3)	2.037(4)	Ni(1)-N(2)	2.081(4)
Ni(1)-N(4)	2.044(4)	Ni(1)-N(72)	2.181(4)
Ni(1)-N(1)	2.076(4)	Ni(1)-N(71)	2.192(4)
N(3)-Ni(1)-N(4)	89.35(14)	N(1)-Ni(1)-N(72)	91.32(16)
N(3)-Ni(1)-N(1)	177.18(17)	N(2)-Ni(1)-N(72)	86.47(15)
N(4)-Ni(1)-N(1)	90.03(14)	N(3)-Ni(1)-N(71)	91.33(15)
N(3)-Ni(1)-N(2)	90.48(14)	N(4)-Ni(1)-N(71)	88.72(14)
N(4)-Ni(1)-N(2)	178.31(16)	N(1)-Ni(1)-N(71)	85.91(15)
N(1)-Ni(1)-N(2)	90.22(14)	N(2)-Ni(1)-N(71)	92.96(14)
N(3)-Ni(1)-N(72)	91.45(17)	N(72)-Ni(1)-N(71)	177.17(16)
N(4)-Ni(1)-N(72)	91.85(15)		
Ni(2)-N(81A)	2.056(5)	Ni(2)-N(82A)	2.058(5)
Ni(2)-N(81)	2.056(5)	Ni(2)-N(121A)	2.193(5)
Ni(2)-N(82)	2.058(5)	Ni(2)-N(121)	2.193(5)
N(81A)-Ni(2)-N(81)	180.0	N(82)-Ni(2)-N(121A)	89.24(19)
N(81A)-Ni(2)-N(82)	90.22(19)	N(82A)-Ni(2)-N(121A)	90.76(19)
N(81)-Ni(2)-N(82)	89.78(19)	N(81A)-Ni(2)-N(121)	92.47(19)
N(81A)-Ni(2)-N(82A)	89.79(19)	N(81)-Ni(2)-N(121)	87.53(19)
N(81)-Ni(2)-N(82A)	90.21(19)	N(82)-Ni(2)-N(121)	90.76(19)
N(82)-Ni(2)-N(82A)	180.0	N(82A)-Ni(2)-N(121)	89.24(19)
N(81A)-Ni(2)-N(121A)	87.53(19)	N(121A)-Ni(2)-N(121)	180.0(2)
N(81)-Ni(2)-N(121A)	92.47(19)		

Symmetry transformations used to generate equivalent atoms: A: -x+3,-y+2,-z+1

Table S31. Bond lengths [Å] and angles [°].

N(1)-C(4)	1.362(5)	C(31)-C(32)	1.377(7)
N(1)-C(1)	1.388(6)	C(31)-C(36)	1.382(7)
N(2)-C(6)	1.353(6)	C(32)-C(33)	1.347(7)
N(2)-C(9)	1.390(6)	C(32)-F(31)	1.361(6)
N(3)-C(11)	1.366(6)	C(33)-F(32)	1.336(6)
N(3)-C(14)	1.394(6)	C(33)-C(34)	1.378(8)
N(4)-C(19)	1.359(6)	C(34)-F(33)	1.348(6)
N(4)-C(16)	1.387(6)	C(34)-C(35)	1.360(8)
C(1)-C(20)	1.371(6)	C(35)-F(34)	1.341(6)
C(1)-C(2)	1.505(6)	C(35)-C(36)	1.376(7)
C(2)-C(21)	1.529(7)	C(36)-F(35)	1.350(6)
C(2)-C(3)	1.541(6)	C(41)-C(46)	1.378(7)
C(3)-C(4)	1.514(6)	C(41)-C(42)	1.385(6)
C(3)-C(22)	1.537(7)	C(42)-F(41)	1.358(5)
C(4)-C(5)	1.403(6)	C(42)-C(43)	1.368(6)
C(5)-C(6)	1.394(6)	C(43)-F(42)	1.338(5)
C(5)-C(41)	1.504(6)	C(43)-C(44)	1.377(7)
C(6)-C(7)	1.500(6)	C(44)-F(43)	1.343(5)
C(7)-C(24)	1.527(7)	C(44)-C(45)	1.364(7)
C(7)-C(8)	1.542(6)	C(45)-F(44)	1.337(6)
C(8)-C(9)	1.516(6)	C(45)-C(46)	1.383(7)
C(8)-C(25)	1.525(7)	C(46)-F(45)	1.342(5)
C(9)-C(10)	1.370(6)	C(51)-C(52)	1.367(7)
C(10)-C(11)	1.418(6)	C(51)-C(56)	1.393(7)
C(10)-C(51)	1.490(6)	C(52)-F(51)	1.349(6)
C(11)-C(12)	1.431(7)	C(52)-C(53)	1.371(7)
C(12)-C(13)	1.354(6)	C(53)-F(52)	1.347(6)
C(13)-C(14)	1.416(7)	C(53)-C(54)	1.381(9)
C(14)-C(15)	1.404(6)	C(54)-F(53)	1.345(6)
C(15)-C(16)	1.391(6)	C(54)-C(55)	1.357(8)
C(15)-C(61)	1.507(6)	C(55)-F(54)	1.356(7)
C(16)-C(17)	1.429(6)	C(55)-C(56)	1.364(7)
C(17)-C(18)	1.354(7)	C(56)-F(55)	1.340(6)
C(18)-C(19)	1.424(6)	C(61)-C(66)	1.356(7)
C(19)-C(20)	1.429(6)	C(61)-C(62)	1.374(7)
C(20)-C(31)	1.488(6)	C(62)-F(61)	1.351(6)
C(21)-N(5')	1.429(16)	C(62)-C(63)	1.380(7)
C(21)-N(5)	1.469(6)	C(63)-F(62)	1.336(6)
C(22)-N(5)	1.461(7)	C(63)-C(64)	1.366(8)
C(22)-N(5')	1.513(17)	C(64)-F(63)	1.350(6)
N(5)-C(23)	1.490(8)	C(64)-C(65)	1.359(8)
N(5')-C(23)	1.504(18)	C(65)-F(64)	1.350(6)
C(24)-N(6)	1.460(6)	C(65)-C(66)	1.392(7)
N(6)-C(26)	1.460(7)	C(66)-F(65)	1.358(6)
N(6)-C(25)	1.466(6)	C(4)-C(3)-C(22)	113.7(4)
C(4)-N(1)-C(1)	108.6(4)	C(4)-C(3)-C(2)	103.1(4)
C(6)-N(2)-C(9)	108.9(4)	C(22)-C(3)-C(2)	104.8(4)
C(11)-N(3)-C(14)	105.1(4)	N(1)-C(4)-C(5)	124.6(4)
C(19)-N(4)-C(16)	105.4(4)	N(1)-C(4)-C(3)	112.5(4)
C(20)-C(1)-N(1)	124.6(4)	C(5)-C(4)-C(3)	122.9(4)
C(20)-C(1)-C(2)	123.5(4)	C(6)-C(5)-C(4)	128.2(4)
N(1)-C(1)-C(2)	111.9(4)	C(6)-C(5)-C(41)	116.7(4)
C(1)-C(2)-C(21)	112.7(4)	C(4)-C(5)-C(41)	115.0(4)
C(1)-C(2)-C(3)	103.1(4)	N(2)-C(6)-C(5)	124.9(4)
C(21)-C(2)-C(3)	103.8(4)	N(2)-C(6)-C(7)	113.4(4)

Table S32. Bond lengths [Å] and angles [°].

C(5)-C(6)-C(7)	121.7(4)	F(62)-C(63)-C(64)	119.7(5)
C(6)-C(7)-C(24)	116.8(4)	F(62)-C(63)-C(62)	121.3(5)
C(6)-C(7)-C(8)	103.1(3)	C(64)-C(63)-C(62)	119.0(5)
C(24)-C(7)-C(8)	104.5(4)	F(63)-C(64)-C(65)	119.6(5)
C(9)-C(8)-C(25)	117.4(4)	F(63)-C(64)-C(63)	119.8(5)
C(9)-C(8)-C(7)	103.3(3)	C(65)-C(64)-C(63)	120.6(5)
C(25)-C(8)-C(7)	104.4(4)	F(64)-C(65)-C(64)	121.2(5)
C(10)-C(9)-N(2)	124.9(4)	F(64)-C(65)-C(66)	120.2(5)
C(10)-C(9)-C(8)	123.7(4)	C(64)-C(65)-C(66)	118.7(5)
N(2)-C(9)-C(8)	111.3(4)	C(61)-C(66)-F(65)	120.4(4)
C(9)-C(10)-C(11)	127.8(4)	C(61)-C(66)-C(65)	122.6(5)
C(9)-C(10)-C(51)	116.9(4)	F(65)-C(66)-C(65)	117.0(5)
C(11)-C(10)-C(51)	115.1(4)	C(75)-N(71)-C(71)	116.9(5)
N(3)-C(11)-C(10)	124.5(4)	F(31)-C(32)-C(31)	118.1(4)
N(3)-C(11)-C(12)	110.4(4)	F(32)-C(33)-C(32)	121.5(5)
C(10)-C(11)-C(12)	125.1(4)	F(32)-C(33)-C(34)	120.1(5)
C(13)-C(12)-C(11)	107.1(4)	C(32)-C(33)-C(34)	118.4(5)
C(12)-C(13)-C(14)	107.1(4)	F(33)-C(34)-C(35)	119.7(5)
N(3)-C(14)-C(15)	122.9(4)	F(33)-C(34)-C(33)	120.4(5)
N(3)-C(14)-C(13)	110.3(4)	C(35)-C(34)-C(33)	119.9(5)
C(15)-C(14)-C(13)	126.7(4)	F(34)-C(35)-C(34)	120.0(5)
C(16)-C(15)-C(14)	127.5(4)	F(34)-C(35)-C(36)	120.3(5)
C(16)-C(15)-C(61)	116.2(4)	C(34)-C(35)-C(36)	119.7(5)
C(14)-C(15)-C(61)	116.0(4)	F(35)-C(36)-C(35)	118.2(4)
N(4)-C(16)-C(15)	124.4(4)	F(35)-C(36)-C(31)	119.3(4)
N(4)-C(16)-C(17)	109.6(4)	C(35)-C(36)-C(31)	122.5(5)
C(15)-C(16)-C(17)	125.8(4)	C(46)-C(41)-C(42)	116.0(4)
C(18)-C(17)-C(16)	107.2(4)	C(46)-C(41)-C(5)	120.2(4)
C(17)-C(18)-C(19)	106.7(4)	C(42)-C(41)-C(5)	123.8(4)
N(4)-C(19)-C(18)	111.0(4)	F(41)-C(42)-C(43)	118.1(4)
N(4)-C(19)-C(20)	124.0(4)	F(41)-C(42)-C(41)	119.0(4)
C(18)-C(19)-C(20)	124.8(4)	C(43)-C(42)-C(41)	122.9(5)
C(1)-C(20)-C(19)	127.8(4)	F(42)-C(43)-C(42)	121.0(5)
C(1)-C(20)-C(31)	116.7(4)	F(42)-C(43)-C(44)	120.2(4)
C(19)-C(20)-C(31)	115.3(4)	C(42)-C(43)-C(44)	118.9(4)
N(5')-C(21)-C(2)	111.8(7)	F(43)-C(44)-C(45)	120.5(5)
N(5)-C(21)-C(2)	102.7(4)	F(43)-C(44)-C(43)	118.8(5)
N(5)-C(22)-C(3)	104.5(4)	C(45)-C(44)-C(43)	120.6(4)
N(5')-C(22)-C(3)	106.7(7)	F(44)-C(45)-C(44)	120.3(4)
C(22)-N(5)-C(21)	104.0(4)	F(44)-C(45)-C(46)	120.8(5)
C(22)-N(5)-C(23)	111.0(4)	C(44)-C(45)-C(46)	118.9(5)
C(21)-N(5)-C(23)	110.3(5)	F(45)-C(46)-C(41)	120.2(4)
C(21)-N(5')-C(23)	111.7(13)	F(45)-C(46)-C(45)	117.1(4)
C(21)-N(5')-C(22)	103.4(11)	C(41)-C(46)-C(45)	122.7(4)
C(23)-N(5')-C(22)	107.4(12)	C(52)-C(51)-C(56)	115.5(4)
N(6)-C(24)-C(7)	102.2(4)	C(52)-C(51)-C(10)	124.4(5)
C(26)-N(6)-C(24)	113.4(4)	C(56)-C(51)-C(10)	120.1(4)
C(26)-N(6)-C(25)	113.5(4)	F(51)-C(52)-C(51)	119.7(4)
C(24)-N(6)-C(25)	104.0(4)	F(51)-C(52)-C(53)	116.9(5)
N(6)-C(25)-C(8)	102.6(4)	C(51)-C(52)-C(53)	123.4(5)
C(32)-C(31)-C(36)	114.6(4)	F(52)-C(53)-C(52)	121.7(6)
C(32)-C(31)-C(20)	121.2(4)	F(52)-C(53)-C(54)	119.0(5)
C(36)-C(31)-C(20)	124.2(4)	C(52)-C(53)-C(54)	119.3(5)
C(33)-C(32)-F(31)	117.0(5)	F(53)-C(54)-C(55)	120.9(6)
C(33)-C(32)-C(31)	124.9(5)	F(53)-C(54)-C(53)	120.2(6)

Table S33. Bond lengths [Å] and angles [°].

C(55)-C(54)-C(53)	118.8(5)	C(66)-C(61)-C(62)	116.9(4)
F(54)-C(55)-C(54)	119.5(5)	C(66)-C(61)-C(15)	121.3(4)
F(54)-C(55)-C(56)	119.6(6)	C(62)-C(61)-C(15)	121.8(5)
C(54)-C(55)-C(56)	120.8(6)	F(61)-C(62)-C(61)	120.5(4)
F(55)-C(56)-C(55)	118.5(5)	F(61)-C(62)-C(63)	117.3(4)
F(55)-C(56)-C(51)	119.4(4)	C(61)-C(62)-C(63)	122.2(5)
C(55)-C(56)-C(51)	122.1(5)		
N(71)-C(75)	1.326(6)	C(72)-C(73)	1.378(8)
N(71)-C(71)	1.334(6)	C(73)-C(74)	1.373(8)
C(71)-C(72)	1.382(7)	C(74)-C(75)	1.390(8)
N(71)-C(71)-C(72)	123.8(5)	C(73)-C(74)-C(75)	118.5(6)
C(73)-C(72)-C(71)	118.3(5)	N(71)-C(75)-C(74)	123.5(5)
C(74)-C(73)-C(72)	118.9(6)		
N(72)-C(76)	1.279(13)	C(78)-C(79)	1.356(15)
N(72)-C(80')	1.281(13)	C(79)-C(80)	1.404(15)
N(72)-C(80)	1.383(12)	C(76')-C(77')	1.381(14)
N(72)-C(76')	1.414(12)	C(77')-C(78')	1.423(18)
C(76)-C(77)	1.400(14)	C(78')-C(79')	1.348(17)
C(77)-C(78)	1.428(17)	C(79')-C(80')	1.425(16)
C(76)-N(72)-C(80)	118.1(8)	N(72)-C(80)-C(79)	120.3(11)
C(80')-N(72)-C(76')	116.8(8)	C(77')-C(76')-N(72)	122.8(11)
N(72)-C(76)-C(77)	126.5(12)	C(76')-C(77')-C(78')	116.1(13)
C(76)-C(77)-C(78)	114.8(14)	C(79')-C(78')-C(77')	121.8(16)
C(79)-C(78)-C(77)	119.8(13)	C(78')-C(79')-C(80')	116.5(15)
C(78)-C(79)-C(80)	119.3(13)	N(72)-C(80')-C(79')	125.5(12)

VI.4 Ni-TPPF$_{20}$ (1)

Table S34.Crystal data and structure refinement for Ni-TPPF$_{20}$ (1).

Identification code	herges99	
Empirical formula	$C_{44}H_8F_{20}N_4Ni$	
Formula weight	1031.25	
Temperature	200(2) K	
Wavelength	0.71073 Å	
Crystal system	Tetragonal	
Space group	I-42d	
Unit cell dimensions	a = 15.4077(6) Å	α= 90°.
	b = 15.4077(6) Å	β= 90°.
	c = 15.3877(7) Å	γ = 90°.
Volume	3653.0(3) Å^3	
Z	4	
Density (calculated)	1.875 Mg/m^3	
Absorption coefficient	0.678 mm^{-1}	
F(000)	2032	
Crystal size	0.15 x 0.2 x 0.2 mm^3	
Theta range for data collection	1.870 to 27.417°.	
Index ranges	-19<=h<=19, -19<=k<=19, -14<=l<=19	
Reflections collected	17088	
Independent reflections	2076 [R(int) = 0.0280]	
Completeness to theta = 25.242°	99.1 %	
Refinement method	Full-matrix least-squares on F^2	
Data / restraints / parameters	2076 / 0 / 157	
Goodness-of-fit on F^2	1.042	
Final R indices [I>2sigma(I)]	R1 = 0.0278, wR2 = 0.0689	
R indices (all data)	R1 = 0.0291, wR2 = 0.0698	
Absolute structure parameter	0.004(4)	
Extinction coefficient	0.0012(5)	
Largest diff. peak and hole	0.223 and -0.269 e.Å^{-3}	

Comments

All non-hydrogen atoms were refined anisotropic. The H atoms were positioned with idealized geometry and refined isotropic with $U_{iso}(H) = 1.2\ U_{eq}(C)$ using a riding model. The absolute structure was determined and is in agreement with the selected setting (Flack-x-parameter: 0.016(21) by classical fit to all intensities and 0.004(4) from 870 selected quotients (Parsons' method)).

Table S35. Atomic coordinates (x 10^4) and equivalent isotropic displacement parameters ($Å^2$x 10^3). U(eq) is defined as one third of the trace of the orthogonalized U^{ij} tensor.

	x	y	z	U(eq)
Ni(1)	5000	5000	0	27(1)
N(1)	3933(1)	4350(1)	5(2)	30(1)
C(1)	3122(2)	4645(2)	241(2)	33(1)
C(2)	2511(2)	3943(2)	233(2)	42(1)
C(3)	2941(2)	3234(2)	-43(3)	43(1)
C(4)	3827(2)	3485(2)	-168(2)	32(1)
C(5)	4486(2)	2910(2)	-354(2)	32(1)
C(6)	4252(2)	2000(2)	-592(2)	33(1)
C(7)	4277(2)	1338(2)	15(2)	39(1)
C(8)	4023(2)	498(2)	-184(2)	41(1)
C(9)	3736(2)	313(2)	-1007(3)	45(1)
C(10)	3699(2)	956(2)	-1628(2)	45(1)
C(11)	3960(2)	1789(2)	-1415(2)	38(1)
F(1)	4547(2)	1505(1)	820(1)	55(1)
F(2)	4064(2)	-129(1)	412(1)	57(1)
F(3)	3492(2)	-497(1)	-1204(2)	67(1)
F(4)	3401(2)	772(2)	-2422(2)	72(1)
F(5)	3930(1)	2394(1)	-2039(1)	51(1)

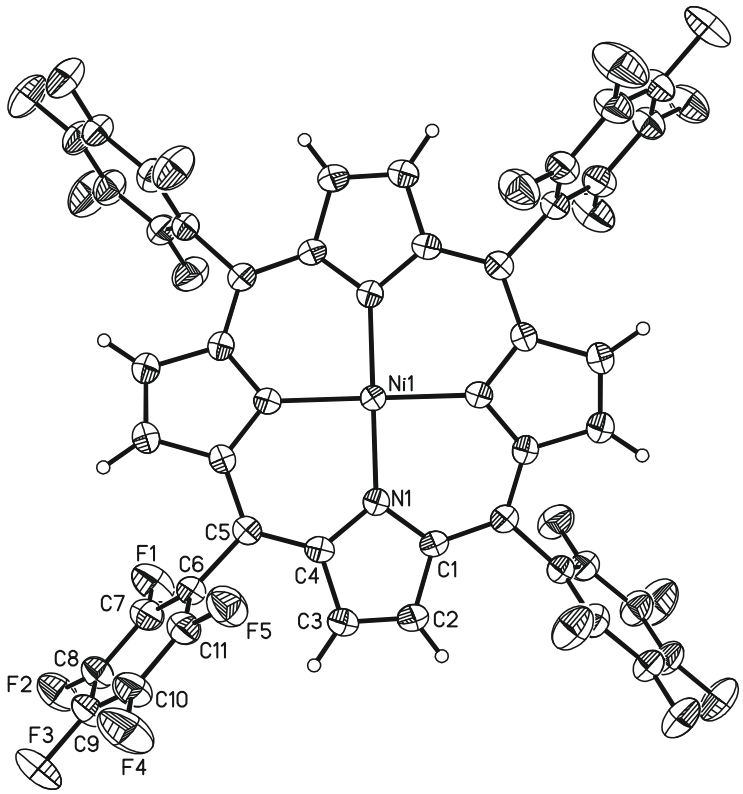

Table S36. Bond lengths [Å] and angles [°].

Ni(1)-N(1)#1	1.925(2)	Ni(1)-N(1)#3	1.925(2)
Ni(1)-N(1)#2	1.925(2)	Ni(1)-N(1)	1.925(2)
N(1)#1-Ni(1)-N(1)#2	90.001(1)	N(1)#1-Ni(1)-N(1)	179.56(15)
N(1)#1-Ni(1)-N(1)#3	90.001(1)	N(1)#2-Ni(1)-N(1)	90.000(1)
N(1)#2-Ni(1)-N(1)#3	179.56(15)	N(1)#3-Ni(1)-N(1)	90.001(1)
C(4)-N(1)-Ni(1)	127.44(18)	C(1)-N(1)-Ni(1)	127.11(17)
N(1)-C(4)	1.368(3)	C(6)-C(7)	1.384(4)
N(1)-C(1)	1.378(4)	C(7)-F(1)	1.331(4)
C(1)-C(5)#3	1.389(4)	C(7)-C(8)	1.385(4)
C(1)-C(2)	1.434(4)	C(8)-F(2)	1.334(4)
C(2)-C(3)	1.346(4)	C(8)-C(9)	1.372(5)
C(3)-C(4)	1.432(4)	C(9)-F(3)	1.338(3)
C(4)-C(5)	1.379(4)	C(9)-C(10)	1.379(5)
C(5)-C(1)#2	1.389(4)	C(10)-F(4)	1.335(4)
C(5)-C(6)	1.492(4)	C(10)-C(11)	1.385(4)
C(6)-C(11)	1.382(4)	C(11)-F(5)	1.339(4)
C(4)-N(1)-C(1)	105.3(2)	F(1)-C(7)-C(6)	119.6(3)
N(1)-C(1)-C(5)#3	124.4(2)	F(1)-C(7)-C(8)	118.3(3)
N(1)-C(1)-C(2)	110.1(2)	C(6)-C(7)-C(8)	122.1(3)
C(5)#3-C(1)-C(2)	125.0(3)	F(2)-C(8)-C(9)	119.9(3)
C(3)-C(2)-C(1)	107.0(3)	F(2)-C(8)-C(7)	120.7(3)
C(2)-C(3)-C(4)	106.9(2)	C(9)-C(8)-C(7)	119.4(3)
N(1)-C(4)-C(5)	125.3(2)	F(3)-C(9)-C(8)	119.6(3)
N(1)-C(4)-C(3)	110.6(2)	F(3)-C(9)-C(10)	120.1(3)
C(5)-C(4)-C(3)	123.8(2)	C(8)-C(9)-C(10)	120.2(3)
C(4)-C(5)-C(1)#2	122.2(2)	F(4)-C(10)-C(9)	119.7(3)
C(4)-C(5)-C(6)	118.4(3)	F(4)-C(10)-C(11)	121.0(3)
C(1)#2-C(5)-C(6)	119.1(3)	C(9)-C(10)-C(11)	119.3(3)
C(11)-C(6)-C(7)	117.0(3)	F(5)-C(11)-C(6)	120.3(3)
C(11)-C(6)-C(5)	121.6(3)	F(5)-C(11)-C(10)	117.7(3)
C(7)-C(6)-C(5)	121.4(3)	C(6)-C(11)-C(10)	122.0(3)

Symmetry transformations used to generate equivalent atoms: #1 -x+1,-y+1,z #2 -y+1,x,-z #3 y,-x+1,-z

Table S37. Anisotropic displacement parameters ($Å^2 x\ 10^3$). The anisotropic displacement factor exponent takes the form: $-2\pi^2[\ h^2\ a^{*2}U^{11} + ... + 2\ h\ k\ a^*\ b^*\ U^{12}\ ]$

	U^{11}	U^{22}	U^{33}	U^{23}	U^{13}	U^{12}
Ni(1)	23(1)	23(1)	36(1)	0	0	0
N(1)	25(1)	25(1)	39(1)	0(1)	2(1)	1(1)
C(1)	23(1)	30(1)	46(2)	0(1)	2(1)	-1(1)
C(2)	26(1)	34(1)	67(2)	-2(1)	6(1)	-3(1)
C(3)	31(1)	30(1)	69(2)	-5(2)	4(2)	-4(1)
C(4)	27(1)	27(1)	42(2)	-2(1)	-1(1)	-3(1)
C(5)	30(1)	26(1)	40(2)	-1(1)	-1(1)	-1(1)
C(6)	28(1)	27(1)	44(2)	-3(1)	1(1)	-1(1)
C(7)	41(2)	34(1)	42(2)	-2(1)	0(1)	-4(1)
C(8)	42(2)	27(1)	54(2)	3(1)	3(1)	-4(1)
C(9)	48(2)	27(1)	60(2)	-7(1)	1(2)	-9(1)
C(10)	51(2)	38(2)	46(2)	-8(1)	-6(1)	-9(1)
C(11)	39(2)	31(1)	45(2)	1(1)	-3(1)	-2(1)
F(1)	79(1)	43(1)	42(1)	2(1)	-8(1)	-14(1)
F(2)	73(1)	35(1)	64(1)	12(1)	2(1)	-12(1)
F(3)	90(2)	31(1)	78(2)	-11(1)	-3(1)	-21(1)
F(4)	106(2)	56(1)	56(1)	-10(1)	-22(1)	-24(1)
F(5)	62(1)	39(1)	50(1)	5(1)	-12(1)	-3(1)

Table S38. Hydrogen coordinates ($x\ 10^4$) and isotropic displacement parameters ($Å^2 x\ 10^{\ 3}$).

	x	y	z	U(eq)
H(2)	1917	3973	392	51
H(3)	2701	2673	-137	52

VI.5 Coordination polymer of 2

Table S39. Crystal data and structure refinement the coordination polymer of 2.

Identification code	herges97	
Empirical formula	$C_{47}H_{15}F_{20}N_5Ni$	
Formula weight	1088.35	
Temperature	170(2) K	
Wavelength	0.71073 Å	
Crystal system	Monoclinic	
Space group	$P2_1/c$	
Unit cell dimensions	a = 15.1307(8) Å	α= 90°.
	b = 13.1247(4) Å	β= 108.180(4)°.
	c = 27.8511(13) Å	γ = 90°.
Volume	5254.7(4) $Å^3$	
Z	4	
Density (calculated)	1.376 Mg/m^3	
Absorption coefficient	0.476 mm^{-1}	
F(000)	2160	
Crystal size	0.14 x 0.05 x 0.04 mm^3	
Theta range for data collection	1.417 to 24.837°.	
Index ranges	-17<=h<=15, -13<=k<=15, -32<=l<=32	
Reflections collected	35365	
Independent reflections	9037 [R(int) = 0.1291]	
Completeness to theta = 25.242°	95.1 %	
Refinement method	Full-matrix least-squares on F^2	
Data / restraints / parameters	9037 / 128 / 758	
Goodness-of-fit on F^2	1.050	
Final R indices [I>2sigma(I)]	R1 = 0.0959, wR2 = 0.2516	
R indices (all data)	R1 = 0.1295, wR2 = 0.2742	
Extinction coefficient	n/a	
Largest diff. peak and hole	1.373 and -0.680 $e.Å^{-3}$	

Comments:

All non-hydrogen atoms were refined anisotropic. The C-H H atoms were positioned with idealized geometry and refined using a riding model. One of the C6F5 rings is disordered and was refined using a split model with restraints and equal site occupation factor. The asymmetric unit contain at least three chloroform molecules, which are disordered and for which no split model can be found. Therefore, the data were corrected for disordered solvent using SQUEEZE in Platon. The low reliabi8lity factors can be traced back to the poor crystallinity and the small size of the crystals. During crystal preparation the crystals immediately start to decompose.

Table S40. Atomic coordinates (x 10^4) and equivalent isotropic displacement parameters ($Å^2$x 10^3). U(eq) is defined as one third of the trace of the orthogonalized U^{ij} tensor.

	x	y	z	U(eq)
Ni(1)	3480(1)	4140(1)	7390(1)	42(1)
N(1)	4635(4)	5049(4)	7436(2)	44(1)
N(2)	3749(3)	4285(4)	8148(2)	41(1)
N(3)	2179(4)	3606(4)	7336(2)	45(1)
N(4)	3060(4)	4274(4)	6626(2)	46(1)
C(1)	4906(5)	5395(5)	7047(2)	45(1)
C(2)	5812(5)	5938(5)	7208(3)	53(2)
C(3)	6140(4)	5826(5)	7776(2)	45(1)
C(4)	5318(4)	5306(4)	7877(2)	43(1)
C(5)	5293(4)	5058(5)	8355(2)	44(1)
C(6)	4564(4)	4578(5)	8485(2)	45(1)
C(7)	4560(5)	4360(5)	9000(2)	51(2)
C(8)	3756(4)	3949(5)	8962(2)	48(2)
C(9)	3218(4)	3907(5)	8438(2)	49(2)
C(10)	2329(4)	3503(5)	8235(2)	45(1)
C(11)	1792(5)	3419(5)	7721(2)	52(2)
C(12)	861(5)	3121(6)	7526(3)	61(2)
C(13)	637(6)	3110(6)	7016(3)	63(2)
C(14)	1470(4)	3429(5)	6898(2)	46(1)
C(15)	1525(4)	3482(5)	6401(2)	45(1)
C(16)	2271(6)	3871(6)	6277(3)	64(2)
C(17)	2312(5)	4000(5)	5785(2)	52(2)
C(18)	3097(5)	4469(5)	5818(2)	50(2)
C(19)	3556(5)	4676(5)	6344(2)	47(1)
C(20)	4404(5)	5221(5)	6527(2)	52(2)
C(21)	5872(5)	7076(5)	7103(2)	48(1)
N(5)	5831(4)	7653(4)	7561(2)	42(1)
C(22)	6359(5)	6977(5)	7974(2)	46(1)
C(23)	4845(5)	7778(6)	7557(3)	62(2)
C(31)	6159(5)	5313(5)	8788(2)	48(1)
C(32)	6971(5)	4735(5)	8863(2)	47(1)
C(33)	7782(5)	4927(6)	9231(2)	57(2)
C(34)	7796(5)	5747(6)	9563(2)	56(2)
C(35)	6997(6)	6286(5)	9511(2)	56(2)
C(36)	6209(4)	6087(4)	9134(2)	42(1)
F(31)	6957(3)	3954(3)	8545(2)	62(1)
F(32)	8534(3)	4414(4)	9280(2)	70(1)
F(33)	8589(3)	5989(4)	9924(2)	71(1)
F(34)	7042(3)	7064(3)	9848(2)	68(1)
F(35)	5461(3)	6673(3)	9081(2)	64(1)
C(41)	1827(5)	3117(6)	8596(2)	55(2)
C(42)	1135(5)	3606(6)	8696(2)	58(2)
C(43)	698(5)	3216(7)	9041(3)	64(2)
C(44)	1006(5)	2301(6)	9265(2)	59(2)
C(45)	1677(5)	1796(7)	9177(3)	62(2)
C(46)	2102(5)	2198(6)	8832(2)	57(2)
F(41)	835(3)	4521(4)	8480(2)	76(1)
F(42)	4(3)	3736(4)	9128(2)	79(1)
F(43)	599(3)	1925(4)	9602(2)	75(1)
F(44)	1975(4)	894(4)	9404(2)	87(1)
F(45)	2794(3)	1629(4)	8751(2)	74(1)

Table S41. Atomic coordinates (x 10^4) and equivalent isotropic displacement parameters ($Å^2$x 10^3). U(eq) is defined as one third of the trace of the orthogonalized U^{ij} tensor.

	x	y	z	U(eq)
C(51)	661(4)	3178(5)	5986(2)	45(1)
C(52)	450(5)	2161(5)	5861(2)	52(2)
C(53)	-307(5)	1883(6)	5478(3)	59(2)
C(54)	-916(5)	2622(6)	5198(2)	54(2)
C(55)	-718(5)	3637(6)	5316(3)	56(2)
C(56)	50(5)	3895(5)	5693(2)	54(2)
F(51)	1020(3)	1445(3)	6123(2)	69(1)
F(52)	-495(4)	884(3)	5371(2)	79(1)
F(53)	-1675(3)	2354(4)	4817(2)	73(1)
F(54)	-1291(3)	4343(4)	5029(2)	78(1)
F(55)	232(3)	4885(3)	5790(2)	72(1)
C(61)	4820(40)	5700(40)	6151(14)	56(12)
C(62)	5480(40)	4920(30)	6042(15)	78(7)
C(63)	5880(20)	5150(20)	5628(10)	87(5)
C(64)	5600(30)	6050(30)	5358(12)	79(5)
C(65)	4960(20)	6700(30)	5459(11)	71(5)
C(66)	4630(30)	6530(40)	5900(30)	57(7)
F(61)	5700(20)	4150(30)	6216(12)	123(11)
F(62)	6471(16)	4564(18)	5523(7)	100(5)
F(63)	5860(20)	6320(30)	4948(11)	137(10)
F(64)	4720(16)	7530(20)	5257(11)	109(6)
F(65)	4018(16)	7020(20)	5983(9)	76(5)
C(61')	4770(50)	5590(40)	6120(18)	65(14)
C(62')	5410(30)	5070(30)	5953(12)	69(10)
C(63')	5560(20)	5640(30)	5491(11)	81(7)
C(64')	5210(20)	6410(20)	5320(10)	74(6)
C(65')	4566(19)	6920(20)	5481(8)	70(6)
C(66')	4410(40)	6410(50)	5860(20)	72(11)
F(62')	6224(16)	4980(20)	5372(8)	123(8)
F(63')	5518(19)	6700(20)	4937(8)	136(11)
F(64')	4290(20)	7769(14)	5212(10)	137(11)
F(65')	3702(15)	7089(18)	6018(10)	77(6)
F(61')	5763(10)	4200(20)	6229(10)	83(7)

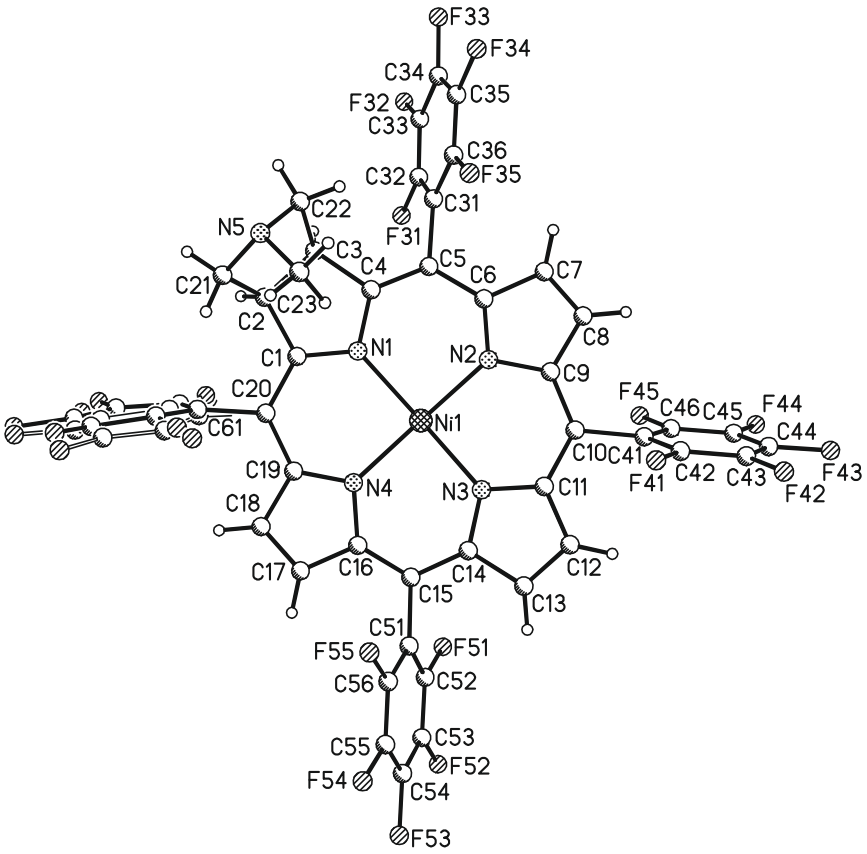

Table S42. Bond lengths [Å] and angles [°].

Ni(1)-N(2)	2.030(5)	Ni(1)-N(1)	2.087(5)
Ni(1)-N(4)	2.031(5)	Ni(1)-N(5)#1	2.198(5)
Ni(1)-N(3)	2.049(5)	N(5)-Ni(1)#2	2.198(5)
N(2)-Ni(1)-N(4)	167.9(2)	N(3)-Ni(1)-N(1)	165.2(2)
N(2)-Ni(1)-N(3)	89.2(2)	N(2)-Ni(1)-N(5)#1	94.67(18)
N(4)-Ni(1)-N(3)	88.4(2)	N(4)-Ni(1)-N(5)#1	97.37(19)
N(2)-Ni(1)-N(1)	89.51(19)	N(3)-Ni(1)-N(5)#1	97.3(2)
N(4)-Ni(1)-N(1)	89.7(2)	N(1)-Ni(1)-N(5)#1	97.6(2)
N(1)-C(1)	1.351(8)	C(5)-C(31)	1.515(9)
N(1)-C(4)	1.379(8)	C(6)-C(7)	1.463(9)
N(2)-C(6)	1.352(8)	C(7)-C(8)	1.305(10)
N(2)-C(9)	1.394(8)	C(8)-C(9)	1.434(8)
N(3)-C(14)	1.370(8)	C(9)-C(10)	1.391(9)
N(3)-C(11)	1.395(9)	C(10)-C(11)	1.413(8)
N(4)-C(19)	1.352(9)	C(10)-C(41)	1.524(9)
N(4)-C(16)	1.388(9)	C(11)-C(12)	1.398(10)
C(1)-C(20)	1.427(8)	C(12)-C(13)	1.354(10)
C(1)-C(2)	1.485(10)	C(13)-C(14)	1.459(10)
C(2)-C(3)	1.510(9)	C(14)-C(15)	1.413(9)
C(2)-C(21)	1.531(9)	C(15)-C(16)	1.377(11)
C(3)-C(4)	1.519(9)	C(15)-C(51)	1.505(8)
C(3)-C(22)	1.606(9)	C(16)-C(17)	1.400(10)
C(4)-C(5)	1.382(8)	C(17)-C(18)	1.316(10)
C(5)-C(6)	1.413(9)	C(18)-C(19)	1.438(8)

Table S43. Bond lengths [Å] and angles [°].

C(19)-C(20)	1.418(10)	C(52)-C(53)	1.348(10)
C(20)-C(61')	1.48(5)	C(53)-F(52)	1.355(8)
C(20)-C(61)	1.51(3)	C(53)-C(54)	1.397(10)
C(21)-N(5)	1.501(7)	C(54)-F(53)	1.345(7)
N(5)-C(22)	1.474(7)	C(54)-C(55)	1.382(10)
N(5)-C(23)	1.499(9)	C(55)-C(56)	1.344(10)
C(31)-C(36)	1.386(9)	C(55)-F(54)	1.349(8)
C(31)-C(32)	1.403(9)	C(56)-F(55)	1.338(8)
C(32)-F(31)	1.351(7)	C(61)-C(66)	1.28(7)
C(32)-C(33)	1.354(10)	C(61)-C(62)	1.53(7)
C(33)-F(32)	1.291(8)	C(62)-F(61)	1.13(6)
C(33)-C(34)	1.416(11)	C(62)-C(63)	1.49(4)
C(34)-F(33)	1.340(8)	C(63)-F(62)	1.28(4)
C(34)-C(35)	1.368(11)	C(63)-C(64)	1.40(5)
C(35)-C(36)	1.347(9)	C(64)-F(63)	1.37(4)
C(35)-F(34)	1.376(7)	C(64)-C(65)	1.38(5)
C(36)-F(35)	1.338(7)	C(65)-F(64)	1.22(4)
C(41)-C(42)	1.329(10)	C(65)-C(66)	1.47(7)
C(41)-C(46)	1.375(10)	C(66)-F(65)	1.22(6)
C(42)-F(41)	1.357(9)	C(61')-C(66')	1.32(8)
C(42)-C(43)	1.419(11)	C(61')-C(62')	1.38(7)
C(43)-F(42)	1.336(9)	C(62')-F(61')	1.39(5)
C(43)-C(44)	1.367(12)	C(62')-C(63')	1.57(4)
C(44)-C(45)	1.299(11)	C(63')-C(64')	1.17(4)
C(44)-F(43)	1.366(8)	C(63')-F(62')	1.44(4)
C(45)-F(44)	1.351(9)	C(64')-F(63')	1.35(4)
C(45)-C(46)	1.414(10)	C(64')-C(65')	1.37(3)
C(46)-F(45)	1.361(9)	C(65')-C(66')	1.34(7)
C(51)-C(52)	1.391(9)	C(65')-F(64')	1.34(3)
C(51)-C(56)	1.391(9)	C(66')-F(65')	1.55(7)
C(52)-F(51)	1.330(8)		
C(1)-N(1)-C(4)	107.6(5)	C(7)-C(8)-C(9)	108.5(6)
C(6)-N(2)-C(9)	105.4(5)	C(10)-C(9)-N(2)	124.1(5)
C(14)-N(3)-C(11)	104.7(5)	C(10)-C(9)-C(8)	126.7(6)
C(19)-N(4)-C(16)	104.7(6)	N(2)-C(9)-C(8)	109.2(5)
N(1)-C(1)-C(20)	124.1(6)	C(9)-C(10)-C(11)	128.2(6)
N(1)-C(1)-C(2)	113.6(5)	C(9)-C(10)-C(41)	118.5(5)
C(20)-C(1)-C(2)	122.2(6)	C(11)-C(10)-C(41)	113.3(6)
C(1)-C(2)-C(3)	104.0(5)	N(3)-C(11)-C(12)	111.3(6)
C(1)-C(2)-C(21)	121.0(6)	N(3)-C(11)-C(10)	121.3(6)
C(3)-C(2)-C(21)	106.1(5)	C(12)-C(11)-C(10)	127.4(6)
C(2)-C(3)-C(4)	102.5(5)	C(13)-C(12)-C(11)	107.7(7)
C(2)-C(3)-C(22)	103.4(5)	C(12)-C(13)-C(14)	106.3(6)
C(4)-C(3)-C(22)	117.0(5)	N(3)-C(14)-C(15)	126.4(6)
N(1)-C(4)-C(5)	124.3(6)	N(3)-C(14)-C(13)	109.9(6)
N(1)-C(4)-C(3)	112.0(5)	C(15)-C(14)-C(13)	123.6(6)
C(5)-C(4)-C(3)	123.6(5)	C(16)-C(15)-C(14)	124.6(6)
C(4)-C(5)-C(6)	127.6(6)	C(16)-C(15)-C(51)	119.2(6)
C(4)-C(5)-C(31)	115.9(6)	C(14)-C(15)-C(51)	115.9(6)
C(6)-C(5)-C(31)	116.4(5)	C(15)-C(16)-N(4)	124.0(6)
N(2)-C(6)-C(5)	124.4(5)	C(15)-C(16)-C(17)	125.5(6)
N(2)-C(6)-C(7)	110.0(5)	N(4)-C(16)-C(17)	110.3(7)
C(5)-C(6)-C(7)	125.5(6)	C(18)-C(17)-C(16)	107.7(6)
C(8)-C(7)-C(6)	106.9(5)	C(17)-C(18)-C(19)	107.3(6)

Table S44. Bond lengths [Å] and angles [°].

N(4)-C(19)-C(20)	126.3(5)	F(51)-C(52)-C(53)	119.2(6)
N(4)-C(19)-C(18)	109.8(6)	F(51)-C(52)-C(51)	118.8(5)
C(20)-C(19)-C(18)	123.9(6)	C(53)-C(52)-C(51)	122.0(6)
C(19)-C(20)-C(1)	125.5(6)	C(52)-C(53)-F(52)	120.3(7)
C(19)-C(20)-C(61')	113(2)	C(52)-C(53)-C(54)	120.2(7)
C(1)-C(20)-C(61')	121(2)	F(52)-C(53)-C(54)	119.5(6)
C(19)-C(20)-C(61)	118.8(19)	F(53)-C(54)-C(55)	120.5(6)
C(1)-C(20)-C(61)	115.6(19)	F(53)-C(54)-C(53)	120.8(6)
N(5)-C(21)-C(2)	107.9(5)	C(55)-C(54)-C(53)	118.7(6)
C(22)-N(5)-C(23)	111.6(5)	C(56)-C(55)-F(54)	121.9(7)
C(22)-N(5)-C(21)	101.7(5)	C(56)-C(55)-C(54)	120.0(6)
C(23)-N(5)-C(21)	110.7(5)	F(54)-C(55)-C(54)	118.1(6)
N(5)-C(22)-C(3)	107.2(4)	F(55)-C(56)-C(55)	118.4(6)
C(36)-C(31)-C(32)	115.9(6)	F(55)-C(56)-C(51)	118.8(6)
C(36)-C(31)-C(5)	124.0(6)	C(55)-C(56)-C(51)	122.8(6)
C(32)-C(31)-C(5)	120.0(6)	C(66)-C(61)-C(62)	120(4)
F(31)-C(32)-C(33)	117.5(6)	C(66)-C(61)-C(20)	132(6)
F(31)-C(32)-C(31)	118.6(5)	C(62)-C(61)-C(20)	108(3)
C(33)-C(32)-C(31)	123.9(6)	F(61)-C(62)-C(63)	112(4)
F(32)-C(33)-C(32)	122.9(7)	F(61)-C(62)-C(61)	130(4)
F(32)-C(33)-C(34)	119.6(6)	C(63)-C(62)-C(61)	118(4)
C(32)-C(33)-C(34)	117.5(7)	F(62)-C(63)-C(64)	120(3)
F(33)-C(34)-C(35)	120.8(6)	F(62)-C(63)-C(62)	122(3)
F(33)-C(34)-C(33)	119.8(7)	C(64)-C(63)-C(62)	117(3)
C(35)-C(34)-C(33)	119.4(6)	F(63)-C(64)-C(65)	115(4)
C(36)-C(35)-C(34)	121.5(6)	F(63)-C(64)-C(63)	123(4)
C(36)-C(35)-F(34)	121.3(6)	C(65)-C(64)-C(63)	122(3)
C(34)-C(35)-F(34)	117.2(6)	F(64)-C(65)-C(64)	125(4)
F(35)-C(36)-C(35)	119.2(5)	F(64)-C(65)-C(66)	113(4)
F(35)-C(36)-C(31)	119.0(5)	C(64)-C(65)-C(66)	121(3)
C(35)-C(36)-C(31)	121.8(6)	F(65)-C(66)-C(61)	113(6)
C(42)-C(41)-C(46)	117.7(7)	F(65)-C(66)-C(65)	123(6)
C(42)-C(41)-C(10)	124.4(7)	C(61)-C(66)-C(65)	121(5)
C(46)-C(41)-C(10)	117.9(6)	C(66')-C(61')-C(62')	116(5)
C(41)-C(42)-F(41)	120.7(7)	C(66')-C(61')-C(20)	119(6)
C(41)-C(42)-C(43)	122.1(7)	C(62')-C(61')-C(20)	124(5)
F(41)-C(42)-C(43)	117.2(7)	F(61')-C(62')-C(61')	114(3)
F(42)-C(43)-C(44)	122.7(7)	F(61')-C(62')-C(63')	136(3)
F(42)-C(43)-C(42)	119.8(8)	C(61')-C(62')-C(63')	110(4)
C(44)-C(43)-C(42)	117.5(7)	C(64')-C(63')-F(62')	133(4)
C(45)-C(44)-F(43)	119.6(7)	C(64')-C(63')-C(62')	125(3)
C(45)-C(44)-C(43)	122.4(7)	F(62')-C(63')-C(62')	101(3)
F(43)-C(44)-C(43)	118.0(7)	C(63')-C(64')-F(63')	110(4)
C(44)-C(45)-F(44)	121.7(7)	C(63')-C(64')-C(65')	125(3)
C(44)-C(45)-C(46)	119.1(7)	F(63')-C(64')-C(65')	125(3)
F(44)-C(45)-C(46)	119.2(7)	C(66')-C(65')-F(64')	139(4)
F(45)-C(46)-C(41)	122.5(6)	C(66')-C(65')-C(64')	110(4)
F(45)-C(46)-C(45)	116.4(7)	F(64')-C(65')-C(64')	111(2)
C(41)-C(46)-C(45)	121.2(7)	C(61')-C(66')-C(65')	134(6)
C(52)-C(51)-C(56)	116.3(5)	C(61')-C(66')-F(65')	121(6)
C(52)-C(51)-C(15)	121.6(5)	C(65')-C(66')-F(65')	104(5)
C(56)-C(51)-C(15)	122.0(6)		

Symmetry transformations used to generate equivalent atoms: #1 -x+1,y-1/2,-z+3/2 #2 -x+1,y+1/2,-z+3/2

Table S45. Anisotropic displacement parameters ($Å^2 x\ 10^3$). The anisotropic displacement factor exponent takes the form: $-2\pi^2[\ h^2\ a^{*2}U^{11} + ... + 2\ h\ k\ a^*\ b^*\ U^{12}\ ]$

	U^{11}	U^{22}	U^{33}	U^{23}	U^{13}	U^{12}
Ni(1)	51(1)	42(1)	36(1)	0(1)	16(1)	1(1)
N(1)	56(3)	39(3)	40(2)	1(2)	18(2)	-1(2)
N(2)	43(3)	39(3)	47(3)	6(2)	23(2)	2(2)
N(3)	47(3)	48(3)	45(3)	3(2)	23(2)	2(2)
N(4)	44(3)	43(3)	52(3)	-6(2)	15(2)	5(2)
C(1)	57(4)	49(3)	31(3)	5(2)	18(2)	10(3)
C(2)	62(4)	44(3)	59(4)	-5(3)	28(3)	-6(3)
C(3)	50(3)	45(3)	46(3)	4(3)	22(3)	12(3)
C(4)	50(3)	40(3)	41(3)	4(2)	16(3)	-2(3)
C(5)	47(3)	45(3)	41(3)	2(2)	17(3)	2(3)
C(6)	53(4)	45(3)	42(3)	3(3)	21(3)	0(3)
C(7)	56(4)	50(4)	40(3)	-9(3)	6(3)	-2(3)
C(8)	50(3)	57(4)	40(3)	4(3)	20(3)	-15(3)
C(9)	47(3)	67(4)	38(3)	2(3)	19(3)	-5(3)
C(10)	40(3)	64(4)	35(3)	1(3)	19(2)	4(3)
C(11)	61(4)	57(4)	41(3)	-2(3)	18(3)	-3(3)
C(12)	57(4)	76(5)	54(4)	4(3)	23(3)	1(4)
C(13)	64(4)	74(5)	61(4)	-2(4)	31(3)	2(4)
C(14)	39(3)	52(3)	44(3)	-3(3)	8(2)	1(3)
C(15)	45(3)	51(3)	39(3)	5(3)	12(2)	-2(3)
C(16)	71(5)	63(4)	46(4)	-6(3)	3(3)	11(4)
C(17)	65(4)	49(4)	40(3)	-3(3)	13(3)	-7(3)
C(18)	61(4)	57(4)	34(3)	-6(3)	16(3)	1(3)
C(19)	54(4)	45(3)	43(3)	0(3)	17(3)	0(3)
C(20)	69(4)	56(4)	34(3)	1(3)	20(3)	-8(3)
C(21)	60(4)	52(4)	37(3)	-6(3)	24(3)	-3(3)
N(5)	49(3)	39(2)	40(2)	-5(2)	15(2)	0(2)
C(22)	55(4)	47(3)	37(3)	2(2)	15(3)	1(3)
C(23)	63(4)	48(4)	84(5)	-6(3)	35(4)	-13(3)
C(31)	55(4)	59(4)	34(3)	3(3)	20(3)	-6(3)
C(32)	60(4)	42(3)	45(3)	1(3)	23(3)	3(3)
C(33)	57(4)	71(5)	44(3)	12(3)	15(3)	2(4)
C(34)	60(4)	64(4)	42(3)	-3(3)	11(3)	-7(3)
C(35)	81(5)	40(3)	46(3)	-3(3)	19(3)	7(3)
C(36)	44(3)	38(3)	43(3)	-4(2)	10(2)	6(2)
F(31)	72(3)	58(2)	57(2)	-1(2)	23(2)	19(2)
F(32)	65(3)	77(3)	72(3)	13(2)	26(2)	27(2)
F(33)	58(2)	86(3)	61(2)	-8(2)	7(2)	-6(2)
F(34)	82(3)	68(3)	53(2)	-24(2)	17(2)	-6(2)
F(35)	75(3)	63(2)	56(2)	-14(2)	21(2)	13(2)
C(41)	49(4)	77(5)	43(3)	6(3)	19(3)	7(3)
C(42)	71(4)	67(4)	44(3)	-6(3)	28(3)	-2(4)
C(43)	58(4)	78(5)	60(4)	-21(4)	26(3)	-12(4)
C(44)	59(4)	83(5)	41(3)	-9(3)	25(3)	-19(4)
C(45)	48(4)	86(5)	49(4)	15(3)	10(3)	-14(4)
C(46)	57(4)	66(4)	50(3)	1(3)	21(3)	-5(3)
F(41)	77(3)	78(3)	79(3)	7(2)	35(2)	8(2)
F(42)	77(3)	95(3)	79(3)	-10(2)	43(2)	-1(3)
F(43)	77(3)	97(3)	59(2)	5(2)	33(2)	-12(3)
F(44)	97(4)	88(3)	84(3)	26(3)	41(3)	4(3)
F(45)	75(3)	80(3)	77(3)	12(2)	40(2)	7(2)
C(51)	43(3)	52(4)	40(3)	-1(3)	10(2)	2(3)

Table S46. Anisotropic displacement parameters ($Å^2 x 10^3$). The anisotropic displacement factor exponent takes the form: $-2\pi^2[h^2 a^{*2} U^{11} + ... + 2 h k a^* b^* U^{12}]$

	U^{11}	U^{22}	U^{33}	U^{23}	U^{13}	U^{12}
C(52)	47(3)	58(4)	49(3)	4(3)	11(3)	10(3)
C(53)	71(5)	56(4)	49(3)	-10(3)	18(3)	-9(3)
C(54)	51(4)	64(4)	42(3)	-2(3)	9(3)	-5(3)
C(55)	54(4)	62(4)	53(4)	3(3)	14(3)	9(3)
C(56)	61(4)	48(4)	49(3)	-1(3)	14(3)	3(3)
F(51)	77(3)	55(2)	67(2)	0(2)	10(2)	4(2)
F(52)	89(3)	59(2)	75(3)	-10(2)	8(2)	-2(2)
F(53)	69(3)	78(3)	61(2)	-7(2)	5(2)	-1(2)
F(54)	80(3)	71(3)	69(3)	3(2)	6(2)	14(2)
F(55)	81(3)	52(2)	74(3)	0(2)	12(2)	1(2)
C(61)	80(20)	60(20)	37(17)	20(15)	31(17)	-16(15)
C(62)	120(19)	66(12)	50(13)	-27(9)	30(12)	-30(14)
C(63)	112(15)	84(11)	74(11)	-33(8)	45(11)	-33(9)
C(64)	79(13)	104(14)	70(12)	-11(9)	46(10)	-47(9)
C(65)	80(16)	78(12)	62(12)	-1(10)	31(9)	-42(8)
C(66)	62(16)	49(12)	68(17)	-9(9)	29(14)	-25(11)
F(61)	190(20)	94(16)	91(17)	-2(12)	48(14)	6(15)
F(62)	97(12)	133(13)	72(11)	-23(9)	29(8)	-15(8)
F(63)	210(20)	148(17)	101(11)	-20(10)	116(13)	-45(14)
F(64)	129(14)	112(12)	75(10)	26(9)	17(11)	-16(9)
F(65)	79(12)	93(11)	54(7)	19(6)	19(7)	18(9)
C(61')	80(20)	59(18)	50(19)	-34(16)	15(15)	-20(15)
C(62')	68(12)	110(20)	45(12)	-1(11)	45(11)	-28(13)
C(63')	82(14)	95(19)	74(15)	-19(13)	36(12)	-16(15)
C(64')	84(16)	93(16)	60(11)	0(10)	43(10)	8(11)
C(65')	77(14)	93(15)	43(9)	14(9)	24(9)	-9(11)
C(66')	80(30)	80(20)	46(10)	2(13)	12(17)	-26(19)
F(62')	99(14)	220(30)	73(11)	-16(12)	58(11)	-21(13)
F(63')	180(20)	190(30)	55(7)	-45(11)	64(11)	-108(19)
F(64')	240(30)	65(9)	69(8)	25(7)	-12(16)	-40(12)
F(65')	87(13)	56(7)	84(9)	-2(6)	22(9)	8(8)
F(61')	41(6)	113(17)	106(16)	-47(11)	38(8)	-2(8)

Table S47. Hydrogen coordinates (x 10^4) and isotropic displacement parameters ($Å^2 x 10^{-3}$).

	x	y	z	U(eq)
H(2)	6255	5565	7070	64
H(3)	6711	5392	7892	54
H(7)	5050	4491	9303	61
H(8)	3559	3718	9236	58
H(12)	459	2955	7717	73
H(13)	53	2931	6781	76
H(17)	1855	3788	5483	62
H(18)	3319	4639	5544	61
H(21A)	6462	7227	7033	58
H(21B)	5348	7279	6804	58
H(22A)	6167	7088	8278	55
H(22B)	7034	7117	8061	55
H(23A)	4546	7108	7526	94
H(23B)	4507	8205	7270	94
H(23C)	4836	8102	7872	94

VII References

(1) Nascimento, B. F.; Rocha Gonsalves, A. M.; Pineiro, M. *Inorg. Chem. Commun.* **2010**, *13*, 395–398.

(2) Stolzenberg, A. M.; Simerly, S. W.; Steffey, B. D.; Haymond, G. S. *J. Am. Chem. Soc.* **1997**, *119*, 11843–11854.

(3) Whitlock, H. W.; Hanauer, R.; Oester, M. Y.; Bower, B. K. *J. Am. Chem. Soc.* **1969**, *91*, 7485–7489.

(4) Bonnett, R.; Nizhnik, A. N.; Berenbaum, M. C. *J. Chem. Soc., Chem. Commun.* **1989**, 1822–1823.

(5) Brückner, C.; Dolphin, D. *Tetrahedron Lett.* **1995**, *36*, 3295–3298.

(6) Brückner, C.; Rettig, S. J.; Dolphin, D. *J. Org. Chem.* **1998**, *63*, 2094–2098.

(7) Chang, C. K.; Sotiriou, C. *J. Org. Chem.* **1985**, *50*, 4989–4991.

(8) Hyland, M. A.; Morton, M. D.; Brückner, C. *J. Org. Chem.* **2012**, *77*, 3038–3048.

(9) Silva, A. M.; Tomé, A. C.; Neves, M. G.; Cavaleiro, J. A. *Tetrahedron Lett.* **2000**, *41*, 3065–3068.

(10) C. Tome, A.; S. S. Lacerda, P.; G. P. M. S. Neves, M.; A. S. Cavaleiro, J. *Chem. Commun.* **1997**, 1199–1200.

(11) Silva, A. M.; Tomé, A. C.; Neves, M. G.; Silva, A. M.; Cavaleiro, J. A.; Perrone, D.; Dondoni, A. *Tetrahedron Lett.* **2002**, *43*, 603–605.

(12) Tomé, A. C.; Lacerda, P. S. S.; Silva, A. M. G.; Neves, M. G. P. M. S.; Cavaleiro, J. A. *J. Porphyrins Phthalocyanines* **2000**, *04*, 532–537.

(13) M. G. Silva, A.; C. Tome, A.; G. P. M. S. Neves, M.; M. S. Silva, A.; A. S. Cavaleiro, J. *Chem. Commun.* **1999**, 1767–1768.

(14) Silva, A. M. G.; Tomé, A. C.; Neves, M. G. P. M. S.; Silva, A. M. S.; Cavaleiro, J. A. S. *J. Org. Chem.* **2005**, *70*, 2306–2314.

(15) de Souza, J. M.; de Assis, F. F.; Carvalho, C. M.; Cavaleiro, J. A.; Brocksom, T. J.; de Oliveira, K. T. *Tetrahedron Lett.* **2014**, *55*, 1491–1495.

(16) del Piero, S.; Melchior, A.; Polese, P.; Portanova, R.; Tolazzi, M. *Ann. Chim.* **2006**, *96*, 29–49.

(17) Gaussian 09, Revision **D.01**, M. J. Frisch, G. W. Trucks, H. B. Schlegel, G. E. Scuseria, M. A. Robb, J. R. Cheeseman, G. Scalmani, V. Barone, B. Mennucci, G. A. Petersson, H. Nakatsuji, M. Caricato, X. Li, H. P. Hratchian, A. F. Izmaylov, J. Bloino, G. Zheng, J. L. Sonnenberg, M. Hada, M. Ehara, K. Toyota, R. Fukuda, J. Hasegawa, M. Ishida, T. Nakajima, Y. Honda, O. Kitao, H. Nakai, T. Vreven, J. A. Montgomery, Jr., J. E. Peralta, F. Ogliaro, M.

Bearpark, J. J. Heyd, E. Brothers, K. N. Kudin, V. N. Staroverov, R. Kobayashi, J. Normand, K. Raghavachari, A. Rendell, J. C. Burant, S. S. Iyengar, J. Tomasi, M. Cossi, N. Rega, J. M. Millam, M. Klene, J. E. Knox, J. B. Cross, V. Bakken, C. Adamo, J. Jaramillo, R. Gomperts, R. E. Stratmann, O. Yazyev, A. J. Austin, R. Cammi, C. Pomelli, J. W. Ochterski, R. L. Martin, K. Morokuma, V. G. Zakrzewski, G. A. Voth, P. Salvador, J. J. Dannenberg, S. Dapprich, A. D. Daniels, Ö. Farkas, J. B. Foresman, J. V. Ortiz, J. Cioslowski, and D. J. Fox, Gaussian, Inc., Wallingford CT, **2009**.

8 Summary

Magnetic bistability has been a typical solid state phenomenon so far. Switching of magnetic properties such as the magnetic susceptibility or the remanent magnetization at room temperature was limited to the solid state.[150] The bistability of these observable magnetic properties is due to cooperative effects between a large number of spin centers. Until recently, single molecular magnetic bistability was restricted to very low temperatures (single molecule magnets, SMM).[151] Five years ago a new approach was developed in our research group which allows the switching of magnetic properties of isolated molecules in homogeneous solution at room temperature.[97] The mechanism was coined Light-Driven Coordination-Induced Spin State Switch (LD-CISSS) and has a number of novel potential applications which can not be realized with the conventional solid state systems. Of particular interest is the spin state switching for the development of switchable contrast agents (CAs) for magnetic resonance imaging (MRI). The clinically applied Gd(III) based CAs improve the contrast of anatomical details of routine MRI examinations.[15] Switchable or responsive CAs could enhance the diagnostic potential of MRI by visualizing physiological parameters like pH or temperature. This is particularly interesting for the detection of tumors and metastases which exhibit a lower pH and a higher temperature than healthy tissue.[152]

This work is devoted to the development of Ni(II)-based CAs which can be switched by irradiation with light. Light is an excellent stimulus for magnetic switching because it can be applied with high temporal and spatial resolution, with different energies (wavelengths) and, most importantly, it leaves not traces and byproducts. Furthermore there is a potential application in interventional radiology. Catheter supported surgeries are routinely applied after strokes or heart attacks.[153] For this purpose a catheter is introduced into the femoral artery and navigated into the brain or heart. The intervention is performed under X-ray imaging control. To control the blood flow during the intervention a bolus of iodine containing CA is administered in regular intervals via the catheter.[154,155] The propagation of the

contrast agent provides important and instant information on the dynamics of the blood flow and on a possible damage of the blood vessels. Thrombi and lesions caused by the intervention in brain arteries lead to an artificial stroke and possible death of the patient.[153] During an intervention, which can take up to two hours, the CA accumulation in the blood may become harmful and reduces the effect of further boluses. Furthermore, the X-ray exposure may cause radiation damages. Therefore, catheter based interventions under MR imaging control are investigated globally. Unfortunately, X-ray imaging control cannot directly replaced by MRI because MRI is inherently slower.[156] Therefore more CA has to be administered and the maximal dose is accumulating much faster. Interventional radiology under MR imaging control is probably only possible with switchable CAs. Once administered the CA concentration during an intervention would be constant and the contrast could be controlled by on and off switching. The light required for switching can be applied via optical fibers through the catheter. The light would switch the CA directly at the site of intervention, where the contrast changes are needed. Light is already a frequently used tool for interventions, for example for atrophying blood vessels.[157] The development of photoswitchable MRI CAs is an important step towards MRI controlled interventions.

The metal complexes investigated in this project contain Ni(II) as the paramagnetic metal ion instead of the commonly applied Gd(III). In contrast to Gd(III) which is always paramagnetic, Ni(II) can be switched between a MRI silent form (diamagnetic) and a MRI active form (paramagnetic). The origin of the effect is the change of coordination number of the Ni-complex from four (square planar) to five (square pyramidal) (Figure 8.1).

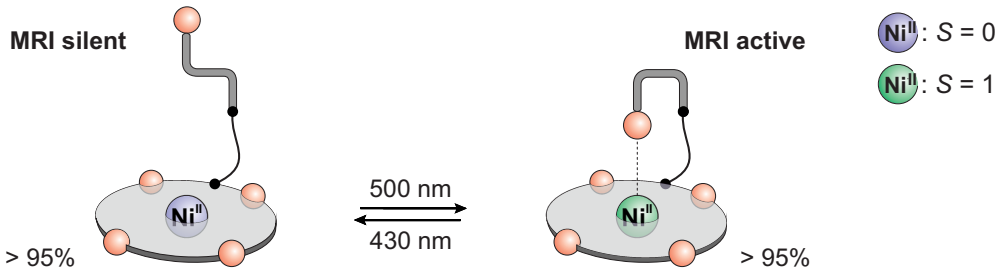

Figure 8.1: The Light-Driven Coordination-Induced Spin State Switch (LD-CISSS) changes the geometry of a Ni-complex from square planar ($S = 0$, diamagnetic) to square pyramidal ($S = 1$, paramagnetic) and thus, from a MRI silent to a MRI active form. In this work the photoconversion substantially increased to better than 95% in both directions.

In this work the photoswitching could be optimized to an almost quantitative conversion between the MRI silent form (>95% upon irradiation with 430 nm) and the MRI active form (>95% upon irradiation with 500 nm). The process is fully reversible and shows no sign of fatigue even after more than 100.000 switching cycles. Ni(II) has not been used or even suggested as the metal ion for CAs so far. Ni(II) complexes have a lower impact on MR images than Gd(III) complexes due to their lower magnetic moment (Ni(II): $S = 1$, Gd(III): $S = 7/2$).[26] However, we were able to demonstrate that the effect of the investigated Ni-complexes (or more precisely Ni-porphyrins) is significant and that the magnetic switching can easily be visualized by MRI (Figure 8.2). It is the first example for a reversible contrast switching by irradiation with light. Since one form is MRI silent, the relative contrast difference between the two forms of the Ni-porphyrin is higher than for any so far presented activatable Gd(III)-based CA.[60] This property is highly beneficial for interventional radiology.

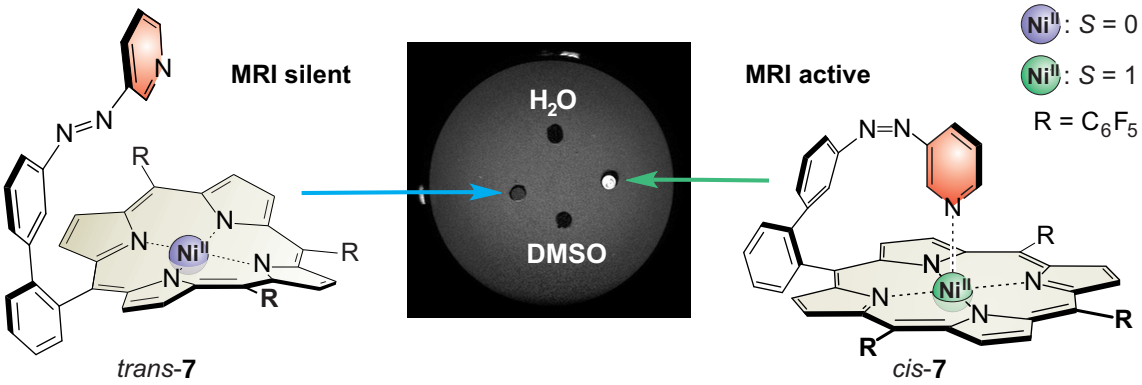

Figure 8.2: Contrast difference between the MRI silent (left) and MRI active form (right) of the Ni-porphyrin **7** (3 T, 3 mmol L^{-1} DMSO solution).

The magnetic switching using light has been performed in a number of organic solvents but not in water, yet. This is due to several problems arising from the properties of water.

1. The Ni-porphyrins used so far are highly hydrophobic and therefore completely insoluble in water.

2. Water is a good ligand and may coordinate to the axial position of a Ni-porphyrin whereby the complex would always be paramagnetic.

3. H-bonding decreases the donor strength of nitrogen based ligands and thus, their association constant could be too low to bind to Ni-porphyrins in water.

For application under *in vivo* conditions water solubility is crucial. Therefore, the investigation of water soluble Ni-porphyrins and their properties was an important issue of this thesis. Three types of water soluble porphyrins are known: porphyrins with cationic, neutral and anionic substituents.[158] Within this thesis a method to functionalize porphyrins with glycerol dendrimers was presented. The dendronized porphyrins are uncharged unlike most of the derivatives documented in the literature so far.[115,140,141] This is advantageous for *in vivo* applications because cationic porphyrins are known to diffuse from the extracellular space into the intracellular space where they can intercalate into DNA duplexes.[159–161] The dendronized Ni-porphyrin exhibits excellent coordination properties. Unlike cationic Ni-porphyrins, water does not coordinate to the Ni(II) to form a paramagnetic diaqua complex.[114,115] However, nitrogen bases like piperidine can still coordinate to the Ni(II) (in contrast to anionic Ni-porphyrins).[142] The resulting paramagnetic complex gives rise to a MRI contrast change (Figure 8.3). Our system is the first example for a Ni-based Coordination-Induced Spin State Switch (CISSS) in water. First cell tests with the dendronized Ni-porphyrin show no toxicity of *in vivo* concentrations ($< 1\,\mathrm{mmol\,L^{-1}}$). The dendron approach is a promising method for the preparation of photoswitchable water soluble Ni-porphyrins.

A further challenge regarding the application of photochromic compounds under *in vivo* conditions is the switching wavelength. The penetration depth of UV and visible light <600 nm through blood supported tissue is below 1 mm.[143,149] Our

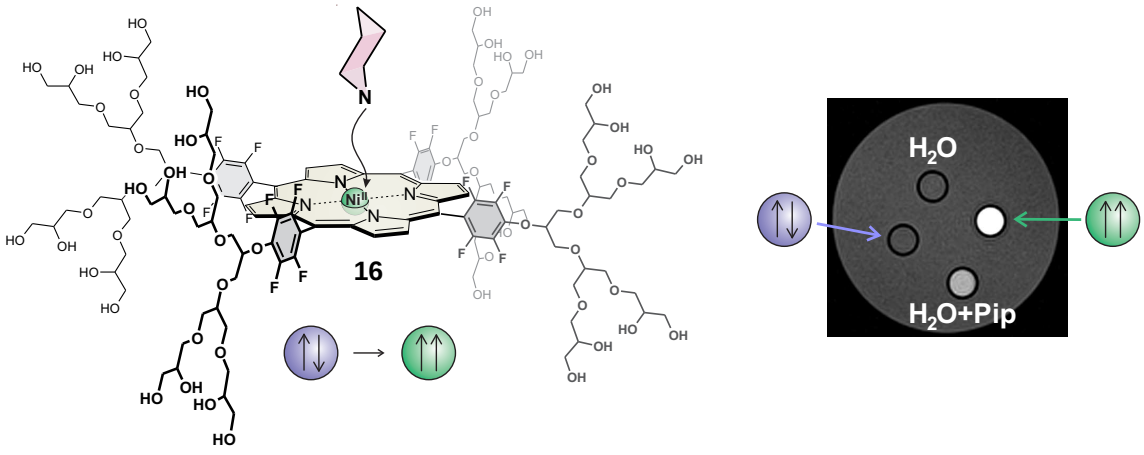

Figure 8.3: The dendronized Ni-porphyrin is diamagnetic in water and becomes paramagnetic upon addition of piperidine (Pip). The two species give rise to different contrasts in MRI (7 T, $2\,\mathrm{mmol\,L^{-1}}$).

porphyrin based contrast agents switch with 430 nm (contrast off) and with 500 nm (contrast on). Applications, therefore, would be restricted to the surface (skin) or transparent organs (e.g. eye, bladder). Consequently, we aimed at shifting the switching wavelengths to the near infrared (NIR, >650 nm). The interval between 650 nm and 950 nm is called the bio-optical window because the penetration depth is up to 10 mm.[143,149] Given the appealing prospect of using light *in vivo* for medical and diagnostic applications, a large number of international groups are aiming at the development of photochromic compounds that switch within the bio-optical window.[162–164] A novel approach pursued within this thesis, is the development of Ni-complexes with bathochromically shifted absorption wavelengths. For this purpose Ni-chlorins (Figure 8.4, green) and Ni-isobacteriochlorins (Figure 8.4, blue) were investigated as square planar platforms for magnetic switching. These compounds are the first non-porphyrin based Ni-complexes performing a CISSS. Besides the expected bathochromic shift of the absorption wavelength (Figure 8.4, top right), improved coordination properties were observed. The association constant K_1 of axial ligands, which is the key parameter for an efficient magnetic switching, has been tremendously increased (Figure 8.4, bottom). Hence, the novel platforms are superior to the so far employed Ni-porphyrins.

The development of clinically applicable photoswitchable MRI contrast agents is a highly challenging project. There are a number of pending questions and a problems

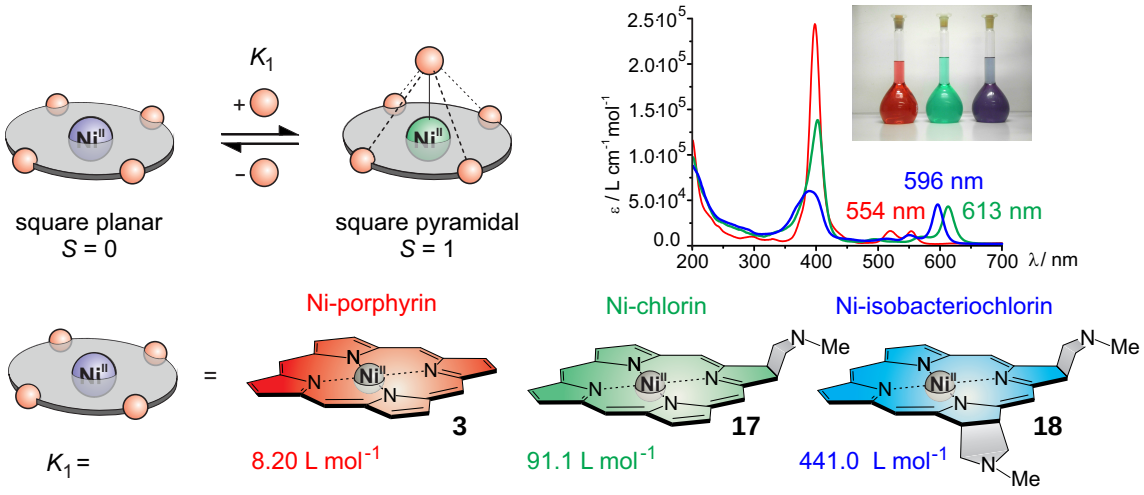

Figure 8.4: The Ni-chlorin (green) and Ni-isobacteriochlorin (blue) are superior square planar platforms for a CISSS due to their increased association constant K_1 and their bathochromic shifted absorption bands. (The axial ligand is pyridine. The *meso*-pentafluorophenyl substituent were omitted for clarity).

to be solved. Some of the most important issues were addressed within this thesis and several important milestones towards in vivo applications have been accomplished. The results clearly indicate that the development of photoswitchable MRI contrast agents on principle is possible and they give direction to future working steps.

9 Prospects

In the more distant future improved versions of the photoswitchable Ni-porphyrins based on the record player (RP) approach may be applied as contrast agents (CAs) for interventional radiology under MRI control. This will require a drastic improvement of MRI methods. Controlling and monitoring interventions with MRI is inherently more difficult than with conventional X-ray imaging control.[156] Digital subtraction angiography (DSA) is a an instructive example for the demonstration of the intricacies of interventional radiology. Currently this method is the state of the art for catheter-based interventions to treat thrombi and aneurysms, the most frequent reasons for strokes.[153] During the intervention the radiologist must know the current position of the catheter in the blood vessel. The catheter is a good X-ray absorber and can be visualized with very low radiation intensities. Hence, the catheter can be dynamically observed with multiple images per second. The cardiovascular system is not X-ray sensitive at all. Therefore, an iodine containing CA is administered through the catheter. By subsequent imaging with high X-ray intensity the propagation of the CA can be observed (Figure 9.1, top). A so called contrast image is obtained depicting a 2D projection of the cardiovascular system in black on a gray background. To remove of any signals not belonging to this system the contrast image is subtracted from a pre-contrast image (the corresponding image that was measured before CA adminstration). The result is a so called road map depicting the projection of the cardiovascular system in white on a gray background. The overlay of current images measured with low X-ray intensities (showing only the catheter) and the road map allows an accurate navigation of the catheter (black) through the blood vessels (white) (Figure 9.1, bottom left). The overlay is accurate as long as the patient does not move. Otherwise, the radiologist might need a more recent road map which includes again a high X-ray exposure for the patient. Without X-ray guidance the interventional treatment of thrombi and aneurysms within the brain would be impossible. Aneurysms are blood filled bulges at a artery wall which are potentially life-threatening. A bursting aneurysm causes a stroke by a

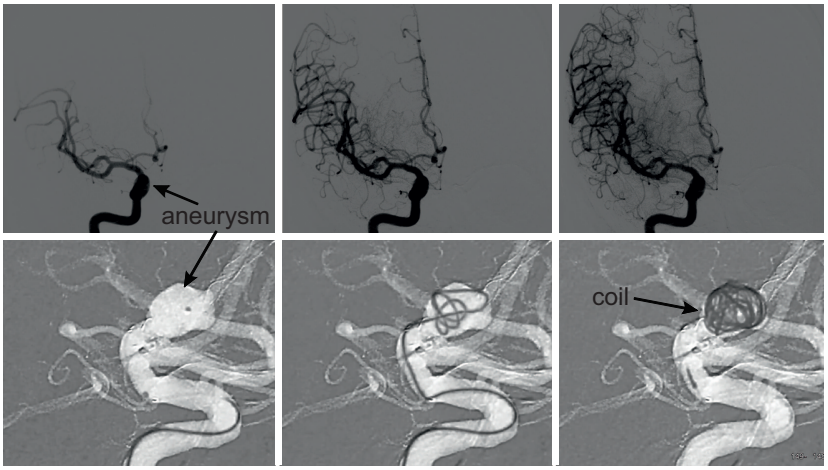

Figure 9.1: X-ray scan of the propagation of a bolus of CA from the tip of a micro catheter into a human brain (top). DSAs of a catheter-based intervention during the coiling of an aneurysm (bottom). The vascular system appears bright on the road map because it is a subtraction image. The image acquisition was performed by Dr. C. Riedel, Clinic for Neuroradiology, Universitätsklinikum Schleswig-Holstein, and reproduced with his permission.

brain hemorrhage.[155] One way to treat an aneurysm is the so called coiling.[153] For this method a catheter is navigated into the blood filled bulge. A very thin platinum wire is pushed through the catheter filling the bulge (Figure 9.1, bottom). Blood is coagulating at the foreign object which stabilizes the artery wall and prevents the bursting of the aneurysm. It would be advantageous to control interventions with MR imaging for two reasons. 1. MRI provides 3D images which are superior to the X-ray provided 2D projections. 2. There is no exposure to ionizing radiation during the intervention. MRI requires paramagnetic CAs instead of the iodine containing CAs used for the X-ray methods. These metal complexes have a half-life of approximately 90 min before they are discharged via the kidney.[136] Frequent road mapping during an intervention would lead to an unhealthy accumulation of the CA. Hence, a photoswitchable CA would be an appropriate tool for MRI guided interventions. The CA would have to be administered intravenously only once. During the intervention the contrast can be switched on to obtain the required road map. The road mapping can easily be repeated if necessary because the photoswitchable CA can be deactivated after every contrast image to obtain another pre-contrast image. The X-ray guided DSA is limited because this deactivation is not possible. For each new road map a further dose of iodine-containing CA has to

be administered. After repeated injection of the CA this may lead to a saturation of the contrast and unhealthy levels of the CA and the intervention may have to be discontinued.

Another possible application of the record player molecules is molecular mathematics. The search for molecular systems that are able to perform Boolean algebra, the basic principle for digital information processing, is a hot topic.[165,166] As shown in section 3.1 the RPs can be used as molecular logic gate with light and pH as inputs and the magnetism (diamagnetic or paramagnetic) as output (AND logic gate, Figure 9.2). Both stimuli are easy to handle and neither interfere with each other nor with the output. Hence, the RPs exhibit a non-destructive read-out. Under neutral or basic conditions (OH^-) the photoswitching between the diamagnetic and paramagnetic state works by irradiation with blue-violet light (435 nm) and green light (500 nm). Under acidic conditions (H^+) there is only diamagnetic Ni-porphyrin due to the protonation of the pyridine which prevents the axial coordination to the Ni(II). The protonated diamagnetic form of the *cis* isomer is stable and can be observed by NMR spectroscopy. Hence, the protonation does not catalyze the thermal relaxation to the *trans* isomer. Irradiation with blue-violet light converts the protonated *cis* isomer to the *trans* isomer. Interestingly the *cis* isomer cannot

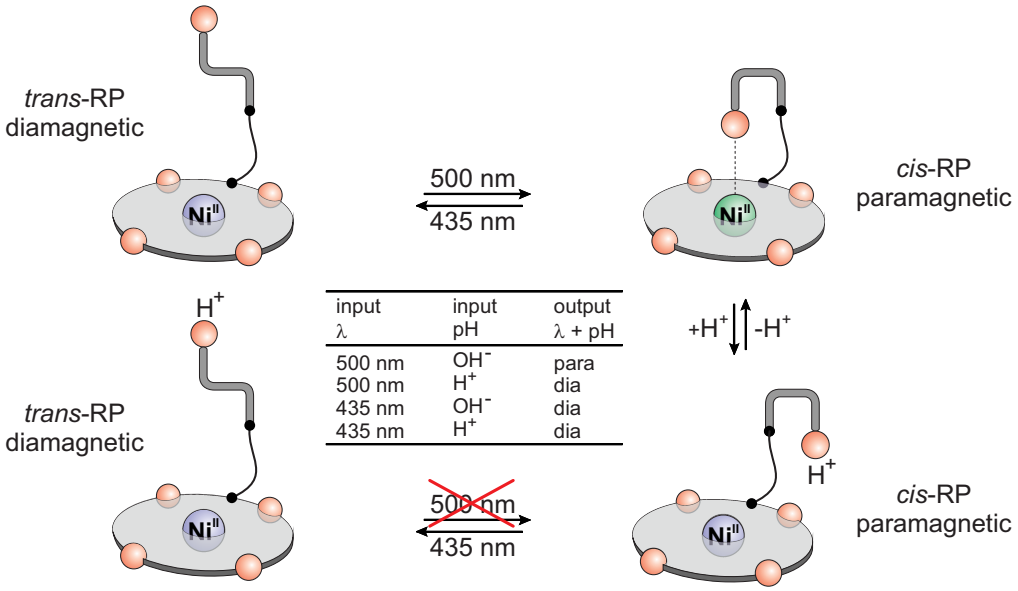

Figure 9.2: RPs can be used to perform Boolean algebra with light and pH as input and the magnetism as output. The truth table for the corresponding AND logic gate is depicted in the middle.

be enriched anymore. The solution must initially be neutralized to obtain the paramagnetic *cis*-RP by irradiation with green light (Figure 9.2). The sensitivity of the switching performance as a function of the pH may later become useful for the design of pH responsive CAs.

The fact that the protonated *trans*-RP cannot switch to the *cis* configuration is very interesting. The intramolecular coordination seems to be somehow crucial for the isomerization. There is further evidence for this assumption (section 3.1 and section 4.1).[167] All experimental results are consistent and strongly suggest that the coordination is directly involved in the mechanism of the *trans* to *cis* photoisomerization of the RPs. The origin of this effect is not yet clarified. It is obvious that the isomerization does not follow the mechanism of conventional azobenzene derivatives. This would require a $\pi\pi^*$ excitation of the azo moiety.[85] The corresponding absorption band of azopyridines is located at 330 nm. Hence, irradiation with 500 nm does not excite the azopyridine but the porphyrin. The isomerization is remarkable because the required green light has a much lower energy than the violet light which is required for conventional azobenzenes. The process has a completely novel mechanism without any precedence in the literature. The order of events seems to be different from the expected one. Instead of 1. isomerization 2. coordination 3. spin change, it is more likely to be 1. spin change 2. coordination 3. isomerization (Figure 9.3). Intramolecular coordination of the *trans* isomer, which

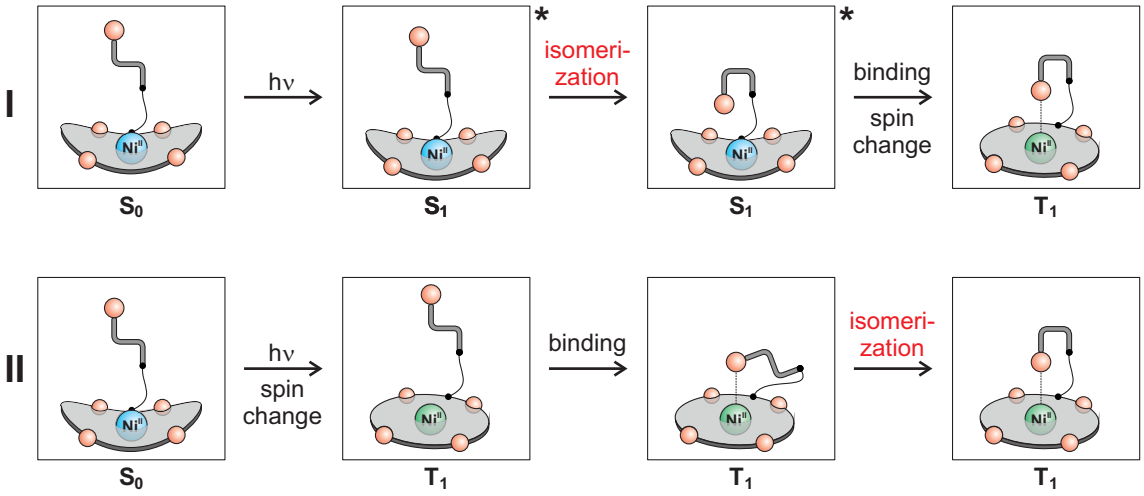

Figure 9.3: The experimentally suggested order of events during the *trans* to *cis* photoisomerization of a RP (II) is different to the expected one (I) which would apply for a mechanism according to regular azobenzene.[85]

is impossible in the diamagnetic spin state, may become possible after the spin change and the associated planarization of the Ni-porphyrin.[167] However, it is known that excited Ni-porphyrins exhibit a fast intersystem crossing (ISC). The lifetime of the resulting triplett state is drastically increasing (from 200 ps to 40 ns) if axial ligands (e.g. pyridine) coordinate to the Ni(II).[110,168,169] The spin switching of a Ni-porphyrin obviously does not necessarily require a photochromic moiety. The azo group merely seems to increase the energetic barrier (E_a) between the HS state and the LS state and thereby prevents an immediate relaxation. Hence, the half-life of the excited triplet state is increased from 40 ns (tetramesityl-Ni-porphyrin, Figure 9.4 left) to more than 400 days (RP **7**, Figure 9.4 right). Further theoretical and experimental investigations aim at a deeper understanding of this isomerization mechanism. This knowledge will be extremely useful for the design of magnetic switches whose isomerizations exhibit higher quantum yields.

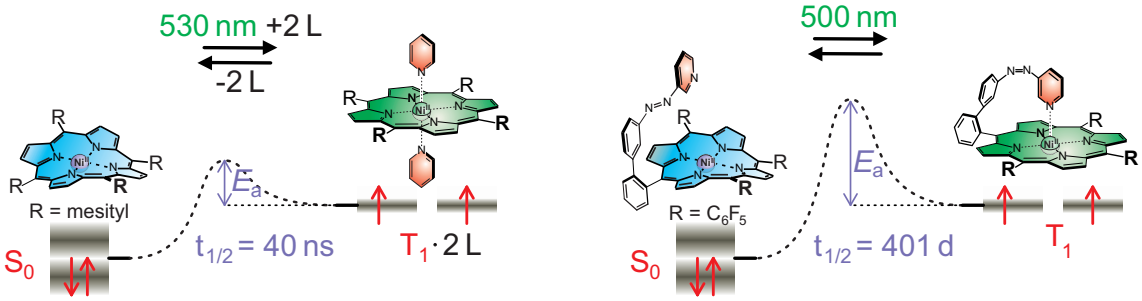

Figure 9.4: The switching mechanism of the RPs (right) seems to be related to the photoinduced ligation of the ordinary Ni-porphyrins (left). The activation barrier (E_a) for the relaxation is drastically increased by the photochromic group which raises the thermal half-life of the excited triplet state.

Since the photochromic group is not crucial to the light-induced spin transition of a Ni-porphyrin there is a chance to design a completely novel kind of magnetic switches. The challenge of this project is to prevent the immediate relaxation of the excited state by increasing the activation barrier (E_a, Figure 9.4) between the LS and the HS state. The proposed Ni-complexes should exhibit an effect that is mechanistically related to the LIESST of Fe(II) complexes (section 1.5).[75,76] Thus, it could be coined Coordination-Induced Excited Spin State Trapping (CIESST). LIESST and CIESST are both caused by an ISC after photoexcitation (Figure 9.5). The changed electronic configurations give rise to a conformational adjustment of the ligands. In the case of the LIESST the metal-ligand distance increases. In the case of the proposed CIESST an axial ligand has to coordinate. The latter

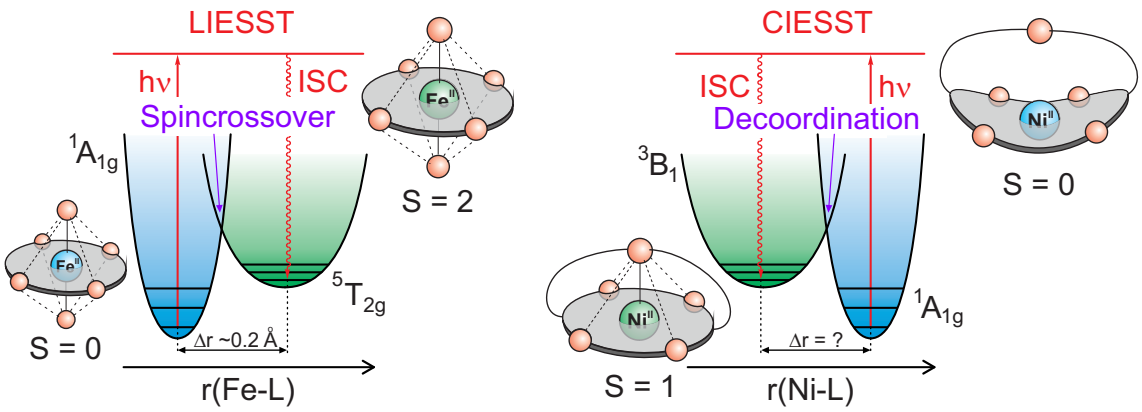

Figure 9.5: Comparison between the LIESST of Fe(II)-complexes (left) and the proposed CIESST of Ni-porphyrins (right). The spin transitions are triggered by the photoexcitation which is followed by an ISC. The Fe(II)-complex increases the distance between the metal and the ligands whereas the Ni-porphyrin reduces the distance to the axial ligand inducing the formation of a coordinative bond.

process exhibits a larger structural transformation and therefore demands more space. Hence, in a potential CIESST complex the axial ligand must be accurately pre-oriented. To realize this the axial ligand could be strapped over the Ni(II) by covalent connections to two opposite *meso*-positions of the porphyrin. The design is well elaborated. After excitation and ISC the porphyrin is flattening. This will tear the ligand towards the Ni(II) which promotes coordination. This intramolecular structural feedback is supposed to stabilize the excited state which may allow spin switching of single molecules. This is not possible with LIESST complexes because they need intermolecular cooperative interactions to stabilize the excited state.[69] CIESST complexes are supposed to give the cooperative feedback intramolecularly which should allow spin switching of non-interacting molecules, e.g. in solution. However, a well designed CIESST complex exhibits a very slight conformational change and thereby also provides a high chance to be switched even in the solid state. This would extend the scope and the possible applications of Ni-porphyrins. They could become a novel class of SCO compounds with reverse SCO properties which would be complementary to the established Fe(II)-complexes.[74,77]

Since the RP approach with Ni-porphyrins was very successful it is worth to investigate if other metalloporphyrins or related complexes exhibit a LD-CISSS as well. The number of suitable metal ions is limited. From the ten 3d transition metals there are

only a few ions that can be considered.[170] Iron in the oxidation states two and three is most promising. For application under ambient conditions Fe(II)-porphyrins are unqualified because they are highly oxidation-sensitive.[171,172] The Fe(III) derivatives are more stable. In contrast to their Ni(II) analogs the Fe(III)-porphyrins are charged and therefore need a counterion. Furthermore the spin state switch occurs during the change from coordination number five to six instead of four to five. Hence, square pyramidal Fe(III)-complexs are required as platforms for a CISSS or LD-CISSS. The photochromic ligand as well as the counteranion have to be carefully chosen to avoid intermediate and admixed spin states which are common for Fe(III)-porphyrins.[170] To simplify the coordination chemistry of the system the exchange of the anionic ligand should be prevented. For this purpose it would be advantageous to attach it covalently to the porphyrin, e.g. strapped by covalent connections to opposite *meso*-positions (Figure 9.6). Upon coordination of the photochromic ligand the proposed Fe(III)-porphyrin is forced to undergo a spin state switch from $S = 5/2$ to $S = 1/2$. This is a larger difference compared to the Ni(II)-porphyrin whose spin state switches from $S = 0$ to $S = 1$. Furthermore the direction of the spin transition is the reversed. The complex with the higher coordination number is LS configured. This may be advantageous for the relaxivity. In contrast to the coordinationally saturated LS complex, the HS Fe(III)-complex can interact via the inner sphere relaxation mechanism (section 1.4) with the solvent.[57] If the proposed Fe(III)-porphyrins perform a LD-CISSS similar to the Ni-porphyrins the relaxivity switching would be superior. The effect would have a much higher impact on a magnetic resonance image which increases the chance for an application as a CA.

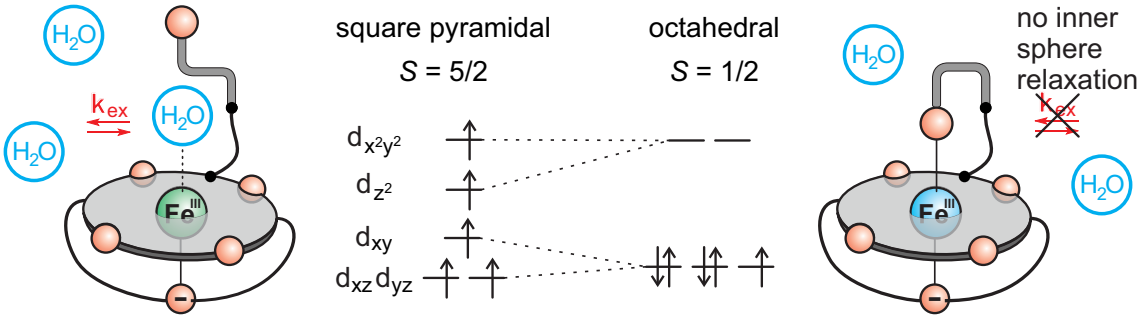

Figure 9.6: The proposed LD-CISSS of an Fe(III)-porphyrin with a strapped ionic axial ligand and a photochromic ligand should be a very efficient switchable CA due to the high magnetic moment of the HS form and the inner sphere relaxation mechanism.

The results of this thesis clearly determine the next steps towards the synthesis of RP-based photoswitchable CAs. The main objectives to be addressed are the design and the synthesis of molecular spin switches that operate in water with near infrared light (>650 nm). In this thesis several problems towards this end have been solved independently. Now, these strategies must be combined in one molecule. A potential photoswitchable contrast agent for *in vivo* applications could look like the structure depicted in Figure 9.7. Every *meso* aryl substituent will be decorated with one glycerol dendrimer for water solubility. Apart from that the aryl substituents are perfluorinated which will provide appropriate electronic properties of the Ni-macrocycle. The porphyrin core will be replaced by macrocycles with absorption bands in the near infrared. Ni-chlorins and Ni-bacteriochlorins have shown to be superior platforms for spin switching. Coordination of axial ligands as well as the absorption properties are improved. The latter is of particular interest for CAs which can be addressed with light within the bio-optical window (650 nm to 950 nm). For this purpose Ni-bacteriochlorins have to be investigated. With absorption wavelengths >700 nm they are best qualified for *in vivo* photoswitching.[134] A pending question for the future concerns the *in vivo* properties of the dendronized RPs. Before a compound may be administered to a human being or even an animal, it has to be tested extensively *in vitro* regarding its toxicity and stability. This process is expensive and should not be started until a larger amounts of the final compound have been obtained. Preliminary tests were promising. The azo group of the RPs obviously is stable under *in vivo* conditions (glutathione test, section 4.1)[173–176] and the dendronized Ni-porpyrin does not exhibit cell toxicity at the physiologically relevant concentrations of $\leq 1\,\mathrm{mmol\,L^{-1}}$ (section 4.1). Hence, the target molecule **19** (Figure 9.7) is a promising candidate for performing a LD-CISSS *in vivo* by irradiation with NIR light and may be the first photoswitchable MRI contrast agent.

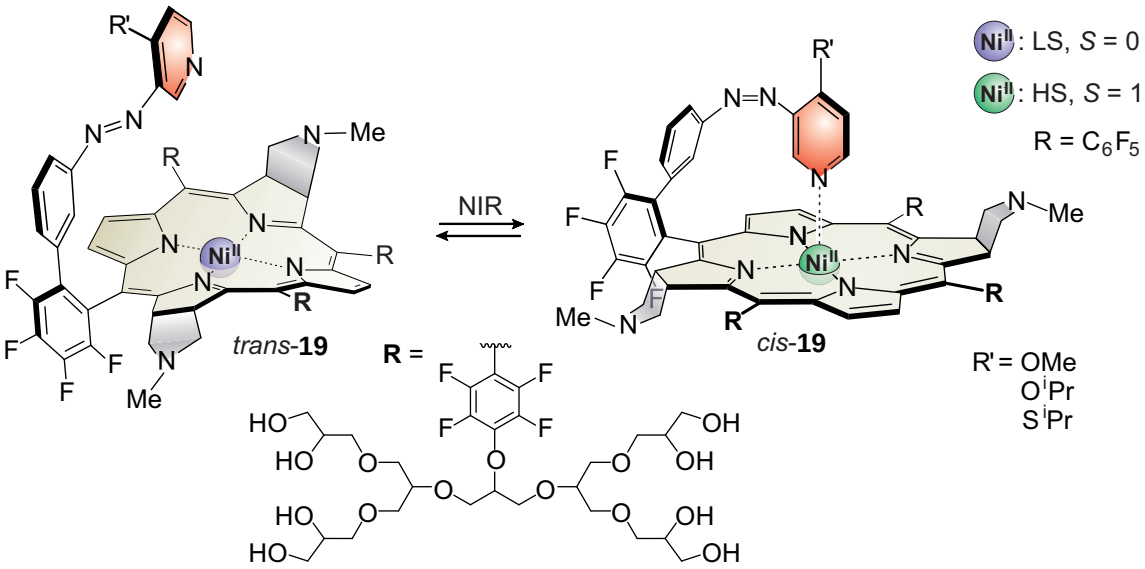

Figure 9.7: Proposed structure of a MRI contrast agent, that can be switched in water with near infrared light. The three glycerol dendrons provide water solubility. The four fluorine atoms at each *meso*-phenyl group tune the electronic properties in such a way that the ligand binding is strongly improved but not yet to such an extend that water would be irreversibly bound to the Ni(II). The electron donating substituents R' in 4-position of the pyridine increase the donor strength of the ligands which enables coordination to the Ni(II) in presence of water. Replacement of the porphyrin core by bacteriochlorin shifts the switching wavelength to the near infrared (700 nm).

10 Bibliography

[1] Haaga, J. R. *CT and MRI of the Whole Body*, 5th ed.; Mosby, 2008.

[2] Lauterbur, P. C. *Nature* **1973**, *242*, 190–191.

[3] Weishaupt, D.; Koechli, V. D.; Marincek, B. *How does MRI work? An Introduction to the Physics and Function of Magnetic Resonance Imaging*, 2nd ed.; Springer, 2006.

[4] Gauglitz, G.; Vo-Dinh, T. *Handbook of Spectroscopy, Volume 2: NMR Spectroscopy*; Wiley-VCH, 2003.

[5] Fry, C. G. *J. Chem. Educ.* **2004**, *81*, 922–932.

[6] Freeman, R. *Magnetic Resonance in Chemistry and Medicine*, 1st ed.; Oxford University Press, 2003.

[7] Grey, M.; Ailinani, J. *CT & MRI Pathology: A Pocket Atlas*, 2nd ed.; Springer, 2012.

[8] Günther, H. *NMR Spectroscopy: Basic Principles, Concepts and Applications in Chemistry*, 3rd ed.; Wiley-VCH, 2013.

[9] Dale, B. M.; Brown, M. A.; Semelka, R. C. *MRI Basic Principles and Applications*, 5th ed.; Wiley-Blackwell, 2015.

[10] Gambhir, S.; Yaghoubi, S. *Cambridge Molecular Imaging Series*; Cambridge University Press, 2010.

[11] Fletcher, L. M.; Barsotti, J. B.; Hornak, J. P. *Magn. Reson. Med.* **1993**, *29*, 623–630.

[12] Friebolin, H. *Basic One- and Two-Dimensional NMR Spectroscopy*, 5th ed.; Wiley-VCH, 2010.

[13] Bakhmutov, V. I. *Practical NMR Relaxation for Chemists*, 1st ed.; John Wiley & Sons Ltd, 2005.

[14] Cowan, B. *Nuclear Magnetic Resonance and Relaxation*; Cambridge University Press, 2005.

[15] Westbrook, C.; Kaut Roth, C.; Talbot, J. *MRI in Practice*, 4th ed.; Wiley-Blackwell, 2011.

[16] Bloch, F.; Hansen, W. W.; Packard, M. *Phys. Rev.* **1946**, *70*, 474–485.

[17] Bloembergen, N.; Purcell, E. M.; Pound, R. V. *Phys. Rev.* **1948**, *73*, 679–712.

[18] Gerthsen, C.; Vogel, H. *Physik*, 17th ed.; Springer, 1993.

[19] Jacques, V.; Dumas, S.; Sun, W.-C.; Troughton, J. S.; Greenfield, M. T.; Caravan, P. *Invest. Radiol.* **2010**, *45*, 613–624.

[20] Kulaksiz, S.; Bau, M. *Appl. Geochem.* **2011**, *26*, 1877–1885.

[21] Hao, D.; Ai, T.; Goerner, F.; Hu, X.; Runge, V. M.; Tweedle, M. *J. Magn. Reson. Imaging* **2012**, *36*, 1060–1071.

[22] de Haen, C. *Top. Magn. Reson. Imaging* **2001**, *12*, 221–230.

[23] Lu, H.; Clingman, C.; Golay, X.; van Zijl, P. C. *Magn. Reson. Med.* **2004**, *52*, 679–682.

[24] Shimada, K.; Nagasaka, T.; Shidahara, M.; Machida, Y.; Tamura, H. *Magn. Reson. Med. Sci.* **2012**, *11*, 265–271.

[25] Tóth, E.; Helm, L.; Merbach, A. *Top. Curr. Chem.* **2002**, *221*, 61–101.

[26] Lauffer, R. B. *Chem. Rev.* **1987**, *87*, 901–927.

[27] Idée, J.-M.; Port, M.; Raynal, I.; Schaefer, M.; Le Greneur, S.; Corot, C. *Fundam. Clin. Pharmacol.* **2006**, *20*, 563–576.

[28] Que, E. L.; Chang, C. J. *Chem. Soc. Rev.* **2010**, *39*, 51–60.

[29] Louie, A. Y.; Huber, M. M.; Ahrens, E. T.; Rothbacher, U.; Moats, R.; Jacobs, R. E.; Fraser, S. E.; Meade, T. J. *Nat. Biotech.* **2000**, *18*, 321–325.

[30] Duimstra, J. A.; Femia, F. J.; Meade, T. J. *J. Am. Chem. Soc.* **2005**, *127*, 12847–12855.

[31] Querol, M.; Chen, J. W.; Weissleder, R.; Bogdanov, A. *Org. Lett.* **2005**, *7*, 1719–1722.

[32] Giardiello, M.; Lowe, M. P.; Botta, M. *Chem. Commun.* **2007**, 4044–4046.

[33] Hanaoka, K.; Kikuchi, K.; Terai, T.; Komatsu, T.; Nagano, T. *Chem. Eur. J.* **2008**, *14*, 987–995.

[34] Mizukami, S.; Takikawa, R.; Sugihara, F.; Hori, Y.; Tochio, H.; Wälchli, M.; Shirakawa, M.; Kikuchi, K. *J. Am. Chem. Soc.* **2008**, *130*, 794–795.

[35] Touti, F.; Maurin, P.; Hasserodt, J. *Angew. Chem. Int. Ed.* **2013**, *52*, 4654–4658.

[36] Aime, S.; Crich, S. G.; Botta, M.; Giovenzana, G.; Palmisano, G.; Sisti, M. *Chem. Commun.* **1999**, 1577–1578.

[37] De Leon-Rodriguez, L. M.; Lubag, A. J. M.; Malloy, C. R.; Martinez, G. V.; Gillies, R. J.; Sherry, A. D. *Acc. Chem. Res.* **2009**, *42*, 948–957.

[38] Hall, J.; Häner, R.; Aime, S.; Botta, M.; Faulkner, S.; Parker, D.; de Sousa, A. S. *New J. Chem.* **1998**, *22*, 627–631.

[39] Lowe, M. P.; Parker, D.; Reany, O.; Aime, S.; Botta, M.; Castellano, G.; Gianolio, E.; Pagliarin, R. *J. Am. Chem. Soc.* **2001**, *123*, 7601–7609.

[40] Tóth, E.; Bolskar, R. D.; Borel, A.; González, G.; Helm, L.; Merbach, A. E.; Sitharaman, B.; Wilson, L. J. *J. Am. Chem. Soc.* **2005**, *127*, 799–805.

[41] Woods, M.; Kiefer, G. E.; Bott, S.; Castillo-Muzquiz, A.; Eshelbrenner, C.; Michaudet, L.; McMillan, K.; Mudigunda, S. D. K.; Ogrin, D.; Tircsó, G.; Zhang, S.; Zhao, P.; Sherry, A. D. *J. Am. Chem. Soc.* **2004**, *126*, 9248–9256.

[42] Zhang, S.; Wu, K.; Sherry, A. D. *Angew. Chem.* **1999**, *111*, 3382–3384.

[43] Aime, S.; Delli Castelli, D.; Fedeli, F.; Terreno, E. *J. Am. Chem. Soc.* **2002**, *124*, 9364–9365.

[44] Trokowski, R.; Zhang, S.; Sherry, A. D. *Bioconjugate Chem.* **2004**, *15*, 1431–1440.

[45] Carrera, C.; Digilio, G.; Baroni, S.; Burgio, D.; Consol, S.; Fedeli, F.; Longo, D.; Mortillaro, A.; Aime, S. *Dalton Trans.* **2007**, 4980–4987.

[46] Li, W.-h.; Fraser, S. E.; Meade, T. J. *J. Am. Chem. Soc.* **1999**, *121*, 1413–1414.

[47] Li, W.-h.; Parigi, G.; Fragai, M.; Luchinat, C.; Meade, T. J. *Inorg. Chem.* **2002**, *41*, 4018–4024.

[48] Dhingra, K.; Fousková, P.; Angelovski, G.; Maier, M. E.; Logothetis, N. K.; Tóth, E. *J. Biol. Inorg. Chem.* **2007**, *13*, 35–46.

[49] Angelovski, G.; Fouskova, P.; Mamedov, I.; Canals, S.; Toth, E.; Logothetis, N. K. *ChemBioChem* **2008**, *9*, 1729–1734.

[50] Dhingra, K.; Maier, M. E.; Beyerlein, M.; Angelovski, G.; Logothetis, N. K. *Chem. Commun.* **2008**, 3444–3446.

[51] Mishra, A.; Fousková, P.; Angelovski, G.; Balogh, E.; Mishra, A. K.; Logothetis, N. K.; Tóth, E. *Inorg. Chem.* **2008**, *47*, 1370–1381.

[52] Que, E. L.; Gianolio, E.; Baker, S. L.; Wong, A. P.; Aime, S.; Chang, C. J. *J. Am. Chem. Soc.* **2009**, *131*, 8527–8536.

[53] Hifumi, H.; Tanimoto, A.; Citterio, D.; Komatsu, H.; Suzuki, K. *The Analyst* **2007**, *132*, 1153–1160.

[54] Hanaoka, K.; Kikuchi, K.; Urano, Y.; Nagano, T. *J. Chem. Soc., Perkin Trans. 2* **2001**, 1840–1843.

[55] Major, J. L.; Parigi, G.; Luchinat, C.; Meade, T. J. *Proc. Natl. Acad. Sci. U.S.A.* **2007**, *104*, 13881–13886.

[56] Major, J. L.; Boiteau, R. M.; Meade, T. J. *Inorg. Chem.* **2008**, *47*, 10788–10795.

[57] Aime, S.; Botta, M.; Fasano, M.; Terreno, E. *Acc. Chem. Res.* **1999**, *32*, 941–949.

[58] Moats, R. A.; Fraser, S. E.; Meade, T. J. *Angew. Chem. Int. Ed. Engl.* **1997**, *36*, 726–728.

[59] Caravan, P.; Ellison, J. J.; McMurry, T. J.; Lauffer, R. B. *Chem. Rev.* **1999**, *99*, 2293–2352.

[60] Tu, C.; Osborne, E.; Louie, A. *Ann. Biomed. Eng.* **2011**, *39*, 1335–1348.

[61] Cambi, L.; Szegö, L. *Ber. dtsch. Chem. Ges. A/B* **1931**, *64*, 2591–2598.

[62] Cambi, L.; Cagnasso, A. *Atti Accad. Naz. Lincei* **1931**, *13*, 809.

[63] Tanabe, Y.; Sugano, S. *J. Phys. Soc. Jpn.* **1954**, *9*, 766–779.

[64] Tanabe, Y.; Sugano, S. *J. Phys. Soc. Jpn.* **1954**, *9*, 753–766.

[65] König, E. *Coord. Chem. Rev.* **1968**, *3*, 471–495.

[66] Zarembowitch, J.; Roux, C.; Boillot, M.-L.; Claude, R.; Itie, J.-P.; Polian, A.; Bolte, M. *Mol. Cryst. Liq. Cryst. Sci. Technol., Sect. A* **1993**, *234*, 247–254.

[67] Granier, T.; Gallois, B.; Gaultier, J.; Real, J. A.; Zarembowitch, J. *Inorg. Chem.* **1993**, *32*, 5305–5312.

[68] Goodwin, H. A. *Coordination Chemistry Reviews* **1976**, *18*, 293–325.

[69] Gütlich, P.; Hauser, A.; Spiering, H. *Angew. Chem. Int. Ed. Engl.* **1994**, *33*, 2024–2054.

[70] Real, J. A.; Gaspar, A. B.; Niel, V.; Muñoz, M. *Coord. Chem. Rev.* **2003**, *236*, 121–141.

[71] Kahn, O.; Martinez, C. J. *Science* **1998**, *279*, 44–48.

[72] Berlinguette, C. P.; Dragulescu-Andrasi, A.; Sieber, A.; Güdel, H.-U.; Achim, C.; Dunbar, K. R. *J. Am. Chem. Soc.* **2005**, *127*, 6766–6779.

[73] Berlinguette, C. P.; Dragulescu-Andrasi, A.; Sieber, A.; Galán-Mascarós, J. R.; Güdel, H.-U.; Achim, C.; Dunbar, K. R. *J. Am. Chem. Soc.* **2004**, *126*, 6222–6223.

[74] Sato, O.; Tao, J.; Zhang, Y.-Z. *Angew. Chem. Int. Ed.* **2007**, *46*, 2152–2187.

[75] Decurtins, S.; Gütlich, P.; Köhler, C.; Spiering, H.; Hauser, A. *Chem. Phys. Lett.* **1984**, *105*, 1–4.

[76] Decurtins, S.; Gutlich, P.; Hasselbach, K. M.; Hauser, A.; Spiering, H. *Inorg. Chem.* **1985**, *24*, 2174–2178.

[77] Real, J. A.; Gaspar, A. B.; Munoz, M. C. *Dalton Trans.* **2005**, 2062–2079.

[78] Hayami, S.; Shigeyoshi, Y.; Akita, M.; Inoue, K.; Kato, K.; Osaka, K.; Takata, M.; Kawajiri, R.; Mitani, T.; Maeda, Y. *Angew. Chem. Int. Ed.* **2005**, *44*, 4899–4903.

[79] Gütlich, P.; Garcia, Y.; Woike, T. *Coord. Chem. Rev.* **2001**, *219-221*, 839–879.

[80] Hirshberg, Y.; Fischer, E. *J. Chem. Phys.* **1955**, *23*, 1723–1723.

[81] Rau, H.; Lueddecke, E. *J. Am. Chem. Soc.* **1982**, *104*, 1616–1620.

[82] Matsuda, K.; Irie, M. *J. Photochem. Photobiol. C: Photochem. Rev.* **2004**, *5*, 169–182.

[83] Minkin, V. I. *Chem. Rev.* **2004**, *104*, 2751–2776.

[84] Natali, M.; Giordani, S. *Chem. Soc. Rev.* **2012**, *41*, 4010–4029.

[85] Bandara, H. M. D.; Burdette, S. C. *Chem. Soc. Rev.* **2012**, *41*, 1809–1825.

[86] Merino, E.; Ribagorda, M. *Beilstein J. Org. Chem.* **2012**, *8*, 1071–1090.

[87] Irie, M.; Fukaminato, T.; Matsuda, K.; Kobatake, S. *Chem. Rev.* **2014**, *114*, 12174–12277.

[88] Klajn, R. *Chem. Soc. Rev.* **2014**, *43*, 148–184.

[89] Roux, C.; Zarembowitch, J.; Gallois, B.; Granier, T.; Claude, R. *Inorg. Chem.* **1994**, *33*, 2273–2279.

[90] Boillot, M.-L.; Roux, C.; Audière, J.-P.; Dausse, A.; Zarembowitch, J. *Inorg. Chem.* **1996**, *35*, 3975–3980.

[91] Boillot, M.-L.; Chantraine, S.; Zarembowitch, J.; Lallemand, J.-Y.; Prunet, J. *New J. Chem.* **1999**, *23*, 179–184.

[92] Takahashi, K.; Hasegawa, Y.; Sakamoto, R.; Nishikawa, M.; Kume, S.; Nishibori, E.; Nishihara, H. *Inorg. Chem.* **2012**, *51*, 5188–5198.

[93] Sour, A.; Boillot, M.-L.; Rivière, E.; Lesot, P. *Eur. J. Inorg. Chem.* **1999**, *1999*, 2117–2119.

[94] Hasegawa, Y.; Kume, S.; Nishihara, H. *Dalton Trans.* **2009**, 280–284.

[95] Nihei, M.; Suzuki, Y.; Kimura, N.; Kera, Y.; Oshio, H. *Chem. Eur. J.* **2013**, *19*, 6946–6949.

[96] Milek, M.; Heinemann, F. W.; Khusniyarov, M. M. *Inorg. Chem.* **2013**, *52*, 11585–11592.

[97] Venkataramani, S.; Jana, U.; Dommaschk, M.; Sönnichsen, F. D.; Tuczek, F.; Herges, R. *Science* **2011**, *331*, 445–448.

[98] Lyaskovskyy, V.; de Bruin, B. *ACS Catal.* **2012**, *2*, 270–279.

[99] Buchanan, R. M.; Pierpont, C. G. *J. Am. Chem. Soc.* **1980**, *102*, 4951–4957.

[100] Hendrickson, D.; Pierpont, C. *Topics in Current Chemistry*; Springer Berlin Heidelberg, 2004; Vol. 234; pp 63–95.

[101] Dei, A.; Gatteschi, D.; Sangregorio, C.; Sorace, L. *Acc. Chem. Res.* **2004**, *37*, 827–835.

[102] Sedó, J.; Saiz-Poseu, J.; Busqué, F.; Ruiz-Molina, D. *Adv. Mater.* **2013**, *25*, 653–701.

[103] Witt, A.; Heinemann, F. W.; Khusniyarov, M. M. *Chem. Sci.* **2015**, *6*, 4599–4609.

[104] Witt, A.; Heinemann, F. W.; Sproules, S.; Khusniyarov, M. M. *Chem. Eur. J.* **2014**, *20*, 11149–11162.

[105] Caughey, W. S.; Deal, R. M.; McLees, B. D.; Alben, J. O. *J. Am. Chem. Soc.* **1962**, *84*, 1735–1736.

[106] Caughey, W. S.; Fujimoto, W. Y.; Johnson, B. P. *Biochemistry* **1966**, *5*, 3830–3843.

[107] Baker, E. W.; Brookhart, M. S.; Corwin, A. H. *J. Am. Chem. Soc.* **1964**, *86*, 4587–4590.

[108] Cole, S. J.; Curthoys, G. C.; Magnusson, E. A.; Phillips, J. N. *Inorg. Chem.* **1972**, *11*, 1024–1028.

[109] Kaplan, W. A.; Scott, R. A.; Suslick, K. S. *J. Am. Chem. Soc.* **1990**, *112*, 1283–1285.

[110] Kim, D.; Su, Y. O.; Spiro, T. G. *Inorg. Chem.* **1986**, *25*, 3988–3993.

[111] McLees, B. D.; Caughey, W. S. *Biochemistry* **1968**, *7*, 642–652.

[112] Song, Y.; Haddad, R. E.; Jia, S.-L.; Hok, S.; Olmstead, M. M.; Nurco, D. J.; Schore, N. E.; Zhang, J.; Ma, J.-G.; Smith, K. M.; Gazeau, S.; Pécaut, J.; Marchon, J.-C.; Medforth, C. J.; Shelnutt, J. A. *J. Am. Chem. Soc.* **2005**, *127*, 1179–1192.

[113] Walker, F. A.; Hui, E.; Walker, J. M. *J. Am. Chem. Soc.* **1975**, *97*, 2390–2397.

[114] Bütje, K.; Nakamoto, K. *Inorg. Chimi. Ac.* **1990**, *167*, 97–108.

[115] La, T.; Richards, R. A.; Lu, R. S.; Bau, R.; Miskelly, G. M. *Inorg. Chem.* **1995**, *34*, 5632–5640.

[116] Thies, S.; Sell, H.; Bornholdt, C.; Schütt, C.; Köhler, F.; Tuczek, F.; Herges, R. *Chem. Eur. J.* **2012**, *18*, 16358–16368.

[117] Thies, S.; Sell, H.; Schütt, C.; Bornholdt, C.; Näther, C.; Tuczek, F.; Herges, R. *J. Am. Chem. Soc.* **2011**, *133*, 16243–16250.

[118] Hund, F. *Zeitschrift für Physik* **1925**, *33*, 345–371.

[119] Venanzi, L. M. *J. Chem. Soc.* **1958**, 719–724.

[120] Goodgame, D. M. L.; Goodgame, M.; Cotton, F. A. *J. Am. Chem. Soc.* **1961**, *83*, 4161–4167.

[121] Chakravorty, A.; Fennessey, J. P.; Holm, R. H. *Inorg. Chem.* **1965**, *4*, 26–33.

[122] Thies, S.; Bornholdt, C.; Köhler, F.; Sönnichsen, F. D.; Näther, C.; Tuczek, F.; Herges, R. *Chem. Eur. J.* **2010**, *16*, 10074–10083.

[123] Adler, A. D.; Longo, F. R.; Finarelli, J. D.; Goldmacher, J.; Assour, J.; Korsakoff, L. *J. Org. Chem.* **1967**, *32*, 476–476.

[124] Longo, F. R.; Finarelli, M. G.; Kim, J. B. *J. Heterocyc. Chem.* **1969**, *6*, 927–931.

[125] Lindsey, J. S.; Wagner, R. W. *J. Org. Chem.* **1989**, *54*, 828–836.

[126] Hampson, G. C.; Robertson, J. M. *J. Chem. Soc.* **1941**, 409–413.

[127] Mostad, A.; Roemming, C. *Acta Chem. Scand.* **1971**, *25*, 3561–3568.

[128] Umemoto, T.; Ohtani, Y.; Tsukamoto, T.; Shimada, T.; Takagi, S. *Chem. Commun.* **2014**, *50*, 314–316.

[129] Otsuki, J.; Narutaki, K. *Bull. Chem. Soc. Jpn.* **2004**, *77*, 1537–1544.

[130] Ayyangar, N.; Naik, S.; Srinivasan, K. *Tetrahedron Lett.* **1989**, *30*, 7253–7256.

[131] Campbell, N.; Henderson, A. W.; Taylor, D. *J. Chem. Soc.* **1953**, 1281–1285.

[132] Cheon, K.-S.; A. Cox, R.; Keum, S.-R.; Buncel, E. *J. Chem. Soc., Perkin Trans. 2* **1998**, 1231–1240.

[133] Faessinger, B. *J. Am. Chem. Soc.* **1951**, *73*, 4606–4608.

[134] Silva, A. M. G.; Tomé, A. C.; Neves, M. G. P. M. S.; Silva, A. M. S.; Cavaleiro, J. A. S. *J. Org. Chem.* **2005**, *70*, 2306–2314.

[135] Reimer, P.; Vosshenrich, R. *Der Radiologe* **2004**, *44*, 273–283.

[136] Adamek, H. E.; Lauenstein, T. C. *MRT in der Gastroenterologie*; Thieme, 2010.

[137] Schmidt, R.; Thews, G. *Physiologie des Menschen*; Springer, 2013.

[138] Lindsey, J. S.; Schreiman, I. C.; Hsu, H. C.; Kearney, P. C.; Marguerettaz, A. M. *J. Org. Chem.* **1987**, *52*, 827–836.

[139] Rohand, T.; Dolusic, E.; Ngo, T. H.; Maes, W.; Dehaen, W. *ARKIVOC* **2007**, 307–324.

[140] Kadish, K. M.; Sazou, D.; Liu, Y. M.; Saoiabi, A.; Ferhat, M.; Guilard, R. *Inorg. Chem.* **1988**, *27*, 1198–1204.

[141] Pasternack, R. F.; Huber, P. R.; Boyd, P.; Engasser, G.; Francesconi, L.; Gibbs, E.; Fasella, P.; Cerio Venturo, G.; Hinds, L. d. *J. Am. Chem. Soc.* **1972**, *94*, 4511–4517.

[142] Ravikant, M.; Reddy, D.; Chandrashekar, T. K. *J. Chem. Soc., Dalton Trans.* **1991**, 2103–2108.

[143] Sternberg, E. D.; Dolphin, D.; Brückner, C. *Tetrahedron* **1998**, *54*, 4151–4202.

[144] Huppelsberg, J.; Walter, K. *Kurzlehrbuch Physiologie*, 3rd ed.; Thieme, 2009.

[145] Pape, H.-C.; Kurtz, A.; Silbernagl, S. *Physiologie*, 7th ed.; Thieme, 2014.

[146] Zwart, A.; van Assendelft, O. W.; Bull, B. S.; England, J. M.; Lewis, S. M.; Zijlstra, W. G. *J. Clin. Pathol.* **1996**, *49*, 271–274.

[147] Lodemann, P.; Schorer, G.; Frey, B. *Ann. Hematol.* **2010**, *89*, 209–209.

[148] Beutler, E.; Waalen, J. *Blood* **2005**, *107*, 1747–1750.

[149] Nyman, E. S.; Hynninen, P. H. *J. Photochem. Photobiol. B: Biology* **2004**, *73*, 1–28.

[150] Halcrow, M. A. *Spin-Crossover Materials*; John Wiley & Sons Ltd, 2013.

[151] Tang, J.; Zhang, P. *Lanthanide Single Molecule Magnets*; Springer, 2015.

[152] Siemann, D. W. *Tumor Microenvironment*; Wiley-Blackwell, 2011.

[153] Lanzer, P. *Catheter-Based Cardiovascular Interventions*; Springer, 2013.

[154] Bryan, N. R. *Introduction to the Science of Medical Imaging*; Cambridge University Press, 2010.

[155] Ginat, D. T.; Small, J. E.; Schaefer, P. W. *Neuroimaging Pharmacopoeia*; Springer, 2006.

[156] Mahnken, A. H.; Wilhelm, K. E.; Ricke, J. *CT- and MR-Guided Interventions in Radiology*; Springer, 2013.

[157] Kandarpa, K. *Peripheral Vascular Interventions*; Wolters Kluwer, 2008.

[158] Kadish, K. M.; Smith, K. M.; Guilard, R. *The Porphyrin Handbook*, 3rd ed.; Academic Press, 2000; Vol. 18.

[159] Pasternack, R. F. *Chirality* **2003**, *15*, 329–332.

[160] Fiel, R.; Howard, J.; Mark, E.; Gupta, N. *Nucleic Acids Res.* **1979**, *6*, 3093–3118.

[161] Fiel, R.; Munson, B. *Nucleic Acids Res.* **1980**, *8*, 2835–2842.

[162] Bléger, D.; Hecht, S. *Angew. Chem. Int. Ed.* **2015**, *54*, 11338–11349.

[163] Cnossen, A.; Hou, L.; Pollard, M. M.; Wesenhagen, P. V.; Browne, W. R.; Feringa, B. L. *J. Am. Chem. Soc.* **2012**, *134*, 17613–17619.

[164] Fredrich, S.; Göstl, R.; Herder, M.; Grubert, L.; Hecht, S. *Angew. Chem. Int. Ed.* **2015**, *55*, 1208–1212.

[165] Szaciłowski, K. *Chem. Rev.* **2008**, *108*, 3481–3548.

[166] Magri, D. C. *New J. Chem.* **2009**, *33*, 457–461.

[167] Alcover-Fortuny, G.; de Graaf, C.; Caballol, R. *Phys. Chem. Chem. Phys.* **2015**, *17*, 217–225.

[168] Kim, D.; Spiro, T. G. *J. Am. Chem. Soc.* **1986**, *108*, 2099–2100.

[169] Shelby, M. L.; Mara, M. W.; Chen, L. X. *Coord. Chem. Rev.* **2014**, *277-278*, 291–299.

[170] Mashiko, T.; Dolphin, D. Comprehensive Coordination Chemistry, eds. G. Wilkinson, R. D. Gillard and J. A. McCleverty, Pergamon, Oxford, 1987.

[171] Shikama, K. *Coord. Chem. Rev.* **1988**, *83*, 73–91.

[172] Huszank, R.; Horvath, O. *Chem. Commun.* **2005**, 224–226.

[173] Kosower, E. M.; Kanety-Londner, H. *J. Am. Chem. Soc.* **1976**, *98*, 3001–3007.

[174] Samanta, S.; McCormick, T. M.; Schmidt, S. K.; Seferos, D. S.; Woolley, G. A. *Chem. Commun.* **2013**, *49*, 10314–10316.

[175] Samanta, S.; Beharry, A. A.; Sadovski, O.; McCormick, T. M.; Babalhavaeji, A.; Tropepe, V.; Woolley, G. A. *J. Am. Chem. Soc.* **2013**, *135*, 9777–9784.

[176] Yang, Y.; Hughes, R. P.; Aprahamian, I. *J. Am. Chem. Soc.* **2014**, *136*, 13190–13193.